Moisture Control and Enclosure Wall Systems

by

John Frederick Straube

A thesis
presented to the University of Waterloo
in fulfilment of the
thesis requirement for the degree of
Doctor of Philosophy
in
Civil Engineering

Waterloo, Ontario, Canada, 1998

The University of Waterloo requires the signatures of all persons using or photocopying this thesis. Please sign below, and give address and date.

Abstract

Moisture Control and Enclosure Wall Systems

Moisture is one of the most important factors affecting building performance and durability, especially in countries with cold climates. Understanding and predicting moisture movement within and through the building enclosure is crucial to the control and the avoidance of moisture-related problems such as corrosion, freeze-thaw, and biological growth.

This thesis comprehensively investigated the control of moisture in above-grade enclosure walls. Emphasis was given to driving rain deposition, rain penetration control, ventilation drying, and pressure moderation. A major review of liquid and vapour moisture storage and transport in porous building materials was undertaken, and the results summarised.

The experimental program involved the temperature, humidity, and moisture monitoring of 26 full-scale test panels exposed to the environment of South-western Ontario for 30 months. Driving rain was measured in the free wind and at 14 locations on a test building. High-speed pressure measurements, of interest to ventilation and pressure moderation, where simultaneously collected at many points. The water permeance of brick veneers under air pressure differences and the moisture absorption of brick were studied in the laboratory.

A method of predicting driving rain was developed and validated with field measurements. The distributions of driving rain event duration, intensity, and direction were investigated. An approximate means of estimating rain deposition on buildings was also developed, supported by measurements and other researchers' results. A rational rain control theory was conceived which led to a useful enclosure classification system. A probabilistic model of rain-building-enclosure interaction was produced which incorporates all of the important variables.

Extensive pressure measurements showed that instantaneous pressure equalisation does not occur. It was also shown that realistic air pressure differences have little effect on the permeance of brick veneers. It was concluded that pressure moderation is not an effective rain control strategy for most walls, especially brick veneers.

The physics of ventilation flow and ventilation drying of walls were formulated. Field measurements of wind pressures and air space moisture content and temperatures behind brick veneers demonstrated the importance of ventilation as a drying mechanism and as a means of resisting inward vapour-drive wetting. It was found that the sun and wind have a large and beneficial influence on ventilation drying. Summer condensation wetting due to inward vapour drives from solar-heated rain-wetted cladding was shown to be a potentially serious performance problem.

Acknowledgments

Thanks are due to the many people who made this thesis and the experimental work possible.

First and foremost, I wish to thank my supervisor Dr Eric Burnett. His confidence in me has allowed me to explore my interests while his guidance ensured that I remained focused. This thesis strongly reflects his philosophy and teaching.

Dr Reinhold Schuster generously offered to be my co-supervisor when Dr Burnett moved on to Penn State. His willing and professional assistance is gratefully acknowledged.

Many friends and fellow students have been very helpful in this work. John deGraauw was always a helpful and knowledgeable sounding board, and Julie Bartlett provided priceless assistance as an informal but strict editor. Reza Erfani and Vipul Acharya helped maintain my sanity, while Gunter Dressler and Torsten Huhse ensured that my work maintained some practical value to builders.

Civil Engineering technicians Terry Ridgeway, Ken Bowman, and Ralph Korchensky were always there to help during the experimental phase. The panels would never have been built without the cheerful, energetic, and skilled assistance of Chris Schumacher.

Finally, the financial support and technical critique of the industrial partners must be recognised for making this work possible as well as directing its scope and direction. These include: Luc Fornoville, Iain Thompson and John Storer-Folt (Canada Brick), John Edgar (Sto Finish Systems), Robert Cardinal (Celfortec), Pierre-Michel Busque (CMHC), John Evans (Roxul Inc.), Keith Wilson (Owens-Corning Canada), Hans Rerup (Durisol Materials Ltd.), and Brad Cobbledick (Brampton Brick).

Nomenclature

A	area, capillary water absorption coefficient
a	acceleration
C_d	drag coefficient, orifice discharge coefficient
C_p	pressure coefficient
c_p	specific heat capacity
D	mass of drained rain water
D_a	adsorbed moisture diffusivity
D_h	hydraulic diameter
D_l	liquid moisture diffusivity
$D_{T.l}$	liquid thermal moisture diffusivity
$D_{T.v}$	vapour thermal moisture diffusivity
$D_{v.K}$	Knudsen vapour diffusivity
D_v	vapour diffusivity
DRF	driving rain factor
d	diameter of orifice, mass fraction of rain water drained
F	force
f	frequency, friction factor
g	acceleration due to gravity, effective surface mass transfer coefficient
H	frequency-domain transfer function
h	height, effective heat transfer coefficient
J	average curvature of meniscus
K	absolute permeability
K_l	liquid moisture permeability
k_a	air permeability
L	flow path length
l	length
l_m	mean free path length of gas molecules between collisions
M	vapour permeance

M%	mass fraction of dryweight that is water
MC	moisture content
m	mass
m_v	mass rate of diffusive vapour flow
m_l	mass rate of capillary liquid flow
m_a	mass rate of adsorbed moisture flow, mass rate of air flow
$m_{v.conv}$	mass rate of convective vapour flow
P	pressure, total pressure
p	partial vapour pressure
Q	volumetric flow rate of air
q	volumetric flow rate of water
R	universal gas constant, thermal or vapour resistance
R_a	gas constant for air
R_{wv}	gas constant for water vapour
RAF	rain admittance factor
RH	relative humidity
r	radius
r_v	rain fall intensity
r_h	driving rain intensity in the free wind
r_{bv}	rain deposition on a vertical building surface
S	frequency spectrum, mass of stored rain water
s	mass fraction of stored rain water
T	absolute temperature, mass of rain water transmitted
t	thickness, time, mass fraction of rain water transmitted
t_a	thickness of adsorbed layer
u	mass of water per unit mass of dry material
V	volume, velocity of wind or water drop or water film
V_a	air volume (in pores)
V_T	total sample volume

W	humidity ratio
w	mass of water per unit volume, width, crack width, airspace width
X	volume fraction
z	height above grade for wind velocity calculations
ψ	porosity, volumetric moisture content
θ	contact angle, wind direction
ϕ	relative humidity, phase shift
σ	interfacial or surface tension
ε	absolute roughness
ξ	slot or opening friction factor
ρ	mass density
δ_a	vapour permeability of air
δ_p	vapour permeability of a porous material
τ	tortuosity factor
μ	dynamic viscocity

Commonly used subscripts

a	adsorbed, air
ab	air barrier
cap	capillary
cav	cavity
conv	convective
eff	effective
i	layer number
l	liquid
m	moisture
sat	saturated
scr	screen
stag	stagnation
v	water vapour, vent

Table of Contents

List of Tables

List of Figures

1. INTRODUCTION

In industrialised countries, most people spend more than 90% of their lives inside buildings. During this time their productivity and quality of life are directly affected by the nature of the enclosed environment. Buildings also represent one of the largest components of any industrialised country's capital wealth. A significant proportion of the total productive effort of a country is expended on producing and maintaining these buildings [1.1]. Between 30% and 50% of all energy is used in the construction and maintenance of buildings, and evidence of the link between this energy consumption and climate change grows stronger with time [1.2].

Buildings and the shelter they provide are clearly important, but a large proportion of all buildings, both new and old, are deficient or inefficient in some way, including durability, utility, appearance, affordability, energy use, occupant health, safety, and productivity. It has recently been estimated that the *premature* deterioration of buildings costs at least 235 - 380 million dollars per annum in Canada [1.3]; several billion dollars are spent annually on the repair and replacement of exterior walls and roofs. Most premature building deterioration is the result of inadequate in-service performance, or even failure, of the building enclosure. Roofing and facade failures, i.e., those involving the above-grade building enclosure, account for the majority of American building defect claims on insurance companies [1.4].

1.1 Moisture and Building Performance Problems

Moisture is one of the most important factors affecting building performance, including durability, especially in countries with cold climates. Understanding and predicting moisture movement within and through both the building and the enclosure is crucial to its control, and the avoidance of moisture-related problems.

Moisture-related problems in the building envelope include:

- leakage of water into the building
- freeze-thaw deterioration of the concrete, stone, and masonry,

- electrochemical corrosion of metal components such as structural framing, reinforcing bars, masonry anchors, ties, flashing, etc.,
- biological, especially fungal (mould, rot, decay) growth, which can damage materials and have a major effect on occupant health,
- chemical deterioration and dissolution of materials such as gypsum sheathing, glued wood products, etc.,
- volume changes (e.g., expansion, shrinkage), which can induce damaging stresses, and
- staining and discoloration of building finishes.

The existing stock of masonry cladding is approximately 2 billion square meters, and in a typical year about 70 million square meters of new masonry is constructed in North America [1.5]. Masonry is especially popular in the residential market; in South-western Ontario the majority of both high- and low-rise residential buildings are clad with a masonry veneer. Despite the outward appearance of durability, however, walls on buildings with masonry veneer cladding have experienced a significant number of performance and durability problems, almost all moisture-related [1.6,1.7].

In Canada, especially over the last fifteen years, a great deal of time and effort has been devoted to the topic of understanding and controlling moisture in building envelopes. The National Research Council of Canada (NRCC) and the Canada Mortgage and Housing Corporation (CMHC) have spent considerable effort supporting work to document, diagnose, and solve moisture-related problems [1.8, 1.9]. Although some of these problems are new, many have existed for decades and have yet to be researched in a systematic and/or detailed manner.

1.2 Research Needs

Computer modelling of the heat, air, and moisture (HAM) transport and storage within building enclosures shows great promise as an aid to the builder designer. These HAM models are still in their infancy although some have proven useful for certain types of problems. There are still some considerable limitations that inherently limit the usefulness of any computer model, even if it could accurately model heat air and moisture movement

within the enclosure. For example, the boundary conditions provided as input are often critical to the accuracy of the results of a simulation.

Driving rain is one of the largest sources of moisture in building enclosures and yet there is practically no theory to predict the amount of driving rain deposition on an enclosure. The moisture flux across and within the exterior cladding, especially of enclosures with absorbent materials (e.g. masonry veneers, stucco, wood), is greater than any other part of the assembly. The importance of rain absorption, shedding, and penetration of the moisture deposited by driving rain has not been studied in any depth, and computer models that do not include driving rain as a boundary conditions are severely limited in application and accuracy.

The drying conditions of the cladding are also not fully understood. For example, the role of ventilation behind the cladding is typically ignored because of its "insignificant" effect, although empirical evidence and years of building tradition suggest otherwise.

Modelling certain aspects of real enclosures systems is also very difficult e.g., interfaces, cracks, air leakage, construction imperfections, connectors, etc. Understanding the role of these imperfections is crucial to the development of sufficiently accurate computer models.

Although various strategies can be used for moisture control in exterior walls, the current consensus regarding wall design in Canada favours multi-layer wall systems employing both a thermally-protected structural component and a drained, vented, and pressure-moderated exterior screen. The popular masonry veneer "rainscreen" wall system for example uses an exterior masonry layer as the screen and an air space and various water barriers to supplement the control of rain penetration. Walls with screens of vinyl siding, natural stone cladding, and even stucco are now also being designed and built using the rainscreen principle.

The air space in such screened wall systems, historically used as a capillary break, can also be used as a drainage plane and to facilitate both pressure moderation and ventilation drying. However, the role of the air space, and its venting, have not been quantified by research or measurements. A significant amount of debate has developed over the need for venting, pressure moderation, and the significance of ventilation drying. All of these questions are especially pressing for masonry claddings.

Some specific building envelope moisture control issues that have not yet been addressed, or have received little attention from other researchers include:

1. The interaction of the wind and rain and their effect on the building envelope;

2. The mechanisms and relative significance of rain wetting, penetration, storage and drainage;

3. The nature, degree, and incidence of pressure moderation across the screen and its significance for moisture control and the reduction of wind loadings, and

4. The nature, relative significance, and incidence of ventilation air flow through wall cavities and the potential for ventilation drying and evaporative drying from the surface.

All of these issues deal predominately with the outer layers (e.g., sheathing, housewraps) or cladding of enclosure walls. Because points 2 through 4 all involve an airspace behind the cladding, the function and significance of airspaces behind claddings in enclosures will be examined in a more general way.

1.3 Objective

The main objective of this thesis is to comprehensively investigate the control of moisture in above-grade enclosure walls. Increasing the understanding of the interaction of the wind, rain, and building enclosure is of special interest. Masonry veneer wall systems will be a focus of the study because of their wide-spread use. As discussed above, pressure moderation and ventilation of the air space are two little understood components of moisture movement in walls and thus will also be given emphasis.

Much of the work can, in principle, be applied to the entire building enclosure. The knowledge generated about realistic boundary conditions will be presented in such a way as to improve the ability of computer models to predict moisture performance.

1.4 Approach

This thesis works towards its objectives from a general to a specific level. Theory is developed and supported or demonstrated with the aid of experimental measurements. The majority of the experimental program was conducted as part of two projects, one supported by a consortium of seven industrial partners and the Ontario government (called the URIF project) and the other an External Research Program grant from the Canada Mortgage and Housing Corporation. Chapter 3 describes the experimental program in general and individual chapters provide more detailed information as required.

To provide a context for discussion, basic moisture control design principles for enclosure walls are outlined in Chapter 2. Although some of these principles are part of what is currently considered "state-of-the-art" in the industry, the rigour of the definitions and the generality of the design approach is new. In Chapter 4, a state-of-the-art review of the physics of moisture storage and transport is presented. No new information is developed in this review, but the synthesis and the completeness of the review is unique, at least in the English language literature.

A method of predicting driving rain is developed in Chapter 5, supported by extensive field measurements and corroborated by the results of other researchers. Chapter 6 presents a theory of rain control that leads to a classification system, rain control strategies for design, and a better understanding of how driving rain is, or can be, controlled by appropriate enclosure design. Building on the theory of the previous chapter, Chapter 7 examines the response of cladding to rain deposition in more depth and consolidates the information from the previous two chapters into a probabilistic model.

One of the mechanisms of rain control is pressure moderation. Previous pressure moderation research is briefly reviewed in Chapter 8. Theory and extensive new field measurements of full-scale walls are used to explore the influence and importance of a range of design variables, and the importance of pressure moderation itself.

Ventilation drying is the subject of Chapter 9. The physics of ventilation drying and air flow through building cavities and vents is developed. A method of assessing the potential for ventilation drying in screened walls is presented and field measurements of wind pressures and lab test data on airflow through vents is used to aid in this assessment. The influence of ventilation on the moisture and temperature conditions within walls is demonstrated with field data.

1.5 References

[1.1] Construction in Canada 1990, Statistics Canada 64-201, Ottawa, 1990.

[1.2] *Global Warming and the Built Environment*, ed. Robert Samuels and Deo Prasad, E and FN Spon, London, 1994.

[1.3] Appendix B of *CSA S478 Guideline on Durability in Buildings*, Decemeber, 1995.

[1.4] Ross, S. S., *Construction disasters: Design Failures, Causes and Prevention.* An Engineering News Record Book, McGraw-Hill Inc., 1984, p. 287.

[1.5] Maurenbrecher, A.H., and Brousseau, R.J., *Review of Corrosion Resistance of Metal Components in Masonry Cladding on Buildings.* Internal Report No. 640, IRC/National Research Council of Canada, Ottawa, February, 1993, p. 8.

[1.6] Drysdale R.G. amd Suter, G.T. *Exterior Wall Construction in High-Rise Buildings: Brick Veneer on Concrete Masonry or Steel Stud Systems.* Canada Mortgage and Housing Corporation, Ottawa, 1991.

[1.7] Grimm, C.T., "Durability of Brick Masonry: A Review of the Literature". *Masonry: Research, Application, and Problems*, ASTM STP 871, J.C. Grogan and J.F. Conway, Eds., ASTM, Philadelphia, 1985, pp. 202-234.

[1.8] *Moisture Problems.* Builders' Series, NHA 6010, Canada Mortgage and Housing Corporation, Ottawa, September, 1988.

[1.9] *Moisture in Canadian Wood-Frame House Construction: Problems, Research, andd Practise from 1975 to 1991.* Report for CMHC by Morrison-Hershfield, September, 1992.

2. ENCLOSURE WALLS AND MOISTURE

The function of buildings and their enclosures, the role moisture plays in the performance and premature deterioration of building enclosures, and the basic wetting, storage, and drying mechanisms in enclosures are briefly outlined in this chapter.

2.1 Buildings

Providing a rigorous definition of the function of a building is not a simple task. However, many writers have reached the conclusion that the primary function of buildings is to provide the desired environment, both inside and immediately outside of the building. This is not to say that buildings are not constructed with aesthetic or symbolic objectives since almost all, from a public museum to a private pumphouse, include some component of sensory appeal and respect cultural expectations while fulfilling their function. The challenge of designers has been to provide the necessary utility (i.e., provide the necessary environment) as well as aesthetics.

There are two fundamental resources in nature which mankind can use to control the built environment: physical barriers and energy. Historically, physical barriers of naturally-occurring topographical features (e.g., caves) and energy in the form of the sun were employed. As technology developed builders used both harvested and manufactured materials as physical barriers, and concentrated energy in the form of fire. In modern times, mankind has increasingly used more sophisticated materials, materials in combination, man-made materials, and vastly greater amounts of energy.

Today, it is generally accepted that humanity should attempt to minimise the use of nature's resources and energy. The ancillary impacts of our activities are being scrutinised like never before because modern civilisation has developed the ability to modify its environment on a grand scale - intentionally and accidentally [2.1]. Therefore, the modern building must minimise the use of both energy and resources (e.g. labour, material, time, capital) while fulfilling its functions.

The physical barrier which assists in the control of the building environment is called the building *enclosure* or *envelope*. The building enclosure developed slowly from a poorly understood and intrinsic part of a building to a distinct component studied by specialists. The functions of the building enclosure will be studied in the following sections.

2.2 The Building Enclosure

The building enclosure is the physical separator between the interior and exterior environments. At the most basic level the enclosure's function is to separate the interior and exterior environments, that is, it is the set of physical building elements that fulfil a major part of a building's function. The functions of the building enclosure can be usefully sub-divided into four more specific functions (Figure 2.1). It:

1. **controls**, limits, and moderates the flow of matter and energy between the interior and exterior environments,

2. **supports**, transfers and/or accommodates structural forces imposed by the interior and exterior environment or from within the enclosure itself, and

3. **finishes** the interface of the enclosure with the interior and exterior environments to meet comfort, aesthetic, and functional (e.g. wear, glare, etc.) requirements.

In many cases, an additional building requirement is imposed and the enclosure also

4. **distributes** services such as power, communication, water, gas, and conditioned air.

The control and support functions are necessary for every part of the enclosure. The finish function is a human requirement; acceptable colours, textures, and patterns are all necessary requirements for the comfort and satisfaction of the occupant but may be eliminated if the enclosure is hidden from view or aesthetics are deemed unimportant. Distribution of services by contrast, is a building function often imposed on the enclosure that may or may not be necessary for every enclosure at all points.

Any required enclosure control function requires the consideration of an enclosure loading. For example, if the function in question is the control of conductive heat transfer, the loading is the temperature difference across the wall.

Perhaps the most important load that the enclosure is required to control is moisture in all its forms; liquid, vapour, and solid. Moisture storage and transport is highly coupled to heat and air transport, especially in cold-climates where the enclosure often has large gradients of temperature and air pressure across it.

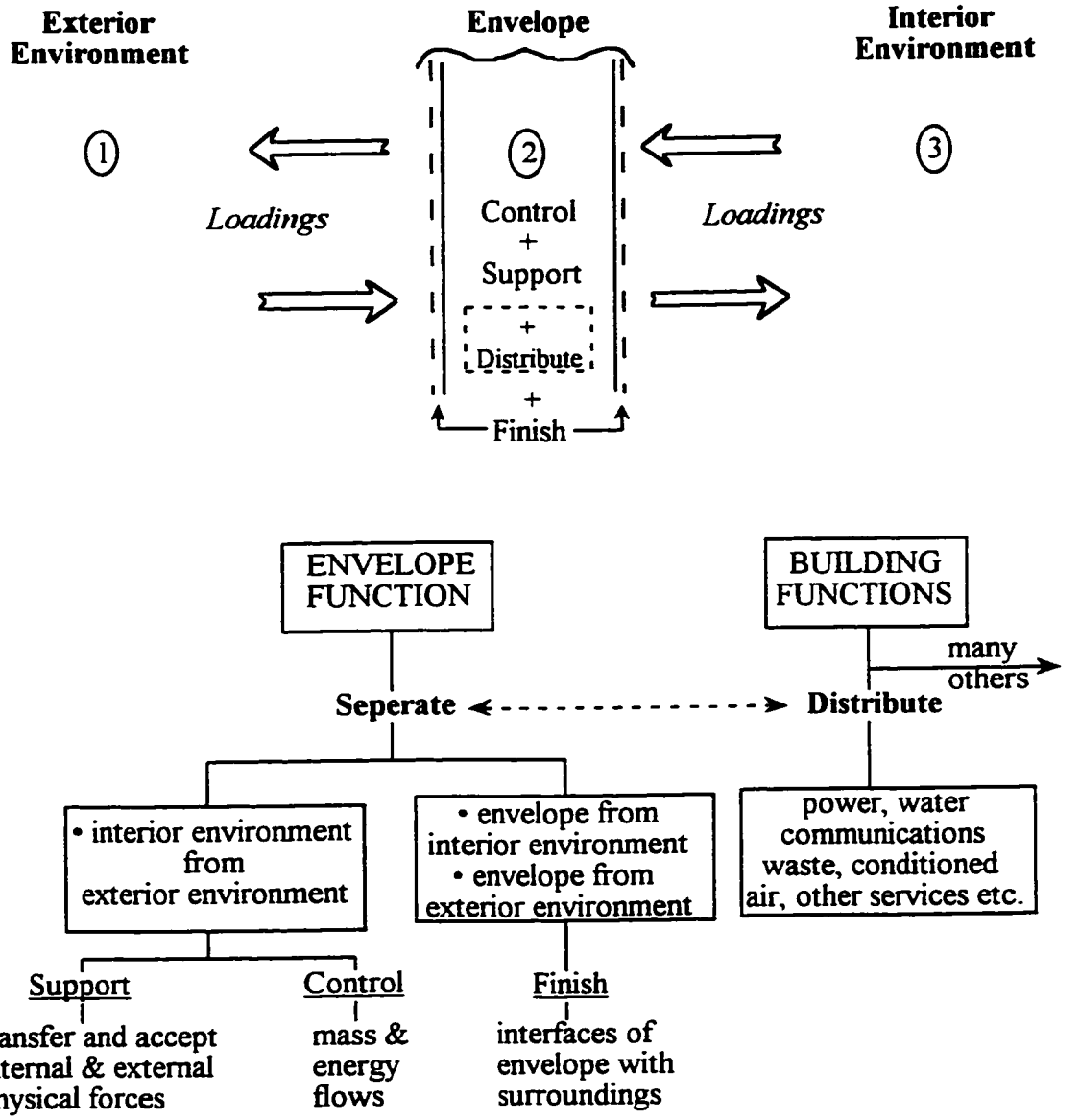

Figure 2.1 Functions of the building enclosure

2.3 Moisture Control and Building Enclosure Systems

2.3.1 Moisture problems

As stated in the introduction, moisture is involved in almost all building enclosure performance problems or deterioration processes, such as:

- leakage of water into the building;
- freeze-thaw deterioration of concrete, stone, and masonry;

- electrochemical corrosion of metal components such as structural framing, reinforcing bars, masonry anchors, ties, flashing, etc.;
- biological, especially fungal (mould, rot, decay) growth, which can have a major effect on occupant health, structural capacity, and appearance;
- the chemical deterioration and dissolution of materials such as gypsum sheathing, wood products, and damaging chemical processes such as carbonation and alkali-aggregate reaction;
- volume changes (expansion, shrinkage) that can cause structural failure, cracking, degradation of appearance, etc.;
- discoloration (staining, 'dusting', irregular wetting, etc.) of building finishes.

For a moisture-related problem to occur, it is necessary for at least four conditions to be satisfied:

1. a *moisture* source must be available,
2. there must be a *route* or means for this moisture to travel,
3. there must be some *driving force* to cause moisture movement, and
4. the material(s) involved must be *susceptible* to moisture damage.

To avoid a moisture problem one could in theory choose to eliminate any one of the four conditions listed above. In reality, it is practically impossible to remove all moisture sources, to build walls with no imperfections, or to remove all forces driving moisture movement. It is also uneconomical to use only materials which are not susceptible to moisture damage. Therefore, in practise, it is often advantageous to address two or more of these prerequisites so as to reduce the probability of having a problem.

Controlling moisture and limiting the risk of a failure by proper design, assembly, and material choices must be the approach taken in the design of building enclosures. This requires an understanding of moisture and moisture control in enclosure systems.

2.3.2 Susceptibility and vulnerability

Different materials and assemblies are susceptible to different kinds of moisture-related damage. Whether a moisture problem occurs depends on whether a susceptible material or assembly is placed in a vulnerable environment. This vulnerability, or more generally, the level of risk associated with a moisture-related problem, should be considered together with the consequences of the problem.

While the susceptibility of a material to a particular problem (e.g. freeze-thaw deterioration) may be measurable (e.g. standardised freeze thaw tests and target criteria for acceptable performance) designers and builders have the responsibility to ensure that a material or assembly is not used in a manner that renders it disproportionately vulnerable, that is, likely to incur a problem.

Moisture vulnerability, or degree of risk, affects the probability of a problem occurring and may be considered to be a function of three potentials:

1. wetting,
2. storage, and
3. drying.

Materials, assemblies, and environments may all be assessed by consideration of these potentials. The environments that the enclosure separates provide both the source of moisture and a sink for moisture that is removed. Therefore, the interior and exterior environment is just as important for assessing vulnerability as the potentials of an assembly. The relevant characteristics of an environment can be grouped together with the characteristics of an enclosure to define an overall (i.e., enclosure plus environment) wetting potential and an overall drying potential.

For example, using a material that is not supposedly susceptible to moisture damage (e.g., good quality, code-acceptable, face brick) in locations with high wetting potential (such as at sills or at corners of high buildings) often leads to a problem. In massive brick walls, the moisture storage capacity is so high that the moisture content of the brickwork never exceeds a performance threshold. In a drier climate, such as the Canadian prairies, the potential for drying is higher than the potential for wetting and again, the moisture content of the brickwork remains below its performance threshold. Just as for brick,

understanding the moisture in materials such as wood and the time of wetness of steel can be used as a measure of their vulnerability to premature deterioration.

Complicating the assessment described above is the fact that the performance thresholds, and even what physical measures one should use to define a threshold, are unknown or poorly defined for most materials and assemblies. The conditions necessary for mould growth and rot in wood are relatively well known combinations of temperature and moisture content. The performance thresholds (i.e. the precise combinations of environmental conditions and material properties) for the onset of freeze-thaw damage in masonry are not as well defined. These performance thresholds will be studied in more depth in Chapter 4.

A better, more quantitative understanding of the wetting, storage, and drying mechanisms of common cladding materials and enclosure assemblies is needed to allow for the quantification of vulnerability.

2.4 Moisture Balance in Enclosure Systems

If a balance between wetting and drying is maintained, moisture will not accumulate over time, and moisture-related problems are unlikely. The extent and duration of wetting, storage, and drying must, however, always be considered when assessing the risk of moisture damage.

Figure 2.2 shows the major wetting and drying processes and the moisture transport mechanisms involved in the movement of moisture into and out of the enclosure. This thesis will primarily consider those portions of the diagram outlined in dashes; that is rain wetting, rain penetration (especially the role of pressure moderation), drainage, and ventilation drying.

The other major wetting mechanism, air leakage and diffusion-induced condensation, has long received attention by researchers [e.g., 2.2] and both simple design tools [2.3] and more detailed and accurate methods of prediction [2.4] have been developed. Since rain wetting, pressure moderation, drainage, and ventilation drying primarily affect the cladding and the cavity, these two components of walls are the focus of this research.

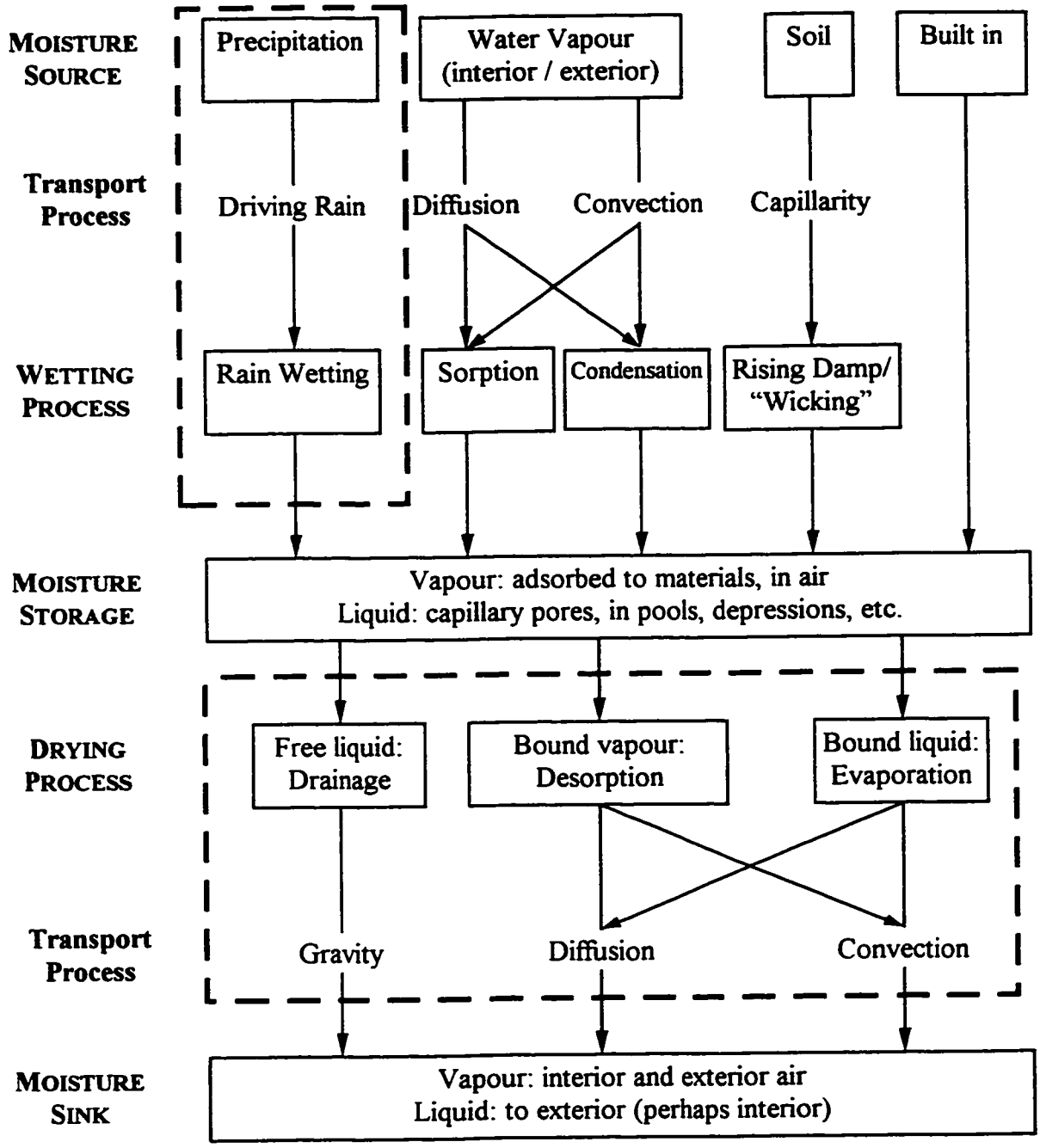

Figure 2.2: Wetting, drying, and moisture storage in the building enclosure

The ability of an assembly to dry and store moisture, as well as its resistance to wetting are of great importance in assessing its vulnerability to moisture-related damage and deterioration. To develop some understanding of how and how much moisture can be removed from a wall by drainage, evaporation, diffusion, and ventilation, it is necessary to

review the fundamental behaviour of moisture in enclosures and the wetting and drying processes in general.

2.4.1 Moisture sources

There are four basic sources of moisture in an enclosure:

1. rain water (or precipitation),
2. water vapour from both the interior and exterior air,
3. moisture built-in during construction or stored moisture from other sources, and
4. moisture from soil adjoining a building enclosure (especially important for enclosures near or below grade level).

Because the exterior and interior environments are the ultimate source of all moisture in an enclosure (other than built-in moisture), characterising the moisture in these environments is critical to moisture control.

2.4.2 Wetting

The moisture from the four sources is transported into the enclosure by several different mechanisms, often considered to be wetting mechanisms. Built-in moisture, of course, requires no transportation process since it is a result of wetting of the material before or during its incorporation into the enclosure.

Other than built-in moisture, which is the result of wetting before or during constrution, the wetting mechanisms can be grouped by the moisture source, e.g.,:

- rain transported by penetration of openings and cracks or absorbed by porous materials,
- water vapour, from diffusion and convection, directly adsorbed by hygroscopic materials or deposited as liquid or frost, and
- soil moisture transported by capillarity.

2.4.3 Storage

The ability of a wall assembly to store moisture may be an important measure of its durability because storage acts as a vital buffer, or capacitor, for times when the rate of moisture deposition (i.e., wetting) exceeds the rate of drying. Deterioration can occur if a materials safe storage capacity is exceeded for long enough. Therefore, the two most important characteristics of moisture storage are how *much* moisture can be stored and for what *duration* without crossing a performance threshold.

Moisture may be stored in enclosures:

- in hygroscopic materials, as water vapour molecules adsorbed to the large internal surface areas of porous materials (e.g., brick, wood, fibrous insulation, paper);
- in the pores of porous materials, and cracks or fissures in non-porous materials, absorbed and held by capillary forces;
- in the air as vapour,
- in pools, small depressions, and other undrained portions or enclosures (e.g., in depressions formed by mortar droppings behind a masonry veneer, in the bottom tracks of steel stud framing);
- as droplets (or frost, even ice), adhered to surfaces by surface tension.

A useful distinction can be made between bound moisture and free moisture. In essence, bound moisture is not free to move under the forces of gravity or normal air pressure — this is normally the water that can actually be seen, and the vapour that can be measured in the air. Bound water is stored water, held in enclosures and materials, and cannot be removed by normal gravity and wind pressure forces.

Free liquid water may exist in an enclosure for short periods of time. For example, it may require between a few seconds and a few minutes for liquid moisture to drain out of an enclosure. For longer time scales, bound water is stored water, and can only be removed by drying mechanisms other than drainage.

2.4.4 Drying

An enclosure's drying potential is an important factor in assessing its vulnerability to moisture problems. Moisture stored within a enclosure can only be removed to the interior or exterior environments. Moisture can, of course, be redistributed within an assembly, but the drying is localised and balanced by wetting in the adjoining areas.

Moisture is usually removed from an enclosure by:

- liquid water drainage, driven by gravity,
- vapour diffusion,
- vapour convection (e.g., air leakage or ventilation).

Before drying can occur, stored moisture must be available either as free water or free vapour, i.e., bound liquid (trapped in undrained enclosures, absorbed by capillary forces) and bound vapour (adsorbed to internal surfaces) must first evaporate or desorb. This requires:

- evaporation, the process of liquid water changing phase to free vapour,
- desorption, the process whereby bound vapour changes to free vapour.

Several mechanisms (such as capillary flow, surface diffusion) aid drying by transporting bound moisture, but these mechanisms do not actually play a role in enclosure drying†. Practical drying modes are often combined mechanisms, e.g., :

- diffusive drying: evaporation and desorption followed by vapour transport by diffusion; and
- convective drying: evaporation and desorption followed by convective transport.

Drainage is capable of removing the greatest volume of water in the shortest period of time. It can therefore be a very important mechanism for moisture control. Provided a

† Bound water transport may theoretically dry an enclosure if the enclosure is in intimate contact with dry soil, or similar. This has limited practical significance, as most building enclosures interface with air, across which bound moisture cannot be transported, or soil, which is almost always wet.

clear drainage path exists (e.g., air spaces, slopes, drainage openings), a proportion of rain water penetration or liquid condensate can flow out of an enclosure assembly.

However, a small but significant amount of water will remain attached to surfaces by surface tension and stored in materials by adsorption and capillary forces even in enclosures with excellent drainage. Materials must be almost saturated by condensation before sufficient volumes of water will bead on the surface for drainage to occur. Therefore it must be assumed that water that cannot be removed by drainage will be stored within a wall.

Under the right conditions, liquid water not drained from an enclosure can be transported out of the enclosure either by diffusion, convection, or advection (i.e., combined diffusion and convection).

Diffusion, especially when driven by large vapour gradients, can remove a significant amount of moisture and be an effective drying mechanism. Diffusive drying is often the most important drying mechanism for enclosures made of absorbent or hygroscopic materials. Since convective flows are normally strictly controlled by designers so as to prevent condensation wetting and convective heat losses ("wind washing"), diffusion is the only transport mechanism still available for the removal of stored moisture.

Convective drying (or air leakage) through the enclosure can, under the proper conditions, move a large quantity of moisture. Air leakage usually leads to condensation wetting under winter conditions. However, periodic reversals of air flow from exfiltration to infiltration (when the wind changes direction for example) can allow drying even under winter conditions. Similarly, winter-time stack-effect-driven infiltration and summer exfiltration can cause drying.

Ventilation drying is a special case of convective drying. It is simply the process of desorption and evaporation followed by convective transport to the exterior environment with air from the exterior. In practise, air flow through a space behind the exterior cladding or roof membrane uses the drier outdoor air to transport water vapour out of the enclosure.

Capillary transport acts to redistribute moisture within a system. For example, water on the back of a brick veneer or wood siding will be drawn to the exterior face where it can evaporate and be removed by convection and distribution.

2.4.5 Moisture sinks

The moisture removed by drying must be transported to the exterior or interior environments. Drainage is the only practical mechanism for the removal of liquid water. Drainage is normally directed to the exterior environment because controlling the entry of water into the building is often one of the most important control functions of the enclosure.

Moisture in vapour form can be removed to the interior or exterior air, where it can then be diluted into these environments. However, diffusive drying can only remove moisture to the exterior if very low permeance polyethylene vapour barriers are used near one face of an enclosure†. Such vapour barriers are commonly used to eliminate diffusion wetting in modern walls and roofs.

Because the exterior and interior environments are the ultimate sink for moisture removed from an enclosure, characterising the moisture in these environments is critical to moisture control.

2.5 Closure

A brief overview of the functions of the building enclosure has been presented in this chapter. A general but complete outline of moisture control, intended as a guiding framework, has also been developed here.

Although the remainder of this thesis considers the control of all sources of moisture, it concentrates on the quantification and prediction of driving rain as a moisture source for above-grade enclosure walls and how this moisture is controlled by an enclosure. Wetting, drying, and storage processes will be reviewed in depth in Chapter 4. Rain, and the interaction of the rain with the wind and the building are studied in Chapters 5 through 8. Ventilation drying has not received wide-spread attention from building science researchers and will be studied in Chapter 9.

† In predominately heating climates the vapour barrier is placed on the warm inside face. This is common practice. In predominately cooling climates theory would require that the barrier be placed near the exterior face. This is less common in practice.

2.6 References

[2.1] Meadows, Donella and Dennis, Randers, Jorgen, *Beyond the Limits*, Chelsea Green, Post Mill, Vermont, 1992.

[2.2] Garden, G.K. *Control of Air Leakage is Important*. Canadian Building Digest 72, National Research Council, Ottawa, 1965. See also CBD's 1, 23 42,104, 107.

[2.3] Handegord, G, Reginato, L. *EMPTIED - Estimating Moisture Performance Through Infiltration, Exfiltration and Diffusion*. A computer program available from Canada Mortgage and Housing Corporation, Ottawa, 1992.

[2.4] Ojanen, T., Kumaran, M.K.,"Air Exfiltration and Moisture Accumulation in Residential Wall Cavities", *Proceedings of ASHRAE/DOE/BETEC Thermal Performance of Exterior Enclosure of Buildings V*, Dec 7-10, Clearwater, Fla., 1992, pp. 491-500.

3. RESEARCH PROGRAM

Much of the research reported in this thesis was part of a larger Ontario government and industry program supported by the University Research Incentive Fund (URIF). This research program involved the construction, instrumentation, and monitoring of 26 full-scale wall panels, the development of a driving rain gauge and the collection and analysis of driving rain data, the measurement of pressure moderation and ventilation, and laboratory tests of some materials used in masonry walls. Canada Mortgage and Housing Corporation (CMHC) also sponsored a smaller study of the performance of wall vents, ventilation pressures, and ventilation drying.

Field and lab test facilities, instrumentation, and details of test wall assembly's construction and materials are summarised in the Appendix A: Construction and Instrumentation Details.

Some of the objectives of this thesis outlined in Section 1.3 were to be met by a combination of field monitoring of different types of screened wall assemblies, laboratory testing of materials and sub-systems, and theoretical analysis. These three components are described in turn below.

3.1 Field Monitoring

Over the past five years the Building Engineering Group (BEG), with funding from a number of projects, has built and equipped an on-campus facility (called the Beghut) for the field testing of building enclosure elements. The exterior environment (wind direction, wind speed, relative humidity, temperature, precipitation, incident solar radiation) can be continuously monitored and the interior environment controlled (to 50% RH, and 21 °C) . This facility is described in detail in Appendix A.

For the URIF project, a total of 26 wall panels (each 2400 x 1200 mm in size) representing 10 types of wall systems were built, instrumented, and installed in the Beghut. The design and instrumentation of the wall panels are described in detail in Chapter 3 of Appendix A. The temperature and moisture conditions within these walls were continuously monitored for 20 months, from September 1995 to April 1997. This period included two winters, and a full calendar year. Air pressures were monitored at high rates on a selective basis (i.e., when wind conditions were appropriate).

3.1.1 Test panels

Each of the ten types of test wall are listed below with an assigned code letter. The walls are also briefly described below and compared in Table 3.1:

1. The B wall is intended to act as a datum, representing typical low-rise, wood frame, brick veneer residential construction practice. This system represents the wall assembly used on large number of low-rise residential buildings.

2. The F wall is intended to act as a datum representing typical commercial steel stud brick veneer construction practice. Following best practice, 50 mm of insulating sheathing was placed outside of the framing and the studspace was only partly-filled (65 mm) with batt insulation.

3. The R wall is a typical low-rise brick veneer wood frame residential wall assembly, except that 50 mm of insulating rock wool cavity filler has been used

4. The W wall is a typical low-rise brick veneer wood frame residential wall assembly, with the exception of the 50 mm of insulating fibreglass cavity filler.

5. The O wall is a typical commercial brick veneer, light-gauge steel frame wall assembly, with the exception of the 50 mm of insulating fibreglass cavity filler and a reduced amount of insulation in the stud space.

6. The prototype D wall is an extension of the concept of a drained, filled-cavity wall, but uses the insulation, a unique insulating and draining material (Durisol), as the structural backing for a hard coat plaster. The plaster coat was vented at regular intervals to encourage air flow through the Durisol.

7. The V wall is a typical low-rise vinyl clad wood frame residential wall assembly with the exception of the 50 mm of rock wool insulating sheathing (normal practise employs OSB or rigid foam insulating sheathing).

8. The E wall is a Sto System Plus1 RS, a pressure moderated EIFS, presently marketed in Canada by Sto Finish Systems.

9. The S wall is a load bearing structural brick wall intended for the low-rise residential market with a unique draining sheathing and insulated inner wythe.

10. The C wall is a structural concrete wall formed from proprietary insulating Durisol Wall Forms clad with brick veneer, intended for use in both the commercial and residential sectors.

Table 3.1: Enclosure Wall Systems in Field Monitoring Program

Code	No.	Cladding	Cavity	Sheathing	Frame	WWB	PAB	PVB
R	4	BV	Full	Rockwool	Wood	Typar	ADA	Poly
E	4	EIFS	Full	Rockwool/ Ext Gypsum	Steel	Stoflex	Stoflex	Stoflex
B	4	BV	Partial	Celfort EXPS	Wood	BP	ADA	Poly
D	4	Durisol	Full	Durisol	Wood	Typar	ADA	Poly
O	3	BV	Full	Fibreglass/ Ext. Gypsum	Steel	Gyp.	Gyp.	Poly
V	2	Vinyl	Full	Rockwool	Wood	Typar	ADA	Poly
S	2	BV	Partial	EXPS	special	None	EXPS	Foil
C	1	BV	Partial	EXPS	Conc.	BP	ADA	Paint
W	1	BV	Full	Fibreglass/ OSB	Wood	BP	ADA	Poly
F	1	BV	Partial	Fibreglass/ Ext Gypsum	Steel	Gyp.	Gyp.	Poly
10	26	16 BV 4 EIFS 4 Durisol 2 Vinyl	8 partial 18 filled		15 wood 8 steel 1 conc. 1special	10Typar 4 Gyp. 4 Stoflex 6 BP	16 ADA 4 Stoflex 4 Gyp 2 EXPS	19 Poly 4 Stoflex 2 foil 1 paint

Notes: All walls finished on the inside with 1/2" drywall, painted with one coat of latex paint on primer.
BV = brickwork veneer EXPS = extruded polystyrene OSB = oriented strand board
WWB = wind/weather barrier PAB = primary air barrier PVB = primary vapour barrier
BP = building paper Gyp = exterior grade gypsum Poly = 0.015 mm polyethylene
Dursiol™ = proprietary insulating, draining, precast cement-bonded wood material
ADA = airtight drywall approach EIFS = Exterior Insulated Finish System
StoFlexyl™ = proprietary polymer-modified cementitious air/vapour barrier

In scope and duration the field monitoring project is unique — not only in Ontario but also in North America. The analysis of the hygrothermal data involved the processing, statistical analysis, and plotting of 30 months of data from over 600 sensors; a total of more than 150 million individual data points. The monitoring of ventilation pressures resulted in the collection of almost 3500 records with 14 million readings, and the high-speed pressure moderation studies required the frequency domain analysis of more than 2 million lines of pressure data.

It is believed that this is the most detailed and fundamental study of driving rain, pressure moderation and ventilation drying ever undertaken in North America.

3.1.2 Driving rain measurement

A driving rain gauge was designed and calibrated. Detailed drawings can be found in Appendix A. A total of 14 driving rain gauges were mounted on the face of the Beghut. A west-facing gauge was installed 3 m above grade on a pole 10m from the west face of the Beghut. Driving rain data was collected from the end of October 1995 to October 1997.

3.1.3 Pressure moderation & ventilation pressure measurements

All of the 26 panels were built with pressure taps. In most cases the pressure at each vent opening and in the centre of the cavity and the centre of the exterior of the cladding was measured. Six of the walls were continuously monitored for a total of about 6 months.

At the same time that pressures were being monitored for pressure moderation performance, pressures driving ventilation flow were also being measured. A second series of measurements were conducted to assess the nature and magnitude of spatial pressure variations on the face of the Beghut.

3.1.4 Cladding and cavity hygrothermal monitoring

The temperature, humidity, and moisture content in the test walls were monitored for two years. The data allowed the moisture content of the wood framing and the air to be analysed. With the aid of the concurrently measured weather conditions, insight into the behaviour of moisture in the enclosure could be developed.

The vapour content of the cavities in the different wall systems provided valuable data describing the wetting and drying mechanisms of the walls.

3.2 Laboratory Testing

3.2.1 Brick veneer water permeance testing

Two brick veneer wall panels were built in the laboratory. Because they were built in the lab, these veneers could be easily tested for rain penetration while providing full access to

the back of the veneer. This allowed the mechanisms and progress of water penetration to be closely observed.

3.2.2 Brick wetting and drying experiments

Dozens of wetting and drying experiments were carried out with the range of different bricks used on the test walls. The intent of these experiments was the confirmation that simple wetting and drying theory could be applied to the claddings used in the full-scale test walls.

3.2.3 Ventilation flow

The flow behaviour of several different orifices, a model of a masonry head joint, and several commercial masonry vent inserts were studied under a range of static and dynamic pressure differences. Flow visualisation was used to aid the understanding of the mechanisms of flow.

3.3 Theoretical Investigations

The theory of wetting and drying of materials, rain fall, wind and its interaction with buildings, and dynamic and low-pressure air flow through wall assemblies were all studied in depth.

Computer simulations of pressure moderation performance and dynamic one-dimensional hygrothermal behaviour were also conducted to explore the influence of variables found to be significant.

3.4 Closure

The research program described above has generated a large amount of data. In the remainder of this thesis, selected experimental results will be used to demonstrate and confirm the theory developed.

4. WETTING, STORAGE AND DRYING PROCESSES

Moisture is one of the most important factors affecting building envelope performance, including durability, since it is involved in almost every material deterioration mechanism. As argued in Chapter 2, the ability of a wall assembly to dry and store moisture, as well as its resistance to wetting are of great importance in assessing its vulnerability to moisture-related damage and deterioration. Understanding and predicting moisture movement within and through the envelope is therefore crucial to the control and understanding of moisture-related problems.

This chapter examines the unique nature of moisture and undertakes a review of the physics of moisture storage, wetting, and drying as related to building envelope performance. The result of microscopic physics on macroscopic building element behaviour is discussed. Finally, a short review of some of the available computerised heat and moisture transport models is presented and discussed.

4.1 Moisture

4.1.1 The water molecule

Water, in all its states, is a molecule with one oxygen and two hydrogen atoms. Hydrogen has a positive charge, and oxygen two negative charges. The water molecule is formed from a covalent bond (one in which each atom shares electrons with the other atoms in the resultant molecule). The two hydrogen molecules are separated by an angle of 104.5°. The covalent OH bond has an average separation distance of about 0.096 nanometers and the equivalent ionic diameter of the molecule is about 0.282 nanometers (Figure 4.1) [4.1,4.2].

It can be seen from the Figure 4.1 that the centroid of the two positive charges is not coincident with the centroid of the two negative charges. This spatially-unbalanced distribution of charges results in a permanent dipole or a polar molecule , i.e., one end is permanently positive and the other end permanently negative.

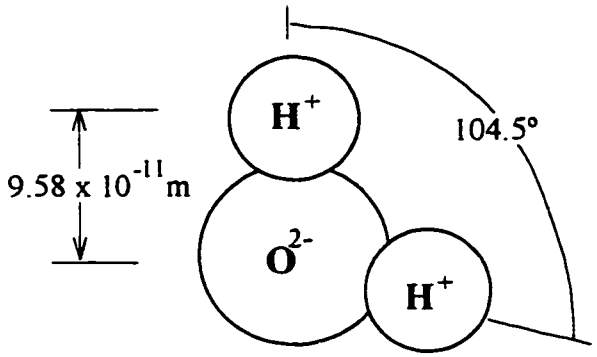

Figure 4.1: The H_20 molecule

The polar nature of the water molecule is pivotal to the way it interacts with other molecules [4.3, 4.4]. The principal force of attraction in water is the orientation effect, i.e., the positive hydrogen of one water molecule attracts the negative oxygen of another and causes the two molecules to link like two magnets.

Another contributor to intermolecular attraction for non-polar molecules is a phenomenon called the dispersion effect. This van der Waals-type attraction is caused when the fluctuation in the electronic cloud of one molecule causes a similar displacement of electrons in a neighbouring molecule. Since the charges will be opposite, an electrical attraction is generated.

The induction or polarizability effect, another van der Waals force, is similar to the dispersion effect but only operates between polar and non-polar molecules. If a (polar) water molecule approaches a molecule with an electron cloud it can influence, the polar nature of the water molecule ensures that an intermolecular electrostatic bond forms in a similar manner to the dispersion effect.

The orientation and dispersion effect alone cannot explain the properties and behaviour of water [4.3]. Hydrogen bonding occurs when the hydrogen atom of one molecule actually forms a weak chemical bond with the oxygen atom of another water molecule (or another solid molecule). Although largely electrostatic in nature, this bonding is different from the orientation and dispersion effect because a partial sharing of an electron (from the hydrogen) s involved. The hydrogen bond is generally weaker than ionic, covalent and metallic interatomic bonds because these bonds involve the complete sharing of electrons, but it is stronger than van der Waals-type intermolecular bonds.

Hydrogen bonding between water molecules explains the viscosity, boiling point, and the strong surface tension of water. Because of hydrogen bonding, water molecules cannot leave the surface of a body of water as readily as they could without this intermolecular attraction. The energy required to break this bond is quite high and partially explains the large amount of energy necessary for the evaporation of water.

Both the dispersion effect and hydrogen bonding cause water to cling to materials, and this in turn results in adsorption and absorption (a result of the important force called capillarity). Capillary rise in small tubes can be quite substantial, easily sufficient to draw water to the top of a 100 m tall tree, or several kilometres up a concrete column.

Liquid water tends to exist in clumps; at room temperature these clumps are about 80 molecules in size (i.e., water behaves more like $H_{160}0_{80}$ [4.5]). As the temperature increases, the clumps break up and become smaller (in the vapour state, the molecules have so much energy that they act individually). The difference in size between the liquid water molecule clumps and the individual vapour molecule explains how materials such as Gore-Tex™ and Tyvek™ can simultaneously be watertight and vapour permeable (i.e., "breathable").

Water has one rare characteristic among matter: as it is cooled close to freezing it expands, contrary to what would be expected. This occurs because ice is a six-sided crystal formed from water molecules (Figure 4.2). Although the energy in the resulting crystal is lowest (and hence stable) the crystal occupies more volume than six individual molecules.

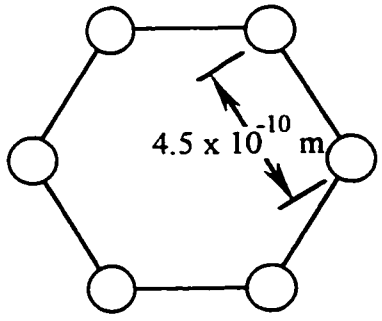

Figure 4.2: Ice crystal

Water crystals begin forming as the temperature approaches zero, but above zero degrees Celsius, the crystals constantly break apart again or are dispersed. As water is cooled it contracts and its density increases; water has its highest density at 4 °C i.e., the molecules

are closest together at this temperature. As the temperature drops further, molecules begin to arrange themselves into ice crystals which occupy more volume; therefore the density decreases. Between 4 °C and 0 °C the volume of water increases by 9% as an increasing proportion of molecules form into crystals. At about 0 °C all of the water molecules are organised into crystals, and as the water freezes, the crystals interconnect and a solid matrix is formed. As the temperature drops further contraction once again takes place as for any other solid, although its density does not drop below liquid water under normal conditions.

The expansion experienced as water is cooled to 0 °C causes frost-jacking forces and may result in freeze-thaw damage to some building materials. Note, however, that the mechanism of freeze-thaw damage in porous brittle materials (i.e., brick, concrete) is far more complicated than simple water expansion.

4.1.2 Moisture states and state changes

In the realm of most building science problems, moisture can exist in all three phases or states (Figure 4.3): solid (ice), liquid (water) and gas (water vapour). A fourth state, the adsorbed state, also exists on a molecular level, with characteristics somewhere between liquid water and vapour.

A gas comprises molecules with a high level of kinetic energy; the molecules move about randomly at a high speed. The root mean square velocity of the molecules is a direct measure of the gas temperature and the partial pressure it exerts. As temperature increases, the molecules collide more often and more energetically with one another. Since a gas molecule can move freely, gaseous matter offers little resistance to change in shape (friction) or to a change in volume (compression), as compared to a liquid or solid.

If a sufficient amount of energy is removed from a gas, the strength of attraction between molecules will eventually become relatively stronger than the kinetic energy of the moving molecules, and the gas will become a liquid. Liquid matter does not strongly resist forces that act to change its shape because the molecules are relatively free to move with respect to each other. However, liquids have sufficient amounts of kinetic energy to resist forces acting to change their volume (e.g. drive the molecules closer). Hence, a liquid retains more shape and offers greater resistance to disturbance than a gas -- this is clearly the case with water vapour and water.

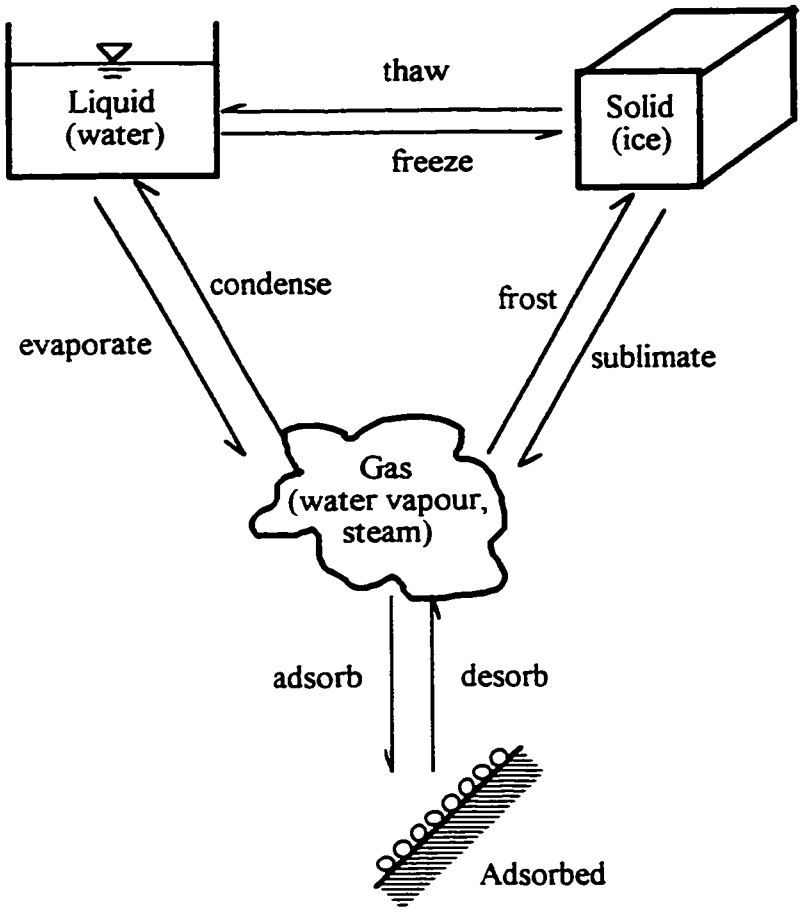

Figure 4.3: Moisture states and state changes
Adapted from [4.6]

By removing even more energy from a material, molecular movement is slowed, and intra-molecular forces begin to dominate -- the molecules cease to move about freely. Hence, solids are characterised by a resistance to change of both shape and volume. Although they remain in a fixed position, they do continue to vibrate. This vibration only ceases when the temperature of the material has reached absolute zero (about -272.15 °C)

The relative forces of attraction between molecules and the kinetic energy of molecules with a certain velocity will clearly vary with different types of molecules and with different mixes of molecules. For example, tungsten becomes a liquid at 3370 °C whereas helium liquefies at -269 °C.

The kinetic theory of matter described above also leads to the expectation that heating a solid, liquid, or gas will cause it to expand. The vibrational or kinetic energy causes

molecules to move farther apart from each other and the same number of molecules will therefore occupy more space.

4.1.2.1 The Adsorbed State

Water exists in another state at normal temperatures, the adsorbed state. Water vapour molecules close to solid molecules can be attracted either by the complementary polar nature of the solid material molecules or can induce polarity in the solid molecules by the dispersion and induction effect. Water vapour molecules may strike a solid surface and rebound, or be captured for a time by attractive forces. During the time that a molecule is held, it is said to be adsorbed. The process is called adsorption. Because of the vibrational and translational energy in single water vapour molecules, any single molecule will only remain adsorbed for a short time (on average this duration is measured in microseconds). The higher the temperature, the higher the energy, and the shorter the residence time of a vapour molecule on a surface. The dynamic equilibrium established at a given temperature results in a stable amount of adsorbed moisture on a surface at that temperature.

Adsorbents are materials that have the ability to adsorb gases. Strictly speaking, desiccants are a subset of adsorbents with a particular affinity for water vapour. Virtually all materials are desiccants, i.e. they attract and hold water vapour. Wood, natural fibres, brick, concrete etc. have a moderate affinity to hold water. However, the term desiccant is normally reserved for materials with a very high affinity toward water (e.g. those used to remove moisture from the air in HVAC systems and equipment); the term hygroscopic is often used to describe those materials which exhibit a moderate affinity. Many porous building materials are hygroscopic, and can store a significant amount of moisture as adsorbed water vapour on their very large internal surface areas.

Because the mobility of the vapour molecule is reduced by the attraction to the surface on which it is adsorbed, the behaviour of adsorbed molecules is different than either the pure liquid or vapour states. Adsorbed water does not freeze until very low temperatures because the reorganisation of the molecules into an ice crystal form is not the lowest energy state. Powers, in his study of cement paste and concrete, calculated that adsorbed water would not form ice crystals (i.e., freeze) above -78 °C [4.7]. However, after several layers of adsorbed water molecules accumulate (usually assumed to be 2 or 3), further layers begin to behave more like liquid water.

Water molecules that are hydrogen bonded to other solid molecules are said to be chemically bound. These bound molecules are not part of the adsorbed state, and typically require much more energy (i.e., heat) to remove.

4.1.2.2 Moisture State Changes

Moisture frequently changes from one state to another, even within a material layer and these state changes can greatly effect building enclosure behaviour. Each state change process is given a name (see Figure 4.3).

The energy used to increase the velocity or vibrations of molecules is called sensible energy or sensible heat (because one can sense an increase in temperature in the material). The sensible energy required to raise a unit mass of material one unit of temperature is called the specific heat capacity of the material. The specific heat capacity is a strong function of temperature and pressure for many gases, but can be assumed to be constant over limited temperature ranges.

Vaporisation is the general term which describes the process by which liquid water changes phase to vapour. Vaporisation can occur at the air-water surface, where it is called evaporation, or within the mass of the liquid water and moves to the surface in bubbles, where it is called boiling. Boiling occurs when the saturation vapour pressure is greater than atmospheric pressure (which occurs at 100 °C for standard atmospheric pressure) whereas evaporation can occur at any temperature. Boiling will occur at a lower temperature on a mountain top because the atmospheric pressure is lower. When vaporisation occurs at temperatures below zero, (or more precisely, from ice), it is called sublimation.

Condensation is the process by which water vapour changes phase to liquid. If water vapour changes directly to the solid state without passing through the liquid phase, the process is called frosting.

When materials change state, additional energy is required to reorganise the molecules into the new state; there is a significant difference in total energy content between a gas and a liquid for example. A state change therefore releases or absorbs a material-specific amount of energy called latent energy or latent heat. Depending on the state change, the latent energy required to change a unit mass of material from one state to another is called the heat of fusion (from solid to liquid) or heat of vaporisation (from liquid to gas)

Water's heat of vaporisation, the energy to evaporate one gram of water, is 2250 J @100 °C (and 2500 J @ 0 °C). Condensation of one gram of water vapour releases the same amount of energy. If water's heat of fusion (the energy required to change ice to water (333 J/g)) and the heat of vaporisation (2250 J/g at 0 °C) are provided, the ice will change state directly to vapour at 0 °C. Figure 4.4 plots a simplified and linearised energy-temperature relationship for water (the numerical values are approximate).

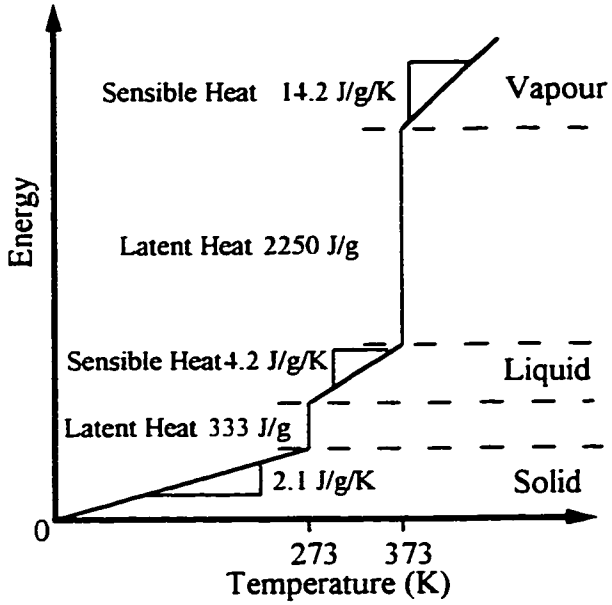

Figure 4.4: Simple linearised energy-temperature relation for water

The heat of adsorption is less than the heat of fusion or vaporisation and varies with the material on which adsorption is occurring and somewhat on temperature. The need for this heat causes hygroscopic materials, such as woollen trousers, to feel cooler in winter when they move quickly from the cold, high RH outdoors to the warm, low RH indoors (e.g., from a high RH to a low RH environment).

4.1.3 Moisture in porous materials

4.1.3.1 The Nature of Porous Materials

Materials with a porous internal structure can store significant amounts of moisture, in vapour, adsorbed, liquid or ice form within this porous structure. Many building materials, e.g., wood, brick, stone and concrete, are porous and have very large internal surface areas. For example, brick typically has an internal surface area of from 0.1 to 5 m^2/g [4.8], and cement paste has internal surfaces totalling about 10 to 100 m^2/g [4.9].

The larger the percentage of volume occupied by smaller pores, the larger the internal surface area. Because of the large internal volume and surface area, some porous building materials can store their own weight in water in their internal pore volume with one-quarter of this amount as adsorbed water vapour on the pore walls (Table 4.1).

Material	Density (Dry) kg/m^3	Open Porosity (%)	MC @ ≅95%RH (M%)	w_{cap} (M%)
Concrete	2200	15-18	4-5	6-8
Brick	1600-2100	11-40	3-8	6-20
Cement Mortar	1800-1900	20-30	5-7	14-20
Softwood	400-600	50-80	20-30	100-200
Fibreboard	240-380	60-80	20-25	100-200
Wood chipboard	700	50-70	15-20	100-150
Expanded polystyrene	32	95	5	> 300
Gypsum (exterior)	1000	70	10	50-100

Note: these values are approximate and from a variety of sources [e.g., 4.10, 4.11, 4.13, 4.28, 4.34, 4.48]

Table 4.1: Moisture contents of some common building materials

The total porosity, ψ_T, of a completely dry porous material is normally defined as the ratio of the total air volume (V_a) to the total volume of the material sample (V_T) or that fraction of the porous volume that is not solid. In terms of fractions, X_i is the volume fraction of the ith component of the total non-solid volume. The total non-solid volume in a porous material can usefully be divided into the volume fraction of pores that are:

- open, interconnected, and with access to the exterior, X_O,
- dead-end pores connected to exterior X_D, (a subset of X_O), and
- closed or sealed pores with no access to the exterior, X_C.

In the assessment of moisture storage, it is the open porosity, $\psi_o = X_O \cdot \psi_T$, that is of interest. Table 4.1 summarises the range of open porosity that can be expected for a number of building materials.

With respect to liquid moisture transport, an effective porosity $\psi_{eff} = (X_O - X_D) \cdot \psi_T$, is used to reflect the fact that dead end pores do not participate in the flow of liquid water through the material.

There are no experimental methods that can accurately and definitively define each of the porosity fractions. However, the open porosity can be approximately measured by various means, including mercury intrusion porisimetery, helium and nitrogen gas adsorption, and vacuum saturation [4.12]. Most methods cannot identify closed pores and sometimes fail to measure very small pores (e.g. less than a few nanometers). Another problem arises when measuring materials whose pore structures change with water content because of shrinkage, swelling, or chemical bonding (e.g., wood, gypsum and some plastics).

The pore size distribution for a representative clay brick is shown in Figure 4.5 as calculated from mercury intrusion testing [4.13, 4.14]. The cumulative percentage of total volume intruded for each of the pore radius ranges is plotted along with the percentage of water absorbed during a vacuum saturation test (25.5% total volume or 88.3% of accessible pore space), and the 24 hour cold immersion test (18.9% of total volume or 65.4% of accessible pore space). The total open porosity (ψ_o) was 28.94%.

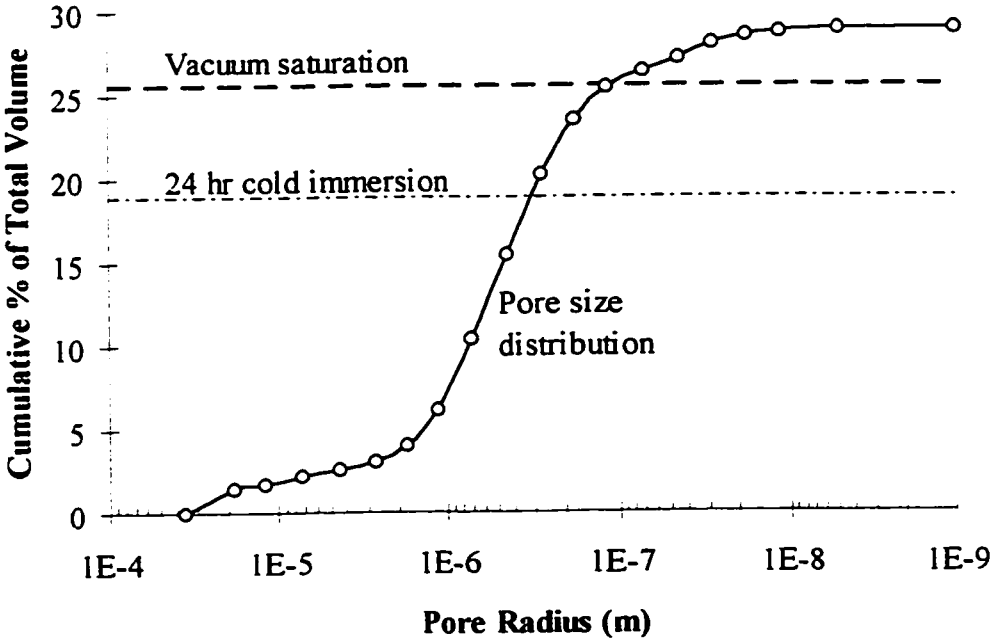

Figure 4.5: Pore size distribution of a representative clay brick [4.15]
Note: A water molecule is approximately 3 x 10^{-10} m in diameter

4.1.3.2 Capillary Moisture Physics

In a porous body which does not have all of its pores filled with water or air (i.e., it is neither fully saturated nor completely dry), it is common to consider three phases: the solid phase, and the two fluid phases: gas (air, including water vapour), and liquid.

The pressure difference between liquid phases that is maintained within a pore space at equilibrium is, by definition, the capillary pressure. The Laplace-Young equation is:

$$P_{cap} = P_{non} - P_{wet} = \sigma \cdot J \qquad \text{(Eq. 4.1)}$$

where P_{cap} is the capillary pressure,

P_{non} is the pressure of the non-wetting fluid,

P_{wet} is the pressure of the wetting fluid,

σ is the interfacial or surface tension between the fluids,

and J is equal to twice the average curvature:

$$J = \frac{1}{r'} + \frac{1}{r''}$$

where r' and r'' are the two radii of the meniscus with the material of the pore walls (Figure 4.6)

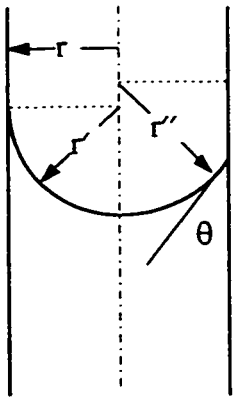

Figure 4.6: Radii and contact angle definitions for the calculation of capillary pressures

It is commonly assumed that the contact angle with all pore walls is the same (e.g. $r' = r''$). This allows for a simplification:

$$J = \frac{2}{r} \cdot \cos\theta \qquad \text{(Eq. 4.2)}$$

where θ is the contact angle of water with the material, and

r is the capillary radius.

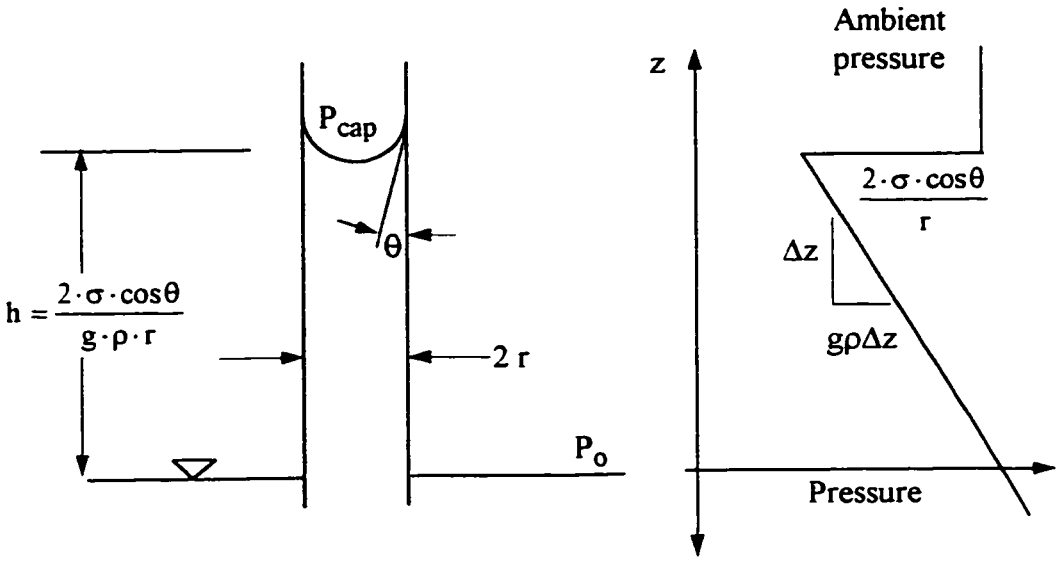

Figure 4.7: Capillary suction of water in a cylindrical tube

For water and air as the wetting and non-wetting fluids respectively, Equation 4.1 can therefore be written as:

$$P_{cap} = P_a - P_w = \sigma \cdot J \qquad \text{(Eq. 4.3)}$$

The Washburn equation can be derived by relating all pressures to atmospheric ($P_a = 0$):

$$P_{cap} = \frac{-2 \cdot \sigma \cdot \cos\theta}{r} \qquad \text{(Eq. 4.4)}$$

where σ is the surface tension (σ =0.072 N/m for distilled water at 20°C)

r is the radius in meters, and

P_{cap} is the capillary pressure.

The negative sign indicates that the capillary force is a suction for contact angles of less than 90° (e.g. for wettable materials). While the contact angle of water with most building materials is assumed to be zero, it may be higher and, as discussed later, a function of the wetting history.

For cracks or non-cylindrical pores, an equivalent hydraulic radius should be used:

$$r_{eff} = \frac{2 \cdot A_{pore}}{\text{perimeter}} \qquad \text{(Eq. 4.5)}$$

= w for a long crack of width w.

Equation 4.4 indicates that water will be drawn into a cylindrical pore of radius r, with a capillary suction pressure of P_{cap} (see Figure 4.7). Simple substitution shows that a 0.3 mm wide crack (an allowable crack width in reinforced concrete design codes) will result in a suction pressure of as much as 350 Pa. Smaller cracks, say 0.05 mm will create larger suctions (2000 Pa)

Using 140° as the contact angle, appropriate for a hydrophobically-treated material (see Section 4.1.4), one can calculate that a pressure of 375 Pa would be required to force water into a crack 0.3 mm wide. This magnitude of pressure can be generated by a strong wind gust or 35 mm of standing water. Pressures of over 1000 Pa would be required to force water into a 0.1 mm wide hydrophobically treated crack -- such wind pressures are much less likely to occur. Even the largest capillary pores or air entrainment pores in concrete will resist very high hydrostatic pressures once treated with a water repellent.

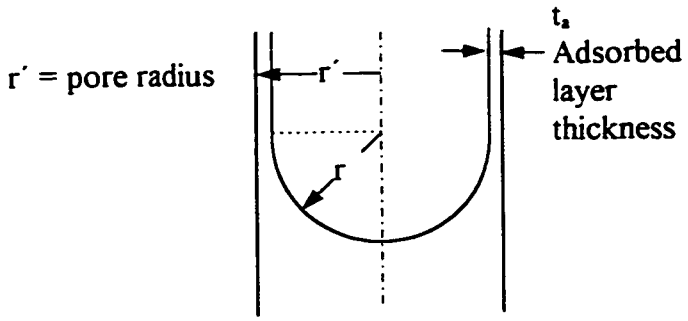

Figure 4.8: Effective radius for small capillaries

The very small capillary pores (e.g. pores in the range of 10 to 1000 nm) that comprise such a significant part of the volume of brick, concrete, and wood will, according to Equation 4.4, generate suctions of 100 kPa to 10 MPa. When considering very small pores sizes, the radius in Equation 4.4 must be adjusted to reflect the size of the adsorbed water layer (see Figure 4.8). Since the thickness of the adsorbed layer is likely to be no

more than about 1 nm, its influence will be negligible for pore radiuses larger than about 10 to 25 nm.

4.1.3.3 Vapour Pressure in Porous Materials

Liquid water open to the air will evaporate until the air reaches its maximum capacity at that temperature: this is the saturation water vapour content of the air. The saturation vapour pressure at any given temperature is merely the density of water vapour molecules in the air at which the amount recaptured by collisions with the water surface are balanced by the amount escaping the surface. Because of the increase in kinetic energy of the water molecules with temperature, more molecules are able to break free as the temperature increases. Hence the saturation vapour pressure increases with temperature in an exponential manner.

The pressure of water is reduced in pores (or over any other sufficiently curved water surface) by an amount described by the Laplace-Young equation. Therefore, within the structure of porous materials there is no simple relationship between maximum vapour pressure (absolute air moisture content) and temperature such as there is over flat water. The reduction in vapour pressure over a curved meniscus (see also Figure 4.7) can be found from the Kelvin equation, which was developed from thermodynamic principles:

$$\ln\left(\frac{P_{cap}}{p_v}\right) = \frac{-2 \cdot \sigma \cdot \cos\theta}{r \cdot \rho \cdot R_{wv} \cdot T} \qquad \text{(Eq. 4.6)}$$

where, ρ is the density of water,

P_{cap} is vapour pressure over the curved surface of water in a capillary pore,

p_v is the vapour pressure at atmospheric pressure (or over flat water) at the same temperature,

R_{wv} is the water vapour gas constant, and other terms are as before.

By noting that the fraction P_{cap} / p_v is relative humidity, Equation 4.6 can be rearranged to give the RH of the ambient air that will cause condensation or saturation of the air (RH = 100%) within a pore of a given radius (this point is sometimes termed capillary condensation):

$$RH = e^{\left(\frac{-2\cdot\sigma\cdot\cos\theta}{r\cdot\rho\cdot R_{wv}\cdot T}\right)} \qquad \text{(Eq. 4.7)}$$

This equation is plotted as a function of effective pore radius at room temperature conditions in Figure 4.9. It can be seen that significant reductions in saturation vapour pressure only occur in pores with an equivalent cylindrical radius of less than about 100 nanometers. Pores in the range of 1 to 10 nanometers will experience condensation for ambient air relative humidities ranging from 8 to 78%. In this range of pore sizes the thickness of adsorbed water layers plays a significant role and cannot be ignored. Note that most materials do not contain a significant volume of pores with an equivalent radius of less than about 100 nanometers, although this small percentage of micropores may be very important to behaviour.

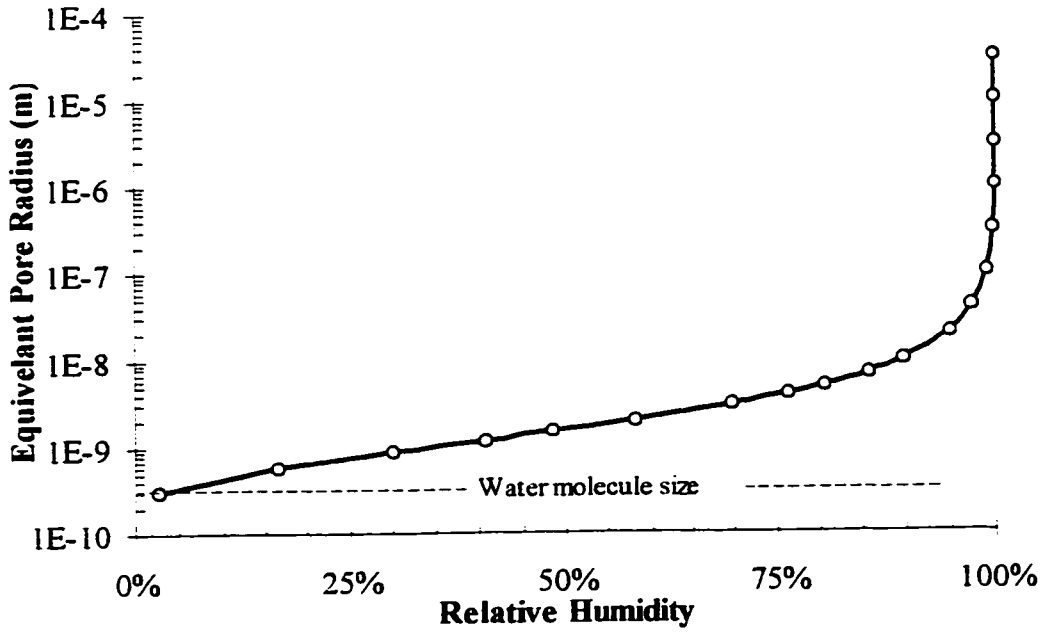

Figure 4.9: Ambient relative humidity at which capillary condensation is predicted to occur by the Kelvin equation

Note that the above theory presumes that cylindrical pores are involved. Scanning electron photographs show that pores are in fact highly irregular agglomerations of crystals and fibres [4.9]. Nevertheless, on an average basis, experimental results show that the cylindrical capillary pore model is a useful and reasonable model for most moisture physics.

4.1.4 Wettable materials and hydrophobicity

All surfaces can be defined as either wettable or non-wettable. Non-wettable surfaces or materials are also called hydrophobic. This property can be defined on a macroscopic level by observing the contact angle between water and the surface. Wettable surfaces have a surface structure that attracts polar water molecules more strongly than other nearby water molecules in the drop. Hydrophobic surfaces actually repel water molecules or have no affinity for them; therefore the inter-water forces are larger than the water-solid forces and a nearly circular drop forms (non-circular because of gravity forces).

Water repellent treatments either change the behaviour of the surface of a material by adding a thin, usually monomolecular layer to the internal surface area of a porous body (as penetrating sealers such as silane and siloxane do to concrete and brick) or provide a thicker (several thousand to millions of molecules thick) coating on the exterior which has itself a hydrophobic surface (e.g. waxes, acrylics, and silicones).

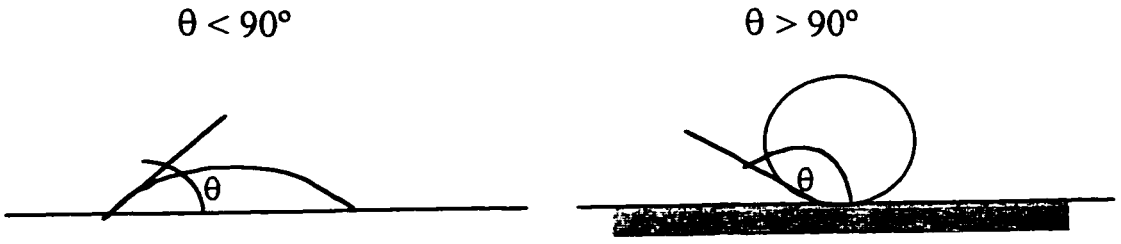

Normal material: "Wettable"

Hydrophobically treated: "Non-wettable"

Figure 4.10: Macroscopic contact angles and wettable materials

A hydrophobic or non-wettable surface is defined as one for which the interfacial contact angle is greater than 90° (Figure 4.10). A hydrophobic treatment (e.g. wax, oil, silicone) will change the contact angle to as much as 140°. Therefore, not only do capillary suctions no longer act, significant hydrostatic pressures are required to push water into a crack or pore of a hydrophobic material. This is significant because most porous building materials used as cladding can be rendered hydrophobic with some form of hydrophobic treatment.

Unlike coatings, some penetrating repellents render a porous material hydrophobic even below the surface. Therefore, if cracks form in service after treatment, significant water pressures can be resisted by the hydrophobic material surface exposed by the crack (Figure 4.11).

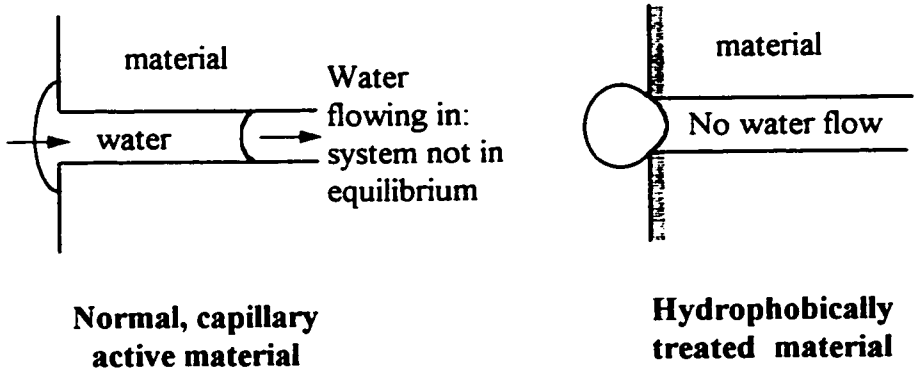

Figure 4.11: Behaviour of pores and cracks

It is normally assumed that the contact angle of water with most porous building materials is zero. However, this angle is difficult to measure on the microscopic level (i.e., within a small pore), and the macroscopic properties shown in large-scale in Figure 4.10 are strongly influenced by surface roughness. Using various Teflon materials, Marrow [4.15] provided strong evidence to suggest that the contact angle θ varies depending on whether the water is advancing (θ_A) (e.g., wetting) or retreating (θ_R) (e.g. drying)[†].

4.2 Moisture Storage in Porous Materials

As noted in Chapter 2, the ability of a material or an assembly to store moisture may be a critical consideration in moisture control for several reasons. Storage provides the buffer in time between the deposition and removal of moisture. The amount and duration of moisture storage can be an important measure of an enclosure's durability. If the volume of stored water exceeds the safe level for a material, and is present for long enough, deterioration can occur. In general, the most important features are how much moisture can be stored and for how long without crossing a performance threshold.

[†] The contact angle change may in fact be an artifact derived from macroscopic measurements of the microscopic interaction of the forces of adsorption and surface tension.

4.2.1 Measures of moisture content

It is important to note the method by which moisture content is reported. Most sources use a gravimetric measure, e.g., kg of water per kg of material, denoted u (kg/kg dry) or M% in this thesis. Volumetric measures also are used, litters of water per cubic meter of material, denoted here as ψ (m^3/m^3) or as V%. Mixed measures are also commonly used, e.g., kg of water per cubic meter of material, or litters of water per kg of material. This commonly used measure will be denoted as w (kg/m^3).

It will be shown in the following sections that equilibrium RH (%) and the moisture content of a porous material are related. Since RH is reasonably easy to measure and performance thresholds are sensitive to it, it is often used as an approximate measure of moisture content. The degree of saturation, S, is the percentage of open pores that are filled with water. It may be expressed as a decimal fraction or percentage, just as relative humidity is. The degree of saturation is very useful when measuring freeze-thaw conditions, and other situations where the materials are highly saturated.

4.2.2 Moisture performance thresholds

For many building products, safe storage capacity is exceeded once the relative humidity exceeds about 80% [4.16]. If the temperature is also between about 15 °C and 30 °C and the pH is less than 10 to 12, significant biological growth [4.17,4.18,4.19] and high surface corrosion rates [4.20] can be expected. Fungal growth essentially ceases below 2 °C [4.21], but both mechanisms can proceed at temperatures as low as freezing, and perhaps lower.

Once initiated, steel corrosion within concrete, masonry mortar, and grout tends to reach a maximum rate in the range of environmental humidity of 85% RH, but corrosion may still occur down to 60% RH [4.22]. Recent research suggests that significant rates of active corrosion are actually unlikely below an internal RH of about 80% [4.23]. Other complementary research also shows that for all practical purposes, corrosion of metal in concrete stops at saturation levels of less than 50% [4.24]. Carbonation of concrete, which eventually leads to a reduction in pH and therefore steel depassivation, occurs most rapidly at an environmental RH of between 40 and 70%.

As the amount of moisture increases, the susceptibility of some materials to deterioration often decreases. For example, when fully saturated, fungal growth slows or stops because

of a lack of oxygen. For the same reason, corrosion of submerged steel and steel reinforcing in fully saturated concrete proceeds at very slow rates. Saturation or submersion also limits the access of carbon dioxide to concrete, and hence carbonation is slowed or stopped. Freeze-thaw damage, however, can only occur in materials which are more than 90% saturated, i.e., typically over about 98% RH.

Non-porous materials, such as steel and most plastics, store small amounts of moisture on their surfaces as adsorbed water, liquid water in drops, and frozen water as ice and frost. However, the amount of water stored on the surface of non-porous materials is very small, and none can be stored within the material. This moisture can, however, still support surface corrosion and fungal growth. In fact, the practically non-existent ability of steel and plastics to store water means that deterioration can begin with even a very small amount of surface water deposition.

4.2.3 Liquid water and ice storage mechanisms

Assuming that water molecules can penetrate all of the open pore volume (a reasonable assumption given the small size, less than 0.3 nanometers, of a lone water molecule), the maximum amount of moisture that can be stored by a material will be governed by both its porosity and the nature of the pore size distribution. Air can also be trapped in dead end pores, and thereby limit the maximum volume of water that can be absorbed[1]. The largest amount of moisture can be stored if a material is first placed in a vacuum chamber, then placed in water, and then atmospheric pressure is reapplied; this procedure eliminates trapped air and ensures that all pores interconnected to the exterior by any path are filled with water. The amount of water stored in such a vacuum saturation test is called the maximum moisture content (w_{max}). The reported vacuum saturation moisture content for materials with very small pores can vary depending on the technique used, especially the degree of vacuum and length of immersion time [4.25].

The equilibrium moisture content of a material in contact with water at atmospheric pressure, is variously termed the capillary saturation moisture content, the free saturation, or the capillary moisture content (w_{cap}). The value of w_{cap} will vary slightly for each sample depending on the test method chosen. In general, test methods ensure that water is available over the entire surface of the sample without generating hydrostatic forces that

[1] The maximum stored will therefore vary between $(X_A - Y \cdot X_D) \cdot \psi_T \cdot V_T$ and $X_A \cdot \psi_T \cdot V_T$, with Y some positive value less than 1.

might drive water into the material. In most tests a material sample is simply placed in a bath of water at room temperature. The amount of water absorbed will asymptotically approach some value, sometimes also called the cold water saturation moisture content. This process may require a few minutes to a few weeks although test standards may specify a duration. Water is actually being forced into the material in these tests by hydrostatic pressure. However, the size of this driving force is small relative to the capillary suction forces. Nevertheless, by leaving a sample immersed in water for a long time, the vacuum saturation moisture content can be approached.

The most accurate tests for capillary saturation are likely those that place a thin sample in a sealed container (so that neither gravity nor evaporation play a role) in capillary contact with water (so that no hydrostatic pressures act).

Once a material has reached capillary saturation, all surface tension forces will be in equilibrium. Therefore, the material will not be able to store any more moisture unless water is forced into the pores by some external force (e.g. hydrostatic head, large air pressures, etc.). The amount of water that can be forced into a material above capillary saturation can be termed $w_{\Delta sat}$. The saturated moisture content, w_{sat}, is therefore simply $w_{cap} + w_{\Delta sat}$.

A sample can also be placed in boiling water (sometimes called the boiling saturation) as a means to accelerate the room temperature or "cold" water saturation test or as a simple means of reaching the maximum saturation value of a vacuum tests. Repeated or long duration boiling will increase the amount of water that is absorbed, and even long-term immersion in cold water may allow the moisture content to approach the maximum moisture content, w_{sat} [4.13]. Reference 4.13 also shows that a 5 hr immersion in boiling water results in approximately the same amount of water absorption as a vacuum saturation test for a wide range of clay bricks. Both test methods only fill about 90% of the pore space accessible to mercury intrusion methods.

It can be concluded that capillary moisture content as measured by most tests lies somewhere in the spectrum between the true capillary moisture content and the vacuum saturation moisture content (in which high levels of vacuum are used in conjunction with long soak times).

The moisture content above which liquid moisture transport begins to occur is termed the critical moisture content (w_{crit}). The critical moisture content is difficult to measure but

generally occurs at a moisture content in equilibrium with an environment of between about 93 and 98% RH for most materials. The critical moisture content is important because it marks the moisture content below which the water in most of the pores is discontinuous at a microscopic level. Therefore, below w_{crit}, moisture moves in a porous material primarily by the mechanisms of vapour diffusion and adsorbed layer diffusion, while above this level capillary conduction is the dominant mode of moisture transport.

The critical moisture content might also be expected to be important for air transport through porous materials because it is assumed that above w_{crit} the liquid water in the majority of pores is interconnected, thereby blocking the passage of air flow. The air permeability is therefore expected to drop dramatically as the moisture content approaches w_{crit}. However, recent experimental evidence strongly suggests that air permeability drops dramatically at w_{cap}, not w_{crit} [4.26]. This is likely the case because capillary transport of liquid water will occur through the smaller pores at low moisture contents, while air will preferentially flow through the largest pores. Since the largest pores become filled only at capillary saturation, it is to be expected that as w_{cap} is approached the air permeability will drop.

4.2.3.1 Capillary Suction Curves

The capillary pressure, capillary suction, or moisture retention curve is a plot of the moisture content as a function of applied pressure air pressure. As can be seen from the Laplace-Young equation (Eq. 4.1), as the atmospheric pressure increases, the water in the pore will seek a new equilibrium. If the exterior air pressure exceeds the capillary pressure predicted by Equation 4.4, liquid water will be expelled from pores with this radius and larger. By successively increasing the air pressure acting on an initially saturated material, the incremental moisture content can be measured from the volume of water expelled. This is the intent of a standard pressure plate test [4.27]

Figure 4.12 is a representative plot of the results of a porous material in a pressure plate test. It can be seen from the plot that the major wetting and drying curves follow different paths. For the same capillary pressure, there are clearly two different moisture contents. This hysteresis is caused by a number of effects [4.28]. The so-called "ink bottle effect" describes the response of moisture to the irregular shape of real pores and capillaries. Figure 4.13 illustrates a hypothetical situation whereby hysteresis would be expected since two equally stable capillary pressures are possible, each with a different moisture content.

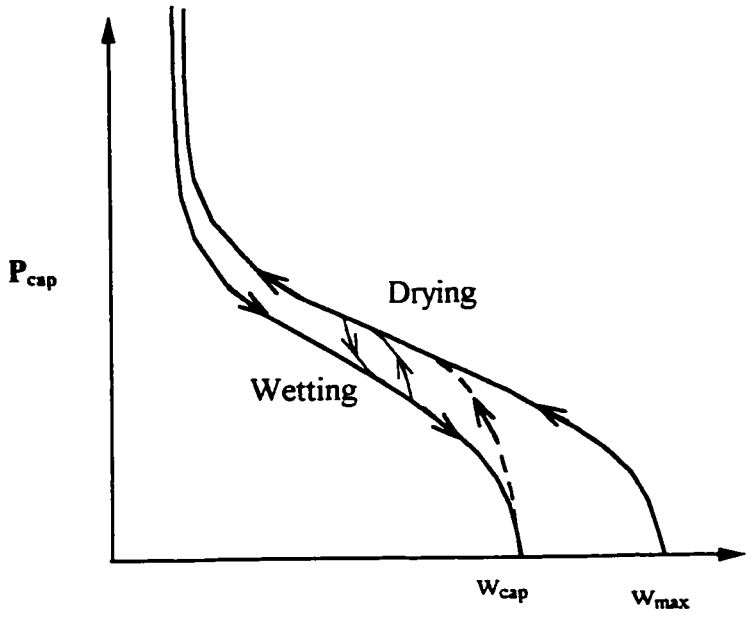

Figure 4.12: Typical Capillary Pressure Curves

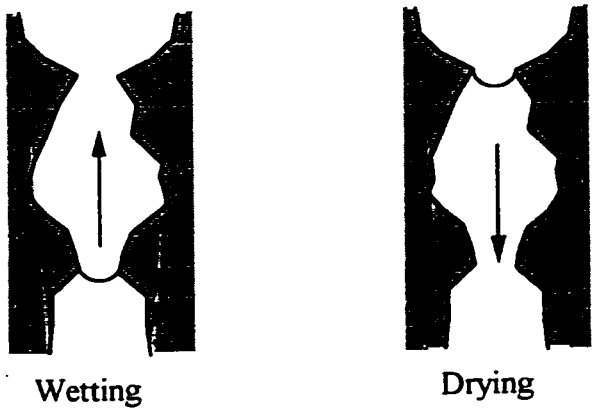

Figure 4.13: Moisture storage hysteresis due to the ink bottle effect

Another proposed explanation for hysterisis is a contact angle that changes depending on whether the capillary meniscus is advancing or retreating. This was discussed earlier. Finally, the behaviour of air in the material will depend on whether wetting or drying is occurring. Trapped air in dead-end pores can retard wetting but have little effect (and may even accelerate) on drying.

It is often assumed that one can trace an average curve between wetting and drying curves. However, the difference can sometimes be quite large and a significant error might accumulate in detailed step-by-step computer simulations. This may be important in wet/dry cycling of materials from almost saturated to almost dry, such as occurs in thin porous cladding elements.

4.2.4 Vapour storage mechanisms

A significant amount of water can be stored in porous bodies in the adsorbed state. This section explores how porous materials store moisture in the vapour or adsorbed phase.

Because the molecular attraction of water to a surface only acts up to about 5 or 6 layers of water molecules, moisture stored by adsorption is usually only significant when materials have large surface areas, i.e., the internal surface area connected to the ambient air is very large per unit volume or per unit mass. This is the case for most common building materials. Even a single or thin layer of adsorbed water molecules will result in significant amounts moisture storage within materials with a very large internal surface area.

All hygroscopic materials attract and adsorb water vapour until they reach equilibrium with the surrounding air. The equilibrium moisture content, however, varies widely with material, temperature, and RH. The amount of moisture stored by adsorption as a function of the vapour concentration (i.e., vapour pressure) in the surrounding air and temperature is shown in Figure 4.14 for a typical hygroscopic material. The vapour pressure is merely a convenient means of measuring the absolute amount of moisture in the air; the humidity ratio can also be used since the two are directly related.

Expressing the response of a hygroscopic material in terms of RH instead of vapour pressure will generally collapse the family of lines shown in Figure 4.14 to the single line shown in Figure 4.15: such a diagram is called the sorption isotherm. Wetting (adsorption) and drying (desorption) follow slightly different paths in most materials for the same reasons that the capillary retention curve does.

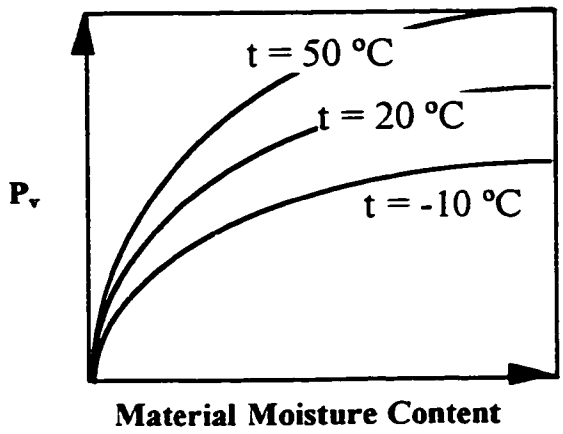

Figure 4.14: Surface vapour pressure of a typical hygroscopic material as a function of temperature and moisture content

Although the sorption isotherm is a very useful and fundamental descriptor of material response, it has not been defined for many building materials and the accuracy and repeatability of available results are poor. Subtle differences in manufacturing or raw material sources can result in significant differences in the sorption isotherm.

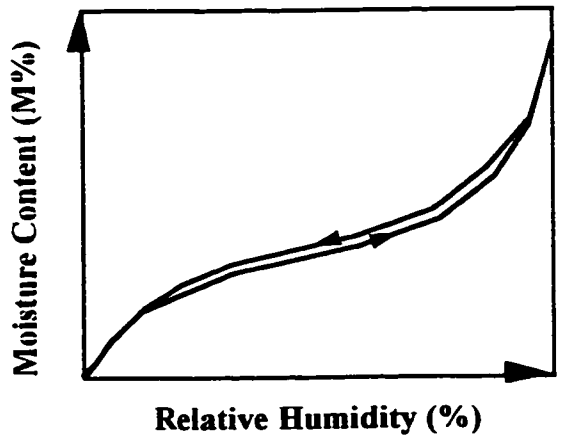

Figure 4.15: Typical sorption isotherm of a hygroscopic material

When a material has adsorbed all the moisture it can by adsorption, further moisture will be stored in pores and cracks within the material by capillary suction (e.g., absorption). For example, wood will adsorb up to approximately 30% moisture content at 98% RH by adsorption, but by placing it in contact with liquid water it can hold two to four times this amount (see Table 4.1). Liquid water (e.g. 100% RH) must be available for absorption to occur. In practical situations, very high relative humidities cannot occur without liquid

condensation forming. Even in laboratory settings, a consistent RH of 95% is difficult to achieve within a chamber without small localised temperature and vapour pressure gradients resulting in surface condensation. Therefore, in practise, adsorption and absorption are often acting together in the RH range of more than about 95%, albeit at different places and times over a sample. This is even more significant in real enclosures because the gradients of moisture and temperature are far greater than in a controlled laboratory setting.

Knowledge of the size and distribution of pores can help predict the vapour pressure within a material. The most widely accepted adsorption theory, termed BET after its developers Brunauer, Emmet, and Teller [4.29], describes and predicts the amount of water vapour that can be expected to be adsorbed onto the internal surface area of various materials up to about 50%RH. Rounsley [4.30] used statistical thermodynamics to improve and extend the BET model and developed the following equation:

$$\frac{X}{X_1} = \frac{C\phi}{1+(C-1)\phi}\left[\frac{1-\phi^n}{1-\phi}\right] \qquad \text{(Eq. 4.8)}$$

where X is the equilibrium moisture content (M%),

X_1 is the moisture content in a mono-layer of adsorbate (M%),

ϕ is the relative humidity,

C is a constant, comprising the heat of adsorption, heat of condensation and the universal gas constant (typically 20 to 50), and

n is the maximum number of layers that can be adsorbed (typically 4 to 6).

Equation 4.8 represents the most probable distribution of adsorbed molecules. The constant C and the number of layers can be found from simple, low-RH adsorption tests. El-Sabaawi and Pei [4.31] and later Tamon, Okazaki, and Toei [4.32, 4.33] combined this background adsorption theory with Kelvin's Law to develop a predictive equation for sorption isotherms given experimental information on adsorption and pore size distribution. Their models accurately predicted the complete sorption isotherm from saturation to complete drying for several materials. These results support the physical validity of their assumptions: adsorption occurs in all pores following the BET/Rounsley model until, as the Kelvin equation predicts, condensation begins to occur within the smallest capillary pores. Experimental results also confirmed that the reduction in pore

size because of the thickness of the adsorbed film must be considered when using Kelvin's equation to assess condensation within the pores. By accounting for both mechanisms (one dominant at low RH and the other at high RH up to saturation) the desorption isotherm can be predicted for some materials (Figure 4.16).

Kuenzel [4.34] used a form of the BET equation with a simple fitting coefficient, b, based on two points: the capillary saturation and the moisture content at 80% RH:

$$w(\phi) = w_{cap} \frac{(b-1)\phi}{b-1} \qquad \text{(Eq. 4.9)}$$

where ϕ is the RH.

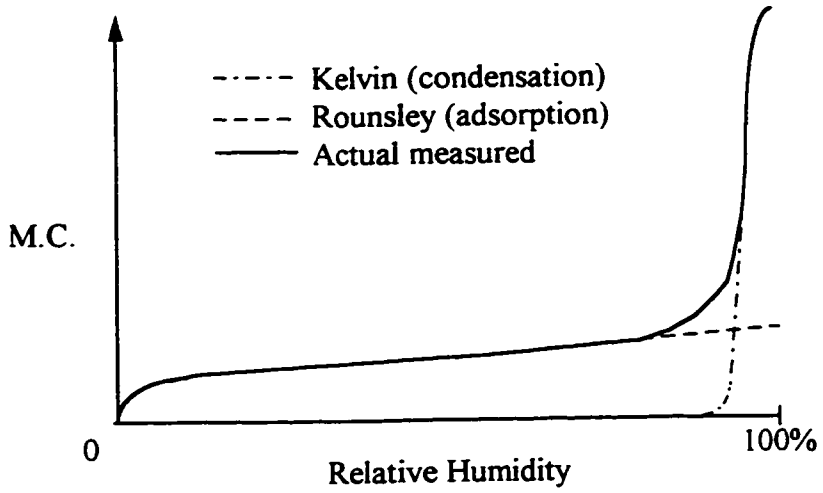

Figure 4.16: Typical predicted sorption isotherm according to Kelvin Equation and modified BET theory

Because the Rounsley equation is valid at RH levels below about 60-90%, Equation 4.9 predicts the sorption isotherm in this region very well. However, because the capillary saturation content is used as a calibration term, and adsorption theory does not apply to capillary saturation, the equation cannot properly predict higher relative humidities. At lower relative humidities the accuracy of Equation 4.9 depends exclusively on the pore size distribution being well distributed over all sizes. It should be noted that Kuenzel intended this equation as a simple approximation if no other information was available.

4.2.5 The moisture storage function

From the discussion above, it can be seen that the moisture storage within porous materials is the result of several mechanisms, with different behaviour due to each. There is a consensus in the modern literature for the qualitative description of the moisture storage function [e.g., 4.11 ,4.34, 4.35], sometimes called the moisture retention curve.

Figure 4.17 shows a typical moisture storage functions. Three clear regimes can be identified:

1. the hygroscopic regime, divided into three sub-regions,
2. the capillary regime, and
3. the over-saturated regime.

In the first sub-regime, labelled A in Figure 4.17, a single layer of adsorbed water molecules forms over the internal surfaces of the material. The strength of the polarity of the water molecule ensures that this is a strong bond.

In sub-regime B, the water molecules in the air are attracted to the first layer of adsorbed molecules and form subsequent layers. Depending on the material (e.g., its contact angle and pore sizes), region B may include from one to many additional layers of adsorbed molecules. Since each layer after the first is held less strongly, the slope of the RH vs. moisture content curve decreases in this region.

In sub-regime C, the layers grow to such a size that they begin to interact and interconnect and significant capillary condensation forms in the mid-sized pores. By applying Kelvin's equation to the pore-size distribution of many materials, a rapidly increasing slope in the sorption isotherm is predicted in this region. For example, from Kelvin's equation, it can be seen that capillary condensation will occur in the smallest pores at mid-range relative humidities (e.g., 8% RH for 1 nanometer pores and 78% RH for 10 nanometer pores). As a result, it can be noted that the greater the proportion of pores smaller than 10 nm, the higher the moisture content in the mid-RH range in the sorption isotherm. Therefore, calcium-silicate brick, which has 10% of its pores less than 10 nm in size, adsorbs significantly more moisture at lower RH's than clay brick, which has almost no pores with a radius less than 10 nm. (Compare Figures 4.18 and 4.19 and note that the total pore volume of concrete is less than half that of clay brick and calcium silicate).

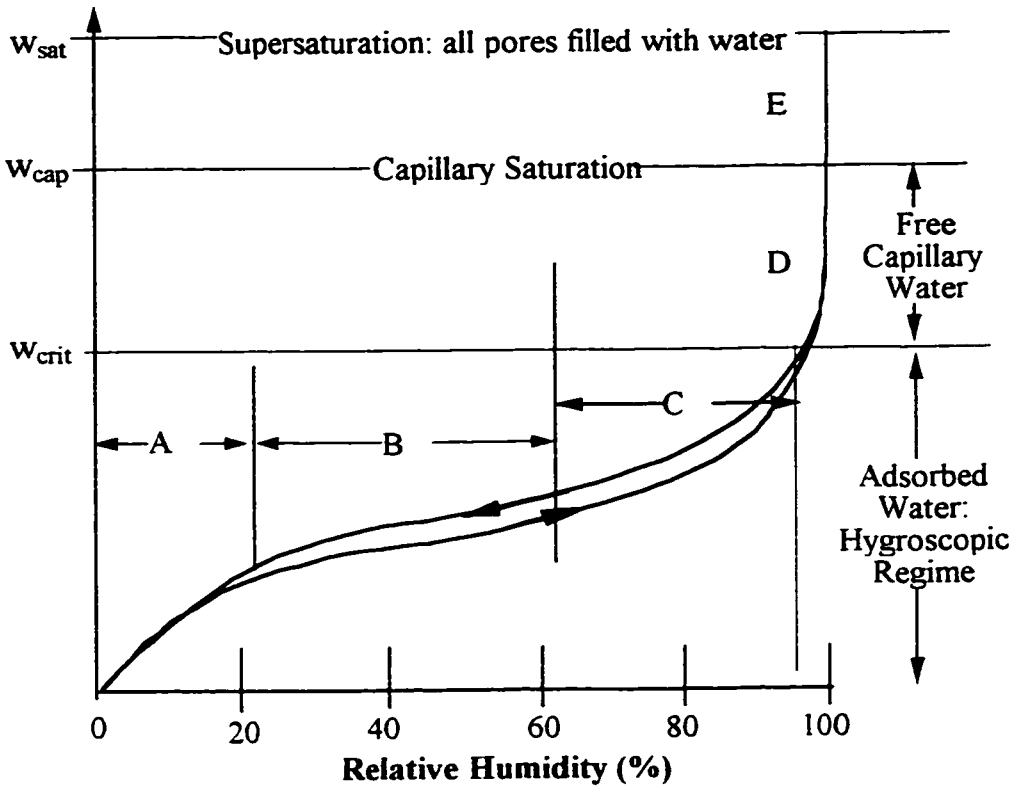

A: Single-layer of adsorbed molecules
B: Multiple layers of adsorbed molecules
C: Interconnected layers, (internal capillary condensation)
D: Free water in Pores, capillary suction
E: Supersaturated Regime

Figure 4.17: Regimes of moisture storage in a hygroscopic porous material

At the highest relative humidities, all but the largest pores are practically filled with water and the capillary regime begins. Kelvin's equation indicates that condensation will occur in pores of 0.1 micrometer radius at relative humidities less than 97.5% RH.

The capillary regime, labelled Region D, is somewhat arbitrarily designated as that part of the moisture storage function above the critical moisture content. Physically, it is presumed that a continuous liquid phase forms. It is characterised by a very steep change in moisture content as the relative humidity changes.

Region E, the supersaturated regime, is characterised by an infinite gradient at 100% RH [4.36]. It is defined as that region between the free capillary saturation moisture content and the fully saturated moisture content. In this region there are no internal forces driving water into or out of a material (since the moisture content is above the capillary saturation content), and the moisture content is independent of RH.

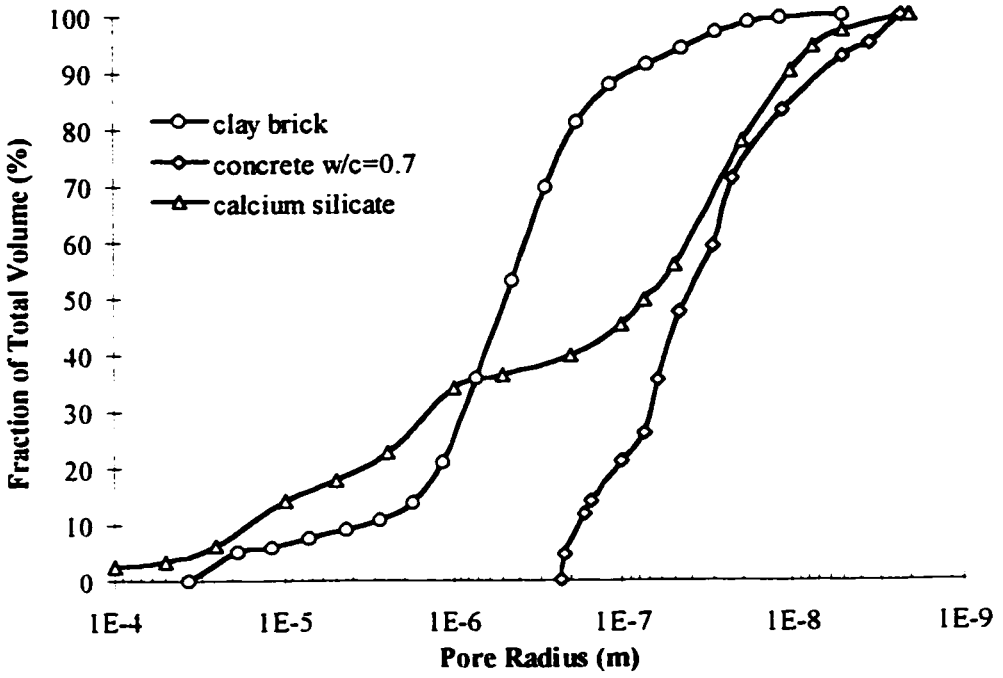

Figure 4.18: Pore size distribution comparison of clay brick, concrete, and calcium silicate

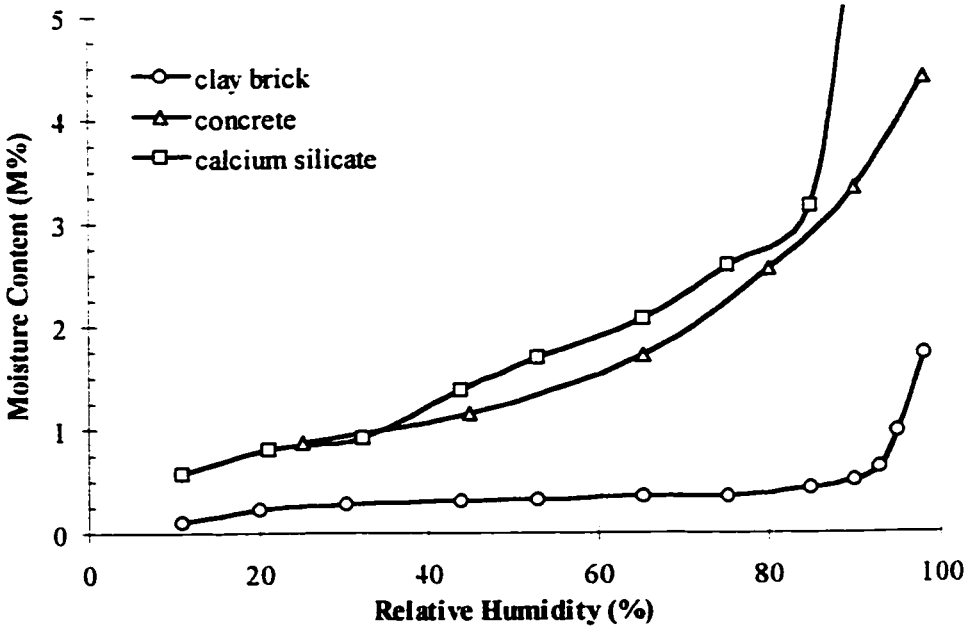

Figure 4.19: Sorption isotherms comparison of clay brick, concrete, and calcium silicate

The complete moisture storage function can be described in the form of a sorption isotherm, with the fast-changing and difficult to measure region above about 95% RH defined in greater detail by the suction curve. The moisture content vs. suction curve at free capillary saturation (w_{cap}, RH =100%) exhibits an infinite slope to the fully saturated moisture content, w_{sat}.

The storage function is typically defined for the hygroscopic regime by conducting a series of gravimetric measurements of a sample after it has reached equilibrium with a specific relative humidity environment. Because of the steep gradient above about 95% RH, it is practically impossible to measure this part of the storage function in the same way as for the hygroscopic region, and other experimental means are used, such as mercury porosimetery and Kelvin's equation or the pressure plate apparatus.

It has become common in building physics to divide the moisture storage function into the hygroscopic region, measured by vapour equilibrium, and the capillary suction or retention curve, measured with a pressure plate apparatus. However, the literature review suggests that theory already exists [e.g.,4.31,4.32] which might allow for the relatively accurate prediction of these curves. Simple low RH adsorption measurements combined with fast mercury intrusion pore size analysis (if this is indeed accurate) is all that is required. It would be very interesting to comprehensively compare theoretical calculations with the present experimental pressure plate apparatus technique used to predict the suction curve.

Descamp [4.26, p.55] compared the suction curves measured with a pressure plate apparatus to those predicted with the Kelvin equation and pore size distribution from a mercury porosimeter. He found a good fit for his sample of calcium-silicate brick but the moisture storage predicted by mercury porisimetery was consistently lower than that measured by the pressure plate.

Krus's [4.48] measurements of sandstones showed some significant differences between the pore size distributions predicted by the two methods. The presence of high levels of salts was also shown to change the results of the pressure plate measurements. More research into the measurement of pore size distribution and the actual moisture storage function is clearly required, although it appears as though presently available theory in the field chemistry and chemical engineering has not yet been fully exploited for building science applications.

4.2.5.1 Significance of the Regions

Some performance thresholds for various building materials and deterioration mechanisms have already been discussed. The description of moisture storage in materials presented above explains the underlying reasons for many of these performance thresholds.

The upper portion of the hygroscopic regime is important because the adsorbed moisture can be both loosely bound and of a sufficient volume to support moisture-related deterioration mechanisms, e.g. mould or fungal growth and corrosion, etc. This upper region is ideal for those deterioration mechanisms that require oxygen as well as moisture.

Although building materials generally operate in the sorption isotherm regime, if wetting occurs, the capillary regime (Region D) is also important. With regard to moisture-related damage, the capillary regime is often critical. Free water can freeze and cause failure in many brittle porous materials. The free water also provides fertile breeding grounds for biological growth and electrolytes for corrosion.

Cyclical wetting and drying, temperature gradients, and freeze-thaw action all result in complex forces which may fill pores that might not be filled in a simple laboratory test of capillary saturation. This over-saturated regime (Region E) can be explored in a laboratory setting by employing various degrees of vacuum saturation. This region is important for some material deterioration mechanisms. For example, bricks and concrete will often experience freeze-thaw failure in after only a few cycles if they become over-saturated. Corrosion and biological growth are usually restricted in this range because the water filled pores restrict the diffusion of oxygen.

Moisture storage in materials also causes small movements that often interfere with the performance of a material's function in an enclosure. If restrained, the movements can generate stresses sufficient to cause material failure. For example, wetting and drying due to adsorption explains why wooden doors tend to be tight in the humid summer and loose-fitting in the dry winter. Drying shrinkage stresses in concrete and the initial expansion of clay bricks can also be explained by the manner in which moisture is stored.

Materials such a wood, mortar, and concrete begin life with all of their pores filled with water. As the material dries, the water vapour pressure in the pores drops and adsorbed water will be tempted to leave the surface of the pores. However, the strength of the bonding between water molecules which comprise the layers results in tension forces as

drying progresses. It is these internal tension forces that causes drying shrinkage stresses and the consequent strain or cracking in wood, concrete, etc.

Conversely, brick begins life at 1000 °C, completely dry. When water vapour enters the pores, compressive forces are developed as water molecules forces themselves onto the brick material (silica-based) and other adsorbed water molecules. This internal compressive force causes the initial expansion of brick, and the wetting expansion of other porous materials.

4.2.6 Moisture storage in enclosure assemblies

Moisture can be stored in a variety of ways in enclosure assemblies, either as vapour, water, or solid (frost, ice). All mechanisms have practical importance, adsorption and absorption of water in hygroscopic materials, free liquid water stored in small depressions or undrained portions of an assembly, and even as droplets or frost on surfaces.

Table 4.2 uses the average values in Table 4.1 to calculate the amount of moisture that can be stored in the materials that comprise a representative wood framed house wall. The wall comprises a 85 mm clay brick veneer with cement mortar (approximately 10 mm wide joints), an airspace, 12.5 mm chipboard sheathing, and a 38x140 mm wood frame at 610 mm centres. The batt insulation, the sheathing paper, and the air in the air space have not been accounted for, since their contribution is small. The interior drywall finish is assumed to be well separated from the exterior by a 6 mil (0.15 mm) polyethylene vapour barrier.

Table 4.2: Moisture contents of a representative wood-framed wall assembly

Material	Dry Density (kg/m^3)	Volume (m^3/m^2)	at ≅ 95%RH (kg/m^2)	at capillary saturation (kg/m^2)
85 mm Brick veneer	1700	0.0765	6.5	13.0
Cement mortar (10% area)	1900	0.0085	1.0	2.4
12.5 mm Chipboard	700	0.0125	1.5	8.7
Wood Studs 38/140@610†	500	0.0277	1.9	7.5
Total		0.1891	10.9	31.6

†Includes two top and one bottom plate and a 38/185 rim joist per 2.6 m height

It is clear from Table 4.2 that a significant amount of water can be stored in such a representative wall. While it is unlikely that the framing will be at 95% RH (in fact,

serious fungal growth would be expected at this moisture content), both the chipboard and the wood framing can safely act as short-term accumulators of moisture, especially in cold weather. It is quite likely that the brickwork will often be at between 95% RH and saturation. The volume of water that can safely be stored in most typical enclosures will therefore be of the order of several to tens of kg per square meter.

Table 4.2 only considers the moisture stored through the absorption and adsorption. A considerable amount of moisture may be stored as trapped liquid water, although this amount is often less than one kg per square meter.

4.3 Moisture Transport in Porous Materials

Moisture transport through porous building materials, especially under combined moisture and temperature gradients, is a complex phenomenon. In fact, no widely accepted theory of combined heat and moisture flow exists, although consensus on the majority of issues is developing. The greatest difficulty exists in extrapolating a model based on the microscopic pore structure of a material and the individual transport phenomenon to the total macroscopic moisture transport behaviour. The majority of the more recent building physics applications appear to have abandoned this approach in favour of the measurement of aggregate macroscopic material properties that can be used in practical numerical finite volume models (see Section 4.6).

Moisture, as a liquid, a adsorbate, or a vapour can move through all porous materials. The coupling of heat and moisture transport and the driving potentials are often different for each phase and each transport mechanism. It is generally agreed that liquid water flows into porous materials driven either by capillary suction and/or by external pressures (e.g. a head of water or, water plus an imposed air pressure). Water vapour transport is driven by differences in vapour pressure. The chemical engineering literature suggests that adsorbed water is driven by mass concentration gradients in the adsorbed layer, although not all of the building science literature recognises this.

The transport of each moisture phase, vapour, adsorbate, and liquid, through porous materials is discussed in turn below.

4.3.1 Water vapour diffusion

Water vapour moves through the building envelope in two primary modes; diffusion and convection. Diffusion is analogous to heat conduction in that the random motion of molecules results in the movement of vapour along a species (i.e. water vapour) mass concentration gradient. Convection is the transport of water vapour by the bulk movement of the air itself.

Fick's Law governs the diffusion of vapour through materials (including air) driven by differences in mass fractions between species. If the pores are of the same order or larger than the mean path length of vapour molecules between collisions (with themselves or with a solid material), diffusive vapour flow through a porous material can be accurately described by Fick's Law. However, if many collisions with the sides of the pore occur, the process is governed by Knudsen transport (also called effusion), and will be slower than vapour transport through air (Figure 4.20).

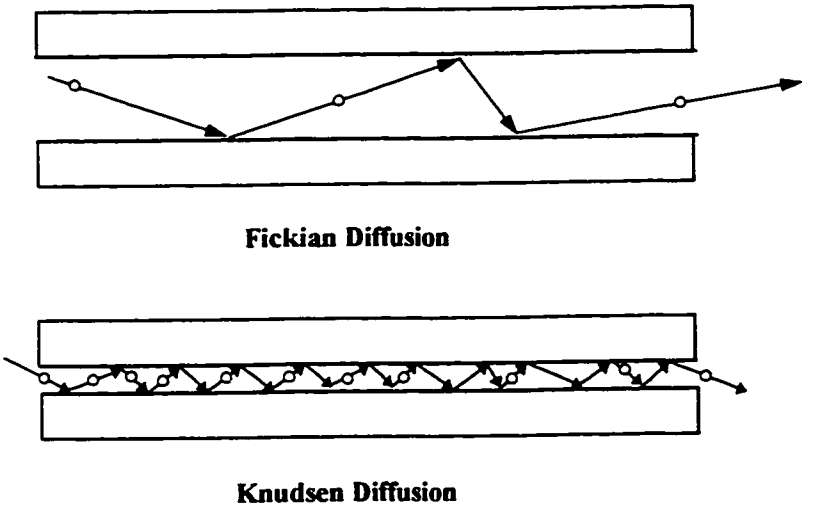

Figure 4.20: Fickian and Knudsen diffusion processes

4.3.1.1 Knudsen Diffusion

The Knudsen number:

$$N_K = \frac{l_m}{2 \cdot r} \qquad \text{(Eq. 4.10)}$$

is the ratio of the mean free path length of a free water vapour molecule between collisions (l_m) to the pore diameter (r). When the pore sizes are large and the vapour pressure high,

N_K <<1 and Fickian diffusion governs. For the case where pores are very small and vapour pressure is low, N_K >>1 and interactions between molecules almost cease and flow is governed by collisions with the pore wall. This type of Knudsen diffusion can be described by [4.37]:

$$m_{v.K} = -D_{v.K} \cdot \frac{M}{R \cdot T} \nabla p_v \qquad \text{(Eq. 4.11)}$$

where

M is the molecular mass of the gas in question

R is the universal gas constant

T is absolute temperature

$D_{v.K}$ is the Knudsen vapour diffusion diffusivity

$$= \frac{2}{3} \cdot r \cdot V_{rms} \cdot \frac{2-f}{f}$$

p_v is the vapour pressure,

r is the pore radius of interest,

V_{rms} is the mean molecular velocity ($= \sqrt{\frac{8 \cdot R \cdot T}{\pi}}$), and

f, the fraction of molecules which undergo diffuse reflections with the pore walls, approaches 1 in pure Knudsen flow. As more molecules collide with one another the fraction f drops and the value of $D_{v.K}$ climbs rapidly.

The mean path length between collisions of a vapour molecule in air can be calculated given the density of vapour molecules (vapour pressure) and the temperature. This path length is approximately 0.1 micrometers for most building science applications (i.e., water vapour in air at room temperatures). Fickian diffusion can therefore be expected to dominate in pores with a radius greater than about 0.1 micrometers (e.g., 7000 water vapour molecule diameters). Since the diameter of a water vapour molecule is of the order of 0.3 nm, vapour transport in pores with a radius of 1 nm (e.g., only 6 molecules across will fill the pore) will be strongly influenced by interference with the pore walls. Some important building materials have a significant volume of pores in the order 1 to 10 nm, e.g., cement paste, calcium-silicate bricks, etc.

If a layer of adsorbed molecules is also present in very small pores, Fickian diffusion is unlikely and Knudsen transport will govern. Knudsen transport will not be significant at high RH's even if the vapour pressure is low (e.g. low vapour molecule density) since the small pores will be filled (because capillary condensation will occur at less than 78% RH in pores with radiuses less than 10 nm).

Although it is often ignored, Knudsen transport would be expected to dominate the vapour transport in pores of less than 10 nm in size at low relative humidities and low vapour pressures. The relative influence of Fickian and Knudsen transport is unclear in the transition regions but Daian [4.38] has proposed a combined vapour diffusivity:

$$D_{v.eff} = D_v / (1 + N_K) \qquad \text{(Eq. 4.12)}$$

where D_v is the Fickian vapour diffusivity.

In most cases, researchers choose to use experimental data which includes both mechanisms rather than using explicit and separate considerations of diffusion and effusion. Separation of the two mechanisms in the study of building enclosures may be useful because the temperature dependence of the two mechanisms can then be accounted for: Knudsen flow varies as $T^{-0.5}$ and Fickian flow varies with $T^{-0.81}$. As second reason is the variable effect of RH and vapour pressure on Knudsen diffusion. In many situations, it may be acceptable to ignore Knudsen transport, but this is not necessarily true in all cases.

4.3.1.2 Fickian Diffusion

The mass rate of Fickian vapour (m_v) diffusion through still (no convection) air can be found from:

$$m_v = -\delta_a \cdot \nabla p_v \qquad \text{(Eq. 4.13)}$$

where δ_a is the vapour permeability of air (kg/(m Pa s)), and

p_v is the vapour pressure (Pa).

The water vapour permeability of still air, δ_a, can be found from Shirmer's widely used equation:

$$\delta_a = 2.0 \times 10^{-7} \cdot T^{0.81} / P_a \qquad \text{(Eq. 4.14)}$$

where P_a is the ambient total pressure (Pa), and

T is the absolute temperature (K)

For an idealised porous body, the ratio of stagnant air permeability to the measured vapour permeability of a dry sample of a porous material (δ_p) should give:

$$\delta_p = \psi_0 \cdot \delta_a \qquad \text{(Eq. 4.15)}$$

where ψ_0 is the open porosity for vapour flow (m^3/m^3)

Equation 4.13 assumes that no vapour can be transported through the solid fraction of a porous material and that vapour flow through pores is exactly the same as vapour flow through still air. Fickian diffusion through porous materials is, however, not exactly the same as diffusion through air. Experimental values of vapour permeability are lower than that predicted by Equations 4.11 and 4.13. As described earlier, the open porosity theory is only valid for a material with pores large enough that vapour molecule collisions with the pore walls do not retard flow (e.g., pure Fickian diffusion). Real materials have a range of pore sizes and complicated interconnectedness, and therefore the actual vapour flow path is considerably longer than the thickness of the sample.

A tortuosity factor†, τ, is defined for real materials which:

1. accounts for the longer flow path,
2. acknowledges that effective porosity, ψ_{eff}, is less than the open porosity, and
3. provides a better match between theory and experimental results.

$$\delta_p = \psi_0 \cdot \delta_a \cdot \tau \qquad \text{(Eq. 4.16)}$$

Pennman originally defined tortuosity as the ratio of the actual vapour molecule path length to specimen thickness [4.39, 4.40] and suggested a constant value of about 0.66, although many references appear to use the constant as an empirical fitting coefficient. However, the tortuosity factor is not likely to be a constant for a given material, since as the moisture content increases, the volume filled with air (and thus available for vapour transport) decreases. Millington and Quirk [4.41] recommended an equation widely used in soil sciences:

† In different literature sources the tortuosity occurs in either the numerator or denominator of Equation 4.16. It is important to be aware of the difference definitions.

$$\tau(\psi) = \frac{(\psi_0 - \psi)^{10/3}}{\psi_0^{3}} \qquad \text{(Eq. 4.17)}$$

which reflects the fact that pores filled with liquid water do participate in vapour flow. More recent results suggest the geometrically derived exponent in the numerator of Equation 4.17 may be too high and a value of just over three (e.g., 3.1 to 3.2) maybe more generally applicable [4.42]. The fact that open porosity is used in Equation 4.17 instead of effective porosity (which is difficult to measure but more realistic) might be one reason why a lower exponent provides a better match to experimental values

It is expected that large pores will obstruct vapour diffusion less because more area will be available for the water molecules to move freely. In small pores, the addition of several layers of adsorbed moisture will have a proportionately larger influence because of the larger reduction in the free area available for vapour molecules to move. As the RH (moisture content) increases, small pores will fill with water from capillary condensation and will also become effectively smaller because of the increased thickness of the adsorbed layers on the pore walls This should result in decreasing vapour permeability with increasing RH, i.e., theory would suggest a vapour permeability plot that steadily decreases with increasing moisture content (and RH).

While the concepts of porosity and tortuosity provide a theoretical background for the prediction of vapour permeability through porous materials, this theory has had limit success in the prediction of the vapour permeability of most porous building materials. Vapour permeability test results actually show different vapour permeabilities and a strong moisture content / RH dependency (Figure 4.21), especially for hygroscopic materials (e.g. see [4.43]).

Various vapour flow enhancement mechanisms have been suggested to explain the observed higher vapour permeability. The "water island" or condensation-evaporation theory proposed by Philip and DeVries [4.44] acknowledges that some capillary condensation has occurred in the smaller pores or in the narrow necks of larger pores, and that this will accelerate the transfer of vapour. This hypothesis suggests that vapour is transported to the meniscus on one side of a pore, where it condenses, while at the same time a water molecule on the meniscus on the other side of the pore would then break free and begin moving along the vapour gradient (Figure 4.22). To reflect the fact that the actual length of vapour diffusion becomes less as more water islands form, this mechanism's effect might be modelled by an enhancement factor that increases with

increasing RH. Once a continuous phase of water forms (the critical moisture content), the enhancement factor should drop, until it reaches zero at capillary saturation (when there should be practically no transport by vapour diffusion).

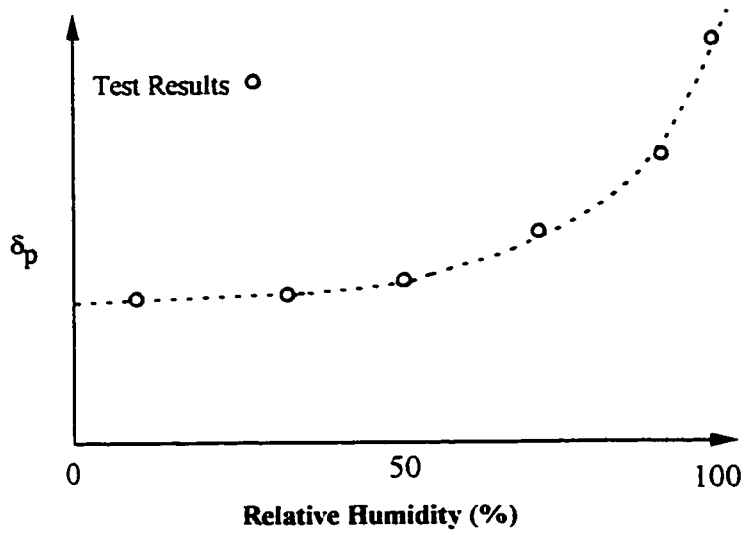

Figure 4.21: Vapour permeability test results for a representative hygroscopic porous material as a function of RH

A related explanation for increased vapour permeability with increasing RH is capillary transport in small pores (micropores) supplementing the mass flow of vapour. This could be termed a "water canal" effect. This mechanism is merely an extension of the evaporation-condensation theory but with liquid flow over larger distances.

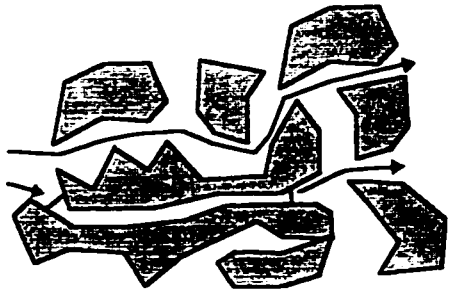

Figure 4.22: Water island / water canal vapour flow enhancement mechanism demonstrating parallel and series moisture flow

Finally, surface diffusion (discussed in the next section) will always be occurring in those pores not small enough to precipitate condensation, but large enough to contain thick adsorbed layers. Both Kuenzel [4.34] and Krus [4.48] maintain that surface diffusion may be sufficient to explain all of the observed increased vapour flow with increasing RH.

It is questionable if any of these enhancement phenomena should be labelled as vapour flow mechanisms (as Philip and de Vries did) or liquid flow mechanisms, since the increased flow is occurring in liquid, vapour and/or the adsorbed states. In reality a combination of series flow (e.g., diffusive vapour transport - condensation - liquid transport - evaporation - diffusive vapour transport) and parallel flow (e.g., surface diffusion in larger pores and capillary flow in smaller pores) is likely occurring. The relative importance of each proposed mechanism will theoretically vary with the pore topology, the pore size distribution, and the actual pore size distributions. In fine-pored materials, such as cement paste, micropore capillary transport will be very important, whereas in materials with mid-sized pores, such as brick, adsorbed flow may be dominant. In all cases there is no reason to believe that the three moisture phases are not interacting and transporting moisture over much of the moisture content range.

The reason for the sensitivity of vapour permeability to RH exhibited in Figure 4.21 is not explicitly addressed in most of the building science literature and is instead simply grouped with vapour flow due to Fickian vapour diffusion.

It is usually assumed that vapour is predominately transported through porous building materials by Fickian diffusion through the larger pores and that what is happening in small pores is not important to the total moisture flux. This may be a reasonable assumption, since the impact of the small pores on total porosity can be small. In any event, Knudsen diffusion, surface diffusion, and liquid flow are all likely taking place in the smaller pores, not Fickian diffusion.

Because the prediction of the vapour permeability of building materials has not received the same amount of attention as it has in other materials (e.g., soils, food, etc.) theory is unable to provide even reasonably useful values for vapour permeability. Therefore standardised tests must be conducted to find empirical material-specific isothermal vapour permeabilities, δ_p. The mass rate of vapour (m_v) diffusion can then be found from:

$$m_v = -\delta_p \cdot \nabla p_v \qquad \text{(Eq. 4.18)}$$

where m_v is the mass density flux of diffusive vapour flow ($kg/m^2 \cdot s$)

δ_p is the measured vapour permeability for a given material (kg/m·Pa·s), and

p_v is the vapour pressure (Pa).

Because this factor accounts for both Fickian and Knudsen transport, tortuosity, surface diffusion, micropore capillary conduction, etc., the measured permeability is only strictly valid for the conditions of the test.

A comprehensive description of vapour flow would have the form:

$$m_v = -D_v(w) \cdot \nabla \rho_v + D_{T,v}(w) \cdot \nabla T \qquad \text{(Eq. 4.19)}$$

$D_v(w)$ is the moisture content water vapour diffusivity (m^2/s),

$D_{T,v}(w)$ is the moisture content thermal vapour diffusivity ($m^2/K \cdot s$),

w is the moisture content (kg/m^3),

ρ_v is the water vapour concentration (kg water vapour / m^3).

The second term in Equation 4.19 describes thermodiffusion, or diffusive flow driven along a thermal gradient. This is also called the Soret effect and can be ignored as negligible in building applications since its value is usually several orders of magnitude less than the vapour (or total moisture) diffusivity [4.11, 4.34, 4.38]. Thermodiffusion is not to be confused with surface diffusion, which is greatly enhanced by thermal gradients because of relative humidity changes with temperature.

In practical situations, Fick's Law for one-dimensional diffusion through an n-layer assembly is normally simplified to:

$$M_V = \frac{1}{\frac{d_1}{\delta_{p,1}} \ldots + \frac{d_x}{\delta_{p,x}} \ldots + \frac{d_n}{\delta_{p,n}}} \cdot \Delta p_V \cdot A \cdot \Delta t \qquad \text{(Eq. 4.20)}$$

where, M_v is the total mass of water vapour transferred,

$\delta_{p,x}$ is the average vapour permeability of layer number x ($kg/(m^2 Pa\ s)$),

d_x is the thickness of material layer x (m),

Δp_V is the vapour pressure difference across the assembly (Pa),

A is the cross-sectional area (m^2), and

Δt is the time interval (s).

Even in the simplified analysis of practical building situations, the vapour permeability of a material layer cannot always be assumed to be constant. A comparison of the wet-cup and dry-cup vapour permeability values from the ASTM E96 test standard is useful for assessing the sensitivity of a material's vapour permeability to changing RH. If the wet-cup and dry-cup values are significantly different, the use of a constant vapour permeability is unlikely to yield accurate results and surface diffusion, or some other flow enhancement mechanism, is likely at work.

The liquid transport of salts to a layer, and the consequent deposition when the liquid water evaporates, can greatly decrease the vapour permeance of the material (by at least an order of magnitude) and result in reduced drying capacity. This effect, combined with subfluoresence (expansion caused when salts recrystalize within a material), has been shown to be the cause of several commonly experienced masonry, stone, and stucco-on-masonry failure mechanisms [4.45]. The effect of dissolved salts on moisture transport has many practical applications but has not been widely studied.

4.3.2 Adsorbed moisture surface diffusion

The thickness of the adsorbed layer of water molecules as a function of water content can be estimated by the modified BET equation. Adsorbed multi-layers are not as strongly tied to the pore walls as the first mono-layer and, of course, the molecules continue to vibrate (with slightly less energy than vapour molecules at the same temperature). If an area with several adsorbed layers adjoins an area with fewer adsorbed layers, there is a likelihood that the more loosely bound molecules from the thicker layer will jump free and settle on the more attractive site with fewer layers. The mass transfer of molecules by this mechanism is commonly termed surface diffusion, but is sometimes more accurately labelled surface flow. It is a diffusion process since the flow is driven by the mass density gradient of adsorbed water molecules.

Okazaki and Tamon [4.46, 4.23] proposed the random walk process or "hopping model" as described above. By accounting for the reduced attraction that holds each subsequent layer of adsorbed molecules to the surface they were able to improve the predictive ability of previous similar models by Hill [4.47].

Despite the strong experimental evidence supporting Okazaki and Tamon's model that has accumulated over time, surface flow is still sometimes modelled as a diffusive process driven by vapour pressure gradients. Adsorbed moisture will clearly be driven along

gradients of mass density. However, the magnitude of the transport function will vary with moisture content. As the RH increases, additional layers of adsorbed molecules will line the capillary walls. Thicker layers of adsorbate are attached less strongly than thin layers and so are more likely to move along the concentration gradient of adsorbed moisture along the pore walls. If a mass density gradient exists adsorbed flow will increase. Although the mass density gradient of adsorbed moisture is the true fundamental transport potential of adsorbed moisture, it is easy and accurate to use the RH or moisture content as a transport potential since the adsorbed layer thickness can be related to the RH and/or moisture content via the sorption isotherm.

The relative significance of adsorbed surface flow can be judged from the internal surface area of a porous material. For materials with a high proportion of small pores (e.g. cement paste, calcium silicate), adsorption tends to play a very significant role in moisture storage and transport. Confusing the issue is the fact that capillary condensation is also more likely in these materials at mid-range RH, and so coincident micropore liquid transport and "water island" effects are also possible.

As discussed in the previous section, the vapour permeability of many materials exhibits a strong moisture content or RH dependency (Figure 4.21). One of the several plausible explanations for this dependency is the surface diffusion of adsorbed water molecules. Hence, while vapour diffusion continues to move water vapour as the moisture content increases, the less-tightly bound adsorbed molecules begin to move from thick layers to thin. This process, shown in Figure 4.23, is well described by both Krus [4.48] and Kuenzel [4.29], and supported by some limited, but strong, experimental evidence. Daian also explicitly considers surface diffusion in his model [4.38,4.49].

Note that the thickness of the adsorbed layers is not a linear function of RH, but rather is a function of the moisture content -- the BET model assumes that each additional layer of adsorbed moisture adds a certain amount of mass. The reason for the distinction between RH and moisture content, which should be directly related by the sorption isotherm, is that the adsorbed moisture diffusivity will change in a more direct way with moisture content.

Surface diffusion would be expected to increase with moisture content. However, a non-linear dependence might be expected for each additional increase in moisture content because each additional layer of adsorbed molecules is held less firmly than the previous. Also, as the RH and the moisture content increase, capillary condensation will occur in the smallest pores. This capillary condensate may aid vapour transport by the water-island

effect and can also move moisture by liquid conduction but it will not allow surface diffusion to occur[†]. As the proportion of condensate-filled pores increases, the rate of surface diffusion will continue to increase in the remaining open pores but the proportion of pores in which surface flow is possible will decrease. As the moisture content increases, capillary condensation will fill pores and counter-act the increasing ease of surface diffusion.

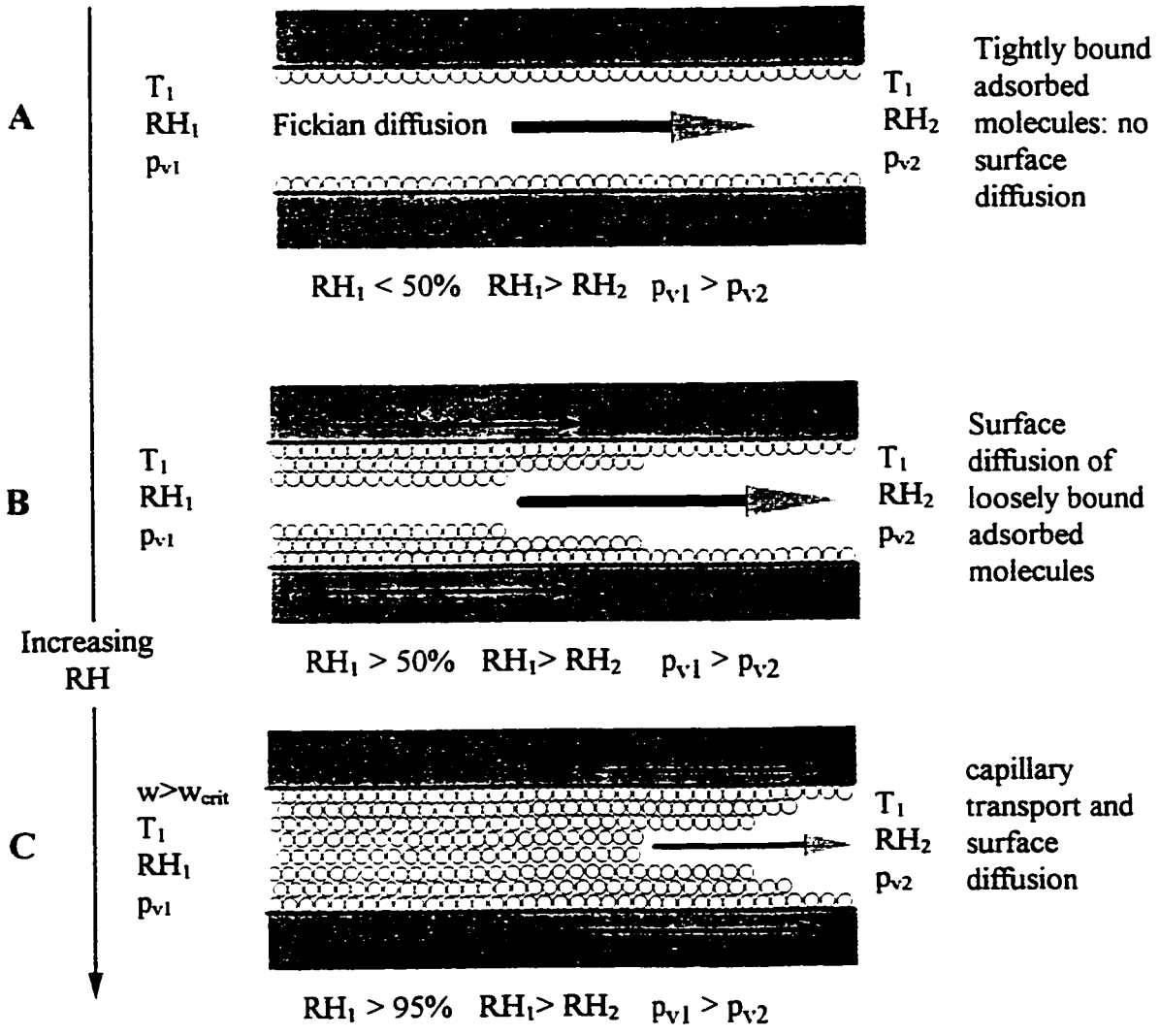

Figure 4.23: Isothermal vapour and surface diffusion as a function of material RH

[†] In fact, surface diffusion is very likely occurring during liquid conduction, since the attraction between the pore walls and nearby water molecules will not change when the pore is filled with water molecules. Adsorbed surface diffusion and liquid capillary transport are likely not physically clearly divided.

The behaviour of some materials under non-isothermal conditions provides strong evidence for the theory presented in Figure 4.23. Under a temperature gradient, the vapour pressure gradient can be sloping in a different direction than the relative humidity gradient (Figure 4.24). Since vapour pressure drives diffusion and relative humidity indirectly drives surface diffusion, complex moisture transport scenarios are possible. As Kuenzel [4.34] pointed out, this is of practical concern because most building enclosures in cold climates during winter separate indoor environments of low RH (30%) and moderate vapour pressure (e.g., 700 Pa) from outdoor environments of high RH (>80%) and low vapour pressure (e.g., < 200 Pa). In this situation surface diffusion is expected to drive flow in the opposite direction as vapour diffusion.

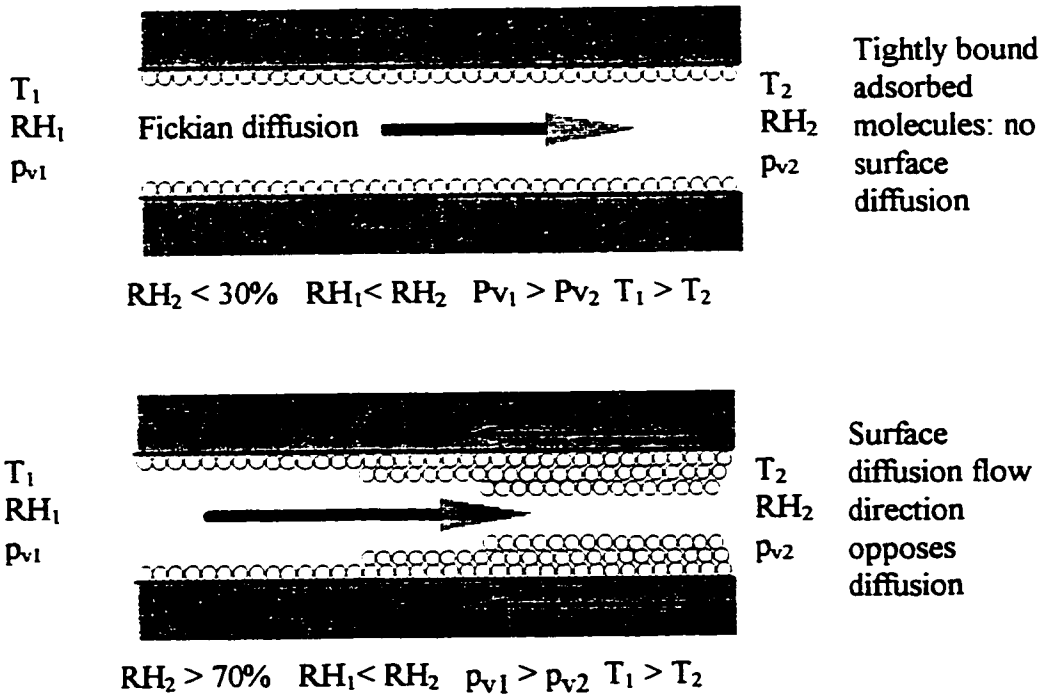

Figure 4.24: Vapour and surface diffusion under a temperature gradient

Under non-isothermal conditions (i.e., most building science situations), serious over- and under-estimations of moisture flow can result from the use of vapour diffusion model to predict surface diffusion. The theory behind Figure 4.24 strongly suggests that surface and vapour diffusion moisture flow should be dealt with as separate mechanisms when predicting moisture flow through porous media with a thermal gradient, especially those materials with a significant proportion of small pores. Moisture transport through materials composed of fine fibres (e.g., paper, cloth, mineral fibre scrims, etc.) may also be strongly influenced by adsorbed surface flow. Confusion is often caused because the

prediction of isothermal flow, (that which is measured in laboratories most of the time) will not be affected by lumping surface diffusion and Fickian vapour diffusion into one mechanism. Under isothermal conditions, a relationship with the same form as vapour diffusion transport (Equation 4.16) can provide accurate predictions, because the relative humidity gradient is directly related to the vapour concentration (or pressure) gradient.

While Kuenzel [4.34] prefers to include the influence of surface diffusion as part of liquid transport, Daian [4.38] and others include it in the vapour flow diffusivity with a special temperature dependency. In either case, the RH dependent nature of the surface diffusion should be taken into account.

For surface diffusion flow, i.e., transport of moisture in the adsorbed phase, the following relationship is recommended:

$$m_a = - D_a(w) \cdot \nabla w \qquad \text{(Eq. 4.21)}$$

where m_a is the mass flux density of adsorbed moisture flow ($kg/m^2 \cdot s$),

w is the moisture content (kg/m^3), and

$D_a(w)$ is the moisture content dependent adsorbed moisture diffusivity (m^2/s)

4.3.3 Liquid moisture transport

This section will consider liquid transport, although it should be clear by this point that the separation of liquid, adsorbed, and vapour phase transport is not clearly delineated, i.e., thick adsorbed layers and capillary condensate in micropores can behave like a liquid.

4.3.3.1 Saturated Flow

Flow through an oversaturated (Region E) porous material under external forces is termed saturated flow. Since internal capillary forces are in equilibrium in this region, moisture flow will not be driven along a gradient in moisture content. Therefore, saturated flow will only occur when driven by gradients of air pressure of hydraulic head. Although saturated flow is not often of practical importance in building science, an understanding may be necessary to describe gravity drainage from saturated porous materials.

Water flow through a fully saturated porous media is usually modelled using Darcy's empirical law:

$$m_l = k_l \cdot \nabla P \qquad \text{(Eq. 4.22)}$$

where m_l is the mass flux density of liquid water flow (kg/m^2 s),

k_l is the hydraulic conductivity (kg/m·s·Pa) and

P is the pressure (also called suction or hydraulic potential) (Pa).

The term hydraulic potential (in units of m of head or Pa) is borrowed from soil science. It can include components of gravity head, air pressure, and differential water pressure.

The hydraulic conductivity or Darcy coefficient is affected by temperature through the temperature dependency of the viscosity of water. A standard means of correcting for temperature in soil science is [4.50]:

$$k_l(T) = \frac{\rho \cdot g}{\mu(T)} \cdot K \qquad \text{(Eq. 4.23)}$$

where K is the intrinsic hydraulic conductivity or permeability coefficient (m^2), a function of the nature of the porous body only

$\mu(T)$ is the temperature dependent dynamic viscosity of water (1000 Pa·s at 20°C),

ρ is the density of water, and g is the acceleration due to gravity.

The temperature effect is not insignificant: the hydraulic conductivity at 0°C is only 56% of the conductivity at 20°C. Below 0°C, the hydraulic conductivity is assumed to be zero.

There have been numerous attempts to predict the hydraulic conductivity from the characteristics of the pore space. For soils, Hazen [4.50] showed that an approximate value for k is given by:

$$k_l = 10^{-8} \cdot D^2_{eff} \qquad \text{(Eq. 4.24)}$$

where D_{eff} is the effective particle size (m).

The value of k_l is in units of m/s for use in Darcy's equation with hydraulic potential expressed in m of head. While predictions can be relatively accurate for materials with unfused, well-graded, spherical particles, (sometimes a practical assumption in soil sciences), the prediction of porous building materials' properties is more difficult.

The Darcy coefficient in Equation 4.22 is reasonably constant so long as the material is fully oversaturated, i.e., so long as all pores remain full. In fact, the Darcy coefficient used in soil science is sensitive to the amount of air in the water: deaired water must be used to ensure that two-phase unsaturated flow permeability is not measured. Depending on the size of the pressure driving flow, small capillaries may not participate in flow if capillary suction is stronger than the applied hydraulic gradient. Water in these small capillaries will be retained by capillarity.

In general, Darcy's law applies to laminar flow (i.e., slow, percolating flow) defined as a Reynolds number of less than about 10. In course-grained materials, Darcy's law may not apply for fully saturated flow, and recourse to the more complete Navier-Stokes equation may be required.

4.3.3.2 Unsaturated Flow

As noted above, in most building science applications unsaturated flow, i.e., two phase (air and water) moisture flow through a porous body is of much more practical interest than saturated flow. Saturated flow is driven primarily by gradients in moisture content which generate gradients in capillary suction pressures. Relative to capillary pressures, wind-induced air pressures, and hydraulic head are rarely large enough to influence unsaturated flow.

Many authors have attempted to model the flow of liquid water through unsaturated media by assuming the pore space is a bundle of parallel tubes, notably Krischer's analysis of the drying process [4.51, 4.52]. The advantage of the parallel-tube approach is that laminar fluid flow through a single pipe can be predicted using the simple Hagen-Poiseuille equation:

$$Q = \frac{\pi \cdot P \cdot r^4}{8 \cdot \mu \cdot L} \qquad \text{(Eq. 4.25)}$$

where Q is the volumetric flow rate of liquid water (m^3/s),

P is the pressure difference (Pa) along the flow path,

r is the equivalent radius of the pore or crack (m),

μ is the dynamic viscosity of water (1000 Pa·s at 20°C) and

L is the length of the flow path (m).

The Hagen-Poiseuille equation can be re-arranged in terms of viscous friction-induced pressure. The fluid friction pressure induced by a flow is:

$$P = \frac{8 \cdot Q \cdot \mu \cdot L}{\pi \cdot r^4} \qquad \text{(Eq. 4.26)}$$

An examination of both forms of the Hagen-Poiseuille equation shows that:

1. the resistance to flow decreases as the fourth power of pore radius,
2. the flow quantity increases linearly with pressure (or capillary suction pressure) and,
3. the flow quantity decreases as the inverse of flow path length.

The absorption of water into a porous material is driven by capillary suction and is slowed by viscous drag with the pore walls. Water absorption cannot, however, move through all pores because of trapped air bubbles in dead end pores; the only means for this air to escape is by gas diffusion into the water, a very slow process.

If a dry material is placed in contact with water, the effective Darcy permeability coefficient will change drastically with moisture content as the smaller pores are filled first (capillary suction draws the water into the smaller pores first) at the expense of the larger pores. However, as Equation 4.26 shows, the resistance to flow increase as the fourth power of pore radius. Therefore, as a material dries and the water content of the material decreases, the largest pores no longer participate in the flow (since they empty first) and the resistance to flow increases.

Water flow through a capillary porous body could be estimated by calculating the flow through each small pore or crack using the Hagen-Poiseulle relation and then summing the results. Unfortunately, the pores in real materials have short lengths (perhaps 3 to 100 times the pore radius), are highly interconnected, and are variable in cross-sectional area.

Series models, which string several different pore sizes and lengths together in series are simple extensions of the parallel tube model which attempt to incorporate some of the variations of the pore space. A major flaw with both the series and parallel-tube approach is that these models ignore the interconnectivity of pores in the direction normal to the flow direction.

Various network models have also been employed using electrical analogies, etc. These models attempt to include the effect of the pore space properties perpendicular to the direction of flow. This approach was first used by Fatt [4.53], but has been revisited by many other researchers. The fundamental difficulty with these approaches is the proper modelling of the pore space: the distribution of size, length, number, and nature of pores are major variables. Although these variables can be manipulated so that a model predicts the measured permeability of a porous material, there is no guarantee that the chosen mix of variables will also predict the behaviour of materials slightly different than the test specimen that was used for calibration.

Percolation theory attempts to more accurately model the behaviour of water flow through a porous body. The advantage of percolation theory is that it accepts that the pore properties are randomly distributed throughout the material. Descamps [4.26] has provided a recent summary of network theory and advanced the use of percolation theory for the prediction of unsaturated liquid moisture flow.

Because a rigorous and reliable theory has yet to be developed, unsaturated flow is often modelled using a moisture content dependent moisture diffusivity:

$$m_l = -D_l(w)\cdot\nabla w \quad + D_{T,l}(w)\cdot \nabla T \qquad \text{(Eq. 4.27)}$$

where m_l is the liquid moisture mass flux density ($kg/m^2 \cdot s$)

$D_l(w)$ is the moisture content dependent liquid moisture diffusivity (m^2/s)

$D_{T,l}(w)$ is the moisture content dependent thermal liquid diffusivity ($m^2/ (K \cdot s)$)

and w is the moisture content (kg/m^3)

The liquid diffusivity is usually derived from experimentally measured isothermal moisture fluxes.

The second term in Equation 4.27 is usually ignored because its effect is one to several orders of magnitude smaller than the isothermal liquid diffusivity [4.39].

4.3.4 The moisture transport function

Equations 4.19 , 4.21 and 4.27 provide general transport functions for unsaturated flow of each of the fluid water phases in a porous material: vapour, adsorbed, and liquid.

(Saturated flow is not generally important in building enclosures). The rate of moisture flow for each phase is governed by material-specific diffusivities. It will be noted that the driving potential for vapour flow and adsorbed and capillary transport are different. Vapour pressure gradients drive vapour diffusion, relative humidity gradients drive surface diffusion, and suction pressure gradients drive liquid flow. The temperature dependencies of each of the diffusivities also varies at a different rate. For all of these reasons, the development of a general moisture transport function for a given material under gradients of moisture content, temperature and vapour pressure is very difficult.

Figure 4.25 shows magnitude and variation of the various isothermal moisture diffusivities as a function of moisture content for a hypothetical hygroscopic porous material at a certain temperature. At the lowest moisture contents, Knudsen diffusion controls vapour flow and tightly bound adsorbed molecules cannot easily move. As the moisture content increases, Fickian vapour diffusion steadily decreases as the smallest pores fill with water. At moisture levels over about 30% RH, surface diffusion of adsorbed moisture begins, and becomes important in the 50 to 90% RH range. Surface diffusion may continue up to full saturation. Liquid transport of condensed water may begin in the smallest pores at moisture contents as low as 30%, but only becomes significant as RH exceeds 90%. At around 95%, liquid transport becomes the dominant mechanism and increases as capillary saturation is approached. By necessity, the liquid moisture diffusivity becomes equal to the hydraulic conductivity when the moisture content surpasses the capillary saturated level (e.g. when $\psi = \psi_{cap}$).

The above is a simplified description for a hypothetical material. Depending on the material and the boundary conditions, each of the three transport functions will have different shapes and magnitudes.

The transport functions for each of the moisture phases are shown and the total moisture diffusivity is assumed to be:

$$D_m(w) = D_v(w) + D_a(w) + D_l(w) \qquad \text{(Eq. 4.28)}$$

The total moisture transport function might have the form:

$$m_m = -D_v(w)\cdot\nabla\rho_v - (D_a(w) + D_l(w))\cdot\nabla w \qquad \text{(Eq. 4.29)}$$

If Equation 4.29 is used in a finite-volume computer program, the important temperature and moisture content dependencies are already incorporated in the choice of driving

potentials and diffusivity functions. Some models use the moisture content (in various forms, e.g., mass or volumetric measures) directly or employ the RH and suction isotherm to couple moisture content with vapour pressure and capillary suction.

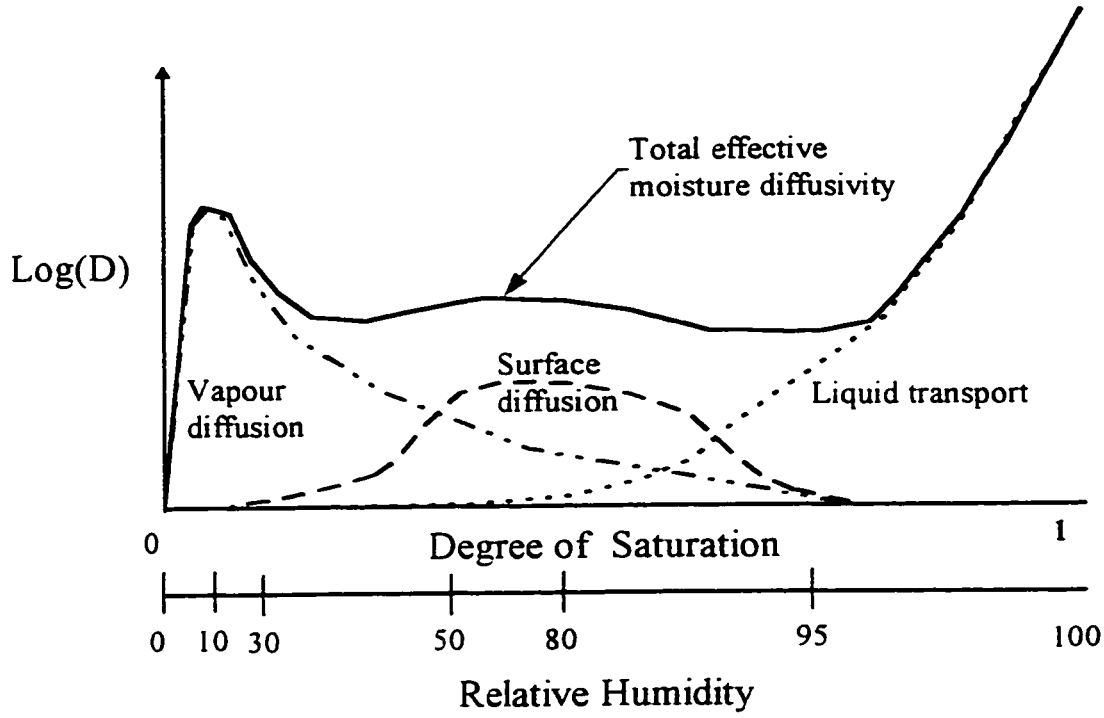

Figure 4.25: Hypothetical total isothermal moisture transport function
Note: The saturation and RH scales are not linearly related because the moisture storage function is not a linear function.

Supported by experimental evidence of simple materials, Imakoma et al [4.54] have shown that the separation of the three moisture transport functions is viable. In fact, using the theory presented above (with detailed quantification of the chemical constants), they have predicted both the moisture storage and moisture transport function from pore size distribution information. Their model accurately predicted experimental results of the drying process. Although much more work is necessary, this is a promising research direction.

4.3.4.1 Experimental Measurements of Total Moisture Diffusivity

The advent of specialised experimental equipment, such as Nuclear Magnetic Resonance (NMR), gamma ray scanning, and neutron transmission, allows highly accurate (e.g., 1-2%), high speed (10 to 60 s per reading) non-intrusive measurements of moisture content with a spatial resolution of 1 to 3 mm. Although these measurements are normally taken

under isothermal conditions, the results they provide are exceptionally useful. Moisture content profiles measured during wetting, redistribution, and drying can be used to calculate a "best-fit" total moisture diffusivity assuming an equation of the form:

$$m_m = D_m(w) \cdot \nabla w \qquad \text{(Eq. 4.30)}$$

Since the coefficient, $D_m(w)$, is an aggregate value which describes the transport of moisture by all mechanisms (e.g. Knudsen and Fickian diffusion, surface diffusion, capillary transport), it is in fact a purely empirical phenomenological factor that is only valid for the conditions of the test. The driving potential shown in Equation 4.30 is the moisture content, but the different driving forces (vapour pressure, RH/suction) will be represented in the total diffusivity calculated from the measured profiles. In isothermal tests, this is valid since vapour pressure is linearly related to RH, and RH and suction stress are essentially the same measure (via Kelvin's equation and the sorption isotherm).

Keey [4.51] was apparently the first to point out what the more detailed measurements of Krus [4.48,4.55], Kuenzel [4.34], Winter [4.56], and Daian [4.38] have all shown: the wetting (suction), redistribution and drying moisture transport functions are different, often by a large margin. Adan's measurements of the moisture diffusivity of gypsum plaster [4.17] has shown that the moisture diffusivity of transient RH variations was significantly different (two or three orders of magnitude) than either the wetting or drying values. Typically, the diffusivity during wetting is an order of magnitude less at low moisture contents than for redistribution. Krus [4.48] found that some materials exhibited a far greater difference (more than two orders of magnitude) while other materials showed almost no difference. Although Pel [4.28] conducted both wetting and drying measurements, he combined the results of the two processes to generate his total diffusivity results and made no comments regarding the need for different diffusivity functions.

Exactly why there is a need for different functions is neither fully understood nor predictable. The different behaviour of porous media to capillary suction and redistribution are, however, qualitatively predicted by the percolation theory discussed earlier. Sorption isotherms and capillary pressure curves also both exhibit hysteresis and various theories to explain this hysteresis have also been presented earlier. As discussed, wetting by immersion in water is expected to occur quickly because the large pores offer less resistance to flow, while redistribution occurs more slowly through the smaller pores which have stronger capillary suction, but more flow resistance.

As part of the Annex 24 project [4.57], samples of carefully selected Eastern white pine were prepared and the total moisture diffusivity calculated from moisture content profiles during wetting by four different groups in four countries. The results are shown in Figure 4.27.

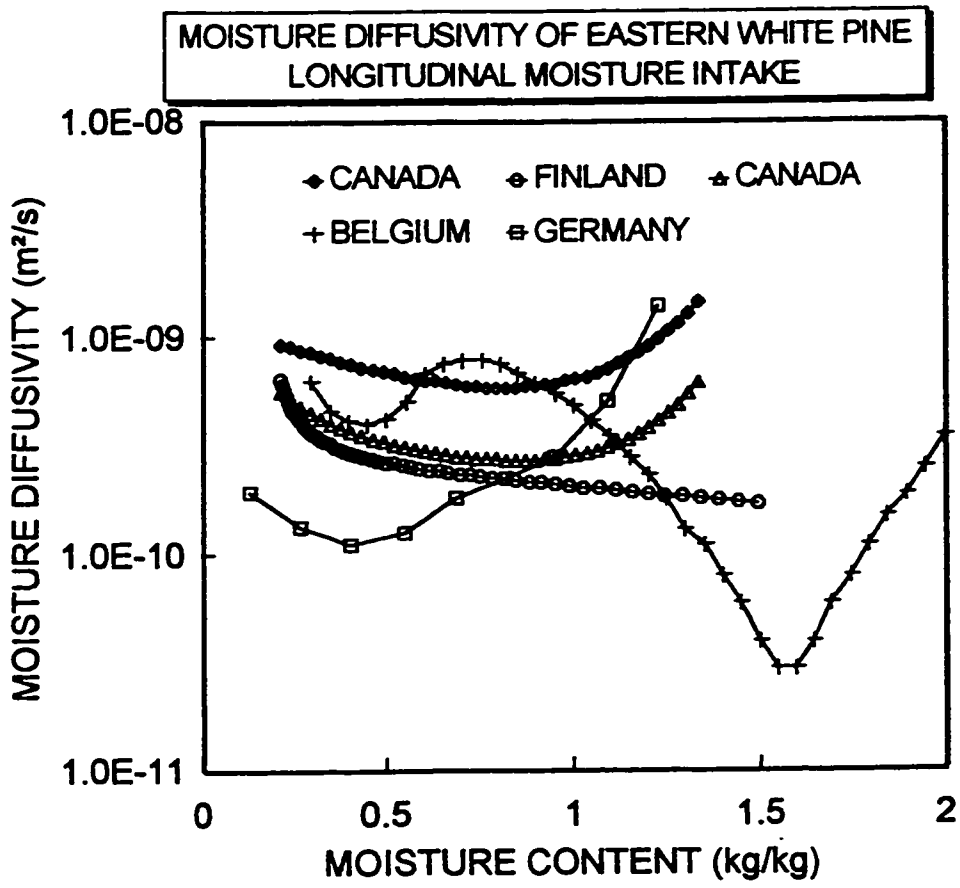

Figure 4.26: Comparison of total moisture diffusivity for pine from same sample by four different laboratories

Two important observations can be made from these results. First, the moisture diffusivity is obviously a material property that is difficult to measure accurately. The values between different materials (calcium-silicate) and between the same materials (pine) measured by different labs exhibits variability of the same order. Secondly, while the magnitude of the results are of the same order of magnitude at high moisture contents, the shape may be quite different, especially at low moisture contents.

Measuring procedures and equipment are apparently not the major or only cause of the different results. As part of the same Annex 24 project, moisture content profiles during

the wetting of a spruce specimen were provided to the same participants. The resulting moisture diffusivities, shown in Figure 4.28, have quite different shapes. Clearly, enough data points must be provided so that the artefacts of interpolation and least-error fits used by different researchers have no effect on the results.

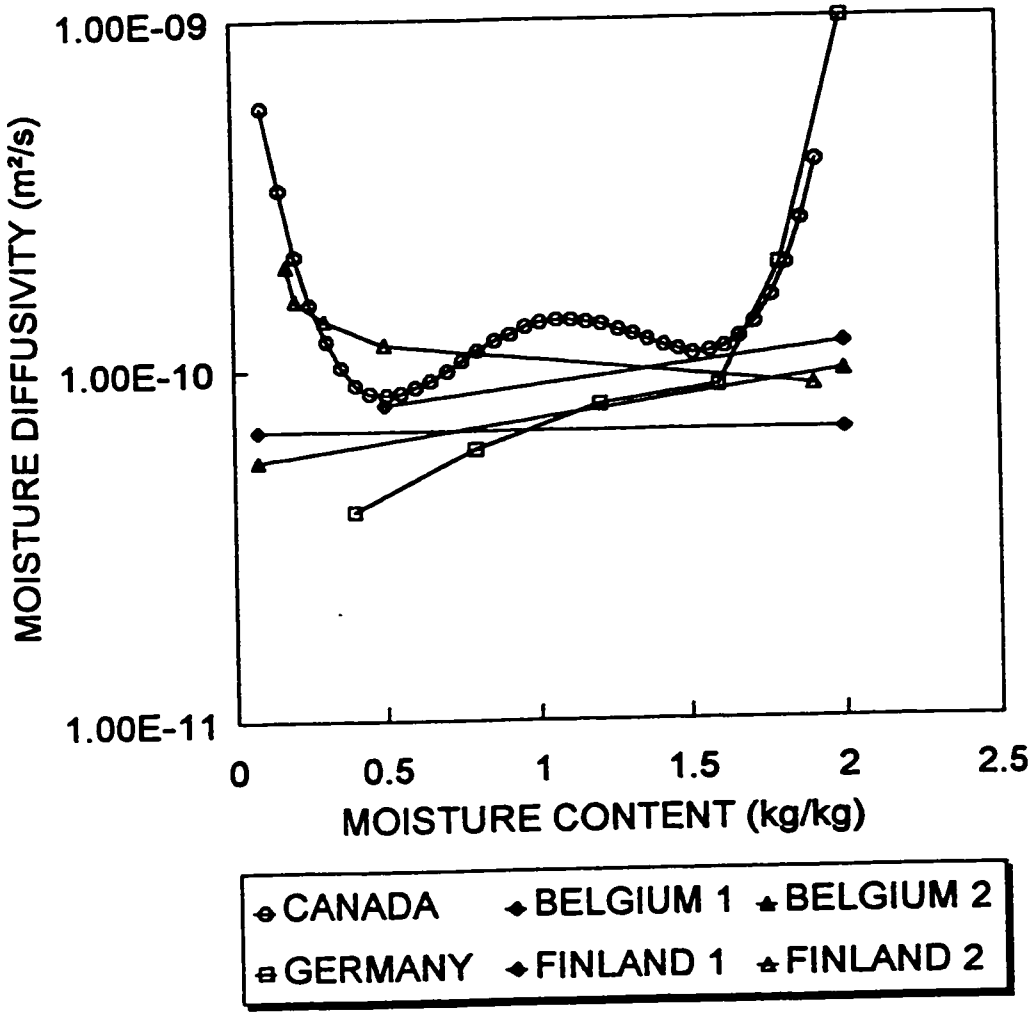

Figure 4.27: Comparison of total moisture diffusivity of a spruce sample calculated from the same measured moisture content profiles

At low moisture contents, the accuracy of measurements tends to be relatively poor, but the transport of moisture is important in this range for the understanding and prediction of drying. It should be noted that Pel [4.28] measured the velocity of the drying front and used this velocity to more accurately calculate the total diffusivity in the low-moisture content drying range. Pel's apparatus also provided a spatial resolution of the order of 1

mm whereas the accuracy of Krus's [4.48] was about 3 mm. Although the low moisture content region is difficult to measure, Pel's characteristic skewed-U shape does match the theory presented earlier. (Note that this shape is dependent on the pore size distribution).

Several researchers have found that an exponential curve fit matches the liquid diffusivity data. A popular form is:

$$D_l(\psi) = D_0 \cdot \exp(\beta \cdot \psi) \qquad \text{(Eq. 4.31)}$$

where D_0 is a constant (m^2/s), and

β is a fitting exponent.

Pel [4.23], who used this form, found that the product $\beta \cdot \psi$ was, as a rough approximation, equal to 7.5 for several inorganic porous building materials, and quotes Kalimeris [4.58], who found the same. This information may be useful for a simple analysis when no other information is available. However, some materials, like gypsum have been found to violate the exponential form.

Kuenzel, who prefers to use a non-dimensional moisture content, w/w_{cap}, has found the following approximation to hold for many inorganic porous materials [4.34]:

$$D_l(w) = 3.8 \cdot (A / w_{cap}) \cdot 1000^{(w/w_{cap})-1} \qquad \text{(Eq. 4.32)}$$

The use of the absorption coefficient, A, and the saturation moisture content, w_{cap}, allows simple lab tests to be used as a guide in generating liquid moisture diffusivity.

4.3.5 Moisture transport across interfaces

Mass transfer (wetting, capillary transport, evaporative drying and diffusion) at exterior surfaces and inter-layer interfaces is another complex aspect of moisture transport through building enclosures. Although the moisture transport function can be used across interfaces, this approach is in fact an approximation. Surface resistance to vapour flow and interface or contact resistance to capillary and adsorbed moisture transport exist and may be significant in some cases.

If two material layers are in direct physical contact, the normal liquid transport function is theoretically valid. However, the definition of "direct contact" is unclear. Since moisture transport primarily occurs through very small capillaries and pores, direct contact is

exceptionally unlikely to occur in real building assemblies. Where such contact is desired, special material layers, like bentonite, might be used as they are in pressure plate apparatus tests.

When materials are not in direct contact, only vapour flow is possible. However, vapour flow can also be interrupted at interfaces. Small interruptions in material contact or changes in thermal resistance will precipitate condensation at interfaces because of small temperature changes across the interface. Many building materials also have higher vapour resistances at their exterior surfaces because of the manufacturing process (e.g., extruded polystyrene exhibits a surface skin, and the outer layers of concrete, plaster and extruded bricks are all more dense and less vapour and liquid permeable).

Because dissolved salts can only be transported in liquid form, not vapour, understanding liquid transport across interfaces is very important for the prevention and understanding of expansive salt recrystallization damage.

4.3.5.1 Liquid Water Transport Across Interfaces

Although wetting of a material by liquid water on the surface is governed by normal liquid transport laws, the effect of interfaces almost always retards liquid water flow, sometimes significantly. Moisture transport across interfaces is a relatively unexplored, yet important area of moisture transport research.

Holm et. al. [4.59] found that the nature of the bond between plaster and brick results in a significant "contact resistance" (to borrow heat flow terminology) that could result in significant errors in modelling moisture behaviour. Krus showed that [4.48] he could model the capillary transport between two material layers (natural stones) if hydraulic contact was ensured through the use of kaolin (a clay with very fine pores and good capillary conductivity). In related research, Groot [4.60] and Brocken [4.61] have also found that there are hydraulic discontinuities in the mortar to brick interface.

Bomberg [4.62] investigated the importance of very small cracks and separations in his work on moisture transport. He showed that for some materials, simple contact ensured much faster moisture transport than across a 1 mm space, but for other materials the 1 mm space affected moisture transport very little.

Clearly, the importance of interface transport depends on the relative magnitude of the test materials' vapour and liquid diffusivities. If two materials which are very capillary active

but reasonably vapour impermeable (e.g., brick and cement plaster), the nature of the interface is critical to moisture transport. Results from the research referenced above suggest that liquid transport will be an order of magnitude less at masonry-mortar interfaces. For materials that are capillary inactive or hydrophobic but vapour permeable (e.g., mineral wool insulation and acrylic stucco), even a visible gap will not significantly reduce the moisture flux between layers.

4.3.5.2 Water Vapour Transport Across Interfaces

Vapour transport within enclosures is rarely influenced by imperfect inter-layer contact since still air is far more vapour permeable than most building materials. However, vapour flow at exterior surfaces is affected by equivalent surface resistances and a combination of convective and diffusive transport effects. Moisture transport from a free surface by pure vapour diffusion is unlikely to occur in most situations since some air flow is always present, either because of driving forces from outside the system or because evaporation induces temperature and vapour gradients that result in air flow.

The mass flow of air across the surface of a material can accelerate drying because moving air over a surface almost eliminates the resistance of stagnant air to diffusion. Exchanging the air adjoining a wet material with dry air ensures that the vapour pressure difference between the air and the material surface (and hence the drying rate) will remain the same. Perfect mixing is a general assumption in building sciences, but the validity of this assumption depends on the vapour pressure differentials, flow rate, and flow path. The air flow also transports the sensible heat energy necessary for the phase change.

The combined effect of diffusion and the convective boundary layer is normally accounted for in the same way as for heat flow at surfaces: by the use of a fictitious equivalent coefficient. Therefore, the rate of vapour transfer for a film of liquid water at an exterior surface to the ambient air can be found from:

$$m_v = g \times \Delta p_v \qquad \text{(Eq. 4.33)}$$

where g is the effective convection-diffusion surface mass transfer coefficient,

and ΔP_v is the difference in vapour pressures between the drying surface and the ambient air.

The magnitude of this surface film coefficient is not well known for the pure diffusive case. In laboratory vapour permeability tests, Burch [4.63] found a water vapour transfer

coefficient of 2.87 x 10^{-6} g/(Pa·m²·s). This value was arrived at by using a special experimental technique to eliminate all convective effects.

In real building science situations thermal- and moisture-induced convective air flows over surfaces are inevitable. Therefore, most coefficients measured in the field are an order of magnitude larger than the purely diffusive case. For example, the mixed diffusive-convective mass transfer coefficient has been reported as ranging from 13.4x10^{-6} g/(Pa·m²·s) for saturated earth in a subfloor crawl space, 25 x10^{-6} g/(Pa·m²·s) for swimming pools during calms [4.64] and between 17 and 102 x10^{-6} g/(Pa·m²·s) for saturated brick wall samples exposed to wind speeds of 1 to 8 m/s [4.65]. Künzel has found that an exterior surface mass transfer coefficient coefficient of 75 x 10^{-6} g/(Pa·m²·s) allowed for good computer model approximations to measured values [4.34] and Karagiozis has used a value of 15 x 10^{-6} g/(Pa·m²·s) in computer modelling [4.66].

The accelerated drying caused by air flowing over a surface can be calculated for many geometric, temperature, and flow conditions by using the Lewis correlation of heat transfer - mass transfer analogy [4.67, 4.68]. The mass transfer coefficient can be defined in terms of the equivalent conductive-convective heat loss coefficient, h_c, as [4.69]:

$$g = \frac{h_c}{R_{wv} \cdot T \cdot \rho \cdot c_p} \qquad \text{(Eq. 4.34)}$$

where R_{WV} is the gas constant for water vapour (J/kg·K),

T is the absolute temperature (K),

ρ is the air density (kg/m³), and

c_p is the specific heat capacity of air (J/kg·K).

This relationship is very useful because h_c has been defined theoretically and empirically for a wide variety of flow conditions and geometries, whereas the mass transfer coefficient, g, is known for only a few cases.

Substituting typical values for air and water vapour into the Lewis correlation, the moisture transfer coefficient, g, can be found as:

$$g = \frac{h_c}{R_{wv} \cdot T \cdot \rho \cdot c_p} = \frac{h_c}{461.5 \cdot 273 \cdot 1.2 \cdot 1004}$$

$$= 6.4 \times 10^{-9} h_c \qquad \text{(Eq. 4.35)}$$

where g is in units of $kg/m^2 \cdot s \cdot Pa$ and h_c is in $W/m^2 \cdot K$

For exterior and interior surfaces under average conditions, typical average heat transfer coefficients are 20 and 8 $W/m^2 \cdot K$ respectively, of which the combined effect of convection and conduction comprises about 15 and 5 $W/m^2 \cdot K$ respectively [4.70]. Average equivalent heat transfer coefficients for interior conditions can be as low as 2 near corners and behind furniture (i.e., conditions with almost no natural or forced convection), and exterior values as low as 10 can occur in sheltered locations on calm days. Figure 4.29 shows the range of values that can be expected for typical cladding materials as a function of windspeed. As can be seen from the intercept value, radiation, conduction and natural convection make up about 8-12 W/m^2 of the heat transfer coefficient and forced convection makes up the rest. For an air velocity of 4 m/s (an average wind speed in most parts of the world) the convective component for brickwork can be seen to be about 15 W/m^2.

The small size (300 x 300 mm) of the specimens used in the experiment results presented in Figure 4.29 suggests that the rate of convection is probably higher than that of a typical 6 m square house wall, or a 20 m square apartment building. Based on work by several other researchers, Duffie and Beckman [4.71] developed a simple equivalent heat transfer equation for solar collectors mounted on buildings:

$$h_c = 8.6\ V^{0.6}/L^{0.4} \geq 5\ W/m^2 \cdot {}^{\circ}C \qquad \text{(Eq. 4.36)}$$

where, V is the wind velocity (m/s)

and L is the cube root of the building volume (m).

For a small, 2-storey house exposed to a 4 m/s windspeed, Equation 4.35 yields a value of 9.6 $W/m^2 \cdot {}^{\circ}C$. A large cubical apartment building of 20 m on a side is predicted to have an average equivalent heat transfer coefficient of about 6 W/m^2. Natural buoyancy and small local wind eddies are likely to ensure that transfer coefficients do not fall below about 5 $W/m^2 \cdot {}^{\circ}C$.

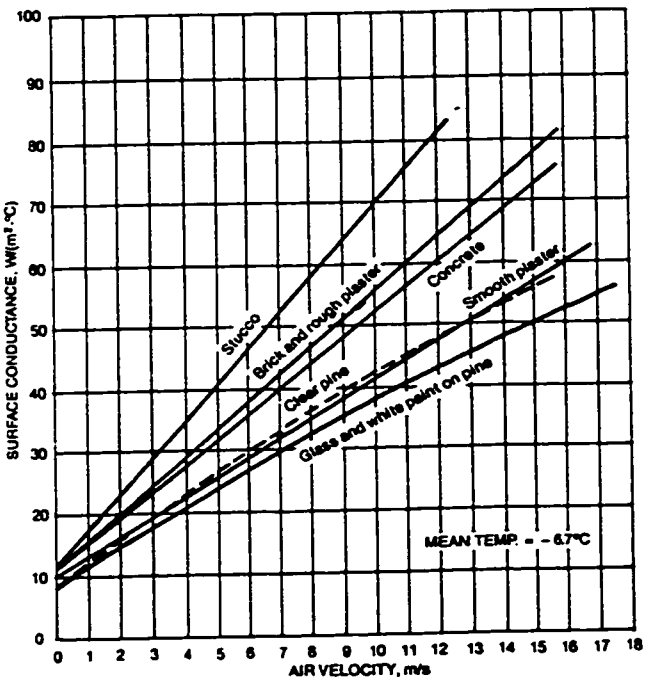

Figure 4.28: Equivalent surface heat transfer coefficients for different 300 mm square surfaces [4.72] (Fig 1, Chpt 22, ASHRAE 1993)

By substituting heat transfer coefficients of 5 and 15 W/m^2 in Equation 4.34, it can be seen that g will typically take on values ranging from 32 and 96 x 10^{-6} g/(Pa·m^2·s) respectively. Higher values near corners and projections and rougher surfaces can be expected. This range of values matches the controlled field measurements of Schwarz [4.65] on building surfaces (he measured values that ranged from 17 to 102 g/Pa·m^2·s) well. It can be concluded that field measurements and calculations from the Lewis correlation match well.

As a surface dries the latent energy required for the evaporation of liquid water will depress the temperature at the surface and hence reduce the vapour pressure, resulting in an apparent mass transfer coefficient that is somewhat lower. Therefore, to predict surface drying, either an accurate assessment of surface temperatures which includes latent heat effects must be conducted or a lower equivalent mass transfer coefficient should be used.

4.3.6 Convective water vapour transport

The convective flow of air can transport significant quantities of water vapour. Air leakage driven by mechanical pressurisation, wind pressures of building stack effect

(forced convection) and internal stack effect (natural convection) cause air flows through and within enclosure assemblies that also transport water vapour.

The flow of air through porous materials is governed by the Navier-Stokes equation. For the laminar flow regime encountered in most porous building materials, Darcy's simplified equation is usually an acceptable approximation:

$$m_a = k_a \cdot \nabla P \qquad \text{(Eq. 4.37)}$$

where m_a is the mass flow rate of air (kg/s),

k_a is the air permeability (kg/m·Pa·s), and

P is the total air pressure (Pa).

Flow through openings and cracks, however, is usually more significant than flow through porous materials. The air permeability of most building materials is less than 10^{-8} kg/m·Pa·s [4.11, 4.73, 4.74], which means that air flow through even small cracks, i.e., of the order of 1 mm, are much more significant to air flow. Low-density mineral fibre insulations are the most important practical exception.

The mass flow rate of water vapour $m_{v,conv}$, due to convective air flow can be described by:

$$m_{v,conv} = m_a \cdot W_a \qquad \text{(Eq. 4.38)}$$

where W_a is the humidity ratio of the air (kg/kg) = M_v / M_a, and

m_a is the mass flow rate of dry air (kg/s).

Very detailed modelling of the physical system, material properties, and fluid dynamics is required to accurately and usefully assess convective vapour transfer. The precise geometry of the flow path is very difficult to define for many building science problems. The extreme sensitivity of the calculated air flow (and thus moisture and heat flow) to the assumptions of how the building system is modelled severely limits the accuracy, and even usefulness, of modelling air flow. Modelling the flows as if it were through a series of cracks, as Kronvall has done in detail [4.73], may be just as useful.

4.4 The Wetting Process

As outlined in Chapter 2, wetting of materials comprising the building envelope occurs primarily because of:

1. condensation of water vapour (transported by diffusion or convection),
2. rain water penetration and absorption, or
3. capillary transport from other wet materials.

Wetting occurs when water vapour is adsorbed, liquid water is drawn into the pores by capillary forces, or external forces drive liquid water into an already saturated material. Moisture is redistributed within the materials and layers of an enclosure assembly primarily by liquid transport (capillary and gravity), adsorbed flow, vapour diffusion and vapour convection.

Inward vapour flows, although strictly a redistribution mechanism, can cause wetting of inner enclosure layers by both adsorption and absorption, Although not widely known, solar heating of the screen (especially brickwork) will often cause evaporation from the interior face of the brickwork and condensation on the interior face of the cavity, sheathing, of inner layers [4.75, 4.76, 4.77]. This mechanism is also significant to heat transfer [4.,78 4.79, 4.80], especially exposed membrane roofs with rain penetration and exfiltration problems.

Exfiltration-induced condensation on the inner face of the wall sheathings, roof membranes, and wall cladding is a relatively common problem which results in slow wetting of surfaces within enclosure assemblies.

Liquid water moving into an ideal, initially dry media generally follows a simplified form of Darcy's equation [4.81]:

$$m_w = A \cdot \sqrt{t} \qquad \text{(Eq. 4.39)}$$

where m_w is the mass of the water absorbed per unit area (kg/m^2),

A is the water absorption coefficient ($kg/m^2\ s^{0.5}$ or $kg/m^2\ hr^{0.5}$)

and t is time (s or hr)

Equation 4.39 is, in fact, a special case of Equation 4.30 that presumes that the moisture diffusivity changes exponentially with moisture content. The value of A is therefore

related to the moisture diffusivity during suction (see also Equation 4.32). Table 4.3 summarises the moisture absorption coefficient for several common building materials from a number of different sources.

Material	A ($kg/m^2/s^{0.5}$]	A ($kg/m^2/hr^{0.5}$]
Water-repellent stucco (per DIN 18550)	< 0.0083	< 0.5
Good quality concrete	0.018	1.08
Cement stucco	0.03 - 0.07	2 - 4
Face brick	0.005 -0.55	0.3 - 33
Cement mortar	0.04 - 0.80	2.4 - 48
Pine: transverse	0.0040	0.240
Pine: longitudinal	0.0163	0.978

Table 4.3: Water absorption coefficients for various materials
Compiled from various sources, including [4.11,4.28,4.34,4.82,4.83, 4.84]

If the rate of water accumulation on the vertical surface of a material is greater than $A \cdot \sqrt{t}$ at any time, the water which is not absorbed will form a film on the surface and eventually drain away, if drainage is allowed.

As discussed earlier, once the wetting stops, e.g., rain or condensation, the nature of the absorption changes (and the liquid moisture diffusivity drops). During wetting, the larger pores transport the largest volume of water, because their resistance to flow is the least. Once wetting of the surface stops, smaller capillaries exert a larger suction and so begin to redistribute the water from the large pores to the smallest. Redistribution takes a longer time because the flow velocity within the small pores is small because viscous forces are large.

4.5 The Drying Process

Water leaves hygroscopic materials in building envelopes by the processes of:

1. drainage of liquid (from Region E to Region D),
2. evaporation/sublimation of liquid/ice (from Region D to Region C),
3. and desorption of adsorbed vapour (from Region C to A).

An initially oversaturated material will first loose moisture by gravity drainage until the capillary saturation moisture content is reached. The remaining liquid moisture in the material is then removed by evaporation at the surface of the material. Liquid water evaporated from the surface is replaced by water that moves through the material toward the relatively drier surface by capillary conduction, driven by the suction gradient. Once the material is no longer saturated, unsaturated flow and desorption begin. The rate of free water evaporation is usually much higher than the rate of desorption. The two processes and their different rates result in a moisture flux (or drying rate) with two reasonably distinct stages (Figure 4.29) [4.85, 4.65]:

> Stage I is the surface-saturated rate of drying. This rate is constant and approximately the same as free-water evaporation under the same conditions; hence it does not vary significantly from material to material.
>
> Stage II is the desorption drying rate. This rate is controlled by material properties (total moisture diffusivity, sorption isotherm), geometry, and the surrounding air conditions. The rate decreases in an approximately exponential manner as the material approaches equilibrium with its environment. The variation of moisture diffusivity with moisture content can dramatically change the shape of this curve.

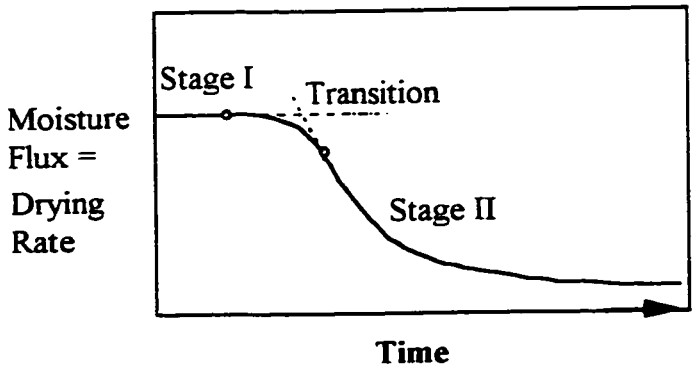

Figure 4.29: Drying stages for a saturated hygroscopic material

Although the rate of Stage I drying is essentially the same as free water under the same conditions [4.85], evaluating the evaporation rate of free water is also difficult. For some materials, geometries, and conditions of surrounding air, the transport of water through the saturated material may not replace the surface water as quickly as it is removed by evaporation; in such rare cases, the flow of water through the material will control the Stage I drying. Provided that free water is available over a constant surface area, the

Stage I drying rate will remain approximately constant with constant air temperature and vapour pressure.

Stage I ends when insufficient liquid water is available at the surface of the porous material. When Stage I begins, all pores are typically full or almost full. As liquid water evaporates from the drying surface, the moisture content at this layer drops and a potential for liquid water flow develops. Water will flow toward the drying surface from the interior of the material at a rate dependent on liquid water diffusivity (D_l) of the material. If the drying rate at the surface exceeds the ability of water to move towards it, drying is restricted and Stage II drying begins. The flow of water towards the drying surface then proceeds by a combination of vapour diffusion, surface diffusion, and unsaturated liquid flow.

As Stage I comes to an end, the plane where liquid water evaporates into the air, often called the drying front, moves below the surface. Stage II drying occurs at a slower rate for two reasons:

- since most porous materials have some internal resistance to water vapour flow, water vapour removal is hindered by the vapour resistance of the material between the exterior surface and the drying front, and
- the vapour pressure immediately over the drying front will be higher because convective effects cannot produce a strong vapour gradient. Since the gradient of vapour pressure from the drying plane is less than if it were at the surface, evaporation from below the surface occurs at a lower rate

Thus, the Stage II drying rate is expected to follow an approximately exponential decay for constant ambient air conditions since the vapour resistance of the material increases inversely as the distance of the drying front from the surface increases. The true shape depends on the moisture-dependent nature of the material's moisture diffusivity.

Except in cases of very high surface evaporation rates and/or thick material layers with low moisture diffusivities, Stage I is approximately the time taken until the material is no longer capillary saturated ($w<w_{cap}$). This is usually a short period of time and can often be ignored. Stage II drying then becomes a drying period during which vapour flow and unsaturated liquid flow dominate.

Consideration of the physics of drying leads to the expectation that layers within an envelope that are initially saturated will exhibit an initially high and constant rate of drying (as all free and surface water is evaporated) and an exponentially decreasing drying rate as all porous materials approach their equilibrium moisture content. Between these two extremes there will be a transition in which drying is due to a combination of the two stages.

Constant air temperature and vapour pressure conditions are not common in the natural environment, and conditions within an envelope might be characterised as "constant" for a few hours at most. During the day, solar radiation may change the temperature of the surface so quickly that even an hourly average is not sufficiently accurate to capture the full range of behaviour. The expected environmental variations can be superimposed on the plot of expected drying to qualitatively gauge actual performance.

4.5.1 Drying of enclosures

Diffusion of water vapour, air movement, desorption, capillarity, evaporation and of course gravity drainage all contribute to the removal of moisture from an enclosure assembly (see Chapter 2). Obviously, considerations of configuration, location and exposure have an influence on the nature and rate of moisture removal.

It is important to note that all of the stored water in an enclosure can only be removed from the enclosure by vapour diffusion and convection, or perhaps by liquid transport through capillary active materials connected to the exterior or interior. Gravity drainage will not remove any water stored in moisture storage regions A through D. Supersaturated materials will drain until they reach capillary saturation if a drainage path is provided.

In an enclosure assembly, drying during both stages will be affected by [4.86, 4.87]:

- the volume, various degrees of wetting/saturation, and the distribution of different materials and different parts of the assembly,
- the amount and nature of moisture flow into the wall (by airflow, diffusion, or rainfall)
- the temperature and vapour pressure conditions and gradients,
- the different sorption isotherms of the hygroscopic materials,

- the vapour resistance of different layers in the wall assembly,
- ventilation air flow, and
- interior and exterior ambient air conditions.

When most non-adsorbed or weakly-adsorbed water has been removed, a continuous and mobile internal water layer no longer exists and further drying must proceed by vapour diffusion and convection only. The material will eventually come to an equilibrium with its environment as predicted by the sorption isotherm.

Cladding, such as brick veneer, concrete, wood, vinyl siding, and some polymer-modified stuccoes have relatively high vapour resistances and will greatly retard drying of the inner layers of a wall by evaporation and diffusion. Ventilation drying is therefore a potentially important drying mechanism. This type of drying will be considered in greater depth in Chapter 9.

4.5.2 Drying by surface evaporation

Evaporation from the surface of saturated porous cladding materials can remove significant volumes of moisture, but its relative importance as a drying mechanism has not been quantified or measured under Canadian conditions.

Lacy [4.88] measured evaporation rates from brickwork in the field and reported maximum rates of 68 g/m^2/hr for a few hours, 20 g/m^2/hr for a few days, and 1- 7 g/m^2/hr for most of the time (when the walls were likely not saturated). Schwarz [4.65] measured rates of between 50 and 400 g/m^2/hr (depending on the influence of solar heating and wind speed) from an artificially saturated surface. Because of the nature of evaporative drying described in the previous section, drying rates of fully saturated materials are likely to be similar for wood, concrete, and stone claddings. Unfortunately, significant evaporative drying can only occur from the outside face and the inner side of the cladding will remain wet for a relatively longer time unless a well ventilated air space is provided behind the cladding. Theoretical calculations [4.89] and laboratory experiments suggest maximum rates of 200 to 400 g/m^2/hr are possible [4.90].

During the first stage of drying, given a mass transfer surface film coefficient, g, the mass transfer due to diffusion alone from a wet surface to the exterior can be found using Equation 4.33.

The vapour pressure at the drying surface is the saturation vapour pressure for that temperature. The use of the saturation vapour pressure at the cladding temperature is a reasonably accurate assumption for moisture contents considerably less than capillary saturation because the shape of the sorption isotherm for most cladding materials is steep in the 90% to 100% RH range (consider the isotherms shown earlier for wood, concrete and clay brick). Wood siding is more hygroscopic than brick, concrete or stucco, and therefore this assumption is not as valid.

Consider a rain saturated (100% RH) masonry wall at 10 °C (P_v= 1230 Pa) and outdoor air at 8°C and 80% RH (860 Pa) with a wind speed of 3 m/s. Using the information from Section 4.3.5.2, the mass transfer coefficient can be found from Equation 4.35 as approximately 50 x 10^{-6}. Therefore, the rate of surface drying rate can be calculated as:

$$m_w = g \times A \times \Delta P \times \Delta t = 50 \times 10^{-6} \times 1\ m^2 \times (1230\text{-}860)\ Pa \times 3600\ s/hr$$

$$= 67\ g/(m^2 \cdot hr)$$

Which is close to both Lacy's and Schwarz's field measurements of the drying rate for saturated brickwork.

Under real conditions the latent energy of evaporation is required to maintain the temperature of the evaporating surface above the ambient temperature. Simple calculations shows that an absorbed solar energy intensity of only 50 W/m^2 is sufficient to provide the latent heat of evaporation for 72 $g/hr/m^2$. Normal daytime solar exposure is in the order of several hundred W/m^2.

As will be shown in Chapter 9, the surface of cladding, especially brickwork, will on average be several degrees above the ambient air temperature. Solar radiation typically increases the temperature of claddings from 20 to 40°C above ambient for several hours on all sunny days. While this solar heating only occurs for orientations exposed to the sun and for a short time, the effect on drying can be very significant because of the very fast increase in vapour pressure with temperature.

The temperature difference in the previous example is rather small. The saturation vapour pressure at 40 °C is 7400 Pa. For the previous example, a cladding temperature of 40 °C would increase the drying rate by a factor of more than 10, to 1170 $g/m^2 \cdot hr$. The moisture within the masonry is unlikely to be transported to the surface at this rate (the drying front

would recede below the surface), but the drying rate would in any event be much larger than the drying rate at a lower temperature.

While the surface may dry quickly, the inability of the cladding material to transport liquid water to the surface fast enough will almost immediately reduce the drying rate to below that predicted by Equation 4.33. The result is that the outside few mm of the cladding will dry very quickly, but depending on the vapour permeance and the speed of capillary redistribution within the material, the material will remain almost saturated some distance inside.

The rate of drying of all but the surface of the cladding is therefore likely to be governed by the ability of the material to transport sufficient water (by capillary conduction) to the surface for evaporation, or the vapour resistance of the material and/or coatings, not by the effective mass transfer coefficient at the surface.

In stagnant air, the mass transfer calculated by the above equations might be substantially reduced by the vapour resistance of the air itself, and by the effect of evaporating water increasing the vapour pressure of air near the surface Stagnant air is only likely to occur in small pockets behind plantings, inside of architectural reveals, etc.

4.6 Computer Model Predictions of Building Enclosure Hygrothermal Performance

Although a general and consistent approach to moisture storage and transport has been presented in the previous sections, predicting the moisture and temperature conditions inside building enclosures is not an easy task. Predicting the durability of enclosures and materials is another entire field of research that requires much more work before the goal of designing and building durable, economical buildings is achieved. This section reviews the practical implementation of computer modelling for assessing and designing building enclosures.

Several comprehensive and informative review papers from chemical engineering [e.g., 4.91] and soil science [e.g.,4.39] appear to provide a more comprehensive view of moisture transport physics than the building science literature. Some of the more recent mathematical models proposed [4.92,4.93] improve upon the more limited models of Philip and de Vries [4.44] and Luikov [4.67] which are so often used as the basis for building enclosure models. The work of Imakoma et al [4.54] also suggests that great

improvements can be made. Building science applications, however, are more dynamic than soil problems, boundary conditions are less accurately known than in chemical process engineering, and unlike most other disciplines, multi-layer assemblies must be dealt with.

4.6.1 Existing computer models

The models that are discussed below have each been implemented in computer programs that use various finite-element or finite-volume schemes. The numerical virtues and difficulties of each approach are not the primary interest here (although this topic is critical for practical computer models).

Each model is based on a certain view of the moisture physics described in the previous sections. One approach is to choose a driving potential and lump all mechanisms into one total moisture diffusivity function. Another approach is to separate vapour diffusion from liquid transport. In the latter case, one can model the flow as either a parallel process (vapour diffusion and capillary transport) or series (i.e., vapour diffusion functions to a certain moisture content, then capillary conduction takes over). In reality the flow is parallel, although the series approach may be sufficiently accurate in some cases.

All of the models (except MATCH, which can use different wetting and drying curves) use an average moisture storage function which does not exhibit hysteresis. Pedersen did show in some limited number of simulations that the hysteresis has little impact on the final result.

The choice of driving potential could be vapour pressure, relative humidity, capillary suction stress, or moisture content. (Chemical potential is another little used potential). The argument against vapour pressure is that it drives only vapour diffusion, and hence is not typically used alone. The disadvantage of using moisture content is that it is discontinuous at material interfaces. Capillary suction is likewise a discontinuous function. Relative humidity does not actually drive liquid or vapour flow but is continuous. All of these potentials are, however, related to one another and can be used with the proper transformations (via Kelvin's equation and the sorption isotherm).

Vapour diffusion is supposedly a well understood transport mechanism, although the measurement and understanding of different vapour flow enhancement mechanisms requires more work before a consensus can be reached. Knudsen diffusion (effusion) is

explicitly ignored by all building models, but is usually implicitly included in the vapour permeability. None of the computer models account for the different temperature dependencies of Fickian and Knudsen diffusion, likely because the differences are small in comparison to the variability of the measured vapour permeability.

Surface diffusion is discussed as a transport mechanism in many of the model developments. Few models explicitly deal with the fact that the adsorbed moisture density gradient is the driving force (except WUFI and Latenite). Surface diffusion may be implicitly included in models that use measured total moisture diffusivities, but many models use material properties that only include capillary flow driven by suction stress (e.g., MOIST). In fact, it is clearly important to understand that moisture flow cannot simply be driven by vapour diffusion or capillary suction, but that surface diffusion also acts and all three mechanisms may be acting at some times.

Liquid conductivity is included in most of the complete models considered here, although some of the earlier and simple models use constant diffusivity (even though it usually varies by several orders of magnitude). Only WUFI includes different functions for wetting, drying, and redistribution, although this may be possible to implement in models like Latenite. This is worrying since Karagiozis et al [4.66, 4.94] have shown, through parametric modelling, that the use of the proper liquid diffusivity is very important for accurate predictions in some applications. If water content is used as a driving potential it must be coupled to the suction curve to avoid the erroneous calculation of liquid flow in the super-saturated region (a fictitious liquid diffusivity might also be used).

Convective vapour transport, i.e., air leakage, is accounted for in some of the most comprehensive models. The proper modelling of convective air flow and its moisture transport is important to some types of buildings. Unfortunately it is even more complex than diffusive and capillary transport, Since almost all building enclosures are designed to have a nearly perfect air barrier, the importance of simulating the effects of air leakage are insignificant next to the need to properly model the flaws in the "perfect" design. Any models that do include air leakage effects must deal with the fact that the results are only as accurate the estimate of the flaw in the air barrier. With these limitations in mind, several of the models that do include air leakage, (notably Latenite and TCCD2) have been shown to be quite useful as research tools.

The **boundary conditions** imposed on the model are often as critical to its usefulness as the proper modelling of the moisture physics. In this regard, both driving rain and solar

radiation must be properly accounted for. Few of the models deal with driving rain, partly because there is little data available. There are some practical situation where driving rain need not be accounted for, namely enclosures with fully-sealed perfect barrier or non-absorbent claddings systems (see Chapter 5). However, the practical value of models that do not account for driving rain deposition is severely curtailed.

For models that include air leakage, accurate and detailed knowledge of wind pressure variations and stack effect pressures is required, but only very rarely available. Interior and exterior temperatures are known with a much greater degree of accuracy than any of the other boundary conditions, and their precise knowledge is usually not that important to the results. The magnitude and variation of interior humidity, which can be critical to the success or failure of a given enclosure in service, is more poorly known although recent research has improved the quality and quantity of available data [4.70].

One of the first relatively complete and useful building envelope models was developed by Kohonen [4.95]. It used vapour pressure (calculated from the moisture isotherm) and temperature as driving potentials. However, as initially implemented, the moisture diffusivity and vapour permeability were constant, and surface diffusion was included as part of the vapour diffusion term.

Ojanen et al built on Kohonen's work to produce TCCD2 [4.96,4.97], a two-dimensional program developed primarily for the analysis of framed building walls. The model uses the same basic physics and mathematical formulation as used in Kohonen's model. A major improvement made over Kohonen's model is the use of moisture content dependent diffusivity. Convection airflow is accounted for as well as condensation and evaporation, but capillary transport and surface diffusion must be lumped into the vapour diffusion process. It has been validated with laboratory experiments and has been shown to provide useful information regarding the impact of convective flows on hygrothermal performance [4.98].

Kerestecioglu et al [4.99, 4.100] have produced a comprehensive and flexible program called FSEC, which contains a library of differential equations, different finite elements, and various functional relationships for materials properties. The authors recognise all of the moisture transport mechanisms, including convection, but in the implementation liquid and vapour flow are described by different sets of equations. Vapour is driven by diffusion and liquid flow by capillary suction. Surface diffusion is not explicitly handled.

Cunningham [4.101] took a simplified approach and used vapour pressure as the only driving potential, as vapour diffusion and convection are assumed to be the only moisture transport mechanisms in this model. The model used the sorption isotherm to couple moisture content to vapour pressure and a linearly varying vapour diffusion coefficient. Despite the extensive simplifications, the model was validated by simple lab tests [4.102] and extensive in-service monitoring [4.103] of roof structures. The limitations of the model are that it cannot deal with rain absorption, situations where capillary active materials are above the critical moisture content, or complex airflows.

Carsten Rode (formerly Pedersen) [4.104, 4.105] used both the sorption and suction curves to define the moisture storage function in his model, MATCH. In the hygroscopic regime the sorption isotherm was used, and moisture transport was assumed to be by vapour flow only, driven by vapour pressure differences and defined by the vapour permeability of the material. In the capillary regime the suction curve was used together with the hydraulic conductivity to model moisture transport. Convection is not accounted for. Some validation has been carried out through the use of his own [4.106] and other researcher's [4.107] lab results, although none of the work has involved driving rain deposition, or similar real-life exposure. MATCH, like the very similar MOIST, can likely be successfully used for the approximate analysis and design of protected membrane roofs and walls with non-absorbent cladding.

Burch's MOIST model [4.108] is similar in most respects to Pedersen's. Moisture transport is modelled as vapour flow driven by vapour pressure gradients and capillary transport driven by capillary pressure gradients. The vapour permeability and hydraulic conductivity are both given as functions of moisture content. The latent heat of phase changes is accounted for as is the increased heat capacity provided by wet materials. Fibrous insulations are assumed to have no moisture storage capacity. No attempt is made to model air leakage but a useful indoor climate model aids the development of realistic indoor climate data. Simple lab validation tests have been conducted in the hygroscopic range [4.109], with good results, and field comparisons [4.110] (without solar exposure, although it can calculate solar effects) have shown reasonable comparison, so long as the moisture content remained in the hygroscopic range and rain deposition was not involved. It is a public-domain package available from the National Institute of Science and Technology.

WALLDRY [4.111, 4.112] is a simple model that attempts to model the drying of framed wall assemblies by separating heat, moisture and air flow. Moisture transport is

considered to be exclusively by vapour diffusion. In field validation trials, the model was unable to capture finer details of the drying process, although in some situations it was able to model some features of the moisture transport process. It is a public-domain package available from the Canada Mortgage and Housing Corporation.

WUFI [4.34, 4.113] was developed by Hartwig Kuenzel but is supported by the comprehensive work of Kiessl, Krus and other workers at the IBP. This model uses a full moisture retention function from the sorption isotherm and suction curve. Surface diffusion and liquid transport are driven by RH (and capillary suction via Kelvin's equation) and governed by a combined moisture diffusivity. Vapour diffusion is considered separately. The vapour and moisture diffusivity can be entered from measurements or approximated from several important behavioural markers, like the absorption coefficient, capillary saturation, and dry-cup vapour permeance. Major features of this model are its ability to provide a reasonable estimate of driving rain deposition as part of its boundary conditions, the use of different liquid moisture diffusivities for suction and redistribution processes, the ease of use, speed of calculation, and degree of validation. The close fit between model predictions and many field validation exercises of a variety of walls and roofs over several years demonstrates the quality and robustness of this model. Its major limitations are its inability to handle air leakage and 2-D assemblies. A two-dimensional version, WUFIZ, exists but is only used as a research tool. WUFI, like MATCH, is commercially available.

Latenite [4.114, 4.115, 4.116] is likely the most comprehensive heat air and moisture model available. Using a complete moisture storage function (e.g. sorption isotherm and suction curve), the model considers vapour and liquid transport separately, driven by vapour pressure and suction respectively. The vapour permeability and liquid diffusivity vary with moisture content (surface diffusion is included in the liquid diffusivity) in an arbitrary way (defined by the user). Air flow, gravity drainage, driving rain deposition, moisture sources (e.g., leaks), wind and stack pressures can all be incorporated into a simulation of up to three dimensions if desired. Driving rain can be comprehensively modelled through the use of a sophisticated commercially-available CFD package as a pre-processor. Stochastic modelling can be used to assess the influence of inaccurate or variable material properties and boundary conditions. Although this model has not been field verified, it was found to be one of the most accurate in the recent IEA Annex 24 comparison project [4.117].

4.7 Closure

This chapter has presented an extensive survey of moisture in building physics from the unique nature of the water molecule, to capillary behaviour, to moisture storage, and transport functions.

This survey, and the short review of some of the available computerised heat and moisture transport models shows that a more comprehensive theory of moisture transport physics for use in building science is needed. For example, the state-of-the-art knowledge in chemical engineering could likely be better exploited.

4.8 References

[4.1] Franks, Flex. *Water*. Royal Chemistry Paperbacks , 1984.

[4.2] *Surface Coatings 3: Waterborne Coatings*, ed. Wilson, Alan, D., Nicholson, John W., Prosser, Harvard J., Elsevier Science Publishers, Essex, England, 1987.

[4.3] Glasstone, S, Lewis, D., *Elements of Physical Chemistry*, van Nostrand & Co., Princeton, 1960.

[4.4] Powers, T., *The Properties of Fresh Concrete*, J. Wiley & Sons, New York, 1968.

[4.5] Cherry, John A., Freeze, Allan .R., *Groundwater*. Prentice-Hall, Englewood Cliffs, N.J., 1979.

[4.6] Kumaran, M.K., Mitalas, G.P., Bomberg, M.T., "Fundamentals of Moisture Transport and Storage in Building Materials", Draft of Chapter 1, *ASTM Moisture Handbook*, ASTM, Philadelphia, 1991.

[4.7] Powers, T., Brownyard, T., "Studies of the Physical Properties of Hardened Portland Cement Paste- Part 8. The Freezing of Water in Hardened Portland Cement Paste", *J. Of Amer. Conc. Inst.*, Vol. 43, Oct 1946 - April 1947.

[4.8] Arnott, M.R., and Litvan, G.G., "Quality-Control Test for Clay Brick Based on Air Permeability", *Amer. Ceramic Soc. Bull.*, Vol 67, No. 8, Aug 1988, pp. 1412-1417.

[4.9] Sereda, P.J., CBD 127 *The Structure of Porous Building Materials*, NRCC, Ottawa, July, 1970.

[4.10] Whiteley, P., Russman, H.D., Bishop, J.D., *Porosity of Building Materials - a Collection of Published Results*, BRE Current Paper 21/77, HMSO, London,1977.

[4.11] Kumaran, M.K., *Task 3:Hygrothermal Properties of Building Materials*, Annex 24, Final Report, International Energy Agency, 1996.

[4.12] Haynes, J.M., "Determination of pore properties of constructional and other materials", *Materials and Structures*, Vol 6, No. 33, May-June 1973, pp. 169-179. Also refer to the 11 other papers in this issue for specific details of each measuring approach.

[4.13] Arnott, M.R., *Investigation of Freeze-Thaw Durability*, CBAC/IRC Industrial Research Fellowship Final Report, National Research Council of Canada, Ottawa, Dec. 1990.

[4.14] Litvan, G.G., "Testing for the Frost-Susceptibility of Bricks", *Special Technical Publication 589*, American Society of Testing and Materials, 1975, pp. 123-132.

[4.15] Morrow, R., *J. Of Canadian Petroleum Technology*, Vol 15, No. 4, pp. 49, 1976 and Vol 14, No. 4, pp. 42, 1975.

[4.16] Sereda, P.J., and Feldman, R.F., CBD 130 *Wetting and Drying of Porous Materials*. NRCC, Ottawa, October, 1970.

[4.17] Adan, O.C.G., *On the Fungal Defacement of Interior Finishes*. Doctoral Dissertation, Eindhoven University of Technology, 1995.

[4.18] Ashton, H.E.,.Canadian Building Digest 124 *Biological Attack on Organic Materials*, NRCC, Ottawa, April, 1970.

[4.19] Baker, M.C., Canadian Building Digest 111 *The Decay of Wood.*, NRCC, Ottawa, March, 1969.

[4.20] Sereda, P.J., Canadian Building Digest 170 *Atmospheric Corrosion of Metals*, NRCC, Ottawa, 1975.

[4.21] *Wood Handbook: Wood as an engineering material.* Forest Products Laboratory, Forest Service, U.S. Dept. Of Agriculture, 1974.

[4.22] *CEB Guide to Durable Concrete Strcutures*, Bulletin d'Information No. 166, ComiteEuro-International d'Beton, 1986.

[4.23] Enevoldsen, J.M., Hansson, C.M., Hope, B.B., "The Influence of Internal Relative Humidity on the Ratoe of Corrosion of Steel Embedded in Concrete and Mortar", *Cem. and Conc. Res.*, Vol. 24, pp. 1373-1382, 1994.

[4.24] Lopez, W., Gonzalez, J.A., "Influence of the Degree of Pore Saturation on the Resistivity of Concrete and the Corrosion Rate in the Presence of Chlorides", *Cem. and Conc. Res.*, Vol. 23, pp. 368-376, 1993.

[4.25] Peake, F. and Ford, R.W., "A Comparison of the Vacuum and Boiling Methods for Measuring the Water Absorption of Bricks", *Trans. J. Br. Ceram. Soc.*, Vol 81, pp. 160-162, 1982.

[4.26] Descamps, Filip, *Continuum and Discrete Modelling of Isothermal Water and Air Transfer in Porous Media*, Doctoral Dissertation, Katholieke Universiteit Leuven, Leuven, Belgium, 1997.

[4.27] Penner, E., "Suction and its use as a measure of moisture contents and potentials in porous materials", Vol. 4, Proc. Of Int. Symp. On Humidity and Moisture, Washington D.C., 1963, Chap 29, pp. 245-252.

[4.28] Pel, Leo, *Moisture Transport in Porous Building Materials*, Doctoral Dissertation, Eindhoven University of Technology, Eindhoven, 1995.

[4.29] Brunauer, P.H., Emmet, P.H., Teller, E., "Adsorption of Gases in Multimolecular Layers", *J. of Amer. Chem. Soc.*, Vol. 60, pp. 309- 319, 1968.

[4.30] Rounsley,R.R., "Multimolecular Adsorption Equation" *J. of Amer. Chem. Soc.*, Vol 7, No. 2, pp. 308 -311, 1961.

[4.31] El-Sabaawi, M., and Pei, D.C., "Moisture Isotherms of Hygroscopic Porous Solids", *Ind. Eng. Chem. Fundam.*, Vol. 16, pp. 321-326, 1977.

[4.32] Tamon, H., Okazaki, M., and Toei, R., "Flow Mechanism of Adsorbate Through Porous Media in Presence of Capillary Condensation", *Amer. Inst. Chem. Eng. Journ.*, Vol 27, No. 2, pp. 271-277, 1981.

[4.33] Toei, R., "Drying mechanism of capillary porous bodies". In *Advances in Drying*, vol. 2., ed. A. Mujumdar, Hemisphere Publishing, Washington, D.C., 1983.

[4.34] Kuenzel, Hartwig, *Verfahren zur ein- und zweidimensionalen Berechnung des gekoppelten Waerme- und Feuchtetransports in Bauteilen mit einfachen Kennwerten*, Doctoral Dissertation, Universität Stuttgart, Germany, 1994.

[4.35] Nevander, L.E., Elmarsson, B., *Fukthandbok*, Svensk Byggtjaenst, Stockholm, October, 1981.

[4.36] Krus, M, Kuenzel, Hartwig, *Fluessigtransport im Uebersaettigungsbereich*, IBP Mitteilung 270, Fraunhofer Institut fuer Bauphysik, Stuttgart, 1995.

[4.37] Quenard, D., Sallee, H., "The Transport of Condensible Water Vapour Through Microporous Building Materials", *Drying '89*, ed. By Arun S. Mujumdar and Michel Roques, Hemisphere Publishing Corp., New York, 1990, pp. 106-112.

[4.38] Daian, J.F., "The Interaction Between Condensed and Gaseous Water During Migration Processes in Porous Media", *Drying '89*, ed. By Arun S. Mujumdar and Michel Roques, Hemisphere Publishing Corp., New York, 1990, pp. 113-118.

[4.39] Hartley, J.G., "Coupled Heat and Moisture Transfer in Soils: A Review". In *Advances in Drying*, vol. 4., ed. A. Mujumdar, Hemisphere Publishing, Washington, D.C., 1987, pp. 199-248.

[4.40] *Handbook of Industrial Drying*, pg. 115, 2nd ed. Vol 1. Hemisphere Publishing, Washington D.C.,1995.

[4.41] Millington, R.J., and Quirk, J.P., "Permeability of Porous Solids", *Trans. Faraday Society.* Vol 57, pp. 1200-1207, 1961.

[4.42] Sallam, A., Jury, W.A., Letey, J., "Measurement of gas diffusion under relatively low air-filled porosity", *Soil Sci. Soc. Amer. J.*, vol 48., pp. 3-6, 1984.

[4.43] Burch, D.M., Thomas, W.C., Fanney, A.H., "Water Vapor Permeability Measurements of Common Building Materials", *ASHRAE Transactions: Symposia*, Atlanta, 1992, pp. 486-494.

[4.44] Philip, J.R., and de Vries, D.A., "Moisture Movement in Porous Materials under Temperature Gradients", *Trans. Amer. Geophys. Union*, Vol 38, 1957 , pp. 222-232.

[4.45] Kuenzel, Helmut, "Trocknungsblockade durch Mauerversalzung", *Bautenschutz - Bausanierung*, 1990.

[4.46] Okazaki, M., Tamon, H., and Toei, R., "Interpretation of Surface Flow Phenomenon of Adsorbed Gases by Hopping Model", *Amer. Inst. Chem. Eng. Journ.*, Vol 27, No. 2, pp. 262-270, 1981.

[4.47] Hill, T.L., "Surface Diffusion and Thermal Transpiration in Fine Tubes and Pores", *J. Chem. Phys.*, Vol 25, pp. 730, 1956.

[4.48] Krus, Martin, *Feuchtetransport- und Speicherkoeffizienten poroser mineralisher Baustoffe. Theoretische Grundlagen und neue Meßtecknken.* Doctoral Dissertation, Universität Stuttgart, Germany, 1995.

[4.49] Daian, J.F., "Experimental and Numerical Study of Drying. Compared Behaviour of Two Building Materials", *Drying '89*, ed. Arun S. Mujumdar and Michel Roques, Hemisphere Publishing Corp., New York, 1990, pp. 76-82.

[4.50] Craig, R.F., *Soil Mechanics*, Fourth Ed., Van Nostrand Reinhold, Wokingham, Berkshire, England, 1987.

[4.51] Keey, R.B., *Drying: Principles and Practice*, Pergamon Press, Oxford, 1972.

[4.52] Krischer, O., *Die wissenschaftlichen Grundlagen der Trocknungstecknik*, Springer Verlag, Berlin, 1963.

[4.53] Fatt, I., "The Network Model of Porous Media", *AIME Petrol. Trans.*, Vol. 207, pp. 144-177, 1956.

[4.54] Imakoma, H., Okazaki, M., Toei, R., "Drying Mechanism of Adsorptive Porous Soids", in *Advances in Drying*, vol. 5., ed. Arun Mujumdar, Hemisphere Publishing, Washington, D.C., 1992, pp. 77-107..

[4.55] Krus, M., "Effect of Different Liquid Water Diffusivities for Wetting and Drying on the Moisture Behaviour", Annex 24 Paper T3-D-92/01, International Energy Agency, 1992.
[4.56] Winter, K., Krus, M., Kuenzel, H., "Feuchtetransport in feinporigen Materialien", *Bauinstandsetzen*, Vol. 3, Heft 1, 1997, pp. 15-28.
[4.57] Kumaran, M.K., *Task 3: Hygrothermal Properties of Building Materials*, Annex 24, Final Report, International Energy Agency, 1996, Appendix I and II.
[4.58] Kalimeris, A.N., *Water flow processes in porous building materials*, Ph.D. thesis, University of Manchester, U.K.,1984.
[4.59] Holm, A., Krus, M., Kenzel, H., "Feuchtetransport ueber Materialgrenzen im Mauerwerk", *Bauinstandsetzen*, Vol. 2, Heft 5, pp. 375-396, 1996.
[4.60] Groot, C.J., "Effects of brick suction on the water distribution in joints investigated with thermal neutrons", *Proc. 5th N.A. Masonry Conf.*, Urbana-Champaign, pp. 723-734, 1990.
[4.61] Brocken, H.J.P., Adan, O.C.G., Pel, L., "Moisture Transport Properties of Mortar and Mortar Joint: a NMR Study", *Heron*, Vol. 42, No. 1, pp. 55-69, 1997.
[4.62] Bomberg. M., *Moisture Flow Through Porous Building Materials*. Report 52, Lund Institute of Technology, Lund Sweden, 1974.
[4.63] Burch, D., Thomas, W.C., Mathena, L.R., Licitra, B.A., Ward, D.B., "Transient Moisture and Heat transfer in Multi-Layer Non-Isothermal Walls - Comparison of Predicted and Measured Results", *Proc. of Thermal Performance of the Exterior Envelopes of Buildings IV*, Orlando, Florida, Dec 4-7, pp. 513 - 531, 1989.
[4.64] Cunningham, M.J., "Further Analytical Studies of Building Cavity Moisture Concentrations," *Building & Environment*, Vol. 19, No. 1, pp. 21-29, 1984.
[4.65] Schwarz, B., *Die Wärme und Stoffübertragung an Außenwandoberflächen.* Doctoral Dissertation, Universität Stuttgart, Germany, 1978.
[4.66] Karagiozis, A., Salonvaara, M., "Hygrothermal Behaviour of a Brick Cavity Wall. Part B: Parametric Study on Material Properties Using Stochastic Modeling", IEA Annex 24 Task 1, Simplified Modeling.
[4.67] Luikov, A.V., *Heat and Mass Transfer in Capillary Porous Bodies.* Permagon Press, Oxford, 1965.
[4.68] Incropera, F.P. and DeWitt, D.P., *Fundamentals of Heat and Mass Transfer.* 3rd ed., John Wiley & Sons, New York, 1990.
[4.69] Kays, W.M.., and Crawford, M.E., *Convective Heat amd Mass Transfer.* McGraw-Hill, New York, 1980.
[4.70] Sanders, C., *Task 2:Environmental Conditions*, Annex 24, Final Report, International Energy Agency, 1996.
[4.71] Duffie, J.A., and Beckman, W.A., *Solar Engineering of Thermal Processes*, John Wiley & Sons, New York, 1980.
[4.72] *Handbook of Fundamentals*, Amer. Society for Heating Ventilating and Air Conditioning Engineers, Atlanta, 1993.
[4.73] Kronvall, J., *Air Flows in Building Components.* Doctoral Dissertation, Lund Institute of Technology, Lund, Sweden, 1980.

[4.74] Bumbaru, D., Jutras, R., Patenaude, A., *Air Permeance of Building Materials.* Report by AIR-IN Inc. for Canada Mortgage and Housing Corp., Ottawa, 1988.

[4.75] Wilson, A.G., "Condensation in Insulated Masonry Walls in Summer", *RILEM/CIB Symposium*, Helsinki, 1965, pp. 2-7.

[4.76] TenWolde, A., Mei, M.T., "Moisture Movement in Walls in a Warm Humid Climate," *Proceedings of Thermal Performance of the Exterior Envelopes of Buildings III*, Clearwater Beach, Florida, Dec 2-5, 1985, pp. 570 - 582.

[4.77] Andersen, N.E.,"Summer Condensation in an Unheated Building", *Proc. of Symposium and Day of Building Physics*, Lund University, Swedish Council for Building Research, August 24-27, 1987, pp. 164-165.

[4.78] Bomberg, M., and Shirtcliffe, C.J., "Influence of moisture and moisture gradients on heat transfer through porous building materials", Thermal Transmission Measurements of Insulation, ASTM STP 660, ed. R.P. Tyre, ASTM, Philadelphia, 1978, pp. 211-233.

[4.79] Cunningham, M.J., Tsongas, G.A., McQuade, D., "Solar-Driven Moisture Transfer Through Absorbent Roofing Materials", *ASHRAE Transactions 96*, Part 1, 1990, pp. 465-471.

[4.80] Hedlin, C.P., "Heat Flow Through a Roof Insulation Having Moisture Contents Between 0 and 1% by Volume, in Summer", *ASHRAE Transactions 94*, 1988, pp. 1579-1594.

[4.81] Hall, C., "Water Movement in Porous Building Materials - I. Unsaturated Flow Theory and its Applications," *Bldg & Environ*, Vol. 12, pp. 177-125, 1977.

[4.82] Lohmeyer, G. *Praktische Bauphysik*, B.G. Teubner, Stuttgart, 1995.

[4.83] Kuenzel, Helmut, "Risse in Bewittertem Holz", *bauen mit holz*, Vol. 95, Heft 12, pp. 1018-1025, 1993.

[4.84] Kuenzel, Helmut, "Der Regenschutz von wasserabweisenden Aussenputz", *Bauphysik*, Vol. 5, 1986.

[4.85] Hall, C., Hoff, W.D., Nixon, M.R., "Water Movement in Porous Building Materials - VI. Evaporation and Drying in Brick and Block Materials", *Bldg & Environ*, Vol. 19, No. 1, pp. 13-20, 1984.

[4.86] Cunningham, M.J., "A New Analytical Approach to the Long Term Behaviour of Moisture Concentrations in Building Cavities - I. Non-Condensing Cavity," *Bldg & Environ*, Vol. 18, No. 3, pp. 109-116, 1983.

[4.87] Cunningham, M.J., "A New Analytical Approach to the Long Term Behaviour of Moisture Concentrations in Building Cavities - II. Condensing Cavity", *Building & Environment*, Vol. 18, No. 3, pp. 117-124, 1983.

[4.88] Lacy, R.E., *Climate and Building in Britain.* HMSO, London, 1977.

[4.89] Straube, J.F., and Burnett, E.F.P., *Vents, Ventilation, and Pressure Moderation.* External Research Program Report for CMHC, Ottawa, Dec. 1995.

[4.90] Hall, C., Hoff, W.D., Nixon, M.R., "Water Movement in Porous Building Materials - VI. Evaporation and Drying in Brick and Block Materials," *Bldg & Environ*, Vol. 19, No. 1, pp. 13-20, 1984.

[4.91] Fortes, M. And Okos, M, "Drying Theories: Their Bases and Limitations as Applied to Foods and Grains", in *Advances in Drying*, vol. 1., ed. A. Mujumdar, Hemisphere Publishing, Washington, D.C., pp. 119-154, 1980.

[4.92] Fortes, M., and Okos, M., "Heat and Mass Transfer in Hygroscopic Capillary Extruded Products", *AIChE Journal*, Vol. 27, No. 2., March 1981, pp. 255-262.

[4.93] Chen, P., and Pei, D., "A Mathematical Model of Drying Processes", *Int. J. Of Heat Mass Transfer*, Vol. 32, No. 2, pp. 297-310, 1989.

[4.94] Karagiozis, A., Salonvaara, M., "Influence of Material Properties on the Hygrothermal Performance of a High-Rise Residentail Wall", *ASHRAE Transactions: Symposia*, CH-95-3-5, pp. 647-655, 1995.

[4.95] Kohonen, R., "Transient Analysis of the Thermal and Moisture Physical Behaviour of Building Constructions", *Bldg and Environ.*, Vol. 19, No. 1, 1984, pp. 1 -11.

[4.96] Ojanen, T., and Kohonen, R., "Hygrothermal Influence of Air Convection in Wall Structures", *Proc. Of Thermal Performance of the Exterior Envelopes of Buildings IV*, Clearwater Beach, Fla., Dec 4-7, 1989, pp. 234-242.

[4.97] Ojanen, T. and Simonson, C., "Convective Moisture Accumulation in Structures with Additional Inside Insulation", *Proc. Of Thermal Performance of the Exterior Envelopes of Buildings VI*, Clearwater Beach, Fla., Dec 4-7, 1995, pp. 745-752.

[4.98] Kohonen, R., "Thermal Effects of Airflows and Moisture on Exterior Wall Structures", *Proc. of Thermal Performance of the Exterior Envelopes of Buildings III*, Clearwater Beach, Florida, Dec 2-5,1985, pp. 583 - 605.

[4.99] Keresteciogiu, A., Swami, M., Fairey, P., Gu, L., Chandra, S., *Modelling Heat Moisture and Contaminant Transport in Buildings: Toward a New Generation Software*, Professional Paper FSEC-PF-165-89, Florida Solar Energy Center, Cape Canaveral, Fla., 1989.

[4.100] Keresteciogiu, A., "Detailed Simulation of Combined Heat and Moisture Transfer in Building Components", *Proc. Of Thermal Performance of the Exterior Envelopes of Buildings IV*, Clearwater Beach, Fla., Dec 4-7, 1989, pp. 477-485.

[4.101] Cunningham, M.J., "Modelling of Moisture Transfer in Structures - I. A Description of a Finite-Difference Nodal Model", *Bldg and Environ.*, Vol. 25, No. 1, pp. 55 -61, 1990.

[4.102] Cunningham, M.J., "Modelling of Moisture Transfer in Structures - II. A Comparison of a Numerical Model, an Analytical Model, and Some Experimental Results", *Bldg and Environ.*, Vol. 25, No. 2, pp. 85 -94, 1990.

[4.103] Cunningham, M.J., "Modelling of Moisture Transfer in Structures - I. A Comparison Between the Numerical Model SMAHT and Field Data", *Bldg and Environ.*, Vol. 29, No. 2, pp. 191 -196, 1994.

[4.104] Pedersen, C.R., "MATCH - A Computer Program for Transient Calculation of Combined Heat and Moisture Transfer", Contribution to CIB-40 Meeting, Victoria, Canada, Sept 11-14, 1989.

[4.105] Pedersen, C.R., "Prediction of Moisture Transfer in Building Constructions", *Bldg and Environ.*, Vol. 27, No. 3, pp. 387-397, 1992.

[4.106] Korsgaard, V., Pedersen, C.R. , "Transient Moisture Distribution in Flat Roofs with Hygro-Diode Vapor Retarder", *Proc. of Thermal Performance of the*

Exterior Envelopes of Buildings IV, Clearwater Beach, Fla., Dec 4-8, 1995, pp. 556-565.

[4.107]Rode, C., Burch, D.M., "Empirical Validation of a Transient Computer Computer Model for Combined Heat and Moisture Transfer", *Proc. of Thermal Performance of the Exterior Envelopes of Buildings VI*, Clearwater Beach, Fla., Dec 4-8, 1995, pp. 283-295.

[4.108]Burch, D.M., Thomas, W.C., Mathena, L.R., Licitra, B.A., and Ward, D.B., "Transient Heat and Moisture transfer in Multi-Layer, Non-Isothermal Walls - Comparison of Predicted and Measured Results", *Proc. of Thermal Performance of the Exterior Envelopes of Buildings IV*, Clearwater Beach, Fla., Dec 4-7, 1989, pp. 513-531.

[4.109]Burch, D.M., Zarr, R.R., Fanney, A.H., "Experimental Validation of a Moisture and Heat transfer Model in the Hygroscopic Regime", *Proc. of Thermal Performance of the Exterior Envelopes of Buildings VI*, Clearwater Beach, Fla., Dec 4-8, 1995, pp. 273-281.

[4.110]TenWolde, A., Carll, C., "Moisture Accumulation in Walls: Comparison of Field and Computer-Predicted Data", *Proc. of Thermal Performance of the Exterior Envelopes of Buildings VI*, Clearwater Beach, Fla., Dec 4-8, 1995, pp. 297-305.

[4.111]*Computer Model of the Drying of the Exterior Portion of Framed Walls - Updated Version*, Prepared by Scanada Consultants Ltd for Morrison Hershfield Ltd., 1986.

[4.112]Schuyler, G.D., Swinton, M., Lankin, J., "Walldry - A Computer Model that Simulates Moisture Migration Through Wood Frame Walls - Comparison to Field Data", *Proc.of Thermal Performance of the Exterior Envelopes of Buildings IV*, Clearwater Beach, Fla., Dec 4-7, 1989, pp. 492-505.

[4.113]Kuenzel, H.M., Kiessl, K., "Calculation of Heat and Moisture Transfer in Exposed Building Components", *Int. J. Heat Mass Transfer*, Vol. 40, No. 1, 1997, pp. 159-167.

[4.114]Karagiozis, A., *Overview of the 2-D Hygrothermal Heat-Moisture Transport Model Latenite*, IRC Internal Report, National Research Council of Canada, Ottawa, 1993.

[4.115]Karagiozis, A. And Solonvaara, M., "Moisture Transport in Building Envelopes Using an Approximate Factorization Solution Method", *CFD Society of Canada Meeting*, Toronto, June 1-3, 1994.

[4.116]Karagiozis, A., "Moisture Engineering", *Proc. of Seventh Conference on Building Science and Technology*, Toronto, March 20-21, 1997, pp. 94-112.

[4.117]Hens, H., *Final Report Task 1: Modelling Common Exercises. Summary Reports.* Annex 24, Heat Air and Moisture Transfer in Insulated Envelope Parts, International Energy Agency, 1996

5. RAIN, DRIVING RAIN, AND ENCLOSURE WALLS

The amount of water deposited on the above-grade building envelope by driving rain is larger than any other source of moisture in almost all building types and climates. Both the deposited rain absorbed by the cladding and water penetration of the cladding can be a significant source of moisture for many deterioration mechanisms. Despite the importance of driving rain to building performance, very little is known about the magnitude, duration, and frequency of driving rain and driving rain deposition on buildings.

The volume of water deposited on a wall system is the result of the interaction between the wind, rain, the building, and the building envelope. The stochastic natures of the wind and rain, and the many variables associated with the building site and geometry makes the prediction of driving rain deposition on a wall a difficult task. Even if the rate of rain deposition on a building surface were known, the relative amounts of absorption, face drainage, and penetration of water will depend on the cladding material, texture, and previous wetting history.

This chapter reviews the nature of rain, and explores the mechanisms involved in wind-rain-building interactions. The rain-wind-building interaction is examined in the following sections, based on previous research by others and supported by experimental measurements of Waterloo, Canada conditions. The interaction is considered below in four parts: the nature of rain, the coincidence of wind and rain at the site, driving rain, and the interaction of building's, wind, and rain.

5.1 Rain

It is generally accepted that condensation of water vapour onto condensation nuclei creates cloud droplets (aided by cooling as a result of air rising). Cloud droplets are perfectly spherical in shape (because surface tension forces are much larger than aerodynamic or gravity forces) and range from 1 to 50 μm in diameter with an average of 10 to 25 μm [5.1, 5.2, 5.3]. Such small drops fall so slowly that their movement is governed by the wind currents aloft and they act as suspended particles.

The precise mechanism of raindrop formation is not known, but the most widely accepted theory is based on ice accumulation around frozen condensation nuclei. Hence, this theory predicts that drops can only form within clouds that are below 0 °C. Because the vapour pressure at the surface of ice is less than that for water, an ice nuclei quickly grows in size by condensation. If the crystal diameter increases to more than about 0.10 to 0.25 mm, it begins falling. As the ice crystal falls through to warmer air layers, the ice melts and a raindrop forms.

If two rain drops in a rainfall touch, they will likely coalesce into a larger drop. Larger drops fall faster and can therefore overtake and absorb smaller drops, further accelerating their fall. However, if the resultant drop becomes too large, aerodynamic forces overcome the surface tension forces holding the drop together and the drop will break apart (both Grey [5.2] and Beard [5.3] suggest that drops with diameters greater than about 6 to 7 mm are unstable). Both the condensation and coalescence mechanisms are likely at work in the formation of most rain drops.

As the rainfall intensity increases, the probability of two raindrops colliding increases and the average raindrop diameter increases. This conclusion is supported by the field measurements of Best [5.4], Laws and Parsons [5.5] and Marshall and Palmer [5.6] but each group developed its own relationship (Markowitz [5.7] provides an excellent summary). More recent researchers have made use of radar readings [5.8, 5.9] and sophisticated electronic drop sizers [5.10, 5.11] to further explore raindrops size distributions. The general conclusion of this body of research is that the nature of the distribution clearly varies not only with rainfall intensity but also with the type of storm, the cloud height, etc. Figure 5.1 is a plot of the relative probability distribution of raindrop diameter as a function of rainfall intensity given by Best [5.4]:

$$F(\emptyset) = 1 - \exp\left\{-\left(\frac{\emptyset}{1.30 \cdot r_h^{0.232}}\right)^{2.245}\right\} \qquad \text{(Eq. 5.1)}$$

where, $F(\emptyset)$ is the cumulative probability distribution of drop diameters for a given rainfall intensity

$\emptyset$ is the equivalent spherical raindrop diameter (mm), and

r_h is the rainfall rate or intensity on a horizontal plane (mm/h).

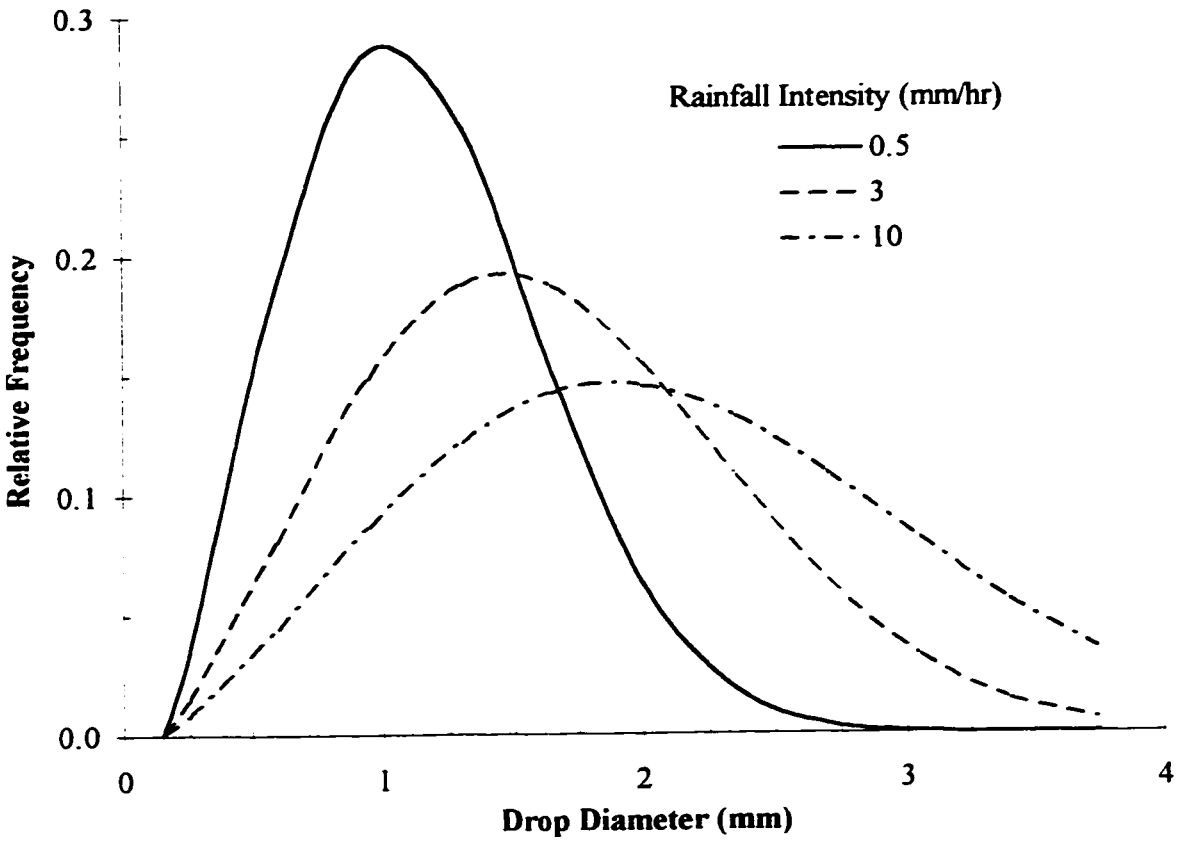

Figure 5.1: Distribution of raindrop sizes with rainfall intensity

While an accurate knowledge distribution of drop sizes may not be available, the physical characteristics of the drops themselves are well understood. Beard [5.3] recently collected the available experimental data of raindrop size, shape, and drag coefficient and, based on fluid dynamics principles, developed general relationships for the terminal velocity of raindrops as a function of air pressure and air temperature. These relationships match most available experimental data, including the comprehensive and widely accepted data of Gunn and Kinzer [5.12]. Figure 5.2 is a plot of this data. Dingle and Lee [5.13] developed a simplified equation, accurate to ±2.5%, for raindrop diameters of more than 0.3 mm: :

$$V_t(Ø) = -.166033 + 4.918440 - .888016Ø^2 + .054888Ø^3 \leq 9.20 \quad \text{(Eq. 5.2)}$$

where, $V_t(Ø)$ is the terminal velocity of a raindrop in still air (m/s).

More precise (± 0.5%) and much more unwieldy equations are available; see Beard [5.3].

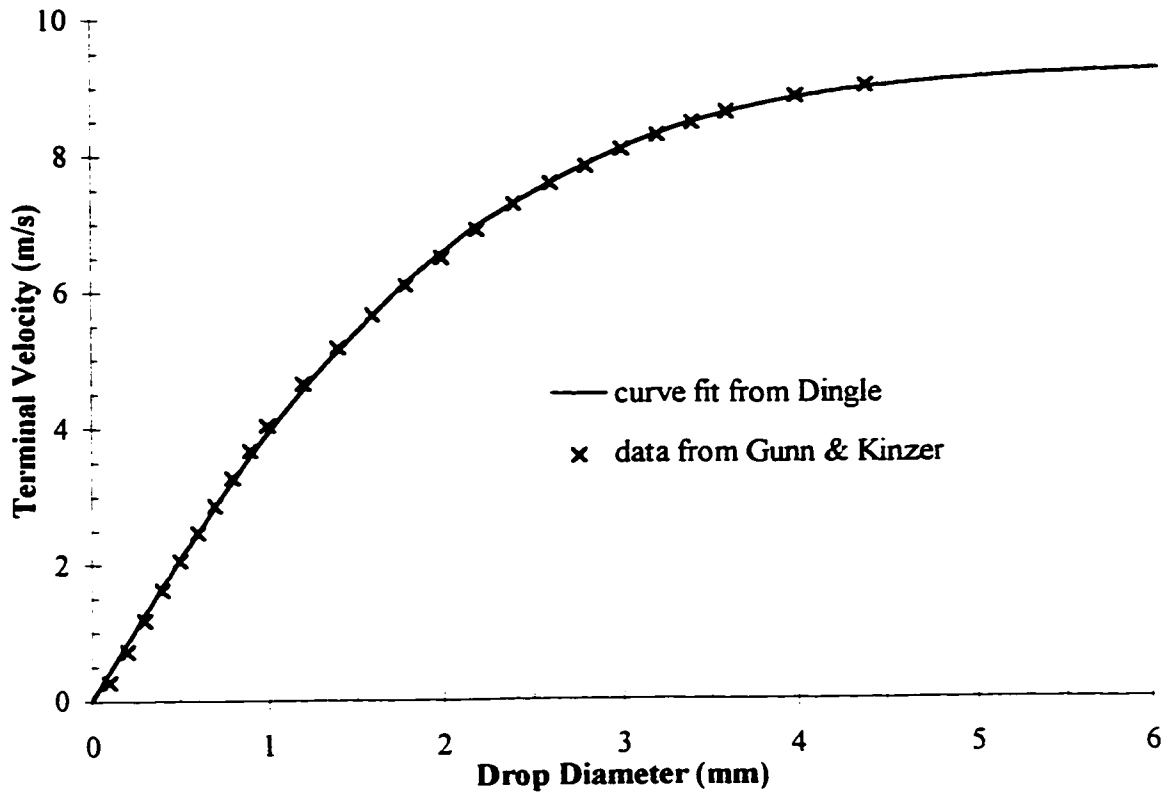

Figure 5.2: Terminal velocity of water droplets in still air

5.2 The Coincidence of Rain And Wind

Since driving rain is not routinely measured by weather stations, the ability to predict driving rain using the available and extensive records of rainfall and wind speed would be useful. It cannot, however, be assumed that the wind and falling rain can be modelled as statistically independent events. In fact, there is strong evidence to suggest that the wind-speed probability distribution is different during rain events [5.14], and it is well documented that the wind direction distribution is different during rain events [5.21,14].

The wind and rain data collected at the test hut over the same three season period as the driving rain (March 1 to October 31) was analysed to examine the coincidence of wind and rain.

Any day with more than 1 mm of total rainfall was considered a rainy day. A total of 77 days (31%) of the days were classified as rainy. Data from 15 minute periods was also

analysed. Of the 23 238 fifteen-minute averaging periods during the 245 days, rain was collected during 1088 (4.7%).

5.2.1 Wind speed during rain

The relative probability distribution of the wind speed during rain and the wind speed during all periods is plotted in Figure 5.3. The average windspeed is about 3 m/s. As expected, the wind speed follows a log-normal distribution. The wind speed during rain is only slightly higher in the mid-range but otherwise follows the same log-normal type of distribution.

While these limited results cannot be used to support any sweeping generalisations, the more comprehensive study of standard weather records by Surry et. al. [5.14] also found a increase in wind speed, especially for small rainfall rates. Nevertheless, the increase is small (of the order of 10%) and the change in windspeed with direction is more significant. The results support the use of the normal wind speed distribution as an approximation for the wind speed-during-rain distribution.

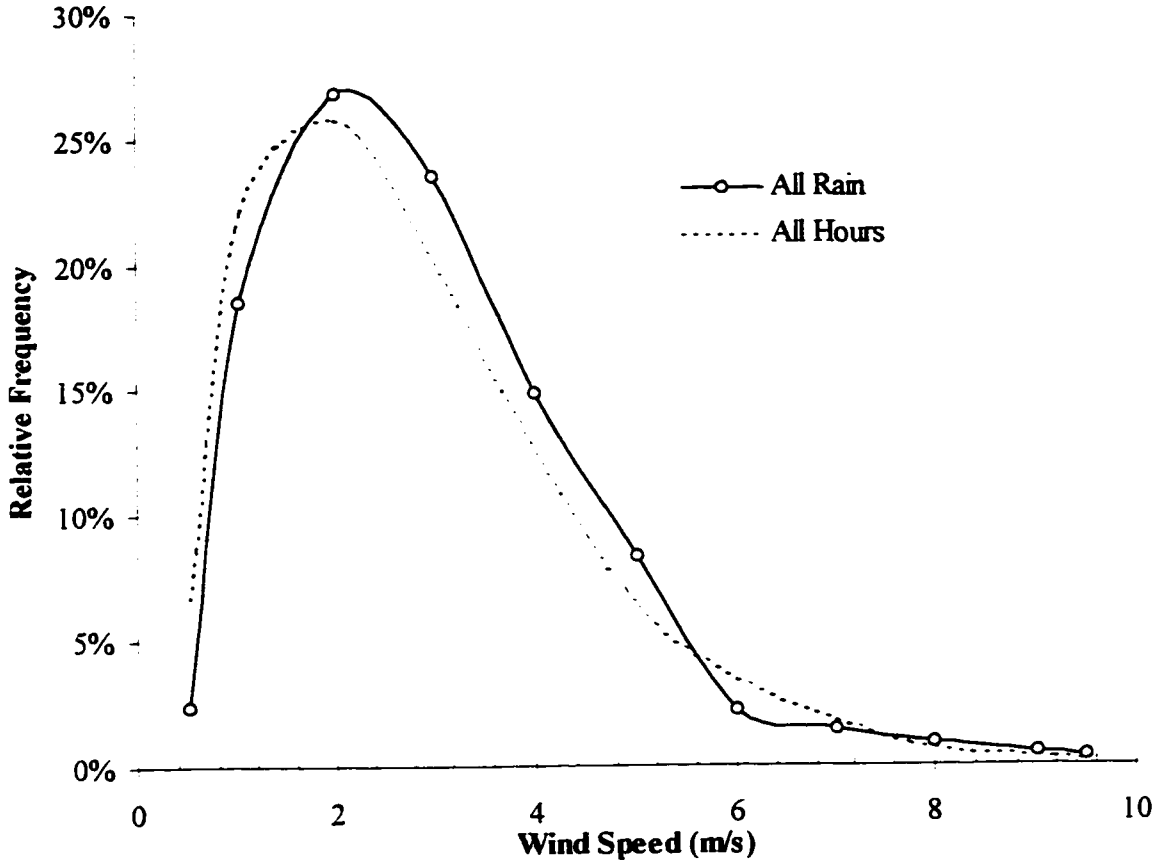

Figure 5.3: Distribution of wind speed during rainfall and all periods

Choi [5.21], in his study of the area around Sydney, found that the use of annual values of the driving rain index (i.e., based on the product of annual average wind speed and average annual rainfall) could result in significant (30-40%) under estimations versus indices based on hourly values.

Bear in mind that the distribution of *extreme* wind speeds during rain will be quite different than the normal wind speed distribution. In fact, the probability of the coincidence of very high wind speeds and high rainfall intensities is quite low because both events are relatively unlikely. Surry et. al. [5.14] found that the extreme wind speed during rain (any rain) was about 10 to 20% lower than the 1-in-10 year design speed for many Canadian locations. Choi also studied the joint probability of extreme wind and rain in Sydney [5.15]. He found that the wind speed during a 10 and 30 mm/hr rainfall were 73% and 29% of the 1-in-10 year speed respectively.

The seasonal wind speed-during-rain distribution for the Beghut test site was also investigated. The differences between the average wind speed distribution and the seasonal distributions were almost the same with and without rain. In all cases there was a bias toward slightly higher average wind speeds during rain. Finally, the wind speed-during-rain distribution was investigated for different rainfall intensities. Although there was no strong correlation between wind speed and rainfall intensity, it was evident that as rainfall intensity increased, there was a bias toward lower wind speeds, approaching those of the average. This trend was also supported by the climate analysis of Surry et al [5.14] for many locations.

The results of the above literature review suggest that the wind speed probability distribution during rainfall is not significantly different during rainfall, although slightly higher, than during all times. Seasonal changes in wind speed distribution are also reflected in the wind speed-during-rain distributions. As the rainfall intensity increases, the wind speed is likely to be slightly lower. These results will, of course, depend on the meteorological causes of rainfall. Waterloo's climate is believed to be representative of many non-coastal, non-mountainous regions.

5.2.2 Wind direction during rain

The wind-direction-during-rainfall distribution was also analysed. As is the case in many locations, driving rain is likely to come from different directions than wind during dry periods. Figure 5.4 shows the wind rose of the probability of wind from each direction during all hours and during rain. There is clearly a significant difference between the two wind roses. North American driving rain maps, however, provide a driving rain index that does not account for the different probabilities of direction. Similarly, the seasonal distribution is quite different. In Waterloo, driving rain is three times more likely to be accompanied by easterly winds than westerly winds in the spring, and southerly rains are only likely in the summer. The distribution of wind direction as a function of rain intensity showed that higher rainfall intensities could be expected from the east, and that light rainfalls were biased from the Northwest.

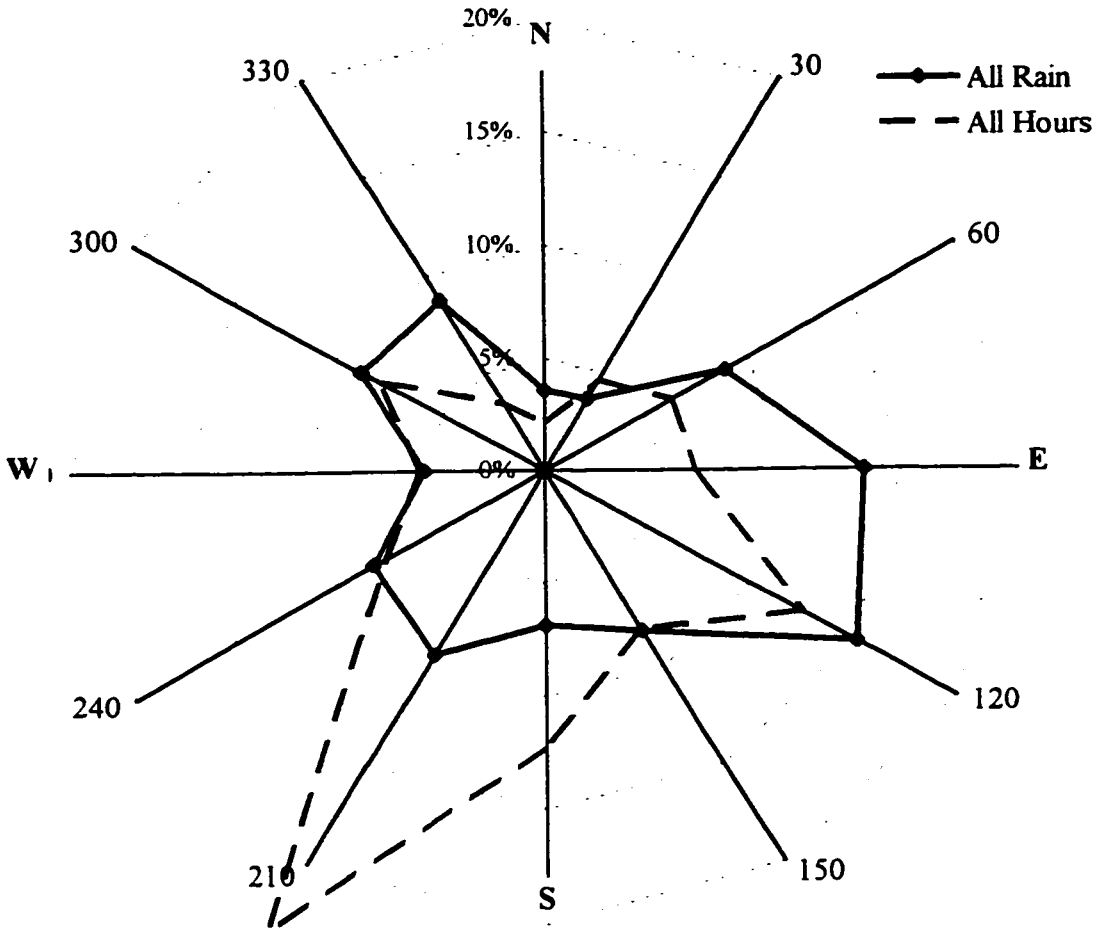

Figure 5.4: Wind direction distribution for Waterloo

Therefore, it can be concluded that the wind direction distribution during rain must be considered, both on an annual and seasonal basis if any reasonably accurate quantification of driving rain is desired. It is presumably for these reasons that some Scandinavian countries have calculated directional driving rain indices for different seasons and/or during periods when freezing could occur [5.16].

As a simple aid for the assessment of the combined influence of the wind and the rain, the Driving Rain Index (DRI) was defined by Lacy as the product of annual average wind speed and total annual rainfall. A more refined DRI was calculated from the present data using the 15 minute average values. The DRI so calculated will be identical to the annual values if the wind speed-during-rain probability distribution is the same as the normal wind speed distribution. This index is plotted versus direction in Figure 5.5. While the index is essentially a plot of the wind speed during rain, when normalised with regard to directional probability, the plot shows that twice the average driving rain can be expected from east,

while less than one quarter the average can be expected from the north. It is interesting to note that the largest directional value is about 10 times the smallest. Choi found the same range of values in his analysis of weather data in Australia [5.21].

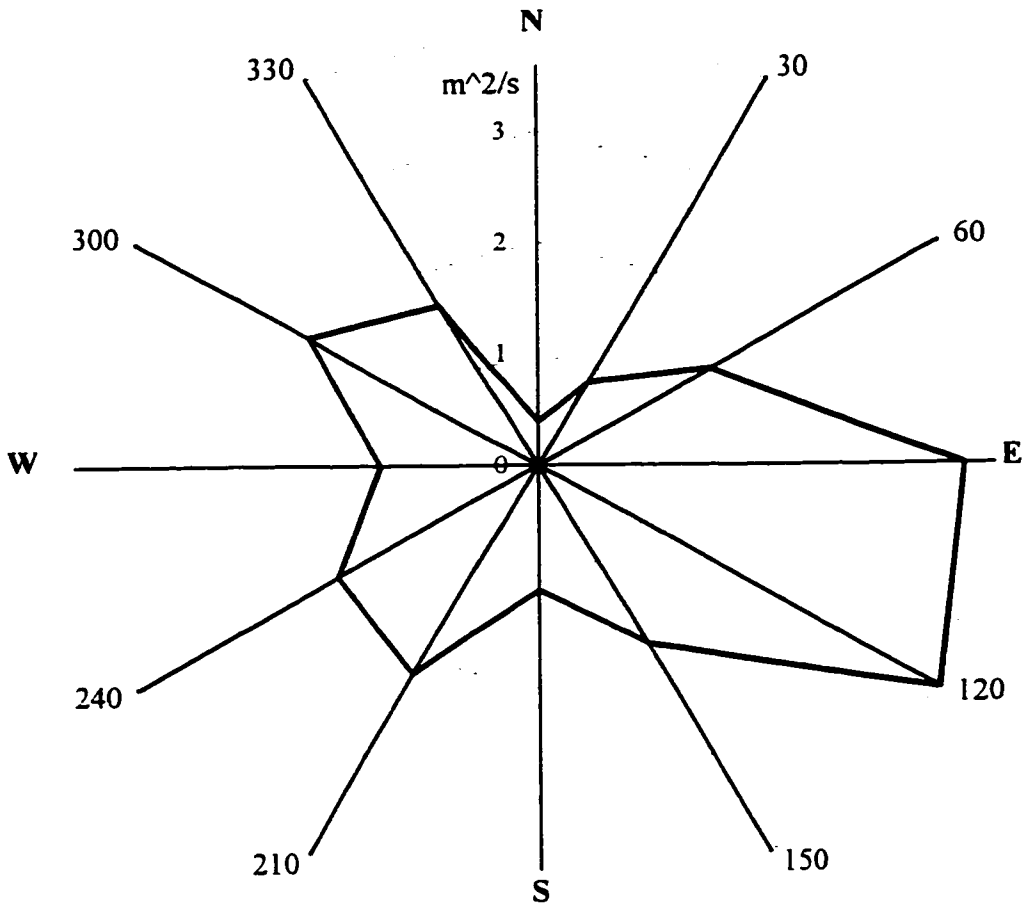

Figure 5.5: Waterloo driving rain index corrected for direction

5.3 Driving Rain

Driving rain can be defined as the amount of rain that passes through an imaginary vertical plane. It is generally accepted that driving rain is primarily a function of wind speed and rainfall intensity, but rain drop diameter and the wind turbulence also play a role. The following sections will examine the nature of the interaction of rain and wind and proposes a means of theoretically predicting driving rain.

5.3.1 Previous research

Lacy [5.17] conducted the seminal English-language field study of driving rain. He developed an equation by combining expressions of the median raindrop size as a function of rainfall intensity from Laws and Parsons [5.5] and the terminal velocity of such raindrops from Best [5.4]. The resulting relationship of wind speed and rainfall intensity to driving rain is:

$$r_V = 0.222 \cdot V \cdot r_h^{0.88} \qquad \text{(Eq. 5.3)}$$

Lacy's comparison of Equation 5.3 with 75 storms (each of more than 10 hours duration and with a total rainfall of more than 5 mm) showed a very good fit. Both because of the lack of other information, and the quality of the fit to the data, Lacy's equation has been the basis of almost all subsequent theoretical and field studies of driving rain.

Lacy's equation is sometimes simplified by assuming that driving rain is a simple linear function of wind speed and rainfall rate. Lacy himself suggested the following widely used simplification:

$$r_V = 0.20 \cdot V \cdot r_h \qquad \text{(Eq. 5.4)}$$

Empirical constants other than 0.20 have been used by different researchers. Using an equation of a form similar to Equation 5.9, Lacy [5.18] calculated a value of 0.208 at Garston, U.K. Based on four years of results, Künzel [5.19] reported a value of 0.23, Frank [5.20] found a value of 0.20, and Choi calculated a value of 0.228 for Sydney, Australia [5.21]. Equation 5.9 assumes a constant DRF and a linear relationship between wind speed, rainfall rate and driving rain. These assumptions form the basis of most of the world's driving rain maps.

The British Standard BS8104 [5.22] codifies the existing knowledge of driving rain. It applies empirical coefficients to Equation 5.4. These coefficients are essentially modifiers of the windspeed to account for topography, but, surprisingly, do not directly factor in the effect of height.

5.3.2 The interaction of wind and rain

All but the largest rain drops reach their terminal velocity within about 20 m of beginning their fall [5.3, 5.12]. For building applications it can be assumed that the drops are at

terminal velocity. Similarly the horizontal velocity of the drops will equal the wind velocity within a short distance. From geometry (Figure 5.6) it can be seen that the fraction of falling rain that will pass through a vertical plane is:

$$r_v = r_h \cdot \frac{V}{V_t} \qquad \text{(Eq. 5.5)}$$

where, r_v is the rate of rain passing through a vertical plane, i.e. driving rain (mm/h = l/m^2/h = kg/m^2/h), and

V is the average wind velocity (m/s).

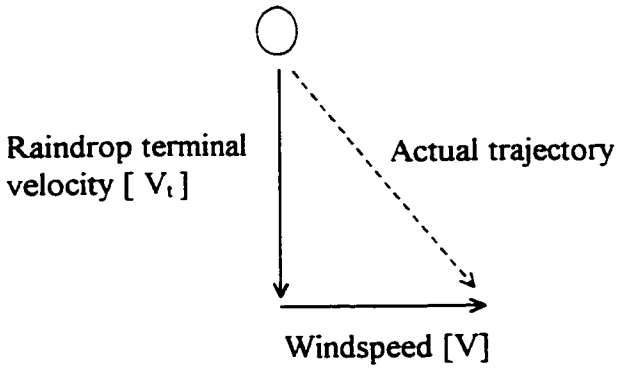

Figure 5.6: Vector analysis of raindrop trajectory

The trajectory of a falling drop will be curved since wind speed decreases significantly with decreasing height above the ground. The angle between the ground and the drop trajectory will decrease as the drop nears the ground.

It is also important to note that the mass of individual raindrops is sufficiently small that falling drops will respond to wind gusts of longer than about several seconds. Gunn and Kinzer's carefully controlled experiments showed that the largest raindrops (i.e., 6 mm diameter) would reach terminal velocity within 12 meters of beginning to fall. Their results included both slip and drag. Smaller drops, like those in most rain events reached terminal velocity much more quickly, within a few meters. Therefore, a droplet's horizontal velocity should reach that of the wind within a few seconds (e.g., 1 to 3).

Very close to the ground (where the wind speed changes quickly with height), at sharp changes in topography (e.g. hill tops), and around buildings (e.g. corners and tops of buildings), the momentum of a drop will cause its velocity components to vary from that

of the wind because the horizontal velocity changes too quickly for the droplet to keep up. This deviation will act to change the value of r_v predicted by Equation 5.5.

The mass of a spherical raindrop, and most raindrops are almost perfectly spherical, is

$$m_{drop} = \frac{4}{3} \cdot \pi \cdot r^3 \cdot \rho_{water} \qquad \text{(Eq. 5.6)}$$

The force required to accelerate a droplet can be found from Newton's law as:

$$F = m_{drop} \cdot a \qquad \text{(Eq. 5.7)}$$

and the drag force provided by air friction is:

$$F_{drag} = \frac{1}{2} \cdot C_d \cdot \rho_{air} \cdot V^2 \qquad \text{(Eq. 5.8)}$$

Neglecting time-dependent momentum effects, a raindrop will be expected to leave the airflow when the force required to accelerate the drop (Equation 5.7) to the speed of the airflow exceeds the drag force imposed by the flow velocity (Equation 5.8).

The wind velocity changes with height according to [5.23]:

$$V(z) = \left(\frac{z}{10}\right)^{\alpha} \cdot V_{10} \qquad \text{(Eq. 5.9)}$$

where, V(z) is the wind velocity (m/s) at a height z (m) above grade,

V_{10} is the velocity at the standard height of 10 m above grade, and

α is the gradient exponent.

The maximum acceleration rate of the wind for which a raindrop will remain in the air flow is plotted in Figure 5.7 for a suburban setting (i.e., α=0.22). As expected, small raindrop diameters will be more affected than large raindrop diameters.

The acceleration (rate of change of wind speed) expected at 3.5 m above grade is plotted in Figure 5.4 because it is at this height that the driving rain gauge is installed at the Beghut. The plot shows that for wind speeds of less than about 3.5 m/s (close to the average wind speed), droplets of more than 3 mm diameter will not follow the trajectory of the wind. Therefore the driving rain, r_v, in Equation 5.5 will be under predicted. At

low wind speeds the effect will be more pronounced. At high windspeeds the effect will be less.

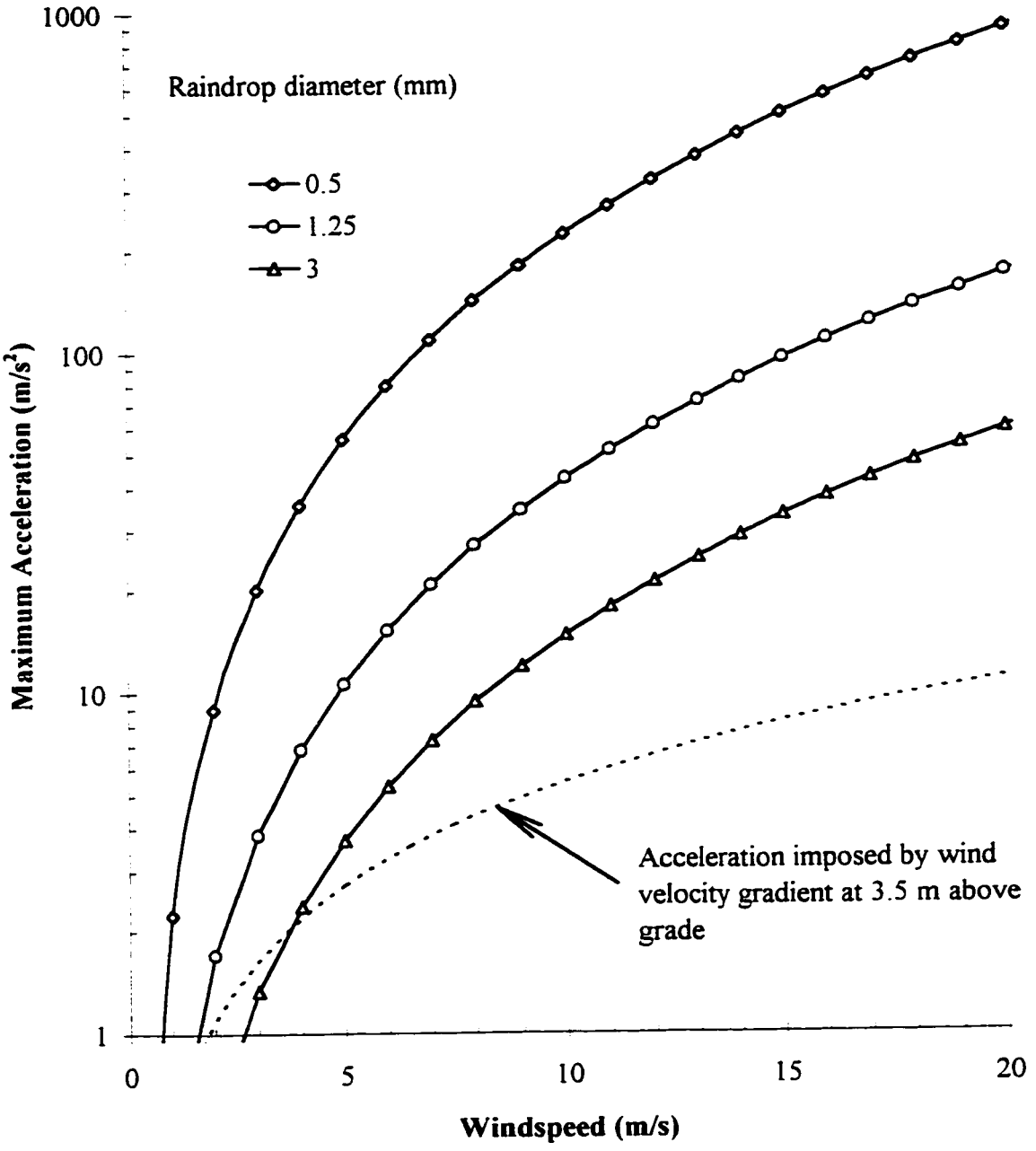

Figure 5.7: Raindrop size versus maximum airflow-induced acceleration

If higher accelerations are encountered, as they will be near building corners, significant deviations from that predicted can be expected.

It is proposed that a theoretically derived and more accurate form of Equation 5.3 is:

$$r_V = DRF(r_h) \cdot V \cdot r_h \qquad \text{(Eq. 5.10)}$$

where, DRF is the driving rain factor (s/m), a function of rainfall intensity.

The proportionality constant in Equation 5.10 relating rain on a vertical plane (driving rain) to rain on horizontal plane (falling rain) is defined here as the Driving Rain Factor (DRF). The empirical coefficients developed by previous researchers can be assumed to be average DRF values which do not account for the rainfall intensity.

However, it can be seen from Equation 5.5 that the DRF defined in equation 5.10 is:

$$DRF = \frac{1}{V_t(\phi)} \qquad \text{(Eq. 5.11)}$$

Therefore, the Driving Rain Factor is neither an empirical fitting factor, nor a "simplification" of Lacy's original empirical fit. The DRF can be directly and precisely found from the inverse of the terminal velocity of the raindrops (i.e., from Equation 5.2).

5.3.3 Field measurements of driving rain

A single free-standing driving gauge has been installed facing due west at a height 3.5 m above grade and 10 m upwind of BEG's test house. The wind, rainfall, and driving rain were collected at 5 minute intervals, and the average stored at 5 minute intervals. This data was analysed over the three season period from March 1, 1996 to October 31, 1996. The location and details of this instrumentation are presented in Appendix A.

Of the more than one thousand 15 minute periods during which it was raining, the DRF factor was calculated using Equation 5.10 for the 147 periods during which the average wind direction was within 30° of due west. The values were adjusted for the cosine of the average horizontal wind angle off perpendicular during each period.

Individual readings, and even average DRF values over the same rain event were found to exhibit considerable scatter. Many comprehensive measurements of raindrop size distributions (from ground and radar measurements) have also found a considerable amount of scatter, and it has been clearly shown that storms of different types have different rain drop size distributions [e.g., 5.10].

Despite the scatter between individual results, the average DRF over all events was found to be 0.215, very similar to the average DRF calculated by other researchers. As expected, the DRF factor varied with rainfall intensity because as the intensity increases, the drop size increases and so in turn does the raindrop terminal velocity. Table 5.1 compares the calculated DRF results (from Equation 5.10) with the values calculated using Lacy's original relationship (Equation 5.3). The average in Table 5.1 is the weighted average for the number of samples in each of the four different rainfall intensity categories.

Table 5.1: Measured DRF versus Lacy's Equation 5.3

Rainfall Intensity (mm/h)	Number of samples (Wind ± 30°)	Measured DRF (Eqn 5.10)	Lacy's DRF (Eqn 5.3)
< 1	43	0.272	0.244
1 - 2.99	55	0.220	0.237
3 - 4.99	23	0.188	0.223
> 5	26	0.136	0.187
Weighted Average	Sum = 147	0.215	0.228

The results in Table 5.1 clearly show that ignoring the effect of raindrop size (as Equation 5.4 does) will result in significant under predictions at higher rainfall intensities, the degree of which depends on the proportion of high and low intensity rainfalls. As Lacy and Choi [5.21] found, the DRF must be a function of rainfall intensity (or, more precisely, raindrop diameter).

Lacy used the following relationship of terminal velocity to rainfall intensity:

$$V_t(\emptyset) = 4.505 \times r_h^{0.123} \qquad \text{(Eq. 5.12)}$$

The median raindrop diameter of each data set of each of the rainfall intensity categories in Table 5.1 was calculated using Equation 5.1. The DRF was then calculated (Equations 5.11) for each data point from the raindrop terminal velocity using both Dingle and Lee's relationship (Equation 5.2) and that used by Lacy (Equation 5.12). Table 5.2 and Figure 5.8 present the results.

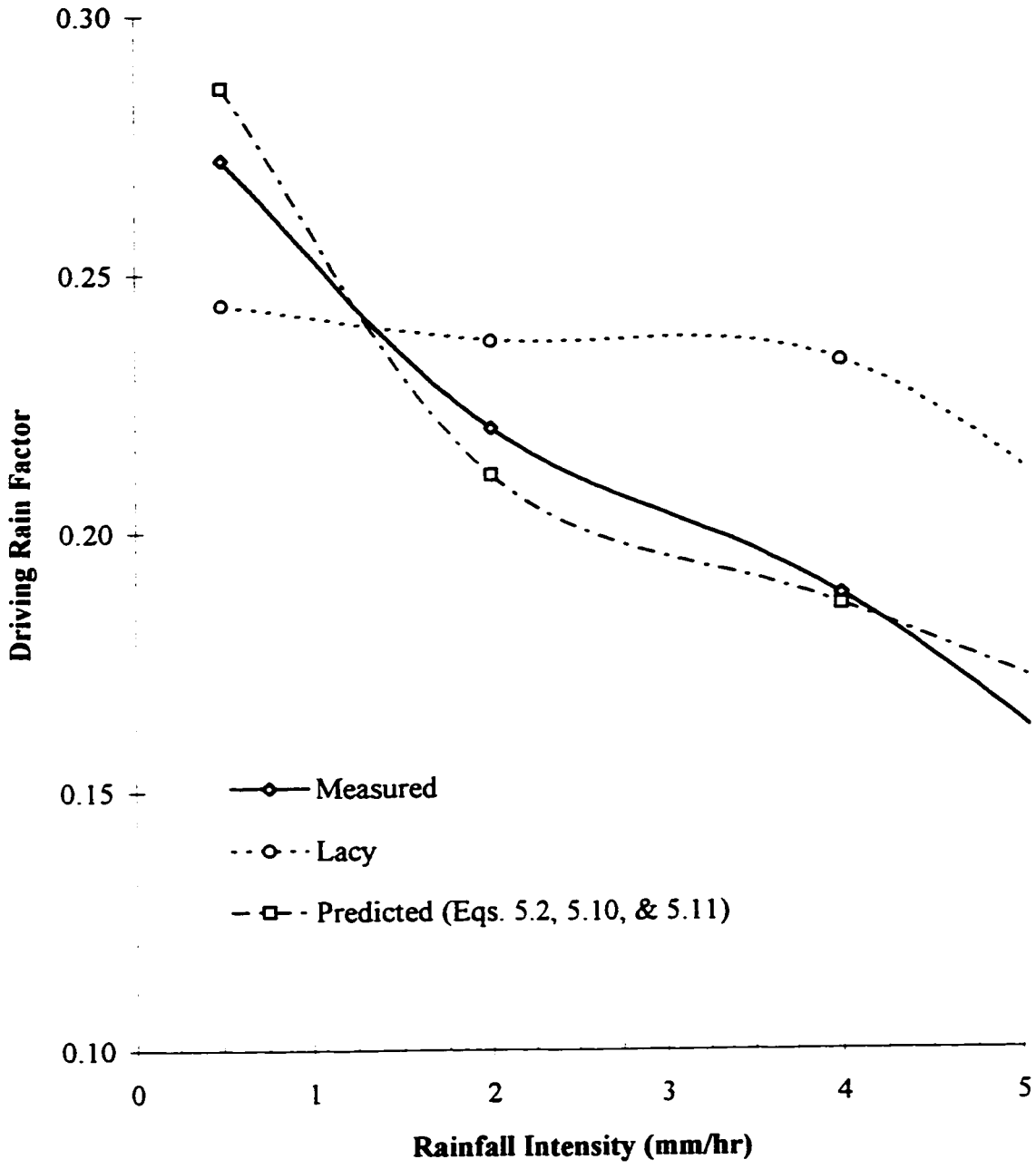

Figure 5.8: Comparison of measured DRF with that calculated by Lacy's method and proposed method

The agreement between the DRF calculated using the procedure recommended here, is seen to be good, especially considering the expected accuracy of the experimental results and the imperfect equations of raindrop diameter distribution. Using a constant DRF value of 0.20 or 0.22 will obviously result in significant errors for all rainfall intensities

other than 1-3 mm/h (the most commonly occurring rainfall intensity). If the average values are used to calculate the DRF, both equations are less accurate.

Table 5.2: Comparison of measured DRF and calculated DRF

Intensity Category (mm/h)	Median Intensity (mm/hr)	Median Drop Diameter (mm)	Measured DRF (Eqn 5.10)	Calculated DRF (Eqn 5.2)	Calculated DRF (Eqn 5.12)
< 1	0.37	0.88	0.272	0.286	0.224
1 - 2.99	1.80	1.27	0.220	0.211	0.216
3 - 4.99	3.60	1.49	0.188	0.186	0.211
> 5	10.26	1.90	0.136	0.158	0.204

Lacy's use of Equation 5.12 (based on the slightly inaccurate data of Laws and Parson) rather then Equation 5.2 (based on the much more comprehensive and widely accepted data of Gunn and Kinzer) resulted in small errors in terminal velocity. Very small errors in predicting the terminal velocity will, however, directly relate to the error in the DRF. Using the improved relationships for raindrop terminal velocity (Equation 5.2) and raindrop size distribution (Equation 5.1) can be seen to greatly improve the match between the experimental data compared to Lacy's equation. Lacy's equation likely fit his storm data well because the terminal velocity relationship of Equation 5.10 was reasonably accurate over the majority of rainfall intensities that he measured.

Although the DRF calculated using Equations 5.2 and 5.11 is typically within 5% of the measured data, it is in error by 15% for the highest rainfall category. As discussed earlier, the wind speed changes quickly with height at the gauge height of 3.5 m. Calculations show that the highest rainfall category contains a high percentage (> 50%) of rain drops large enough that they will fail to match the change in horizontal wind speed at the heights and wind speeds measured. If this is the case, it would mean that the equality in Equation 5.3 is no longer true. Until more data is analysed it is unlikely that any further analysis can significantly improve the fit demonstrated here.

The change of the DRF with rainfall intensity is important for the extrapolation of driving rain data collected by researchers to the values needed for assessing likely extreme values. During rare rain events, say with intensities of more than 25 mm/h, the median drop size

will be larger (2.3 mm), the terminal velocity higher (7 m/s) and the driving rain factor will therefore become quite small (0.140).

For routine estimations of rainfall over longer averaging times, e.g. for the analysis of typical in-service conditions, the use of Equation 5.10 with a DRF of 0.22 is appropriate. For more detailed studies and for the assessment of extreme rain conditions, the more detailed approach developed here may be warranted. Hygrothermal computer models which make use of detailed time-series weather files can, with little computational effort, calculate the driving rain approaching a building for every 15 min. or 1 hour period. Since real data appears to have a random scatter superimposed on the raindrop distribution, more sophisticated approaches could apply an appropriate random function to the raindrop distribution while remaining within the bounds of measured distributions.

5.3.4 Duration and intensity of rainfall and driving rain

The duration of rain fall also has a decided effect on the response of the building envelope. To assess the duration of rainfall, a rain event was defined as any period of rainfall within a 24 hour period with a total of at least 1 mm rainfall and uninterrupted by a period of longer than 12 hours. Using this definition, 60 rain events were so classified in the period considered.

The cumulative frequency of the rain event duration is plotted in Figure 5.9. As can be seen, the majority of events are less than about 8 hours long. Künzel [5.24], based on a different definition, found 60% of rain events at his South German location to be less than 8 hours long. These conclusions are sensitive to the choice of rain event definition, but do provide an indication of the range of durations that can be expected.

The cumulative frequency of rain intensity is plotted in Figure 5.10. The average intensity of rainfall was found to be about 3.4 mm/hr, but the distribution was skewed to lower rainfall intensities so that the median value was 1.8 mm/hr. For hydrological calculations, intensity-duration-frequency curves are often used. Such a plot (Figure 5.11), based on long term meteorological data, shows that intense rain falls may occur for short periods of time, but, as expected, the intensity will decrease as the duration increases. Such plots are generally available and can be used to guide the choice of extreme rainfall intensities. As discussed earlier, wind speeds during extreme rainfalls are likely to be significantly lower than design values.

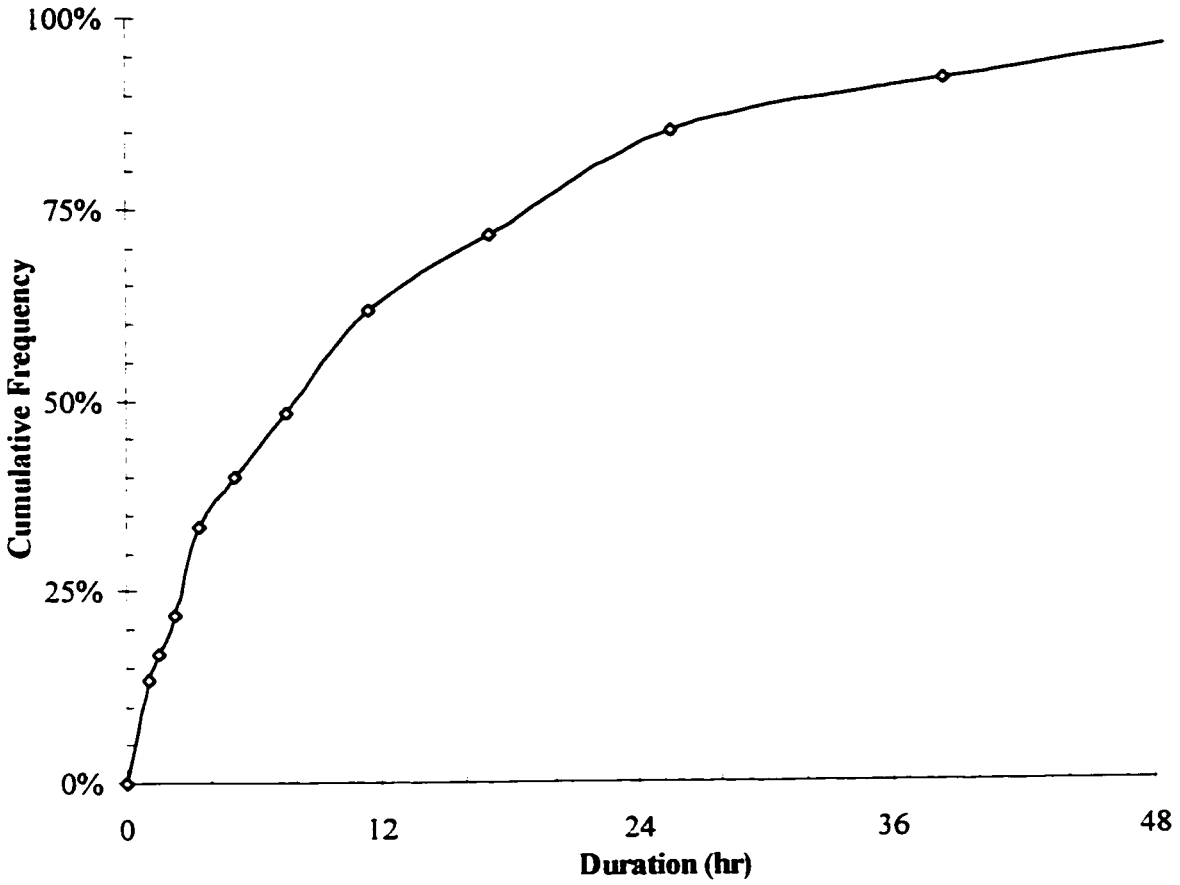

Figure 5.9: Cumulative frequency of rainfall duration

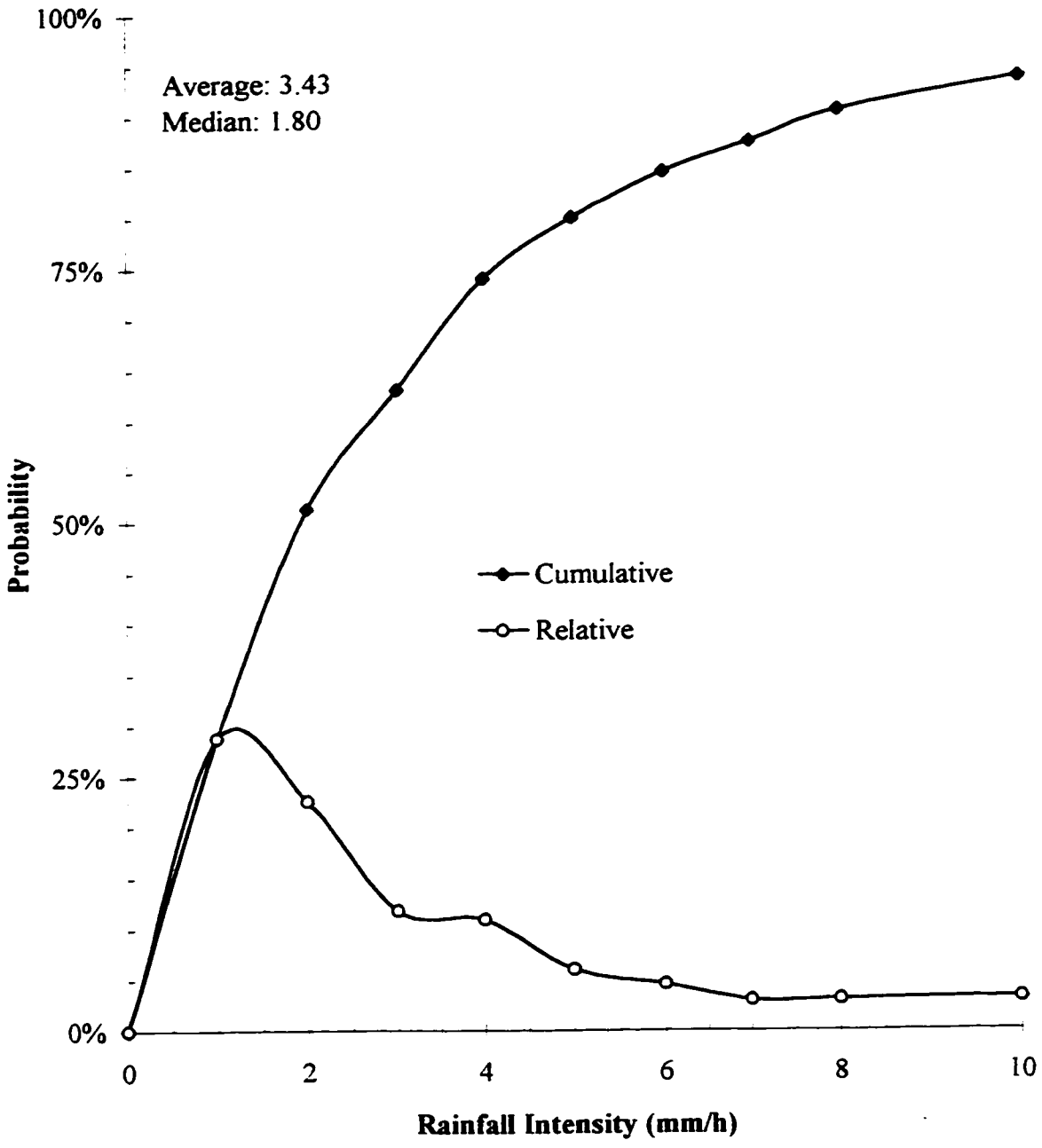

Figure 5.10: Distribution of rainfall intensity (based on 15 minute averages)

The distribution of the driving rain intensity (as measured by the gauge on the free-standing pole) is plotted in Figure 5.12. It should be noted that that the average value for driving rain is only 2.1 mm/hr and that 90% of driving rain has an intensity of less than 5 mm/hr.

The application of DRF and wind velocity information (from Equation 5.7) in Equation 5.10 shows that even for great heights (e.g., z=100 m, where the velocity is usually less than twice the velocity at 10 m above grade), driving rain intensity will often be much lower than commonly specified in test standards. The implications of this observation are addressed in Chapter 6.

The average and the median of the intensity of driving rain is less than that for rainfall (Figure 5.10). The average driving rain value is 61% of the falling rain intensity (2.09 Vs 3.43 mm/hr). This ratio is approximately the product of the average DRF and average wind speed (i.e., 0.2 x 3 m/s = 0.60, not including rain during calm periods).

All of the above merely provides an outline of the influence that site-specific weather and climate can have on driving rain calculations. Similar analysis can be conducted for any site given data with sufficient temporal resolution (preferably hourly). The exact nature of the rainfall-during-wind and wind-during-rainfall probability distributions need to be defined more accurately if driving rain at different sites are to be quantitatively assessed.

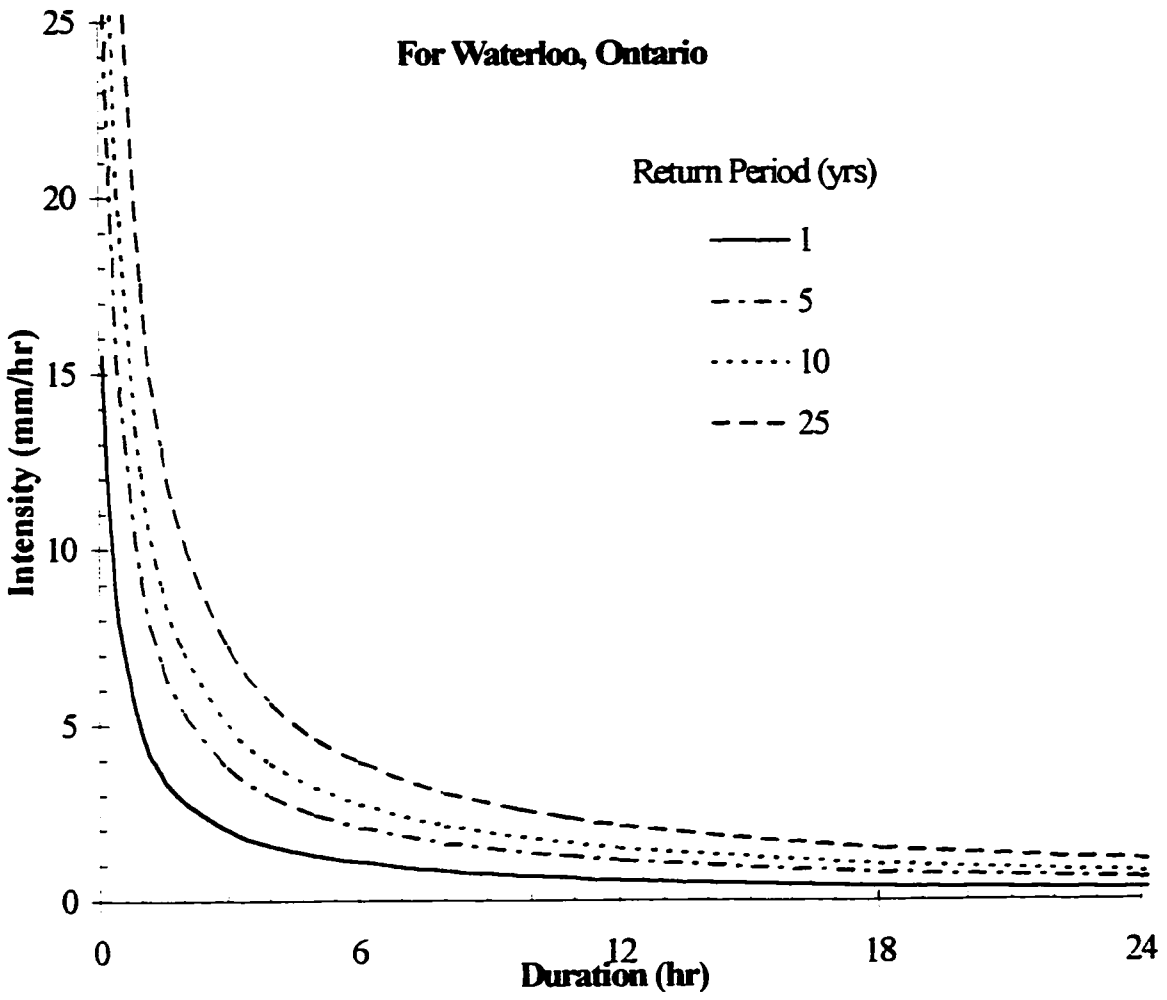

Figure 5.11: Intensity-Duration-Frequency curves for Waterloo

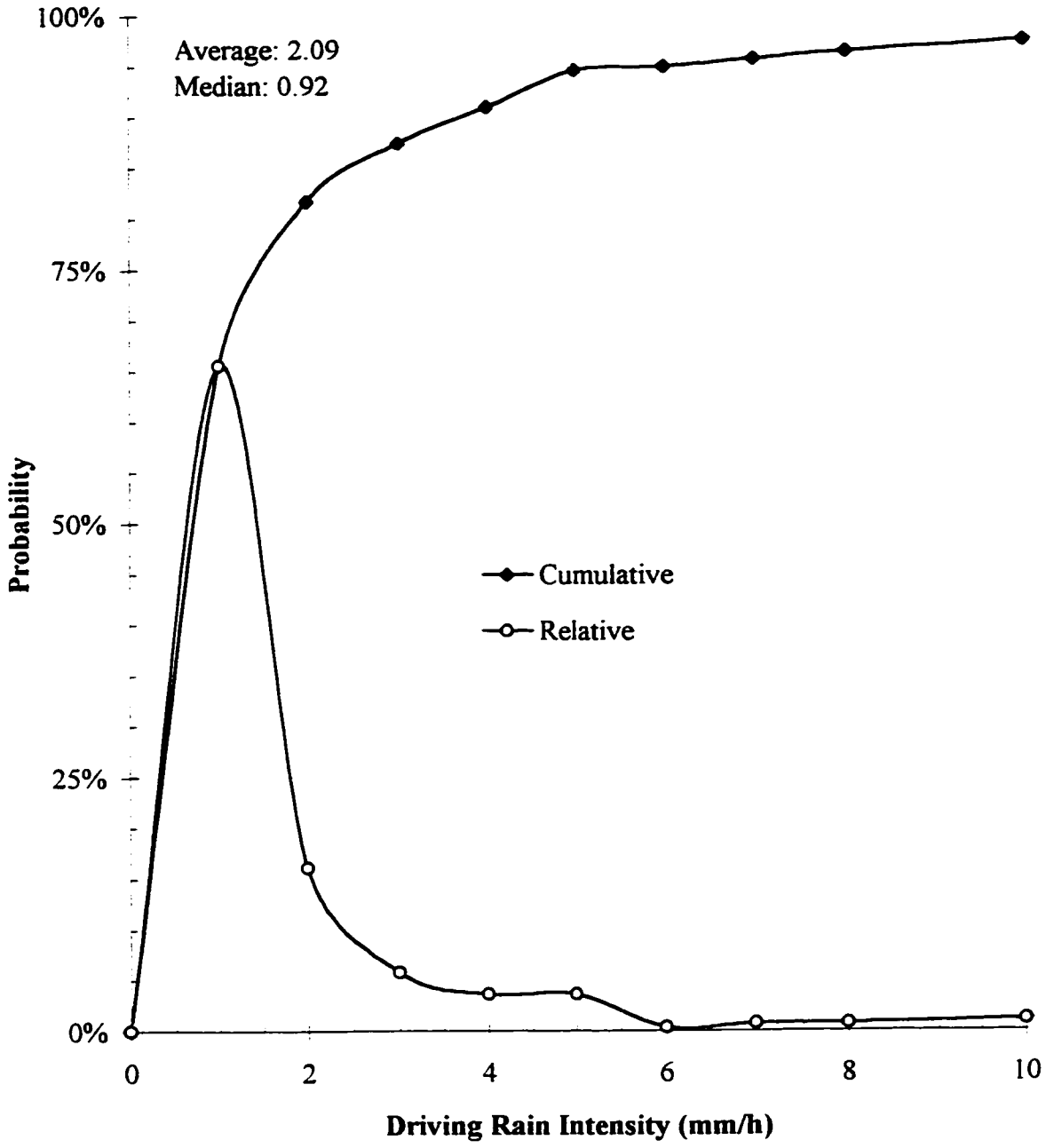

Figure 5.12: Distribution of driving rain intensity (based on 15 minute averages)

5.4 Interaction of Wind, Rain, and the Building Enclosure

As the wind encounters a building, stream lines and pressure gradients form around the building. While it is clear that driving rain is re-directed by these streams of air, accounting for this effect is difficult. As was discussed earlier, the reason it is difficult to predict the concentration of rain around buildings is that the raindrop trajectory will usually depart from that of the wind velocity vector. Given the wind velocity vector, the droplet drag coefficient, size, and size distribution, it should be relatively easy to calculate the rain deposition. However, the wind velocity vector cannot be calculated easily and can be accurately estimated only occasionally. While there are many Computational Fluid Dynamics (CFD) models available, all require large computer resources and none are sufficiently accurate or practical to be used for commercial building design. A practical and reasonably accurate approximation would be very useful.

To predict driving rain deposition on the vertical face of a building an extension of the previously developed model of driving rain in the free wind can be written:

$$r_{bv} = RAF \cdot DRF(r_h) \cdot \cos(\theta) \cdot V(z) \cdot r_h = RAF \cdot \cos(\theta) \cdot r_v \qquad \text{(Eq. 5.13)}$$

where r_{bv} is the rain deposition rate on a vertical building surface ($l/m^2/h$),

$V(z)$ is the wind speed at the height of interest (m/s),

θ is the angle between the normal to the wall and the wind direction, and

RAF is the rain admittance function, where $RAF = r_{bv} \div (r_v \cdot \cos(\theta))$.

A rain admittance function (RAF) is defined here as factor to transform driving rain at some horizontal distance (i.e. outside of the region disturbed by the building) to deposited rain on the building. The RAF accounts for the effect of the building on driving rain in the unobstructed wind. Based on the nature of building-rain interaction, it is likely that the RAF will be a strong function of the building's shape (aerodynamics) and the angle of attack of the wind. It is likely that the RAF is a function of raindrop size and size distribution, and wind speed.

The British Standard employs a similar wall factor, W, but modifies the wind direction using a different procedure.

5.4.1 Previous research

The literature contains only a few references of simultaneous measurements of driving rain in the environment and driving-rain deposition on a building. Recently, some researchers have pursued a computational fluid dynamics (CFD) approach [5.25] while others have begun wind tunnel modelling [5.26] to the help predict driving rain deposition on buildings.

Driving rain deposition studies in the literature usually report driving rain as a fraction of that collected in the free wind or simply as volumes collected. However, the RAF can often be calculated from published data. In most cases, the value of RAF is less than 1.0, and for low-rise, rectangular buildings the value near the centre can be assumed to be about 0.3. Sandin [5.27, 5.28] reported values of 0.3 (near the lower centre) to 1.0 (upper corners) in studies of driving rain on low-rise rectangular buildings. Lacy [5.18] reported values of 0.3 for the middle, and about 0.5 for the corner of a low-rise wall over a wide range of wind speeds and rainfall intensities. Henriques [5.29] measured an RAF value of 0.6 on the centreline of a low-rise building, but the gauge was mounted near the top of the partially-obstructed building at an unreported height above the free-wind gauge. Flori [5.30] found a RAF value of almost 0.6 and, more importantly, reported increasing values of the RAF factor (up to 1.2) as the wind angle changed from normal to the wall to parallel to the wall.

These values of RAF have been calculated from driving rain measured at the same height in the free wind for low-rise (less than 10m) buildings. Higher up a tall building, the driving rain intensity will be greater because wind speeds increase with height according to the power law (Equation 5.7). Lacy's [5.18] measurements near the top corner of a highly-exposed ten-storey apartment building suggest a RAF value of 1.0. However, Lacy reported that the amount of rain received a meter from the edge of the building appeared to be even greater.

Schwarz [5.31] measured driving rain deposition on an 18-story building for a seven-month period. The RAF factor was calculated to be 0.5 for the 10 m height. Extrapolating wind speed data higher up the tall building studied by Schwarz (using the appropriate power law), the RAF for other heights on the building can be calculated from his data. The calculated RAF for the ninth and sixteenth storeys was no different than that for the third story at 10 m above grade. The RAF calculated for the upper corners of the building, however, ranged from 0.9 to 1.0.

The results presented above (RAF = 0.3 to 0.5 for the centre of a building and RAF = 0.9 to 1.0 for edges and corners) match Sandin's results for a low-rise building. An important implication of these results is that driving rain deposition increases with height at the same rate as wind speed. The RAF also appears to be scale-independent, probably in a similar way as mean wind pressure gradients can be scaled for buildings of the same geometry.

Note that all of the measurements reported above are averaged over several rain events, or even over several years. The RAF is likely to vary with the wind speed and rain drop diameters of the individual storm, much like the DRF. However, unlike the DRF and windspeed, we do not now have sufficient information about the flow of wind around buildings to analytically predict the DRF (computer models like Choi's attempt to do this). Therefore, it is both difficult and impractical to attempt the calculation of more detailed RAF values. A larger database of field readings would however be invaluable in the assessment of the factors that affect RAF, and its variability.

Choi's CFD model [5.25] was used to assess extreme events, and so the results are difficult to compare to the field measurements by other researchers reported earlier. He calculated the amount of rain falling on a tall, narrow building with 3 horizontal and 4 vertical zones (a total of 12). For a 10 m/s wind speed and 10 mm/hr rainfall, he calculated a DRF of 0.48 in the top corner zone. Given the area over which the rain was calculated was equal to one-third the width and one-quarter the height, the RAF for smaller zones near the edges would likely be at least one. The importance of these theoretical RAF values is the trends exhibited by the RAF as a function of wind speed and rainfall intensity. Choi found that the RAF increased weakly with rainfall intensity (the maximum RAF increased by 25% for a fivefold increase in rainfall intensity to 50 mm/hr), and with strongly with wind speed (a 70% increase for a 300% increase in wind speed). The RAF changed by a factor of less than 2 for a combined 300% increase in wind speed and 500% increase in rainfall intensity.

Karagiozis [5.32] has conducted some of the most sophisticated CFD modelling. Because the results were presented as r_{bv}/r_h, they are difficult to cast into the form of a RAF. The results did show very little sensitivity to rainfall intensity despite the previously demonstrated influence of intensity on DRF. However, all of his simulations involved high rainfall rates, e.g., 10 mm/hr to 50 mm/hr. The rain deposition was linearly rated to wind speed (as predicted by Equation 5.13) except at the very top, where upward flow velocities appeared to distort this relationship (as expected). Rain deposition at the centre

was predicted to be about 1/3 that near the top, where an RAF of slightly more than 1.0 can be estimated from the data provided in the paper[†] .

Although there is not a large amount of data available, Figure 5.13 is a summary plot of the essentially consistent results available for the RAF of high and low-rise buildings.

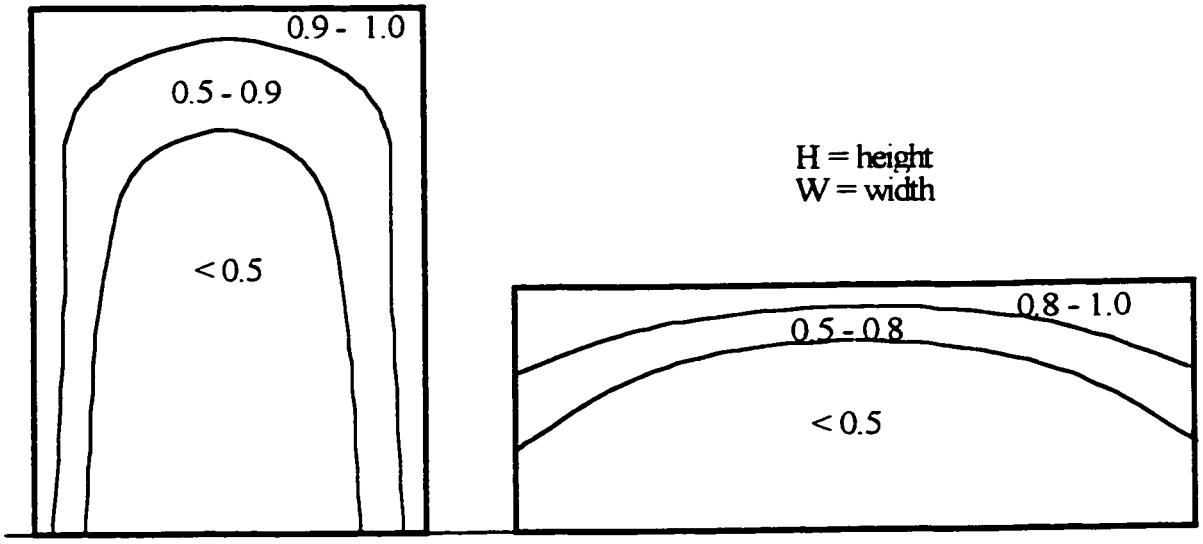

Figure 5.13: Rain Admittance Factor calculated from literature sources

5.4.2 Rain deposition measurements

A total of 14 driving rain gauges are mounted on the four faces of BEG's test house. The east and west elevations of the building have six gauges each, while the north and south each have one. The total driving rain captured by the gauges mounted on the east and west elevations for the same period of 245 days analysed earlier was analysed.

The actual amount of rain collected in the middle of each orientation is plotted as a function of frequency in Figure 5.14. These values do not include freezing rain or rain during the winter because such rain is difficult to measure. The east face clearly receives the most driving rain, almost 100 mm/year, while the north face receives one-third as much (30 mm/year). The seasonal distribution is also interesting. The west face receives the most in the summer, although the south face receives almost as much as the east and west.

[†] The wind speed at the top of the building was not given so the speed at gradient height was used to calculate the RAF from the results. The paper did give the exposure as suburban (α=0.22)

Using the actual measured amount of driving rain collected, the RAF was calculated for the total period for gauges of the west face. Similarly, using the DRF calculated as described earlier, the RAF for the gauges on the east face were calculated. Figure 5.15 plots these results.

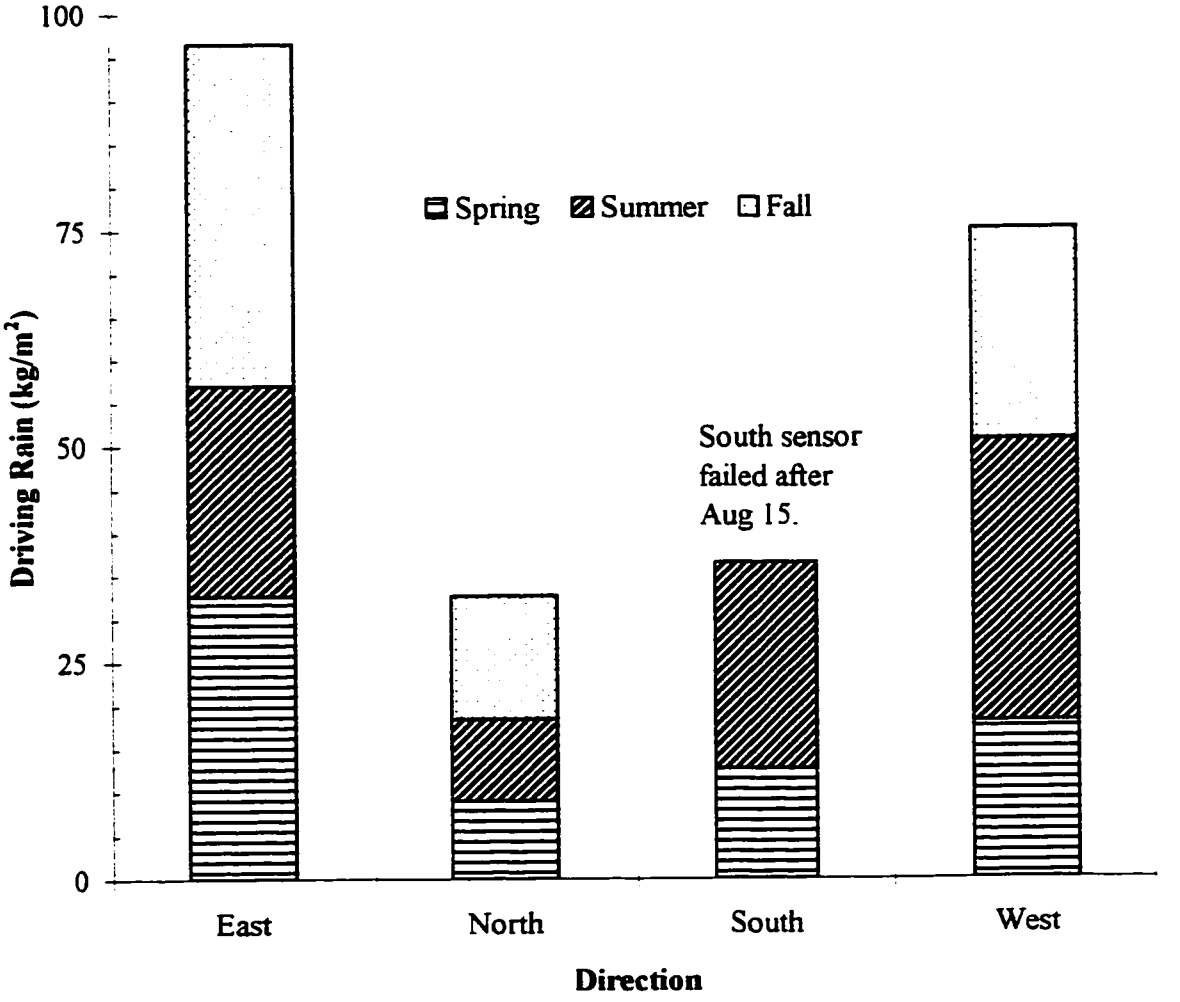

Figure 5.14: Measured driving rain deposition as a function of direction and season

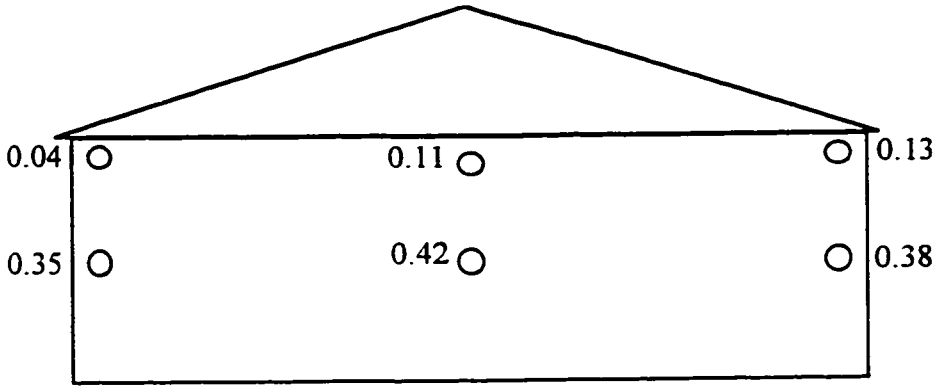

Measured Average RAF values for West Elevation

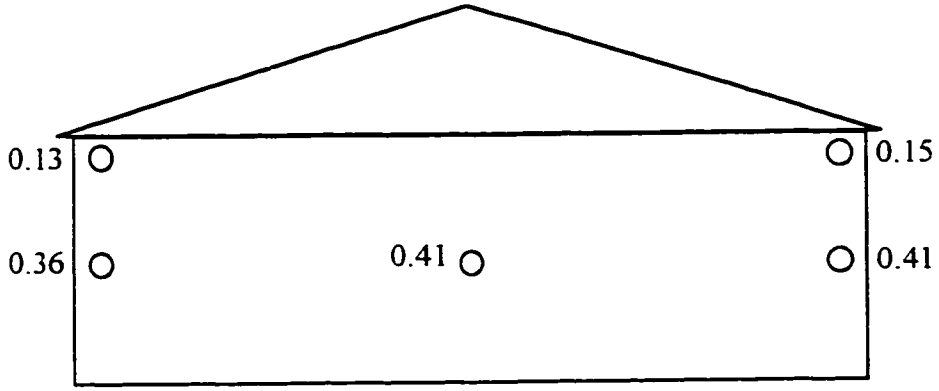

Measured Average RAF values for East Elevation

Figure 5.15: Measured Rain Admittance Factor at the Beghut

As can be seen from a comparison of Figure 5.13 and Figure 5.15, there are some obvious and significant differences. The four upper corner gauges consistently have a much smaller RAF than expected. This is due to 2 factors. The plots in Figure 5.13 are based on results from buildings with blunt top edges. Hence, the flow over and around these buildings is characterised by high lateral and vertical accelerations of the air mass near these building edges. The raindrops in the airflow will be unable to undergo such high accelerations and will leave the airflow on a trajectory less steep than the wind. This results in a concentration of rain drops at corners and sharp changes. The peaked roof of the test building reduces the rate of acceleration required for the air mass to rise up and over the building. Since the sides of the hut are reasonably blunt, the mid-height corner gauges capture the expected amount of rain.

The test hut also has a small overhang (approximately 200 mm). The overhang helps control more than just near-vertical rainfall, as observation and long-term experience of vernacular buildings show. By trapping upward flowing air near the top of the wall, an overhang will move the point of maximum vertical acceleration in the airflow further from the wall (Figure 5.16). Hence, when rain leaves the air flow, it is further from the wall and may fall downward completely missing the wall. At high wind speeds this effect will be small, but for the majority of rain events, a significant reduction of average RAF may be achieved.

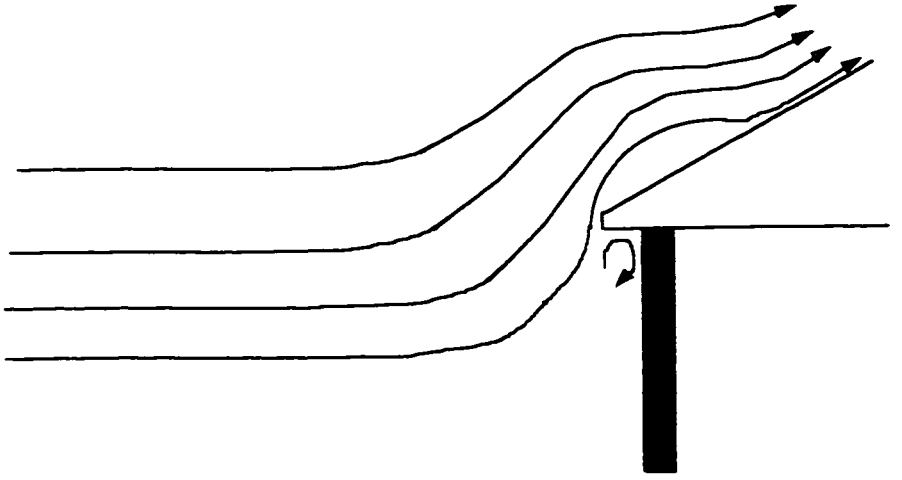

Figure 5.16: Influence of overhangs on airflow around Beghut

The beneficial effects of both overhangs and peaked roofs has qualitatively been observed in wind tunnel modelling of tall buildings [5.26]. A recent field survey of rain-related moisture damage in three and four storey structures in Vancouver showed a strong relation between the size of the overhang and the amount of damage [5.33]. The effect of overhangs on the airflow can likely have a significant beneficial effect on even relatively large multi-storey buildings and overhangs can and perhaps should be used as part of a rain control strategy.

5.4.3 Rainwater on walls

How water behaves once it strikes a wall is highly dependent on the nature of the wall and, to some extent, the location of the wall on the building. Rain water deposited on the surface of a wall will either be shed (i.e., flow away along the outer surface of the wall), absorbed by capillarity or otherwise stored in the wall material, or can penetrate further into the wall. The behaviour of rainwater on and in walls will be explored in more depth in the following two chapters.

5.5 Conclusions

A theoretical model of predicting driving rain in the environment has been developed in this chapter. This model improves on Lacy's mostly empirical work, especially for rain intensities other than the average. Comparison of predictions with field measurements and other researchers' work shows good agreement.

The field measurements also show that typical rain events are much less intense than widely believed: 90% of rain events resulted in driving rain deposition of less than 5 mm/hr. This implies that rain absorption can play an important role in cladding response to rain. Rain events also tend to be an average of about 8 hours long, but this statistic is dependent on the definition of event. Both of these conclusions are believed to be reasonably true for many of the inhabited parts of North America. However, the influence of hurricanes and ocean-driven storms along the eastern seaboard and Gulf coast greatly increases the amount of rain, and will likely increase the intensity and duration of rainfalls as well.

Describing the rain wetting of building facades, both under service and extreme conditions requires more work. Methods to quantify the coincidence of wind and rain and the seasonal and directional changes in driving rain from existing long-term weather records should be developed. More detailed field measurements, both to confirm the present DRF calculations, especially during extreme events, and to extend the existing body of RAF values are sorely needed, if only to calibrate and validate computer models and wind tunnel techniques. A significant amount of research is required to understand the effect of wind speed, wind direction and rain intensity on the RAF.

Using the driving rain theory developed in this chapter and hourly weather data tapes will allow for much more accurate assessments of driving rain exposure, regardless of the climate. Building designers and researchers are now in a position to approximate the amount of driving rain likely to be deposited on a building either during a storm, over a season, or over a year. The information is immediately useful for hygrothermal analysis computer programs that already use hourly weather data but require some means of assessing the driving rain moisture load. This knowledge can and should be used to properly design rain control measures and develop and implement appropriate test methods and performance models.

5.6 References

[5.1] Barry, R.G., and Chorley, R.J., *Atmosphere Weather and Climate*, 6 ed., Routledge, New York, 1992.

[5.2] *Handbook on the Principles of Hydrology*, ed. Donald M. Grey, National Research Council of Canada, Ottawa, 1970, pp. 2.2-2.3.

[5.3] Beard, K.V., "Terminal Velocity and Shape of Cloud and Precipitation Drops Aloft", *J. of the Atmospheric Sciences*, Vol. 33, 1976, pp. 851-864.

[5.4] Best, A.C., "The Size Distribution of Raindrops", *Quart. J. Royal Meteor. Soc.*, Vol. 76, 1950, pp. 16-36.

[5.5] Laws, J.O., and Parsons, D.A., "Relation of raindrop size to intensity", *Amer. Geophys. Union Trans.*, No. 24, pt. 2, pp. 453-460, 1943.

[5.6] Marshall, J. S., and Palmer, W. M., "The distribution of raindrops with size", *J of Meteor.*, Vol. 5, Aug. 1948, pp.165-166.

[5.7] Markowitz, A.M., "Raindrop Size Distribution Expressions", *J. of Appl. Meteor.*, Vol. 15, pp. 1029-1031, 1976.

[5.8] Rogers, R.R., and Pilie, R.J.,"Radar Measurements of Drop-Size Distribution", *J. of the Atmospheric Sciences*, Vol 10, Nov. 1962, pp. 503-506.

[5.9] Caton, P.G., "A study of the raindrop-size distributions in the free atmosphere", *Quart. J. Royal Meteor. Soc.*, Vol 92, 1966, pp. 15-30.

[5.10] Dingle, A.N. and Hardy, K.R., "The description of rain by means of sequential rainddrop-size distributions", *Quart. J. Royal Meteor. Soc.*, Vol. 88, 1962, pp. 301-314.

[5.11] Bradley, S.G., and Stow, C.D., "The Measurement of Charge and Size of Raindrops: Part II. Results and Analysis at Ground Level", *J. of Appl. Meteor.* Vol 13, Feb 1974, pp. 131 - 147.

[5.12] Gunn, R, and Kinzer, G.D., "The terminal velocity of fall for water drops in stagnant air", *J. Meteor.*, Vol 6, pp. 243-248, 1949.

[5.13] Dingle, A.N., and Lee, Y., "Terminal Fall Speeds of Raindrops", *J. of Appl. Meteor.*, Vol 11, August 1972, pp. 877 - 879.

[5.14] Surry, D., Skerlj, P. , Mikitiuk, M.J., "An Exploratory Study of the Climatic Relationships between Rain and Wind," Final Report BLWT-SS22-1994, Faculty of Engineering Science, University of Western Ontario, London, September, 1994.

[5.15] Choi, E.C.C., "Determination of wind-driven rain intensity on building faces", *J. of Wind Eng. and Indus. Aerodynamics*, Vol 51, 1994, pp. 55-69.

[5.16] Nevander, L.E., Elmarsson, B., *Fukthandbok*, Svensk Byggtjaenst, Stockholm, October, 1981.

[5.17] Lacy, R.E., "Driving-Rain Maps and the Onslaught of Rain on Buildings". *Proceedings of RILEM/CIB Symposium on Moisture Problems in Buildings*, Helsinki, 1965.

[5.18] Lacy, R.E., "Driving Rain at Garston, U.K.", *CIB Bulletin*, No. 4, pp. 6-9, 1964.

[5.19] Künzel, H.M., *Bestimmung der Schlagregenbelastung von Fassadenflächen*. Fraunhofer-Institut für Bauphysik, Mitteilung 263, No. 21, 1994.

[5.20] Frank, W. *Entwicklung von Regen and Wind auf Gebaeudefassaden*, Verlag Ernst & Sohn, Bertichte aus der Bauforschung, 1973, Vol 86, pp. 17-40.

[5.21] Choi, E.C.C., "Parameters Affecting the Intensity of Wind-Driven Rain on the Front Face of a Building", *Proceedings of the Invitational Seminar of Wind, Rain, and the Building Envelope*, University of Western Ontario, London, Canada, May 16-18, 1994.

[5.22] BSI. *British standard code of practise for assessing the expossure of walls to wind-driven rain*, BS 8104, British Standards Institution 1992.

[5.23] Commentary to the National Building Code of Canada, Chpt 4: Commentary B, Wind Loads, 1990. Many other sources are also available.

[5.24] Künzel, H.M., *Regendaten für Berechnung des Feuchtetransports*, Fraunhofer Institut für Bauphysik, Mitteilung 265, 1994.

[5.25] Choi, E.C.C., "Determination of the wind-driven-rain intensity on building faces", *J. of Wind Eng. and Indus. Aerodynamics*, Vol 51, 1994, pp. 55-69.

[5.26] Inculet, D.R., Surry, D., "Simulation of Wind-Driven Rain and Wetting Patterns on Buildings," Report BLWT-SS30-1994, Faculty of Engineering Science, University of Western Ontario, London, November, 1994.

[5.27] Sandin, K., "The Moisture Conditions in Aerated Lightweight Concrete Walls", *Proc. of Symposium and Day of Building Physics*, Lund University, August 24-27, 1987, Swedish Council for Building Research, 1988, pp. 216-220.

[5.28] Sandin, K., *Skalmurskonstruktionens fukt- och temperaturbetingelser*. Rapport R43:1991 Byggforskningsrådet, Stockholm, Sweden, 1991.

[5.29] Henriques, F.M.A., "Quantification of wind-driven rain - an experimental approach", *Building Research and Information*, Vol. 20, No. 5, 1992, pp. 295-297.

[5.30] Flori, J-P., *Influence des Conditions Climatiques sur le Mouillage et le sechalge d'une Facade Vertical*, Cahiers du CTSB 2606, Sept. 1992.

[5.31] Schwarz, B., "Witterungsbeansphruchung von Hochhausfassaden," *HLH* Bd. 24, Nr. 12, 1973, pp. 376-384.

[5.32] Karagiozis, A. And Hadjisophocleous, G. "Wind-Driven Rain on High-rise Buldings", *Proc. Of Thermal Performance of Exterior Envelope of Buildings VI*, December 1995, pp. 399-406.

[5.33] *Rain Penetration Control: Applying Current Knowledge*. Draft Morrison-Heshfield Report for CMHC, Ottawa, January 5, 1998.

6. RAIN CONTROL THEORY

The design of the enclosure to control rain penetration and rain shedding is typically based on experience, rules of thumb, and traditional details. Unlike heat flow, vapour diffusion, exfiltration, etc. there is no rain control *theory* to aid the designer or analyst of enclosures.

The last chapter presented theoretical and empirical means of predicting the amount of driving rain that can be expected to be deposited on a vertical above-grade building enclosure. The objective of this chapter is to develop a rational and rigorous means of describing, understanding, and classifying rain control for the above-grade enclosure. Such description and classification is needed because it:

- aids designers in understanding the function of each layer and material in an assembly. Such understanding will result in better enclosure designs that more reliably and economically meet a project's performance requirements.
- allows water penetration tests to be developed and applied that impose realistic loads and that more closely match likely service conditions. The results of such testing can also be more accurately interpreted to aid the prediction of actual performance under extreme and typical loadings.
- provides a means for the accurate assessment of the reasons for enclosure failures and therefore proper repair and retrofit strategies.

What happens to rainwater deposited on an enclosure wall is discussed first. The relative amount of water dealt with by each fraction, and at which layer is shown to be a rational means of describing the behaviour of an envelope exposed to rain.

6.1 Drainage, Storage, and Transmission

Rain deposited on a wall can either be drained (the term shed is often used in the context of the exterior surface of a wall, or surface drainage), stored (absorbed by capillarity or attached by surface tension), or transmitted further into the wall (rain penetration or infiltration are other common terms). At the exterior surface of a wall, some of the water deposited might be removed from the surface by features such as drips and ledges. Each layer within a multi-layer wall responds in a similar manner to that described above.

If water penetrates through an entire wall assembly, that assembly has failed to control rain penetration. However, complete water penetration of the enclosure is not necessary for failure since transmission of rain water into any sensitive layer of a wall assembly may also cause damage, degrade performance, and affect durability. Although all water theoretically causes wetting, in a practical sense only the water that is stored for longer than a few minutes (see Chapter 2) will be considered to have caused wetting, i.e., it must be subsequently removed by one of the drying mechanisms described in Chapters 2 and 4.

The above reasoning can be made more rigorous by applying simple mathematical rules. Consider the enclosure assembly element shown in Figure 6.1. This n-layer wall system can be discretised into smaller sub-elements, each chosen to be sufficiently small so that the drainage, storage and transmission characteristics are constant over the element.

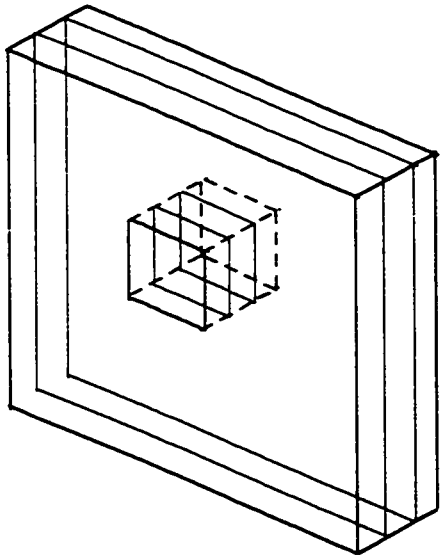

Figure 6.1: Discretisation of enclosure into sub-elements and layers

At each layer i, the water from the previous layer, i-1, must be either stored (S_i), drained (D_i) or transmitted to the next layer (T_i) (Figure 6.2). Since the sub-element under consideration is one-dimensional, drainage is considered as water that leaves the assembly. In a 2-D (height and layers) or 3-D (height, width, layers) analysis, drainage ($D_{i,x,y}$) may subsequently become stored ($S_{i,x,y}$) or transmitted water ($T_{i,x,y}$) in an adjoining sub-element.

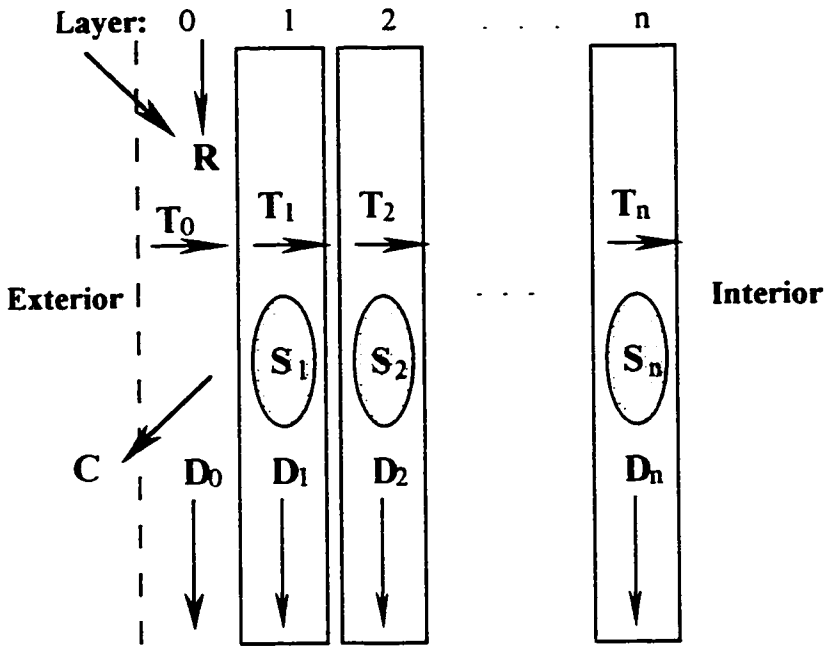

R = rain deposition and drainage from above
D = drainage (or shedding on outside layer)
S = storage: capillary absorption + surface tension
T = transmission
C = reflected drops, water cast off of surface

Figure 6.2: Distribution of rain within a multi-layer enclosure assembly

From observation of Figure 6.2 and conservation of mass:

$$\sum_{i=0}^{n} D_i + \sum_{i=0}^{n} S_i + T_n = R - C \qquad \text{(Eq. 6.1)}$$

for any given period of time, ranging from a few seconds to an entire rain event. This constant relationship will henceforth be termed the DST ratio for brevity. R is the amount of surface water both from rain deposition (r_{bv} from Chapter 5) and drainage from above. C is the amount of water that is deposited on the enclosure, but splashes back, is removed from the surface flow by features such as drips, ledges, etc.

To provide a completely general analysis, a layer can be used to model both materials and interfaces, since interfaces between enclosure layers will often have an important influence on storage, drainage and transmission characteristics. This can be accomplished by

treating each interface as a small airspace. In real assemblies this is often how the interfaces actually behave (i.e., as two surfaces).

Water does not drain *in* a layer such as an airspace, but rather water flows along a surface, e.g., the interface between the back of the cladding and the airspace or the interface between roofing paper and a roof shingle. The use and definition of layers and interfaces in the model depends on the need and on the analyst's modelling preferences.

It is also useful to define an imaginary outer surface layer, layer zero. This imaginary layer allows one to consider surface drainage as this layer's drainage (D_0), water beading on the surface as storage (S_0), and transmission (T_0) as the water that penetrates the outer surface. Therefore,

$$D_0 + S_0 + T_0 = R - C \qquad \text{(Eq. 6.2)}$$

S_0 is almost always a negligible quantity for walls, although it can be significant for low-slope and flat roofs. By contrast, C is usually zero for roofs (rain drops may splash back from the surface on impact, but eventually end up on the roof), but can be quite significant for walls, especially for those walls with many drips and projections.

For walls, S_0 can be assumed to be almost zero and Equation 6.2 rewritten as:

$$D_0 + T_0 = R - C \qquad \text{(Eq. 6.3)}$$

which merely states the obvious fact that rain water deposited on a wall can either penetrate (T_0) or be drained (D_0). Cast off water, C, includes water that breaks free of the surface because of drops shattering on impact, surface projections, flashings, etc.

Since, the total amount of rainwater that reaches an interior wall layer (T_{i-1}) acts as if rain were being deposited, then for any given layer,

$$D_i + S_i + T_i = T_{i-1} \text{ for all layers } i = 1 \text{ to } n \qquad \text{(Eq. 6.4)}$$

It is useful to non-dimensionalise values on a per layer basis, thereby providing *fractions* of rainwater. Since $D_i + S_i + T_i = T_{i-1}$, then

$$\frac{D_i + S_i + T_i}{T_{i-1}} = 1.0 \quad \text{or,} \qquad \text{(Eq. 6.5)}$$

$$d_i + s_i + t_i = 1.0 \qquad \text{(Eq. 6.6)}$$

where the lower case letters are used to denote non-dimensionalised fractions.

The materials and arrangement of most practical assemblies is such that water cannot penetrate further than a specific layer, k, $k \leq n$, or it will be considered to have failed to control rainwater. In the case of k=n, every layer of the assembly is presumed to be tolerant to rain wetting. (Note: the assessment of layer k is limited by the fact that failure cannot be defined simply as the presence of moisture; the amount of moisture and the length of time are obviously important as well. However, from a design point of view, one can usually choose a layer beyond which rain water should not penetrate, e.g., into the studspace of a framed wall, or onto the drywall finish of a concrete masonry wall).

The description given above is valid for time scales of perhaps a few minutes. Because drainage is not instantaneous and rain intensity varies, mass may be not be conserved for very short time scales (e.g., a few seconds) since water may accumulate in a film before draining from the sub-element.

However, in longer time scales the relative fractions will change: as the amount stored in a layer increases, the rate of storage (absorption) will decrease (see Chapter 4) and as the intensity of deposition increases, the ability of materials to absorb water will decrease. An extreme example is highly absorbent cladding during low intensity rain events. Rain water deposited on the surface of the cladding will first be absorbed, perhaps for some time. Eventually, the surface will become saturated and absorption will stop. At this point surface drainage and transmission will begin. This behaviour is examined in the next chapter.

The above analysis of rainwater movement leads to a series of related conclusions:

1. the relative amount of water dealt with by each part of the DST ratio, and at which layer(s) is a rational means of describing the behaviour of an envelope exposed to rain;

2. because the response of materials and interfaces changes due to changes in moisture content, temperature, time, etc., enclosure response is a function of the same variables;

3. based on the previous conclusions, the rate and duration of rain deposition, the time between rain events, and the drying of the envelope, i.e., the environmental conditions preceding the time in question, may all influence the behaviour of an enclosure to a driving rain event.

These conclusions have significance for understanding the in-service performance and interpreting the results of rain penetration testing, both in the lab and the field.

6.2 Rain Control Strategies

Several different strategies are used to control or prevent rain penetration through building enclosures. The behaviour of an enclosure system may change with time, rainfall intensity, temperature, etc. However, a designer must chose a strategy so that s/he can design and specify a system, and typically this means the system must be designed for the worst likely rain scenario. In some cases this "worst case" is an intense short-duration rain storm. In other cases, the worst case may be a long-duration moderately intense storm. The three choices that are available to designers are discussed below in the context of drainage, storage, and transmission.

As has been discussed above, the intended or actual response of an envelope to driving rain can largely be described by the relative fractions of rainwater dealt with by each mechanism at each wall layer. Regardless of the control strategy, the amount of water drained from the surface is D_0 and the amount that penetrates the outer surface of the envelope is T_0. Bear in mind that R is the volume of rainwater deposited on the surface or drained from above and C is the amount of previously deposited water removed.

6.2.1 Perfect Barrier Systems

A multi-layer envelope may contain a single layer where the amount of rainwater transmitted inward must be zero, i.e., at one layer, j:

$$T_j = t_j = 0, \quad j \leq k, \qquad \text{(Eq. 6.7)}$$

Such a rain control strategy has been termed "face-sealed" by some groups. Although the perfectly water-impermeable layer j is often located on the exterior face of an assembly, e.g., for an EIFS cladding, j=1 and t_1=0, it need not be so. Therefore, the more generally accurate term "perfect barrier" system is preferred[1]. Since the transmission characteristics of the perfect barrier layer is almost always moisture content independent in practical systems, the rain control performance of a perfect barrier system is independent of previous weather conditions. Perfect barriers with j greater than 1 must also provide

[1] It may seem that "perfect barrier" is a redundant term, but the building industry almost always uses the term barrier in a relative, not absolute sense (e.g., vapour barrier, moisture barrier). Therefore it is deemed necessary to qualify the barrier as being perfect.

drainage or storage for layers $n < j$, e.g., inverted roofs may be perfect barrier systems, but they must still provide drainage.

In the special but common case of a face-sealed perfect barrier envelope $j = 1$, and the following characteristics apply:

$$T_1 = t_1 = 0 \qquad \text{(Eq. 6.8)}$$

and so,

$$D_0 = R - C \qquad \text{(Eq. 6.9)}$$

i.e., all driving rain deposition and surface drainage from above must be drained on the surface. Drainage and storage within the assembly therefore do not play a role in providing rain control in functional face-sealed perfect barrier systems.

6.2.2 Mass Systems

The oldest rain control strategy is to provide an assembly with enough mass to absorb all rainwater that is not drained or otherwise removed from the outer surface. By draining or absorbing all rain water, such an assembly can prevent inward transmission, i.e.,

$$\sum_{i=0}^{\leq k} S_i = T_0 \qquad \text{(Eq. 6.10)}$$

Although envelopes employing this strategy might be termed "storage" systems, "mass" is generally used because a large quantity of material is usually required to provide sufficient storage. Unlike perfect barrier or drained-screened systems the maximum quantity of rain that can be controlled is limited by the storage capacity available. Therefore, the performance of mass systems is highly dependent on weather conditions, e.g. if a series of rain events occurs and drying conditions are poor, the storage capacity may be exceeded and failure to control rain will result. Also, unlike perfect barrier or screened systems (see next), mass systems do need to use drainage within the assembly.

The storage capacity of the system is not the only characteristic in such a system that is important in rain control. The water permeance of the various layers and interfaces can play a critical role. For example, consider a 300 mm thick solid multi-wythe brick masonry wall with a certain amount of storage capacity. By applying a thin 15 mm

cement-based rendering, the storage capacity is only marginally increased, but the permeance of this outer layer is so low, even when cracked, that the rain penetration control is vastly improved.

Similarly, any treatment that reduces surface water absorption while not reducing the water storage capacity of a wall will increase the ability for the assembly to control rain. However, if water is not absorbed at the surface it will increase the frequency and duration of a film of flowing water on the surface of the enclosure. This in turn will increase the likelihood of rain penetration through flaws, cracks, and other openings, intentional or not, in the enclosure.

Therefore, the rain control of mass systems will be dependent on the storage mass provided for the permeability provided. If the water permeance of a material or assemblage were constant, then the measure would be moisture storage divided by water permeance. Since permeance is typically a function of a number of variables a simple ratio is not sufficient, and an assessment of the likely average or extreme permeance (depending on need) must be made.

6.2.3 Drained-Screened Systems

Another approach to controlling rain water is to accept that some water will penetrate the outer surface (hence the cladding "screens" rain) *and* provides drainage to remove it. The drainage need not be provided at one layer only. In fact, if drainage were to be provided at one layer only, the wall would be acting as a perfect barrier system, since for any layer j where $D_j = T_0$, $t_j = 0$, is the definition of a perfect barrier. Drained-screened walls instead control rain penetration by reducing the amount of water transmitted at each of several layers, i.e.:

$$\sum_{i=0}^{\leq k} D_i = T_0 \qquad \text{(Eq. 6.11)}$$

Since the dominant control mechanism is drainage, envelopes using such a strategy are sometimes called "drained" systems. However, the layered and screening nature of the assembly is also important in this approach. The defining characteristic of a screened-drained wall system is that the drainage need not be complete at any one layer, nor does transmission need to be completely controlled at any given layer, nor is storage required.

Because drained enclosure systems control rain penetration by reducing the successive fractions of water that are transmitted inward, the following relation can be defined:

$$\prod_{i=1}^{\leq k} t_i \approx 0 \qquad \text{(Eq. 6.12)}$$

The practical implications of Equation 6.12 can be better understood by considering an example assembly with three layers, each with a small penetration fraction, say 10%. The amount of rain penetrating the third layer would be $0.1 \cdot 0.1 \cdot 0.1 \cdot (T_0) = 0.001 \cdot (T_0)$. If all rain deposited on the envelope where to penetrate the screen ($T_0 = R - C$), the amount of water penetrating the third layer during a typical heavy rain storm would be 0.1% of 5 $l/m^2/hr$, or 5 $ml/m^2/hr$! Providing even a small amount of storage in the third layer will ensure that rain penetration is controlled. In fact, failure to control rainwater in such walls is usually the result of a failure to drain since the required amount of drainage equals $0.999 \cdot (T_1)$. This line of reasoning supports the "drained" part of the label applied to this type of system.

The term "rainscreen" has been rather loosely applied by practitioners and researchers to several special cases of drained walls, especially those that use several layers and several mechanisms to control rain. A rainscreen system typically contains a drainage layer as the second layer of the assembly, (i.e. $d_2 \approx 1.0$). The first layer is the screen, and the second layer is often the backside of the screen. Almost without exception, functional rain screen walls provide several additional drainage layers, for example, an airspace and sheathing paper. Modern windows, car doors, and two-stage joints are exceptions, in that they typically have precisely two layers (hence two stage). Although these types of joints provide an "almost" perfect inner layer, the intent of the outer layer is to significantly reduce the potential for any water on the second layer.

Pressure-equalised rainscreens are a very special case of drained-screened systems that moderate wind pressure to reduce the transmission fraction of the screen. The screen is, of course, much more than a rain screen in these wall systems, it is also a screen to the sun, impact, etc.

6.3 Actual Envelope Behaviour

Many functional envelope systems may actually perform quite differently than designed during most rain events. For example, if drainage, storage or both are provided in an

envelope designed and/or built as a perfect barrier system, the perfect barrier need not be perfect.

Exterior Insulation and Finish Systems (EIFS) are one of the most popular and contentious face-sealed perfect barrier enclosure wall systems. The existence of cracked, perforated (by windows, doors, etc.) and otherwise imperfect Exterior Insulation and Finish Systems (EIFS) has been widely documented. For example, in a recent survey of 50 EIFS-clad buildings, Kenney and Piper [6.1] found 91% of the buildings over 9 years old to have lamina cracks large enough for water penetration. There are, however, millions of square meters of EIFS in North America that continue to control rain. This is not necessarily because the lamina (the plane assumed by designers to be perfectly watertight) allows no transmission, but rather that the substrate has sufficient storage to store the small fraction t_1, that penetrates. In other cases, this storage capacity may act in conjunction with drainage that is inadvertently provided by interface layers and large pored or fibrous insulation materials. In most cases, EIFS fail because of very high exposure and poor detailing of the joints and penetrations (e.g., windows).

It is likely that many rain control failures of EIFS are the result of extreme exposure conditions and insufficient safe storage capacity behind the (often) somewhat less-than-perfect lamina. The inability of some types of EIFS systems to dry once rain penetrates often results in other serious performance and durability problems (for example, the well-publicised cases in Wilmington, North Carolina)

As noted earlier, a "rain screen" drained system typically contains a drainage layer as the second layer of the assembly, (i.e. $D_2 \approx 1.0$). In the popular brick veneer rain screen wall system, drainage is provided along both the inside face of the veneer, layer 2, and the outside face of the inner wythe, layer 4. The airspace acts as a capillary break so that the fraction crossing it is as small as possible, $t_3 \approx 0$. Provided drainage is provided, usually in the form of an unobstructed air space, such a wall system will control rain independently of moisture content. The critical characteristic of a drained wall system is that the drainage need not be perfect at any one layer, nor does transmission need to be completely controlled. Several "almost perfect" layers, each with the ability to drain, act in conjunction to control rain water.

Storage may also play an important role in drained-screened wall systems. For example, in most masonry veneers, S_1 = R-C during many rain events (which typically have rain deposition rates less than the masonry absorption rates: see Chapter 7) and therefore no

water is available to be shed or transmitted inward. However, during extended rainy periods and intense rain events, the veneer may become saturated, and some water will penetrate the permeable veneer (since masonry veneers are remarkably water permeable). The layers behind the veneer only need to perform their drainage function during extreme events, and it is therefore only during these events that drainage becomes critical. Inspection of many functional veneer walls shows that drainage is often blocked by mortar bridges and dams. The exposure conditions and storage capacity of such walls suggest that they are actually behaving as mass walls, with several low transmittance layers (e.g. the sheathing paper) behind the storage. While these walls may be functional, if they are used in an area with more driving rain deposition (e.g., near the top of high rise buildings) or less drying potential (e.g., Halifax, Vancouver or other rainy, coastal climates), the storage capacity is likely to be exceeded and rain control failure will result.

6.3.1 Roof Systems

Low-slope roof assemblies provide many examples of the perfect barrier approach. An inverted roof is one which has a waterproof membrane (t = 0) located below several layers of moisture tolerant materials such as crushed stone (i=1) , a geotextile (i=2), and extruded polystyrene insulation (i=3). In this assembly, $T_4 = 0$, and usually k=4. It is an accepted fact that a large fraction of water is drained along the top of the insulation (typically, $d_2 \cong 70\%$) in these systems. Nevertheless, the success of the design rests on the perfection of the protected membrane layer.

Most low-slope roofs are still designed with exposed membranes, i.e., face-sealed perfect barrier systems. Because of the often shorter-than-desired life-span of these roofs, a new philosophy has recently arisen [6.2]. This philosophy accepts the fact that the exposed membrane will not be perfect for the design life of the roof. Numerous layers of storage are provided, typically in the form of insulating fibreboard, which are sized to allow for the safe storage of moisture equal to T_1. Solar heating and appropriately vapour permeable inner layers assist in removing this water by evaporation and diffusion to the interior. This type of roof is therefore a mass system, with a very low transmittance outer layer and enhanced drying potential to the interior (ensured by not providing an interior polyethylene vapour barrier).

Sloped shingled roofs are drained-screened systems with the unique characteristic that the majority of drainage occurs on the surface. The overlapping shingles however, provide a second drainage layer. If the roof deck is covered with a water resistant roofing paper, as

is sometimes done in high rain exposure locales, this provides a third layer of drainage. In all cases, the roof sheathing acts as a final drainage plane and a storage layer. It is clear from the theory presented here that increasing the number of layers in a drained-screened enclosure system will provide more protection against higher rain loads. Asphalt shingle roofs provide a practical example of this theory. For lower-slope shingle applications (for slopes between 1:12 and 3:12) shingle manufacturers generally recommend doubling the layers of shingles, i.e., providing a total of 4 drainage layers.

In summary, it can be concluded that the rain control of a perfect barrier envelope is dependent on a single layer resisting all inward water transmission, a mass system relies on sufficient storage capacity, and a drained-screened system depends on drainage at other than the outside surface. As has been pointed out above, despite the fraction that dominates, all fractions play a role in almost all wall systems. If some storage and drainage is possible in walls designed as perfect barriers, these walls may not fail even if and when the perfect barrier is less than perfect. In the same way, many drained screened walls may, in fact, have poor drainage and therefore can only function if sufficient storage is available. However, the designer is often concerned with the behaviour of the wall under extreme events, and should choose a rain control strategy from one of the three.

6.4 Wall Categorisation

An enclosure wall categorisation system based on the above analysis is presented in Figure 6.3. This categorisation system has been developed over the last several years [6.3, 6.4]. The categorisation system is based on the method by which the wall system controls rain penetration. Because the control of rainwater penetration has historically been a major function of above-grade enclosure walls, the categorisation is generally useful. The categorisation is independent of materials, building function, or design intent. Although the focus of this research is on wall systems, the theory and the classification system can be extended to the other enclosure systems.

Walls can be considered to be comprised of elements and the joints between these elements. Both the elements and joints may be classified in the same manner, but the classification of the joints in any given system may be quite different than for the element. This distinction is critical for some systems; perfect barrier elements made of modern materials rarely fail, but the joints between the elements is a common source of problems, e.g., window openings in EIFS, joints between metal panels, etc.

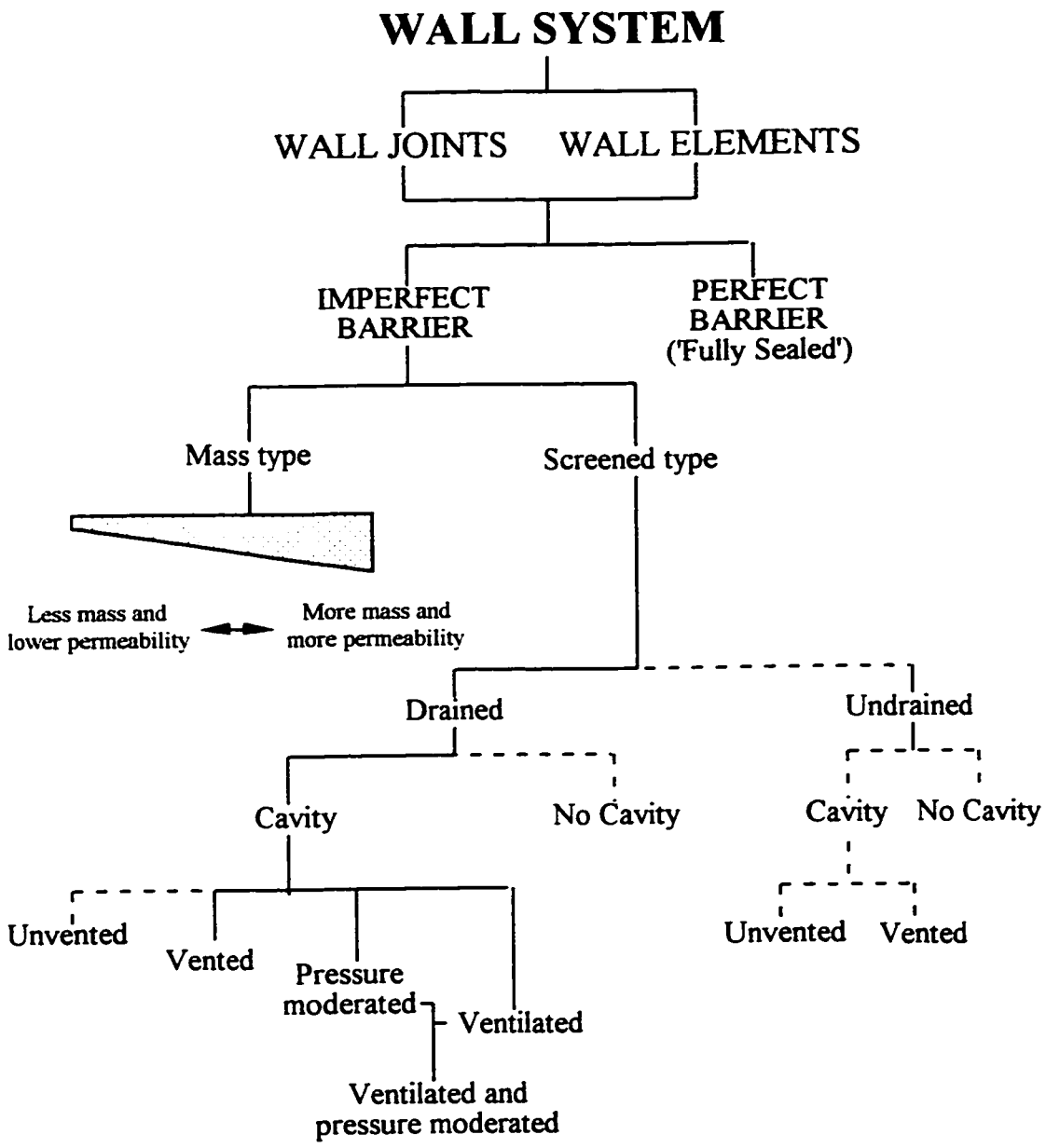

Notes:

The walls are categorized based on actual behavior, not necessarily design intent.
For the purposes of this classification system, the following definitions are necessary:
Drained: the majority of the water that penetrates the screen is removed by gravity.
Cavity: a clear space or a filled space that facilitates gravity drainage and air flow and resists the lateral transfer of water (a capillary break).
Vented: allows some degree of water vapor diffusion through vents and by air mixing.
Ventilated: allows a significant flow of air largely to promote drying by mass vapour movement.
Pressure-moderated: an approach that moderates air pressure differences across the screen.

Figure 6.3: Wall categorisation system (by rain penetration Control)

The primary and initial classification is whether a wall is a perfect barrier or an imperfect barrier.

Perfect barriers stop all water penetration at a single plane, much as a perfect air barrier would prevent air flow. Examples of perfect barrier walls are some window frames, EIFS, and metal and glass curtain wall systems. Because it is very difficult to build and maintain a perfect barrier wall, most walls are designed as, or perform as, imperfect barrier wall systems of either the mass type or the screened type.

Mass systems control rain penetration by absorbing and storing rain water which penetrates the exterior surface. In a functional mass wall this moisture is eventually removed by evaporative drying before it reaches the inner surface of the wall. Some examples of mass walls include adobe, solid multi-wythe brick masonry, and single-wythe block masonry. Undrained masonry cavity walls (i.e., those with blocked airspaces or weep holes) often behave as multi-layer mass walls.

Drained-screened walls control rain penetration by draining any water that is not shed from the front face. Such walls are also imperfect-barrier type wall systems in that this approach acknowledges that some rain water will penetrate the outer surface. Supplementary mechanisms, such as a capillary breaks, storage, and multiple drainage planes are usually employed to resist further inward movement of the water that penetrates the screen. The dashed lines in the figure indicate that, while undesirable, undrained walls do exist. Some examples of drained wall systems include cavity walls, brick and stone veneer, vinyl siding, two-stage joints, and drained EIFS. It should be noted that the outer layer of a multi-layer drained wall is much more than a rain screen; it must also resist wind, snow, solar radiation, impact, etc.

Although the above is all that is necessary to classify a design, the multiple and important roles of airspaces and cavities means that further practical classifications are possible.

6.4.1 The function of the cavity

A cavity behind the cladding of a drained-screened wall system provides a capillary break and a clear path for both gravity drainage and air flow. A cavity is defined for our

purposes as any continuous space behind the screen, which may be filled with a porous material, that fulfils these functions. An air space is the unfilled part of the cavity. [†]

Although not part of the primary classification system, it is practical to further sub-divide those enclosure wall systems that have a cavity behind an outer screen:

1. An *unvented* system has no openings connecting the air in the cavity with the exterior. The exterior cladding or finish of such walls usually behaves as an air barrier.

2. A *vented wall* system allows some degree of water vapour diffusion and air mixing between the cavity and the exterior. Venting may be explicitly provided (e.g., in the form of unfilled head joints in brick veneers) or it may be provided implicitly by the nature of the cladding (e.g., in the form of openings and cracks in overlapping wood siding).

3. By increasing the flow of air into and through the cavity, a relatively large volume of water vapour can be transported from the cavity. Such a *ventilated* wall will assist the drying of both the inner wythe and the cladding by providing a mechanism for the removal of water that does not drain from behind the cladding. Ventilation may also remove water vapour that may have diffused outward from within the wall. The distinction between vented and ventilated walls is not clear — it is presumed here that ventilated walls are those that have a "significant" amount of airflow. The relative significance of various flow volumes will be discussed in Chapter 9.

4. A *pressure moderated* wall system promotes the moderation of wind-induced pressure differences across the cladding. The proper choice of venting, i.e., size, number, and location, and the division of the cavity into stiff, airtight compartments are necessary requirements. Although such walls have heretofore been described as pressure equalised rainscreens (PER) in Canada, instantaneous pressure equalisation rarely occurs in reality and the screen deals with more than rain — hence the more realistic term, "pressure moderated screened" or "pressure moderated drained" wall, is preferred.

Based on its potential benefits, a drained and vented wall that is both pressure moderated and ventilated is not only feasible, it should be the *preferred* solution for most applications.

[†] From a structural point of view, a cavity is the space between two masonry wythes or between cladding and framing. It may be empty, completely filled or partially filled by insulation. From a moisture control standpoint it is the functions previously listed that are important.

6.5 Conclusions

The rain control theory developed in this chapter provides a rigorous and practical means of understanding the function of each layer and material in an assembly, and also leads to a useful classification system.

The theory will also aid the development of more realistic test standards and provide the means for a more accurate assessment of the reasons for enclosure failures and therefore the proper repair and retrofit strategies.

6.6 References

[6.1] Kenney, R.J., Piper, R.S., "Proposed Material and Application Standards for More Durable Exterior Insulation and Finish Systems", *Development, Use, and Performance of Exterior Insulation and Finish Systems, ASTM STP 1187*, Mark Williams and Richard Lampo, Eds., American Society of Testing and Materials, Philadelphia, 1995, pp 56-73.

[6.2] Desjarlais, A.O., "Self-Drying Roofs: What!? No Dripping!" *Proceedings of Thermal Performance of the Exterior Envelopes of Buildings VI*, Clearwater Beach, Florida, Dec. 2-5, 1995, pp. 763-773.

[6.3] Straube, J.F., *The Performance of Wall Systems Screened with Brick Veneer*. M.A.Sc. Thesis, Civil Eng. Dept., University of Waterloo, 1993.

[6.4] Straube, J.F., and Burnett, E.F.P., "Rain Control and Screened Wall Systems", *Proceedings of the Seventh Conference on Building Science and Technology*, Toronto, Mar. 20-21, 1997, pp.17-37.

7. CLADDING RESPONSE TO DRIVING RAIN

The drainage, storage, and transmission characteristics discussed in the previous chapter are directly related to cladding response. Enclosure performance and durability are also affected by the DST ratio because:

1. the amount of water drained on the surface is important since this water is available for penetration through openings and is the primary cause of staining and streaking;

2. the amount of water that is stored (i.e., absorbed and trapped) is important since this water increases the moisture content of the cladding material(s), and hence may place the materials in a moisture content range that leads to deterioration;

3. the amount of water that is transmitted through the cladding is important since this water is a source of wetting for materials within the enclosure assembly.

As discussed in the previous chapter, the time-dependent and wetting-history-dependent behaviour of cladding can change the relative importance of each of the factors with time. This chapter will quantify this dependency using the driving rain duration and intensity information presented in Chapter 5.

This chapter will examine the response of the cladding to driving rain deposition in more detail. The interaction of rain absorption, surface drainage, and penetration will be examined in more detail

7.1 Rain Absorption and Surface Drainage

Different surface materials and textures will respond differently to rain that is deposited. The fraction that is drained at the surface greatly influences the amount of water that must be controlled on the surface. For example, as has been argued in the previous chapters, during most rain events a large proportion of water falling onto a masonry veneer screen is likely to be absorbed by the masonry. If the masonry becomes saturated or the intensity of rainfall is high, rainwater will begin to be drained on the surface and transmitted through the veneer. A glass-and-metal curtain wall will respond quite differently. Surface drainage will begin very shortly after rain is deposited on the wall, and large surface flows of water can be expected during most rainfalls. Most wall systems' behaviour lies

somewhere between these two extremes. For example, polymer-based (PB) EIFS absorb very little water whereas normal cement-based (CB) stuccoes behave like very thin masonry veneers.

As described in the previous chapter, rainwater striking a wall can be drained at the surface, absorbed by the surface, or penetrate through the outer surface. It is useful to consider the surface of the enclosure as though it were made of a number of small 2-D surface elements, each with different rain loading (e.g., DRF and RAF) and response characteristics. The nature of surfaces above and beside the cladding element being considered will play a role in cladding response since water draining or blown from these surfaces may add to the water load on a particular element.

Claddings that are either non-absorbent or absorb very little water, are simpler to analyse. If water is deposited on a non-absorbent or hydrophobically-treated cladding, at a rate higher than capillary suction can absorb, or on an already saturated porous material, a surface film will form and water will be drained away on the surface. In these situations, even low rainfall rates and short durations will cause a surface film of flowing water to form. This film of water is directed by gravity, wind, and surface features. Any imperfections in a non-absorbent cladding will be more likely to allow water penetration than an absorbent cladding, because the probability of water being present on the surface is higher, and the quantity of water penetration will be higher because the amount of water on the surface is higher.

Therefore, two of the most important wall characteristics affecting the amount and behaviour of surface water on a wall is the water absorptance and moisture storage capacity of the cladding. However, many inter-related material, assembly, and building characteristics will have an effect on the absorptance of the cladding and how water behaves on the surface of a building. Some of the most important characteristics include:

- the rate of water deposition,
- the moisture content of the surface,
- the duration of the rain event,
- the previous wetting and drying history of the cladding,
- the surface texture and larger surface features, and

These characteristics have an impact over every element of the building enclosure, and the total response is the integration of the individual elemental response. The characteristics of the cladding elements above and beside the one in question is of course important, because their characteristics influence the amount of water drained or blown (by the wind) onto the element of interest. A practical example is that of a band of windows over a band of masonry: since the glass will immediately drain all deposited rain water, the masonry below will be exposed to a much higher rain load than if the entire building were masonry. In practise, large drips on the window sills could be used to reduce and distribute the rain load on the masonry.

It is difficult to assess the influence of cladding imperfections without using probabilistic models (as described in Chapter 5). However, we know very little about the probability distribution of the occurrence, size, spatial variation of flaws in cladding. Therefore, from a design point of view, one must design details that reduce the probability of workmanship and materials flaws, provide surface features (such as overhangs, drips, etc.) that direct, control and remove surface water. The above actions reduce the probability of flaws, the probability of water on the surface, or the amount of water on the surface (all of which influence the probability and severity of water penetration through flaws). Therefore, the "state-of-the-art" design approach is to presume that some water penetration will occur and provide both a means of removing this moisture (e.g., drained-screened walls) and a moisture-tolerant assembly (e.g., balanced wetting and drying and moisture storage: mass walls).

Comparatively simple probabilistic and deterministic methods can potentially be used to assess the response of enclosures with claddings that exhibit essentially time-independent response (e.g., metal cladding or glass curtainwalls). The response of absorbent claddings such as brick, wood, and cement- or lime-based stuccoes, however, requires much more detailed analysis to assess the effect of prior wetting and drying, rainfall intensity and rainfall duration.

Any detailed analysis becomes very complicated because of site, weather, and assembly specific characteristics. For these reasons only an outline of cladding response is provided here, with special emphasis on brickwork veneers.

7.1.1 Surface film thickness and velocity

Reference has already been made several times to the importance of the film of water that can form on the surface of cladding during rain deposition. This sub-section describes the surface that can be expected to form on the surface of a smooth cladding during rain deposition.

Deposited water that is not absorbed will initially begin to accumulate as a series of beads adhered by surface tension. Very quickly, however, the beads of water will begin to flow downward, coalescing into trickles of water. As more water is added the trickles grow in size until they form a sheet or film of water. Very coarse textured surfaces, such as some stuccoes and natural split-faced block, will encourage water to remain adhered and stationary because of their large specific surface area†. Very smooth and/or hydrophobic surfaces will encourage water to flow.

Given the normal range of rain deposition (see Chapter 5), typically 1 - 5 mm/hr and very rarely more than 25 mm/hr, the thickness and velocity of any film is expected to be very small.

However, the amount of water on the surface of a building will accumulate with height if surface features do not collect and remove the water from the building's face. Table 7.1 shows that significant quantities of water can accumulate with height, even with reasonably low rain fall rates. For example, a tall (50m) building with a non-absorptive cladding will accumulate 500 kg/hr/m width in a reasonably intense 10 mm/hr rain storm.

The surface film thickness and velocity can be approximately calculated using basic fluid mechanics if one assumes that all rain deposited forms a well-distributed film over a smooth surface. The average flow velocity can be calculated as the volumetric flow rate divided by the area of flow. For a unit width:

$$V_f = (R - C - A - E) / (\rho_w \cdot t_f) \qquad \text{(Eq. 7.1)}$$

where V_f is the average film velocity (m/s)

R is the rate of water deposition ($kg/m^2/s$),

C is the rate at which water is removed from the surface ($kg/m^2/s$),

† Specific surface area, as used here, is the actual surface area divided by the surface area of a flat plane within the same perimeter.

A is the rate of water absorption ($kg/m^2/s$)

E is the rate of evaporation ($kg/m^2/s$)

ρ_w is the density of water (approximately 1000 kg/m^3)

t_f is the film thickness (m)

Table 7.1: Water accumulation (kg/hr/m width) as a function of rain deposition and collection height

Deposition Rate†	Collection Height (or Building Height) (m)					
(mm/hr)	2.5	5	7.5	10	25	50
1	2.5	5	7.5	10	25	50
3	7.5	15	22.5	30	75	150
5	12.5	25	37.5	50	125	250
10	25	50	75	100	250	500
25	62.5	125	187.5	250	625	1250
50	125	250	375	500	1250	2500
75	187.5	375	562.5	750	1875	3750
100	250	500	750	1000	2500	5000

† This rate refers to the rain deposition rate less absorption, evaporation, and removal by drips, flashing

The analysis can be simplified by assuming that the C, A, and E terms are zero, or by using an effective deposition rate that accounts for these factors (i.e., R_{eff} = R-C-A-E). For a deposition rate of 0.01 $kg/m^2/s$ (approximately equal to 36 mm/hr) and a film thickness of 0.1 mm, the velocity would be 0.1 m/s.

The velocity of the film can be calculated from the balance of forces acting on the surface: the shear force restricting the flow at the wall surface and the force of gravity driving water downward. This balance of forces can be written for a unit width:

$$F_{gravity} = F_{drag}$$

$$m \cdot a \cdot L = \text{Drag coefficient} \cdot P_{dynamic}$$

$$(\rho_w \times t_f \times L) \times g = C_D \times L \times (\rho_w \times v_f^2 / 2) \quad \text{(Eq. 7.2)}$$

where g is the acceleration due to gravity,

L is the length of sheet of water being considered (the height of the building),

C_D is the surface drag coefficient.

The surface drag coefficient for laminar flow over a smooth flat plate was solved analytically by Blasius [7.1] and shown to be, on average:

$$C_D = 1.328 / (Re_L)^{0.5} \quad \text{(Eq. 7.3)}$$

Empirical methods must be used for turbulent flow and the following relationship is widely accepted [7.1]:

$$C_D = 0.455 / (\log(Re_L))^{2.58} \quad \text{(Eq. 7.4)}$$

where Re_L is the Reynolds number (using length as its dimension)

$$= v_f L / \mu.$$

where v_f is the velocity of the falling water film, and

ν is the dynamic viscosity of water, (about 1×10^{-6} m^2/s).

The division between fully laminar and fully turbulent flow lies approximately between 0.5 to 1.0×10^{-6}. More detailed analysis can be conducted that account for the changing friction coefficient in the transition region, but the improved accuracy is not warranted for this study, since the accuracy of the boundary conditions is relatively low.

A force balance of Equation 7.2 can be re-written:

$$t_f = C_D \times v_f^2 / (2\,g) \quad \text{(Eq. 7.5)}$$

The surface drag coefficient is a function of Reynolds number (a function of film velocity and building height) and flow regime (e.g., laminar or turbulent).

Equations 7.4 has been solved numerically for a series of different building heights and driving rain intensity rates. For all but the lowest driving rain rates, the flow was found to be in the turbulent regime.

The results, plotted in Figure 7.1 for collection heights of 10 m and 50 m, show that the film thickness and velocity can be expected to be in the range of 0.05 to 1 mm and 0.1 to 1 m/s respectively over the range of reasonable rainfall intensities. This range of values is reasonably likely to occur on buildings with smooth and reasonably flat cladding, e.g., glass, metal, smooth painted stucco, polished natural stone, and flat concrete cast onto metal forms.

Materials such as textured stucco and EIFS, wood, brick, and concrete cast on wood will create much more friction. Experiments with sand-roughened plates have generated the following relation for an average turbulent-flow drag coefficients [7.1]:

$$C_D = [1.89 + 1.62 \cdot \log(L/k)]^{-2.50} \qquad \text{(Eq. 7.6)}$$

where k is the average height of the roughness elements.

This relation presumes that the boundary layer develops early and quickly, and would be valid for collection heights of more than about 5 m.

Figure 7.2 compares the results of calculations assuming a smooth flat wall and rough plate wall for a collection height of 50 m. The rough wall has been assumed to have an average surface roughness of 5 mm. As expected, the roughness reduces the velocity and increases the film thickness, but the changes are not very significant even though a 5 mm average roughness height would be perceived as a very rough surface.

Horizontal surface interruptions and wind on the surface will also affect the surface film thickness and speed.

The results of these calculations confirm that the surface film will be quite thin, less than 1 mm, in almost all situations. Therefore, the amount of water spanning openings and cracks in the cladding is actually quite small.

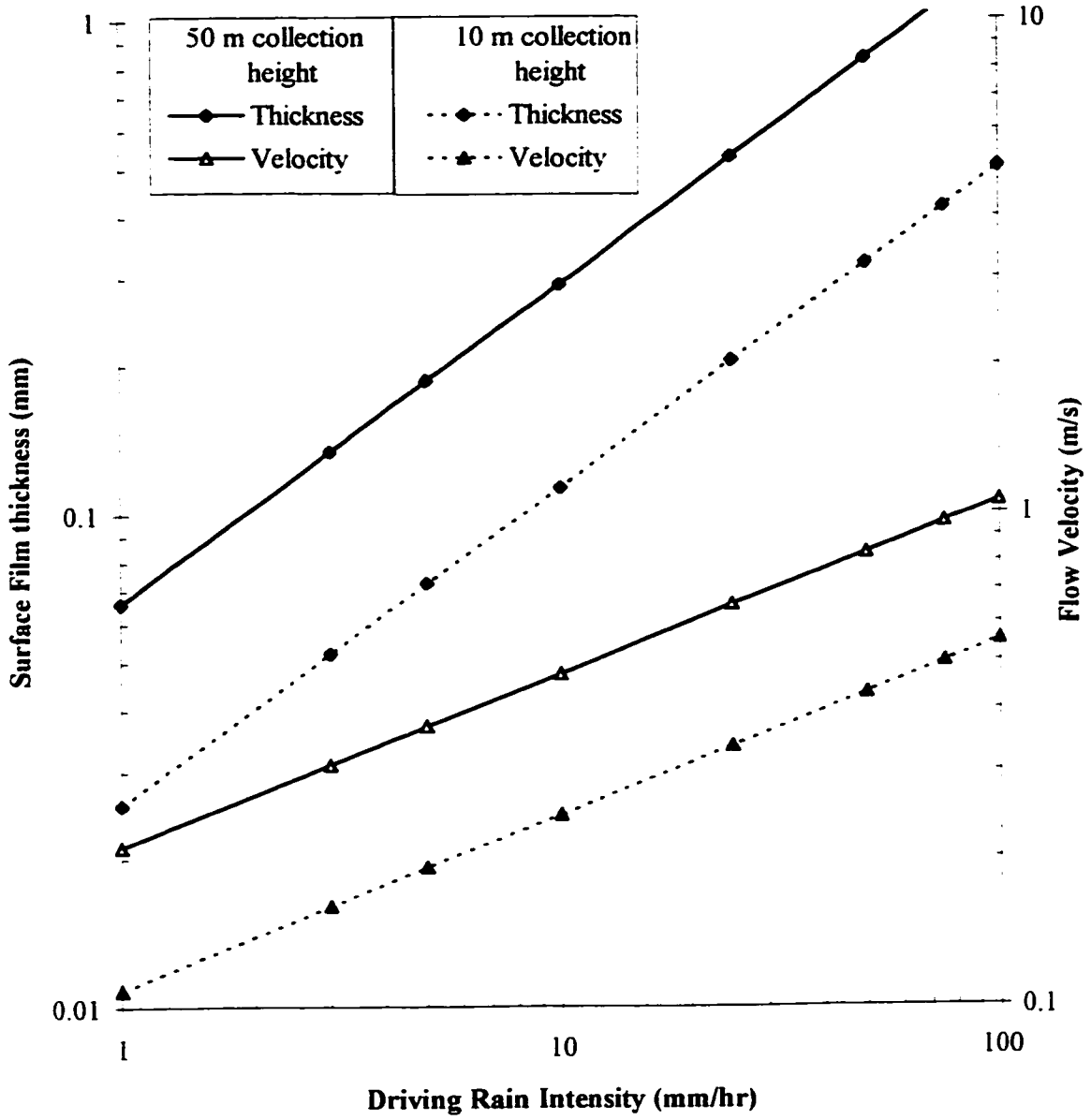

Figure 7.1: Surface film velocity and thickness vs. driving rain intensity and collection height

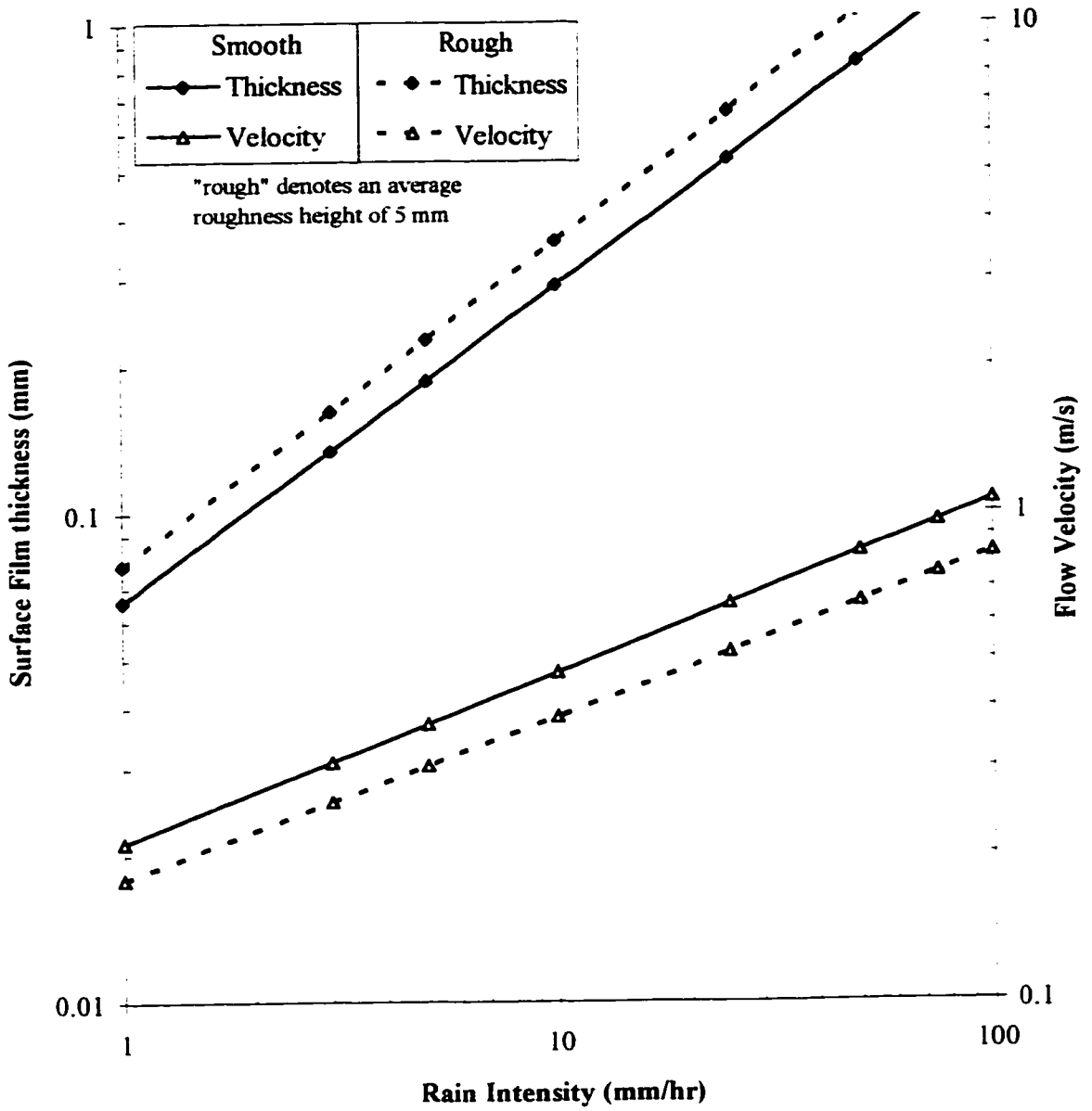

Figure 7.2: Surface film velocity and thickness vs. driving rain intensity and surface roughness

Note: for 50 m rain collection height

7.1.2 Evaporation rates during rain

The rates of absorption and evaporation have not been considered in the results presented in Figure 7.1. Evaporation rates for surface films are not necessarily insignificant because of the very large surface area. As discussed in Chapter 4, the evaporation rate from a water surface can be found from:

$$E = g \times A \times \Delta P$$

where g ranges from about 30 x 10^{-6} to 100 x 10^{-6} g/Pa/s/m^2 for calm and windy conditions respectively.

The difference in vapour pressure between the water and the air is difficult to assess since it varies over a wide range. In most situations with wind-driven rain, the outdoor relative humidity is more than 90%, and often nearly 100%. The temperature of the rain itself is usually the same temperature as the air (because of convective heat transfer during the raindrops' fall) but may be slightly colder than the air if insufficient distance has been travelled by the drop since it thawed from its ice-crystal beginnings. Once a droplet strikes the wall, the temperature of the resulting film will rise (because the cladding will usually be warmer than the exterior air) and the cladding temperature will drop as it gives up its energy to heat the drop. Therefore, the vapour pressure may range from almost zero to more than 100 Pa. (Note: the difference in vapour pressure between air at 15 °C and 90% RH and water at 15°C is 170 Pa).

Choosing low values (calm day, small vapour pressure difference) yields,

$$E = 30 \times 10^{-6} \times 1\ m^2 \times 10\ Pa \times 3600\ s/hr = 1\ g/(m^2 \cdot hr)$$

and choosing high values (windy day, large vapour pressure difference):

$$E = 100 \times 10^{-6} \times 1\ m^2 \times 100\ Pa \times 3600\ s/hr = 36\ g/(m^2 \cdot hr)$$

Therefore, it is unlikely that evaporation plays a strong role during rain. Even assuming surface film temperatures of 3 °C above ambient air temperature will yield evaporation rates of at most 100 g/(m^2·hr). While these are not insignificant drying rates, they are less than 10% of even low intensity driving rain deposition (e.g., 1mm/hr = 1 kg/(m^2·hr)).

7.1.3 Absorption rates during rain

As discussed in depth in Chapter 4, capillary suction will draw water into many of the porous materials used as cladding (such as brick, mortar, concrete, natural stone). Recall that the simplified version of Darcy's law for unsaturated flow states that the moisture content of an initially-dry material will absorb moisture as:

$$m_w = A \cdot \sqrt{t} \qquad \text{(Eq. 4.39)}$$

where m_w is the mass of the water absorbed per unit area (kg/m^2),

A is the water absorption coefficient ($kg/m^2\ s^{0.5}$ or $kg/m^2\ hr^{0.5}$)

and t is time (s or hr)

A is normally measured in units of $kg/m^2/hr^{0.5}$, although the units of $kg/m^2\ s^{0.5}$ are also used.

The rate of water absorption at t time is therefore:

$$\frac{dm_w}{dt} = \frac{A}{2 \cdot \sqrt{t}} \qquad \text{(Eq. 7.7)}$$

Therefore, the rate of water absorption can be found as a function of the time from the start of wetting and the sorptivity.

The time-dependent nature of the problem must be appreciated. If the material has previously been saturated, and has not had sufficient time or weather to dry, the sorptivity will be lower than predicted. This would be the case after several rain events in cool and humid conditions. For claddings with significant moisture storage capacity (e.g., concrete and brick panels), this limitation is not severe. For thin claddings such as wood and stucco, the storage capacity may quickly be exhausted in rainy climates. Only climate and material specific numerical simulations on an hourly basis or shorter can overcome the limitations of this theoretical development.

7.1.4 Brick wetting and drying experiments

Many European researchers have conducted sorptivity tests of various building materials. Their results are summarised in Table 4.3. This table indicates that a broad range of values are possible, from zero for glazed bricks to as much as 33 $kg/m^2/hr^{0.5}$ for very porous mud bricks.

Arnott tested thousands of Canadian clay bricks from six different plants with a full range of firing [7.2]. He did not explicitly measure sorptivity, but the reported values from the extended IRA tests can be reinterpreted as sorptivity values. All of the bricks followed the square root law of Equation 7.6, and in almost all cases, higher firing temperatures resulted in lower sorptivity. The sorptivity of these bricks ranged from a low of 4.6 to a

high of 16.8 $kg/m^2/hr^{0.5}$. Note that one type of brick, no longer in production, exhibited almost no absorption and is not included in this range.

Several similar sorptivity experiments were conducted to demonstrate and confirm the principles described out above. One dozen clay brick from each of Canada's two largest manufacturers, representing a full range of burning, were tested. The test involved placing the finished brick face down in a dish with the water level controlled to maintain about 1 mm of immersion. The brick were removed and weighed to the nearest tenth of a gram and replaced within 30 seconds. The test was run for up to 168 hours, although most brick were saturated long before this time.

Figure 7.3 plots the moisture content versus weight for the most and least absorbent bricks provided by the two manufacturers. The sorptivity of this clay brick, which represents a broad range of Canadian brick, exhibited a range of 0.25 to 7.5 $kg/m^2/hr^{0.5}$. The low sorptivity brick (CB-1) was intentionally burned harder than is normal (and exhibited some surface glazing on its back face).

The straight line drawn through the data points when plotted against the square root of time demonstrates the practical validity of the square root law. As expected, there was a sharp change in absorption rate when the wetting front reached the back of the brick. Once the initial absorption into the brick was complete, the rate of absorption dropped by an order of magnitude, as the smallest pores were filled, and the air diffused out of the dead end pores.

It should also be noted that the time to saturation varied from under 4 hours to more than 160 hours, and the more absorbent bricks were almost always those with the most storage capacity.

7.1.5 Implications for brickwork response

Equation 4.39 predicts that one square meter of typically absorbent brick, A = 2.5 $kg/m^2/hr^{0.5}$ will absorb 2.5 kg/m^2 after one hour if continually supplied with water, and 5 kg/m^2 if continually supplied for 4 hours. A sorptivity of 2.5 is also a reasonable value for cement and cement-lime stuccoes.

From Equations 4.39 and 7.7 it can be seen that the total amount of water that can be absorbed will increase with the square root of time, while the rate of absorption will

decrease with square root of time. As discussed in Chapter 5, the total volume of rainfall is also likely to increase with time at a decreasing rate.

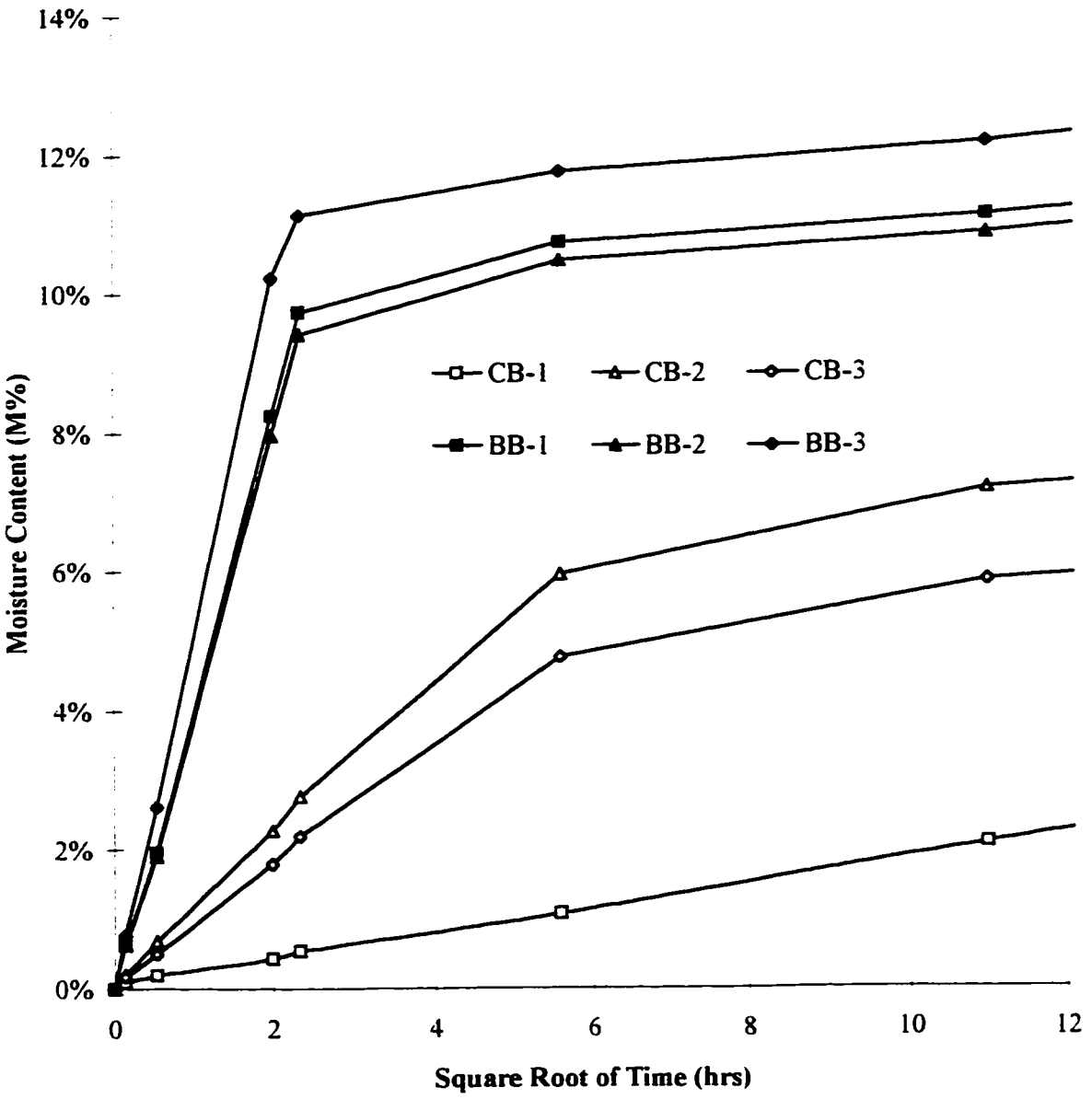

Figure 7.3: Moisture absorption versus square root of time for Canadian bricks

The information on the typical duration and intensity of driving rain events presented in Chapter 5 is useful for the assessment of the likely behaviour of different absorptive wall assemblies. Figure 7.4 is a plot of the average deposition of rainwater as a function of storm duration for three driving rain storms and three material absorptivities.

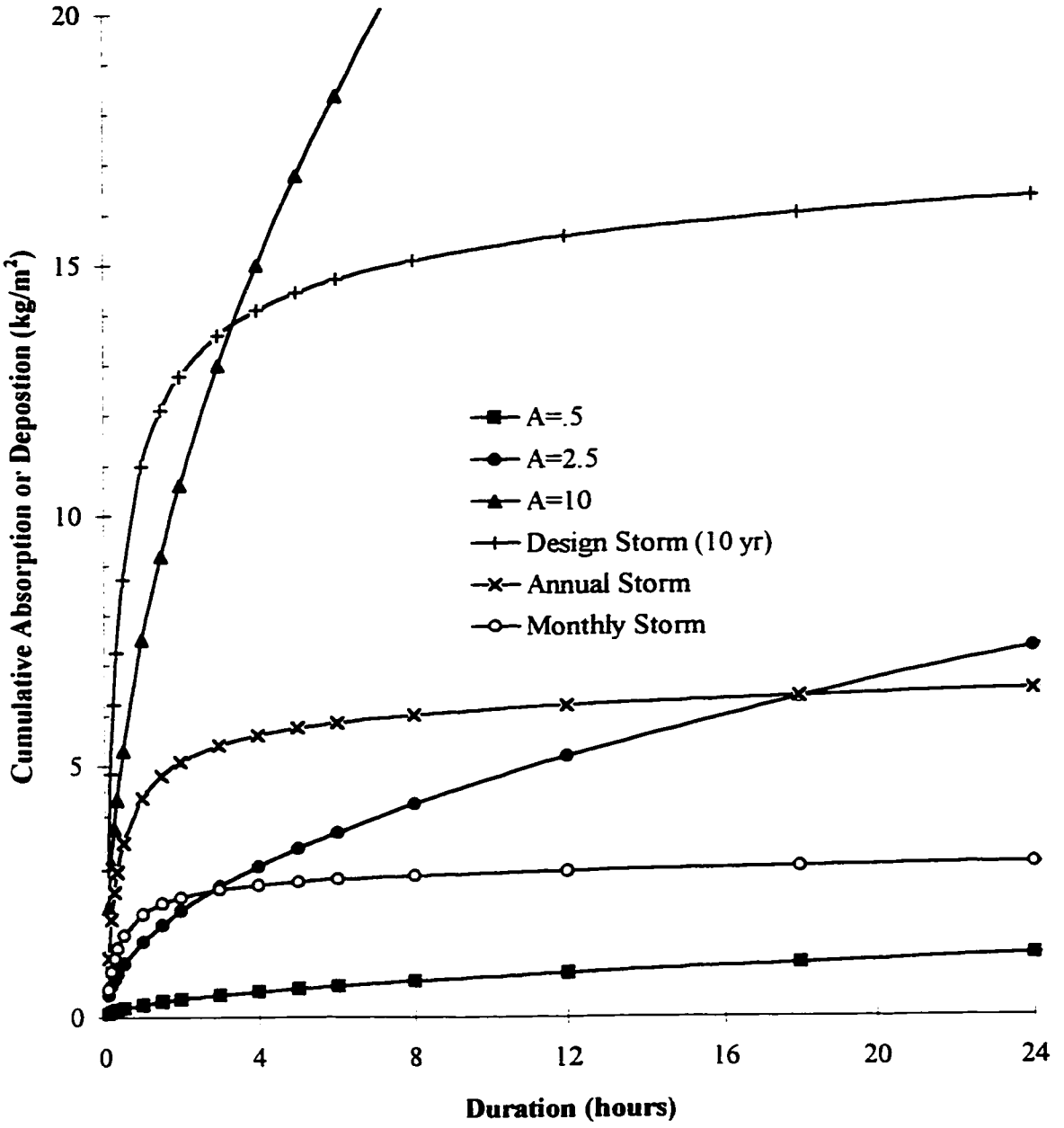

Figure 7.4: Rain deposition and absorption for representative scenarios

The intensity-duration-frequency relationship plotted in Chapter 5 (Figure 5.11) was used to define a monthly storm, a storm with a 1 year return period, and a storm with a 10 year return period. The curves of deposition versus time represent an enclosure at the top of a 10 m high building during a storm with a 4.5 m/s windspeed (i.e., more than average) perpendicular to the wall, (RAF=1.0).

The absorption has also been plotted in Figure 7.4 for three representative water absorption coefficients using Equation 7.7. A value of 0.5 kg/m^2/hr is the upper threshold of what is considered a water repellent stucco by the German DIN Code 18550 [7.3]. A value of 2.5 is a reasonable value for lime-cement stucco, and a value of 10 is representative of an absorptive brick.

It can be seen that even highly absorbent claddings will not absorb the rain water deposited by intense and short rain falls. However, Figure 5.9 shows that half of all rain events of were from 4 to 20 hours long. The average rain deposition intensity reported in Chapter 5 is 2.1 mm/hr at 3.5 m above grade: at 10 m above grade, this amount would be 2.65 mm/hr. The monthly storm shown in Figure 7.4 is therefore a reasonable but slight overestimation of an "average" storm (note that the windspeed chosen for this analysis is higher than average). For monthly storms of 4 to 20 hours duration, dry brickwork can absorb much of the rain deposited.

The more sheltered areas near the middle of buildings will experience 1/3 to 1/2 of this loading (i.e., RAF=0.3 to 0.5). This reduced loading will reduce the probability of surface water significantly.

The implications of this behaviour are important for building performance. Since brickwork initially absorbs water at a relatively high rate (1-10 kg/m^2/hr) the rate of absorption may often be more than the rate of deposition. As has been shown in Chapter 4, typical brickwork veneers can store a total of 5-10 kg/m^2. This leads to the conclusion that many brick veneers will shed water only during statistically less likely high intensity and/or long duration driving rain events. If the climate does not favour drying, or rainfalls occur often, the brickwork will remain saturated or nearly so, and rain penetration control failures become more likely.

Walls clad with metal, glass, EIFS, and polished granite will absorb almost no water and will have flowing water on their surface for almost all driving rain events. Hence, water penetration through joints and openings will always be more likely, simply because the joints are much more likely to be exposed to water.

It can therefore be concluded that claddings which have very low absorptions will drain a high ratio of deposited rain and increase the water load on the joints in the system. It can also be expected that joints in systems with little absorption will be exposed to an order of magnitude more water much more often than the joints in walls with more absorptive

claddings (e.g., brick, wood). These conclusions are important because joints are still typically designed as perfect barriers, and field experience has shown that they rarely perform in this way.

7.2 Water Permeance of Masonry Veneers

Several dozen tests of water permeance were conducted on the two laboratory brick veneer panels built as part of the URIF project (see Appendix A). The Canada Brick panel was tested in the laboratory under a range of conditions. Although pressure differences of -500 to 750 Pa could be imposed and accurately measured, the majority of the testing was conducted with no air pressure difference imposed across the veneer. The fraction of applied water that was transmitted across, shed from the face, absorbed by the veneer, or drained off the back in each test was measured and recorded at 30-second intervals by load cells and an automated data acquisition system.

The fraction of applied water that was transmitted across, shed, and absorbed by the initially dry, well-built clay brick veneer (made of well-burned Canada Brick bricks) in such a test is plotted in Figure 7.5.

It can be seen that water penetration did not occur for more than 30 minutes—even though water was applied at the standard ASTM E331 [7.4] rate of 3.33 $l/m^2/min$ (204 mm/hr), about 50 times what might be considered a "typical" rain event (see Chapter 5). However, once the brickwork had become almost saturated, about 2% of the applied water penetrated. Despite the severity of the test, the amount of water transmitted through this veneer in one hour (2 l/m^2 = 2 mm/hr) can easily be drained by a properly designed and built assembly. If a more realistic rate of water were to be applied (e.g., 1 to 10 mm/hr), water would take much longer to penetrate (because it would be absorbed by the masonry), but the *fraction* that penetrated would be higher (as high as 80% according to [7.7]), while the *rate* of penetration would be much lower.

The U.K. Building Research Establishment has conducted a long-term research program into the water permeance of brick masonry and has published a number of reports and papers regarding its research. All the tests conducted on brick veneer walls in the field have resulted in water penetration values quite similar to those measured in the tests reported here. Several other researchers in the U.S. and U.K. have conducted realistic laboratory and field testing as well. The results of some of these tests are presented in

Table 7.2, together with the results of a literature review [7.5] of dozens of similar tests in the laboratory and in the field. All of the values have been standardised to mm/hr.

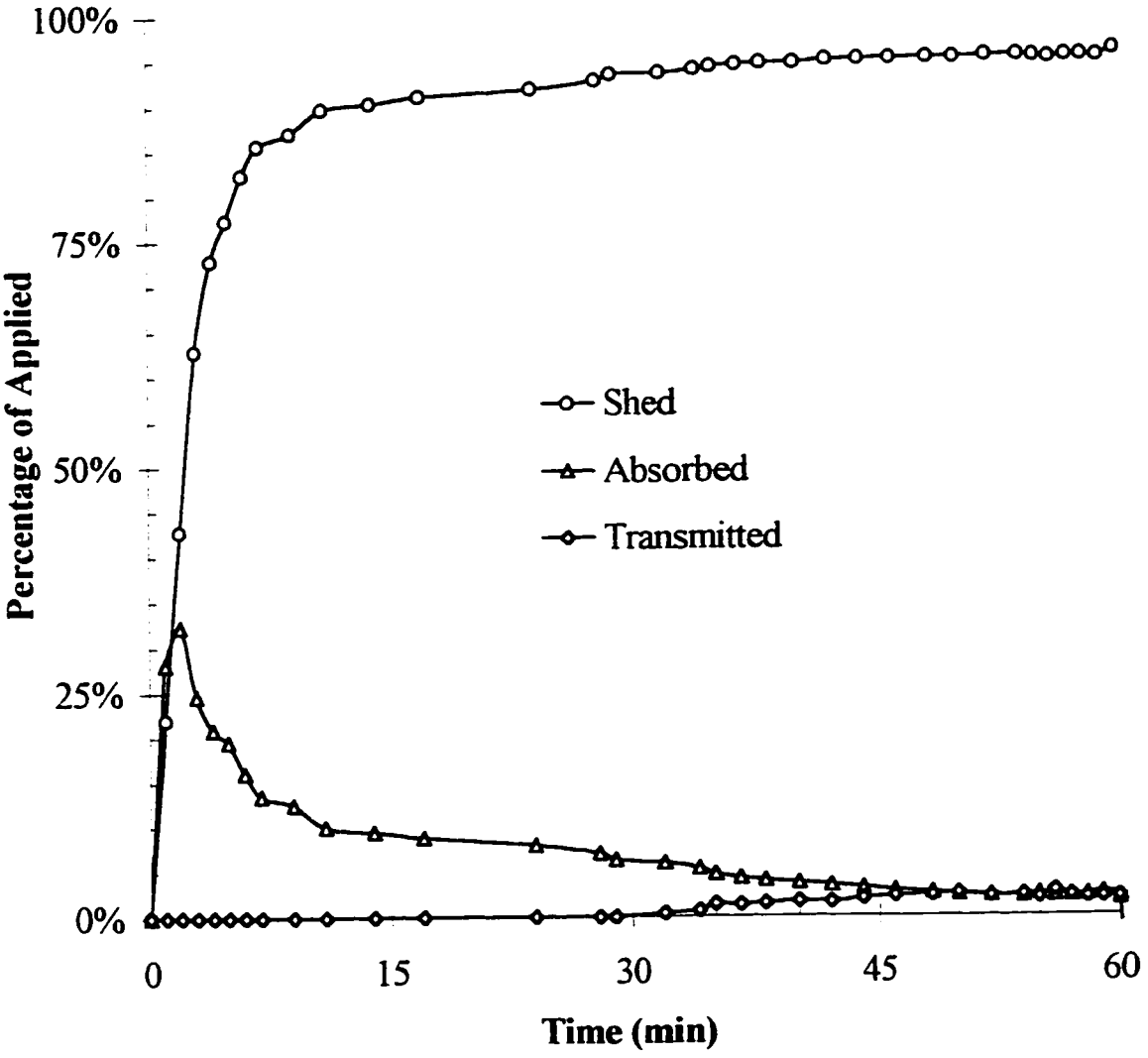

Figure 7.5: Percentage of water shed, absorbed and transmitted through brick veneer during testing

Note: No air pressure was applied. Veneer initially surface dry.

Table 7.2: Comparison of zero-pressure difference brick veneer water permeance

Source [Reference]	Application Rate mm/hr	Leakage Rate Range mm/hr	Passing %	Comments
[7.6] ASTM E514	134			Solid walls, "mass" systems ΔP=479 Pa
[7.4] ASTM E331	204			Curtain walls, "Perfect barriers", ΔP=137 Pa
[7.5] 1992 Beghut tests	336	1.4 - 3.5	0.4-1.0	Field tests of 5 walls as part of another project
[7.7]Table 1	3.0	0.5 - 0.76	17.0-25.0	Note low application rate, 6 h test duration
[7.8] Figure 6	336	1.2 - 1.4	0.4	laboratory test
[7.8] Figure 4	9.0	0.06 - 1.60	0.7-18.0	laboratory tests
[7.9] Table 1	1.62	0.34 - 1.40	21.0-88.0	multiple field tests
[7.10] Table 1	1.62	0.94 - 1.46	58.0-90.0	laboratory test
[7.11] Fig. 1	16.8	0.006 - 1.5	0.0 - 9.0	intermittent spray- 50/50 on/off
[7.12] Fig. 25 (concrete)	60 - 180	3.0 - 5.1	5.0 - 2.8	Max/min application rate relates to max/min leakage

The almost-unanimous conclusions of these tests can be summarised as follows:

1. All brickwork veneers can be expected to absorb the majority of driving rain initially.
2. Once saturated, a significant fraction of the 1 to 5 mm/hr typically imposed by driving rain will penetrate through the veneer.
3. Almost all of the penetration rates are in the range of 1 to 3 mm/hr, although concrete brick masonry appears to have a higher rate.
4. The application rate does not play a strong role in the penetration rate but does strongly affect the time to saturation.

Another important point must be emphasised. In other research, it has been postulated that water penetrates almost exclusively through the interfacial cracks between the mortar and brick at head joints [7.5]. Capillary suction draws the water in (with pressures of up

to 750 Pa) and gravity head within the head joints will drive the water out. The relative size of the capillary suction pressures versus likely air pressures leads to the conclusion that wind-induced air pressure differences are not the only cause of masonry veneer water permeance. This conclusion is studied further next.

7.2.1 Air pressures and masonry veneer permeance

No air pressure was applied across the veneers in the test results plotted in Figure 7.5. Although it is a commonly held belief that air pressure differences are the *primary* cause of water penetration of masonry veneers, there is little scientific support for this contention. There are at least three reasons why this belief may have arisen. Air pressure differences *are* important for mass walls, such as multi-wythe and TTW brick walls. Tests of face-sealed EIFS, curtain walls, and windows also show that air pressure is often the most important penetration force for these perfect barrier systems. Finally, it has often been observed that walls leak when it is very windy during rain. Only the last point is relevant to drained-screened walls, but the observation of rain-wind-leak coincidence merely supports the fact that rain is deposited on a wall only when it is windy, not necessarily the assertion that wind pressure is the major cause of rain water penetration.

Figure 7.6 is a plot of the steady-state (i.e. after at least an hour of testing) water permeance of the same clay brick veneer shown in Figure 7.5 as a function of the sustained air pressure differences. While sustained air pressure differences clearly increase the amount of water penetration, water will penetrate even with a *suction* pressure applied. These tests demonstrate that water will always penetrate a brickwork veneer and, therefore, that a means of drainage behind the screen is always necessary.

More than a dozen tests were conduct to generate the curve shown in Figure 7.6. A range of pressures from -120 to +120 Pa were applied in more than a dozen different tests. The tests were conducted after the test wall had been previously saturated by several hours of continuous spraying.

Although a 100 Pa pressure difference may not appear to be a large or even a significant pressure (compared to the wind pressures specified in design codes or standard tests), pressures of 100 Pa across the screen are actually unlikely. Average hourly wind speeds at 10 m above grade are in the range of 3 to 4 m/s for most North American locations. This wind speed will impose a pressure difference of less than 10 Pa across the envelope of a low-rise building. Even for a 50 m tall building in the suburbs the pressure will be less

than 25 Pa. Therefore, under average conditions the wind pressure across the envelope of a 10 m and 50 m high building can be estimated as 10 and 25 Pa respectively.

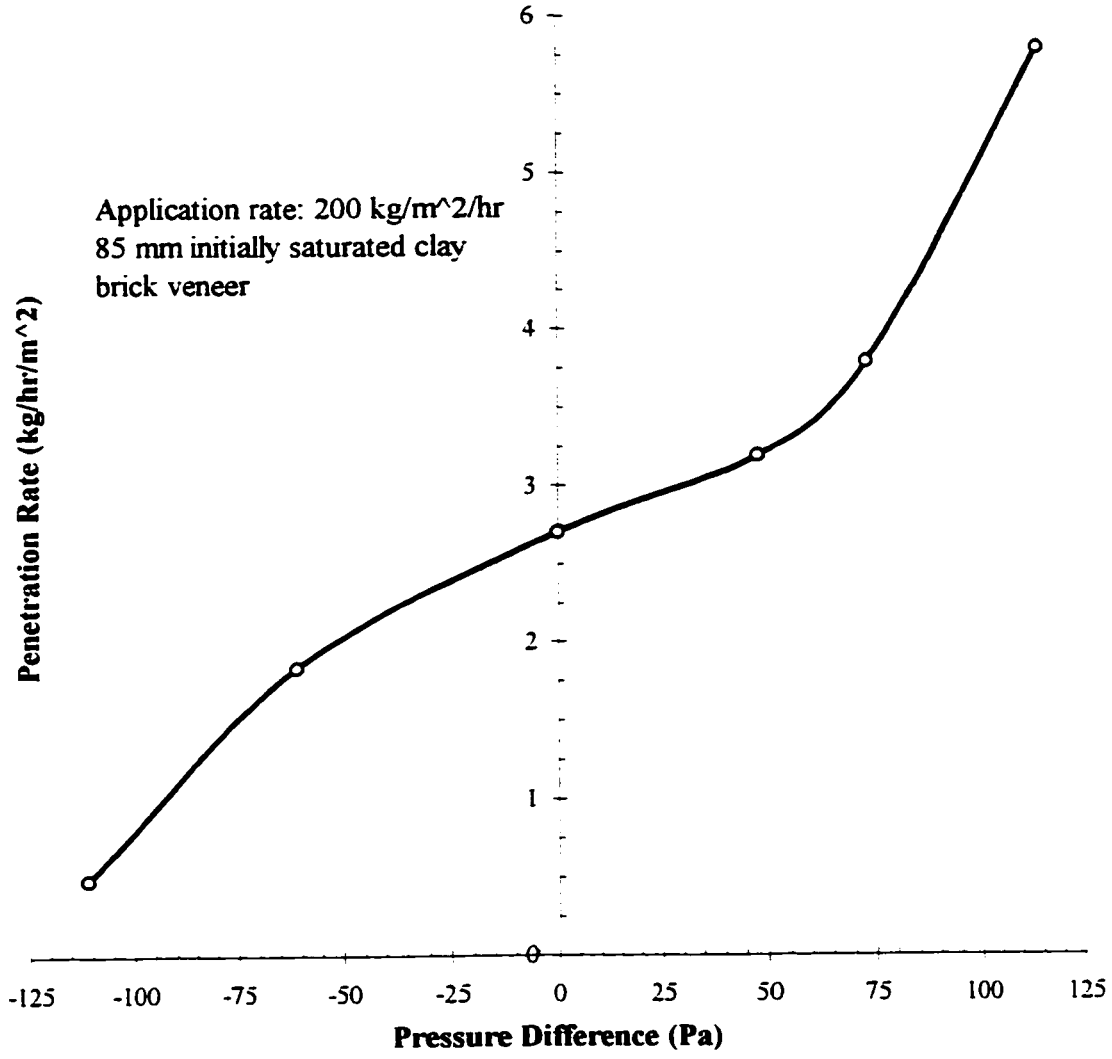

Figure 7.6: Steady-state water permeance vs. air Pressure Difference

Based on the log-normal distribution of wind speed, it can be shown that the average hourly wind pressure acting across the envelope for 99% of the time will be no more than four times the average pressure (therefore, 40 and 100 Pa respectively). Using the gust factor approach it can be calculated that wind gusts of about three seconds duration or longer can increase these pressures by no more than 50% (to 60 and 150 Pa respectively).

From the above it should be clear that it is quite unlikely that sustained wind pressure differences of more than 100 Pa will act across the envelope of most buildings most of the

time. During the small percentage of time that high wind pressures act, it will be raining only during a small fraction of that time, i.e., the coincidence of rain and high winds are rare. In fact, according to a review of weather records, the maximum hourly average wind pressure at 10 m during rainfall reaches 250 Pa for less than one hour every 10 years in most Canadian locations [7.13].

Coastal locations may indeed experience higher driving rain pressures, and the coincidence of high winds and rain is more likely in climates with more rain. Assuming that the wind speed during rain distribution is not much different than the known wind speed distribution (see Chapter 4), a climate such as Halifax, with 1381 mm of annual precipitation, is more likely to experience high winds with rain than Saskatoon, with only 353 mm of annual precipitation. Nevertheless, for the vast majority of North America, sustained air pressures of much more than 200 Pa are very unlikely. Most of the vast amount of masonry veneer permeance literature, however, is based on this magnitude of pressure difference.

Screened walls (masonry veneers, vinyl siding, etc.) almost always contain a cavity vented to the exterior. Using basic orifice flow equations it can be shown that the average pressure acting across the *screen* (not the envelope) in a screened wall system should be less than 5% of the pressure across the envelope if the ratio of vent area to air barrier leakage area is more than about 5:1 (see Chapter 8). This ratio of venting to leakage area can be achieved by masonry veneers built according to the masonry code or Part 9 of the NBCC.

Therefore, for a properly-built vented veneer or cavity wall, the 1 hour-in-10 year 250 Pa wind pressure during rain would result in a pressure difference of less than 15 Pa across the screen. For most rain storms therefore, sustained pressure differences across the screen should be only a few pascals.

Walls often perform poorly because design or construction errors result in systems that are much more air permeable or more poorly vented than required. As a result, sustained pressures of 100 Pa may act across the screen, and in the case of masonry veneers, this will increase water transmission somewhat. Even so, the amount of water which penetrates the screen in most rain events will be so small that proper drainage, if provided, should remove it.

7.3 Probabilistic Assessment

The volume of water impinging on a wall system is the result of the stochastic interaction of the wind, rain, building, and building envelope. The complex natures of the wind and rain, and the many factors of building site, geometry, cladding material, etc. make the prediction of driving rain a difficult task.

A model is proposed here which attempts to identify and link together all of the most important factors in this complex interaction. Because neither the wind nor rain are deterministic, at least parts of the model must be probabilistic. An analytical solution is intractable because of the number of interactions, and their probabilistic, dynamic nature, although a Monte-Carlo simulation might be used. Much of the frequency-domain description of the wind and wind pressures can be considered directly as the product of each of the spectral density functions and admittance function. However, the rain and wall behaviour will need to be considered for each orientation, wind direction, and cladding area as a distribution constructed from many point-wise multiplications of all of the factors.

The model outlined below provides a probabilistic measure of the air pressures across the screen and the volume of rain water that is absorbed, shed, and penetrates the screen of a unit area of wall on a building. The pressure information can be used to define the extreme loads and thus conduct a structural analysis of the screen, air barrier, and connectors in pressure moderated wall systems. The amount of water absorbed by the screen can be used to assess the assembly's susceptibility to various moisture problems, such as freeze-thaw damage. The amount of water which penetrates the screen is a useful measure of the potential for corrosion and water penetration damage.

The most important use of the model, even an approximate one, is a ranking of the relative importance of different factors affecting rain control. For example, the impact of different cladding types (absorbent, non-absorbent, pressure moderated), building type (high-rise, low-rise), site (Halifax, Toronto, Calgary), location on building (upper corner, centre), etc. would yield very useful information. Building designers need such information to design more economical and more durable buildings. Researchers can use such information to focus their efforts on those problems with the greatest significance.

The model approaches the problem by considering rain and wind as separate, independent events, and dividing the wind, driving rain, and building interaction into three parts; the

weather at the site, which is unaffected by buildings; building considerations, i.e., how the building interacts with the wind and rain; and wall considerations, i.e., how the wall affects water deposited on the building envelope. Each part of the model is considered in turn below.

7.3.1 Weather at Site

The proposed model considers the probability distribution of the wind speed, wind direction, and horizontal rainfall intensity. As described in Chapter 5, for a given rainfall intensity there is a particular rain drop distribution. The ratio of rain on a vertical plane (driving rain) to rain on horizontal plane (falling rain) is the driving rain factor (DRF); this factor is a function of the rain drop diameter. Figure 7.7 graphically shows the probabilistic interaction of wind and rain as described by the model.

The model assumes that the wind and falling rain can be modelled as separate events which interact at various stages. As discussed in Chapter 5, this is not precisely correct. However, using the wind speed and direction probability distributions during rain events is likely a reasonable approximation.

The wind probability distribution is relatively well known (the average hourly wind speed fits a log-normal distribution), and statistical values have been documented. However, for shorter time scales, the wind speed behaves almost randomly. By transforming the wind speed from the time domain to the frequency domain, it has been found that the wind fits a well-defined distribution, which is a function of only the wind speed and terrain type [7.14, 7.15]. The remainder of the model considers the wind speed and wind pressures in the frequency domain.

The output of this part of the model is the spectral density function of the wind and a probability distribution of driving rain intensity in the environment for each wind speed and direction.

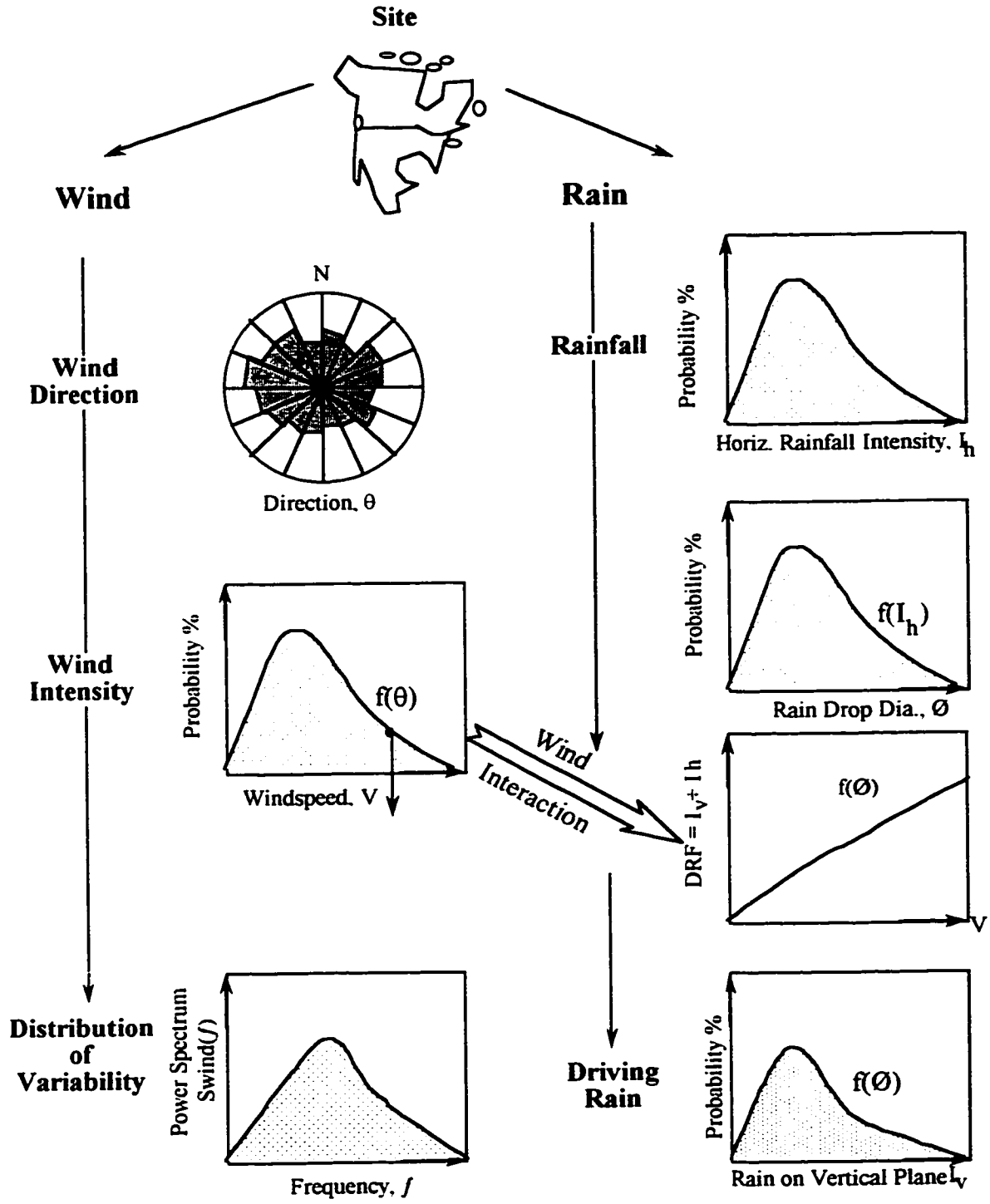

Definitions: I_h horizontal rainfall intensity; I_V vertical rainfall intensity, V wind velocity, q wind direction, Ø rain drop diameter, f frequency, $S_{wind}(f)$ spectral density function of wind velocity

Figure 7.7: Probabilistic assessment of site

7.3.2 Building Considerations

The second stage of the model (Figure 7.8) considers an arbitrary area of the building envelope. The model employs the aerodynamic admittance function, commonly used in wind engineering, to transform the spectral distribution of the wind in the environment to wind pressures on the cladding. The aerodynamic admittance function (AAF) will be a unique function for a particular building geometry and surrounding terrain and obstacles. The AAF is different for each location on the building, but with experience, it can be roughly approximated. The major factors affecting the AAF are dealt with earlier in the model, namely the wind speed and wind direction.

The rain admittance factor transforms the probability distribution of driving rain in the environment to deposited rain on the building. Although there is no explicit link allowing interaction between the wind and rain, the interaction is implicitly contained in the wind speed and wind direction variables which are included earlier in the model. It is postulated that the RAF is a function of raindrop diameter, although this has yet to be proven.

The shape of the RAF used in the figure suggests that at high wind speeds the amount of driving rain deposited on a building might be greater than that in the environment (i.e., RAF > 1.0). Although this may be possible in the upper corners and very near edges, both the literature reviewed earlier and the field measurements presented made earlier suggest that the RAF will be less than 1.0 for most parts of most buildings.

The output from this part of the model is the spectral density function for wind pressures on the cladding, and a probability distribution of the rate of water deposition on a given part of the envelope.

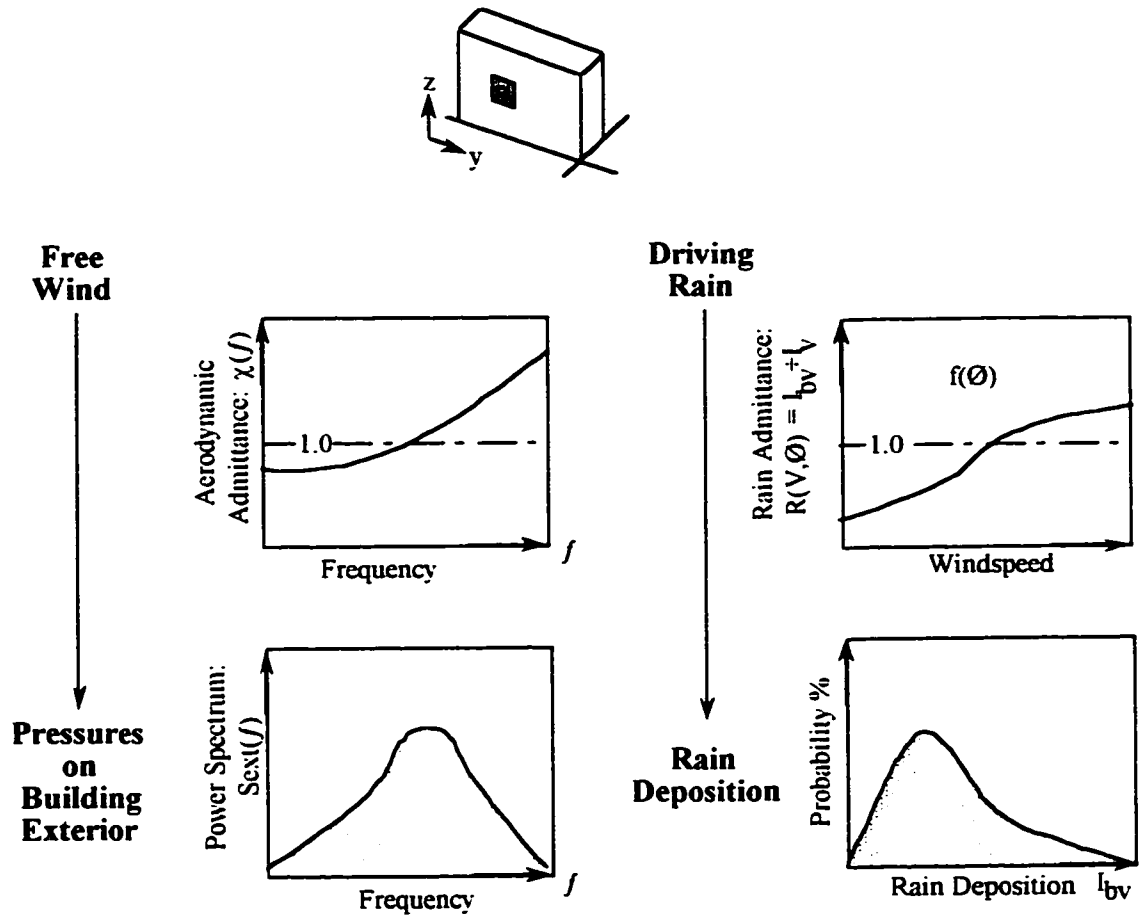

Definitions: I_{bv} intensity of driving rain deposited on a vertical building surface; $\chi(f)$ aerodynamic admittance function, $S_{ext}(f)$ spectral density function of wind pressures on exterior of the building.

Figure 7.8: Probabilistic assessment of building

7.3.3 Wall Considerations

How water behaves once it strikes a wall is very dependent on the nature of the wall, and to some extent, the location of the wall on the building. Some of the most important wall characteristics such as the absorbency and surface texture have been discussed previously. The nature of surfaces above and beside the wall of interest also play a role since water draining or blown from these surfaces will add to the water on the wall. The rate of water deposition, the moisture content of the surface, and the duration of the rain event all have a very important effect on how water behaves on the surface of a building.

The model (Figure 7.9) deals with these many issues by introducing a Surface Admittance Function (SAF) which correlates the amount of water on the surface of the cladding with

the intensity of rainfall. This function will be strongly influenced by the adjoining materials and their nature and area. The SAF will also vary with the moisture content of the screen but this depends on the surfaces previous history of wetting and drying. Simplifying assumptions may be necessary to overcome this problem.

Moisture on the surface of a wall can be absorbed, drained (i.e. shed), or penetrate into the wall. To account for each, an drainage/storage/transmission (DST) fraction is defined, a function of the amount of water on the surface, the pressure difference acting, and the moisture content and absorption coefficient of the material. The DST fraction will need to be measured from laboratory and field tests of different types of cladding, although, engineering judgement can also be used to estimate reasonable values.

Pressure moderated screened wall system create further complexity because the pressure across the screen may be important to the penetration of the screen. As demonstrated earlier, air pressure differences are not necessarily a very important water penetration force for masonry veneer walls. However, for walls made of impervious materials water flow through small cracks, joints, and imperfections driven by air pressure may be the primary water penetration mechanism.

Chapter 8 deals with air pressure moderation in more depth. As described in Chapter 8, a screen admittance function can be used to transform pressures on the exterior of the screen to pressures acting across the screen. Three issues need to be resolved. First, a method of predicting the value of this function has not yet been developed. Although there are some computer simulations available, none has yet been shown to accurately model the response of walls in the field. Second, the influence of spatio-temporal wind pressure variations has been shown to be a critically important factor affecting the ability of walls to pressure moderate. Although the effect of spatial variations can likely be introduced in the screen admittance function, a method of doing this has not yet been developed. Finally, the effect of the duration of a pressure difference on the amount of water penetration through screen materials has not been examined. Transforming the spectrum of pressures across the screen back to the time domain may be necessary.

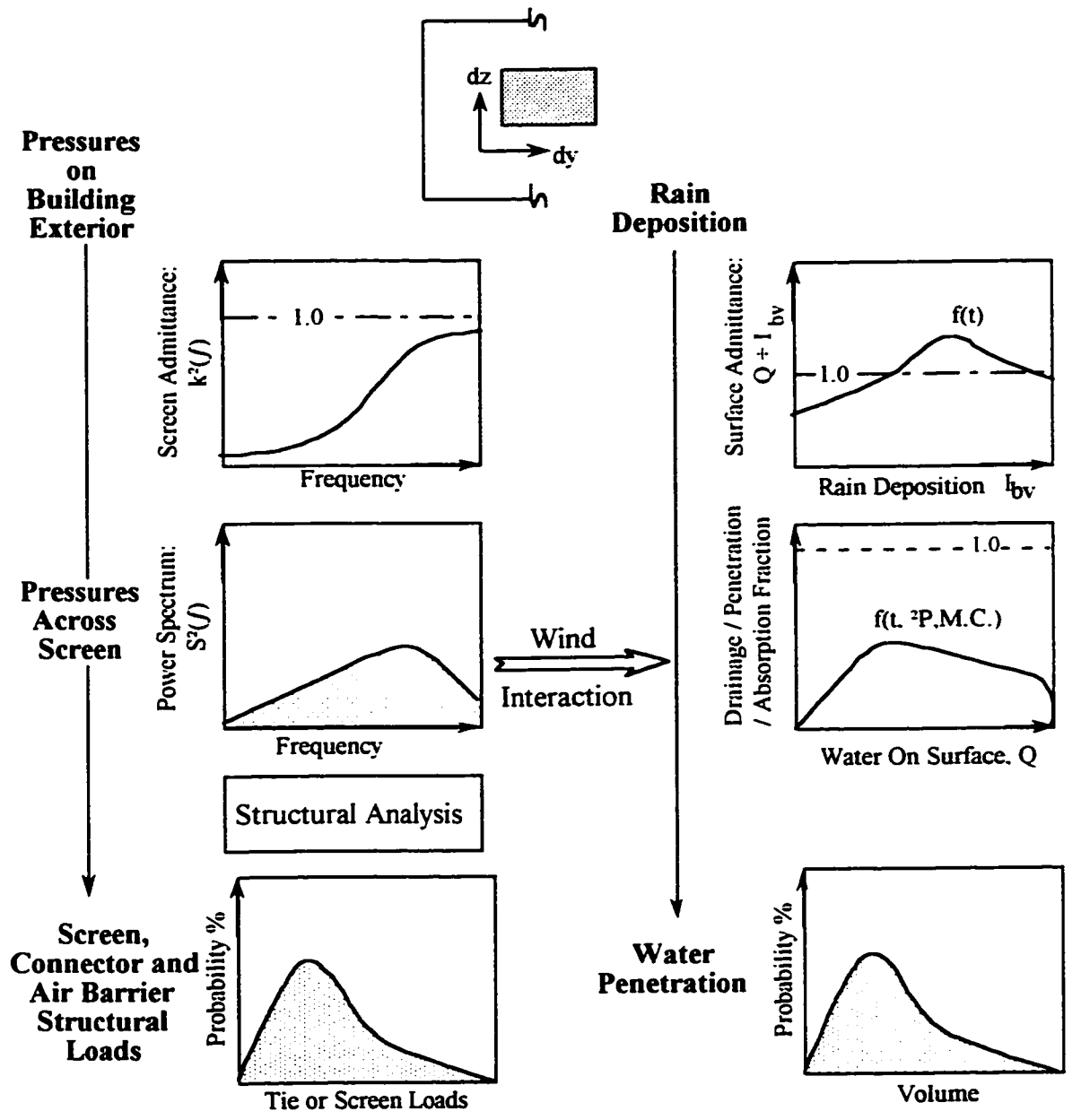

Definitions: $k_\Delta(f)$ screen admittance function, $S_\Delta(f)$ spectral density function of pressure differences acting across the screen.

Figure 7.9: Probabilistic assessment of enclosure

7.4 Conclusions

The examination of cladding response presented in this chapter leads to the following conclusions:

- Many brick veneers and other absorbent claddings can be expected to absorb a significant percentage of the rain fall that is deposited
- The thickness of the film of water that forms over a wall during rain deposition can be expected to be less than 1 mm for most claddings, even those with rough textured. This should guide designers of water penetration tests.
- Absorption by the cladding reduces the volume and the probability of water on the surface. This in turn reduces the probability of rain penetration problems.

The behaviour of masonry veneers under driving rain has been demonstrated with the aid of lab tests. It was show that realistic (i.e., statistically likely) air pressure differences do not have a very significant influence on the water permeance of masonry veneer walls. Thus, air pressure difference should not dominate rain control design. Drainage must be provided in any case, and the increased amount of water penetration caused by air pressure differences will not change the need for or type of drainage.

A probabilistic model has been presented that incorporates all of the important factors which affect the rain penetration control of enclosure walls. Given sufficient climatic information, this model can be used to quantify the risk of rain deposition and penetration as well as to assess the relative importance of each factor.

7.5 References

[7.1] White, F.M., *Viscous Fluid Flow*. McGraw-Hill, New York, 1991.

[7.2] Arnott, M.R., *Investigation of Freeze-Thaw Durability*, CBAC/IRC Industrial Research Fellowship Final Report, National Research Council of Canada, Ottawa, Dec. 1990.

[7.3] DIN 18550 *Putz, Teil 1*, Jan, 1985.

[7.4] ASTM E331-84. *Standard Test Method for Water Penetration of Exterior Windows, Curtain Walls, and Doors by Uniform Static Air Pressure Difference*, ASTM, Philadelphia, 1984.

[7.5] Straube, J.F., *The Performance of Wall Systems Screened with Brick Veneer*. M.A.Sc. Thesis, Civil Engineering Department, University of Waterloo, 1993.

[7.6] ASTM E514-86. *Standard Test Method for Water Permeance of Masonry*, ASTM, Philadelphia, 1986.

[7.7] Whiteside, A.J., Newman, A.J., Kloss, P.B., Willis, W."Full-Scale Testing of the Resistance to Water Penetration of Seven Cavity Fills", *Bldg. and Environ.*, Vol. 15, pp. 109-118, 1980.

[7.8] Newman, A.J., and Whiteside, D.,"Water and Air Penetration Through Brick Walls - A Theoretical and Experimental Study", *Trans. J. Br. Ceram. Soc.*, Vol. 80, pp. 17-26, 1981.

[7.9] Whiteside, A.J., Newman, A.J., Kloss, P.B., Willis, W."Full-Scale Water Penetration Tests on Twelve Cavity Fills- Part I. Nine Retrofit Fills", *Bldg. and Environ.*, Vol. 17, pp. 175-191, 1982.

[7.10] Whiteside, A.J., Newman, A.J., Kloss, P.B., Willis, W."Full-Scale Water Penetration Tests on Twelve Cavity Fills- Part II. Three Built-in Fills", *Bldg. and Environ.*, Vol. 17, pp. 193-207, 1982.

[7.11] Newman, A.J., and Whiteside, D.,"Water and Air Penetration Through Masonry Walls - A Device for the Measurement of Air Leakage in-Situ", *Trans. J. Br. Ceram. Soc.*, Vol. 83, pp. 190-195, 1984.

[7.12] Rathbone, A.J.,*Rain and Air Penetration Performance of Concrete Blockwork*, Technical Report 553, Cement and Concrete Association, Wexham Springs, UK, 1982.

[7.13] Surry, D., Skerlj, P. , Mikitiuk, M.J., "An Exploratory Study of the Climatic Relationships between Rain and Wind," Final Report BLWT-SS22-1994, Faculty of Engineering Science, University of Western Ontario, London, September, 1994.

[7.14] Van der Hoven, I., "Power spectrum of horizontal wind speed in the frequency range from 0.0007 to 900 cy./hour", *Journal of Meteorology*, Vol. 14, 1957, p. 160.

[7.15] Davenport, A.G., "The Spectrum of Horizontal Gustiness Near the Ground in High Winds", *Quarterly Journal of the Royal Meteorological Society*, Vol. 87, 1961, pp. 194 - 211.

8. PRESSURE MODERATION

Many researchers, designers, and builders consider Pressure-Equalised Rainscreens (PER) to be the state-of-the-art with respect to enclosure wall design†. This approach is also considered to be best practise for walls with brick veneer, EIFS, and vinyl screens. Both CMHC and IRC/NRCC have supported the view that pressure equalisation is both a powerful means of rain control and achievable in practice.

This chapter reviews the theory of pressure moderation, reviews other research into pressure moderation, and presents and analyses new field results. A comprehensive review of the historical development of pressure-moderated screened walls has already been conducted in [8.1]. The URIF project provided the opportunity to collect more detailed and comprehensive field pressure moderation measurements on brick veneers than ever before. The results of these measurements are summarised and discussed here.

8.1 Theory and Previous Research

The goal of a pressure moderated enclosure design is to reduce wind-induced air pressure differences across the screen. There are two reasons why the reduction of pressure differences across the screen is desirable:

- the amount of rainwater that will be forced across the screen or through vent openings *by air pressures* will be reduced, and
- the screen, and its connectors to the main structure, *may* not need to be designed to carry the entire wind load.

Historically, rainwater penetration control was the primary goal of pressure equalisation, although the potential for reductions in wind loadings, on the cladding and the structural connections between the cladding and the main structure, was always considered. Confusion has sometimes resulted because different researchers have studied one or the other of these two primary goals of pressure moderation.

† As described in Chapter 5, the more general term "screen" is preferred to rainscreen since much more than rain is screened by the outermost wall layer ("rainscreen"). Also, the more technically correct term pressure moderation has been used throughout this thesis because previous work has shown that instantaneous pressure equalization rarely occurs in service.

All pressure-moderated elements of an envelope, whether wall, window frame, or joint, have three basic components (Figure 8.1):

1. a screen,
2. an air chamber sealed from the building interior by an air barrier, and
3. an air vent (or vents) connecting the chamber to the exterior through the screen .

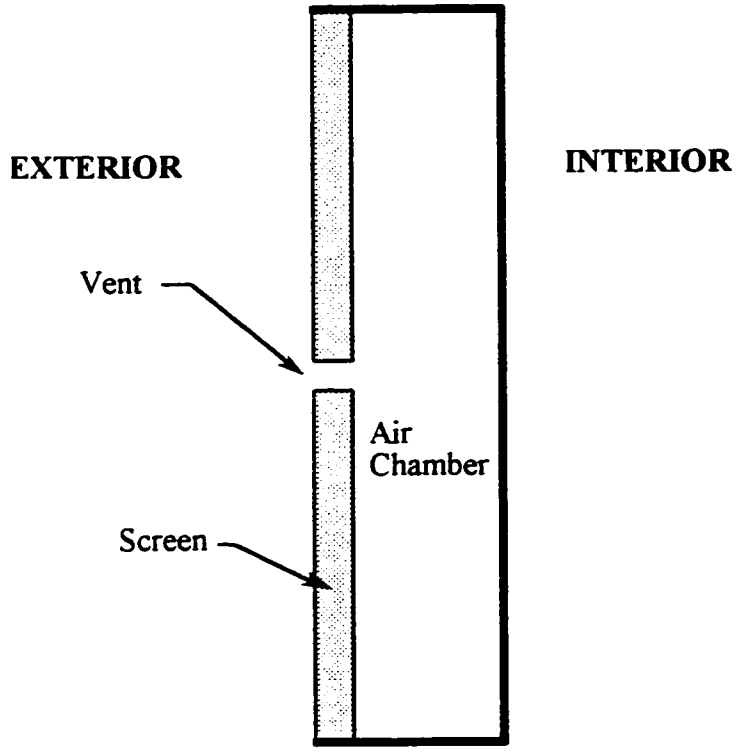

Figure 8.1: Basic components of a pressure-moderated enclosure system

Of course, wall systems must fulfil many other envelope functions as well. This means that a pressure-moderated wall is composed of more than the three basic components shown in Figure 8.1. Since water will penetrate the screen (the basic assumption in all screened walls), drainage is also very important for the control of rainwater penetration. At the same time, the control of heat, air, and water vapour flow cannot be compromised—that is, an enclosure design must balance the benefits of various rain-control strategies with the equally important needs of controlling air leakage, energy consumption, etc. Therefore, although this chapter focuses chiefly on pressure

moderation and the control of rain penetration, the reader should bear in mind that the sometimes-conflicting requirements of other envelope control and support functions also need to be addressed where appropriate.

The components of a more realistic pressure-moderated enclosure wall system are shown in Figure 8.2. It should be evident from this figure that the absolute and relative locations of the air barrier, water barrier, and the support and control elements of the inner wythe are not fixed. For example, in some wall systems, insulation is used to protect the air barrier, and it is therefore placed inside the air chamber. The air and water barrier may be the same material, may be located next to one another, or may be completely separated. In many systems, the air barrier is located close to the interior face of the wall assembly (e.g., the air tight drywall approach). The vertical supports for the screen (e.g., a shelf angle in brick veneer construction), the base flashing, and horizontal compartment separators often occupy the same location (and may even be the same component). These complications do not change the functions of the components, but they may affect the requirements for good performance. For example, an air barrier located on the inner face of the wall will remain warm and protected (and thus the requirement for durability will be less), but the volume of the air chamber may be larger and may negatively affect the capacity for pressure-moderation.

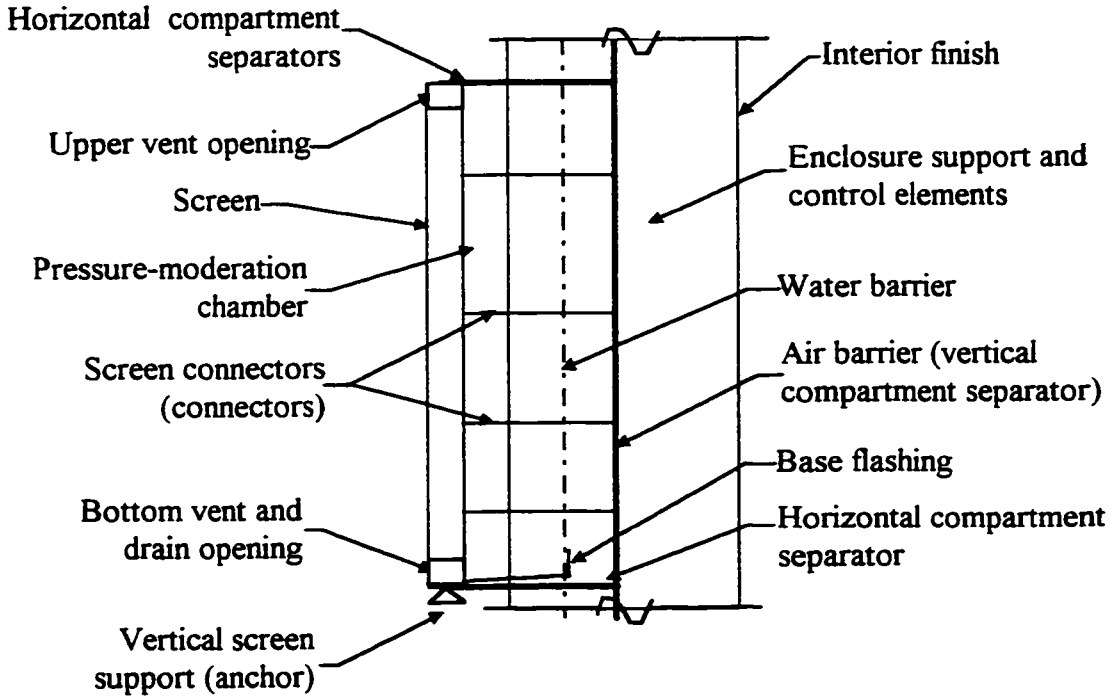

Figure 8.2: Schematic of pressure-moderated wall system components

8.1.1 Factors affecting pressure moderation

The theory and research conducted to date has resulted in a consensus view of the factors that affect pressure moderation performance. The relative importance of each factor, and requirements for design are not yet fully established.

It is argued here that, on a general level, pressure moderation performance depends on two general classes of factors:

- the enclosure system characteristics, and
- the nature of the wind loading.

The *enclosure system characteristics* can be further sub-divided into categories of characteristics that

- minimise the volume of flow required to achieve pressure equalisation, and
- maximise the flow of air into the chamber.

Factors included under the first category are:

1. the volume of air in the chamber;
2. the spatial extent of the chamber, i.e. compartmentalisation;
3. chamber deformability (this includes the flexibility of both the screen and the air barrier); and
4. air barrier leakage, or more precisely, the nature and amount of air barrier permeance.

The second category includes factors such as:

5. venting, or more precisely the nature and amount of screen air permeance;
6. the air flow characteristics within the chamber; and
7. the spatial distribution of venting across the screen.

The *wind load characteristics* that affect pressure moderation are:

1. the mean pressure across the enclosure system;

2. the mean gradients (in two dimensions) across the exterior of each compartment;

3. the time-varying pressures across the system; and

4. the instantaneous pressure field acting across the exterior of each compartment (i.e., the spatio-temporal pressure variations).

Almost all of the existing PER research has examined wall characteristics, although it has been shown in most field research that the characteristics of the wind tend to govern the performance of most common wall systems. Lab tests of pressure equalisation, the basis of most design recommendations, are of the spatially-uniform, temporally dynamic type. It is, however, widely recognised that most screened and vented walls will be almost pressure equalised if exposed to a steady, spatially-uniform pressure (as in most lab tests), but very few wall systems can significantly moderate very short-duration, localised, and high-intensity pulses of pressure.

Requirements for air-barrier tightness, venting area, air-barrier stiffness, etc., have been developed by various organisations — primarily IRC [8.2]. Based on lab tests which applied large sinusoidally-varying but spatially-uniform pressures [8.3] and simple computer models, requirements for air barrier tightness, venting area, air barrier stiffness, etc. have been developed [8.2].

Recommended values for venting are from 1 to 2% of related wall area and at least 40 times the equivalent air barrier leakage area. Chamber depths should be from 50 to 300 mm (the minimum value is based on the need to ensure drainage), and all sides of the chamber should be stiff. These preliminary requirements are sometimes conflicting and it can be shown that they are difficult to implement in practice for some wall systems [8.4]. For example, achieving more than about 0.3% vent area in brick veneers is practically difficult, and this makes the 40:1 ratio impractical.

8.1.2 Static pressure moderation

Static pressure moderation is the term used here to describe the performance of a system under a time-invariant pressures, e.g., long-term averages. If a wall system can be approximately modelled as one shown in Figure 8.1, the following analysis, first presented by Latta [8.5], is appropriate.

Air flow through both intentional vents, as well as cracks and openings in the screen or the air barrier can be reasonably accurately modelled by a power law equation of the form:

$$Q = C_d \times A \times \Delta P^n \qquad \text{(Eq. 8.1)}$$

where Q is the air flow,

C_d is the flow coefficient,

A is the area of the opening,

ΔP is the pressure difference acting across the opening, and

n is the flow exponent

Latta assumed perfect sharp-edged orifices for both the screen venting and the air barrier leakage. Such idealised openings have a flow exponent of 0.5. Therefore,

$$Q_{scr} = C_{d,scr} \times A_{scr} \times \Delta P_{scr}^{0.5} \text{ and} \qquad \text{(Eq. 8.2a)}$$

$$Q_{ab} = C_{d,ab} \times A_{ab} \times \Delta P_{ab}^{0.5} \qquad \text{(Eq 8.2b)}$$

Under steady-state pressure differences, the flow of air through the screen must equal the flow through the air barrier imperfections, e.g.,

$$Q_{scr} = Q_{ab} = Q_{total}$$

so,

$$C_{d,scr} \times A_{scr} \times \Delta P_{scr}^{0.5} = C_{d,ab} \times A_{ab} \times \Delta P_{ab}^{0.5}$$

and therefore,

$$\frac{A_{scr}^2}{A_{ab}^2} = \frac{\Delta P_{ab}}{\Delta P_{scr}}. \qquad \text{(Eq. 8.3)}$$

Using Equation 8.3, the ratio of the pressure drop across the air barrier and across the screen can be calculated for steady-state conditions, regardless of the size of the pressure drop or the amount of air flow. The ratio of screen venting to air barrier leakage is the only parameter that affects static pressure moderation. Supported by the results of Equation 8.3, Latta concluded that a wall with a venting-to-leakage ratio of 10:1 would be 99% pressure moderated, i.e., practically pressure equalised. Changing the flow

exponents to more realistic values (e.g., 0.65 to 0.80 for air barrier leakage) does not significantly change the results of this analysis.

It is expected that the average chamber pressure measured in field tests can be related to the average exterior pressure by the simple orifice flow expression given in Equations 8.3.

8.1.3 Dynamic pressure moderation

It has long been recognised that the dynamic and spatially varying nature of the wind has an effect on the actual pressure moderation performance of a wall. However, only in the last fifteen years has research been directed toward assessing the actual dynamic response.

Killip and Cheetham [8.6] were the first to perform laboratory tests of dynamic pressure variations. Using a small scale experimental set-up with turbulent (not modelled on the wind) flow, they concluded that a venting-to-leakage ratio of 2.5 to 4 times that proposed by Latta was required. This research generated the recommendation that the venting area should be from 25 to 40 times the equivalent air barrier leakage area.

The IRC conducted much more comprehensive and detailed research into the effects of dynamic wind pressures on pressure moderation performance [8.7, 8.3]. Large sinusoidal pressure variations were imposed on full scale wall assemblies, and the response of walls plotted as a function of the frequency of the pressure variation. (Note that this type of testing accounts for the dynamic nature of the wind, but does not assess the influence of spatial pressure variations). These lab tests showed that the pressures in the airspace behind the screen followed the ideal gas law rather closely, i.e., the major determinant of response speed was the compressibility of the air.

Holmes developed an analytical solution of the response of a vented chamber to an instantaneous exterior pressure change [8.8]. Harris extended the analysis to include leakage from the chamber [8.9]. This theory predicts very fast response to exterior pressure changes, in the order of 0.1 seconds, for typical enclosure wall arrangements. Because brick veneers tend to have low vent areas and most walls have imperfect air barriers, their response is relatively slow, but pressure equalisation is still expected at frequencies of 1 Hz.

Computer models based on the compressibility of air have also been developed [8.1]. The results of computer simulations have lead to the same conclusion as the analytical solutions: pressure-moderated walls designed with vent areas of more than 0.1 %, and a

vent-to-leakage area ratio of more than 10 should be able to moderate spatially-uniform exterior pressure variations quickly, (i.e., >95% pressure moderation at 1 Hz).

8.1.4 Spatial pressure variations

The study of wind pressures on buildings over the last three decades has shown that significant mean and short-term pressure variations are present over all faces of a building. The more complex the geometry of the building and the more turbulent the wind, the greater the spatial pressure variations.

The mean and short-term spatial variations of the wind can affect pressure moderation for two reasons. One concern is that spatial pressure variations allow pressures to occur across the screen which cannot be equalised by flow since they occur at some distance from the vents. A second concern is that spatial differences which exist for long enough may induce flow in one vent, through the air space, and out another vent. These longer-duration flows could draw water into the chamber. By separating a wall into properly sized compartments the mean and temporal-spatial variations that occur will be relatively small.

The average spatial variations can be described by the hourly average pressure gradients, typical plots of which can be found in many design codes. The study of short-term spatial-temporal variations has only recently been studied in depth. Surry, Skerlj, and Inculet have used orthonormal decomposition to condense pressure gradients (both average and long-term) from a wide range of building shapes to statistically significant average values [8.10, 8.11, 8.12]. This work has shown that the mean and instantaneous pressure gradients across the face of a building near the top and side edges of a building are much larger than near the middle. Gradients due to short-duration wind gusts are especially severe. Based on its own and other wind-tunnel studies, these researchers recommend a maximum compartment area of 1 m^2 to achieve 80% dynamic pressure moderation. Even "static" pressure moderation can be negatively affected by the steep average gradients near edges. As shown in Chapter 5, the top and side edges of a building are precisely where most of the water is deposited by driving rain.

Experience with testing small panel, well-vented European rainscreen overcladding has shown that while a reduction in wind load can be achieved, the spatial variations remain. In fact, Cook states that "The principal loads on the outer skin and its fixings comes from the variation in pressure distribution over the skin" [8.13]. In one of the few detailed non-

IRC field studies of pressure moderation, it was concluded that spatial variations governed the wind load on slate panels, but that, not surprisingly, pressure moderation of average pressures (static pressure moderation) was achieved [8.14].

Cook [8.13], Gerhardt [8.15, 8.16], and Solliec [8.14] have all found that wind loads on the cladding can be predicted given the pressure field (e.g., the spatial pressure variations) and the flow characteristics of the system. The compressibility of air simply does not govern the response of typical wall systems under realistic wind loads.

Although some best practise guides suggest that a single large vent is the best distribution of vents [8.2], this is not supported by theory or field and wind tunnel measurements. Distributing vents over the compartment should increase the averaging of compartment pressures (and thus increase the pressure moderation over the entire screen area). If, however, spatial variations are large relative to the mean pressure, the increased air flow through more than one vent could result in inertial effects reducing the response time and decreasing overall performance. There has been no field evidence to suggest that the latter mechanism has any significance.

8.1.5 Previous field monitoring

Although theoretical and lab studies provided some information about the performance of pressure moderated wall systems, the field performance needed to be confirmed.

To fill the need for field results, the IRC comprehensively monitored two full-scale buildings in the early 1980's. One building was a high-rise precast concrete clad office tower in Montreal (Place Air Canada) and the other was a low-rise brick veneer court house in Lethbridge, Alberta.

The monitoring of Place Air Canada showed that the static pressure moderation of this tightly compartmentalised and airtight wall system was excellent, but that short term (a few seconds) pressure differences could exist because of spatial pressure variations in the wind. The Lethbridge Court House monitoring showed static pressure moderation of about 50%, and short-term pressure moderation of as little as 10%.

More recent field monitoring by others has shown that typical brick veneer walls may moderate only 50% [8.17] and glass curtainwall spandrels may moderate only 25% [8.18] of the static pressures. Dynamic performance was not measured in these studies. The

lack of sufficient vent area, blocked air spaces, and leaky air barriers probably account for the lack of steady-state (long-term) pressure moderation in many typical walls.

Field monitoring of the pressure-moderation performance of several brick veneer panels at the Beghut was conducted as part of a previous project [8.19]. This monitoring showed that the airtight and tightly compartmentalised (1.2 by 2.4 m) panels provided a high degree of static pressure moderation, but short-term gusts were poorly moderated.

The fact that the results of lab tests and computer simulations, both which assume a dynamic but spatially uniform wind pressure, match well, while field measurements show inferior performance is strong evidence that spatial pressure variations are very important.

Several significant conclusions can be drawn from the few reported field measurements of pressure-moderated walls:

- the wind's temporally and spatially varying nature affects the extent, frequency, and nature of pressure moderation performance,

- the probability of high wind speeds is low, the stagnation pressures generated by wind most of the time are low, and the amount of time that high winds and rain occur together is very low, (see Chapters 5 and 7), and

- theoretical predictions based on the compressibility of air and assuming a spatially-uniform pressure cannot predict dynamic pressure moderation of large (> 1 m^2) panels.

8.1.6 Rain penetration control

Even a high degree of pressure moderation may not reduce rainwater penetration in many systems. Many forces drive water across the enclosure and pressure moderation only reduces air pressure differences, it does not address any other concerns. Rain water can also penetrate the screen as a result of the forces of gravity, capillarity, surface tension, etc. Any water penetration of the screen as a result of forces other than air-pressure differences will, of course, decrease the relative contribution that pressure moderation can make to the amount of rain that penetrates the screen.

The nature of capillary water flow through cracks and pores in screen materials like brick veneers, is such that air pressure plays a small role in driving water across the screen. For these screens, pressure moderation can do little to improve rain penetration control.

Walls that are labelled "pressure-equalised rainscreens" by their designers often have screens that allow water to penetrate, either due to gravity-assisted capillarity or through unintentional openings. Masonry veneer walls are the most common example; the rain penetration of brickwork is discussed in detail in Chapter 7 and the water permeance shown to be relatively insensitive to air pressure differences. These walls must be designed and built with meticulous attention to proper drainage and to the water resistance of the secondary water barrier, since water will penetrate the screen regardless of whether or not air pressure differences exist across the screen.

Theoretically, pressure moderation can only provide a useful increase in rain control for screens that exhibit little or no leakage at zero air pressure difference and significantly increased leakage at reasonably likely static air pressure differences. Screens that meet these requirements are some natural stone veneers, metal panel systems, and glass and metal framing elements of curtainwall systems or windows. Hence, any benefit from moderating the pressure difference across the screen would be a reduction in structural wind loads. All screen materials that are impervious to water can be designed to resist rainwater penetration by proper detailing without any assistance from pressure moderation. In most cases, this detailing involves surface and interstitial drainage and capillary breaks. Some of these features also will result in some degree of pressure moderation.

As described in the previous chapter, the *joints* between elements made of non-absorbent cladding materials usually experience much higher rain loadings since the screen drains water rather than absorbing it. These joints are exposed to all of the environmental loadings of the screen and may not be built water-tight, or may not remain perfectly water-tight (e.g., caulked joints). Designing such joints to be drained and pressure-moderated is theoretically compelling and has been shown to be successful both in laboratory and natural-exposure tests [8.20, 8.21, 8.22, 8.23, 8.24, 8.25] as well as in practice. (The two-stage joint, when properly drained and pressure-moderated, is an example). Therefore, there is little need to pressure moderate water impermeable screens and the design emphasis should be on the pressure moderation of the joints between elements.

Drainage must always be provided in pressure moderated systems because:

- pressure moderation can never be expected to be perfect, and
- air pressure is not the only water penetration mechanism.

This conclusion leads from the fact that pressure moderation *merely augments* a drained-screen's ability to control rain penetration by reducing the load on the drainage system.

Capillary suction pressures of a few hundred to a few thousand pascals may draw water into small openings such as failed sealant bond lines, cracked stucco and concrete, and small construction joints in metal curtainwalls. This water will be retained in the crack by surface tension forces until disturbed by a larger force. Wind pressures can be this force. Pressure moderation can be beneficial by reducing the peak pressures acting on these surface tension films to a level low enough that the surface tension force holding the water in the crack or opening is not exceeded. This is unlikely to be the case in practise.

Therefore, only screened enclosure systems in which:

- air pressure differences are the *only* rain penetration force *and*
- instantaneous pressure equalisation can be achieved under all conditions

do not need to provide drainage or storage for rain penetration control. Since there are few, if any, practical examples of such enclosure systems, it must be concluded that pressure moderation can only reduce the load on the drainage system (or the storage capacity in mass walls).

Provided sufficient drainage capacity exists, pressure moderation provides little benefit in controlling rain penetration. However, pressure moderation can *aid* rain penetration control in enclosure systems which:

- rely on storage within or behind the air space, or
- have limited or imperfect drainage, or
- have air pressures as the primary penetration force.

Therefore, even without a knowledge of actual in-service PM performance, two significant conclusions can be made:

1. Screened wall systems with a water permeable screen should be designed with drainage and/or storage. Their performance will not be much improved by dynamic pressure moderation.

2. The rain penetration control of enclosure systems for which both air pressure differences are important rain penetration forces, and which have little storage capacity (e.g., EIFS, metal panels, windows, vinyl siding) can potentially benefit from pressure moderation.

8.1.7 Structural load reduction

The wind loads that must be transferred by a PM wall system to the main structural system of the building are the same as other types of wall systems. However, the manner in which these loads are transferred and the nature of the load distribution can be quite different.

Well-vented and properly compartmentalised PM systems may allow a significant redistribution of wind loads from the screen to the sides of the chamber (the air barrier and compartment separators). Potential savings can be achieved if the air barrier system transfers most of the wind loads to the structural sub-systems under all conditions, because the cladding then does not need to be designed to carry these loads. In many screened wall systems currently being built, it is well accepted that the cladding does carry a significant percentage of the wind load. Nevertheless, the air barrier system and its structural supports must still be designed for the full wind load. If the load distribution between the cladding and air barrier could be predicted, each component of the wall could be "optimally" designed for the load it actually must support. It is presently common practise to design both the cladding (e.g., brick veneer) and the air barrier system (e.g., the drywall on steel studs) for the full wind load.

With regard to structural loads and pressure moderation, there are several potential problems that must be addressed:

- The structural system of screen and air barrier may not allow for a reduction in screen stresses or deflections in some situations. For example, if the structural system supporting the air barrier is more flexible than the screen, wind load shed from the screen by pressure moderation will be redistributed back to the screen by the connectors to maintain geometrical compatibility. This is the situation with most steel-stud-supported masonry veneers.

- Because structural design must be based on extreme loads, the level of pressure moderation performance and reliability required for load reduction are much more stringent than for rain penetration control. Cladding in Canada (most countries have similar requirements) must be designed to withstand the worst loading expected in 10 years. This translates to the worst second in 10 years, or one second in 315 million.

- The actual distribution of wind loads is dynamic and not easily predicted. Depending on the type of loading, the cladding may in one instant carry a large load while in the next instant the air barrier system may carry the full load. Other components in a wall system also carry loads. Housewraps, rigid insulation, and any other material that has any resistance to airflow will share some of the load. Even under static pressure differentials it is far from obvious which wall components are carrying what share of the total imposed wind load.

Several researchers have attempted to assess the influence of pressure moderation on cladding and connector loads. Gerhardt and his co-workers have conducted the most detailed studies of such load reductions, both in the wind tunnel and the field [8.15, 8.16]. This work was conducted on panellised systems with large vent areas, clear air spaces, and good air barriers. They found that load reductions of 40% could be achieved if the proper amount of venting was provided. They also showed that the possible load reduction was strongly affected by the height-to-width ratio of the building and the amount of air permeance through the cladding and air space (defined by the vent area and the unobstructed area of the air flow gap behind the screen). The nature of the wind (e.g., open country of city exposure) played a smaller role. By decreasing the size of the airflow gap behind the cladding, cladding loads were reduced because the friction acted to compartmentalise the system. The minimum vent area considered was 0.5% of wall area.

Egner conducted a series of dynamic load tests on small (up to 1.35 m) cladding panels [8.26]. The test panels were well compartmentalised, and small enough that the spatial wind pressure variations would have little effect. The smallest vent area investigated was 1% of wall area. He developed an equation for the fraction of the total wind load taken by the cladding panel for frequencies less than 3 Hz:

$$f = 1.13 \cdot a_{flow} \cdot a_{vent}^{-0.87} \leq 1 \qquad \text{(Eq. 8.4)}$$

where a_{flow} is the area of the thinnest section of the airspace behind the cladding through which air can flow divided by the area of the cladding panel

a_{vent} is the area of the thinnest section of the airflow path connecting the exterior to the airspace behind the cladding divided by the area of the cladding.

A unit width of a 2.4 m high brick veneer wall with a 25 mm air space has a flow area of 0.025/(2.4 · 1.0) = 1%. If open head joints are provided at 600 mm centres, top and bottom, the vent area is (2 · 0.01 · 0.065) / (2.4 · 0.6) = 0.09%. Egner's equation predicts a load fraction of 1.0 -- no load reduction. Load reductions are predicted only if the vent area is increased to more than 0.6%. Equation 8.4 also predicts a load reduction of 38% for a vent area of 1%. Such large vent areas are difficult to achieve in practical brick veneers without, for example, the use of continuous slots along the top. These results are more conservative than other analytical procedures.

The European pressure moderation research appears to be following their previous ventilation research, i.e., the emphasis is on panellised systems and large vent areas are always recommended.

Calculations by Solliec et al suggest that load reductions of as much as 60% might be achieved by proper design of air permeable cladding [8.14]. Note that these results imply a very flexible cladding with a stiff backup, perfect equalisation of mean pressures and a reasonably high degree of pressure moderation at 1 Hz (about 50%).

8.2 Field Monitoring Program

All of the test panels built as part of the URIF project were instrumented with pressure taps to allow for pressure moderation performance measurement (see Appendix A). Several different panels oriented in different directions, and built with different air space sizes etc. were monitored. The test panels, experimental set-up, monitoring protocol, and analysis methods are described in this section. The following sections present and analyse the results.

8.2.1 Test panel description

All of the brick veneer panels were 1.2 m wide and 2.4 m high. They were vented with four open head joints, each approximately 10 x 65 mm, two at the top and two at the bottom (total vent area = 2600 mm^2). This vent area is approximately equal to 0.1% of the wall area and is at least 50 times the leakage area of the panel.

Note that all of the panels tested were built better than could be expected of a real wall: the inner layer of sealed drywall acted as a perfect air barrier, the 1.2 m wide by 2.4 m high compartment size is quite small (better than most brick veneer compartmentalisation recommendations), and the 4 open head joints provide more vent area than in most practical brick veneer walls (but much less than the recommended 1 to 2%).

Although all of the brick veneer walls monitored are ideal with respect to actual practise, they are far from ideal with respect to most accepted guidelines. Wall systems such as some European cladding panel systems, that incorporate tighter compartmentalisation, much greater vent areas (usually 1 to 3%) in the form of perimeter joints (i.e., a form that acts to "smooth out" spatial pressure variations, can be expected to perform in a much different manner.

The monitored wall panels were shown to be practically airtight, i.e., air-leakage testing of the inner air barrier revealed no measurable leakage. Panel B was intentionally made more leaky during some monitoring periods by opening a 38 mm diameter hole in the lower middle of the drywall (total leakage area = 1,134 mm^2, equivalent to a vent area to leakage area ratio of 2.3:1).

None of the test panels were located at the corners of the Beghut. Because of spatial pressure variations, which are much greater near corners, wall panels located near building edges are expected to have much less dynamic pressure moderation than the panel results reported here.

The size of the pressure-moderation chamber in the brick veneer panels is difficult to define. Theoretically, the depth of the chamber extends from the back of the brick veneer to the air barrier (the drywall in the brick veneer panels). In practice, however, the housewrap or the rigid sheathing acts as the back of the chamber instead of the primary air barrier doing so. Therefore, the panels acted as if they had a chamber depth of 30 mm in the datum panels, 50 mm in the R panels, and 75 mm in the O panels.

The EIFS panels contained a pressure-moderation chamber that was 75 mm deep, 1.2 m wide, and 2.0 m high and filled with Roxul Lamella Wallboard. Venting was provided by a continuous vent strip along the bottom of the fill (see Appendix A). Continuous, diamond-shaped columns of air, about 19 mm square, ran vertically at 200 mm centres from the vent strip to the top of the pressure chamber.

8.2.2 Experimental set-up and monitoring protocol

The test panels were instrumented with numerous pressure taps. The field monitoring program involved continuous pressure measurement (at 3 Hz) at eight locations: at the four vent holes, at the centre of the exterior face, and at mid-height, the top, and the bottom of the airspace. Wind speed and direction at 3.5 m and 10 m above grade were monitored concurrently. The instrumentation used and the exact location of the pressure taps are described in detail in Appendix A: Construction and Instrumentation.

It was necessary to monitor each wall for some time to obtain meaningful results (i.e., until high enough winds from the proper direction occurred). The west-facing (prevailing wind direction) datum wall was monitored for more than 4 months under 4 different venting and air barrier leakage scenarios. The east-facing B, E, and R walls, and the west-facing O wall were each monitored for at least one month each.

The data was collected in approximately 15-minute segments: at least 5 segments were collected for each of 5 wind-speed categories and 12 wind-direction categories for each wall and each venting and air barrier leakage combination. Each record contained 2048 entries, each entry spaced at 1/3 of a second. Each entry of eight pressure measurements, wind speed and direction measurements was collected at a rate of about 1 kHz, e.g., the ten readings were taken in the space of 1/100 of a second.

8.2.3 Analysis technique

A windspeed or pressure signal can be considered to be made up a normally distributed random component and an average component. While the average and standard deviation of such a signal provide useful information, these time-domain statistical measures do not provide much information about the distribution of gust pressures, nor the length of gusts. This information is obviously very important for an assessment of pressure moderation performance.

Like most random signals, a wind pressure signal can be approximated by an infinite series of sinusoidal waves, each with a unique frequency (f), amplitude (A), and phase shift (ϕ):

$$P_{wind}(t) = \overline{P_{wind}} + \int_0^{\infty} A_{wind}(f) \cdot \sin[2\pi \cdot f \cdot t + \phi_{wind}(f)]\, df + n(t) \quad \text{(Eq. 8.5)}$$

where $P_{wind}(t)$ is the instantaneous wind pressure,

$\overline{P_{wind}}$ is the average wind pressure over the entire period,

n(t) is a random component not described by the equation.

Based on a vast body of measurements, it is widely accepted that the wind can be accurately statistically described in the frequency domain, even though this description is an estimation. (The relative size of the term n(t) is an indicator of the accuracy of the approximation). The most useful general descriptor is the power spectrum, a plot of the amplitude A versus frequency *f*. The power spectrum varies with wind speed and terrain; this variation is described in many references including the Commentary to the National Building Code [8.27]

Pressures on the face of a building are different than pressures in the free wind because the airflow is modified by the presence of the building. Frequency domain methods are also useful to describe these pressure variations, especially since the random component of building pressures is not necessarily normally distributed (e.g., the standard deviation is a less reliable measure). The following equation can be used:

$$P_{ext}(t) = \overline{P_{ext}} + \int_0^{\infty} A_{ext}(f) \cdot \sin[2\pi \cdot f \cdot t + \phi_{ext}(f)]\, df \qquad \text{(Eq. 8.6)}$$

Although the pressure within the chamber of a pressure moderated wall system is expected to follow the exterior wind pressure, some attenuation and time lag is expected. Assuming the that the response of the chamber to exterior pressures is linear (and based on the lab-tests referenced earlier, this is at least a good approximation) the response of the chamber to a single sinusoidally varying exterior pressure can be described by:

$$P_c(t) = \overline{P_c} + k \cdot A_{ext} \cdot \sin[2\pi \cdot f \cdot t + \phi] \qquad \text{(Eq. 8.7)}$$

where $P_c(t)$ is the instantaneous chamber pressure at time t

$\overline{P_c}$ is the average chamber pressure

k is the amplitude attenuation coefficient, the ratio of the chamber amplitude to exterior amplitude,

ϕ is the phase shift, the angular displacement of the chamber pressure relative to the exterior pressure (where 2π radians are one period, 1/f).

This is the equation used to describe lab test results which impose a single frequency sine wave to a wall system and measure the response.

For many superimposed frequencies, a real wind pressure for example, the following equation can be expected to apply (provided that the response is still linear):

$$P_c(t) = \overline{P_c} + \int_0^{\infty} k(f) \cdot A_{ext}(f) \cdot \sin[2\pi \cdot f \cdot t + \phi(f)]\, df \qquad \text{(Eq. 8.8)}$$

The amplitude attenuation and the phase shift together describe the frequency-dependent response of the chamber pressure to a random exterior pressure.

The power spectrum of many random signals can be approximated by using the Fourier transform of a record of measurements. The mathematical foundation of the Fourier technique means that N/2 estimates can be calculated from N measurements. The very efficient Fast Fourier Transform (FFT) method requires N to be a power of 2, i.e., records with 128, 1024, or 4096 measurements are acceptable, whereas records with 100 or 2000 are not. The Fourier method approximates a random signal with a series of sinusoids of the following form:

$$x(t) \cong \sum_{i=1}^{N/2} A_i \cdot \sin(2\pi \cdot f_i \cdot t + \phi_i) \qquad \text{N, even} \qquad \text{(Eq. 8.9)}$$

where x(t) is the estimated value of the random signal at time t

A_i, f_i, and ϕ_i are the amplitude, frequency, and phase shift of the ith component

N is the number of discrete measurements of the real signal.

By calculating the Fourier transform of a real signal, the frequency dependent amplitude and phase shift can be estimated. The transform of a signal x will be denoted $S_x(f)$ throughout this thesis.

The function relating a systems output with to input is termed the transfer function in communications theory. Since this transfer function is often frequency dependent, the term frequency response function is often used. This function can be found from [8.1]:

$$H_{ext\rightarrow c}(f) = \frac{S_c(f)}{S_{ext}(f)} \qquad \text{(Eq. 8.10)}$$

where $H(f)$ is the frequency-dependent transfer function and the subscript indicates the relationship between the system's input (exterior) and output (chamber), and

$S_c(f)$ and the $S_{ext}(f)$ transforms of the chamber pressure and the applied pressure respectively.

The amplitude attenuation and phase shift between two signals can then be found from:

$$k(f) = |H_{ext\rightarrow c}(f)| \qquad \text{(Eq. 8.11)}$$

$$\phi(f) = \tan^{-1}\left(\frac{Im[H_{ext\rightarrow c}(f)]}{Re[H_{ext\rightarrow c}(f)]}\right) \qquad \text{(Eq. 8.12)}$$

where Im and Re are the real and imaginary parts of the complex function H.

The value that is of most interest is the pressure difference across the screen, $P_{\Delta scr}$. Using a similar development as above, a more compact description of pressure moderation performance is provided by the fraction of the exterior amplitude that generates a pressure across the screen, e.g.,

$$k_\Delta = \frac{A_\Delta}{A_{ext}} \qquad \text{(Eq. 8.13)}$$

which becomes, over the frequency domain:

$$H_{ext\rightarrow\Delta}(f) = \frac{S_\Delta(f)}{S_{ext}(f)} \qquad \text{(Eq. 8.14)}$$

$$k_\Delta(f) = |H_{ext\rightarrow\Delta}(f)| \qquad \text{(Eq. 8.15)}$$

$$\phi_\Delta(f) = \tan^{-1}\left(\frac{Im[H_{ext\rightarrow\Delta}(f)]}{Re[H_{ext\rightarrow\Delta}(f)]}\right) \qquad \text{(Eq. 8.16)}$$

The $k_{\Delta}(f)$ function is an excellent measure of the magnitude of the pressure difference across the screen. In the time-domain, the wind and wind-induced pressures on a building never behave the same way twice, whereas in the frequency domain the short-term variations do (this is why the power spectrum is so useful for assessing wind loads). Since a unique value is calculated for each frequency, the function is theoretically independent of the frequency spectrum of the applied wind. These features mean that the $k_{\Delta}(f)$ function allows repeatable and comparable results, results that can also be compared to single-frequency lab tests.

There are some limitations to the chosen frequency domain approach however. The basic assumptions in the development are that the wind is a stationary signal (the mean does not change over the record) and that the process connecting the pressures outside and in the chamber are linear. The former assumption can be overcome by analysing only records that are stationary. A simple means of checking is to calculate the average of three or five contiguous blocks of a record. If the average of each is similar, the record is stationary. This is common practise by researchers measuring wind in the field. During some weather events (e.g., thunderstorms), stationary records are impossible to collect because the wind velocity is increasing or decreasing.

The linearity of the process connecting the interior and exterior pressures is a more serious limitation -- in walls where inertia, flow through vents, wall stiffness, and similar non-linear processes dominate, the analysis method described above may not provide repeatable results. In the walls being analysed in this thesis, the range of pressures and the physical nature of the walls are not likely to cause significant non-linearities. This contention is supported by lab tests and field measurements. Linear computer models are able to predict the pressures in the chamber reasonably well. Also, the repeatability of the results reported later strongly support the assumption of linear processes.

8.2.4 Wind record selection criteria

To simplify analysis and to allow for meaningful comparisons, the analysis that follows concentrates on the response of the panels to wind conditions that favour instantaneous pressure equalisation and rain deposition, i.e., positive windward pressures. Records during which the wind speed was high (over 4 m/s) and stationary, and the mean wind direction was almost perpendicular to the wall being monitored (mean wind direction less than ±30° off perpendicular) were analysed in depth. These records have the highest positive windward pressures and some of the smallest spatial variations in the wind

pressures. The nature of the wind is such that even with these restrictions, instantaneous wind direction variations of ±75° and windspeeds of ±50% of the mean windspeed were commonly observed over the course of a 15 minute record.

The frequency-domain method of analysis was used because it ensures that measurements taken at different times will yield similar results for broadly similar wind conditions. However, it was found to be difficult to analyse the results of the pressures under glancing wind conditions (angles > ±60° off normal) because the exterior pressure would change from positive to negative very quickly. The frequency domain analysis gave what are believed to be incorrect, or at least not useful, results Wind conditions such as these do not cause the deposition of much rain and so are not important for rain control.

It is important to note, however, that cladding design is often governed by peak suction pressures and these typically occur under wind angles of about 100 - 120° off normal. The pressure variations in the separation zone of a building are very difficult to describe because two different types of flow processes are involved, and the type of process can change quickly between attached and fully detached flow.

In this thesis, all frequency-domain plots have been calculated from a minimum of five 15-minute-long wind-pressure records collected under similar wind speed and wind direction conditions. The pressures acting at the middle of the panel on the exterior, the pressure moderation chamber, and the inside have been used in all calculations because they are considered to be the most representative or average values.

The average, standard deviation, peak loads, and correlations between all of the signals were also calculated from the time-domain records using standard methods.

8.3 Results and Analysis

In general, the results of the pressure moderation performance monitoring support the comments made earlier in the review of previous research and literature. However, the influence of air-barrier leakage and the amount and location of venting was also studied in the experimental program.

The monitoring showed that all of the wall systems exhibit a relatively high degree of static pressure moderation (over time periods longer than five minutes) but very little pressure moderation of short-term wind gusts.

The degree of static pressure moderation is very high (well over 90%) for situations where the pressure field acting over the wall is relatively stable, e.g., under nearly perpendicular (±30°) winds or under suction pressures on the leeward face. Steady-state pressure moderation was found to be slightly lower, in the order of 75 to 90%, for highly erratic wind-direction variations and glancing wind angles (where the pressure on the wall changes rapidly from positive to negative).

Pressure changes of a few seconds duration and shorter were not well moderated by any of the wall systems. Large pressure spikes often last for only a few seconds. Note that in the National Building Code, the design wind pressures for buildings, for example, are based on a gust of 3 to 5 seconds' duration [8.27], and the cladding or other small components are designed for the equivalent of an approximately 1-second gust or less [8.28].

For most of the brick-veneer records analysed, the spatial correlation between the readings at the centre pressure tap and the corners of the panel was relatively high, between 90 and 94%: this means that there were no large *average* gradients across the face of the panel. This range of values is similar to wind-tunnel studies of the spatial coherence of pressures across a panel on a high-rise building [8.29]. However, average gradients near building corners can be much higher, and short-term spatial pressure variations can be very large indeed.

The single variable that correlated most strongly (usually about 70%) with the pressure difference across the screen was the difference between the pressure at the centre of the panel and the average of the pressures at all four vent holes. This result means that on average 70% of the difference in pressure across the screen was due to spatial pressure variations. The correlation of the chamber pressure with the top vent pressures was always higher than was the case with the bottom vent pressures; this result is likely because top vents are usually exposed to higher pressures than bottom vents.

There was a small positive correlation (30-35%) between the pressure at the middle exterior of the panel and the pressure difference across the screen. This result means that on average, the greater the wind pressure, the greater the pressure difference across the screen.

8.3.1 Standard brick veneer

Most of the monitoring was conducted on the datum (B) panels, and so most of the analysis concerns this commonly used wall system. This panel was 1.2 m wide, 2.4 m high, contained a 30 mm airspace vented with two open head joints (each 10 mm x 65 mm in size) at both the top and bottom. The drywall air barriers was confirmed to be airtight.

Figure 8.3 is a plot of the pressure-moderation performance of the datum panel under nearly perpendicular wind conditions. The figure is a plot of the percentage of wind pressures moderated as a function of frequency (or, 1÷ wind gust duration). Therefore, 100% indicates that no pressure was acting across the screen and that full, instantaneous pressure equalisation occurred. A value of 25% at 2 Hz (a gust lasting 0.5 seconds) means that 75% of the wind-gust pressure acted across the screen

Figure 8.3 shows that the static pressure moderation of the brick-veneer wall is almost 97% under pseudo-static conditions (a 100-second gust can, for practical purposes be considered a static pressure). However, pressure changes shorter than about 5 seconds long are moderated by less than 50% for wind directions nearly perpendicular to the wall.

A wall system similar to the datum wall has also been tested in the laboratory by NRCC/IRC [8.30] and the pressure-moderation performance predicted using a computer program developed by the author (BEG-RAIN [8.1]). The results of these predictions, which match one another, is plotted in Figure 8.3. Both the IRC laboratory testing and the computer modelling suggest that dynamic pressure moderation should be about 95% at 1 Hz, whereas the field results show that the moderation is almost zero at this frequency. Unlike the lab and computer results, the field results incorporate the effect of spatial wind pressure variations. The discrepancy between lab, computer, and field results is convincing evidence of the importance of spatial variations to pressure moderation performance.

1 This is a program based on the compressibility of ideal gases. It uses sinusoidal loading conditions and includes the important wall characteristics.

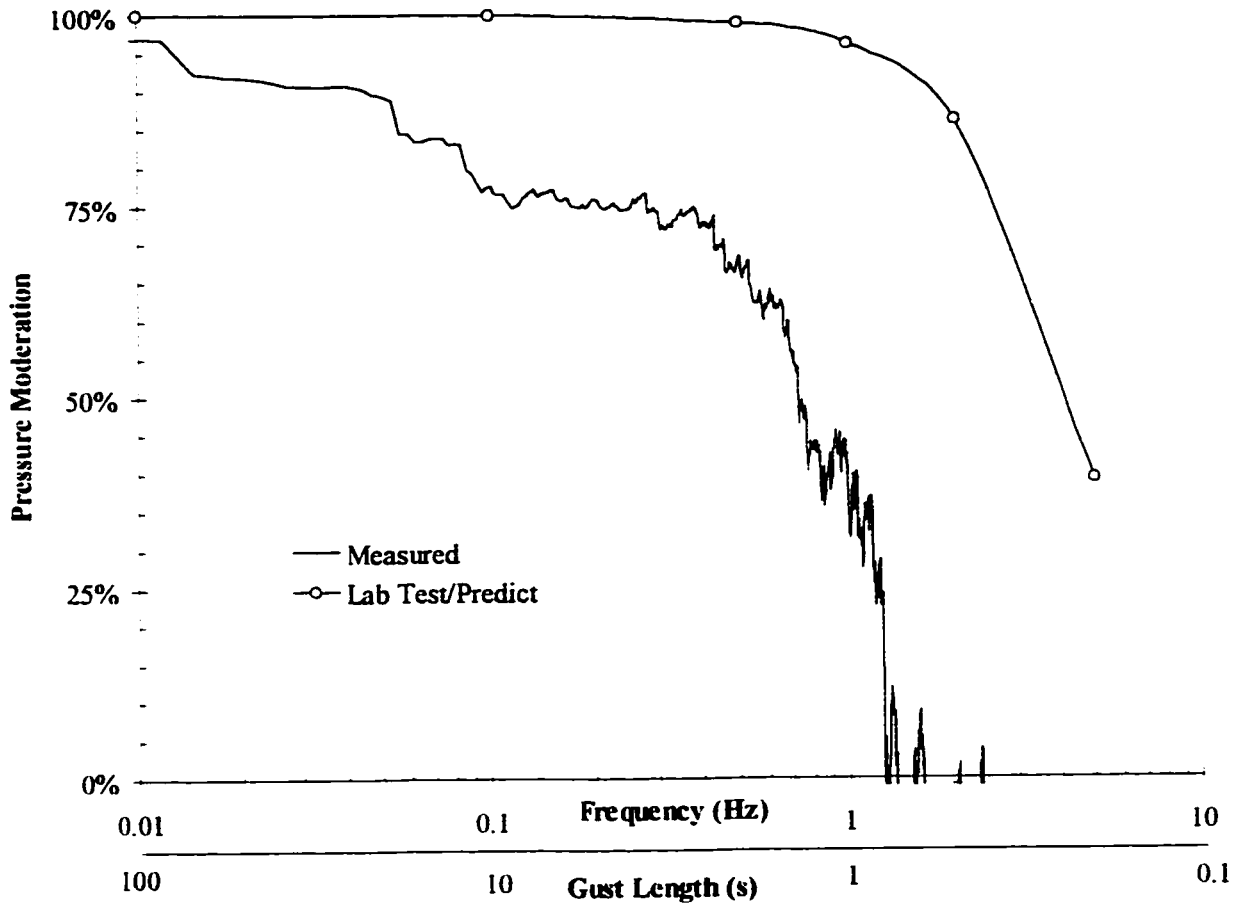

Figure 8.3: Pressure-moderation performance of brick-veneer panel as measured in the field, the lab, and predicted by computer model

Note: Panel BW with perfect air barrier, 30 mm air space and 4 open head joints. Wind Direction ±30°.

The lack of pressure *equalisation* is mostly due to the spatial variation of the wind pressure, not the slow temporal response of the wall system to gusts. Because of spatial variations, the pressure acting over the central part of the wall can be quite different from the pressure acting at the vents, although the pressure in the cavity responds only to the pressure at the vents. The pressures acting at each vent opening are quite different, especially in turbulent winds. Turbulent winds are the result of rough upstream fetches (e.g., cities) and by building-induced turbulence near building corners, at aerodynamic discontinuities, etc. Therefore, while the panel may be able to respond quickly to temporal variations (e.g., those imposed by laboratory tests and computer models), the spatial pressure variations (and gradients) on the panel reduce the achievable degree of moderation, especially at high frequencies.

In summary, although the pressure-moderation performance of a wall panel can be "tested" in the laboratory or predicted by simple computer models, the actual pressure-moderation performance of most properly designed and built walls will be governed by spatial wind-pressure variations, not the wall design or temporal wind-pressure variations. Therefore computer modelling or lab testing, while useful, may provide misleading results and foster unrealisable expectations for performance.

8.3.2 Exterior insulated finish system (EIFS)

Figure 8.4 plots the pressure-moderation performance of the EIFS panel studied. The frequency-based analysis clearly shows how the response deteriorates with decreasing gust duration. Compared to Figure 8.3 it can be seen that less pressure moderation is occurring at all frequencies. This response was unexpected because the vent area is quite high: several percent of the wall area. However, the vent is located only at the bottom in the form of a strip that runs the full width of the panel, at about 0.5 m above grade.

The pressure-moderation performance of the EIFS panel appears to have been restricted by the spatial gradients of the wind near the ground at the Beghut test site. While the pressures near the ground do change quickly with increasing height at the Beghut, similar pressure gradients can also occur higher up on the corners of a large building. The pressure-moderation performance of the similarly vented panels installed on a tall building will be significantly better near the middle of the building, where spatial gradients are small. The performance will be very similar to that measured at the Beghut when the panels are used near building edges where gradients are large (and rain deposition is the greatest).

Correlations were calculated to gain a better understanding of the behaviour and to provide more information regarding the average performance. The correlation between the pressure in the vertical air slots and the centre of the rigid fibrous insulation was between 98 and 99%, i.e., on average these pressures were almost always exactly the same. The air pressures at the middle of the chamber were, on average, well correlated (about 95%) with the pressures at the vent slot. Thus, the chamber was exhibiting a high degree of pressure moderation relative to the pressures acting at the slot. It would therefore appear that the pressure-moderation performance was chiefly affected by the location of the vents. Another potential contributor to poorer performance is the relatively large volume of the pressure chamber, although the vent area provided should be large enough to compensate for this larger volume.

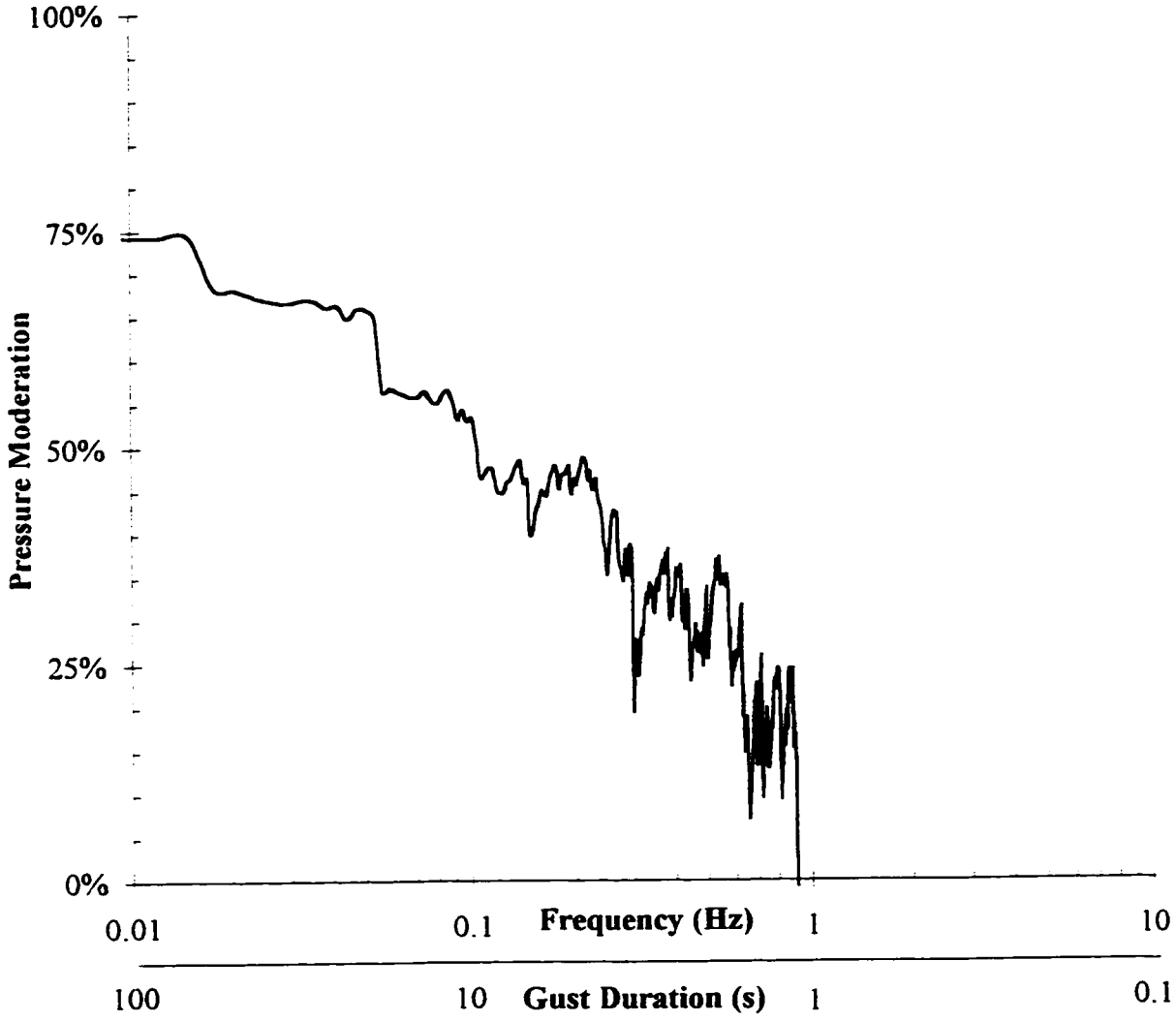

Figure 8.4: Pressure-moderation performance of Sto System Plus 1 RS EIFS

Note: Perfect air barrier. Wind Direction ±30°

8.3.3 Filled-cavity brick veneers

Both the R and the O walls were monitored. Both of the panels exhibited pressure moderation performance that was essentially the same but slightly lower than that of the datum panel (Figure 8.5). While the cavity fills do retard ventilation, the small amount of airflow required for pressure moderation is clearly not restricted by the mid- to high-density cavity fill products used in these panels. The small reduction in performance may be due to the larger chamber volume in these panels.

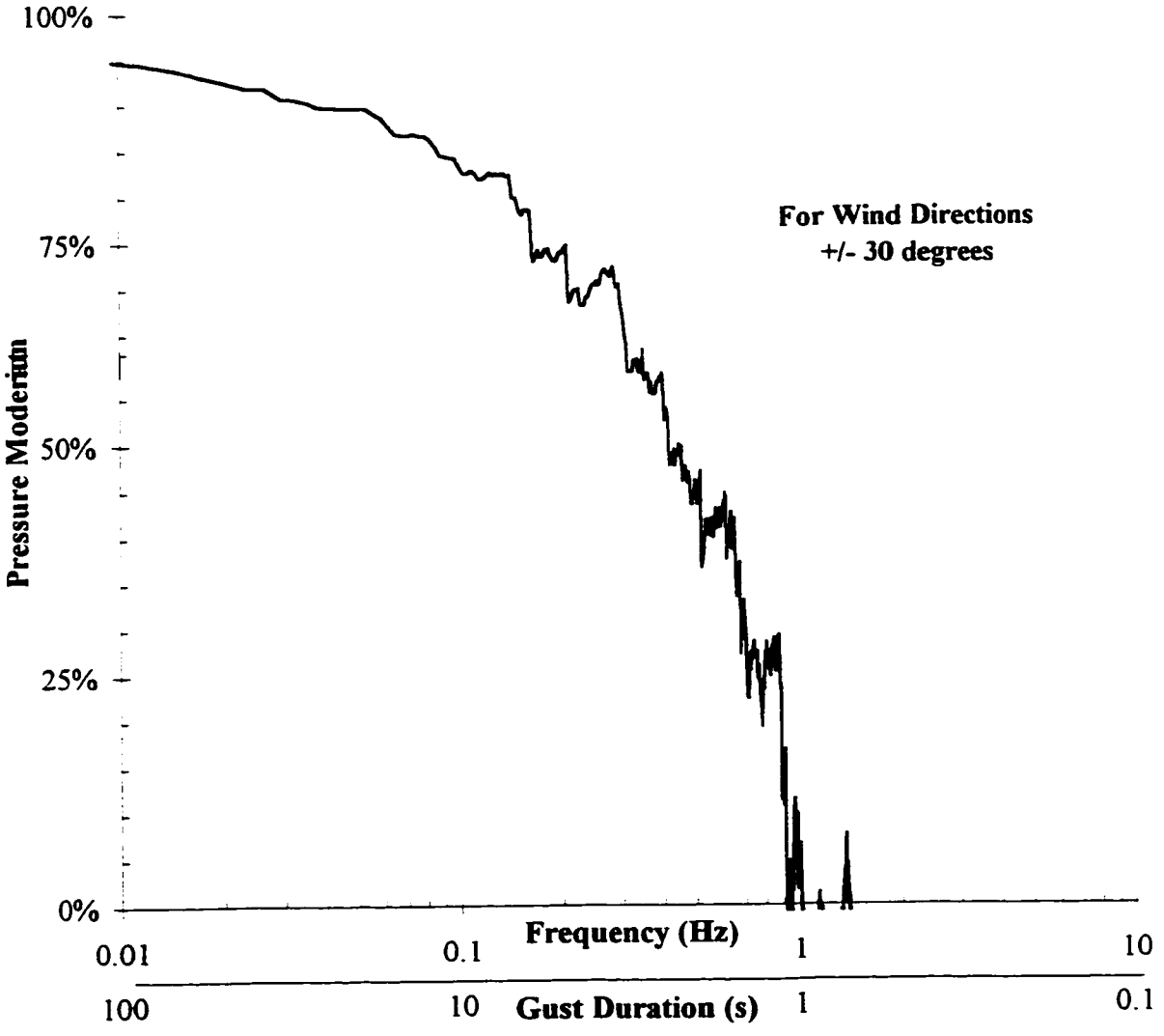

Figure 8.5: Pressure moderation performance of filled-cavity walls

8.4 Parametric Assessment

Although the characteristics of the wind will, in many cases, limit the maximum achievable degree of pressure moderation, wall characteristics do have an effect, especially at low frequencies. Important variables are the amount of leakage through the air barrier, the total venting area, the vent location, and the wind direction.

Air barrier leakage can have a significant effect on pressure-moderation performance. The larger the ratio of vent area to air-barrier-leakage area, the higher the degree of pressure moderation.

Another common concern is the proper location of the vent openings themselves. The IRC recommends that all vent openings be placed along the bottom [8.2]. However, Inculet [8.31] calculations of spatial wind variations strongly indicate that distributing the vent openings over the compartment will result in the best performance.

These parameters were studied by conducting simple experiments on datum panel BW. The datum panel was chosen since it is a commonly used wall system and the results should therefore be relevant to many similar wall systems. After monitoring for several months, a single characteristic was changed, and the wall monitored for another month. The results are presented and discussed below.

8.4.1 Effect of air barrier leakage

Figure 8.5 compares the performance of datum panel BW with and without a hole in the primary air barrier. Increasing the equivalent leakage area from almost zero to 1134 mm^2, has the effect of reducing the ratio of venting area to air-barrier-leakage area from nearly infinity to about 2.5:1. The results show that static pressure moderation was reduced (to about 85%) and that the degree of dynamic pressure moderation was similarly reduced, i.e., the performance was about 85% of the airtight response over the entire frequency range.

Based on Equation 8.3, static pressure moderation can be calculated from:

$$\text{Static pressure moderation} = 1 - (A_{leak}^2 \div A_{vent}^2)$$

Applying Equation 8.3 to panel BW with a leaky air barrier and a 2.5:1 vent:leakage ratio results in a predicted pressure moderation of about 84%. Therefore, simple theory provides a close match with the measurements. This evidence suggests that Equation 8.3

can be used to provide a relatively accurate assessment of long-term pressure response when both the equivalent air leakage area and vent area are known.

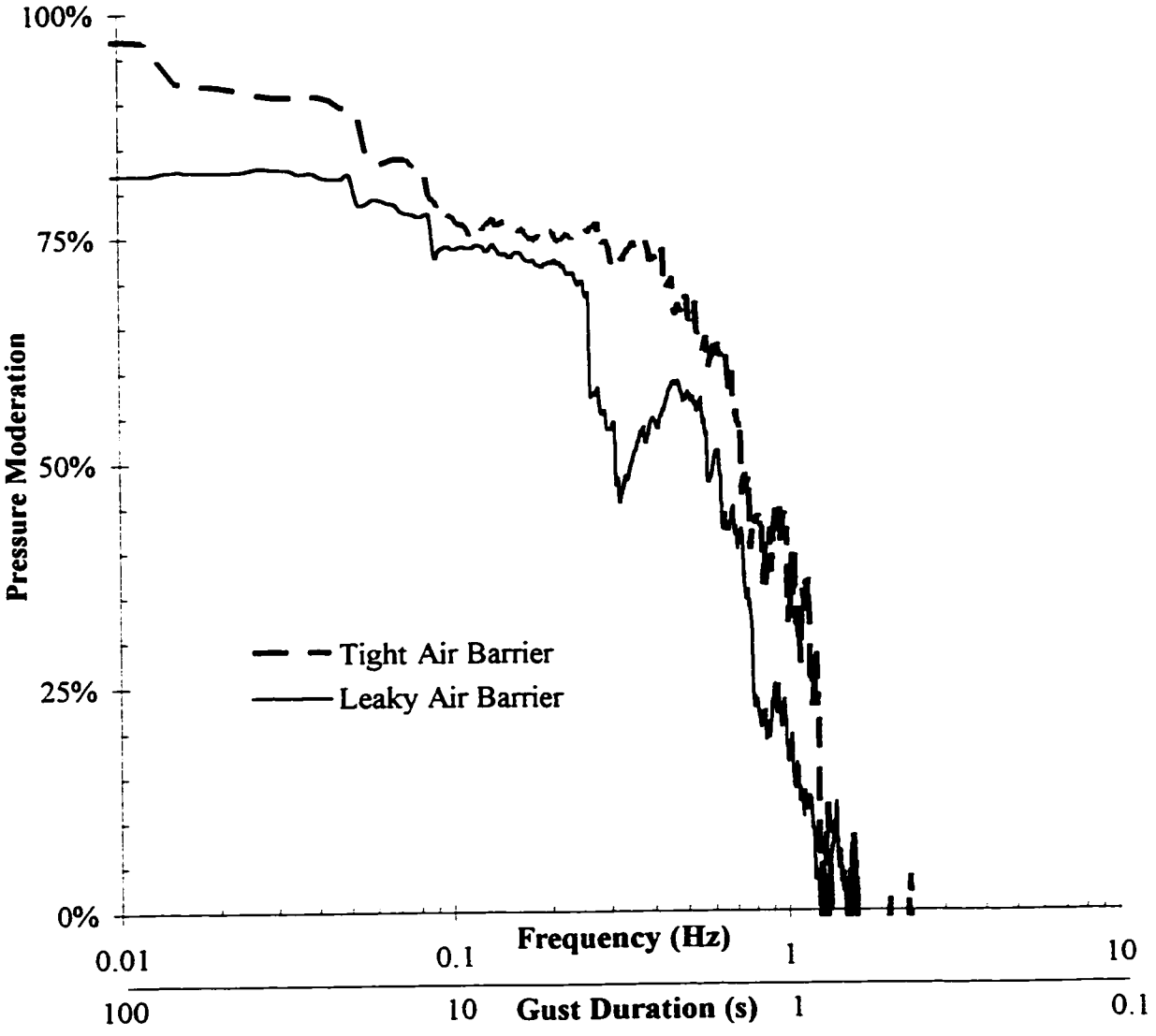

Figure 8.6: Pressure-moderation performance of panel BW with leaky air barrier

Vent to Leakage Ratio = 2.5:1. Wind Direction ±30°

8.4.2 Influence of total venting area

Recent references [8.2] recommend a total venting area of 1 to 2% of the wall area. For a storey-high brick veneer wall system, the 1% requirement translates into about 35 open head joints per running metre of wall. Note that a metre of wall normally has only 2 to 6 head joints per metre. The walls tested in this project contained 4 open head joints per 1.2 m x 2.4 m panel: this is equivalent to approximately 0.1% of wall area. Although this amount of venting is much less than that recommended (by a factor of at least ten), it is much more than is normally provided (by a factor of about 2 to 5). Note that open head joints all along the bottom course of a veneer at 800 mm on centre provides only 0.04%. In practice, head joints are often provided with inserts to protect against the entry of insects, driving rain, etc. It should also be noted that tests (presented in Chapter 9) have shown that most commercially available vent inserts drastically reduce air flow (by an order of magnitude), and hence significantly reduce the effective vent area.

As reported in Section 8.1.2, the 0.1% vent area allows for more than 95% pressure moderation of long-duration wind-pressure changes (longer than 100 s). Measurements of panel BW were also taken with the vent area reduced by half (by sealing two of the four vents). During one two-week period the top vents were closed, and during the next two-week period one top vent and one bottom vent were closed.

Comparison of the results in Figure 8.7 with Figures 8.3 and 8.6 shows that the reduced vent area significantly affected the pressure-moderation performance. The effect of reducing the vent area is almost the same as that produced by greatly increasing the leakage area. In the context of these tests, it appears that a vent area of least 0.1% of wall area should be provided for any significant degree of pressure-moderation performance to be achieved under these ideal conditions.

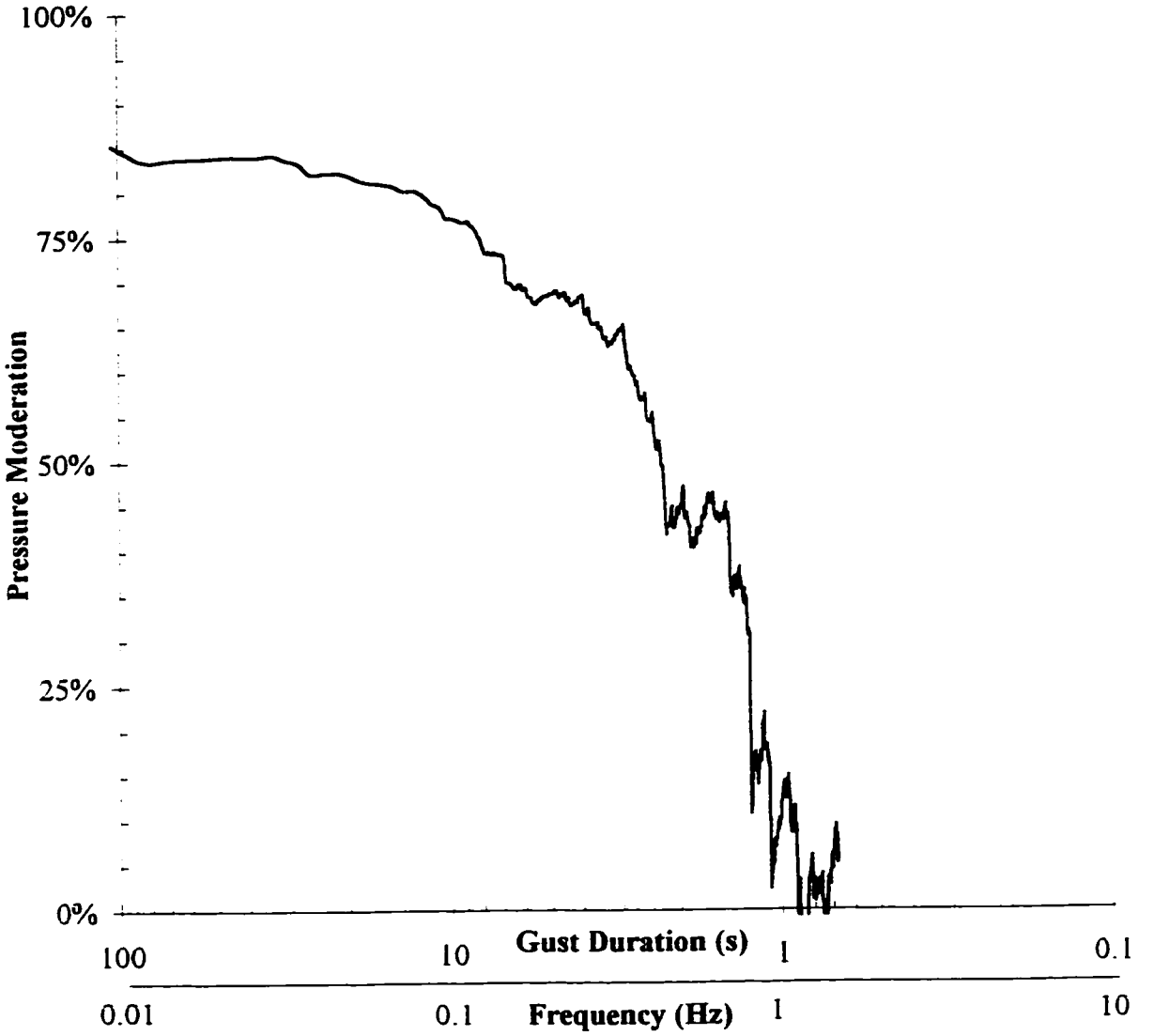

Figure 8.7: Pressure-moderation performance of panel BW with reduced vent area

Note: Vents were open head joints, located at the top and bottom, diagonally separated on the panel. Total vent area: 1400 mm^2 = 0.05% of Wall Area. Wind Direction ±30°

8.4.3 Vent location

The location of vents on the wall is another important issue. Is it better to locate vents at the top and bottom or only at the bottom? In an attempt to provide an answer to this question, pressures were monitored for one month with only the bottom vents open and for one month with one top and one bottom vent open.

Figure 8.8 shows the results. The pressure-moderation performance clearly was not strongly affected by whether the vents were located at the top and bottom or only at the bottom. This result was somewhat surprising because there is an average gradient of wind pressure, increasing from the bottom of the panel to the top, and it was therefore expected that the bottom-only location would be inferior. In actuality little effect was apparent, although the bottom-only venting did slightly reduce the degree of pressure moderation of the low-frequency, long-duration gusts. The bottom-only location also appears to result in slightly better performance in the high frequency range, although the results in this range are less accurate.

Locating the vents at the top *and* bottom of the cavity has three distinct advantages, however:

1. Locating vents at both the top and bottom will permit and promote ventilation drying.
2. Locating vents at the top is an easy and simple way to double the vent area so that a greater degree of pressure moderation can occur.
3. A more practical consideration is the fact that vents at the bottom of a wall are much more likely to be blocked by mortar than those at the top.

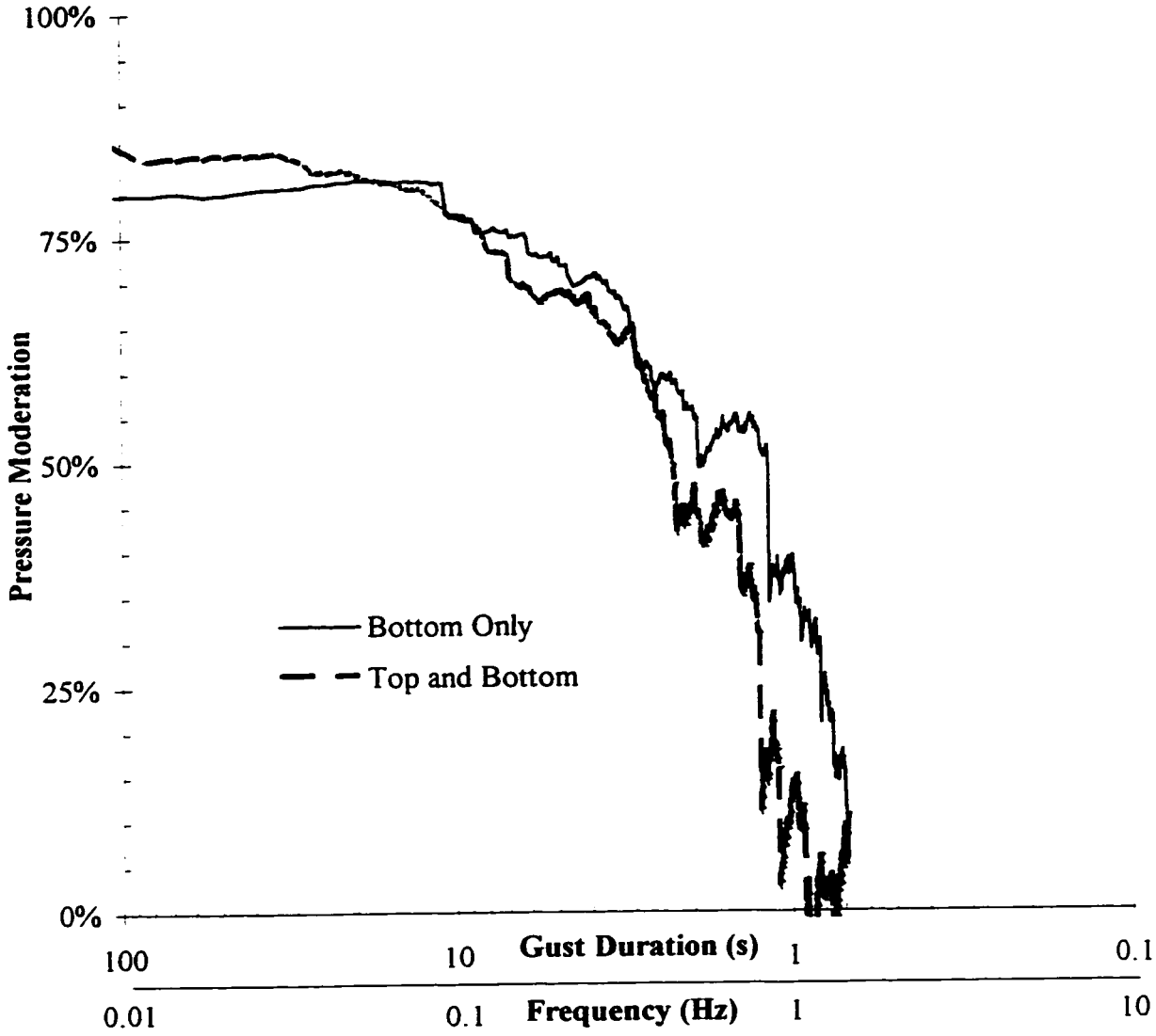

Figure 8.8: Pressure-moderation performance of panel BW — influence of vent locations

Wind Direction ±30°

8.4.4 Influence of wind direction

It has long been suspected that the location of the wall on a building and the wind direction would have an effect on the pressure-moderation performance. The analysis presented above is for wind directions almost normal to the wall, and for walls near the middle of the building. A limited analysis of walls near the corner of the Beghut and under different wind angles has been conducted.

As expected, the pressure-moderation signature does not change near corners, since it is a measure of the wall response. However, the wind contains more high-frequency / short-duration gusts (the wind is more turbulent), and hence a larger proportion of the gusts are moderated to a lesser degree. The likely consequence is poorer pressure-moderation performance. Unfortunately, the areas of a building likely to receive the most driving rain (edges and corners) are also the areas where dynamic pressure moderation is the most difficult to achieve. In these areas the area of the compartments in the test panels would have to be much smaller in order to achieve the same level of performance as at the middle of the building.

No panels can be installed very near the corner (e.g., within 10% of the building width). However, wind under glancing angles creates large mean spatial pressure gradients. As discussed in Section 8.2.4, the frequency-domain signature was very different under these conditions. The pressures were low and often changed sign. Methods of analysing this response need to be developed.

8.5 Peak Loading of the Screen

The analysis and presentation of the previous results has concentrated on the dynamic behaviour of the wall during the majority of the time. For structural design purposes, however, it is the peak loads on the screen that are of interest. This section analyses the same pressure records in the time domain so that the peak loads can be found.

8.5.1 Analysis method

While the frequency-domain results shown earlier are very descriptive of in-service behaviour, they do not clearly show the effect of wind pressures on the structural loading of the screen. Design wind loads are typically presented in the form of pressure coefficients, which are applied to the stagnation wind pressure calculated for a particular site and building height.

The equivalent static wind-induced pressure on a building face is often expressed as a fraction of some reference pressure, usually either the stagnation pressure at the top of a tall building, the eaves height for buildings with pitched roofs, or 10 m above the ground. A pressure coefficient is defined as the ratio of the pressure of interest (e.g., the pressure across the enclosure) to the average stagnation pressure of the wind. Pressure coefficients normalise the wind loads so that the pressures measured in wind tunnels or on test

buildings like the Beghut can be used on actual buildings in different locations. This pressure coefficient, C_p, is defined as:

$$C_{wall} = \frac{P}{P_{stag}} \qquad \text{(Eq. 8.17)}$$

The stagnation pressure is approximately equal to:

$$P_{stag} = 0.647 \times V^2$$

where V is the wind velocity in m/s, and

P_{stag} is the stagnation pressure in Pa.

The actual pressure acting on a building or component can then be calculated by using the appropriate pressure coefficient:

$$P = C_p \cdot P_{stag} = C_p \cdot 0.647 \times V^2 \qquad \text{(Eq. 8.18)}$$

where C_p is the pressure coefficient (no units), and

P is the actual pressure in Pa.

Pressure coefficients are usually based on the hourly average wind velocity. Additional factors are applied to reflect the influence of wind gusts, terrain conditions, and the height of the building or building element.

The monitoring program measured all pressures with reference to the interior of the Beghut. Therefore, a wall pressure coefficient was defined as:

$$C_{wall} = \frac{\Delta P_{wall}}{P_{stag}} \qquad \text{(Eq. 8.19)}$$

where C_{wall} is the pressure coefficient (no units),

ΔP_{wall} is the pressure across the entire wall, which would normally be calculated as

$\Delta P_{wall} = P_{ext} - P_{int}$, and

P_{stag} is the average stagnation pressure, calculated from the windspeed measured at 10 m using $P_{stag} = 1/2 \cdot \rho \cdot V^2$, $\rho = 1.2$ kg/m^3.

8.5.2 Results

The pressure across the wall, ΔP_{wall}, was calculated using various averaging times. For example, for a 30-second averaging time, 90 samples (taken at 3 Hz) were averaged to calculate the average coefficient, the maximum, and the minimum. Since a 15-minute record contains 30 unique 30-second records, the process was repeated 30 times and 30 different coefficients for maxima, averages, and minima were calculated

The average of these maxima, minima and averages is plotted for 5 different records in Figure 8.9 as a function of averaging time. The vertical bars show the range of values recorded for the different records considered. Figure 8.9 shows that the average pressure coefficient across a panel located near the middle of the windward face of the BEGHUT is about 0.8. This value is close to the results of wind tunnel and field studies of buildings similar to the Beghut. The fact that the average coefficient does not change with averaging time indicates that the record was stationary.

It can also be seen that gusts of 1-second duration may occur that are as much as four times the average stagnation pressure. Even on the windward face, the pressure can change to suction (indicated by a negative pressure coefficient). Figure 8.9 shows that the minimum pressures recorded are suction gusts with a magnitude of about half the average stagnation pressure. These data describe the wind-building interaction only and are the same for all panels located near the middle of the windward side of the Beghut.

As the averaging time is decreased, the wind pressures are higher. The National Building Code assumes an averaging time of about one second for cladding and three seconds for the building structure as a whole. While pressures that act for less than one second have significance for some lightweight claddings and non-adhered roof membranes, a one second averaging period is reasonable for the design of heavy brick veneer and natural stone screens.

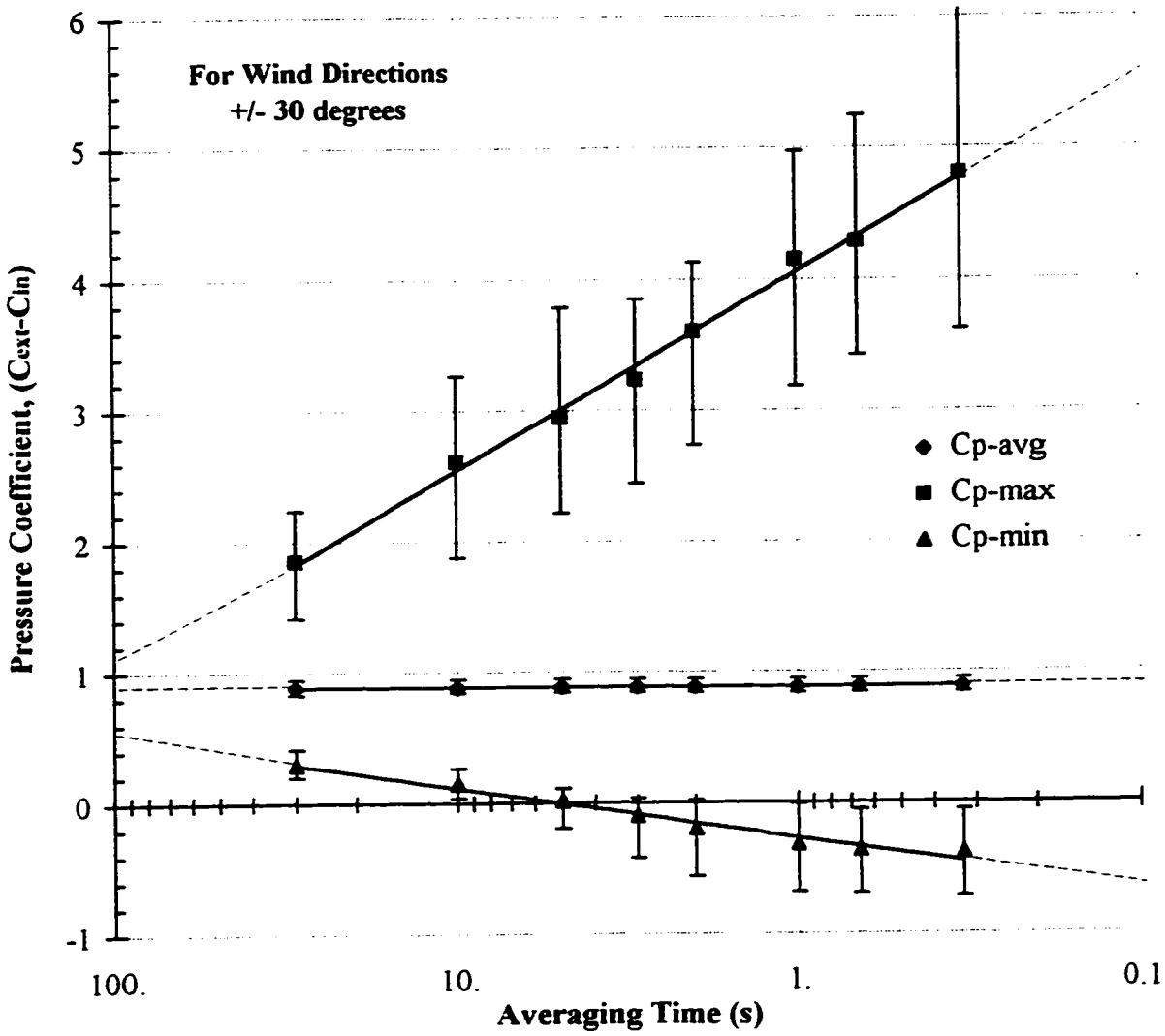

Figure 8.9: Pressure coefficient for a windward wall in the Beghut as a function of averaging time

Wind Direction: ±30° off perpendicular

A rainscreen coefficient was defined as the ratio of the pressure acting across the screen to the average stagnation pressure:

$$C_{screen} = \frac{\Delta P_{screen}}{P_{stag}} \qquad \text{(Eq. 8.20)}$$

where C_{screen} is the pressure coefficient (no units),

ΔP_{screen} is the pressure acting across the screen, and

is P_{stag} is the stagnation pressure at 10 m above grade.

Figure 8.10 plots the pressure coefficient for the air pressure acting across the screen of the datum panel BW. Just as the frequency domain plots showed, this plot confirms that, on average, the pressures are almost equalised. However, when short-term effects are accounted for, it can be seen that pressures as much as two times the stagnation pressure itself can occur.

As an aid to the interpretation of these data, consider the following example. If the wind has an hourly average speed of 10 m/s (quite a stormy day), then the stagnation pressure at 10 m above grade will be:

$$P_{stag} = 0.647 \times 10^2 = 65 \text{ Pa}$$

For a 1-second averaging period (appropriate for cladding design), Figure 8.9 provides a coefficient of about +4 for positive pressures and -0.4 for negative pressures, and so

$$P_{wall.\,max} = C_{p.max} \times P_{stag} = 4 \times 65 = 270 \text{ Pa}$$

$$P_{wall.min} = C_{p.min} \times P_{stag} = -0.4 \times 65 = -27 \text{ Pa}$$

The brick veneer screen should also be designed for the pressure acting across it. Figure 8.10 shows a screen coefficient value of about 1.1 for a 1-second averaging time, so:

$$P_{screen.max} = C_{screeen.max} \times P_{stag} = 1.1 \times 65 = 71.5 \text{ Pa}$$

In this case, the design load for the brick veneer is only about one quarter of that on the enclosure itself. Such an analysis suggests that some useful reduction in screen design loads might be possible in well-vented, airtight walls that have appropriately stiff backups (e.g., concrete block).

Note, however, that the screen pressure coefficient for suction pressures under glancing wind angles has not been analysed. The wind loads that tend to govern a design are suction loads on the side walls of a building. No attempt has been made to assess this situation, although the existing wind loading information in the literature indicates that the pressure moderation would be less successful in this region of the building (because of very turbulent wind conditions).

Also, since it is likely that the backup portion of the wall is significantly more flexible (e.g., wood or steel stud framing) than the masonry veneer, much of the wind load may be transferred back to the veneer through the brick ties as a consequence of composite structural action. Therefore, any reduction in wind loading would only be a benefit if the backup structure was significantly stiffer than the cladding. This is clearly the case with panellised systems.

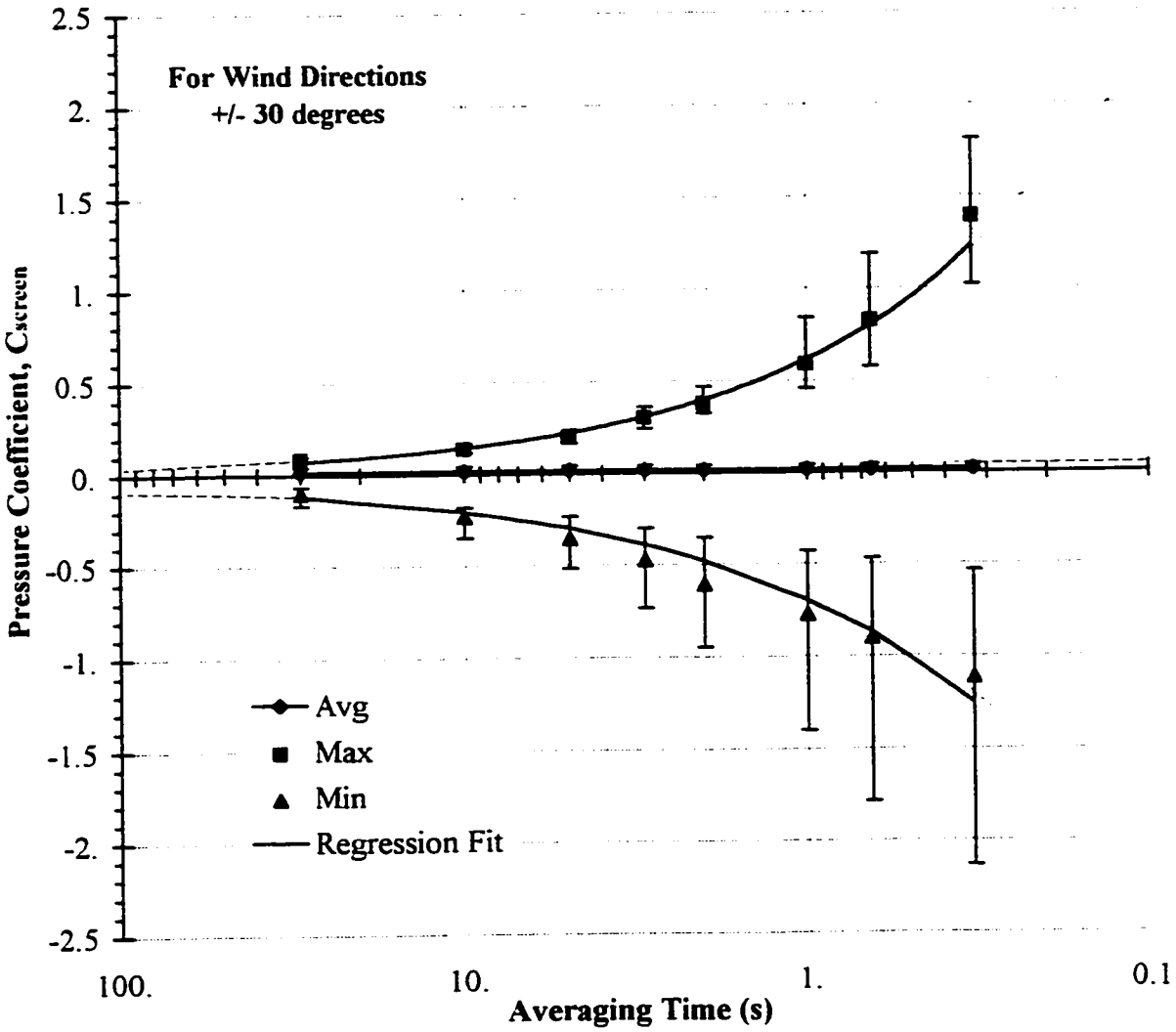

Figure 8.10: Pressure coefficient across brick veneer of panel BW as a function of averaging time

Wind Direction ±30°

It would be conservative to continue to design both the air barrier system and the masonry veneer to each resist the full wind load. However, savings are likely possible, especially

for walls that are well vented. Before any consideration is given to screen load reductions due to pressure moderation, the designer must realise that the performance of such a structural design is dependent on the probability of the specified amount of venting and airtightness being provided. While it may be reasonable to rely on venting and airtightness being provided in some prefabricated systems (e.g., metal cladding), it is clearly not realistic for site-built masonry veneers.

8.6 Conclusions and Implications

The results of the pressure moderation performance monitoring, theoretical considerations, lab and field experience have generated a series of important conclusions.

The wind rarely blows hard enough to generate significant pressures (i.e., greater than about 100 Pa) across the envelope of a low-rise building, even one as exposed as the Beghut. High wind pressures (greater than 100 Pa), especially in conjunction with rain, are rare (see also Chapter 5: Driving Rain). Both wind direction and speed can change drastically and very quickly (see also Chapter 9).

Based on average values, pressure differences across the screen can be well moderated — almost equalised — provided that the wind is not exceptionally turbulent and that the wall is well-vented, airtight and somewhat compartmentalised. Long-term, "static" pressure moderation can be quite high (more than 90%) so long as sufficient venting is provided to accommodate the air-barrier leakage. Providing vent areas of at least 5 times the equivalent air-barrier leakage area *in service* will permit about 94% static pressure moderation. Actually achieving this level of venting in the field may require considerably more vent area than typically specified if realistic estimates of air-barrier leakage are considered. Blocked vents, vent inserts, and weep tubes all restrict the vent area to such an extent that the backup may need to be unreasonably/impractically airtight to allow high levels of static pressure moderation to be achieved.

The degree of pressure moderation of short-term gusts (less than a few seconds long) is rather limited for brick veneers. This conclusion is also valid for any wall system with little venting (<0.5% of wall area) and with compartment sizes greater than about 1.5 m.

The dynamic pressure-moderation response *of a wall system* can be tested in the laboratory and/or predicted by special computer models. However, short-term pressure moderation of even well-vented, airtight and tightly compartmentalised walls will be poor

because dynamic pressure-moderation performance is governed by the spatial variations of the wind pressures in typical walls, not by the wall characteristics. Pressure moderation is expected to be worst at upper and side edges of buildings, the same areas of cladding that receive the most driving rain. Measured pressure moderation of one-second gusts was less than 33%, and even three-second gusts were only moderated by 40% in the well-built brick veneer panels exposed to a nearly perpendicular wind direction.

Wind directions other than perpendicular will increase the spatial and temporal variations of pressure on the face of a building and therefore negatively affect the pressure-moderation performance. Because the pressures are often much lower and even negative under these conditions, and because rain wetting is less intense, rain penetration is probably not seriously affected by the reduced pressure-moderation performance.

The degree of pressure-moderation performance is a function of both the characteristics of the wall and the wind. Wall characteristics, e.g., area of venting, air tightness, etc., are of only secondary significance for dynamic pressure moderation. Based on the available research, vent area appears to be the wall system characteristic with the greatest influence on pressure-moderation performance. The spatial extent of gusts is likely the most important wind characteristic affecting the degree of pressure moderation, but the speed of the gust (i.e., frequency) and, to a lesser extent, the magnitude of the gust also play a role. Even in walls compartmentalised at 1.2 x 2.4 m spacings, it is the spatio-temporal variations of the wind that will govern the performance of most pressure-moderated wall systems.

As shown in Chapter 7, brickwork veneers are water permeable, even when no air-pressure difference is applied. Therefore pressure moderation can only reduce — not eliminate — rain penetration. Even perfect, instantaneous pressure moderation cannot eliminate rain water penetration of a brickwork veneer. Although it is difficult to precisely quantify the relative significance of pressure moderation for rain penetration control at this time, it is clearly not that important for brick veneers.

The rain control of all types of screened walls, including EIFS, can benefit from the contribution from pressure moderation when the appropriate amounts of venting and compartmentalisation are used. Spatial pressure gradients will reduce pressure-moderation performance at the upper and side edges of buildings, the same areas of cladding that receive the most driving rain.

The rain control performance of masonry veneers can be improved only marginally by dynamic pressure moderation because:

- the testing reported in Chapter 7 shows that mechanisms other than air pressure are the primary cause of water leakage through masonry,
- a masonry veneer drained-screen wall design must presume that the veneer will leak significant quantities of water and so drainage is critical and must be provided in nay case, and
- pressure moderation of gusts is very difficult, not because of the wall design, but primarily because of the spatial variability of wind pressures.

The rain control of drained-screen walls with relatively water-impermeable screens (e.g., EIFS, vinyl, precast concrete) may benefit from pressure moderation because air pressure differences are often the most important mechanism by which water can penetrate the screen. Even so, these systems more often experience rain control problems at joints, windows, or other penetrations. These joints should be designed as drained screens and not as perfect barrier systems.

In all cases, drainage is absolutely essential for good rain control in screened wall systems, and is certainly more important than any contribution from pressure moderation. At this time pressure moderation may be a beneficial characteristic to strive for, but many other characteristics are more important. Any contribution to rain penetration control or screen or connector load reduction should be regarded as possible but not as a quantifiable nor reliable benefit. Factors such as exposure conditions, the control of rain water on the surface, drainage, and the quality of workmanship will all play a larger role in the control of rain penetration than pressure moderation. Even if walls could be made to pressure-equalise instantaneously, poorly installed flashing, joints, windows and brickwork can still cause failure, as field experience suggests are in fact the problems.

It may be possible to safely design the enclosure for lower wind loads if a greater understanding of the structural distribution of static and gust pressures could be developed. Any possible load reductions should only be implemented once the relative stiffnesses of the cladding and backup, and the reliability of venting, air flow and air barrier tightness, have been carefully assessed.

8.7 References

[8.1] Straube, J.F., *The Performance of Wall Systems Screened with Brick Veneer.* M.A.Sc. Thesis, Civil Engineering Department, University of Waterloo, 1993.

[8.2] Baskaran, A., *Review of Design Guidelines for Pressure Equalized Rainscreen Walls* , Internal Report No. 629, IRC/NRCC, Ottawa, March 1992.

[8.3] Poirier, G.F., Brown, W.C., Baskaran, A., "Pressure Equalization and the Control of Rainwater Penetration", *Proc. Sixth Conference on Building Science & Technology, Toronto*, March 5-6, 1992, pp.45-64.

[8.4] Burnett, E.F.P., and Straube, J.F.,"The Brick Veneer Screened Wall", *Proceedings of the Seventh Canadian Masonry Symposium*, Hamilton, Canada, June, 1995, pp.651-662.

[8.5] Latta, J.K., *Walls, Windows, and Roofs for the Canadian Climate*, Special Technical Publication No. 1 of the Division of Building Research, Ottawa, 1973

[8.6] Killip, I.R., and Cheetham, D.W., "The Prevention of Rain Penetration through External Walls and Joints by Means of Pressure Equalization", *Bldg. And Environ.*, Vol. 19, No. 2, 1984, pp. 81-91.

[8.7] *Assessment of the Air Leakage and Rain Penetration Control Performance of a Prefabricated Brick Wall Test Specimen*, Report for J.C. Perreault & Sons and Vet-O-Vitz Masonry Systems Inc. By the Institute for Research in Construction/National Research Council of Canada, Report CR6016.2), Ottawa, 1990.

[8.8] Holmes, J.D., "Mean and fluctuating pressures induced by the wind". *Proc. of the 5th International Wind Eng. Conf.*, Fort Collins, Colorado, ed. J.E. Cermak, 1980.

[8.9] Harris, R.I., "The propogation of internal pressures in buildings", *J. of Wind Eng. and Industr. Aero.*, Vol 34, pp. 169-184, 1990.

[8.10] Inculet, D., Surry, D., Davenport, A.G., "Unsteady Pressure Gradients and Their Implications for Pressure-Equalized Rainscreens", *Proc. of ICBEST '97*, Bath, U.K., pp. 457-463, 1997.

[8.11] Skerlj, P.F., Surry, D., *A Study of Mean Pressure Gradients, Mean Cavity Pressures, and Resulting Residual Mean Pressures Across a Rainscreen for a Representative Building*, Report by BLWTL, The University of Western Ontario for CMHC, Ottawa, Sept, 1994.

[8.12] Inculet, D., Surry, D., *The Influence of Unsteady Pressure Gradients on Compartmentalization Requirements for Pressure-Equalized Rainscreens*, Report by BLWTL, The University of Western Ontario for CMHC, Ottawa, June, 1996.

[8.13] Cook, N.J., "Dynamic response of single-ply membrane roofing systems". *J. of Wind Eng. and Industr. Aero.*, Vol 41-44, pp. 1525-1536, 1992.

[8.14] Solliec, C., Barnaud, G., Chaibi, A., "Procedure de dimensionnement au vent des bardages et vetures: appoches experimentale et numerique", *J. of Wind Eng. and Industr. Aero.*, Vol 48, pp. 95-110, 1993.

[8.15] Gerhardt, H.J., and Janser, F., "Wind Loads on Wind Permeable Facades", *J. Of Wind Eng. and Industr. Aero.*, Vol 53, pp. 37-48, 1994.

[8.16] Gerhardt, H.J., and Krueger, O., "Double Skin Glass Facades - Investiagtions into the Load Sharing Possibilities", *Proc. of ICBEST '97*, Bath, U.K., pp. 335-339, 1997.

[8.17] Laviolette, S., and Keller, H., *Performance Monitoring of a Brick Veneer / Steel Stud Wall System*, CMHC Research Report by Keller Engineering, June, 1993.

[8.18] Quirouette, R., *Laboratory Investigation and Field Monitoring of Pressure-Equalized Rainscreen Walls*, CMHC Research Report, September, 1996.

[8.19] Straube, J.F., and Burnett, E.F.P., *The Zero-Cavity and DPV Wall Project*, Research Report for CMHC by the Building Engineering Group, December, 1995.

[8.20] Herbert, M.R., *Open-jointed Rain Screen Claddings*. Building Research Establishment, Current Paper CP89/74, HMSO Garston, U.K., 1974.

[8.21] Isaaksen, T., "Rain Leakage Tests of Open Joints in Ventilated Calddings", *Weathertight Joints for Walls: Proc. Of the Int. CIB Symp.*, Oslo, Norway, Sept. 25-28, 1967, pp. 349-354.

[8.22] Harrison, H.W., and Bonshor, R.B., *Weatherproofing of Joints: a Systematic Approach to Design*. Building Research Establishment, Current Paper CP29/70, HMSO Garston, U.K., 1970.

[8.23] Herbert, M.R., and Harrison, H.W., *New Ways with Weatherproof Joints*. Building Research Establishment, Current Paper CP90/74, HMSO Garston, U.K., 1974.

[8.24] Bishop, D., Webster, C.J., and Herbert, M.R., "The performance of drained joints", *Weathertight Joints for Walls: Proc. Of the Int. CIB Symp.*, Oslo, Norway, Sept. 25-28, 1967, pp. 241-248.

[8.25] Isaaksen, T., "Rain leakage tests on trhough-joints", *Weathertight Joints for Walls: Proc. Of the Int. CIB Symp.*, Oslo, Norway, Sept. 25-28, 1967, pp. 265-269.

[8.26] Egner, R., *Zum Tragverhalen von Fassadenelementen aus Aluminium bei Windbelastung*, Doctoral Dissertation, University of Karlsruhe, 1993.

[8.27] *Supplement to the National Building Code of Canada*, 1990, Section 4, para 11.

[8.28] *The Assessment of Wind Loads. Part 4: Terrain and building factors and gust peak factors*, BRE Digest 346, August 1989, Garston, UK. This is an example of a concise source. There are many other references that discuss the time scale of gusts.

[8.29] Wacker, J., "Flucutating wind load on cladding elements and roof pavers". *J. Of Wind Eng. and Industr. Aero.*, Vol 38, pp. 405-418, 1989.

[8.30] Brown, W.C., and Ullett, J., *Measured Pressure-Equalized Performance of a Brick Veneer / Steel Stud Assembly*, NRC/IRC Client Report A-3028.4 for CMHC, June, 1995.

[8.31] Inculet, D.R., *Pressure-Equalisation of Rainscreen Cladding*, M.A.Sc. Thesis, University of Western Ontario, 1990.

9. VENTILATION DRYING

The last four chapters examined the nature and control of rain wetting using various strategies and mechanisms. The moisture control strategy that was developed in Chapter 2 recommended that more attention be given to drying mechanisms. This chapter examines the drying of cladding and other parts of an enclosure assembly by ventilation.

As has been discussed earlier, it must be assumed that some proportion of moisture, from whatever source, that enters the envelope will be stored in some way in the enclosure. Drainage is often touted as the most important drying mechanism, and has received much attention of late with regard to drained screened wall systems such as brick veneer, EIFS, wood siding, stucco, etc. Drained-screened systems are often recommended as the best systems for all but the driest climates. This chapter will show, however, that drainage does not necessarily remove sufficient moisture to ensure proper enclosure performance -- other drying mechanisms, essentially diffusive drying and ventilation, must be provided.

Diffusive drying is fairly well understood and appreciated, although the precise calculation of such drying is still not very accurate because of our limited knowledge of moisture transport properties through porous materials. One drying mechanism that has not received the attention it is due is ventilation.

Most cladding systems have relatively low vapour permeability and therefore tend to restrict diffusive drying. Moisture trapped in or behind the cladding can be transported into the enclosure by solar-driven diffusion, especially in air-conditioned buildings. Rather than control vapour diffusion, a 6 mil vapour barrier close to the interior can, in many instances, exacerbate wetting and greatly retard drying. Ventilation of the space behind the cladding can be an important means of both drying and avoiding inward vapour drive wetting.

The objective of this chapter is to develop the physics of ventilation drying, and to demonstrate the drying potential of this mechanism through theory supported by field measurements.

9.1 Background

Enclosure systems constructed of hygroscopic porous materials (e.g., wood, stucco, brick) can store very significant quantities of water (see Table 4.2). Chapter 4 described how the capillary forces in a porous building material such as wood, stucco, and brick will continue to absorb water until the material's moisture content reaches its capillary saturation moisture content. Conversely, it can be assumed that drainage cannot begin until either the saturation moisture content is reached, or the rate of wetting exceeds the rate of absorption.

With regard to the latter point, it can be shown that most wetting mechanisms deposit water slowly enough that the majority of the water can be absorbed by many materials. For example, condensate tends to deposit moisture slowly and therefore often allows the material on which condensation occurs (e.g., brick veneer, gypsum or waferboard sheathing) sufficient time to absorb the deposited moisture. Driving rain deposition occurs slowly enough that brick veneers and many plasters can absorb a large proportion of the water (Chapter 7). Therefore, it is reasonable to assume that in most common building enclosure wetting situations, a material must reach capillary saturation before sufficient volumes of water will bead on the surface and consequently allow drainage to occur.

The threshold moisture content level that corresponds to most moisture-related damage mechanisms is often equivalent to that material's moisture content at approximately 80%RH (see Chapter 4). Figure 9.1 plots the moisture content (in weight percent) versus relative humidity for several common building materials, and tabulates the difference between capillary saturation moisture content and the "safe" moisture content level at 80%RH.

Figure 9.1 effectively demonstrates that since any water below saturation cannot be removed by drainage, a significant amount of moisture must be removed by other mechanisms in order to reduce the moisture content to below the "safe" level.

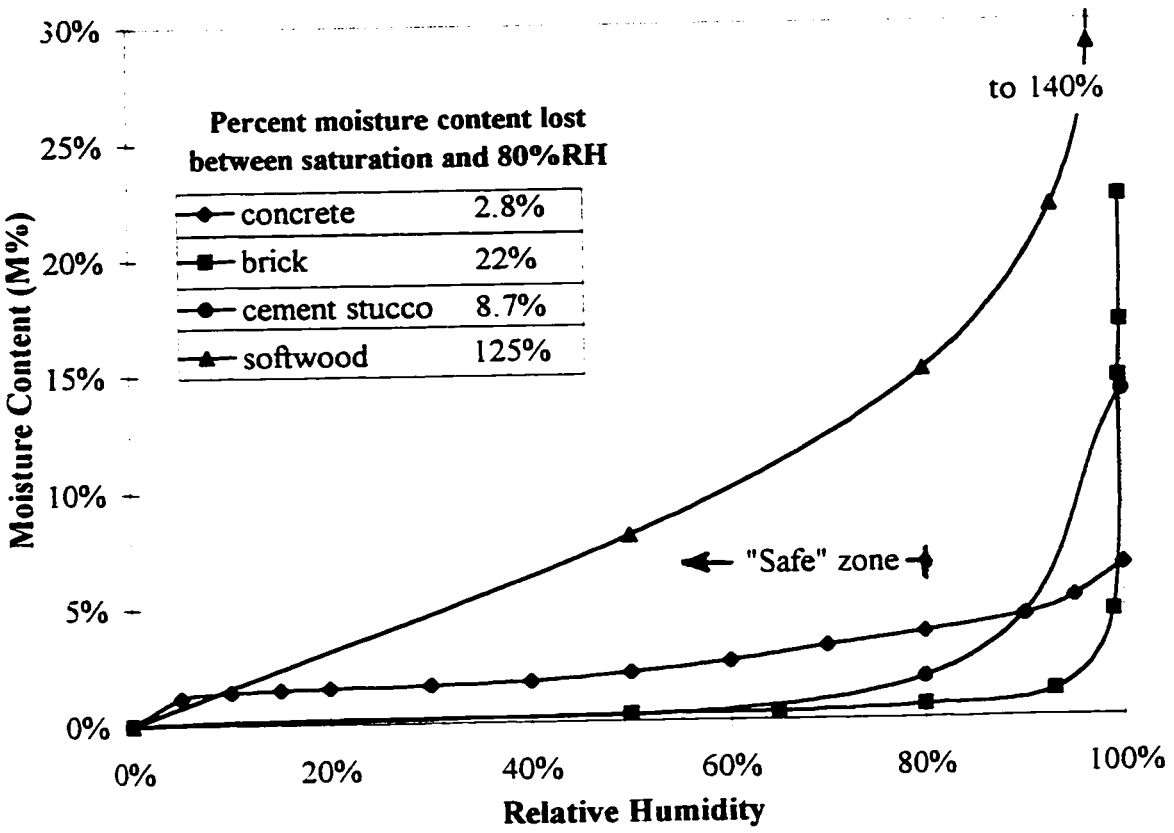

Figure 9.1: Sorption isotherms of some cladding materials

Once stored in the cladding or inner layers (e.g., wood framing, concrete block, and OSB sheathing) moisture can in practise only be removed in vapour form. Water from within cladding can be transported by capillarity to, or near the surface, where it can evaporate from the exterior surface to the ambient air. Alternatively, drying can proceed toward the interior of the assembly, where the vapour can be adsorbed by hygroscopic materials, or pass through to the interior air. Materials within the assembly and not in capillary contact with the cladding can only dry by vapour diffusion through the cladding or towards the interior.

In summary, moisture can be removed from a drained-screened enclosure wall in a variety of ways (Figure 9.2):

1. drainage of free water, driven by gravity
2. capillary transport of bound liquid water to, and evaporation from, the outer surface of the screen

3. diffusion and/or convection of water vapour outward through the screen, and inward into the wall or building interior; and

4. convective flow of exterior air through the air space, (e.g., ventilation).

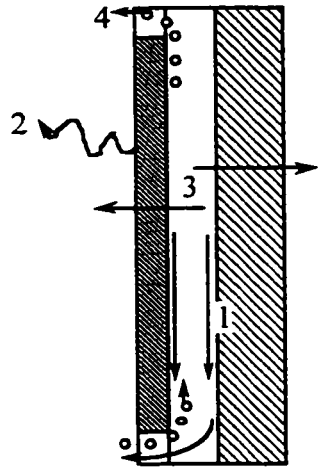

Figure 9.2: Moisture removal mechanisms in multi-layer enclosure walls with vented airspaces

Capillary transport to drier adjoining materials is a redistribution mechanism that may result in local drying but is not for the assembly as a whole.

Other wall systems, e.g., those without vents, solid walls, or walls with complete capillary contact, will of course have fewer possible drying mechanisms.

A layer of 6 mille (0.15 mm) thick polyethylene is placed just outside of the interior finish in many areas of North America, either because of building codes requirements or because it is deemed good practice. The water vapour permeance of 0.15 mm polyethylene is generally considered to be about 3 ng/Pa·s·m^2. This permeance is so low that little inward drying can be expected. Therefore, drying of most modern North American walls can only proceed to the exterior, although significant amounts of moisture redistribution from outer layers to inner, or vice versa, may occur.

The diffusive drying of the inner layers of a wall to the outside will be greatly retarded by cladding with low vapour permeance. For example, ASHRAE [9.1] gives the water vapour permeance of 90 mm thick brickwork as 45 ng/Pa·s·m^2; this qualifies it as a Type 2 vapour barrier. Values used in Britain [9.2, 9.3] range of from 25 to 100 ng/Pa·s·m^2 and in Germany they range from as low as 20 to as high as 400 ng/Pa·s·m^2. Recent Canadian measurements produced vapour permeance values for brick of about 25 to 30 ng/Pa·s·m^2

at low relative humidities and 45 to 50 ng/Pa·s·m^2 at over 91% RH [9.4]. The vapour permeance of vinyl siding has not been quantified, but since PVC is essentially vapour impermeable, ventilation is the only means by which vapour can leave an airtight assembly clad with vinyl. Most synthetic stuccoes (EIFS) have a relatively high vapour permeance, e.g., the Canadian Construction Materials Centre requires at least 170 ng/Pa·s·m^2 [9.5] and many manufacturers quote values of 200 to over 1000 ng/Pa·s·m^2.

Ventilating the space behind the cladding with outdoor air therefore offers two major benefits:

1. relatively dry outside air flow allows evaporative drying of the inside face of the cladding and outside face of the inner cavity wall, and

2. water vapour diffusing through the inner parts of the wall can bypass the vapour diffusion resistance of the cladding and be carried outside.

Thus, ventilation can theoretically increase the drying potential of walls, especially in wall assemblies that store significant amounts of water in the cladding. It can also reduce the potential for and severity of wetting by condensation and inward vapour drives.

9.2 Codes and Regulations

Although building codes and regulations may prescribe minimum values for ventilation flow or venting area for roofs and crawl spaces, rules for walls are rarely codified. The 1990 National Building Code of Canada (5.2.1.2.(1)) [9.6] requires that where a layer outside the layer with the major thermal resistance significantly resists water vapour flow :

> *an air space ventilated to the outside or other method of equal effectiveness shall be provided for removing water vapour that may pass from the high vapour pressure side through the material with the major thermal resistance.*

This clause obviously applies to most claddings – masonry, vinyl and wood siding, and sheet metal all have low vapour permeance ratings – and a vented air space is traditionally provided in most wall assemblies designed with these materials.

The Canadian masonry construction standard (CAN3-A371-M84)[9.7] requires (§ 5.12.1) that weepholes with an area of at least 70 mm^2 every 600 mm be provided at the base of every masonry veneer wall. This amounts to a vent area of 0.005% of wall area for a 2.4 m high wall and 0.002% for a 5 m high wall. The same clause adds, in a note, that:

Venting is often required in conjunction with weepholes to permit cavity walls and veneer walls to function properly.

The recent American masonry standard ACI 530-95/ASCE-95/TMS 402-95 *Building Code Requirements for Masonry Structures* [9.8] contains a new chapter on masonry veneers. Clauses 12.8.3, 12.9.4, and 12.10.2 require a minimum 1 inch (25.4 mm) airspace; this requirement is provided to ensure sufficient drainage, not ventilation. There is no minimum requirement for venting. Clause 12.2.2 requires that weepholes have a minimum dimension of 3/16 inch (5 mm) and be spaced less than 33 inches (825 mm) on centre.

The Brick Institute of America's Technical Note # 27 [9.9] provides widely respected advice on brick masonry screened walls. It suggests that a minimum cavity depth of 50 mm and vent openings at the top and bottom be provided. Although there is no mention of a minimum absolute venting area, the Note states that open head joints at a maximum of 600 mm o.c. at the top and bottom of the cavity are acceptable (a vent area of less than 0.1 %) as are 10 mm diameter tubes at 400 mm o.c. (a vent area of less than 0.008%).

Other building codes more precisely prescribe the measures required to ensure that some ventilation occurs. For example the German masonry design standard, DIN 1053 [9.10] requires in Clause 8.4.3.2 (double wythe masonry with air space) an airspace at least 40 mm deep and vent openings, top and bottom, with a minimum area of 7500 mm^2 per 20 m^2 of wall; this is approximately 0.0375% of wall area. The code for stone and ceramic facade cladding panels, DIN 18 515 [9.11], requires a minimum airspace of 20 mm, and horizontal slots top and bottom with a vent area of between 1 and 3% of the wall area. The code for ventilated facade cladding in general, DIN 18 516 [9.12], requires a minimum 20 mm air space and 5000 mm^2 of vent area per m length of wall, with no opening dimension less than 20 mm.

The German moisture protection standard, DIN 4108 [9.13], prescribes procedures, and material and climate values to be used in calculating the resistance of a building assembly to condensation and driving rain. Using a simple steady-state Glaser diffusion analysis, DIN 4108 requires the calculation of the diffusion condensation volume during 1440 h of cold weather and the subsequent evaporation and diffusive drying during 2160 h of summer weather. The standard requires that the moisture content in the materials not exceed given values and that annual evaporation exceed annual condensation. Most natural stone claddings fail to meet these calculations because the vapour resistance of the

cladding is quite high. Based on long experience, a prescriptive clause in the code exempts such assemblies from these requirements if an airspace behind the cladding is ventilated. DIN 4108 provides vapour permeance values for two classes of bricks: Klinker (hard burned face brick), with a value of between 20 to 40 ng/Pa·s·m^2 and Ziegel (normal structural brickwork), with a value of 200 to 400 ng/Pa·s·m^2. It is specified that the Klinker class of hard-burned bricks should not be used in brick veneer walls that do not meet the ventilation requirements of DIN 1053 Clause 8.4.3.2 (see above).

In general, European codes are much more explicit and require significantly greater venting area and airspace depths than North American codes. North American designers and builders would undoubtedly benefit from more information about how much and what kind of venting to provide in walls.

9.3 Research by Others

A literature survey found that almost all building-related vent and ventilation drying research found has been conducted in Europe. Much of the available research focuses on drained and back-ventilated panel systems and does not consider ventilation of brick veneer walls.

Several comprehensive studies of ventilation mechanics have been conducted in Europe. The German texts, *Belüftete Dach- und Wandkonstruktionen: Bauphysikalische Grundlagen des Wärme- and Feuchteschutzes* (Ventilated Roof and Wall Constructions: Building Physics Fundamentals for Heat and Moisture Protection) by K.W. Liersch [9.14] and *Praktische Bauphysik* (Practical Building Physics) by G. Lohmeyer [9.15], and Chapter 2 of the Dutch text *Bouwfysica 1: Warme- en massatransport* (Building Physics 1: Heat and Mass Transport) by Hugo Hens [9.16] contain excellent background information of ventilation flow mechanics. These texts also indicate how important wall ventilation is considered to be in designing standard wall panel cladding in continental Europe. The design procedures presented in these texts focus on increasing ventilation flow in open-joint cladding systems. Little guidance is provided for a designer wishing to *quantify* ventilation drying or use brick veneer, EIFS, vinyl, etc. as the cladding.

In Canada, Guy and Stathopoulus [9.17] conducted an analytical study of the effect of stack-effect-driven ventilation behind cladding. They reported that a cooling load reduction of 35% of the extreme design value could be achieved using a storey height of 2.4 m, a cavity of 30 to 40 mm, and a vent area of 100% of the cross-sectional area of the

cavity (i.e., a 30 to 40 mm continuous slot). Halving the venting area reduced the savings to 29% and doubling the insulation value of the inner wythe at the same time cut the savings further, to 20%. Reducing the emissivities (from 0.9 to 0.4) and decreasing the venting area to 25% of the cavity area resulted in savings of as much as 50%. The effect of wind was not taken into account in their analysis. The cooling effect of ventilation in winter will, however, increase heating energy consumption. This research showed that ventilation of a well-insulated wall will not reduce heat gain without large air spaces and very generous venting.

The Fraunhofer-Institut für Bauphysik conducted some important research by field monitoring ventilation flow and drying effectiveness for different types of panel cladding. One project measured the ventilation velocity and air exchange rate behind asbestos cement and wood siding with various types of cavities and venting arrangements. The cladding was installed over initially wet, aerated concrete blockwork and the moisture content (and hence drying rate) of these blocks was monitored over a period of two years. A complementary project involved the field measurement of ventilation behind large cladding panels on a three-storey building. The details of the research are contained in two research reports [9.18,9.19] but most of the conclusions can be found in the more readily accessible reference [9.20]. A summary of the important findings is presented below:

- The size of the vent openings and the presence of an unobstructed cavity were found to be the most important wall characteristics affecting ventilation flow .

- The three most important forces affecting ventilation drying were found to be wind-induced pressure differences, solar-induced buoyancy (stack effect), and solar heating. Solar heating was important because it increased the air temperature of the cavity air and thus allowed the transport of a much larger volume of water vapour.

- Hourly average air velocities of 0.05 to 0.15 m/s were measured in the wall cavities when the windspeed was between 1 to 3 m/s. Wind direction influenced the ventilation air velocity more than windspeed did. Cavity air temperatures of 20 °C above the exterior induced cavity air velocities of more than 0.20 m/s even when the wind velocity was under 1 m/s. Hourly average cavity air velocities of over 0.25 m/s were recorded when the windspeed was over 7 m/s.

- Walls with non-airtight joints (e.g., slate, shingles) were also shown to be ventilated (using tracer gas techniques), albeit less than intentionally vented walls. The greater the number of joints and the leakier the joint, the more ventilated the cavity. The pumping action of the wind was postulated as the ventilation mechanism in these walls.

- It was observed that with sufficient ventilation, condensation on the backside of the cladding rarely occurred.

The researchers drew the following conclusions:

- a clear cavity depth (i.e., accounting for tolerances and potential blockage) of 20 mm is generally sufficient for panel-type cladding;

- although a large vent area is not absolutely necessary for acceptable wall performance, it is a practical means of removing trapped moisture, i.e., increasing the drying potential;

- ventilation is less important if the backup wall or cladding has a low vapour resistance, or if the cladding itself is relatively air permeable.

The report recommended that:

- the cladding should always be left open at the bottom to allow drainage of any condensate which may form on the backside of cladding;

- effort be expended on ensuring that no water bridges can occur if materials which are sensitive to moisture are used in the backup wall; and

- the size of the upper and lower vent openings should be as large as possible, especially for backup walls which have high levels of built-in moisture.

Schwarz, also from the Institut für Bauphysik, instrumented an apartment building to measure the velocity of the air flow in the cavity [9.21]. The 18-storey building in Hamburg, Germany, was clad with a 1.25 m x 1.35 m open-jointed panel cladding system. He measured velocities of 0.2 to 0.6 m/s under a range of windspeeds (at 10 m) of 0 to 5 m/s. He found little relationship between building height and cavity ventilation velocity. It was also found that although lower velocities in the cavity were measured for the lee side than the windward side, the cavity air velocity on the lee side was usually stable at around

0.2 m/s for the normal range of wind velocities. The air exchange rate was therefore several hundred exchanges per hour, and the researchers concluded that vapour diffusion played a completely insignificant role in the transfer of vapour from inside to outside.

The Norwegian Building Research Institute has measured the pressure gradient in an airspace behind vertical wood siding on a rotatable test house in Trondheim, Norway [9.22]. The objective of these studies was the assessment of the cooling effect of air blowing across and through the fibrous insulation adjacent to the air space. They found that a wind barrier (not an air barrier) is essential to reduce convective heat loss through low-density fibrous insulations. This work also showed that the mean pressure gradient behind the siding was highly correlated with windspeed and wind direction. The influence of solar heating was not reported. Maximum pressure gradients in the cavity of almost 100 Pa/m were measured during storms with very high wind speeds (about 30 m/s). Average pressure gradients for all wind directions for a mean windspeed of 3 m/s were found to be between 0.1 to 0.5 Pa/m.

Akoestisch Advies Bureau Peutz & Associes BV [9.23], a Dutch consulting group, conducted both a theoretical and wind tunnel study of the potential for ventilation in an open-jointed, small-panel cladding product. Their analysis and measurements suggested that properly designed cladding products could, on average, have ventilation velocities of 0.5 to 3 m/s. For Dutch conditions, such large velocities would result in enough ventilation to ensure that condensation would not occur on the backside of panels for typical backup wall assemblies. The panel sizes examined, ranging from 200 to 800 mm in height, were installed over a 20 mm cavity and had full-length open joints 20 mm wide.

9.3.1 Ventilation and masonry veneers

Reports of ventilation drying studies in masonry veneer wall systems are more difficult to find, and the results tend to be much less conclusive.

Kenneth Sandin [9.24] of Lund University, Sweden, conducted what is perhaps the most extensive study of ventilation behind brick veneers. The work involved a field study of different types of brick-veneer clad, wood-frame wall systems for the Swedish Byggforskningsrådet (Building Research Council). The 20 mm wide air spaces in the 2.45 m high and 1.25 m wide test panels were vented by a single head joint in the bottom and a continuous slot under the eaves. In his measurements of cavity air exchange rates, he found the open head joint did increase air space exchange rates compared to the rates

achieved by drainage tubes. In typical weather conditions, air exchange rates of 0.3 to 8 per hour were measured. However, when an entire brick was removed from a panel with a 50 mm airspace substantial ventilation rates, of 3 to 25 changes per hour were measured. Although wind was thought to be the primary ventilation mechanism, ventilation rates during periods when the cladding was warmer than the outside air were almost always higher than when the cladding was at the same temperature as the outside air. In other published work [9.25, 9.26], he has questioned the effectiveness of ventilation in a climate (similar but somewhat wetter than most of Canada) where ventilation drying might remove 3 kg of moisture per month and driving rain could deposit 20 to 50 kg/month. However, the published data clearly shows that a wide, well-vented cavity significantly reduced the air moisture content of the cavity and reduced the potential for inward vapour drive wetting.

The Fraunhofer-Institut für Bauphysik has also conducted field monitoring of the moisture content of brick veneers in walls with and without (the cavity was filled with insulation) an air space [9.27]. Over about two years, approximately 100 gravimetric measurements were made of several different walls assemblies built in accordance with DIN 1053. The authors concluded that the presence of an air space had no effect on the moisture content of the brick veneer.

The German Institut für Ziegelforschung (Institute for Brick Research) conducted a unique field study of the effect of ventilation on the drying of brickwork [9.28]. A test building was constructed (in Essen, Germany) with a 40 mm deep cavity and vented at the top by a 30 mm open joint under the eaves and at open head joints in the bottom course (every 250 mm). The average ventilation velocity measured was about 0.1 m/s for an average windspeed of 2.6 m/s. This ventilation velocity was deemed to be slow enough that the insulation value of the air space was not significantly affected and yet resulted in an average of 100 air exchanges per hour. Measurements of the moisture content of the brickwork immediately after construction showed that drying occurred faster on the cavity side than on the outside. Within three weeks the brickwork dropped from 12% moisture content by volume to about 1.5%. In a personal discussion, the research engineer (Jung) indicated that the major obstacle to significant ventilation drying in brick veneer walls was mortar obstructions in the cavity. Specifying a 50 mm cavity and large venting areas would, in his opinion, achieve practical results similar to those obtained in the more controlled study.

The Laboratorium voor Bouwfysica in Belgium conducted a series of field, laboratory, and theoretical studies of masonry cavity walls. In a summary report [9.29] the issue of ventilation behind brick veneers was addressed. It was shown that ventilation has practically no effect on the heat transmission values of the air space, however, it was also found to be difficult to quantify the benefit of ventilation to moisture removal rates. Although it is recommended that ventilation continue to be used in veneer walls with air spaces, the author then states that only drain openings are required in cavities filled with insulation because the ventilation rates would be very low in any case. This is also the approach taken in the German masonry code, DIN 1053.

In a more recent study by the same laboratory, Hens [9.30] reported controlled laboratory experiments in which air (at 21 °C and 50% RH) was forced into a 70 mm airspace between two masonry wythes. The results showed that ventilation drying accounted for 30 and 37% of total drying at ventilation rates of 5 and 17.6 $m^3/(m^2\ h)$ respectively. The remainder of the drying was presumed to be by evaporation from the exterior surface.

In a second set of experiments, the same walls were ventilated with 1.8 $m^3/(m^2\ h)$ of air at 6.5 °C and 89% RH while an interior wall temperature of 21 °C was maintained. This wall exhibited no ventilation drying. Based on this evidence the authors concluded that ventilation does not contribute to drying.

The lab experiments described above employed relatively high air flows: it will be shown later that flows of 0.2- 2 $m^3/(m^2\ h)$ might be expected in well-built brick veneer walls. The influence of solar radiation, however, was not accounted for. The vapour pressure difference between the saturated outer wythe and the ventilation air was about 1100 Pa in the first experiment. In the second experiment, the difference in vapour pressure between the saturated brick and the ventilation air was at most 100 Pa, more likely it was 40 or 50 Pa. In any wall exposed to the sun, the temperature of the veneer and the air space will be considerably higher than the ambient temperature. If the sun was shining while the outdoor temperature was 6.5 °C, the airspace temperature would likely be much more than this. If higher temperature conditions are considered, the vapour pressure difference, would be between 500 to 1000 Pa, and a considerable amount of ventilation drying could be expected, perhaps 20% of the total drying.

9.3.2 Discussion

There remains a serious lack of quantitative information of the effect of ventilation on wall performance. The present design trend in Europe appears to be away from ventilation and toward more vapour diffusive claddings and paint systems. Little research is being conducted on ventilated-panel systems because it is generally believed by the research and building communities that following the present codes will result in satisfactory performance.

The influence of ventilation on brick veneer walls is little understood and requires much more research before any conclusions can be drawn. It can be stated that ventilation of brick veneers is not likely to be the most powerful drying mechanism: evaporation from the surface of the brick will generally be much more important. However, the extra drying capacity provided by significant ventilation may tilt the moisture balance in the favour of durable performance. The greatest restriction to ventilation flow in brick veneers are the limited vents areas commonly used, and the potential for airspaces blocked by mortar.

Ventilation drying may aid the drying of the materials behind a vapour impermeable cladding. This is just as important as the drying of the cladding itself. Because of the use of a capillary break behind the cladding (to control rain penetration), materials on the inside of the airspace cannot dry directly to the outdoors by surface evaporation, and must dry into the cavity air.

A major obstacle in assessing ventilation drying is the inability of instrumentation to measure the moisture content of masonry veneers in situ. Because the ventilation pressures and flows are so small and the drying rates so low, the accuracy and resolution of most instruments cannot directly capture the effects. However, the difference in moisture content between a 97% degree of saturation and 93% is likely the difference between a brick vulnerable to freeze-thaw damage and one that is safe.

9.4 Forces Driving Ventilation Flow

In this section the primary forces that drive the flow of air through an air space are identified and described. The intention is to document, quantify, and discuss the relative significance of these forces and the variables affecting ventilation driving forces.

There are two primary forces driving ventilation: thermally induced buoyancy (stack effect) and wind pressures. Thermal and wind pumping, and moisture-induced buoyancy effects may be secondary forces.

9.4.1 Thermal buoyancy

Solar radiation can cause cladding temperatures of more than 40 °C above ambient under some conditions. Heat energy is transferred to the air in the cavity, reducing its density. As the sun sets or passes by the face of a wall, the cladding will lose its heat to the exterior until the next day when the cycle begins again. The effect of temperature on air density can generate small but significant ventilation pressures.

The difference in density between exterior and cavity air results in buoyancy and a pressure difference (Figure 9.3). This buoyancy phenomenon is often described as the stack effect, and its effect can easily be calculated.

The density of dry air varies with temperature approximately as:

$$\rho_a = \frac{351.99}{T_a} + \frac{344.84}{T_a^2} \qquad \text{(Eq. 9.1)}$$

where T is the temperature in degrees Kelvin and ρ_a is the density in kg/m^3

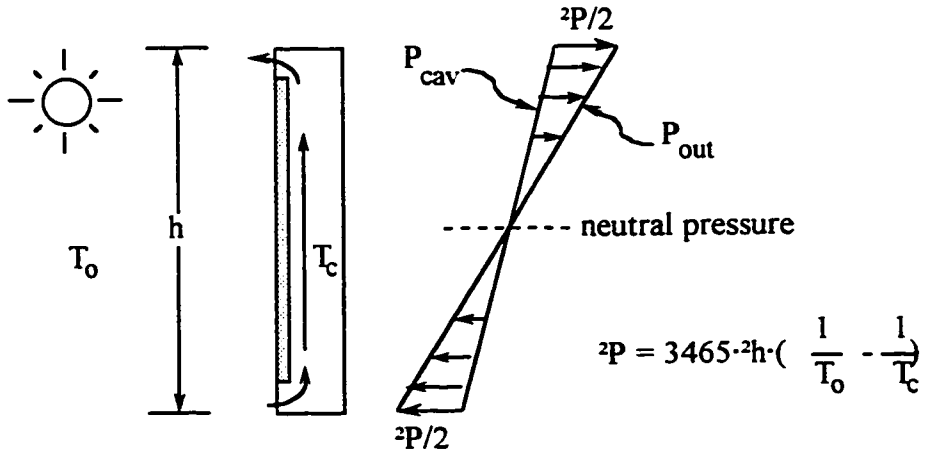

Figure 9.3: Thermal buoyancy

The greater the height of the column of air in the cavity, the greater the potential difference in pressure. In Pascals, the pressure difference generated by a temperature difference between cavity and outdoor air is therefore:

$$\Delta P = \left[\left(\frac{352.0}{T_c} + \frac{344.8}{T_{c^2}} \right) - \left(\frac{352.0}{T_o} + \frac{344.8}{T_{o^2}} \right)\right] \cdot h \cdot 9.81 \quad \text{(Eq. 9.2)}$$

or more approximately, at standard temperature and pressure,

$$\Delta P = 3465 \cdot \Delta h \cdot \left(\frac{1}{T_o} - \frac{1}{T_c} \right) \quad \text{(Eq. 9.3)}$$

where T is in Kelvin, pressure is in Pascals, and

h, the vertical distance between vent openings, is in m.

Table 9.1 provides a summary of a reasonable range of conditions and the thermal buoyancy pressures that might be generated by temperature differences. In general the cavity air will be warmer than the exterior air. However, for lightweight cladding, night-time black sky radiation can cause the cladding temperature to drop as much as 3-5 °C below ambient. For most cladding types, a temperature difference of 10°C will occur for a significant proportion of the time, 30°C will occasionally occur, and a difference of at least 3°C will occur for most of the time.

Table 9.1: Ventilation pressures due to thermal buoyancy (Pa)

For 0° C outdoor temp	*Temperature Difference (Cavity - Exterior)*		
Cavity Height (m)	±3 °C ΔP (Pa)	10 °C ΔP (Pa)	30 °C ΔP (Pa)
2.4	0.33	1.08	3.02
3.0	0.41	1.34	3.77
3.6	0.49	1.61	4.53
4.8	0.66	2.15	6.03
6.0	0.83	2.69	7.54

For a temperature difference between the exterior air and the cavity of 10 °C, the pressure difference between the top and bottom of the cavity due to buoyancy over a typical 2.4 m high cavity is about 1 Pa. For tall cavities, the pressure will be proportionately higher. However, if sufficient venting is provided, the temperature in the cavity may drop as heat

energy is removed by the ventilation air. Because of the low heat capacity of air, very high ventilation flows are required to generate significant cooling effects.

9.4.2 Thermal pumping

The daily cycle of heating and cooling of the air in the cavity will generate one diurnal cycle of expansion and contraction of the cavity air volume. As the air in the cavity expands, it is forced out through the vents or any other openings (including small pores and cracks in the cladding). Using the equation for air density as a function of temperature, the volume of air movement through the cavity due to expansion and contraction can be calculated. Over the typical range of air temperatures encountered in buildings, the change in air density is almost linear and, just as for thermal buoyancy, a simplified equation can be derived:

$$\Delta V = 0.003546 \cdot \Delta T \cdot V \qquad \text{(Eq. 9.4)}$$

where ΔV is the change in cavity volume, V, due to the rise (or fall) of the cavity temperature of ΔT (in Kelvin).

Note that the influence of this venting mechanism, sometimes called thermal pumping, is independent of the venting area. In all practical cases the mass exchange of air due to thermal pumping is volumetrically *very* small. For example, for a meter width of 2.5 m high, 25 mm deep air space, a 30 °C temperature rise will result in the expulsion of: $3.546 \cdot 30 \cdot (2.5 * 0.025) \div 1000 = 0.00665$ m^3 = 6.65 litres of air. Since this occurs only once per day, the equivalent ventilation rate is 0.000077 litres per second.

Although thermal pumping results in the movement of a very small volume of air, it occurs in all walls, regardless of the size of the intentional vent areas. For walls with no vents, an air exchange will still take place unless the cladding is perfectly airtight (not the case in practice) or is very flexible.

9.4.3 Wind pressures

Wind pressures are often more significant for ventilation than thermally induced pressures; this has been confirmed by most of the research reviewed in Section 9.3. When the wind blows, gradients of pressure form over all of the surfaces of a building. These gradients in pressure are due to the vertical gradient of wind velocity (i.e., wind speed increases with

height) and the horizontal and vertical gradients which form as wind flows around a structure . In relative terms, vertical gradients will be greater on short squat buildings and horizontal gradients will be larger on tall, slender buildings.

Vents that are separated by even a small distance will be exposed to different pressures because of these gradients in pressure. As shown in Figure 9.4, there is a relatively constant average gradient and an almost random, instantaneous short-term gradient. The pressure difference between the two vent locations can drive ventilation air flow. Ventilation can occur through two vents separated either horizontally or vertically.

The mean pressure gradients on many different buildings have been studied extensively. The distribution of mean pressure coefficients for common building types is shown in Figure 9.5. (Note, in this context, mean is an "appropriately long time", usually 15 minutes to one hour). Within reason, the lines of equal pressure in these figures can be scaled to match the size of the building. This scaling implies that the larger the building, the smaller the pressure variation over a fixed floor height. Therefore, the ventilating pressures over a floor height on an exposed three-storey building are expected to be much more than in a thirty-storey building with the same aspect ratio.

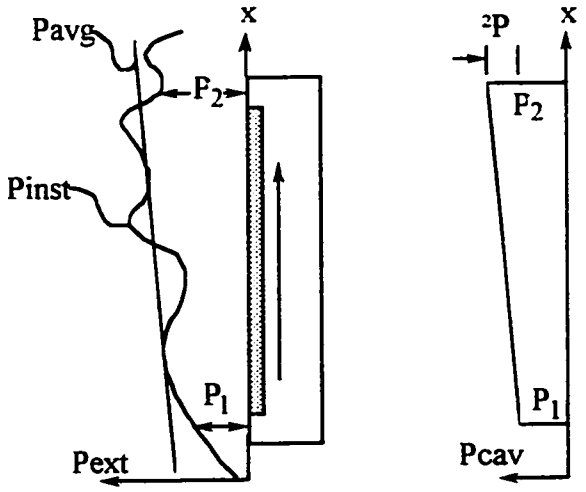

Figure 9.4: Wind-induced ventilation pressures

When exposed to a wind acting perpendicular to the face, a typical, rectangular apartment building will have a pressure coefficient value of 0.7 or 0.8 near the centre. This value will drop quickly to 0 or less near the edges . If the wind acts at 45° to the face, the maximum mean pressures might be slightly lower and will reduce to zero or less at the edges. Walls

parallel to the wind flow will generally experience negative pressures (which can be just as effective for ventilation as positive pressures) with significant gradients.

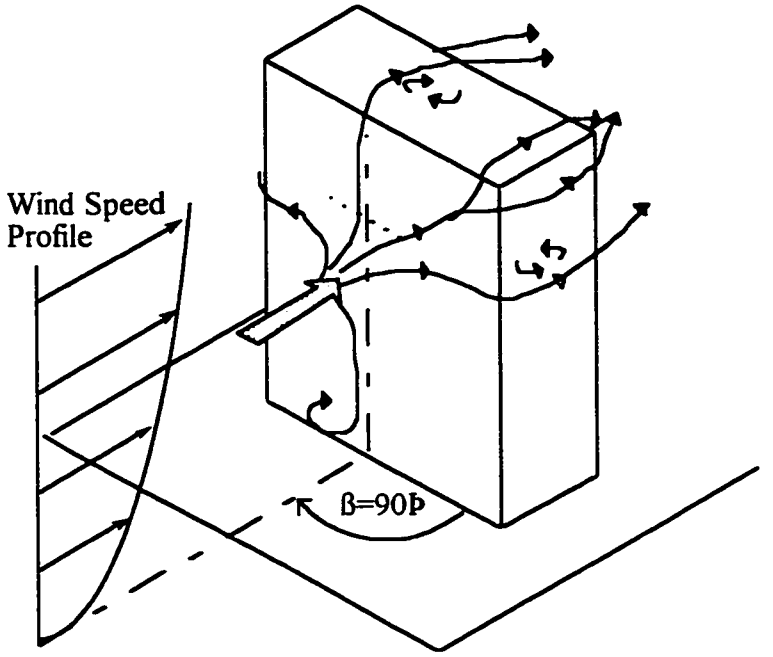

Wind Streamlines On A Building Face

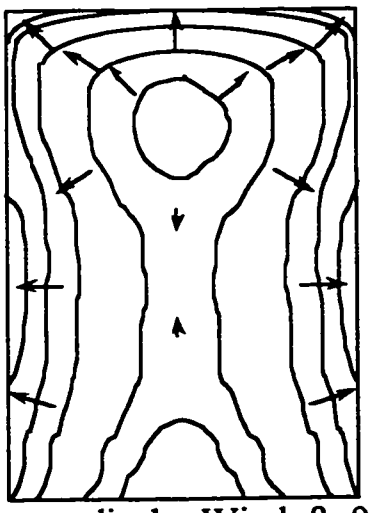

Perpendicular Wind: ß=90Þ

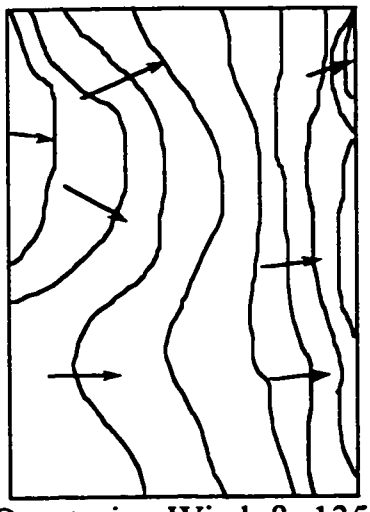

Quartering Wind: ß=135Þ

Mean Windward Face Pressure Distributions & Secondary Flows

Figure 9.5: Wind, air flow , and pressure gradients on a building

Pressures on the leeward faces will be negative and more uniform than on the other faces. A recent wind-tunnel study [9.31, 9.32] of mean pressure gradients on the face of large apartment building models by the Boundary Layer Wind Tunnel Laboratory at the University of Western Ontario provides some very useful information regarding the potential size of ventilation pressures.

Section 9.7 presents some experimentally measured pressure differences.

9.4.4 Wind pumping

A cavity with one vent hole is normally considered vented but can, to some extent, be "ventilated" by wind-induced pressures in a manner similar to thermal pumping. The changing wind pressures at the vent hole location will compress and decompress the volume of air in the cavity. Thus, a small volume or slug of air will move into and out of the cavity. Over the period of hours or days, the volume of air displaced will accumulate. Although only air near the vent hole itself is exchanged, air has a very low vapour diffusion resistance and moisture in the cavity somewhere other than the vent hole can move rapidly to the vent hole by diffusion and convection (induced by both thermal and vapour differences throughout the cavity volume) within the cavity.

The change in volume due to compressibility (i.e., the volume of air exchange from pumping) because of an increase in exterior pressure can be calculated from Charles' Law as:

$$\Delta V_{puming} = \frac{\Delta P}{P} \cdot V_{cavity} \qquad \text{(Eq. 9.5)}$$

where V_{cavity} is the air volume of the cavity

ΔP is the pressure change

P is the absolute atmospheric pressure (typically about 101 300 Pa)

The above relationship is based on the assumption that the volume of the cavity does not change. Cavities formed by flexible materials (e.g., those with non-adhered membranes as air barriers) will allow a much greater volume of air movement.

Figure 9.6 plots the ventilation flow rate as a function of the gust rate for two common walls: a one square meter cladding panel over a 25 mm air space and a floor height brick

veneer over a 50 mm air space. Measured pressures confirm that the gust rate is typically in the 1 to 10 Pa/s range for the vast majority of the time. On average the pumping ventilation rate is likely to be less than 0.01 litres per second. For gust rates of between 10 and 100 Pa/second, the ventilation flow rate is small but may be reasonably useful (e.g., less than about 0.1 litres per second).These results have two implications.

First, a relatively small transfer of air takes place because of pumping; it is not a very efficient means of ventilation. Unless the cavity has a flexible wall (which is very detrimental to pressure moderation performance), the ventilation flow is unlikely to be beneficial. Nevertheless, for walls clad with vinyl siding (which have a vent opening only at the bottom of the "airspace") over building paper or housewrap (very flexible), this pumping may be the most important ventilation mechanism.

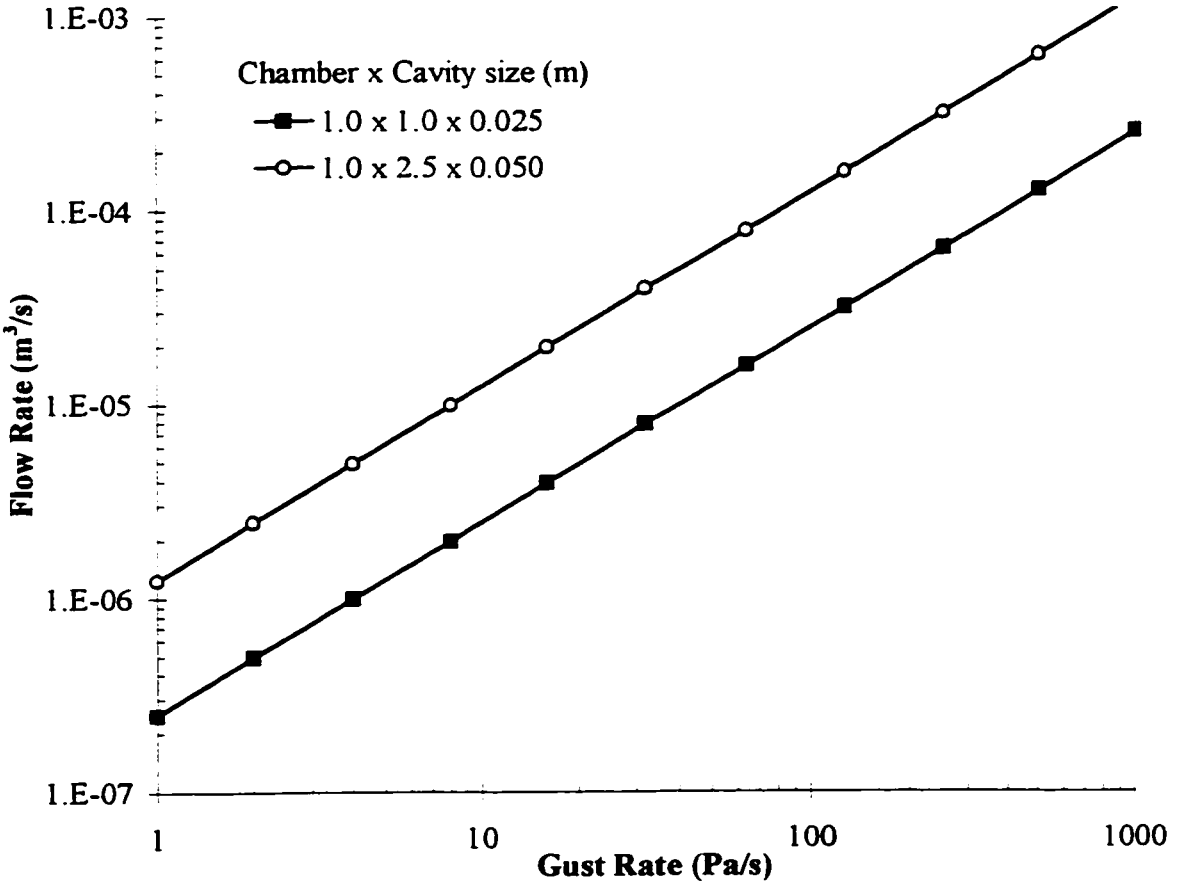

Figure 9.6: Ventilation flow as a function of gust speed

Secondly, consider pressure moderation across the screen. The flow of air necessary to moderate a significant percentage of the pressures acting on the screen is very small. Flows of 0.1 lps are easily achieved through most wall vents with very little restriction and hence pressure drop (e.g., the pressure drop across an open head joint would be less than 0.1 Pascals). Higher gust rates, e.g., 500 or 1000 Pa/s, which may occur for a few seconds per storm, will still only require flow rates of less than 1 litre per second to equalise pressures. These flow rates through an open head joint produce a pressure drop of about 3 Pa through an open head joint, i.e., only 0.3% of the applied pressure gust rate!

Hence, if compressibility of the air were the limiting factor, the pressure variations that a pressure moderated wall is exposed to could be well moderated – practically equalised – by small flows of air through relatively small vent areas. As described in the previous chapter, the degree of pressure moderation is generally controlled by the size of spatial pressure variations, not by the venting area. From a practical design point of view, this means that the level of pressure moderation can be increased by increasing compartmentalisation (an expensive solution) and not simply by increasing vent area (a relatively inexpensive solution).

9.4.5 Moisture buoyancy

As described earlier, temperature affects air density. The moisture content of air also affects the air density slightly. Air with water vapour has a lower density than dry air. Employing ideal gas law relationships [9.1], one can calculate the mass of water vapour as:

$$w_w = \frac{p_v V}{R_{wv} T}$$

where

w_w is the mass of water vapour (kg)

p_v is the partial pressures of water vapour (Pa)

V is the volume of moist air (m^3), and

R_{wv} is the gas constants for water vapour (461.5 J/kg·K).

The difference in density of two air masses at the same temperature but with different moisture contents can cause convective air flow within the cavity. Such convection is useful because it ensures that moisture is well distributed and mixed throughout the air in the cavity.

The difference in air moisture content between the cavity and the outside generates buoyancy forces which drive air flow in the same manner as thermal buoyancy. Table 9.2 contains the results of calculations of the pressure difference generated by moisture buoyancy alone in wall cavities of different heights with a saturated inner wythe (i.e., 100% RH). The exterior air was assumed to be at 10 °C and 85% RH. Changing the exterior temperature changes the results significantly because the relationship between vapour pressure and air temperature is highly non-linear. Increasing the outdoor temperature to 20 °C almost doubles the calculated pressures, and reducing the outdoor temperature to 0 °C will decrease the results by almost 40%.

Table 9.2: Moisture buoyancy ventilation pressures (Pa)

	Temperature Difference Between Airspace and Exterior		
Cavity Height (m)	**3 °C**	**10 °C**	**30 °C**
1.0	0.03	0.09	0.42
2.4	0.08	0.22	1.01
3.6	0.12	0.33	1.51
4.8	0.16	0.44	2.02
6.0	0.20	0.54	2.52

Note: Outdoor air at 10 °C and 85%RH.

For the case where the outside temperature is 3 °C cooler than in a 2.4 m high cavity , a driving pressure of only about 0.08 Pa would be generated. If the outdoor air is 30 °C cooler (e.g., a sunny day), pressures of 1.0 Pa would be generated, even with outdoor humidities of 85%.

A comparison of these results to the thermal buoyancy results shows that moisture buoyancy is a smaller but not insignificant ventilation driving force. The size of the moisture buoyancy force is highly dependent on the exterior air conditions. While thermal

buoyancy will act whenever the cavity temperature is greater than ambient, moisture buoyancy occurs only when the cavity air has a higher moisture content than the ambient, i.e., when the sides of the air space are wet and the exterior air is dry. These are precisely the conditions amenable to powerful ventilation drying.

On a calm sunny day in the spring or fall, a wall with a wet screen or inner wythe may be subject to combined moisture and thermal buoyancy pressures of 3 to 5 Pa for several hours per day. The moisture buoyancy pressures will steadily decrease as the inner wythe or screen dries and increase dramatically under solar heating. Naturally, wind pressures may augment or detract from these pressures.

9.5 Ventilation Drying Physics

To simplify calculations it is assumed in the development below that the materials comprising the sides of a cavity are wet (e.g., at or almost at 100% RH) and provided with a constant supply of water by capillary conduction from the body of the materials. If sufficient energy is available, liquid water will evaporate at the surface and enter the air of the cavity. The magnitude of this vapour transfer can be calculated using the equivalent mass transfer coefficients given earlier.

Ventilation will assist drying by replacing the moist air in this cavity by drier outdoor air and by educing the boundary layer vapour resistance of surfaces. Both of these mechanisms will be examined in the following two sections.

9.5.1 Air exchange

The process of moisture movement (at a known evaporation or desorption rate) from cavity materials to a well-mixed chamber can be represented schematically as in Figure 9.7. A well-mixed chamber is a reasonable assumption because variable wind pressures, internal convection (as a result of temperature and moisture buoyancy) and the low vapour diffusion resistance of air will allow for fast redistribution of water vapour throughout the air space. If the rate of ventilation flow is high, the air space will not contain well-mixed air, but drying will proceed at such a high rate that this inaccurate assumption does not effect most results.

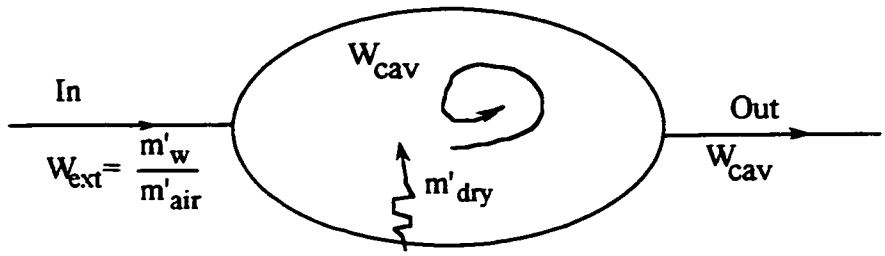

Figure 9.7: Simple mixing chamber model of cavity

The flow rate of vapour into the cavity (from the exterior air or, perhaps, from exfiltration of interior air) plus the flow rate of vapour because of drying will determine the water vapour balance of the air space and therefore the driving potential for further drying. In terms of mass fractions (i.e. humidity ratios):

$$W_{cav} = \frac{(W_{ext} \cdot m_{air} + m_{dry})}{m_{air}} = W_{ext} + \frac{m'_{dry}}{m'_{air}} \qquad \text{(Eq. 9.6)}$$

where W_{cav} is the humidity ratio of the cavity air (kg water/kg air),

W_{ext} is the humidity ratio of the exterior or ventilating air (kg water/kg air),

m_w is the mass flow rate of water vapour in the ventilating air (kg water /time),

m_{air} is the mass flow rate of ventilating air (kg air /time), and

m_{dry} is the drying rate of the materials adjoining the air space (kg water /time).

The exterior humidity ratio is a climatic boundary condition that will vary with each analysis. The rate of ventilation airflow can be assessed using the methodology and information presented in Section 9.7. The drying rate into the air space can be assessed using the information in Section 9.4.2

9.5.2 Cavity surface drying

As discussed in Chapter 4, the surface mass transfer coefficient can be calculated by using the Lewis correlation of heat transfer - mass transfer analogy. The surface vapour flow coefficient in terms of the convective heat loss coefficient, h_c, was shown to be:

$$g = 6.4 \times 10^{-6} h_c \qquad \text{(Eq. 4.35)}$$

Convective heat transfer coefficients within airspaces depend primarily on the flow velocity (Reynolds number), the flow regime (laminar or turbulent), the properties of the gas (Prandtl number), and the geometry of the flow channel [9.33]. A relationship for forced convective heat transfer of air in the laminar flow (slow flow) regime between parallel plates [9.34] is:

$$h_c = k/D_h \cdot \left[3.66 + \frac{0.104 \cdot Re \cdot Pr \cdot D_h / L}{1 + 0.016 \cdot (Re \cdot Pr \cdot D_h / L)^{0.8}}\right] \qquad \text{(Eq. 9.7)}$$

where, h_c is the convective heat transfer coefficient,

Re is the dimensionless Reynolds number as before,

Pr is Prandtl number the dimensionless ratio of a fluids propensity to propagate shear to its propensity to propagate thermal energy (Pr is about 0.71 for air at room temperature),

D_h is the hydraulic diameter (twice the cavity width),

k is the thermal conductivity of air (about 0.026 W/m°C at room temperature), and

L is the length of the flow path.

For Reynolds numbers of 10 to 2300 (i.e., laminar flow) in cavities between 25 to 50 mm wide and 2.5 m high at normal temperatures the heat transfer coefficient predicted by Equation 9.2 for these typical wall conditions ranges from 3.8 to 4.4 W/m^2. (The range of Reynolds numbers that can be expected for common air space situation will be discussed later)

Therefore, from the Lewis correlation, the moisture transfer coefficient, g, for the above conditions can be found as:

$$g = 6.4 \times 10^{-6} h_c = 24 \text{ to } 28 \times 10^{-6} \text{ g/s·m}^2\text{·Pa}.$$

Note that, not surprisingly, the mass transfer of water from a wet surface exposed to air flow is much greater than that for stagnant air (which is in the range of 1.5×10^{-5}) and less than for an exterior surface (which is about 75×10^{-6}).

The calculation of the evaporation rate from fully saturated cavity sides using the above coefficients is very high, and should be considered as an upper limit. For example, the

transfer of moisture from a completely saturated brick veneer at 20°C ($p_{v,sat}$ = 2300 Pa) to cavity air at 19°C and 80% RH (P_v = 1650 Pa) would be:

$$m_v = g \cdot \Delta p_v \cdot \Delta t = 25 \cdot x\ 10^{-6} \cdot (2300 - 1650) = 0.01625\ g/s/m^2 \text{ or } 58\ g/hr/m^2.$$

Naturally, the ventilation air flow through the cavity is insufficient to carry all of this evaporated moisture away and the RH of the cavity would quickly reach equilibrium with the wetted face of the cavity, e.g., measurements would indicate a very high RH. The rate of energy required to evaporate this moisture (2500 J/g x 0.01625 g/s/m^2 = 40.6 W/m^2) may also not be available. The extraction of the heat of vaporisation from the material surface at high evaporation rates will cause a significant drop in surface temperature and a consequent reduction in evaporation rate. Eventually, an equilibrium will be reached between the ability of the material and the flowing air to transport energy for evaporation to the surface and the ability of the ventilation air to remove moisture from the surface.

9.5.3 Solar effects

When the sun shines on a wall, it does so with an intensity of as much as 1000 W/m^2. More typically, the sun delivers 100 to 700 W/m^2 during sunny periods to most wall orientations [9.35]. Even north walls will receive more than 100 W/m^2 during daylight hours. Dark-coloured and rough-textured walls will absorb more than 80% of the incident solar energy, and smooth white walls in the field absorb at least 30% (atmospheric pollution of cladding surfaces makes a lower value impractical) [9.1].

The absorbed solar energy increases the temperature of the cladding and outer layers of the wall while also providing energy for the evaporation of liquid water. A shown in the previous example, an absorbed intensity of less than 50 W/m^2 is sufficient to provide the latent heat required to evaporate more than the ability for normal rates of air exchange to remove moisture from the air space.

9.5.4 Measured cladding and airspace temperatures

The cladding temperatures for all of for the test walls where measured every 5 minutes over the duration of the URIF project. The average temperatures for February 1996 and 1997 were calculated for the brick, EIFS and vinyl wall. The average air temperature over these two period was -5.2 °C and -2.6 °C respectively. Note that the south orientation

will receive the most solar energy in February. The differences between the average cladding temperature and the average air temperature are tabulated in Table 9.3.

The south-facing brick wall was, on average, 7.3 °C warmer than the air temperature for the entire month of February 1996 while there was practically no difference between the air temperature and the white-coloured EIFS temperature. Changing the solar absorptance of the EIFS resulted in a general increase in its temperature, but its lack of thermal mass did not allow the temperature to reach that of the brick.

In general, red brick veneers were from 2 to 7 °C above the exterior air temperature in winter, and 4 to 8 °C warmer in summer. The air space behind the brick veneer was usually 4 to 8 °C warmer than the exterior in summer and winter. This difference in temperature between the air and the cladding is primarily due to solar effects, although it is estimated that about 0.5 °C of the total temperature drop is due to the insulating effect of the exterior boundary layer.

Table 9.3: Average difference between ambient air temperature and cladding temperatures for February 1996/1997

	Brick (dark red)	EIFS (brown)	EIFS (white)	Vinyl (grey)
North	3.3 / 5.1	2.3	1.7	--/ -1.1
South	7.3 / 6.7	2.5	0.1	--/ 0.0
East	3.1 / 4.5	1.1	-0.8	--
West	2.1 / 1.7	1.5	-0.3	--

Although many walls were studied in depth, Wall FE, a well-insulated east-facing brick veneer wall with a clear 30 mm air space is used to demonstrate the results. Figure 9.8 presents a plot of the cumulative distribution of exterior air temperature and brick veneer temperatures (actually measured 10 mm below the surface) for a three month summer period (a total of about 2800 hourly averages). Because of solar heating the brickwork temperature is higher on average (by almost 7 °C) and more variable than the exterior. This temperature difference significantly increases the potential for drying from both faces

of the cladding, but the small thermal gradient from the exterior to the interior will on average drive moisture inwards by vapour diffusion and surface diffusion.

The temperature difference between the air space and the exterior air is very important for ventilation drying. Figure 9.9 compares the distribution of this temperature difference for the air space in Wall FE when the wall was vented (summer 1996) and unvented (summer 1997).

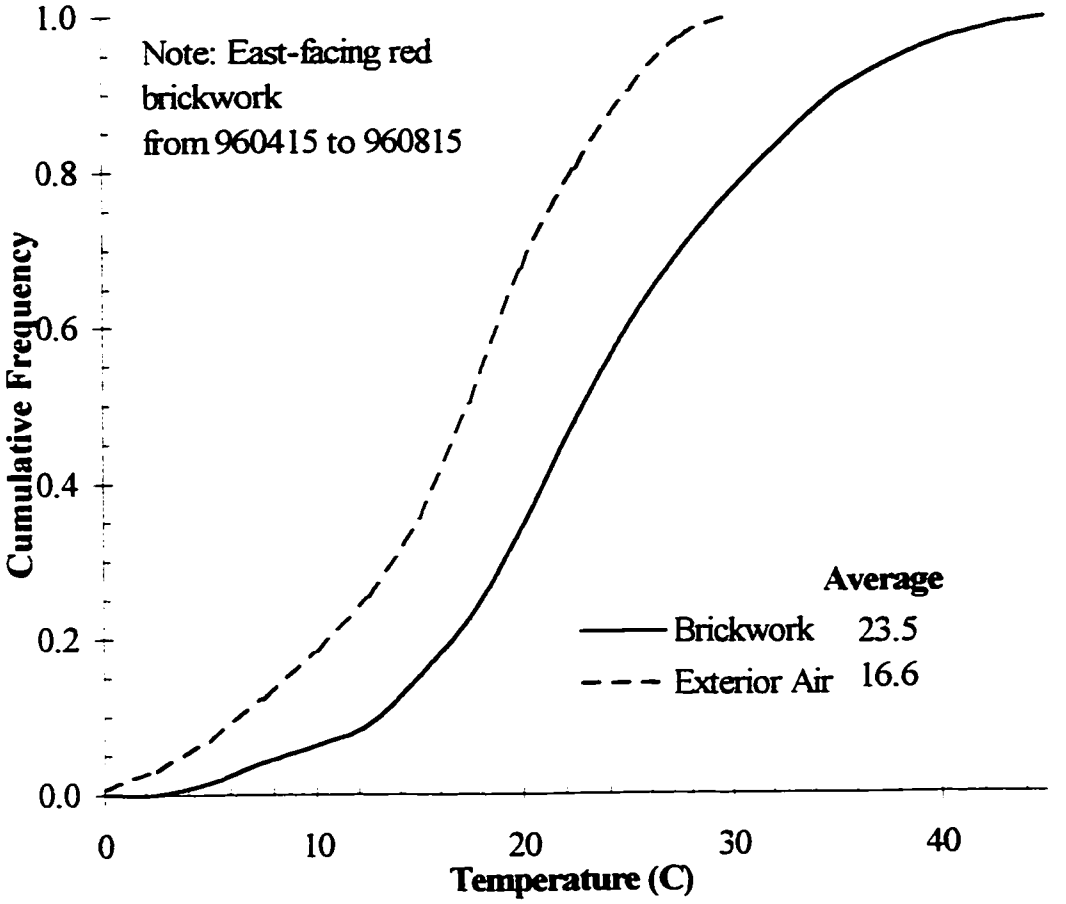

Figure 9.8: Distribution of cladding vs. exterior air temperature over summer period

Two important points are illustrated by the data in the plot. First, the average temperature in the air space is considerably higher than the exterior air temperature (by about 5 °C) and this difference is less than the difference between the exterior surface and the outdoor air. This data, and analysis of many more walls at the Beghut, show that the air space is on average slightly cooler than the face of the brickwork. This cooler air space temperature is due both to ventilation cooling and the moderating effect of the brickwork.

Secondly, the difference in the temperature of the vented and unvented wall configuration is practically negligible, given the accuracy of the data. A temperature decrease of the order of 0.4 °C might theoretically be expected to be due to ventilation flow. Hence, the assumption that ventilation air flow will not cool a wall is valid even for a well-vented brick veneer.

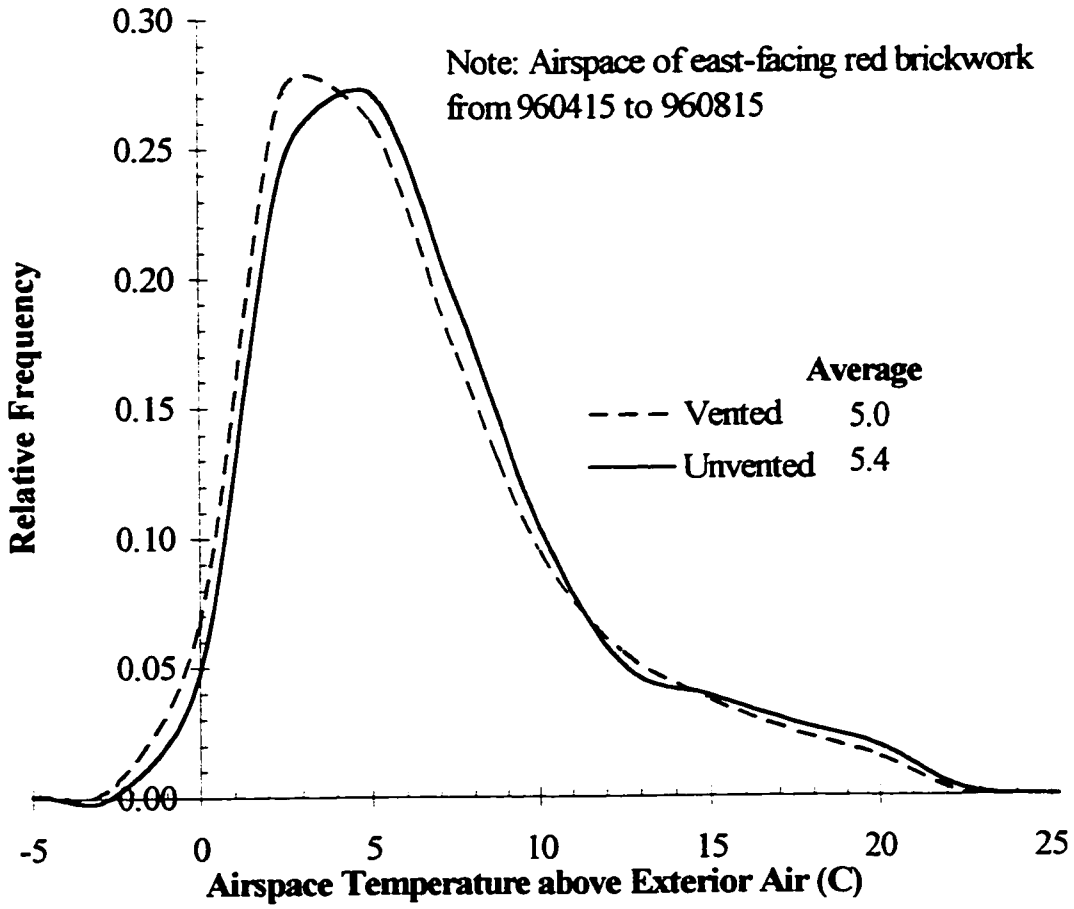

Figure 9.9: Distribution of difference between air space vs. exterior air temperature for vented and unvented brick veneer wall

Because the vapour carrying capacity of air is nonlinearly related to temperature, the amount of time that the air space is more than about 10 °C above the exterior will have a disproportionate effect on the drying potential. This is discussed further in Section 9.9.

9.5.5 Summary

The calculations presented in the previous sections lead to the following important conclusion:

> Because the transfer rate of moisture from a wetted surface to the air is high, and the volume of air in the cavity is low, it follows that for all practical building cavity situations, the rate at which moisture can be removed from saturated materials along the sides of the air space will be dictated by the rate at which moisture in the air leaves the cavity.

With reference to the stages of drying described in Chapter 4, the above statement can be expected to be true for the initial portion of Stage 2 drying as well as Stage 1 drying.

The rate of drying from the exterior surface of the cladding by contrast is likely to be governed by the ability of the material to transport sufficient water to the surface for evaporation.

9.6 Airflow Through Vents

As has been stated in the literature review, one of the most important wall characteristics influencing ventilation flow is the resistance to airflow through the vents. Because brick veneer walls contain relatively few vents, the resistance imposed by the vents is even more significant. This section experimentally examines air flow through a range of common wall vents and compares the experimental results to theory.

9.6.1 Vent types

Vents for use in screened wall systems can be divided into three broad types (Figure 9.10):

- **Small circular openings and rounded slots**. Window frames, curtain walls and some types of contact siding (vinyl) often use circular or oval openings of 3 to 6 mm in one dimension and 3 to 25 mm in the other. These vents are usually in a thin material (0.5 to 3 mm thick) such as aluminum, PVC, etc.

  Flow through circular, sharp-edged orifices has been extensively studied. Theoretically, the sharp-edged circular orifice is also the easiest to analyse and hence has been chosen as the behavioural datum for this work. Also, flow through non-circular orifices is often analysed by considering an equivalent diameter

circular orifice. Therefore, a range of orifices with both sharp edges and square edges have been studied and compared to the results of existing theory and other published research. A variety of orifice sizes (from 1 mm Ø to > 22 mm Ø) in 3 mm thick plate have been studied. To test the applicability of the equivalent diameter circular orifice theory to brick vents, a 19 mm Ø x 90 mm long pipe was considered and compared to orifices in thin plate.

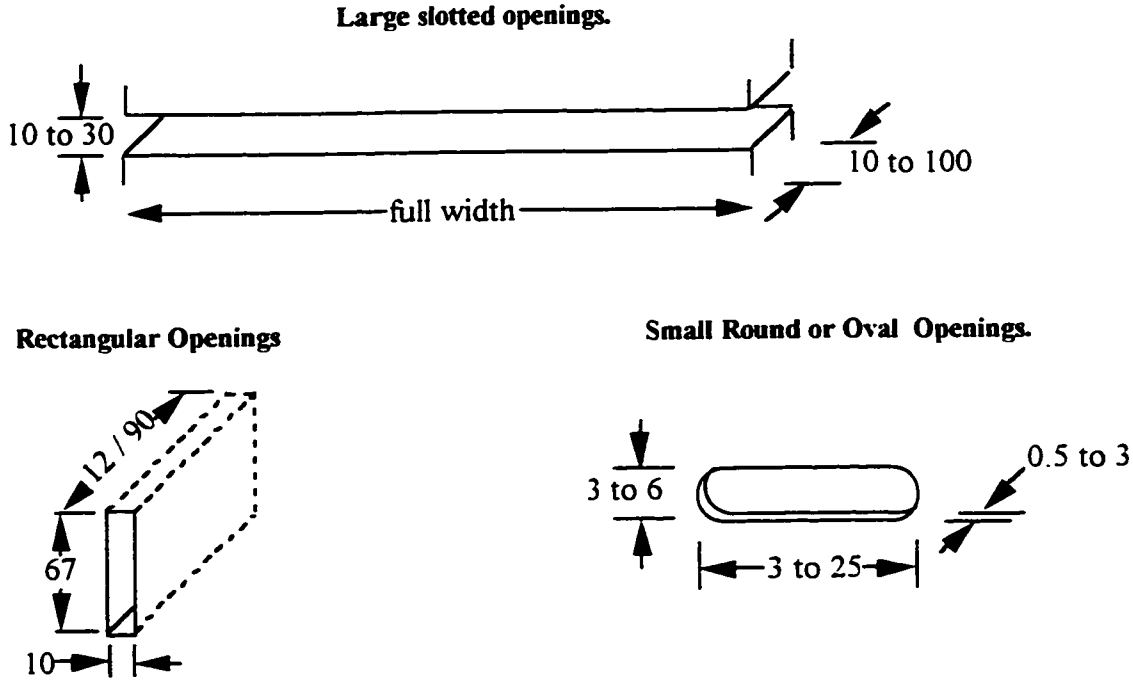

Figure 9.10: Typical vent geometries and sizes

- **Deep rectangular openings**. These openings are used predominantly in masonry veneers. As such, the standard size is 10 wide, 60 to 80 mm high in elevation, and 85 to 90 mm deep.

  Because masonry veneer walls are very common the behaviour of relatively standard open head joints has been a focus of the experimentation. The ratio of height-to-width (10:65) and width-to-depth (10:90) places an open head joint brick vent in a relatively unexplored area of orifice flow. Brick vents cannot be assumed to behave as an infinitely wide slot (i.e., ignoring the effect of the two short sides). They are too deep to behave as a square-edged orifice and too shallow to act as a pipe. In practice, vent inserts are often used to resist direct rain penetration and to keep insects out; it was thought that these inserts might affect

the air flow characteristics. The performance of four types of commercially available vent inserts has therefore also been evaluated.

- **Large slotted openings.** Open joints, for whatever reason, in natural stone cladding, precast panels, and other panel cladding systems are common. Many European drained and back-ventilated systems utilise a series of horizontal openings at the panel joints. Depending on the nature of the screen, the width ranges from about 5 mm to 20 mm and the depth (thickness of the screen) from about 10 to 100 mm.

  Semi-continuous slots (i.e., slots with a length many times their height or width) are sometimes used for venting cavities in the building envelope. Slots of this nature, because of the large venting area, provide comparatively little resistance to airflow. The width-to-height aspect ratio of a brick vent (approximately 1:7) represents one extreme of expected deep slot behaviour. A higher aspect ratio (1:15) and shallower (i.e., thinner cladding) slot will provide less resistance to flow; such slots can be realistically modelled as infinite-length, square-edged orifices.

9.6.2 Orifice flow: Basic theory

The volumetric fluid flow rate through a sharp-edged orifice as a function of a pressure difference is usually described by the relationship [9.36]:

$$Q = C_d \cdot A \cdot \sqrt{\frac{2 \cdot \Delta P}{\rho}}, \qquad \text{(Eq. 9.8)}$$

where Q is the flow rate,

A is the area of the orifice,

ρ is the mass density of the fluid,

ΔP is the air pressure difference, and

C_d is a factor that accounts for friction and turbulence losses.

This relationship can be derived from Bernoulli's basic flow equation. The value of C_d (the so-called discharge coefficient) must be applied to match actual measurements and can be derived analytically only for some unique situations. The discharge coefficient comprises two parts: the contraction coefficient, C_c, and the velocity coefficient, C_v. The

former coefficient accounts for the fact that the flow narrows as it flows through the orifice. The second coefficient accounts for losses due to friction and turbulence.

For turbulent flow through a circular sharp-edged orifice, Kirchoff calculated a discharge coefficient of $\pi/(\pi+2) = 0.611$; this is still commonly used as a datum in much of the building science literature.

Flow through deep orifices, cracks, or slots can be better described by the more general power law expression:

$$Q = C_d \cdot A \cdot \left(\frac{2 \cdot \Delta P}{\rho}\right)^n \qquad \text{(Eq. 9.9)}$$

where all variables are as before but the square root has been replaced by the flow exponent, n.

For sharp orifices and large openings and turbulent flow, the equation simplifies to the same equation as before (i.e., n = 0.5). For laminar flow, the choice of a higher value of n (but always less than 1.0) provides a better fit to the data and is theoretically more acceptable. A flow exponent of 0.5 indicates that the flow is completely turbulent. An exponent of 1.0 indicates that the flow is completely laminar.

Although the power law form is widely used to relate the pressure drop and the flow rate through building envelope assemblies and components, it should be noted there is still debate in the literature over the validity of this law [9.37, 9.38, 9.39, 9.40], especially at low flows and for small opening sizes. Quadratic expressions, for example, are more dimensionally consistent and just as accurate. ASHRAE [9.1, pg. 2.13, Fig. 18] suggests that the power law can be used to describe flow through normal orifices for Reynolds numbers as low as 100 (the Reynolds number, discussed later, is a non-dimensional number which relates inertial to viscous forces in fluid flow). The discharge coefficient for an orifice is predicted to remain between 0.60 for 0.70 for most practical flow conditions. Until more compelling experimental results prove otherwise, the power law is likely appropriate and presumably sufficiently accurate for the vent openings of interest and the flow rates that occur in wall vents.

Orifices that are very carefully calibrated for use as international (e.g., ISO) or industry (e.g., ASTM) standards generally have higher discharge coefficients than that derived by Kirchoff, and, more importantly, the discharge coefficients vary with the speed of the flow

(more precisely, with the Reynolds number). These standards also tend to restrict the minimum orifice size to 12 mm. At very high flows, the discharge coefficient will often converge to a value of 0.61, but flows this high may not occur in building envelopes. The standards rigidly define the location at which the pressure is measured in order to ensure repeatable results. However, the choice of pressure tap size and location is based on practical application and not theoretical considerations; therefore, measured discharge coefficients rarely match theoretically derived values [9.41].

9.6.3 Static pressure vent tests

The measurement of the flow characteristics of the various vent types over a range of steady-state flow rates were conducted to allow the more accurate assessment of ventilation air flow. Note, however, that ventilation flow are likely to be very slow and somewhat variable, and pressure moderation flows are likely to be highly variable about a mean that is often close to zero. Matching results from steady-state flow to more realistic conditions has been attempted so that existing research can be used to validate and extend our results.

9.6.4 Objective

The objective of the static vent flow experiments was to characterise a vent in terms of the discharge coefficient , C_d, and the flow exponent, n. These values can then be compared to other research as well as providing a full description of the volume of air flow that can be expected when a vent is under a given air pressure difference.

9.6.5 Apparatus

The apparatus developed to conduct the steady-state flow experiments consisted of a fan to produce the flow, 50 mm ducts to transfer the air flow, valves to regulate the flow, and a 1.2 m long, 250 mm diameter plexiglass pipe to which one of the vents could be attached. Instrumentation included a group of parallel flowmeters that could measure flows (from 0.02 l/min to 200 l/min), and pressure transducers or a Betz manometer to accurately measure the pressure drop (from 0.1 Pa to 3000 Pa) with better than 1% total accuracy. The pressure difference was measured between the pressure in the large pipe and the ambient pressure in the lab.

The plexiglass pipe served several functions. Its length ensured that flow from the fan was stabilised before reaching the vent test section. Its diameter was chosen so that the vent would be exposed to an approaching flow very similar to that in actual wall vent (i.e., the diameter of the pipe was very large in relation to the diameter of the vent). The volume of the pipe was such that it acted as a reservoir and ensured that small, short-term flow variations were damped out. The transparent pipe also permitted the nature of the flow to be observed, i.e., smoke could be added to the air flow and the nature of the flow could be clearly observed.

The commercial vent inserts tested are shown in Figure 9.11.

9.6.6 Procedure

Before beginning each series of steady-state tests, the vent test section was installed and the vent opening tightly sealed. The leaks in the test system (air flow through connections, seals, etc.) were then found by applying several large pressures and measuring the flow. Because the system was exceptionally tight, pressures of over 500 Pa were often needed to generate measurable system leakage.

The vent was unsealed and the flow and related pressure were recorded at 15 to 30 points in roughly equal steps of increasing pressure and then in steps of decreasing pressure. Three or more similar runs were generally conducted. The temperature of the air was relatively constant and an average of 25 °C during all tests.

The discharge coefficient and flow exponent were calculated from the recorded data using a least-squares regression analysis.

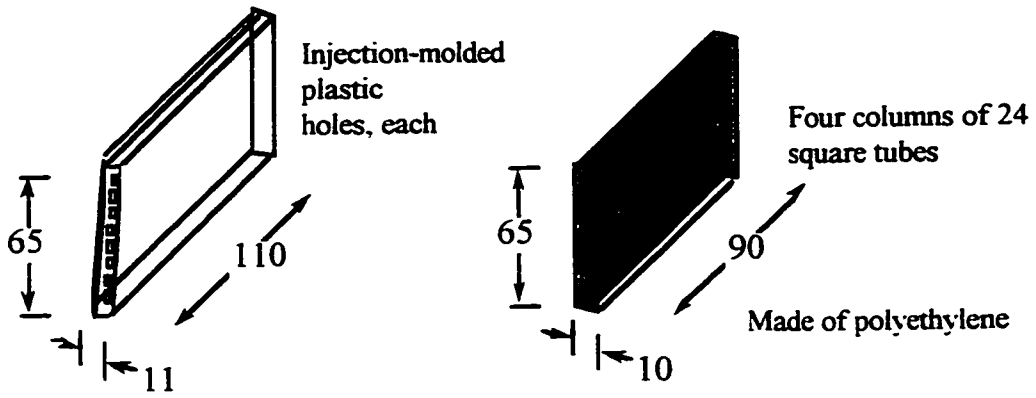

Cavity Trays of Yeovil

Cell Vent

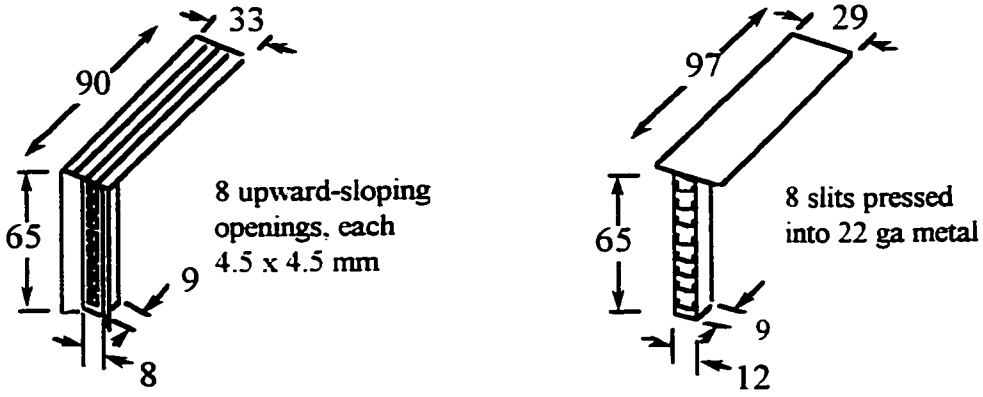

Goodco

Aircraft Style

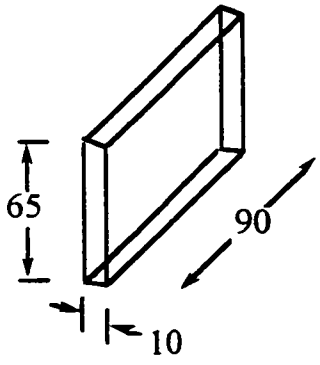

Open Head Joint

Figure 9.11: Commercial masonry veneer vent inserts tested

9.6.7 Results

From the literature review and flow visualisation experiments, an understanding of the behavioural aspects of orifice flow was developed. Figure 9.12 and the discussion below summarises this behaviour.

Flow through sharp-edged orifices (thickness-to-diameter ratio = t:d < 0.5) was similar to theory – air was attracted from all directions on the high pressure side and the flow contracted just past the upstream edge of the entrance. The exit stream was a relatively sharply defined sharp cone with an angle of 10 to 15 degrees off the centreline, even at very low flows. This behaviour did not change over the range of pressures tested (1 to 500 Pa). The contraction coefficient, C_c, is indicated in Figure 9.12a.

Flow through deeper orifices (larger t:d ratio), such as the open brick head joint and the 90 mm deep pipe, behaved as shown in Figure 9.12b and c. For low flows or shallow orifices the flow expanded past the entrance and, although it began to interact with the exit edge, it remained separated or detached flow. As the flow was increased, or the orifice was made deeper, the flow would reattach to the sides of the orifice before exiting. This latter behaviour was unstable, and flow could switch between attached and unattached flow at the same flow level – this change in behaviour may result in a change in the flow vs. pressure plot and generate hysteresis effects during a test.

When the orifice is many times deeper than its diameter, the flow consistently reattaches to the side of the orifice and takes on a stable velocity profile. The reattachment may occur after as little as 10 diameters from the entrance but may require as much as 100 diameters [9.49]. If the flow is slow enough, it behaves laminarly and a parabolic velocity distribution forms. Once the flow passes a threshold flow level and becomes turbulent, a blunter power-law profile forms. For the deep orifices typically used in buildings (i.e., a t:d ratio less than about 8), reattachment would not occur for pressure differences greater than about 0.1 Pascals.

The steady-state flow test results (summarised in Table 9.3) show that simple orifice theory (i.e., C_d=0.61 and n= 0.5) is relatively accurate for the tested orifices with a diameter of more than 12 mm (t/d < 0.25), as the ISO orifice flow meter standard suggests [9.42]. The small holes (t/d > 0.5) have higher C_d values (and therefore higher flows) than predicted by simple theory. This behaviour is predicted by more complex theory and has

been measured by other researchers. In fact, the measured discharge coefficients for the tests with t/d > 0.5 are in good agreement with some of the literature [9.43].

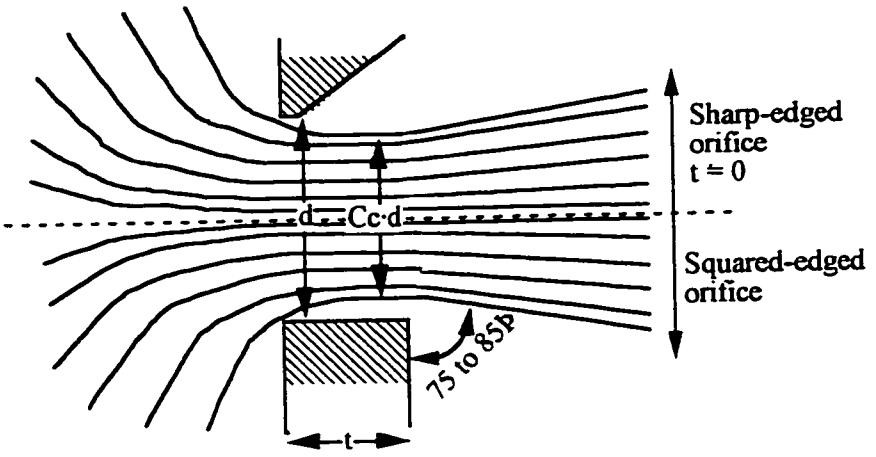

(i) Orifice: t/d < 0.5

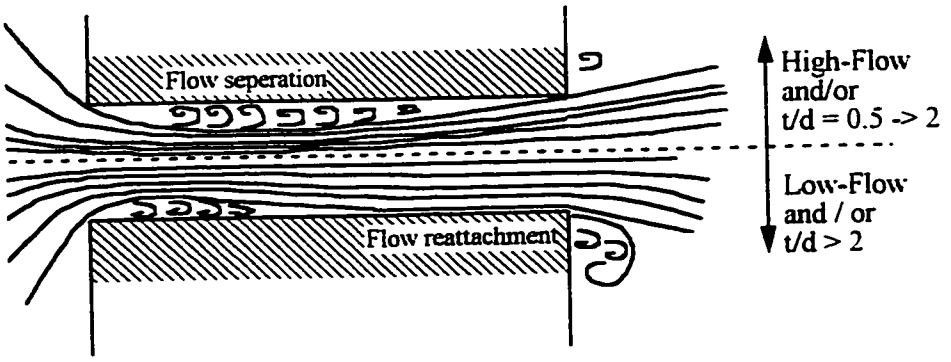

(ii) Deep Orifice Flow: 10 < t/d < 0.5

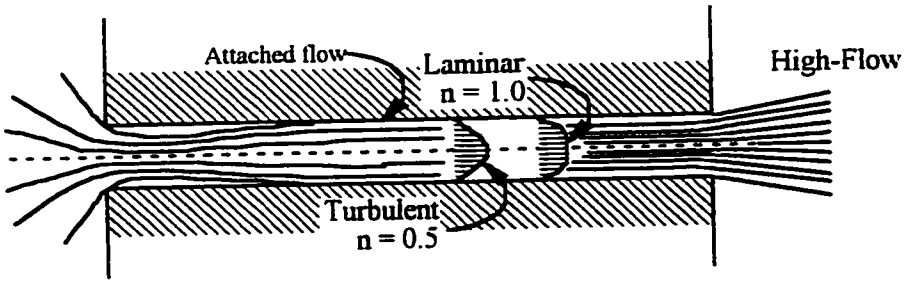

(iii) Pipe Flow: t/d >> 10

$$Q = C_d \cdot A_{vent} \cdot \left(\frac{2 \cdot \Delta p}{\rho}\right)^n \qquad C_d = C_c \cdot C_v$$

Figure 9.12: Generalised observed steady flow behaviour through building vents

Table 9.3: Sharp-edged orifice flow coefficients from steady-state flow tests

Orifice Dia. (d) x Depth (t) [mm]	Depth (t): Diameter (d) (t:d)	Pressure / Reynolds # Range (Pa/#)	Discharge Coefficient (C_d)	Flow Exponent (n)
25.4 x 3.0	0.12	5-250 / 3227-23085	0.652	0.503
22.65 x 3.0	0.13	5-250 / 2838-20301	0.643	0.503
19.0 x 90.0	4.73	5-250 / 2465-17293	0.673	0.498†
15.8 x 3.0	0.19	5-500 / 2078-21068	0.675	0.503
12.0 x 3.0	0.25	5-500 / 1598-17119	0.666	0.515
6.0 x 3.0	0.50	5-75 / 920-3496	0.804	0.493†
3.0 x 3.0	1.00	5-500 / 527-5443	0.894	0.507
3 (square-edged)x 3	1.00	5-500/ 515-5393	0.868	0.510
1.5 x 3.0	2.00	5-500 / 248-2941	0.789	0.537

Note: Linear regression best-fit to flow equation $Q = C_d \cdot A \cdot (\Delta P)^n$. Simple theory: $C_d = 0.611$, $n = 0.5$

† The value for n cannot, theoretically, be less than 0.5. Experimental scatter explains these values.

The results for the 15.8 mm Ø orifice are close to simple theory, whereas the 12 mm, 6 mm, and 3 mm have increasing values for C_d with flow exponents of almost 0.5. The 1.5 mm Ø orifice has a smaller C_d than the 6 mm orifice but the flow exponent is larger than 0.5; hence, for the very small orifices, flow at a given pressure is proportionally higher than predicted by simple orifice theory. The flow exponent begins to diverge from 0.5 for the smallest orifice because the t:d ratio approaches 2, and thus flow behaves slightly more like laminar pipe flow (note, for laminar flow n=1.0) despite the sharp-edged bevel. The brick vent and inserts discussed below also clearly show how the flow exponent reflects the flow regime. For diameter-to-thickness ratios of more than 2, the flow coefficient appears to stabilise at about 0.65 with a flow exponent of 0.50.

The 90 mm deep pipe behaved remarkably like an orifice since, over the pressure differences tested, it was observed that the flow did not reattach to the sides of the pipe. The flow in a smaller diameter pipe (say 3 or 6 mm diameter) might have reattached to the sides of the tube and resulted in more laminar flow (i.e., $n > 0.5$).

The Reynolds number range of the tests is also presented in the table. The lowest Reynolds number test for the 1.5 mm orifice was about 250, well within range for which the discharge coefficient should be valid for. For the larger orifices, such as the 12.0 mm orifice, the ASHRAE limit of applicability ($Re \geq 100\pm$)[9.1] is equivalent to a pressure of only 0.025 Pa, at a predicted flow of 0.015 litres per second.

The brick vent (C_d=0.63, n=0.56), despite its rectangular aspect ratio and depth, behaved in a very similar manner to a large orifice. The discharge coefficient for the brick vent inserts was not calculated because measuring the area of the openings in the inserts is difficult. Instead, an equivalent discharge coefficient was calculated based on the full area of the vent (10 x 65 mm). This method of presentation is also more useful for comparing the venting efficiency of the different products to each other and to an open head joint. The flow exponent calculated from the results of the open brick vent tests indicates that flow begins to diverge slightly from perfect turbulent flow, almost certainly because of the vent's depth. It is expected that, at very low pressure differences (much less than 0.1 Pa), the flow exponent will be higher because the flow will reattach to the sides of the vents.

The discharge coefficient and flow exponent of the vent inserts are presented in Table 9.4. Not surprisingly, the Cell-Vent (n=0.72), essentially a series of 1 mm square pipes 90 mm long, behaves in a manner much closer to laminar flow than any other configuration. The other vent inserts did not modify the nature of the flow significantly.

Figure 9.9 plots the pressure-flow relationship of the masonry vents. The commercially available inserts severely restricted the flow of air. The best insert, Cell-Vent, restricted flow to less than 15% of the flow through an open head joint. The Goodco, Yeovil, and aircraft-style inserts all restricted flow to between 5 and 8% of the flow through an unobstructed vent. Clearly, the flow restriction of all the vent inserts may have serious negative implications for both ventilation and pressure-moderation.

Table 9.4: Orifice flow coefficients from masonry vent insert tests

Masonry Vent Type (10 x 65 mm head joint)	Discharge Coefficient (Cd)	Flow Exponent (n)
Open	0.626	0.555
Cell-Vent	0.089	0.720
Goodco	0.047	0.515
Yeovil	0.056	0.555
Aircraft	0.030	0.497

Note: Linear regression best-fit to flow equation $Q = C_d \cdot A \cdot (\Delta P)^n$. Area based on an open head joint.

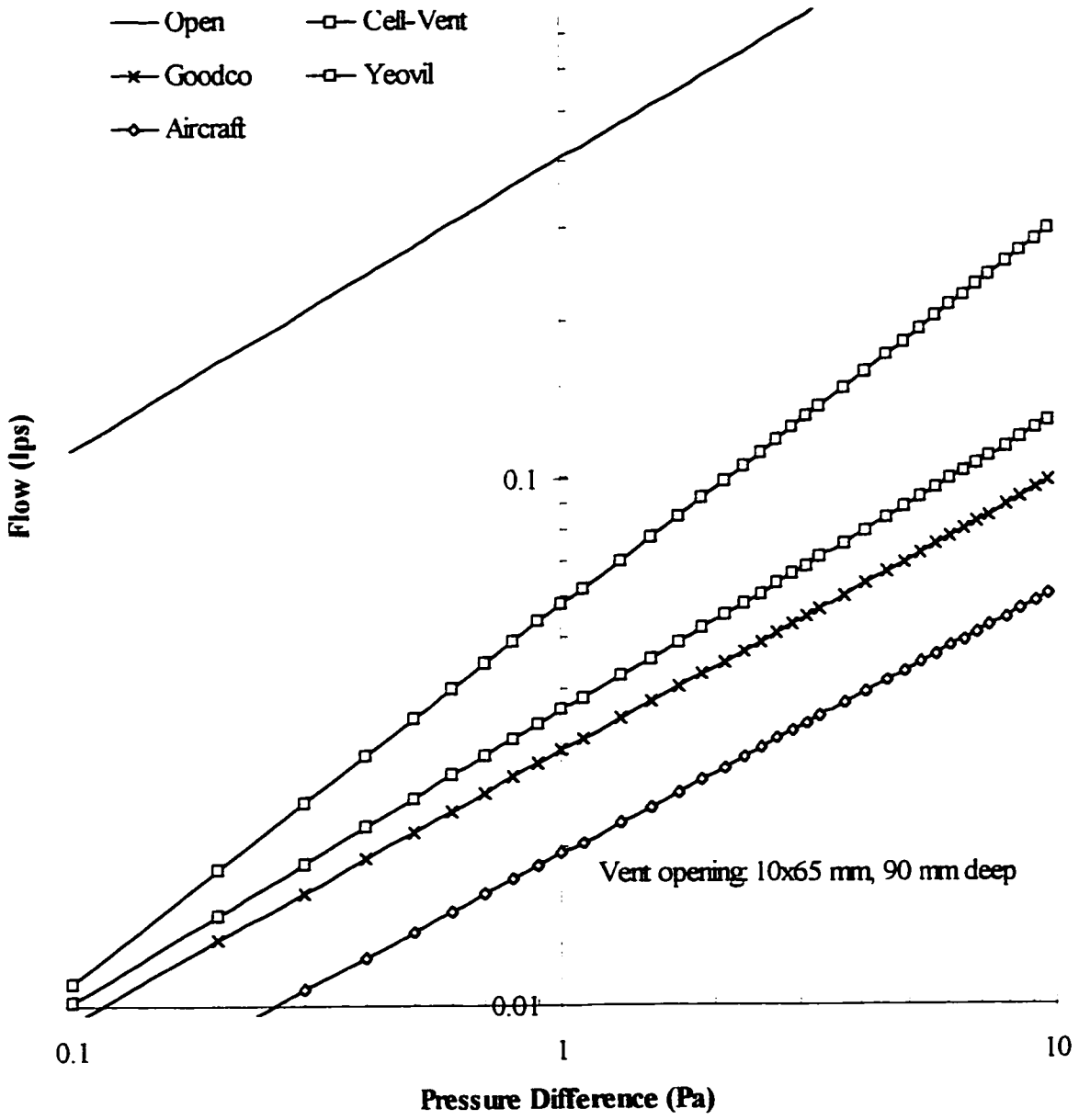

Figure 9.13: Masonry vent static pressure test results

9.7 Ventilation Wind Pressure Measurements

Field measurements of the wind and wind pressures on a real building were undertaken to provide information about the size of ventilation pressures in service. The intent was to gain a better understanding of normal conditions, not extreme events.

The major variables affecting the ventilation pressures acting on a building are:

1) the size and aspect ratio of the building,
2) the windspeed
3) wind direction, and
4) the location of the vents, on the building and relative to one another

The field monitoring program devised would quantify the last three variables. Measuring ventilation pressures in the field has been very difficult in the past because such pressures are small and variable. Advances in pressure measuring technology have removed some of these difficulties.

The monitoring was conducted on the west wall of the Beghut over the period of November to December, 1995. Figure 9.14 presents a summary of the five venting configurations (labelled 1 to 5) comprehensively measured, the dimensions of the test house, and locations of the pressure taps (labelled A to F).

The wind speed, wind direction, absolute stagnation pressure at point A, and the pressure difference between point A and the point of interest (pressure taps B to F) was measured every second. Every 15 minutes the average and standard deviation was calculated, the record was classified according to wind speed and wind direction and the results saved to disk. Each of the five venting configurations shown in Figure 9.14 was monitored for a minimum of one week. Over approximately six weeks, some 3500 records were collected.

The first 5 minutes of a record collected during the field monitoring is presented in Figure 9.15. These pressures were recorded for vent configuration # 1 with the wind coming from 30° south of due west at an average velocity of 4.4 m/s (slightly higher than the annual average wind speed) at 10 m. The record was intentionally chosen to include periods with low windspeeds (as low as 2 m/s) and high windspeeds (over 7 m/s) although this range is not uncommon in the other records. The figure also plots the maximum difference measured between the top and bottom vents, the ventilation pressure. The

following characteristics, which apply to many of the records and match the present understanding of the wind, should be noted:

- as is widely known, the wind speed, wind direction and wind pressures all exhibit large, short-term variations about their mean values,
- the wind speed results in relatively small stagnation pressures at the centre of the panel (normally between 5 and 20 Pa),
- high pressures are well correlated with high wind speeds and vice versa,
- the ventilation pressure is significantly smaller than the stagnation pressure, and equally variable.

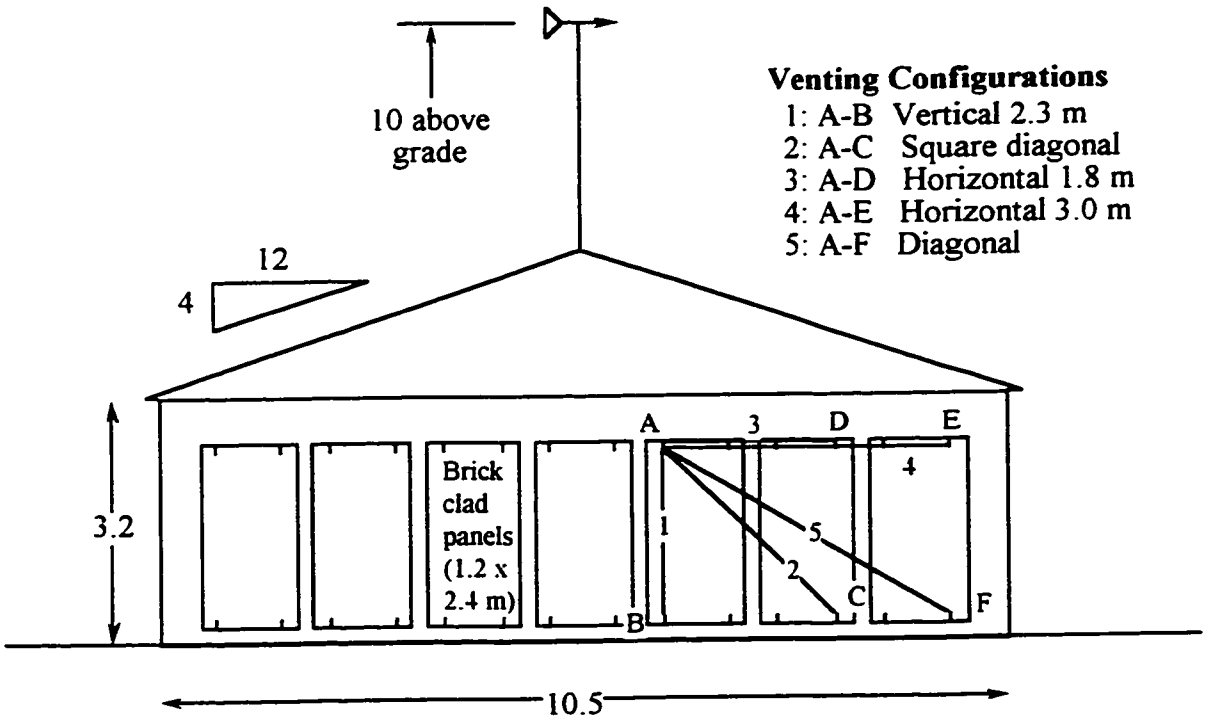

Figure 9.14: Set-up for field monitoring of ventilation pressures

For this particular wind direction and venting configuration:

- the difference in pressure between the top and bottom vents for this particular record is about 1/4 of the total pressure at the centre. For the purposes of ventilation, this is a relatively large force.

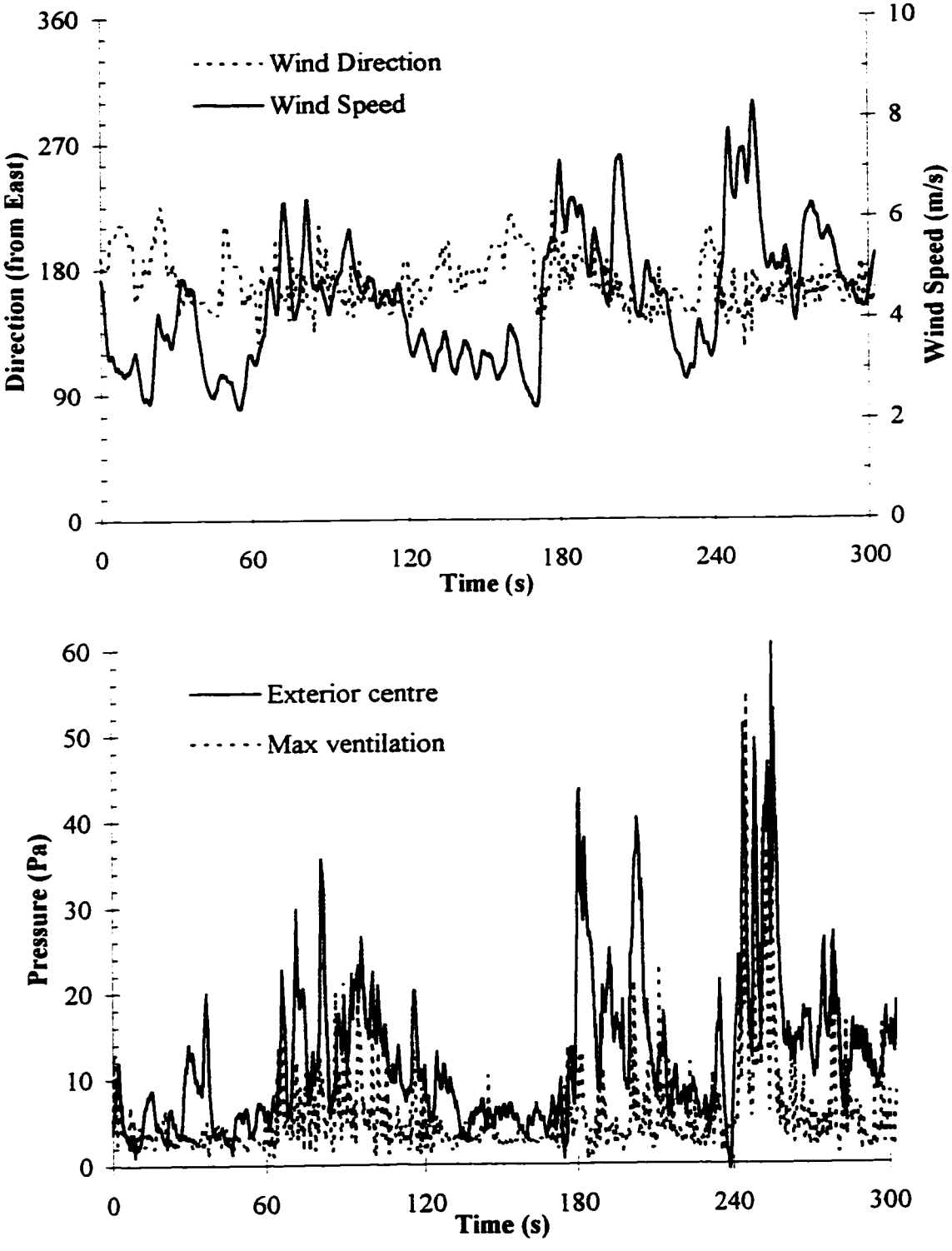

Note: West-facing panel. Venting configuration #1. Avg. windspeed 4.4 m/s.

Figure 9.15: Example ventilation pressure and wind record

- the pressure at the centre of the panel and the pressure driving ventilation are somewhat positively correlated. As the pressure increases so often does the ventilation pressure.

Although the stagnation pressures at the centre of the panel and the ventilation pressures vary between all of the records, the values could be non-dimensionalised by calculating ventilation pressure coefficients, i.e. the ratio of the ventilation pressure to the calculated stagnation pressure of the wind. These ventilation pressure coefficients for each record were calculated using the average stagnation pressure at the eaves height of the Beghut (3.2 m above grade), the typical reference location for a low-rise building with a pitched roof, and the average measured ventilation pressure:

$$C_{p,v} = \frac{\Delta P_{vent}}{P_{stag}} \qquad \text{(Eq. 9.10)}$$

where P_{stag} is the average stagnation pressure at the Beghut's eaves height , and

ΔP_{vent} is the average measured ventilation pressure.

The average calculated ventilation coefficient is a useful means of examining the influence of vent configuration and wind direction. The coefficient was calculated for all of the many records collected during the field monitoring. Appendix B contains plots of the average ventilation pressure for windward and leeward directions versus wind stagnation pressure.

9.7.1 Mean spatial gradients

The wind pressure gradients on the face of a building vary in space and time. Only the mean spatial pressure gradients across the building face are discussed below, although the short-duration dynamic gradients, called spatio-temporal in the literature, may also be important for ventilation and are dealt with in the next section.

Figure 9.16 summarises the mean values of the ventilation pressure coefficient from the field monitoring of each of the configurations shown in Figure 9.14 for all wind directions and speeds and for each wind direction. The value for the mean ventilation coefficient is based on from 10 to 150 records for that wind direction. The mean ventilation coefficient (based on from 421 to 1047 records) for all wind directions for each venting configuration

is shown in the first bar graph of Figure 9.16. The remaining five plots present the average ventilation coefficients for each wind direction for each of the five venting configurations.

Appendix B contains statistical summary data and relative frequency plots for each venting configuration. Figure 9.17 Compares the cumulative frequency of the actual ventilation pressures measure for each of the configuration. Note that this plot contains the results of the average ventilation pressure of 3287 records without consideration for the wind direction.

Several important conclusions can be drawn from these results. Vent configuration #1 (two vents separated vertically by 2.4 m) had by far the largest average ventilation coefficient (0.18) and was the only configuration in which the ventilation pressures consistently acted in one direction, regardless of the wind direction. The actual ventilation pressures were, on average, the highest (at 1.0 Pa) for this configuration. These results justify the common belief that the best vent locations to encourage ventilation are at the top and bottom of an airspace.

The ventilation pressures for most venting configurations were higher for wind acting directly on the wall (west), but could still be significant when the wind came from the other direction (easterly). Hence, ventilation flow can occur even on the lee side of a building.

Consideration of the percentage of time that the wind acts from a certain direction and the average annual wind speed from that direction allows the calculation of mean annual ventilation pressures for the test walls in Beghut. In Figure 9.18 the ventilation *potential* for each orientation is plotted for the different configurations. The potential was calculated as the product of the ventilation coefficient, the mean wind speed, and the number of hours per year that the wind blows from this direction. The potential is expressed in units of pascal-hours per year and is valid for Waterloo, Ontario and the vent configurations tested on the Beghut.

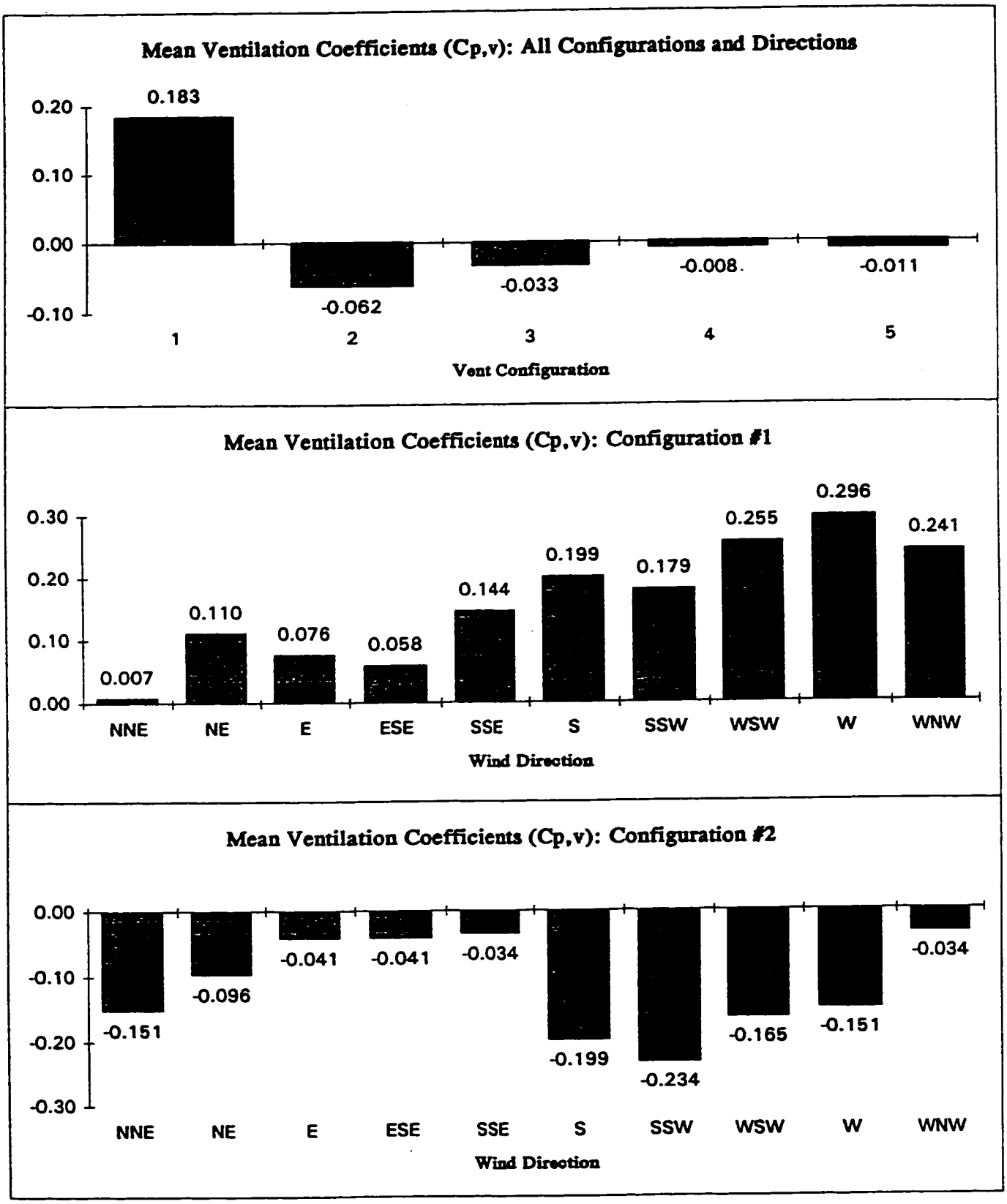

Figure 9.16a: Mean ventilation coefficients (Avg., Configurations #1 and #2)

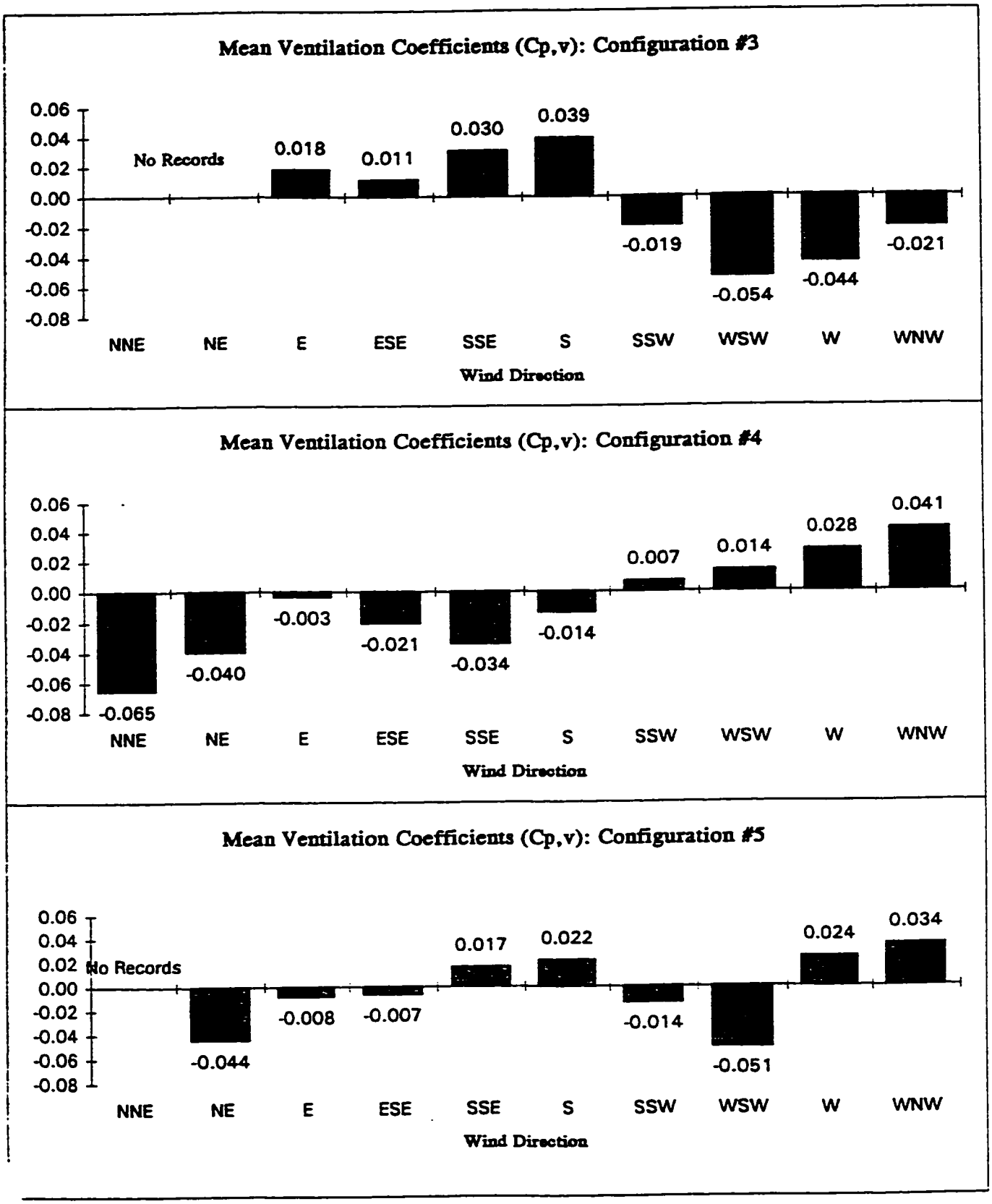

Figure 9.16b: Mean ventilation coefficients (Configurations #3, #4 and #5)

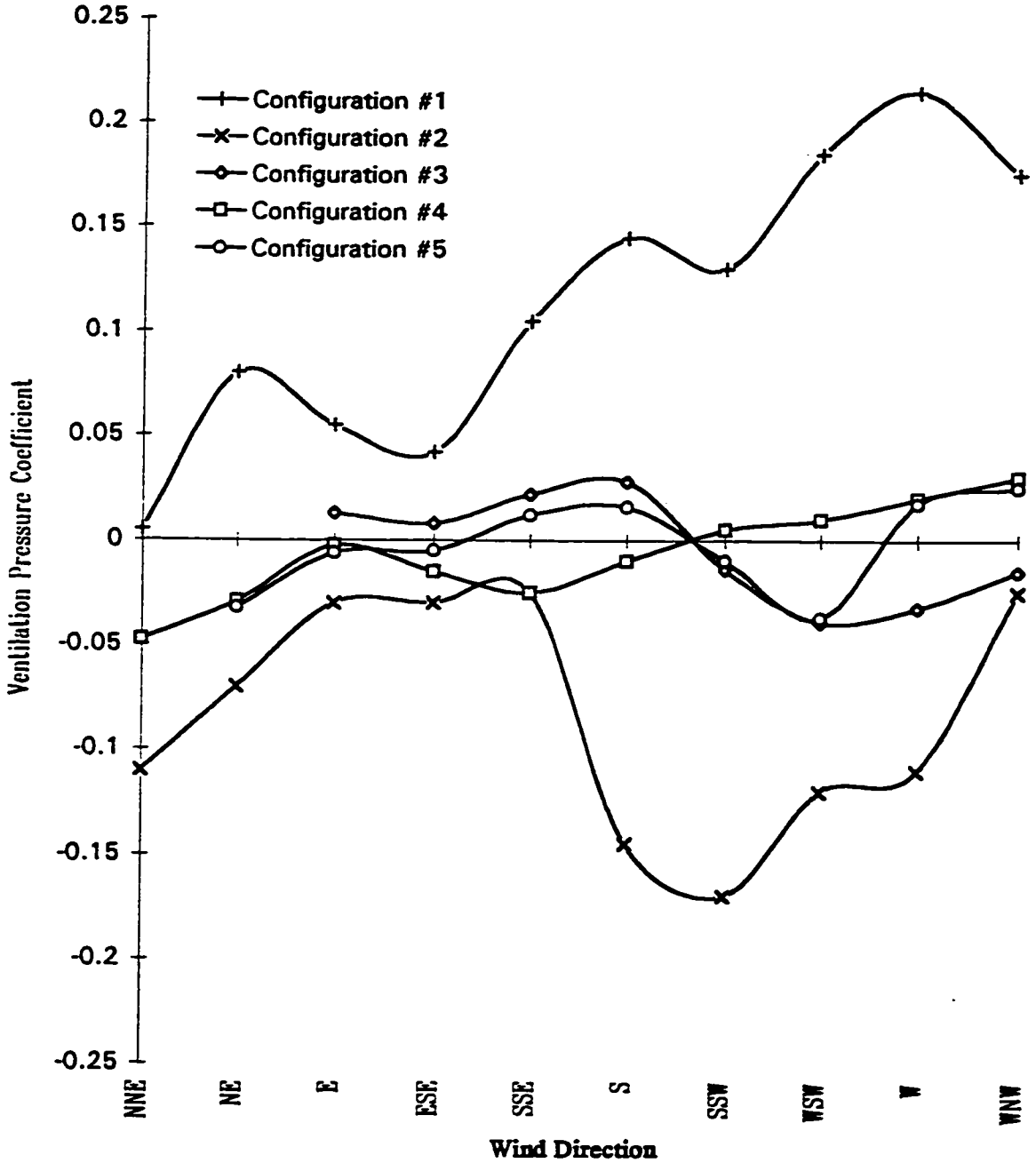

Figure 9.16c: Mean ventilation coefficients (All Directions and Configurations)

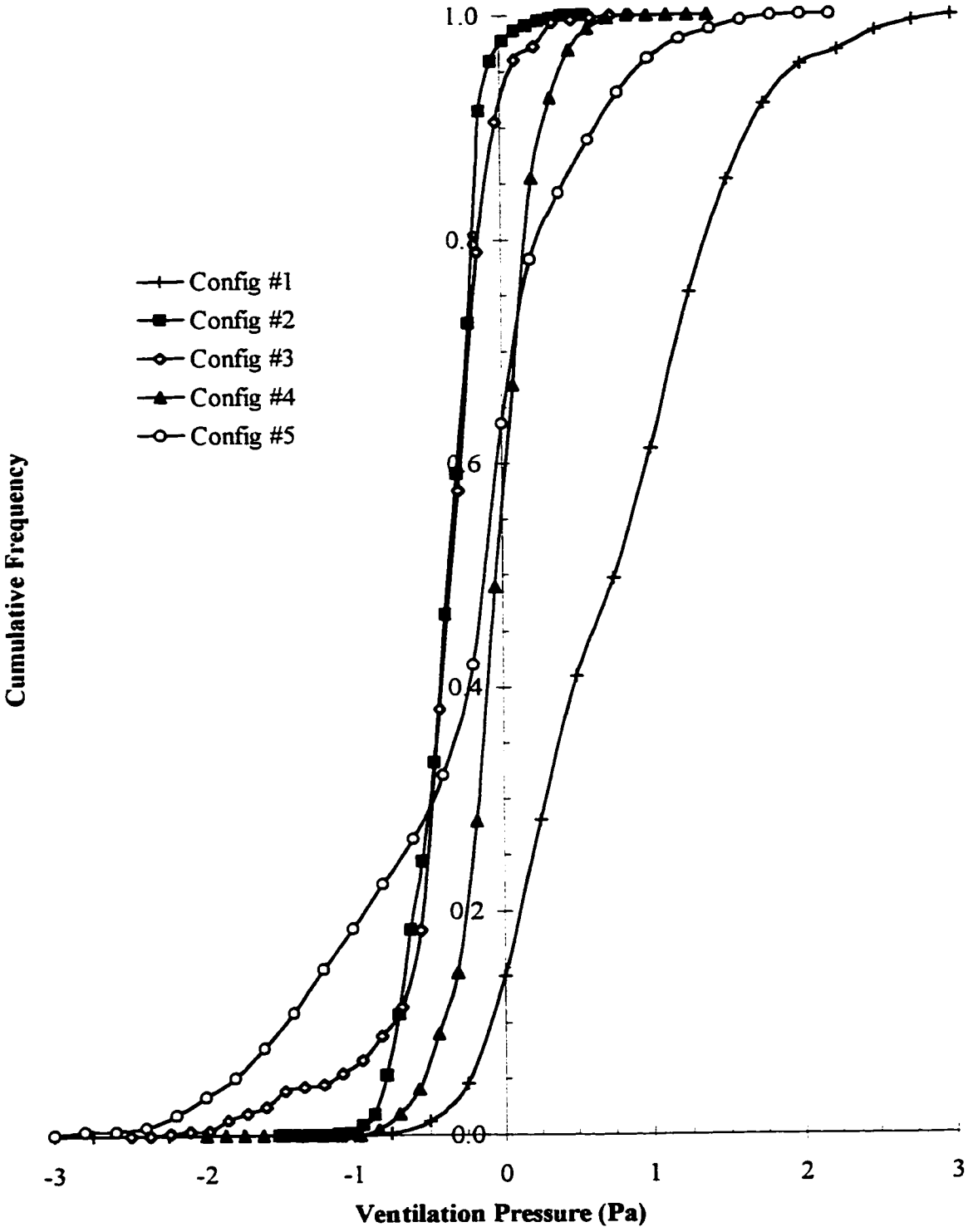

Figure 9.17: Cumulative frequency of average ventilation pressure for all records

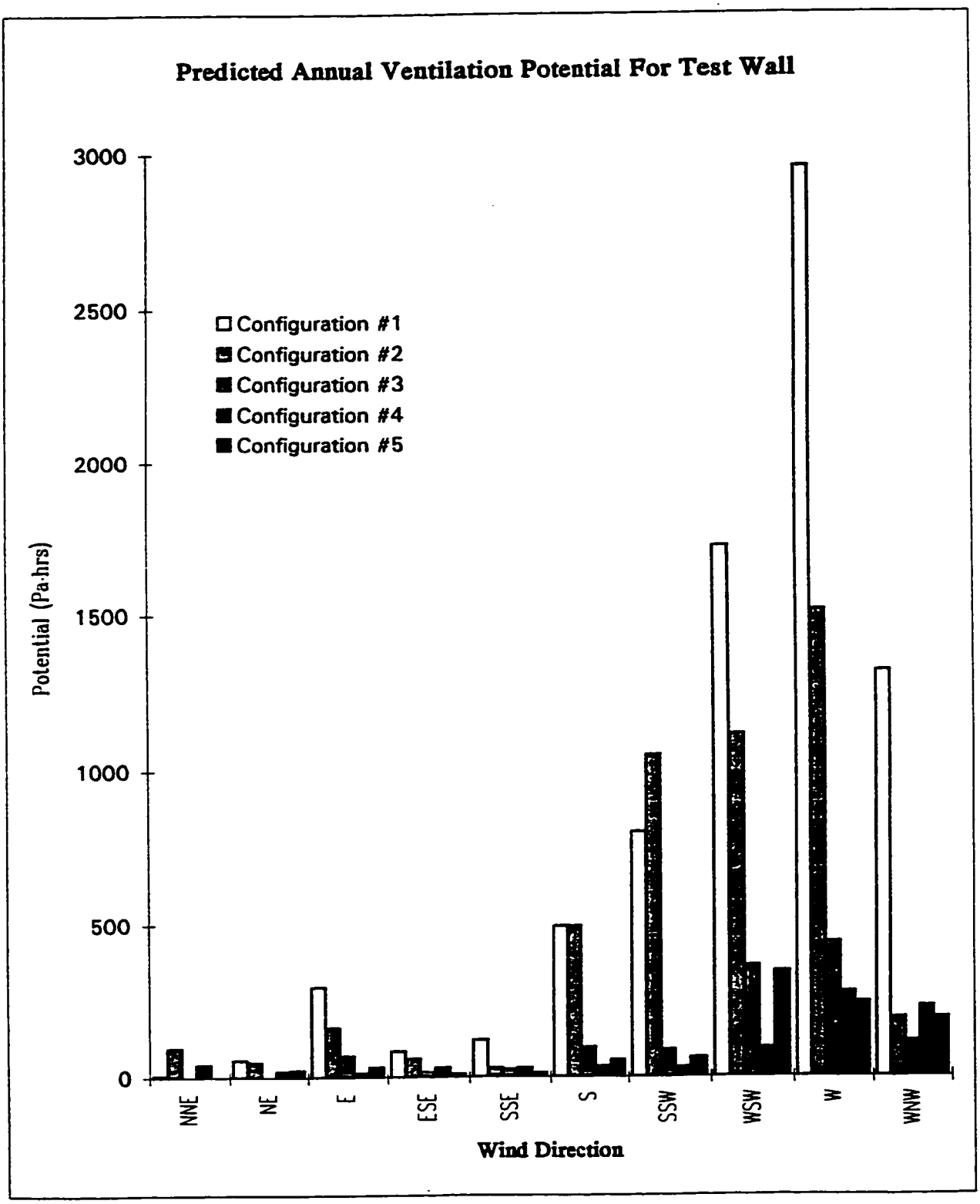

Figure 9.18: Ventilation flow potential for test wall

It is clear from Figure 9.18 that some orientations, and some parts of a wall, will receive several hundred times more wind-driven ventilation than others and that the location of the vents on the wall can have almost as large an influence. In Waterloo, the wind is predominately from the west and hence walls exposed to the west receive the most wind-driven ventilation. In Waterloo, however, the highest load of driving rain wetting is from the east. The leeward side of a building will also usually have the highest amount of exfiltration condensation wetting.

9.7.2 Dynamic spatial variations

Short-duration (i.e., less than about 3-5 seconds) gusts can occur over small regions of a building and create temporary but large pressure gradients. Quantifying the influence of these variations on ventilation has not been attempted but some pertinent comments and observations can be made.

One approach to assessing the influence of dynamic spatial variations is to use statistical measures of the variability of the ventilation pressures. For example, although the smallest ventilation coefficient for venting configuration #1 ($C_{p,v} = 0.007$ for wind from the NNE) suggests little ventilation action, the average standard deviation of the vent pressures for this direction category was 0.5 Pa. This indicates that the flow direction was constantly changing but still acting to ventilate the wall. Hence the average value is misleading, and the standard deviation provides a better measure of the likely ventilation potential.

As another example, consider the ventilation coefficients over all wind directions for venting configuration #5. Although these coefficients are quite small (in the order of 2-3%) and the average measured ventilation pressure was only -0.27 Pa, the average standard deviation was 1.82 Pascals (see Appendix B). This large variability is likely to force a significant amount of air movement through the cavity. In fact, the high standard deviation likely has just as significant an effect on ventilation flow as an average 1 Pa pressure difference.

The spatial extent of gusts is directly related to the wavelength of the wind (i.e., velocity ÷ frequency) and turbulence [9.44]. As the wavelength increases so does the size of the gust. For a given velocity, as frequency increases (i.e., the gust duration decreases) the size of the gust decreases. For a given frequency, as velocity increases so does the spatial extent of the gust. As turbulence increases, the size of the gusts decreases.

In a very simple analysis it is possible to postulate a 'gust size' from the statistical information collected from wind measurements. One suggestion is that a typical gust size in the wind will be of the order of 1/5 to 1/8 of the wavelength and somewhat smaller in more turbulent regions on building faces [9.45]. For a velocity of 10 m/s (a strong wind) and a gust duration of three seconds, a typical gust size would be (1/8 to 1/5) · 10÷(1/3) = 4 to 6 m in size. For a 4 m/s wind (an average velocity), the same 3-second gust would have a size of 1.5 to 2.4 m. For a one-second duration gust under similar wind speed conditions, the gust size would be 1.25 to 2.0 and 0.5 to 0.8 m respectively. Therefore, short-duration gusts can realistically be expected to envelope only a few of the many vents in a well-vented wall system. Near building edges or on complicated geometries, the turbulence will be significant and the gust sizes will be relatively small.

If the gusts are large enough to simultaneously envelop all vents connected to a cavity, no ventilation will occur because the pressure acting on all vents will be similar. However, a short-duration gust acting over only one vent will force air into the cavity at the vent over which it acts. Although this may occur for a short time only, flow through the cavity can be significant. For walls with a single vent the compression of the air by temporal pressure variations is so small that little mixing can be expected.

Ventilation flow through windows is somewhat similar to building cavities in that spatio-temporal pressure variations drive the ventilation. Although difficult to predict, some research in this direction [9.46, 9.47] has shown that significant ventilation rates can be achieved by this mechanism alone.

9.8 Predicting Ventilation Flow

In this section fluid mechanics is applied to predict air flow through vents and cavities. The previous sections outlined the potential driving forces and their magnitude. This section considers the resistance to ventilation flow (friction in various forms) in the form of pressure losses. A ventilation flow system balances the driving forces and the resisting forces.

Figure 9.19 presents a simplification of ventilation flow mechanics through a wall cavity (either vertically or horizontally). The resistance to flow from points A to B and C to D is due to the vents. From points B to C, the flow resistance is due to friction with the cavity walls.

Ventilation flow can be seen to be analogous to flow through an orifice into a rectangular duct and out again through an orifice. Predicting the resistance to ventilation air flow in this simplified model is developed by first examining the flow through the cavity and then the flow through the vents.

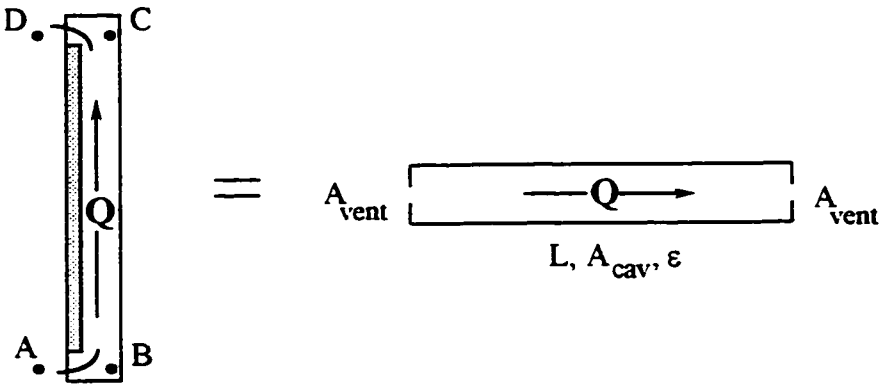

Figure 9.19: Air flow model of an air space in a wall

9.8.1 Air Flow in Cavities

Resistance to air flow in the cavity (between points B and C in Figure 9.19) is theoretically dependent primarily on three characteristics:

1. flow velocity
2. roughness of the sides, and
3. the size (depth) and shape of the cavity.

In practice, a fourth characteristic, the number and size of obstructions and degree of baffling, can be very important. Because this fourth characteristic depends mostly on workmanship, it is difficult to quantify. Nevertheless, it is dealt with below.

Friction varies significantly with velocity – the friction depends on whether the flow is laminar or turbulent. In laminar flow the shear between particles is relatively powerful and causes the air to flow smoothly. In turbulent flow, the inertia of individual air particles exceeds the shear between particles. For internal flows (flow where the air is confined on all sides) the transition between laminar and turbulent flow occurs when the Reynolds number lies between 2000 to 3000. The Reynolds number is a dimensionless measure of the ratio of viscous to inertial forces. For standard air conditions the Reynolds number can be found from the following equation [9.1]:

$$Re = 66\,400 \cdot D_h \cdot V \qquad \text{(Eq. 9.11)}$$

where, Re is the Reynolds number,

D_h is the hydraulic diameter (or equivalent diameter), and

V is the velocity of the flow.

The hydraulic diameter of an air space can be defined as:

$$D_h = \frac{4 \cdot A}{p} \qquad \text{(Eq. 9.12)}$$

where $A = b \cdot d$ is the cross sectional area of an air space b wide and d deep, and

$p = 2 \cdot d$ is the perimeter.

Therefore, for a cavity the hydraulic diameter is

$$D_h = 4\ b \cdot d \div 2\ b = 2\ d \qquad \text{(Eq. 9.13)}$$

Figure 9.19 shows plots of the flow rate through cavities and vents versus the Reynolds number and indicates those regions of flow velocity or flow rate that are laminar and those that are turbulent. This plot shows that flow can normally be assumed to be laminar over the typical velocities expected in cavity ventilation. In laminar flow, the pressure drop across the cavity will vary linearly with velocity. If the flow increases sufficiently, it becomes turbulent and friction will then increase faster than flow rate. This fact can be used in design to naturally limit ventilation flows to velocities that are less likely to entrain water into the cavity through the vents.

The Darcy-Weisbach equation is commonly used [9.36] to give the pressure drop due to friction in fluid flow through pipes and airflow through ducts:

$$\Delta P_{pipe} = f \cdot (L / D_h) \cdot P_{stag} \qquad \text{(Eq. 9.14)}$$

where f is the friction factor (this accounts for flow velocity and pipe roughness),

L is the length of the pipe, D_h is the hydraulic diameter, and

P_{stag} is the stagnation pressure of the air flow, which can be calculated as

$P_{stag} = 0.5 \cdot \rho \cdot V^2 = 0.6 \cdot V^2$ for $\rho_{air} = 1.2\ kg/m^3$.

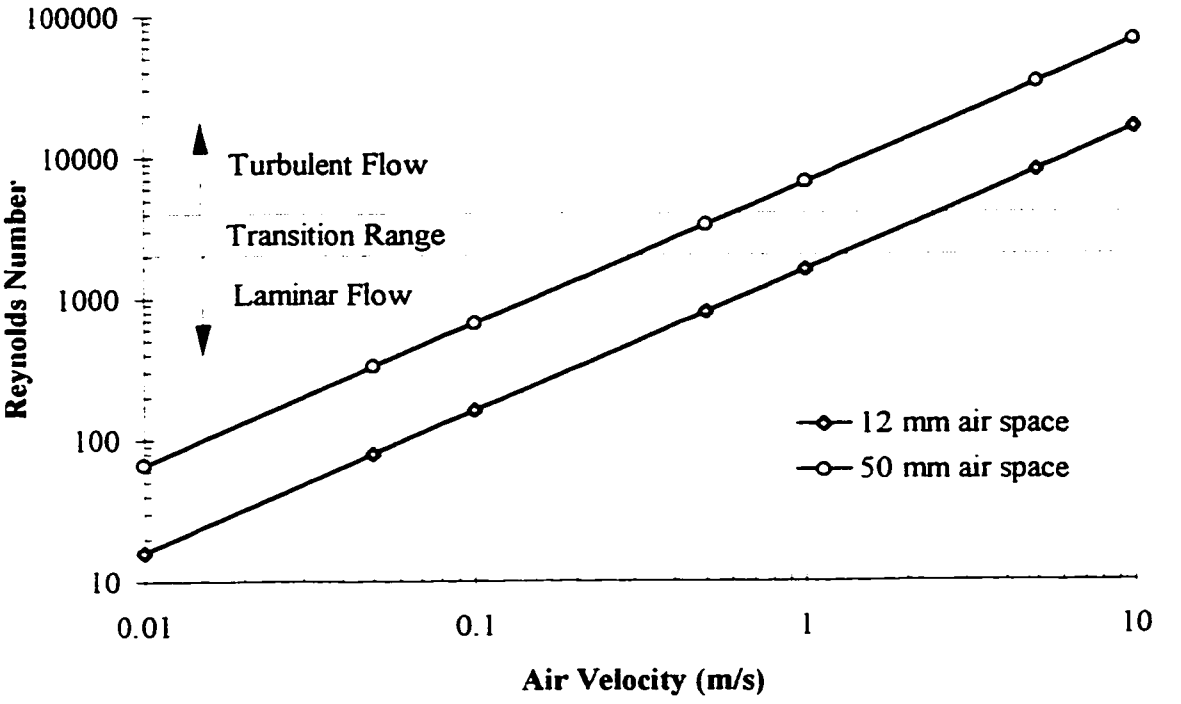

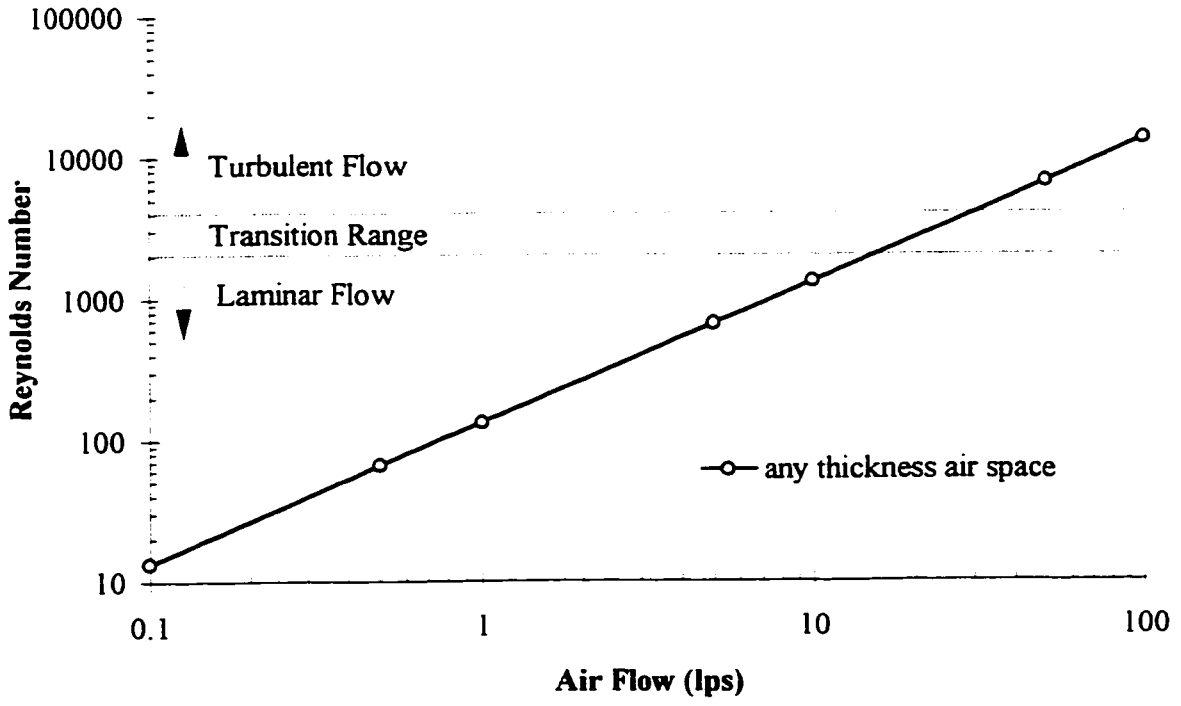

Figure 9.20: Laminar and Turbulent Flow Ranges in Wall Cavities

For laminar flow the friction factor varies simply with the flow rate but also depends on the shape of the duct. For the two extremes of shape [9.48, 9.49]:

$f = 64/(\mathrm{Re}\cdot\gamma)$, circular ducts, and

$f = 96/(\mathrm{Re}\cdot\gamma)$, channel flow (as in a cavity).

A blockage factor, γ, has been included to account for very rough and/or partially obstructed cavities. This factor is approximately equal to the average reduction in cross-sectional area caused by the protrusions from the side of the cavity. For clear cavities $\gamma=1$. For cavities with small protrusions, say the mortar from bed joints in a carefully constructed brick veneer or a stone veneer with the normal number of anchors, a γ value of 0.8 might be appropriate. Since many brick veneers have partially blocked cavities, the value of γ may be significantly less than 0.8.

For turbulent flow, the friction factor varies considerably with flow and roughness. However, a simplified approximation developed by Altshul-Tsal [9.1] is:

$$f = 0.11 \cdot \left(\frac{\varepsilon}{D_h} + \frac{68}{\mathrm{Re}}\right)^{.25}, \text{ for } f > 0.018 \qquad \text{(Eq. 9.15)}$$

where ε is the absolute roughness. This is defined as the average height of the projections divided by cavity width.

For ventilation flow through an enclosed cavity, it can be assumed that the flow will be laminar. Flow velocity is merely flow volume divided by flow area (V= Q/A). Combining equations, therefore, the pressure loss of laminar air flow through a wall cavity can be estimated as:

$$\Delta P_{\text{cavity}} = \frac{V\cdot h}{692\cdot\gamma\cdot Dh^2} = \frac{Q\cdot h}{4610\cdot\gamma\cdot b\cdot d^3} \qquad \text{(Eq. 9.16)}$$

where d is the cavity depth,

h is the cavity height,

b is the cavity width,

γ is a blockage factor, and

Q is the flow volume (all in consistent units).

9.8.2 Flow through vents

Two practical building-related cases should be considered: discrete vents that act as orifices, and continuous slots. Using the standard sharp-edged orifice flow coefficient, the pressure drop across a vent hole acting as an orifice can be calculated as:

$$\Delta P_{vent} = \left(\frac{Q}{0.65 \cdot A_{vent}} \right)^2$$

Section 9.5 dealt with theoretical and measured vent flow behaviour and should be referred to for different flow coefficients and exponents substituted in the equation for more accuracy.

The change in direction from horizontal to vertical flow is not likely to be a significant factor for most ventilation flow situations because the flow velocity is so slow. Although this assumption needs to be proven, it is based on the observation that discrete vents provide such a large proportion of the total flow resistance in walls that the resistance to a direction change in an open cavity is, in relative terms, not significant. A small increase in flow resistance (in the order of 10% of vent resistance) might be in order for high entrance flows, whereas at very low flows (typical ventilation conditions) no increase would be necessary.

9.8.3 Flow through slots

For the situation where a continuous (or semi-continuous) slot is provided as a vent, the cavity tends to provide a significant proportion of the flow resistance, and the change in direction at the vent becomes important. Based on European research [9.14, 9.16] and North American HVAC practice [9.1], the following approach is suggested.

Losses are based on a fraction of the dynamic velocity pressure as:

$$\Delta P_{slot} = f\,(L / D_h)\, P_{stag} = \xi \cdot P_V = \xi \cdot (0.5 \cdot \rho_{air} \cdot V^2) \qquad \text{(Eq. 9.17)}$$

$$= \xi \cdot 0.6 \cdot V^2 = \xi \cdot 0.6 \cdot \left(\frac{Q}{b \cdot d}\right)^2$$

where ξ is a friction factor,

V is the flow velocity, and

$\rho_{air} = 1.2\ kg/m^3$.

The flow velocity is referenced to the flow in the venting slot, not the flow velocity in the cavity.

The following values of ξ have long been used in practice by European designers:

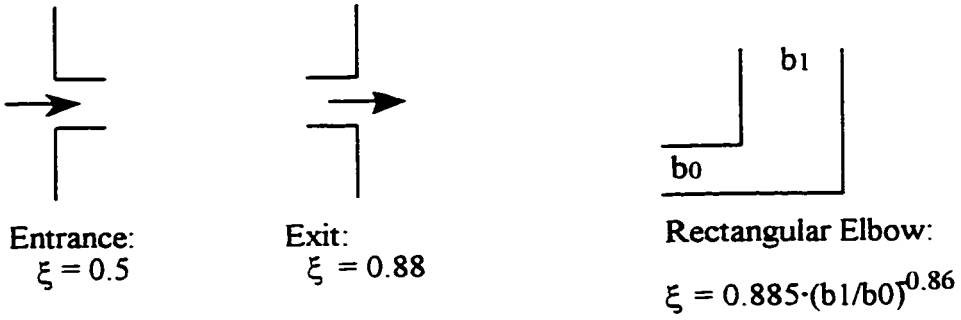

Figure 9.21: Friction coefficients for duct flow

Note that for slots, the change in direction is more significant to flow resistance and should be accounted for.

9.8.4 Wall system flow

At equilibrium, the pressure drop across two vent holes and cavity will equal the pressure drop due to external driving forces, or

$$\Delta P_{drive} = \Delta P_{vent\_entrance} + \Delta P_{cavity} + \Delta P_{vent\_exit} \qquad \text{(Eq. 9.18)}$$

For many wall systems with discrete vents and laminar flow the entrance and exit vents will be of the same type and can be lumped together (for other systems the flow may enter and leave via different vent types) and the above equation simplified to:

$$\Delta P_{drive} = 2 \cdot \Delta P_{vent} + \Delta P_{cavity} = 2 \cdot \left(\frac{Q}{0.62 \cdot A_{vent}}\right)^2 + \frac{Q \cdot h}{4610 \cdot \gamma \cdot b \cdot d^3} \qquad \text{(Eq. 9.19)}$$

In the case of discrete vents, the value of b is the horizontal spacing between vents.

For a panel system with continuous open slots:

$$\Delta P_{drive} = \Delta P_{slot} + \Delta P_{cavity}$$

$$= \xi \cdot 0.6 \cdot \left(\frac{Q}{b \cdot d}\right)^2 + \frac{Q \cdot h}{4610 \cdot b \cdot d^3} \qquad \text{(Eq. 9.20)}$$

where, assuming the same slot at the top and bottom of the cavity, the slot entrance, exit, and direction change resistance can be lumped together as

$\xi = 0.5 + 2 \cdot \{0.885 \cdot (d/ds)^{-0.86}\} + .884$, ds is the slot height

Note: In the case of a panel system with slots, b can be chosen as either a unit width or the width of one panel.

Therefore, with a knowledge of the driving forces and the characteristics of the wall system, the ventilation flow can readily be calculated. Figure 9.22 shows plots for the flow rate through the cavities of typical wall systems and a likely range of driving forces. A blockage factor of 1, relatively unlikely in brick veneer walls, was used to generate Figure 9.22.

Walls # 1 and #2 in Figure 9.22 represent ideal versions of walls that are presently being built. Because of blockage, the flow rates are likely to be smaller than shown. Wall #3 represents a wall designed to increase ventilation; vent area is three times as large as normal and the cavity is twice as deep (to reduce the chance of blockage). It can be seen that the flow through this wall is at least twice as much as Walls #1 and #2. Wall #4 represents a panel cladding system applied to a five-storey building. The ventilation flow through the cavity of this system is more than ten times the flow through a typical brick veneer wall.

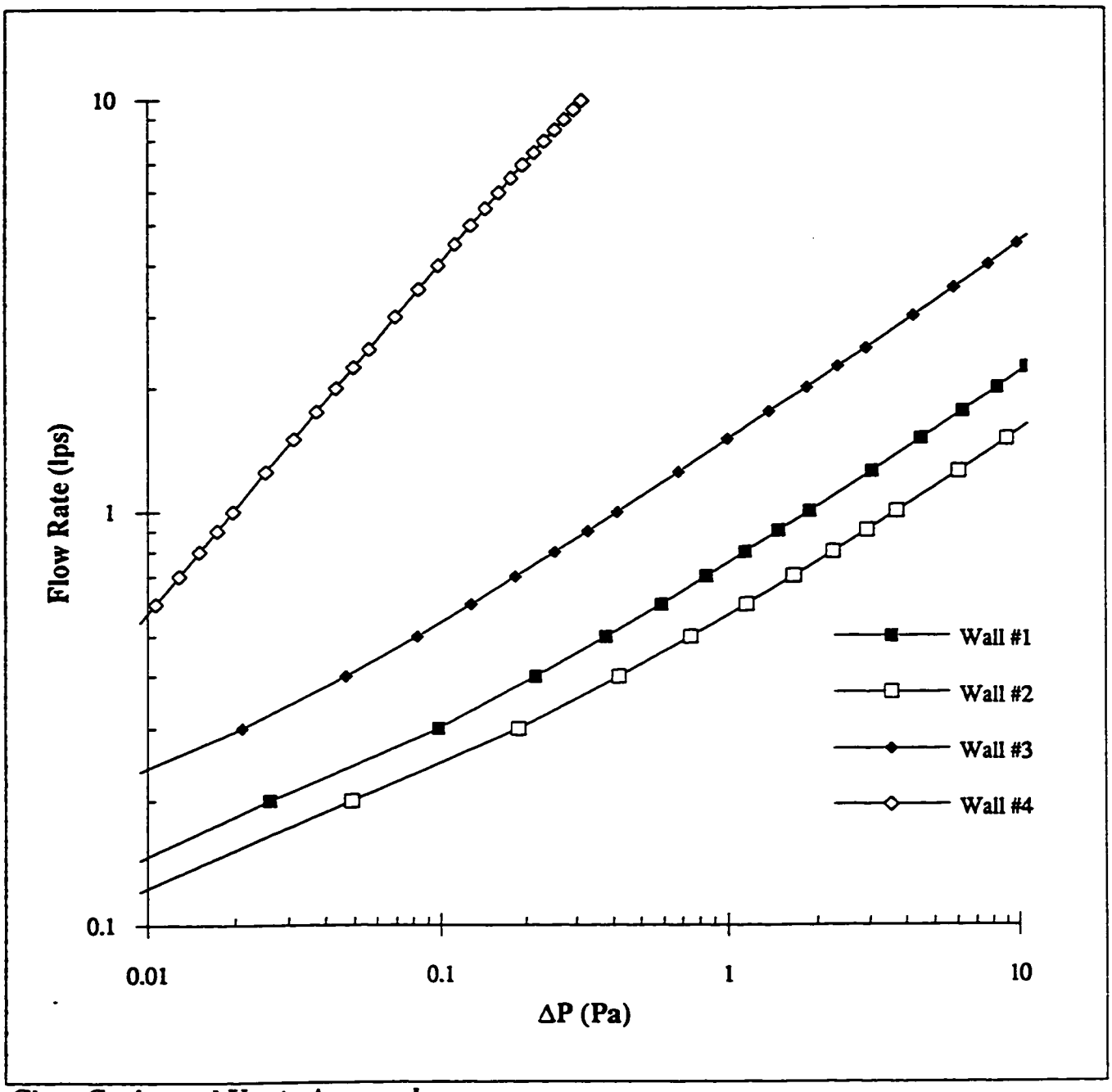

Clear Cavity and Vents Assumed.

Wall #1: 2.4 m high, 25 mm deep cavity, full-width 12 mm slot top and 10 x 65 vent @ 600 bottom
Wall #2: 2.4 m high, 25 mm deep cavity, 10 x 65 vent @ 600 o.c. top and bottom
Wall #3: 2.4 m high, 50 mm deep cavity, 10 x 65 vent @ 200 o.c. top and bottom
Wall #4: 12 m high (5 stories), 50 mm deep cavity, full-width 12 mm slot top and bottom

Figure 9.22: Ventilation flow versus driving pressure for some typical walls

9.9 Assessing Ventilation Drying

Given a knowledge of the quantity and quality (i.e., temperature and moisture content) of ventilating air, an estimate of the maximum drying capacity can be made. However, several simplifying assumptions need to be made:

1. the air in the space must be considered to be well mixed, i.e., the moisture content is constant over the whole air space

2. the rate of drying must be controlled by the rate of ventilation flow not the rate of evaporation from the material along the side of the air space

3. temperature conditions are not modified by the drying process

Field monitoring of various wall systems has shown that the first assumption is quite accurate under most conditions, i.e., the difference in relative humidity between the top and bottom of a clear air space is very small. Because the vapour permeance of air is so high it is difficult for large gradients of air moisture content to form in clear air spaces. This assumption is no longer valid under high flow conditions near the inlet vent.

The second assumption is valid given that the ventilation flow rate is low and the sides of the air space are wet. When the materials drop below saturation, this assumption becomes progressively less accurate. Thus, calculations based on this assumption are maximum drying rates, or drying rates when the air space sides are saturated; however, it is precisely these conditions that one is trying to alleviate with ventilation drying.

The validity of the final assumption depends on the drying rate. As demonstrated earlier, at low ventilation rates the specific heat capacity of air is too low to change the temperature conditions of the air space air or sides. At low drying rates, the amount of latent heat required to evaporate moisture is very small and has little effect on temperatures. Very high drying rates, such as would occur during a sunny period immediately after a rain event, will depress the temperature noticeably. This assumption limits the accuracy of calculations during extreme events, i.e., most of the time the third assumption is valid.

In summary, the three assumptions listed above are valid for low ventilation flows (i.e., those typically experienced) and walls that have wet materials (i.e., those walls that require drying).

9.9.1 Example calculation

Consider a well-built brick veneer wall system with a 50 mm air space and open head joint vents spaced a 600 mm o.c. top and bottom. Assume that a layer of 12.7 mm chipboard sheathing (density 700 kg/m^3) has been saturated by exfiltration condensation.

If exterior conditions are 7 °C and 85% RH (851 Pa), the outdoor air can store 6.6 g per m^3. If the sun shines on the wall, the air space temperature will rise to at least 20 °C above the outdoors for 6 to 8 hours, and the air in the space will be nearly 100%RH (as it must be if the materials lining the sides of the air space are saturated); air at 27 °C can store 27.6 g per m^3. The difference between interior and exterior air of more than 20 g per m^3 is the amount that can be removed by ventilation. As discussed earlier, ventilation flows of 0.2 - 2 m^3/m^2·h might be expected in the wall. This flow rate is so small that it generates flow velocities of only 2.6 to 26 mm/s. Over an 8 hour period at a flow rate of 1 m^3/m^2·h, the moisture content of the materials lining the airspace can drop by 160 g; this would reduce the moisture content of the chipboard by almost 2%.

Diffusion drying of the sheathing can be calculated in a similar manner. If the sheathing is at 27 °C and 100%RH (3567 Pa), drying by diffusion would be:

$$(3567\text{-}851)\ \text{Pa} \times 46\ \text{ng/Pa·s·m}^2 \times 3600\ \text{s/hr} \times 8\ \text{hrs} = 3.6\ \text{g}$$

In this realistic example, ventilation drying removed more than 40 times as much stored moisture than diffusion drying.

9.9.2 Equivalent vapour permeance

As has been emphasised earlier, the potential of ventilation is important to screened cavity walls because the screen often has a relatively high vapour resistance (e.g., brickwork, inorganic siding, steel, and stone). However, because air flow can be a much more powerful water-vapour transport mechanism than diffusion, it must be taken into account. The concept of an equivalent water-vapour permeance (which accounts for ventilation) of a cavity with an air exchange rate is developed here as a means of assessing the potential effectiveness of ventilation.

Using the assumptions listed earlier, it is possible to generate a combined or effective vapour permeance of a wall layer which includes the effects of both diffusion and ventilation air flow. The mass of water in air can be found from a form of the ideal gas law:

$$w_v = \frac{p_v \cdot V}{R_{wv} \cdot T} \qquad \text{(Eq. 9.21)}$$

where w_v is the mass of water (kg),

p_v is the vapour pressure of water (Pa),

V is the volume of air (m^3),

R_{wv} is the gas constant for water (461.5 J/kg·K), and

T is the temperature (K).

For a difference in vapour pressure, assuming well-mixed air, the mass of water transported by an air volume exchange is:

$$\Delta w_v = \frac{\Delta p_v \cdot \Delta V}{R_{wv} \cdot T} \qquad \text{(Eq. 9.22)}$$

assuming that the temperature difference between the air streams is small. If the temperature difference is not small, and accuracy is important, Equation 9.21 should be evaluated at each temperature.

The property that defines the amount of diffusive water vapour transport across a material layer is called the water-vapour permeance. For a unit change in vapour pressure and volumetric flow rate, yields a system property which can be considered to be the *equivalent vapour permeance* of the cladding due to ventilation air flow.

For an air flow rate of 0.00028 $m^3/m^2 \cdot s$ (i.e., 1 $m^3/m^2 \cdot hr$), a vapour pressure difference of 1 Pa, and a mean temperature of 15 °C, the mass of water transferred, is:

$$\Delta w_w = \frac{1 \cdot 0.0028}{461.5 \cdot (273+15)} \cdot 10^{12} \text{ ng/kg}$$

$$= 2100 \text{ ng / s·m}^2\text{·Pa.}$$

This value of permeance is over forty times that of a 90 mm brick masonry veneer -- this is the same conclusion reached in the previous example. Such calculations indicate that, at the very least, small rates ventilation can play a very important role in bypassing the vapour resistance of the cladding. Even with a ventilation rate of only 0.1 m^3/hr, the transfer of vapour out of the cavity by mass transport is likely to be four to five times greater than that by diffusion alone.

The air velocity in a cavity 2.5 m high and 50 mm deep necessary to generate 1 $m^3/m^2 \cdot hr$ of air flow is 0.006 m/s. Compare this velocity to the range of velocities (of 0.05 to 0.5 m/s) measured in the field by some researchers. A velocity of 0.006 m/s is so small that it is exceptionally difficult to measure and the pressures necessary to generate this small flow rate are generally considered so small as to be insignificant (i.e., $\Delta P << 1$ Pascal). Ventilation drying may have been dismissed in much of the literature because of the difficulty of measuring such small velocities and pressures. However, the preceding examples confirms that very small ventilation rates can have a dramatic influence on the actual vapour permeance of the cladding.

To account for the resistance of the brickwork, a parallel circuit analogy can be used, and an equivalent resistance and permeance calculated:

$$\frac{1}{R_{equiv}} = \frac{1}{R_{v,vent}} + \frac{1}{R_{v,screen}} = M_{v.vent} + M_{v.screen}$$

In this case the vapour diffusion resistance of the screen is negligible. Even with a ventilation rate of only 0.1 m^3/hr, the transfer of vapour out of the cavity by mass transport is likely to be from four to five times greater than by diffusion. Table 9.5 lists the equivalent ventilation vapour permeance of a screened wall for various ventilation rates.

For some claddings (vinyl siding, metal panels), the resistance to vapour diffusion is very high and the satisfactory performance of the wall assemblies can only really be explained by the ventilation, albeit exceedingly small, of the airspace often through small unintentional openings. The concept of equivalent vapour permeance allows for a rational assessment of the importance of ventilation air flow to drying. The important role of the sun and the wind are clear from the assumptions that need to be made for these calculations.

Table 9.5: Equivalent vapour permeance for various ventilation flow rates

Ventilation Flow Rate ($l / m^2 \cdot s$)	Equivalent Vapour Permeance ($ng / s \cdot m^2 \cdot Pa$)
0.05	375
0.10	750
0.25	1 875
0.50	3 750
1.00	7 500
3.00	22 600

Note: By comparison, the vapour permeance of brickwork and wood siding is approx. 50 $ng \cdot s \cdot m^2$ /Pa

9.9.3 Ventilation drying potentials

The equivalent ventilation permeance can easily be substituted for the permeance of brick veneer in a standard Glaser vapour flow analysis. From such analysis it can be shown that a relatively small ventilation rate (e.g., less than 0.25 lps) will greatly reduce the chance of condensation on the backside of a brick veneer.

By making the drying assumptions described earlier (i.e., the cavity sides are saturated and the drying rate is controlled by the ventilation rate), and using the concept of equivalent permeance developed above, the maximum ventilation drying rate can be calculated for various cavity and exterior weather conditions. It is then a rather simple task to generate drying potential curves given the monthly average exterior conditions.

Figure 9.23 presents the results of such calculations based on equivalent permeance and using average weather data for Waterloo, Ont. (i.e., the vapour pressure of exterior air and the vapour pressure within a saturated airspace) for four months of the year. For example, given a ventilation flow rate of only 0.1 $l/s \cdot m^2$, a drying rate of up to 10 $g/m^2 \cdot day$ can be achieved in January and about 100 $g/m^2 \cdot day$ in July. As demonstrated earlier, flow rates of 0.5 to 1 $l/s \cdot m^2$ could likely be achieved in practice with proper ventilated wall design and construction. Figure 9.23 indicates that ventilation rates of this magnitude can remove moisture, even in the winter.

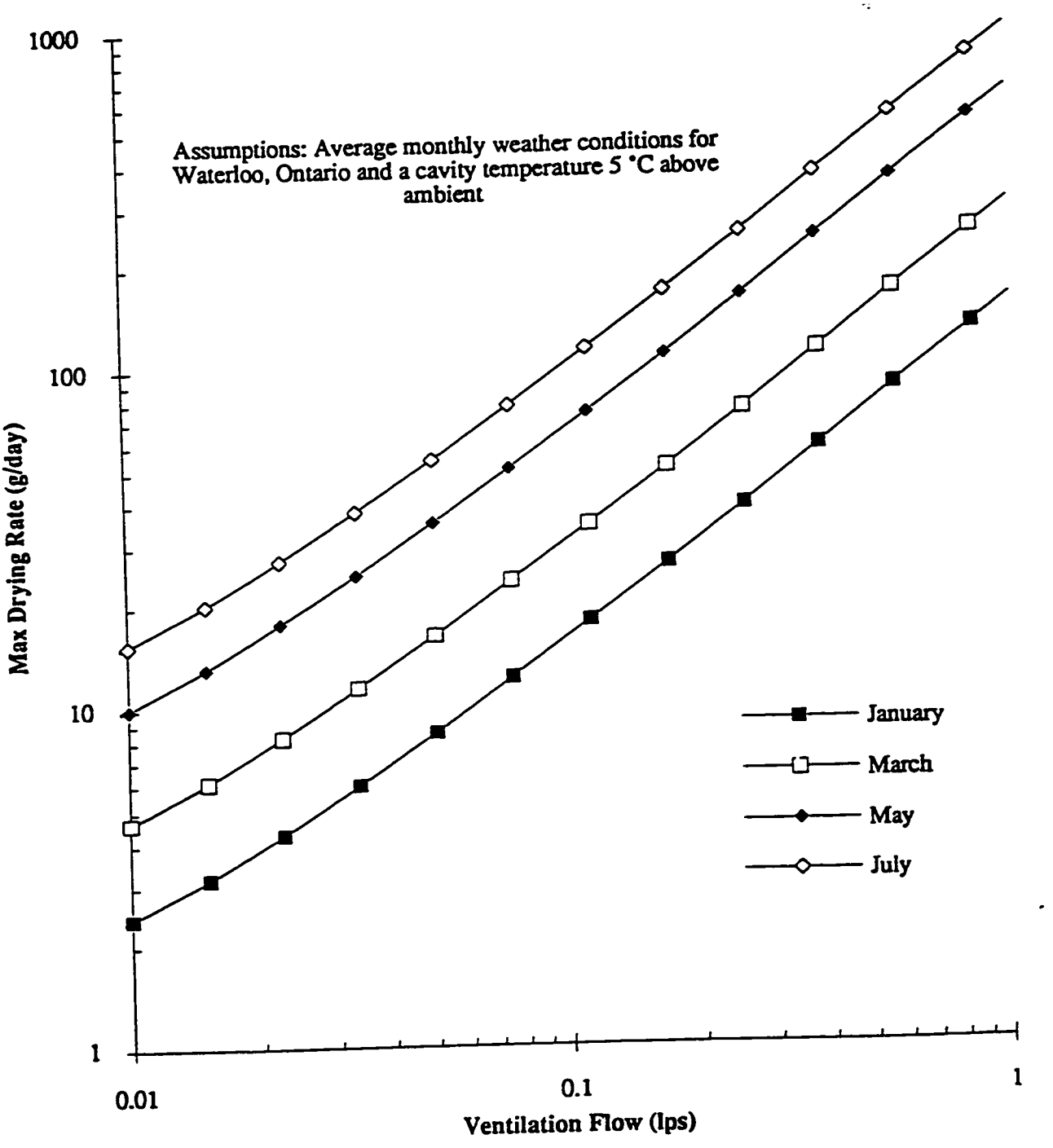

Figure 9.23: Ventilation drying potential versus ventilation flow for Waterloo, Ont.

9.9.4 Moisture from the interior

To this point, only moisture stored within the wall has been considered. Ventilation may also be able to reduce the potential of wetting from several sources.

Calculating the vapour gradient through a typical wood-frame house wall with a low vapour permeance cladding in a cold climate will show that diffusion condensation can often occur. In a ventilated wall, the vapour pressure in the cavity would be depressed and diffusion condensation might be avoided

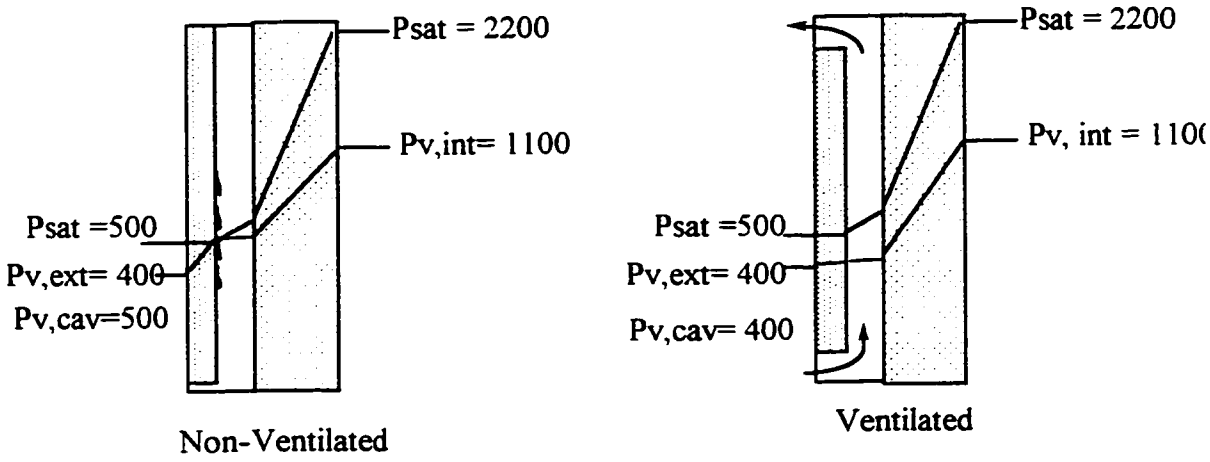

Note: Vapour pressures in Pascals

Figure 9.24: Effect of ventilation on diffusion condensation behind low vapour permeance cladding

If air leaks through imperfections in the air barrier system of the assembly, considerable amounts of water may be deposited on the rear of the cladding by exfiltration condensation. This type of wetting can be very significant in cold climates. Ventilation not only acts to remove moisture stored from this wetting mechanism, it can also reduce the probability of it occurring. By maintaining the RH of the cavity at close to exterior conditions, a ventilated cavity may act like a ventilated attic -- so long as a sufficient amount of ventilation occurs, moist air leaking into the cavity will be diluted and removed to the exterior before condensation can occur.

For example, consider air at -4 °C (an average temperature over the three winter months), and 85% RH which contains 3.0 g/m^3. A brick veneer airspace will be several degrees

warmer, and so ventilation air warmed to 0 °C within the air space can contain 4.9 g/m^3 at saturation. Indoor air at 20 °C and 30% RH which contains 5.3 g/m^3, may leak into the space through the air barrier. If ventilation can remove the excess (5.3 - 4.9 = 0.4 g) of moisture, condensation on the back of the cladding will be prevented. Therefore, each cubic meter of leaking air will deliver 0.4 g more moisture than the air in the airspace can store, but each cubic meter of ventilation can remove 1.9 g (4.9 - 3.0) of moisture. In this scenario, 1 m^3/m^2/hr of ventilation could prevent condensation due to as much as 4.75 m^3/m^2/hr of air leakage.

Ventilation can also be used to control inward vapour drives. As discussed briefly in Chapter 4, moisture from saturated cladding will be evaporated because of solar heating. The high vapour pressure generated can drive significant amounts of vapour inward, where it can condense on the cooler polyethylene vapour retarder. By allowing the vapour to escape to the exterior by convection, ventilation reduces this possibility, and also hastens the drying of the cladding so that it no longer evaporates into the airspace.

9.9.5 Controlling ventilation wetting

Only the drying potential has explicitly been examined in this chapter. There are, however, cases where ventilation may cause wetting. For ventilation to be of benefit, its drying potential must be significantly higher than its wetting potential.

For thermally lightweight cladding with well ventilated cavities (metal cladding systems are especially vulnerable) and roofs, night time condensation can cause wetting. For example, in Forest's study of attics with lightweight roof sheathing (plywood and shingles) and high ventilation rates (2 to 20 air changes per hour), it was found that night-time ventilation could often cause condensation wetting [9.50]. Even in this study, however, the best performance was found by ventilating well since interior moisture leaking through the ceiling added a moisture load to the attic space. Although roofs receive more solar radiation in the summer than walls, they are more susceptible to ventilation wetting because the solar gain is not stored in lightweight roofs and the high rates of ventilation remove some of the heat gain. At night, night-sky radiation causes a much greater temperature depression for roofs than walls (the temperature reduction is normally assumed to be at least twice as large as for walls).

Ventilation of crawl spaces can cause wetting even more often than ventilation of roofs. In this case, the ventilation air is cooled (raising its humidity) because the earth in the

crawl space is a cold surface. Exacerbating crawlspace moisture problems is the almost limitless supply of moisture available from the earth. In climates and weather conditions where the dewpoint of the outdoor air often exceeds the expected crawl space soil temperature, ventilation is likely to cause wetting and should be avoided.

Maximum and minimum venting areas for these systems must be carefully chosen by considering the climate, the quality of the air barrier system, solar exposure, and the interior environment.

For most wall systems, the cladding is warmer than the outdoor air (because of solar heating, thermal mass, and in winter, outward heat flow) and the possibility and duration of condensation within the cavity is small. This danger of ventilation-induced condensation exists only if radiation losses reduce the temperature of the cladding below ambient. The possibility of night time condensation on the inner face of brick veneers can be practically ruled out because of solar absorption and heat capacity.

If the cavity is faced on the inside with a highly vapour and air-permeable insulation (e.g., mineral fibre insulation), condensation on the underlying sheathing may occur in air-conditioned buildings. This is unlikely to be a problem for most wall assemblies because the summertime temperature difference between outdoor and indoor air rarely exceeds 10°C and a barrier to air and water flow is often located outside some insulation.

Because significant inward-acting summertime vapour drives occur in all veneer walls and excessive wind and convective cooling will occur in low-density fibrous insulated sheathing, a facing should be provided on the exterior (cavity) face of these products. Such a facing will greatly reduce the probability of summertime condensation induced by ventilation and inward diffusion, as well as reducing convective heat loss.

The addition of vent openings increases the chance of wind driven rain penetrating into the cavity. While it is felt that the amount of water penetration through most vents is small or negligible, this question deserves further research.

9.10 Field Measurements

The absolute air moisture content was calculated on a hourly basis over the summer period (from April 15, 1996, to August 15, 1996) for each of the panels in the URIF project that contained a filled cavity or air space. Walls B, F, and C are brick veneer walls with clear well-vented air spaces. Walls R, W, D, and O are also brick veneer walls, but the cavity has been completely filled with fibrous insulation. While this insulation may be air permeable, it provides too much air flow resistance to allow ventilation air flow. Walls V and E are clad with vinyl siding and EIFS system respectively. They are both well-vented but not ventilated.

Table 9.6 summarises the average calculated amount of moisture in the air space/cavity less that in the outdoor air, i.e., the moisture excess.

Table 9.6: Excess moisture content of cavity air (g/m^3) from April 15, 1996, to August 15, 1996

Wall	N	S	E	W
B	0.0	0.5	1.0	1.3
R	4.1	6.3	6.6	3.4
W	N.A.	N.A.	5.6	N.A.
E	-0.1	-0.3	0.0	0.8
D	2.8	5.8	6.4	5.3
F	N.A.	N.A.	1.4	N.A.
C	N.A.	0.8	N.A.	N.A.
V	-1.5	-1.4	N.A.	N.A.
O	3.7	N.A.	N.A.	7.8

Notes: Exterior air moisture content over the period was 9.1 g/m^3. Some wall panels/instruments did not face all orientations: this is indicated with a "N.A." symbol.

While the RH in the B wall air space was usually just as high as in the middle of the cavity insulation in the walls which had their cavities filled with fibrous insulation, the actual moisture content of the air in most of the filled-cavity walls was significantly higher than in walls with clear air spaces (e.g., B, C and F) during the later spring, summer and early fall.

The average moisture content of the air in the air space of the well vented brick veneer clad B, F, and C walls was slightly higher than that of the exterior air. During the summer period, the average moisture content of the air space of the B, F, and C walls was about 10 g/m^3, (about 10% above the exterior) ranging from about 0 to 1.4 g more than the exterior air moisture content during this period.

Although walls E and V do not contain an air space, both are designed to act as if they have vented cavities. Primarily because both wall types E and V both have non-absorbent cladding, the air moisture content ranged from 0 to -1.5 g/m^3 below the outdoor air. For unknown reasons, of the four EIFS panels only the west-facing wall showed slightly more cavity moisture than ambient.

These results indicate that ventilation or venting allows the moisture content of the air to be approximately the same in the air space as in the outdoor air. Absorbent claddings will tend to have slightly higher moisture in the air space because these claddings retain rain water, while non-absorbent claddings will tend to have slightly less moisture than outdoors (because solar heating maintains the materials at a higher temperature).

To assess the effect on ventilation drying potential of the temperature difference between the cavity air and the exterior (shown earlier in Figure 9.9), the saturation moisture content was calculated based on the cavity air temperature for the vented wall FE. This moisture was subtracted from the actual ambient air moisture content for the same summer period as Figure 9.9. Figure 9.25 plots the cumulative distribution of this difference, or moisture content excess.

On average, the excess was 8.9 g/m3, indicating a large ventilation drying potential. Of course as the wall drys, the actual excess will drop until it approaches that of the exterior air. The data presented in Table 9.6 shows that while this brick veneer wall never dried completely, it was considerably drier than saturation, likely partially due to ventilation drying.

The moisture content of the air in all of the filled-cavity walls (which are essentially vented but unventilated) was considerably higher than the exterior air. For example, walls RE, RS, WE, and OW were all seriously affected by summertime inward vapour drive wetting, and all exhibited cavity air moisture contents of 6 to 7 g/m^3 (50 to 60%) more than the exterior air (which averaged 9.1 g/m^3) over the entire period. For shorter periods, the difference could be even larger. On a daily-average basis, for example, wall RE exhibited

an excess of at least 15 g/m^3 for several days. On an hourly basis, excess values of 30 or more frequently occurred during solar heating. In winter the amount of moisture in the cavity air had normally dropped to close to that in the exterior air, just as in the ventilated, partially-filled walls.

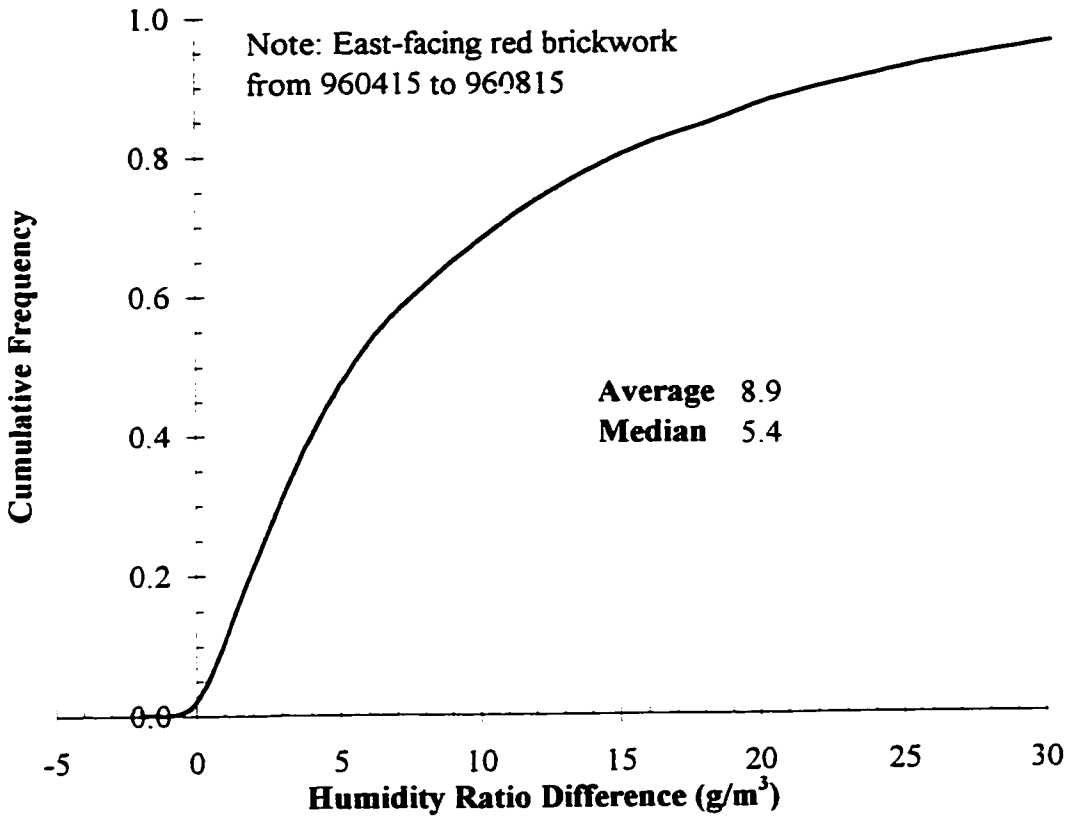

Figure 9.25: Maximum possible moisture content excess for vented brick veneer wall

The B walls exhibited large daily variations in air space moisture content. Typically the moisture content of the air in the cavity would surge above the exterior (about double the exterior value in summer) for several hours as solar heating drove vapour from the brickwork (Figure 9.26). As the wall cooled it would adsorb water, dragging the moisture content of the cavity down, sometimes below that of the exterior. The filled cavity walls behaved in the same way, except that the amount of moisture in the air was almost twice that in the B wall and the moisture content never dropped to that in the exterior air (Figure 9.27).

The plot of the calculated saturation moisture at the poly shows that condensation could often occur on the poly, i.e., inward vapour drive wetting was occurring. The wood

framing in Wall RE became quite wet during the summer, peaking at approximately 45%. The moisture content of the framing in Wall BE peaked at 12%.

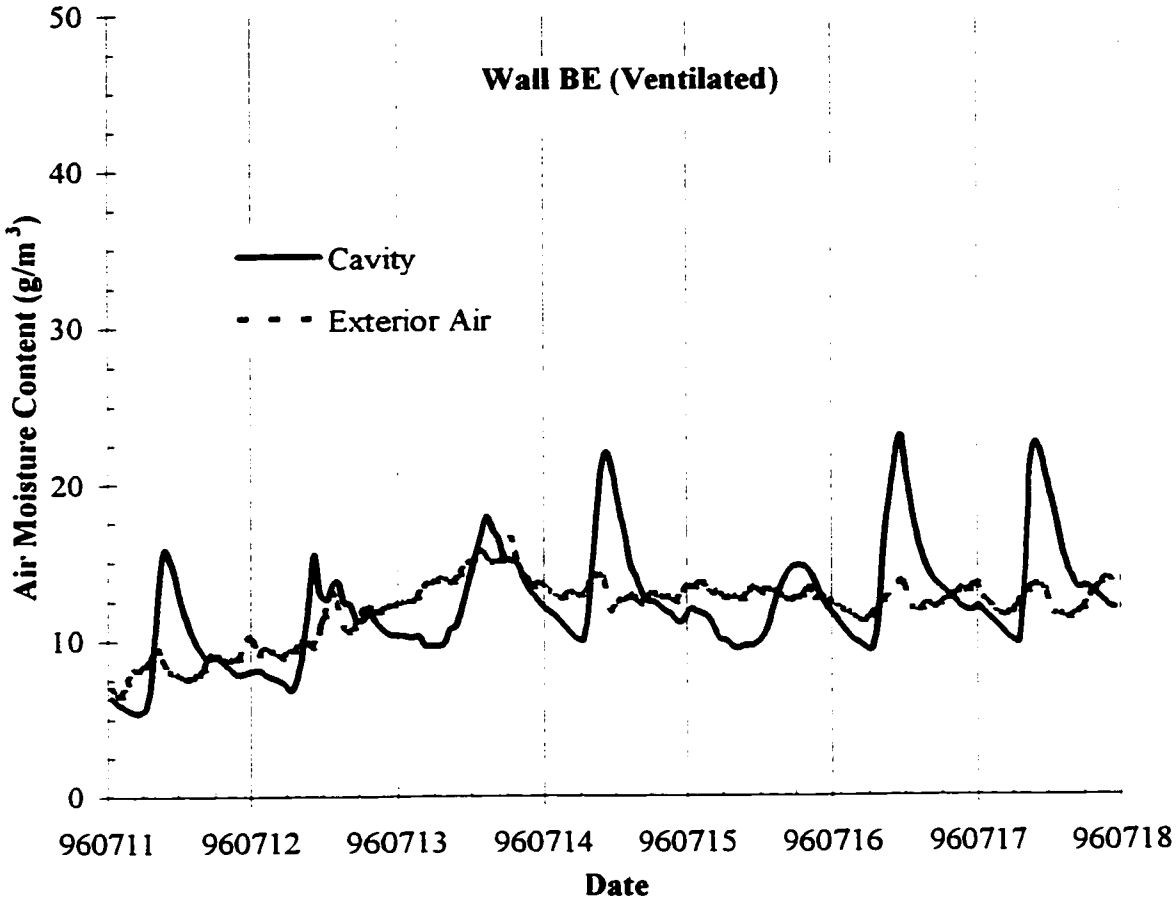

Figure 9.26: Air space moisture content for a vented brick veneer over a representative summer week

The EIFS wall acted as a vented (i.e., the moisture content of the air in the cavity followed that of the exterior even though there was no ventilation flow) and drained filled-cavity wall with a non-absorbent and water-impermeable screen. The RH in the filled cavity of these EIFS walls followed a sinusoidal variation, with a minimum RH in the winter (about 45% RH) and a peak (of about 80%) in the late summer / early fall. This RH variation is due to the variation in the temperature at the middle of the filled-cavity insulation. The absolute moisture content of the air in the mineral wool behind the screen was usually lower than that in the exterior but often varied above the exterior for short periods of time. Note that panel EE had a slightly cracked lamina (caused by vandalism) from late 1995 onward. The presence of this circular (about 70 mm diameter), approximately 0.1

mm wide crack did not have any noticeable affect on the moisture in the mineral fibre insulation.

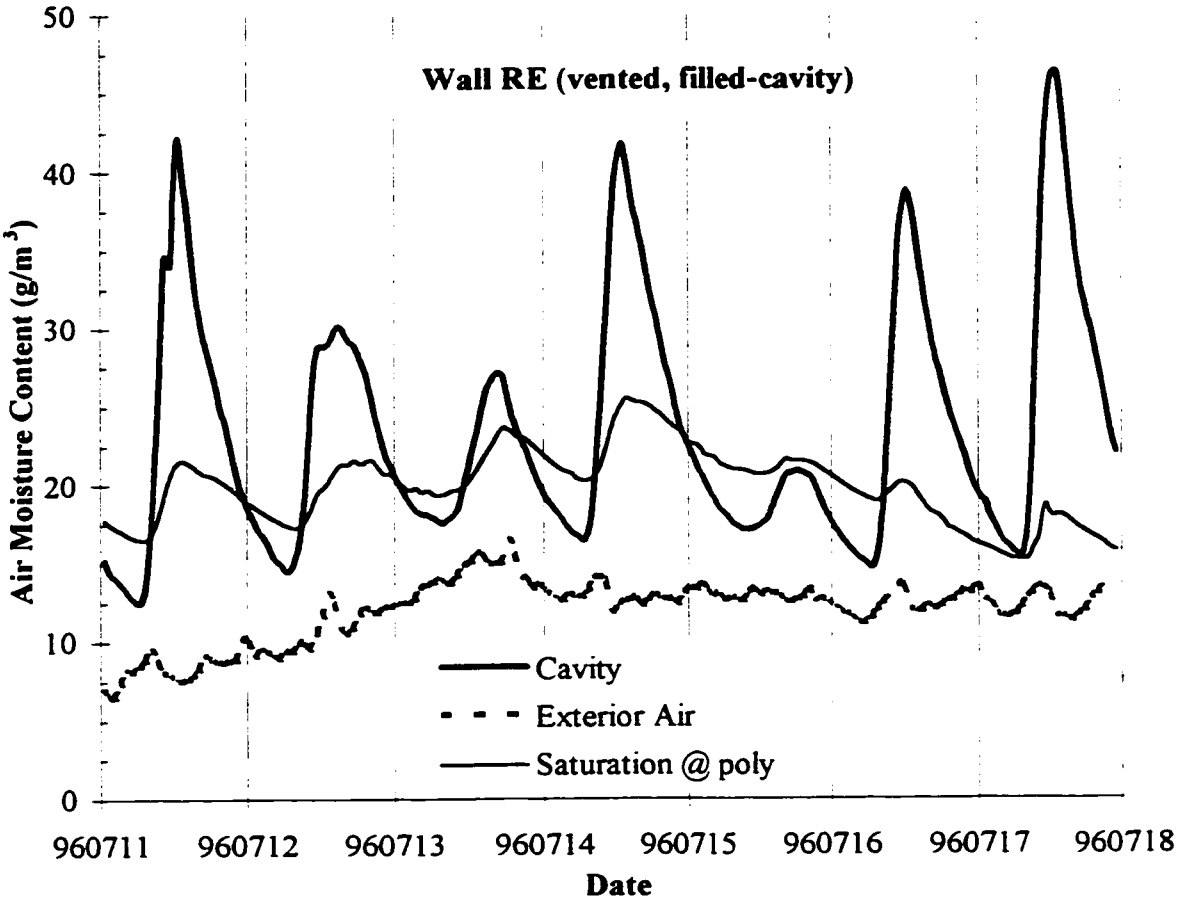

Figure 9.27: Cavity air moisture content for a filled-cavity brick veneer over a representative summer week

Figure 9.28 plots the framing moisture content of two different east-facing brick veneer panels (Walls FE and BE) over the period of a year. The line labelled "vented" is for 1996, and that labelled "unvented" is for 1997. The plot of wall panel BE is for 1997 (1996 was essentially the same). During the summer of 1996 the moisture content of the vented Wall FE climbed to almost 15%. This is not a dangerous level, but clearly shows that a small amount of summertime inward vapour drive wetting could occur in the Wall FE. Wall BE exhibited no such wetting because of the relatively vapour resistant exterior sheathing (EXPS). It is clear that sealing the vent openings on June 1, 1997 (Day 211)

had a significant impact on the moisture content of Wall A. This wetting was further investigated.

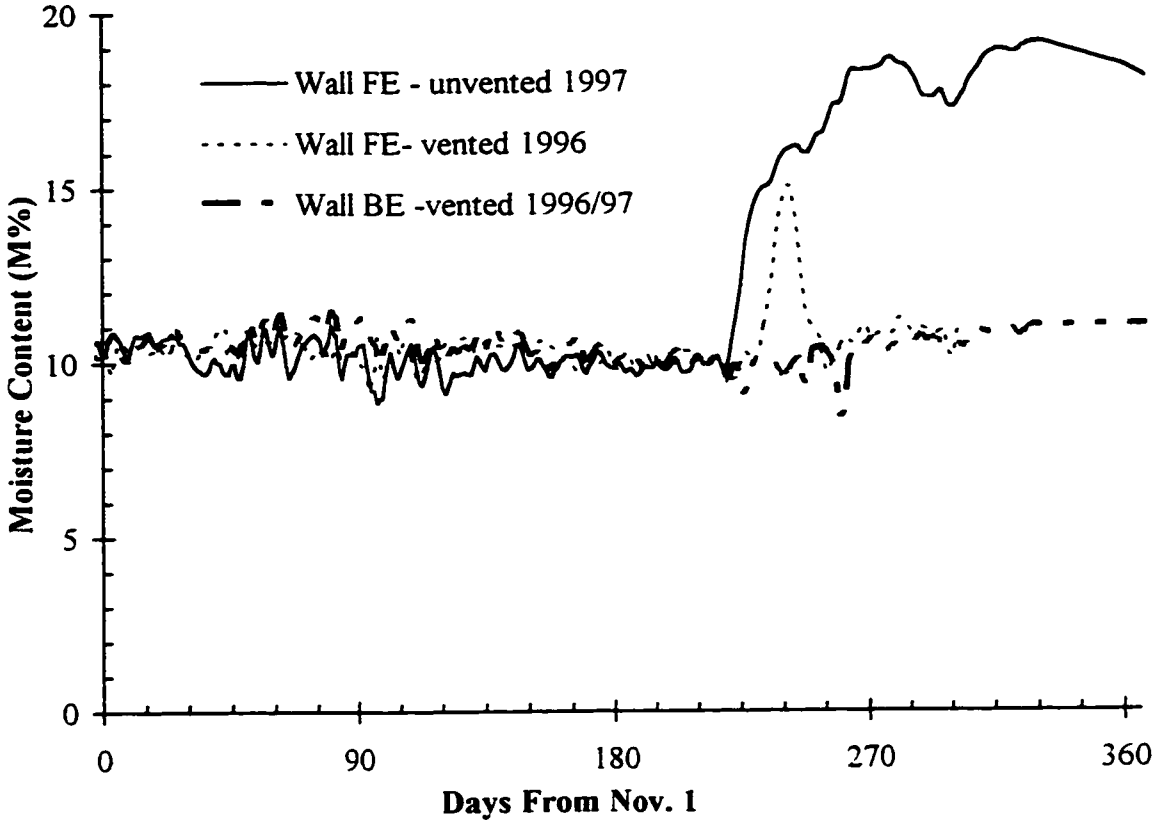

Figure 9.28: Framing moisture content vs. time

The temperature and relative humidity measurements within the wall cavities were used to calculate the moisture content of the air. Over the summer period, the average moisture content of the exterior air in 1996 was 9.6 g/m^3. Over the summer period in 1997, the average exterior air content was 9.1 g/m^3. The average moisture content of the air in the airspace of the well-vented Wall FE was 10.9 g/m^3: about 1.3 g/m^3 higher than the exterior. During the following summer when Wall FE was unvented, the moisture content in the airspace was 13.1 g/m^3, 4 g/m^3 or 44% above the exterior. The well-vented east-facing Wall BE acted as a control specimen. Its air space moisture content was 1.0 g/m^3 (11%) above the exterior during the same period of 1996, and had a moisture excess of only 0.41 g/m^3 during 1997.

Figure 9.29 compares the moisture content of the air in the studspace, air space, and exterior over a typical week during July for Wall FE when it was vented (1996) and when

it was unvented (1997). The moisture content in the air space is clearly much more closely coupled to the exterior in the vented case than the unvented case. Water vapour that is driven off hygroscopic materials, especially the brickwork, by solar heating enters the cavity air, but is unable to leave by ventilation in the unvented wall.

The close correlation of the studspace and air space moisture contents in both the unvented and vented case indicate that the veneer is acting somewhat like an exterior vapour barrier and that the gypsum sheathing is not controlling the flow of vapour from the air space to studspace. The high air moisture contents in the studspace of the unvented wall show that condensation because of inward vapour drives is often occurring.

These plots demonstrate both how ventilation can promote drying, and how it can prevent wetting from inward vapour drives in the summer.

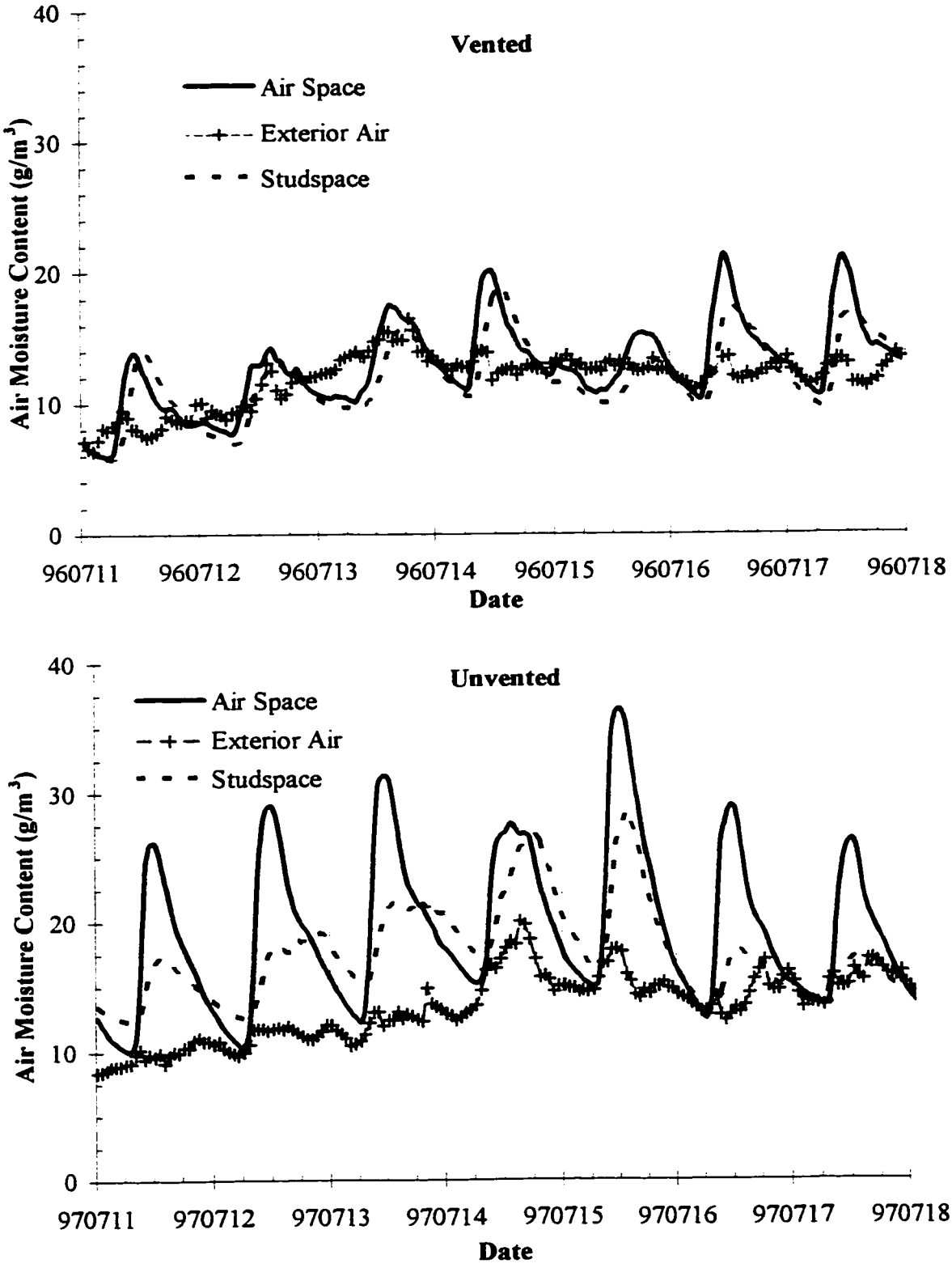

Figure 9.29: Hourly moisture content of Wall FE - vented vs. unvented

9.11 Conclusions

This chapter has undertaken a detailed review of ventilation research, developed theory to approximate both ventilation flow and ventilation drying, and presented field and laboratory data that demonstrate the potential for ventilation drying. The following paragraphs summarise the conclusions developed throughout the chapter.

Ventilation is primarily driven by a combination of wind pressures and thermal buoyancy. The provision of vent openings at the top and bottom of the cavity will generally allow the most ventilation by these mechanisms. Field monitoring showed that wind pressures driving ventilation can be expected to be in the order of 1 Pascal. The flow behind brick veneers generated by these pressures will be in the order of 0.1 to 1.0 litre per second per m^2. Panel systems can easily achieve useful levels of ventilation flow. Normal amounts of ventilation will not provide cooling benefits in brick veneer walls, although some small amount of cooling may be generated by very well ventilated cladding systems.

In normal walls, the ventilation drying rate will be governed by the ventilation flow rate, not the ability for wet materials to evaporate moisture into the air space. Solar heating greatly affects the potential for ventilation drying, by increasing both the thermal buoyancy and the moisture carrying capacity of the air. Ventilation flows can be expected to remove from 10 to 1000 $g/m^2/day$ of moisture from saturated materials behind the cladding, depending on the exterior environment.

Full-scale testing has shown that standard (10 x 65 x 90 deep) open head joints in masonry veneers can be considered to behave as orifices with a flow coefficient of approximately 0.65 and a flow exponent of 0.55. All of the commercially available masonry veneer vent inserts tested greatly restricted flow, some by an order of magnitude.

Although ventilation drying can be recommended as a design strategy, the current practise for brick veneers does not reliably ensure a significant amount of ventilation. To achieve the full benefit of ventilation drying, more vent area and clear air spaces must be specified. Air space widths of 40 to 50 mm are likely required to prevent blockage and thus ensure flow. Those commercially available vent inserts tested provide too much flow resistance to be practical. The use of open head joints at 600 mm centres, top and bottom, and air spaces of over 40 mm should be considered the minimum level of venting required to provide measurable benefit to brick veneer walls.

9.12 References

[9.1] ASHRAE, 1997. *1997 ASHRAE Handbook - Fundamentals*, Atlanta: American Society of Heating Refrigerating, and Air-Conditioning Engineers, Inc.

[9.2] *Condensation*. Building Research Establishment Digest No. 110, HMSO, London, 1972.

[9.3] *British Standard 5250:1989 Control of Condensation in Buildings*, British Standards Institute, London, 1989.

[9.4] Salonvaara, M., and Karagiozis, A.N., "The Influence of Waterproof Coating on the Hygrothermal Perfromance of a Brick Facade Wall System", Water Leakage Through Building Facades, ASTM STP 1314, R.J. Kudder and J.L. Erdly, Eds., ASTM 1998, pp. 295-311.

[9.5] *Technical Guide for Exterior Insulation and Finish Systems Class PB*. Canadian Construction Materials Center, Ottawa, 1996.

[9.6] *National Building Code of Canada 1990*, National Research Council of Canada, Ottawa, 1990.

[9.7] CAN3-A371-M84 *Masonry Construction for Buildings*, Canadian Standards Association, Rexdale, 1984.

[9.8] ACI 530-95/ASCE-95/TMS 402-95 *Building Code Requirements for Masonry Structures*, The Masonry Society, 1995.

[9.9] *Brick Masonry Rain Screen Walls*. Technical Note No. 27 (revised), Brick Institute of America, Reston, Virginia, August 1994.

[9.10] DIN 1053 *Mauerwerk*, Feb., 1990.

[9.11] DIN 18 515 *Aussenwandbekleidung*, Apr. 1993.

[9.12] DIN 18 516 *Aussenwandbekleidung, hinterlueftet*, Jan. 1990.

[9.13] DIN 4108 *Waermeschutz in Hochbau, Teil 3: Klimabedingter Feuchteschutz*, August 1981, *Teil 4, Waerme- und Feuchteschutztechnische Kennwerte*, Nov, 1991, and *Teil 5, Berechnungsverfahren*, Aug 1981.

[9.14] Liersch, K.W., *Belüftete Dach- und Wandkonstruktionen: Bauphysikalische Grundlagen des Wärme- and Feuchteschutzes* , Bauverlag, Berlin, 1981.

[9.15] Lohmeyer, G. *Praktische Bauphysik*, B.G. Teubner, Stuttgart, 1995.

[9.16] Hens, H., *Bouwfysica 1: Warme- En Massatransport*. Leuven, Belgium, 1992.

[9.17] Guy, R.W. and Stathopoulus, T., "Mechanisms of Pressure Differences Across Building Facades," *First Annual Conference on Building Science*, London, Ont., March 4-5, 1982.

[9.18] Popp, W., Mayer, E., Künzel, H., "Untersuchungen über die Belüftung des Luftraumes hinter vorgesetzten Fassadenbekleidung aus kleinformatigen Elementen", Fraunhofer Institut für Bauphysik, Forschungsbericht B Ho 22/80, April, 1980.

[9.19] Mayer, E., Künzel, H., "Untersuchungen über die notwendige Hinterlüftung an Außenwandbekeidung aus großformatigen Bauteilen," Fraunhofer Institut für Bauphysik, Forschungsbericht B Ho 1/83, March, 1983.

[9.20] Künzel, H., Mayer, E., "Untersuchung über die notwendige Hinterlüftung an Außenwandbekeidung aus großformatigen Bauteilen", Schriftenreihe Bundesminister für Raumordnung, Bauwesen, und Städtebau, 3/1983.

[9.21] Schwarz, B., "Witterungsbeansphruchung von Hochhausfassaden," *HLH* Bd. 24, Nr. 12, pp. 376-384, 1973.

[9.22] Uvsløkk, S., "The Importance of Wind Barriers for Insulated Wood Frame Constructions," *Proc. of Symposium and Day of Building Physics*, Lund University, August 24-27, 1987, Swedish Council for Building Research, 1988, pp. 262-267.

[9.23] *Research of the Natural Ventilation Behind, and Condensation On, Trespa Volkern Facade Siding*, Report E108-1, Akoestisch Advies Bureau Peutz & Associes B.V., Netherlands, Jan., 1984.

[9.24] Sandin, K., *Skalmurskonstruktionens fukt- och temperaturbetingelser*. Rapport R43:1991 Byggforskningsrådet, Stockholm, Sweden, 1991.

[9.25] Sandin, K., "Moisture Conditions in Cavity Walls With Wooden Framework", *Building Research and Information*, Vol. 21, No. 4, 1993, pp. 235-238.

[9.26] Sandin, K., "Temperature and Moisture Conditions in Cavity Walls," *CIB W67 Symposium on Energy Moisture and Climate in Buildings*, Rotterdam, Netherlands, September 3-6, 1990.

[9.27] Künzel, H., Mayer, E., *Wärme- und Regenschutz bei zweischaligem Sichtmauerwerk mit Kerndämmung*. BMFT-Forschungbericht T84-191, 1984.

[9.28] Jung, E. "Dauerstandverhalten von Verblendziegelmauerwerk unter Witterunsbeansphruchung und Auswirkungen von Kerndämm-Maßnahmen, " *Baustoffindustrie*, No. 6, November, 1985, pp. 185-188.

[9.29] Hens, H., *Buitenwandoplossingen voor de residentiële bouw:De Spouwmuur*, Laboratorium voor Bouwfysica, Katholieke Universiteit, Leuven, Belgium, 1984.

[9.30] Hens, H., Fatin, A., "Heat-Air-Moisture Design of Masonry Cavity Walls: Theoretical and Experimental Results and Practice", *ASHRAE Tansactions: Symposia*, CH-95-3-2, pp. 607-626, 1995.

[9.31] Skerlj, P. , Surry, D., *A Study of the Mean Pressure Gradients, Mean Cavity Pressures, and Resulting Residual Mean Pressures across a Rainscreen for a Representative Building*, Final Report BLWT-SS23-1994, Faculty of Engineering Science, University of Western Ontario, London, September, 1994.

[9.32] Lin, J.X., Surry, D., Inculet, D.R., *A Study of the Characteristic Shapes of Mean Pressures and Their Gradients on Buildings in Realistic Surroundings*, Report BLWT-SS3-1995, Faculty of Engineering Science, University of Western Ontario, London, March, 1995.

[9.33] Kays, W.M., and Crawford, M.E., *Convective Heat and Mass Transfer*. McGraw-Hill, New York, 1980.

[9.34] Wolf, H., *Heat Transfer*. Harper and Row, New York, 1983.

[9.35] Duffie, J. and Beckman, W., *Solar Engineering of Thermal Processes*, John Wiley & Sons, 1980.

[9.36] Streeter, V, Wylie, E., *Fluid Mechanics*, 8th ed. McGraw-Hill, New York, 1985.

[9.37] Baker, P.H., Sharples, S., Ward, I.C., "Air Flow Through Cracks," *Building & Environment*, Vol. 22, No. 4, 1987, pp. 293-304.
[9.38] Etheridge, D.W., "Crack Flow Equations and Scale Effects," *Building & Environment*, Vol. 12, 1977, pp. 181-189.
[9.39] Liddament, M.W., "Power Law Rules - OK?" *Air Infiltration Review*, Vol. 8, No. 2, February 1987, pp. 4-6.
[9.40] Etheridge, D.W.,"The Rule of the Power Law - an Alternative View," Correspondence in *Air Infiltration Review*, Vol. 8, No. 4, August 1987, pp. 4-5.
[9.41] Miller, R.W. *Flow Measurement Engineering Handbook.* McGraw-Hill, New York, 1989.
[9.42] ISO Standard 5167-1980. *Measurement of fluid flow by means of orifice plates, nozzles and venturi tubes inserted in curcular cross-section conduits running full.* ISO, Switzerland, 1980.
[9.43] Lichtarowicz, A., Duggins, R.K., Markland, E., "Discharge Coefficients for Incompressible Non-Cavitating Flow Through Long Orifices," *J. Mechanical Engineering Science*, Vol. 7, No. 2, 1965, pp. 210 - 219.
[9.44] Lawson, T.V., *Wind Effects on Buildings, Volume 1: Design Applications.* Applied Science Publishers, London, 1980.
[9.45] Aynsley, R.M., Melbourne, W., and Vickery, B.J., *Architectural Aerodynamics.* Applied Science Publishers, London, 1977, p.98.
[9.46] Crommelin, R.D., Vrins, E.M.H., "Ventilation Through a Single Opening in a Scale Model," *Air Infiltration Review*, Vol. 9, No. 3, May 1989, pp. 11-13.
[9.47] Rao, J. and Haghighat, F, "Wind-Induced Fluctuating Airflow in Buildings", *Proc. 12th AIVC Conference*, Ottawa, September 1991, pp. 111-121.
[9.48] Kronvall, J., *Air Flows in Building Components.* Doctoral Dissertation, Lund University, Lund, Sweden, 1980.
[9.49] White, F., *Viscous Fluid Flow*, 2nd ed. McGraw-Hill, New York, 1991.
[9.50] Forest, T.W., and Walker, I., *Attic Ventilation and Moisture,* Univ. of Alta report for CMHC, Ottawa, March, 1993.

10. CONCLUSIONS

The control of moisture in above-grade enclosure walls has been comprehensively investigated in this thesis. The moisture balance of wetting, storage, and drying has been used as a framework, but emphasis was given to driving rain deposition, rain penetration control, ventilation drying, and pressure moderation. Because of the prevalence and popularity of brick veneer cladding, wall systems of this type have been a focus for much of the work.

The most important and general conclusions will be briefly repeated here.

Driving Rain

A relatively simple procedure for predicting driving rain in the wind was developed and validated with field measurements. It was shown the driving rain varied linearly with windspeed, rainfall, and a non-linear rainfall-intensity-dependent factor (termed the Driving Rain Factor). The seasonal and directional variation of driving rain was examined, as was the distribution of intensity and rain event duration. This site-specific analysis showed that the amount of driving rain can vary significantly (by a factor of ten) for different orientations, that the intensity is often less than 5 $kg/m^2/hr$, and that the duration of a rain event is usually between 4 and 20 hours.

Rain Wetting of Walls

The application of another factor (termed the Rain Admittance Factor, RAF) allowed the rain deposition on the test building to be estimated. Interpretation of other researchers' results supports the contention that this approach can be used for other building sizes and shapes in other climates. Results from a tall building strongly suggest that the RAF can be scaled for different building heights if the variation of wind speed with height is accounted for. It is recommended that more field monitoring and computer modelling be conducted to develop a database of Rain Admittance Factors for different building shapes and sizes.

Controlling Rain Penetration

A rain control theory was developed which led to a useful enclosure classification system. This theory is generally applicable because it is based on the physical processes of rain water movement (storage, drainage, transmission), not on building tradition, design intent,

or climate. Study of cladding response resulted in the conclusion that rain absorption and storage by the cladding can change the response, the possibility of rain penetration, and the need for drainage.

Pressure Moderation

Frequency domain analysis methods have been proved to be a repeatable and useful means of analysing pressure moderation performance. The extensive dynamic field pressure measurements showed that instantaneous pressure equalisation does not occur. The degree of pressure moderation achieved is limited by dynamic spatial wind pressure variations in wall systems with large compartments; in the walls tested, a well-built 1.2m x 2.4m panel was found to moderate only 50% of the dynamic pressures at 1 Hz. Computer and analytical models based on the compressibility of air greatly over-estimate dynamic pressure moderation because they do not account for spatial pressure variations. The amount of venting and the quality of the air barrier were shown to be the most important wall characteristics affecting pressure moderation.

Controlled laboratory tests showed that realistic air pressure differences do not greatly increase the rain permeance of brick veneers and, just as significantly, that all brick veneers should be expected to be water permeable. Therefore, it was concluded that pressure moderation is not an important or highly effective mechanism for controlling rain penetration strategy for most walls, especially brick veneers. Venting walls, as current good practise requires, does provide useful moderation of average wind pressures, and is a useful feature. Drainage should always be provided in veneer walls unless a climate- and exposure-appropriate amount of moisture storage is provided (i.e., a mass wall).

Preliminary results indicate that the combined static and dynamic pressure moderation reduced the structural loads acting on the brick veneer of the test panels under pressures from wind directions normal to the panel. Much more work needs to be done to quantify the potential load reductions under glancing wind directions (which generally govern design).

Ventilation and Ventilation Drying

A significant amount of potentially damaging moisture that cannot be removed by drainage will be stored in screened-drained walls, especially those constructed of absorbent materials. This stored moisture may cause performance and durability problems if not removed, and can also cause wetting of inner enclosure layers if transported inward by

solar-driven vapour diffusion. Several of the test panels, all of which had restricted ventilation capacity, exhibited serious summer condensation wetting by this mechanism. These conclusions are valid for all absorbent cladding materials, e.g., brick, stucco, and wood, and are especially significant for air-conditioned buildings. Ventilation is one means of controlling this wetting mechanism, appropriate vapour resistance behind the cladding and on the exterior of the insulation is another.

Ventilation flow and ventilation drying of walls were studied in depth with the aid of available physics. Both calculations and the review of previous research suggest that beneficial ventilation drying can be realised if sufficient venting is provided.

The concept of equivalent vapour permeance was introduced as a simple aid for the approximate prediction of ventilation drying. The use of equivalent vapour permeance allows designers and analysts to easily approximate the potential magnitude of ventilation drying. It was concluded that the sun and wind have a large and beneficial influence on ventilation drying; their effect must be accounted for in any assessment of ventilation drying.

The field measurement of wind pressures, air space moisture contents, and temperatures behind brick veneers demonstrate the importance of ventilation both as a drying mechanism and as a means of resisting inward vapour drive wetting. In general, current brick veneer construction practise does not fully develop the potential benefits of ventilation drying. More venting and clear air spaces are required to fully exploit the potential benefits.

Appendix A: Construction and Instrumentation Details

Natural Exposure Test Facility Description

Test Panel Description

Instrumentation and Construction Details

Timetable of Events

A1. THE BEGHUT

A1.1 Introduction

This chapter begins with a description of the natural exposure and test facility, the Beghut, in which the panels are installed. The design and instrumentation of the Beghut are described in Section A3.2.

A1.2 Beghut Design and Details

Sections A3.2.1 and A3.2.2 describe the design and instrumentation of the natural exposure and test facility into which the test panels were installed.

A1.2.1 Description of Beghut

The Building Engineering Group's outdoor full-scale permanent natural exposure, test and demonstration facility is known as the Beghut. The facility, which is located on the University of Waterloo campus, is a square building approximately 10.5 x 10.5 m (34.5 x 34.5') in plan and 3.0 m (9'-10") high floor to ceiling. The walls are oriented in the four cardinal directions. The roof is peaked to the centre with a slope of 1-in-3. A pipe mast rising from the central peak of the roof supports a weather station at 10 m (34'-6") above grade. A second weather station is located 10.0 m (34'-6") from the centre of the west wall at 3.5 m (11'-6") above grade.

An air-to-air heat pump heating and cooling unit, and supplementary humidification units maintain the interior climate at 21 °C and 50% relative humidity. A floor-mounted air distribution system is used to distribute the conditioned air evenly. Four symmetrically mounted ceiling fans are used to prevent vertical and horizontal stagnation.

The structure is of wood post-and-beam construction with a trussed roof. The foundation is a 1.2 m (4') high, 250 mm (10") thick unreinforced concrete wall on a 500 mm (20") wide, 300 mm (12") deep strip footing. The floor consists of a 100 mm (4") thick concrete slab-on-grade placed on a polyethylene moisture barrier and 150 mm (6") of granular fill. The corner columns and ring beam are sheathed with plywood, insulated with 150 mm (6") fibreglass batts, and clad with aluminum siding. The roof system comprises asphalt shingles, building paper, and plywood sheathing, with an additional ice

and water shield extending 600 mm (24") up from the eaves. A construction plan of the Beghut is provided in Figure 3.2.

The roof overhang (200 mm) is sized to prevent shading from the sun under most conditions. The small overhang and the drip-edge in lieu of eavestroughs provides very little direct protection from rainfall.

The post-and-beam method of framing allows for installation of seven test panels in each side (28 total) of approximately 1.2 m (4') wide by 2.4 m (8') in height. This project uses 27 of the wall panel spaces. The last space is reserved for the door, currently on the north side of the building. Figure 3.2 shows the location of each of the panels in the Beghut.

The test hut is sited on relatively flat land and is fully exposed to winds from most directions. A two-storey office building located approximately 30 m (100') to the north-west and a four-storey office building located about 120 m (400') to the west provide some shelter from these directions.

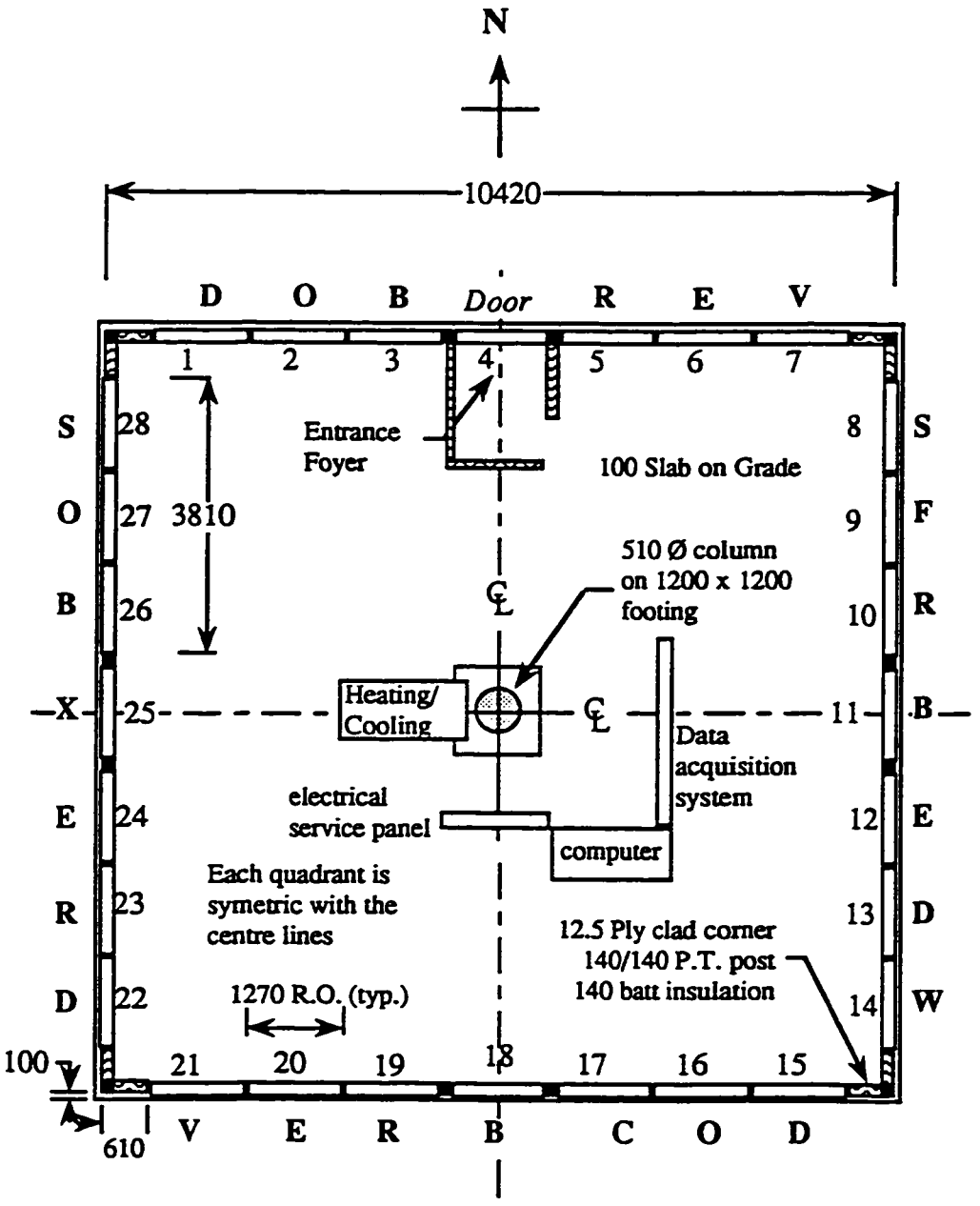

Note: All dimensions in mm

Figure A1.1 - Plan of the Beghut

A1.2.2 Exterior Environmental Instrumentation

The locations of sensors on the weather stations and elevations of the Beghut are illustrated in Figure 3.3.

The weather station on top of the Beghut has instrumentation to measure wind speed and direction, exterior temperature, exterior RH, horizontal solar radiation, and rainfall. The wind speed and direction are measured at the meteorological standard height of 10 m above grade. The instruments include:

- A Young™ Model 05103 Wind Monitor measures horizontal wind speed and wind direction through a propeller mounted on the front of a vane. The monitor provides a linear DC voltage proportional to direction and linearly increasing magnitude AC voltage as wind speed increases. The instrument has a speed range from 1.0 m/s to 50 m/s with a distance constant of 2.7 m for 63% recovery (this means that in a 2.7 m/s wind, 63% of an instantaneous wind speed change will be measured within 1 second). The direction is accurate to within 5 degrees in wind speeds over 1.5 m/s.

- A Vaisala™ HMP 35A with integral solar radiation and precipitation shield is used to measure relative humidity and temperature. To measure RH, the instrument uses a HUMICAP® sensor and a platinum Pt 100 RTD. The RH sensor has a range of 0 to 100% RH with an accuracy of approximately ±2% RH and repeatability of better than 1% RH per year. The humidity sensor produces a linearly-varying output in the range of 0 to 1 volt DC which is directly measured by the hardware and calculated as RH by the software. The temperature sensor varies in resistance at about 0.38 Ohms/°C; the voltage drop of a small current flow across this resistance is measured and converted into a temperature value by the software.

- The incident horizontal solar radiation is measured by an Eppley™ pyranometer. The calibration accounts for the international standard solar spectrum and measures +/- 105 degrees from vertical. This device, recently calibrated by the Atmospheric Environment Service, generates a small voltage signal proportional to the solar radiation.

- A Rimco™ tipping bucket rain gauge is used to measure horizontal rainfall. The collector is a meteorological standard 8" diameter funnel, plated with gold to reduce surface tension effects. The bucket tips once for each 0.2 mm of rainfall. The

resulting electrical pulse is measured by a dedicated counter chip. Because the gauge is mounted more than 15 feet off the ground, the catch is reduced by wind effects. According to Grey's Handbook of Hydrology, a 10% increase was used to allow for true catch at grade level.

A second weather station is located 10 m (34'-6") from the center of the west wall of the Beghut. This second weather station has instruments to measure wind speed, wind direction and driving rain. These instruments include:

- The Mamac Systems™ Model WE-105-2 Wind Speed and Direction transducer comprises a 400 mm (16") long vane attached to a potentiometer and a three cup anemometer driving a generator. The wind speed range is from 0.5 to 44.4 m/s (0 to 100 miles per hour) and direction ranges from 0 to 360 degrees within 5 degrees.

- A driving rain collector similar in design to those mounted on the walls faces due west. A modified tipping bucket rain gauge (by Jarek™) provides a pulse output for every 0.226 liters per square meter of driving rain collected.

Several instruments are mounted on the walls of the Beghut to measure driving rain on each face. Driving rain is not typically measured and standard instruments are not available. A driving rain collector was developed and 15 have been manufactured and installed. The collector is approximately 200 mm in diameter and made of PVC. The collected water is directed to a 38 mm diameter pipe and the hydraulic pressure head is measured by a pressure transducer, recorded by the data acquisition system during every scan. Figure A1.2 provides more details of the driving rain gauge. Figure A1.3 indicated the location of these gauges on the Beghut.

A1.2.3 Interior Environmental Instrumentation

The interior environment is measured by a Vaisala™ HMP 35A RH transducer accurate to +/- 2%RH. The sensor is located near the middle of the Beghut at a height of 1.8 m above the floor. A 3000 Ohm YSI™ thermistor, accurate to within 0.2 °C, measures the interior temperature. The temperature sensor is located near the RH sensor.

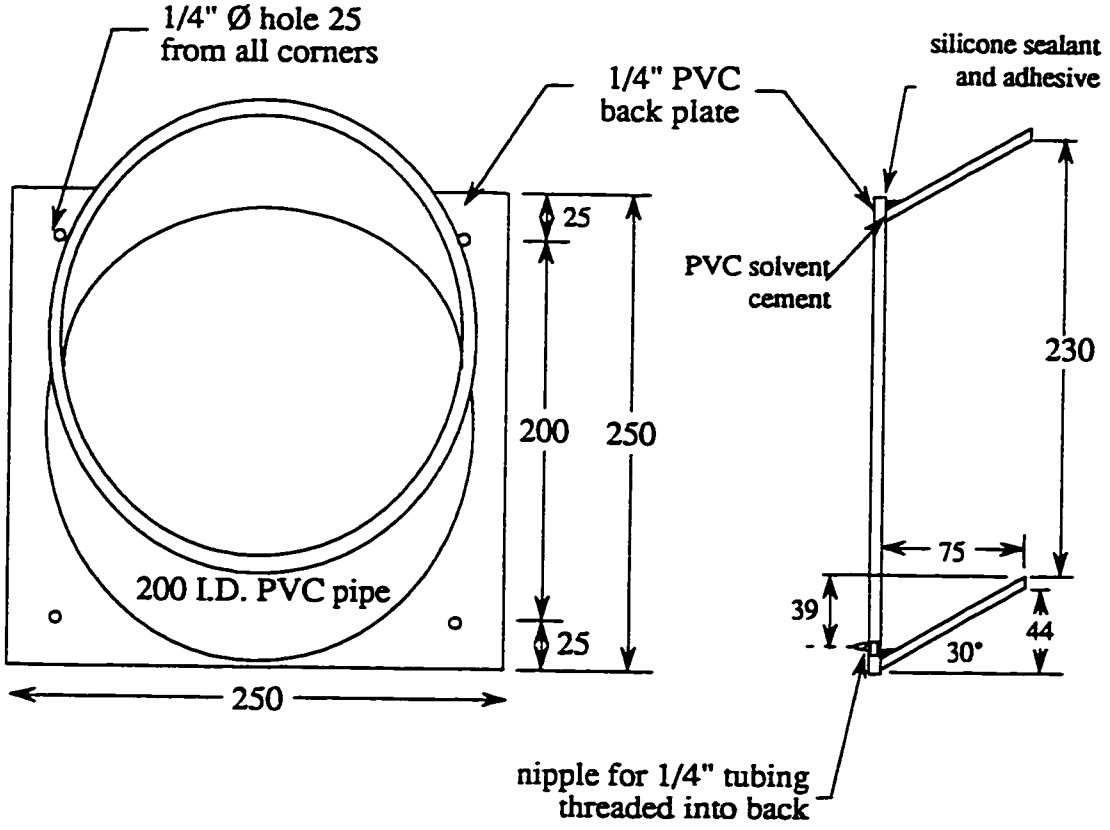

Figure A1.2 -Driving Rain Gauge

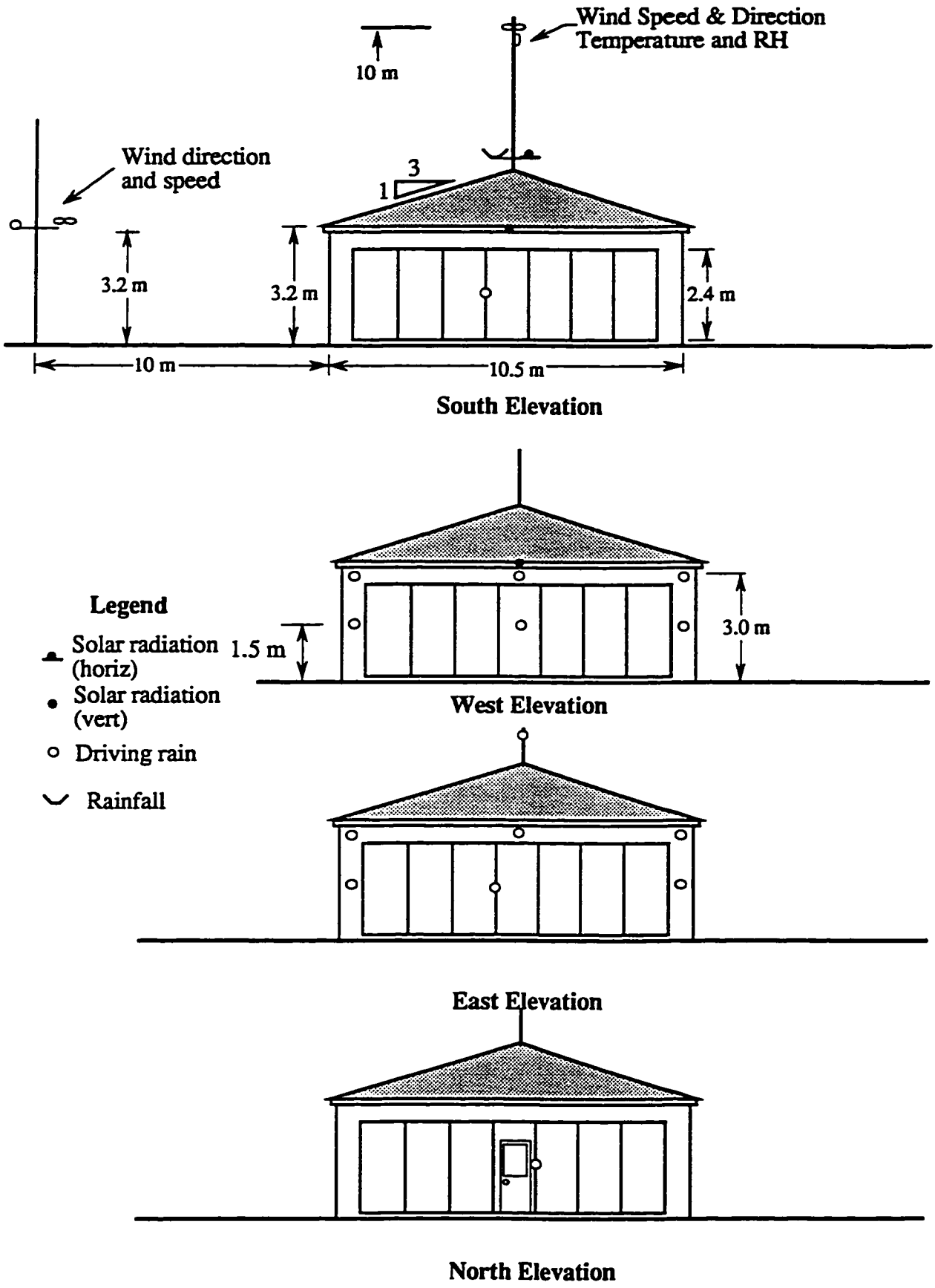

Figure A1.3 - Location of meteorological sensors on Beghut

A2. WALL PANEL DESIGN, DETAILS & INSTRUMENTATION

This chapter comprises ten similar sections, one for each of the different wall systems plus sections for the mockup veneers built in the lab and the Beghut. Each section is similar in structure and intent. The design, construction and instrumentation details for each wall system are discussed along with a brief explanation of the design and construction details that make each wall type unique. All of the wall systems were designed / developed with the full participation and involvement of each sponsor.

Construction and installation procedures typical of all of the walls are presented in Section A3. Section A4 outlines the instrumentation procedure and provides specific details for each type of instrument installed in the test panels.

For convenience, the wall panel descriptions and drawings are summarized in Table A2.1.

Wall System Code	Description (Section)	Horizontal Section (Figure)	Vertical Section (Figure)	Instrumentation Isometric (Figure)
R	A2.1	A2.R1	A2.R2	A2.R4
V	A2.2	A2.V1	A2.V2	A2.V4
O	A2.3	A2.O1	A2.O2	A2.O4
F	A2.4	A2.F1	A2.F2	A2.F4
W	A2.5	A2.W1	A2.W2	A2.W4
D	A2.6	A2.D1	A2.D2	A2.D4
C	A2.7	A2.C1	A2.C2	A2.C4
E	A2.8	A2.E1	A2.E2	A2.E4
B	A2.9	A2.B1	A2.B2	A2.B4
S	A2.10	A2.S1	A2.S2	A2.S4
X	A2.11		A2.X1	

Table A2.1 - Wall system descriptions and drawings

A2.1 Roxul R Panels

The R panel is a wood framed, brick veneer, filled-cavity wall assembly intended for use in low-rise residential buildings. The assembly is typical of current residential construction practice except that the cavity behind the exterior brick veneer has been filled with a draining insulation. A single layer of Typar™ is positioned and sealed directly at the inner face of the cavity to act as a wind and water barrier and a secondary air barrier. From the inside, the wall consists of (Figure A.R1):

- taped and painted 13 mm (1/2") drywall,
- 0.15 mm (0.006") polyethylene vapour barrier,
- 38 x 89 mm (2 x 4" nom.) wood framing (see Section A3.1),
- Roxul Flexi-batt™ insulation in the stud space (R 13),
- a single layer of Typar™ housewrap, sealed with sheathing tape,
- a nominal 60 mm (2-3/8") wide vented cavity occupied by 50 mm (2") of Roxul RXL 20™, used as an insulating and draining cavity fill,
- a finger space of not more than 10 mm (3/8"), and
- an 85 mm (3-3/8") brick veneer screen with vents and weep holes (see Section A3.3).

Construction of the wood stud frames for the R panels was carried out in the laboratory as described in Section A4.1. Only materials which are specific to the R panels are discussed in this section. Refer to Section A3.1 for the construction of the typical wall panel frame. The R wall panels were completed in the following sequence:

1. The Typar™ housewrap was installed on the exterior of the frame using 10 mm (3/8") staples at 200 mm (8") spacing. Sheathing tape was carefully applied to seal the housewrap to the sides of the panel to prevent leakage around the edges.

2. The standard 600 mm (24") high pieces of Roxul RXL 20™ insulation were cut to 405 or 810 mm (16 or 32") in length, and the vertical joints were staggered over the studs (see Figure A.R3). This was done in order to ensure representative jointing. The Roxul RXL 20™ was temporarily fastened with plastic-headed nails to prevent the insulation from falling out prior to the installation of the brick ties.

3. The wall was transported to the Beghut and installed using the procedure outlined in Section A3.2.

4. The brick veneer was installed as described in Section A3.3.

The design of the R wall was developed in conjunction with Roxul. RXL 20, a fibrous rock wool insulation, was used as the draining and insulating cavity fill because of its relatively lower cost and greater air and water permeability. A list of some of the physical properties of RXL 20 are listed in Table A.R1.

	Metric	Imperial
Dimensions (as delivered)	50 x 610 x 1220 mm	2 x 24 x 48"
Thermal resistance (ASTM-C518)	RSI = 1.44 $m^2 \cdot °C/W$	R = 8.2 H °F ft^2 / BTU
Density (ASTM-C303)	32 kg/m^3	2.0 $lb./ft^3$

Table A.R1: Some physical properties of Roxul RXL 20™

The lower density and fibrous nature of RXL 20™ renders it vulnerable to damage during handling, installation and construction. Contact with trowels, bricks and masons' hands tended to damage the insulation. This would appear to be an issue. To make the RXL 20™ more robust, we would suggest that either a reinforcing scrim be applied to one or both sides, the binder content be increased, or the density of the product be increased.

The brickwork on the first panel to be clad (R west) was initially laid as close as practical to the cavity insulation i.e. essentially without a finger space. The masons found that they had some difficulties in keeping the brickwork plumb because of the lateral pressure exerted by the mortar as it squeezed out of the bed joint against the insulation. Also, if the

insulation was not perfectly plumb, the mason had no space to move the veneer inwards; although compressible, the RXL 20™ exerted enough outward force to displace freshly laid bricks. The brick veneer on this test panel was removed and rebuilt with a finger space of not more than 10 mm (3/8"). All of the remaining filled-cavity (R, O, and W) walls were constructed with a similar finger space.

During construction of the panels, the RXL 20™ was temporarily fastened with plastic-headed nails. The brickwork was anchored to the frame using Helifix Tim™ ties. As the brickwork was installed, the construction team recognized the need to address practical issues such as:

- how to fasten the RXL 20™ to the wall - nails, brick ties, special staples, adhesives?
- when to fasten it - immediately after the framing or immediately before the brickwork? The ability of the RXL 20™ to resist up to several weeks of exposure to job site conditions must also be considered. Although experience has shown that exposure of the RXL 20™ does not damage it, how it is fastened and the mechanical damage from construction traffic must be considered.
- who will fasten it - the framers, the masons, or a separate trade?

The frame, cavity insulation, and brickwork of the R test panels were instrumented following the typical instrumentation layout and procedure outlined in Section A3.5. Additional temperature sensors were installed in the north and south panels. These were located in the right-hand stud at the intersection with the top and bottom plates. The instrumentation layout specific to the R test panels is illustrated in Figure A.R2.

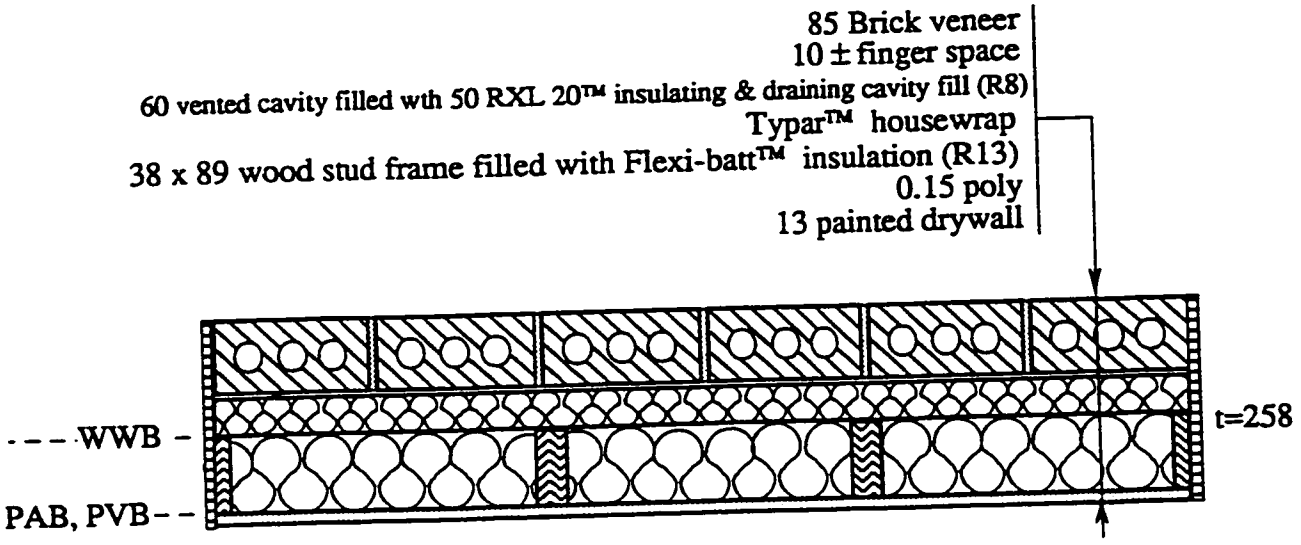

Code (R) **Residential Filled-Cavity Wall Section** (4)

All dimensions in mm unless noted otherwise

Control Layers
PAB : Primary Air Barrier
PVR: Primary Vapour Barrier
WWB: Weather and Wind Barrier

Figure A.R1 - Horizontal section through R wall panel

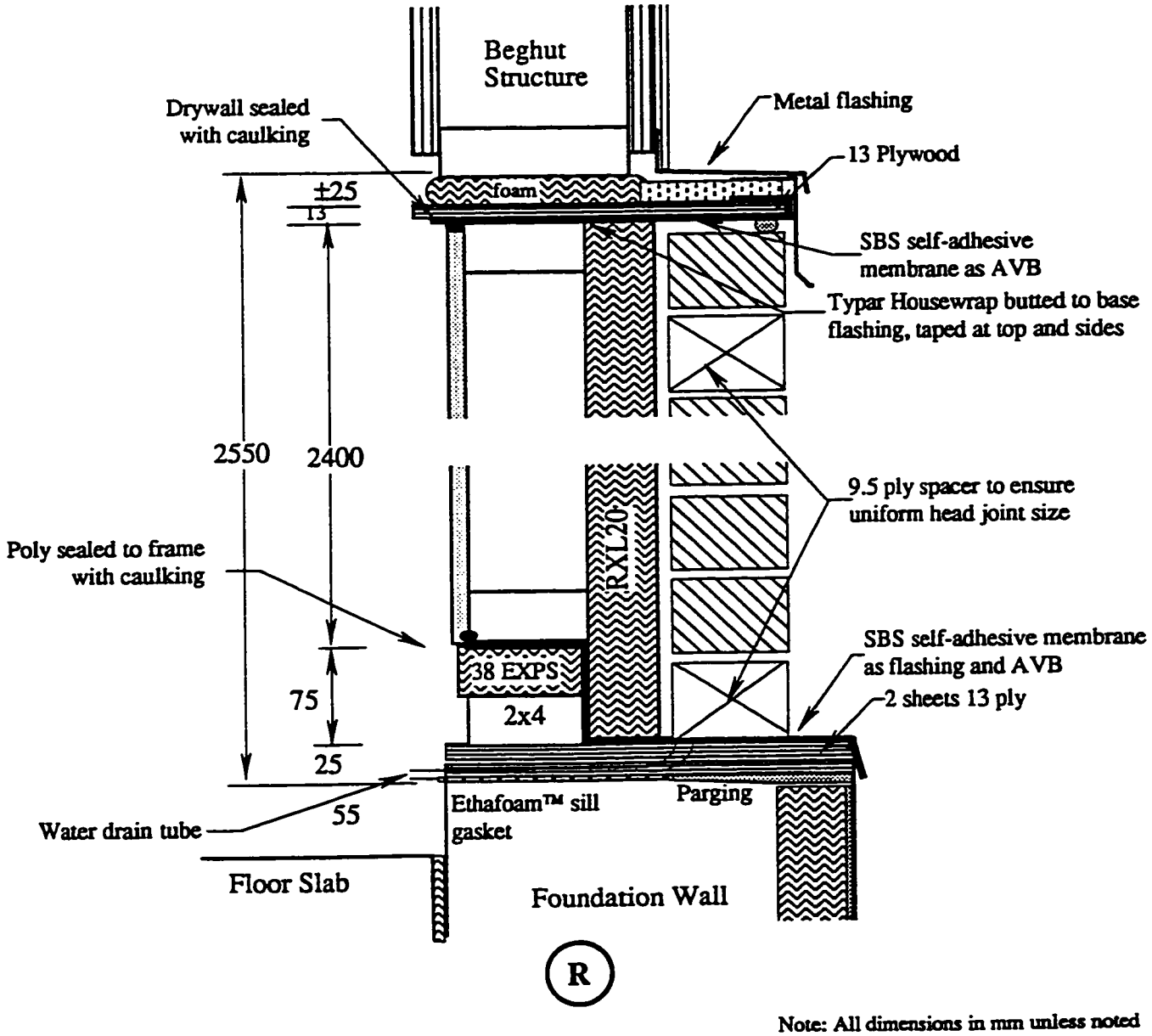

Figure A.R2 - Vertical section through R wall panel

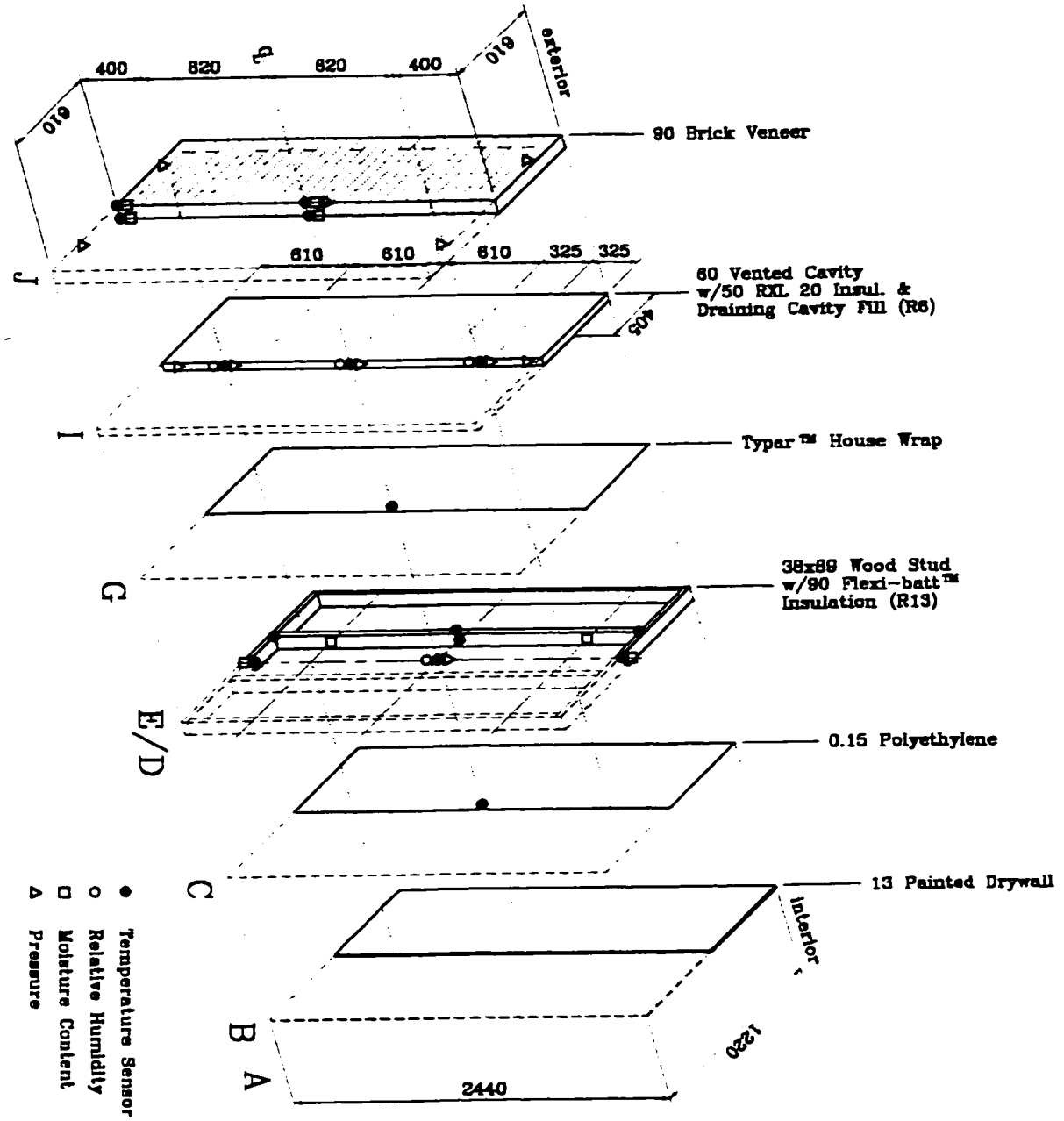

Figure A.R3 - Instrumentation isometric for R wall panel

A2.2 Roxul V Wall

The V panel is a wood-framed wall, clad with horizontal vinyl siding, intended for use in low-rise residential buildings. The assembly is typical of current residential construction practice except for the type of fibrous insulating sheathing used. From the inside, the wall assembly consists of (Figure A.V1):

- taped and painted 13 mm (1/2") drywall,
- 0.15 mm (0.006") polyethylene vapour barrier,
- 38 x 89 mm (2 x 4" nom.) wood framing (see Section A3.1),
- Roxul Flexi-batt™ insulation in the stud space (R13),
- 38 mm (1-1/2") RXL 40™ as an insulating sheathing (R6),
- a single layer of Typar™ housewrap that is sealed with sheathing tape, and
- double 100 mm (4") horizontal vinyl siding.

Construction of the wood-stud frames for the V panels was carried out in the laboratory as described in Section A3.1. Only materials which are specific to the V panels are discussed in this section. Refer to Section A3.1 for the construction of the typical wall panel frame. The V wall panels were completed in the following sequence:

1. The standard 610 mm (24") high pieces of RXL 40™ insulation were cut to 405 or 810 mm (16 or 32") in length and the vertical joints were staggered and over the studs (see Figure A.3.7). This was done to ensure representative jointing. The RXL 40 was attached using 50 mm (2") plastic headed nails at 610 mm (24") spacing.

2. The Typar™ housewrap was installed on the exterior of the RXL 40™. Sheathing tape was used to prevent leakage around the edges of the panel and to temporarily hold the housewrap until the siding was applied.

3. The vinyl siding was precut in 1220 mm (48") long pieces and attached to the stud frame with 50 mm (2") long plastic-headed nails directly through the Typar™ and the RXL 40™.

4. The wall was transported to the Beghut and installed using the procedure outlined in Section A3.2.

The design of the V wall was developed in conjunction with Roxul. The RXL 40™ was used as the insulating sheathing because of its density and stiffness. Some of the physical properties of RXL 40™ are listed in Table A.V1.

	Metric	Imperial
Dimensions (as delivered)	38 x 610 x 1220 mm	1-1/2 x 24 x 48"
Thermal resistance (ASTM-C518)	RSI = 1.16 m^2•C°/W	R = 6.55 H°F ft^2 /BTU
Density (ASTM-C303)	64 kg/m^3	A2.0 lb./ft^3

Table A.V1 - Some physical properties of Roxul RXL 40™

As built, the assembly required three layers of fasteners, one each for the RXL 40™, Typar™, and vinyl siding. Since only the last of these is necessary in the completed assembly, further consideration should be given to the methods of fastening:

- the RXL 40™ to the stud frame - nails, special staples?
- the Typar™ to the RXL 40™ and/or the frame - special staples, adhesives?
- the vinyl siding to the studs - nails, staples?

The frame and the cavity insulation of the V test panels were instrumented following the typical instrumentation layout and procedure outlined in Section A3.5. Additional temperature sensors were installed in the batt insulation, outside of the Vaisala RH sensor cover to provide a check on the difference in temperature measurements inside and outside of the RH sensor. Temperature sensors were also placed on the inside surface of the vinyl siding and on the outside surface of the Typar housewrap. An RH sensor and 3 pressure taps were installed in the space behind the siding. Three corresponding pressure taps were installed on the face of the siding. The instrumentation layout specific to the V test panels is illustrated in Figure A.V2.

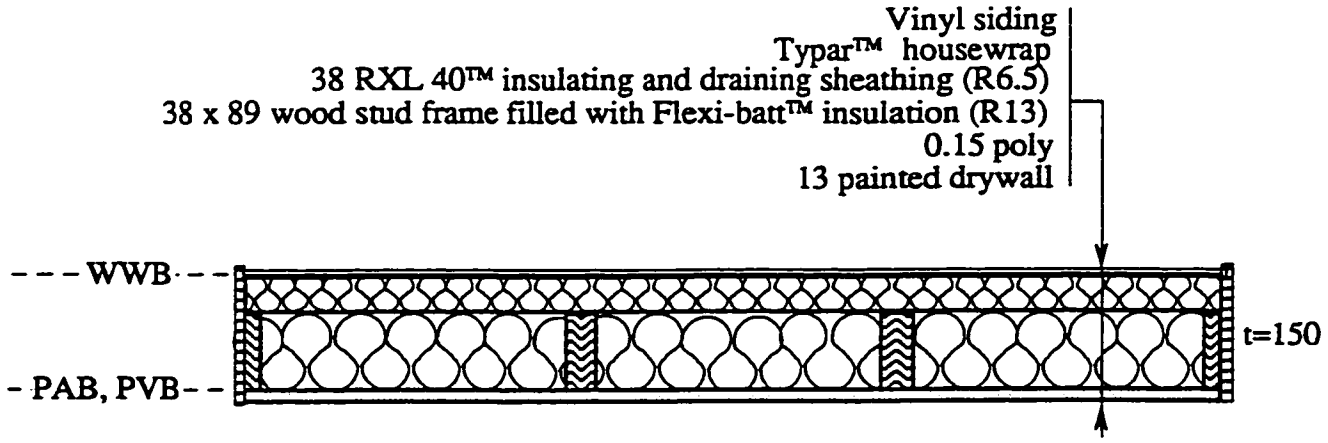

Code (V) **Vinyl-Clad Residential Draining Wall Section** (2)

Control Layers
PAB : Primary Air Barrier
PVR: Primary Vapour Barrier
WWB: Weather and Wind Barrier

All dimensions in mm unless noted otherwise

Figure A.V1 - Horizontal section through V wall panel

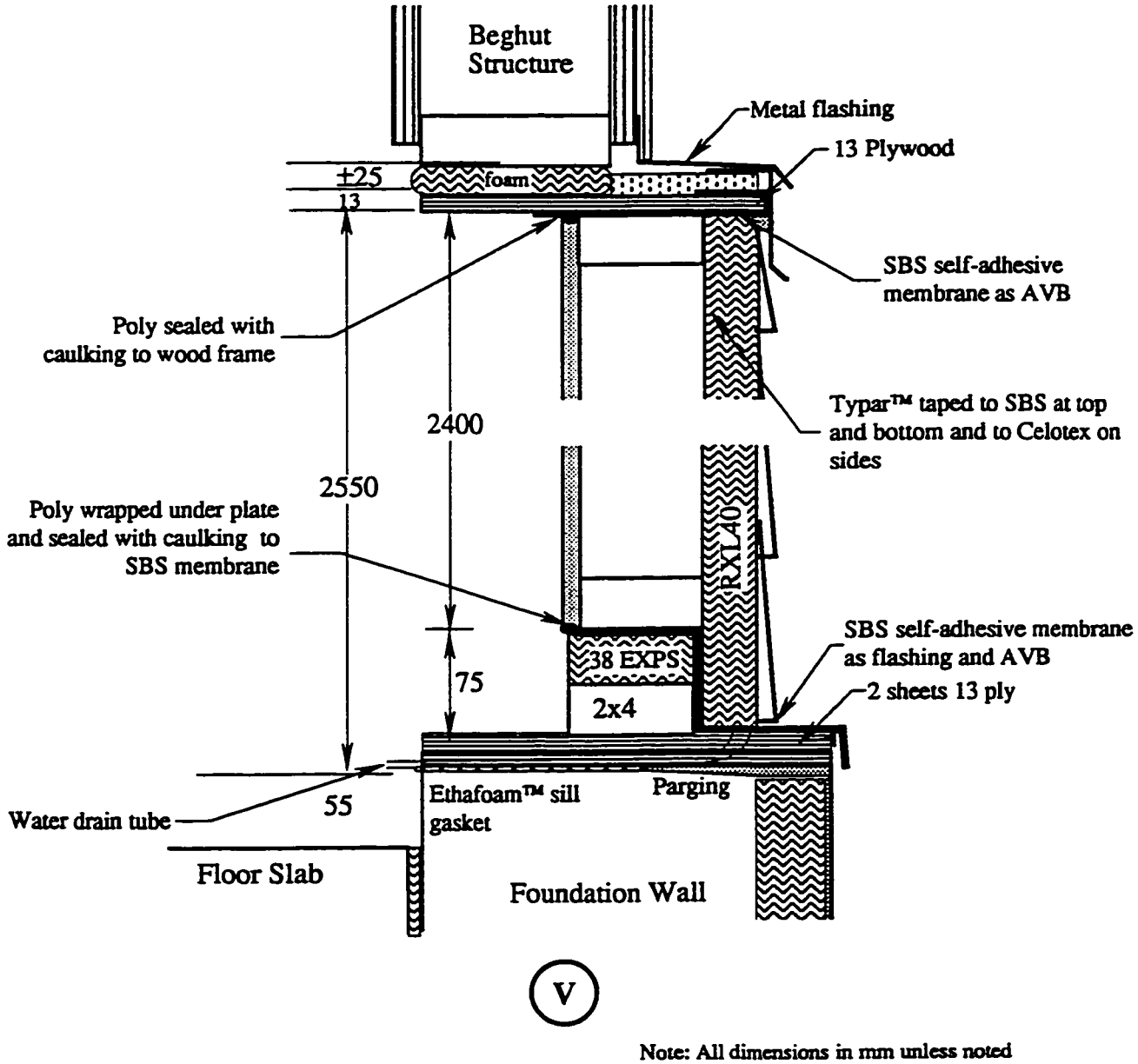

Figure A.V2 - Vertical section through V panel

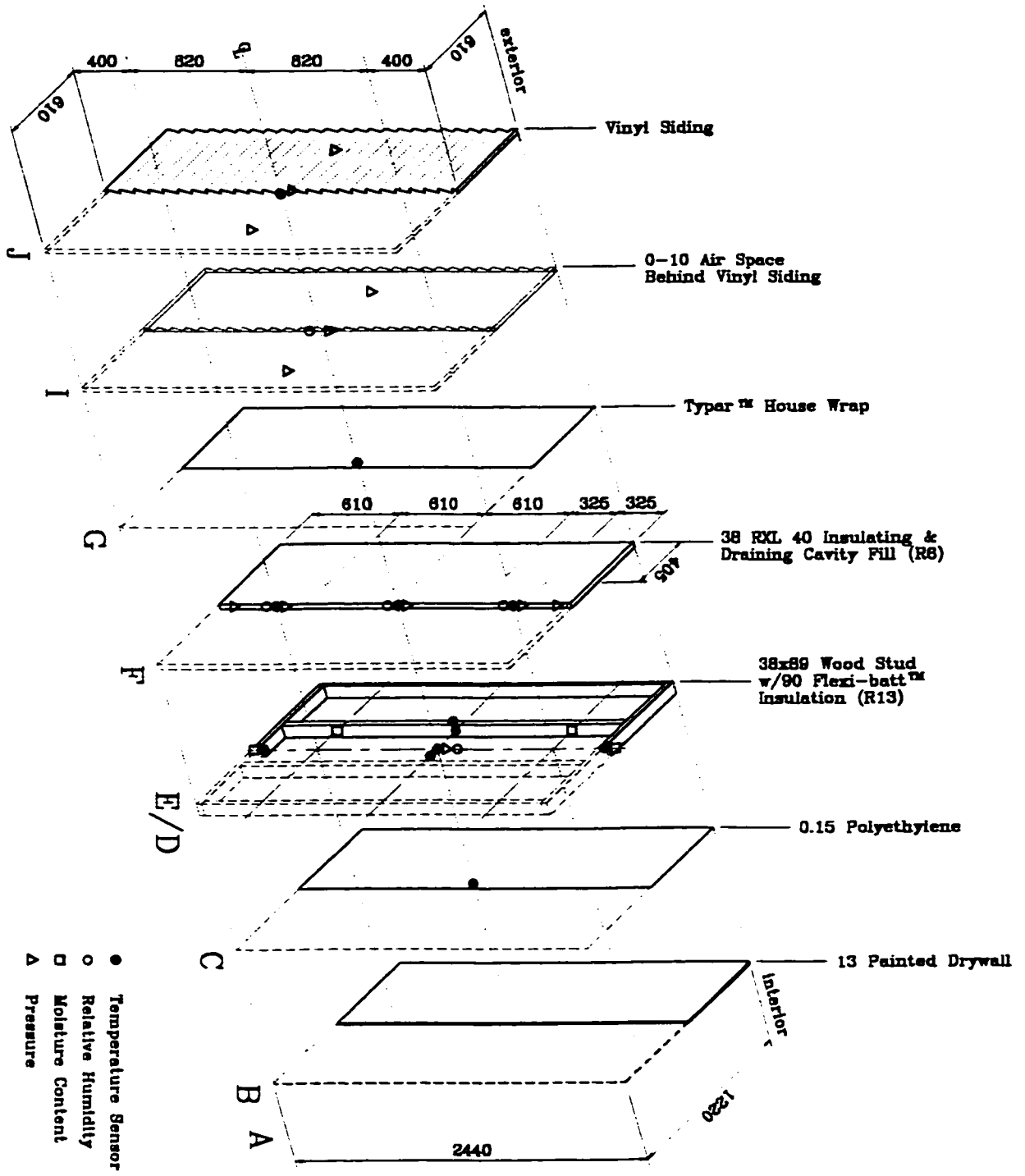

Figure A.V3 - Instrumentation isometric for V panel

A2.3 Owens-Corning O Panels

The O panel is a steel-framed, brick-veneer, filled-cavity wall intended for use in commercial buildings. The composition of the O wall is typical of current commercial construction practice with the exception of the Dritherm insulating and draining cavity fill. From the inside, the wall consists of (Figure A.O1):

- taped and painted 13 mm (1/2") drywall,
- 0.15 mm (0.006") polyethylene vapour barrier,
- a 38 x 89 mm (2 x 4") 20 gauge steel framing (see Section A3.1),
- 65 mm (2-1/2") Friction Fit batt (R8) in the stud space,
- a 13 mm (1/2") exterior gypsum sheathing as a rigid air barrier with joints sealed using 150 mm (6") wide strips of Bakor Blueskin SA™,
- 75 mm (3") vented cavity with Dritherm insulating and draining cavity fill,
- a finger space of not more than 10 mm (3/8"), and
- an 85 mm (3-3/8") brick veneer screen with vents and weep holes (see Section A3.3).

Construction of the steel frames for the O panels was carried out in the laboratory as described in Section A3.1. Only materials which are specific to the O panels are discussed in this section. Refer to Section A3.1 for the construction of the typical wall panel frame. The O wall panels were completed in the following sequence:

1. The 65 mm (2-1/2") batts were fixed in the stud space with sheathing tape to prevent them from falling out of position while the panel was transported. Wire clips would typically be used in industry.
2. The standard 1220 x 2440 mm (4 x 8') sheet of 13 mm (1/2") exterior gypsum sheathing was cut into four pieces to make two vertical joints and one horizontal joint This was done in order to ensure representative jointing. Each piece of gypsum was attached using 32 mm (1-1/4") drywall screws at 200 mm (8") spacing around the perimeter and 400 mm (16") spacing in the field.

3. The joints in the drywall were sealed using 150 mm (6") wide strips of Bakor Blueskin SA™ overlapped 50 mm (2"). These strips were also used to seal the gypsum to the sides of the panel.

4. The Dritherm insulation was delivered from the manufacturer in the United Kingdom. The standard 455 mm (18") high pieces were cut to 405 or 810 mm (16 or 32") in length so that the vertical joints were staggered and over the studs in order to ensure representative jointing. The Dritherm was temporarily fastened to the wood framing with plastic-headed nails to prevent the insulation from falling out prior to the installation of the brick ties.

5. The wall was transported to the Beghut and installed using the procedure outlined in Section A3.2.

6. The brick veneer was installed as described in Section A3.3.

The O wall was designed in coordination with Owens-Corning. Dritherm was used as the draining and insulating cavity fill because it is presently used as a partial or complete cavity fill in the UK for masonry walls. A list of some of the physical properties of Dritherm insulation is provided in Table A.O1.

	Metric	Imperial
Dimensions (as delivered)	75 x 455 x 1200 mm	3 x 18 x 48"
Thermal resistance (ASTM-C518)	RSI = 2.03 $m^2 \cdot C°/W$	R = 11.50 $ft^2 \cdot h \cdot °F/Btu$
Density (ASTM-C303)	16.8 kg/m^3	1.05 $lb./ft^3$

Table A.O1 - Some physical properties of Dritherm™

During the construction of the O panels, the Dritherm was temporarily fastened to the wood framing with plastic-headed nails. The brickwork was installed using prototype lag bolt fasteners and trapezoidal ties. This created the same concerns as for the Roxul products

The frame, cavity insulation and brickwork of the O test panels were instrumented following the typical instrumentation layout and procedure outlined in Section A3.5. Additional temperature sensors were installed in the north and south panels. These were located in the right-hand stud at the intersection of the top and bottom tracks. The instrumentation layout specific to the O test panels is illustrated in Figure A.O2.

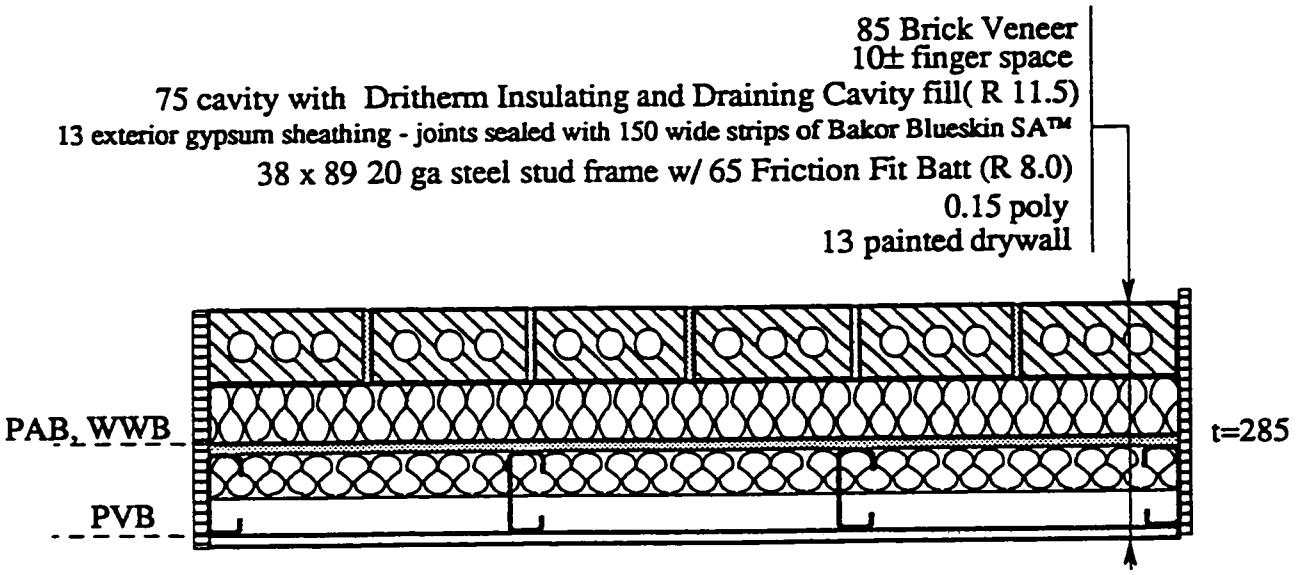

CODE: (O) **Filled-Cavity Wall Section: Commercial** **(3)**

All dimensions in mm unless noted

Control Layers

PAB : Primary Air Barrier
PVB: Primary Vapour Barrier
WWB: Wind and Weather Barrier

Figure A.O1 - Horizontal section of O panel

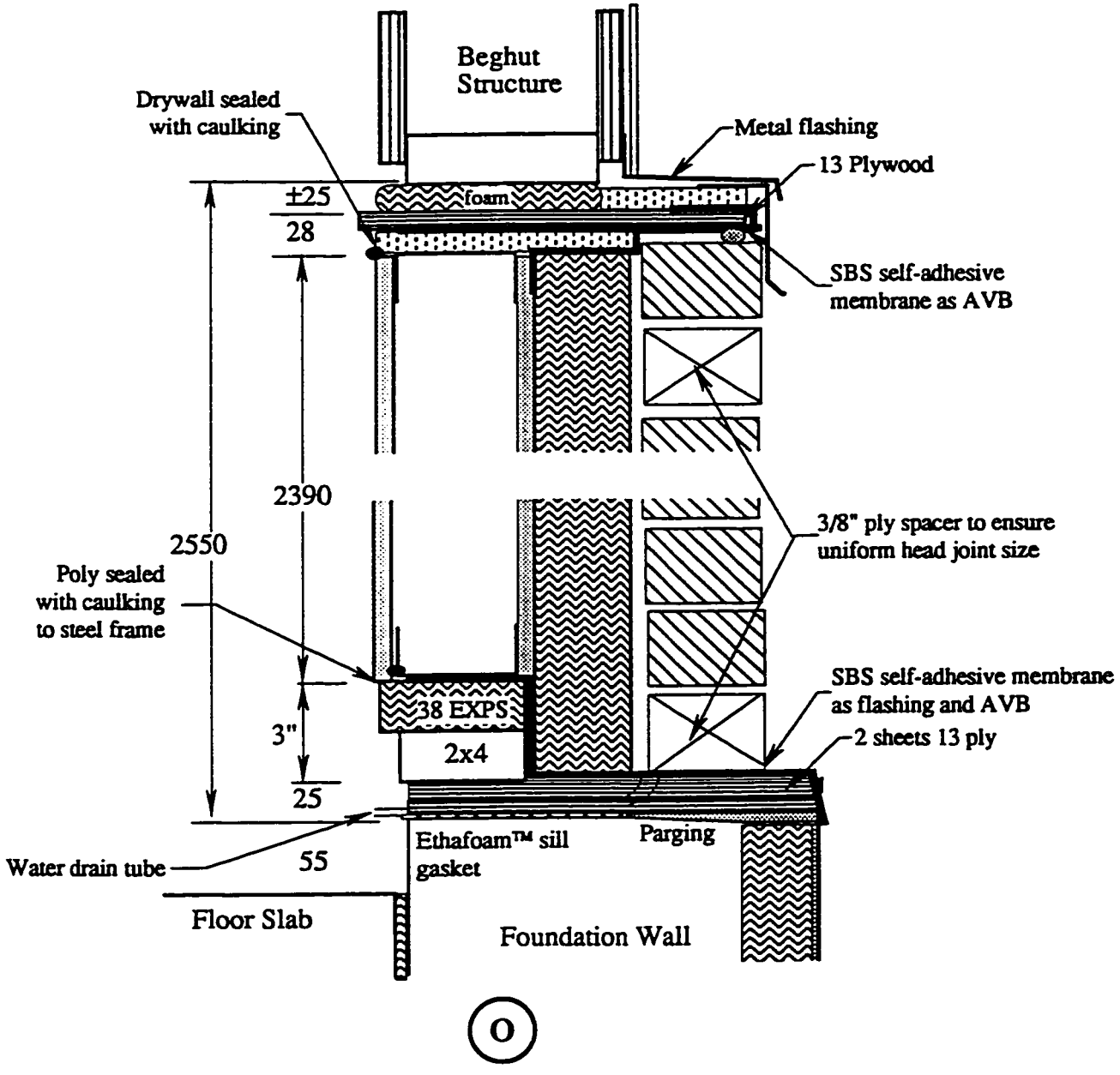

Figure A.O2 - Vertical section of O panel

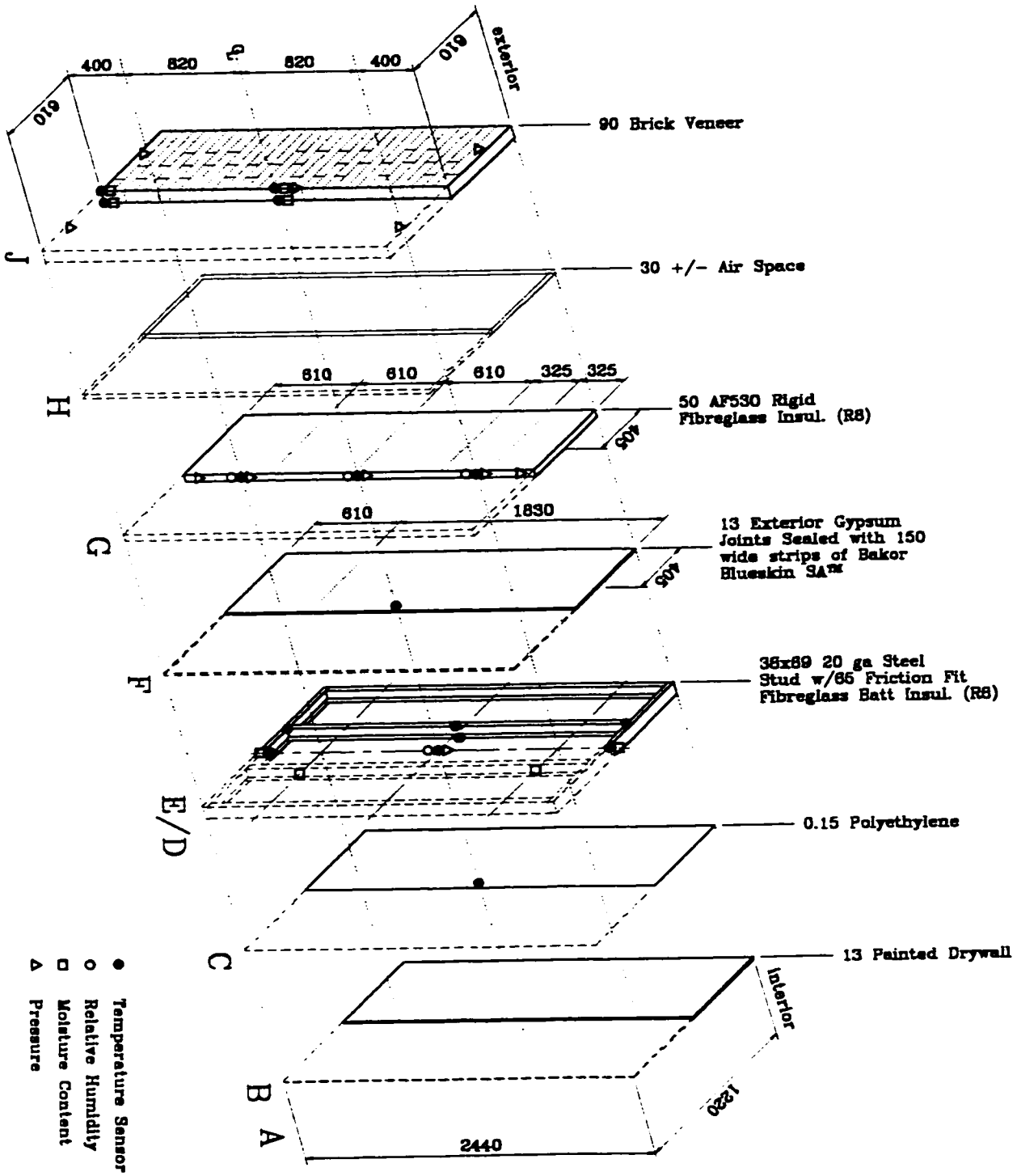

Figure A.O3 - Instrumentation isometric for O panel

A2.4 Owens-Corning F Panel

The F panel is a steel-framed, brick-veneer, cavity wall intended for use in commercial buildings. The composition of the F wall is typical of current commercial construction practice and is intended to act as a datum wall for commercial construction. From the inside, the wall consists of (Figure A.F1):

- taped and painted 13 mm (1/2") drywall,
- 0.15 mm (0.006") polyethylene vapour barrier,
- a 38 x 89 mm (2 x 4") 20 ga. steel framing (see Section A3.1),
- 65 mm (2-1/2") Friction Fit batt (R8) in the stud space,
- a 13 mm (1/2") exterior gypsum sheathing as a rigid air barrier- joints sealed with 150 mm (6") wide strips of Bakor Blueskin SA™,
- 50 mm (2") AF530 Insulation (R8)
- a ±30 mm (1-1/4") air space, and
- an 85 mm (3-3/8") brick veneer screen with vents and weep holes (see Section A3.3).

Construction of the steel frames for the F panel was carried out in the laboratory as described in Section A3.1. Only materials which are specific to the F panel are discussed in this section. Refer to Section A3.1 for the construction of the typical wall panel frame. The F wall panel was completed in the following sequence:

1. The 65 mm (2-1/2") batts were fixed in the stud space with sheathing tape to prevent them from falling out of position while the panel was horizontal.
2. The standard 1220 x 2440 mm (4 x 8') sheet of 13 mm (1/2") exterior gypsum sheathing was cut into four pieces to make two vertical joints and one horizontal joint (See Fig. 3.F3a). This was done to ensure representative jointing. Each piece of gypsum was attached using 32 mm (1-1/4") drywall screws at 200 mm (8") spacing around the perimeter and 400 mm (16") spacing in the field.

3. The joints in the drywall were sealed using 150 mm (6") wide strips of Bakor Blueskin SA™ overlapped 50 mm (2"). These strips were also used to seal the gypsum to the sides of the panel.

4. The standard 600 mm (24") high pieces of AF530 were cut to 405 or 810 mm (16 or 32") long so that the vertical joints were staggered and over the studs (see Fig. 3.F3b).

5. The wall was transported to the Beghut and installed using the procedure outlined in Section A3.2.

6. The brick veneer was installed as described in Section A3.3.

The F wall was designed in conjunction with Owens-Corning. The AF530 insulation is recommended by the manufacturer for use in commercial cavity-wall applications. Its rigidity makes it easy to work with and durable. Some of the physical properties of AF530 are listed in Table A.F1.

	Metric	Imperial
Dimensions (as delivered)	51 x 610 x 1220 mm	2 x 24 x 48"
Thermal resistance (ASTM-C518)	RSI = 1.46 $m^2 \cdot C°/W$	R = 8.34 $ft^2 \cdot h \cdot °F/Btu$
Density (ASTM-C303)	48.1 kg/m^3	3 $lb./ft^3$

Table A.F1 - Some physical properties of Owens-Corning AF530™

The brickwork was anchored to the backup using prototype lag bolt fasteners and trapezoidal ties (see Section 3.A2.4). This raises the same issues as in the other systems.

The frame, cavity insulation and brickwork of the F test panel was instrumented following the typical instrumentation layout and procedure outlined in Section A3.5. The instrumentation layout specific to the F test panel is illustrated in Figure A.F2.

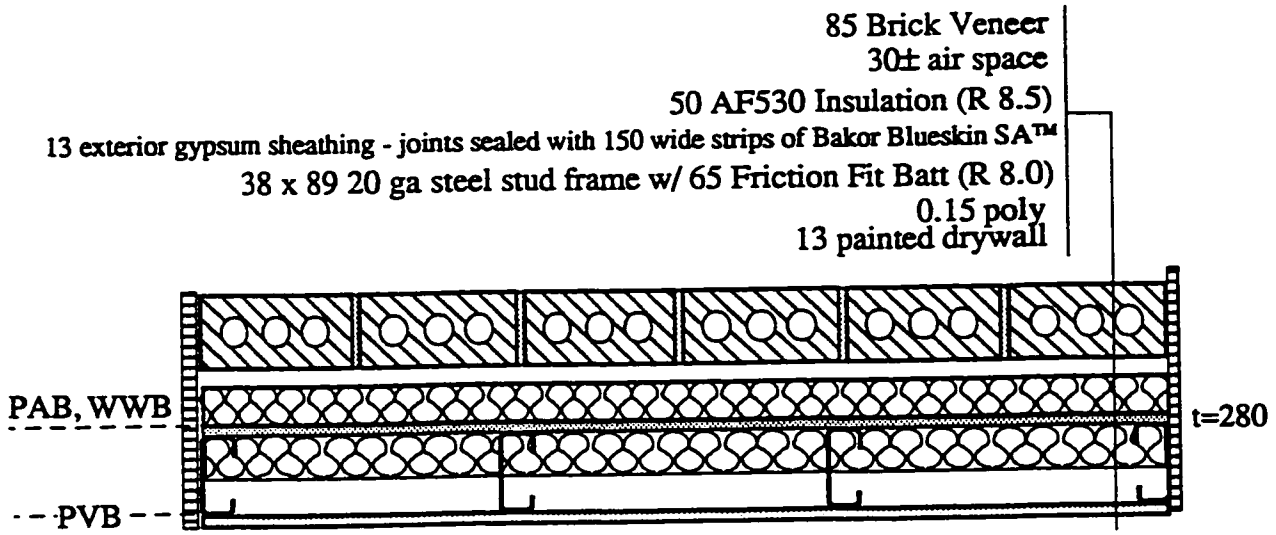

CODE: (F) **Clear Cavity Wall Section: Commercial Datum** (1)

Control Layers

PAB : Primary Air Barrier
PVB: Primary Vapour Barrier
WWB: Wind and Weather Barrier

All dimensions in mm unless noted

Figure A.F1 - Horizontal section through F wall panel

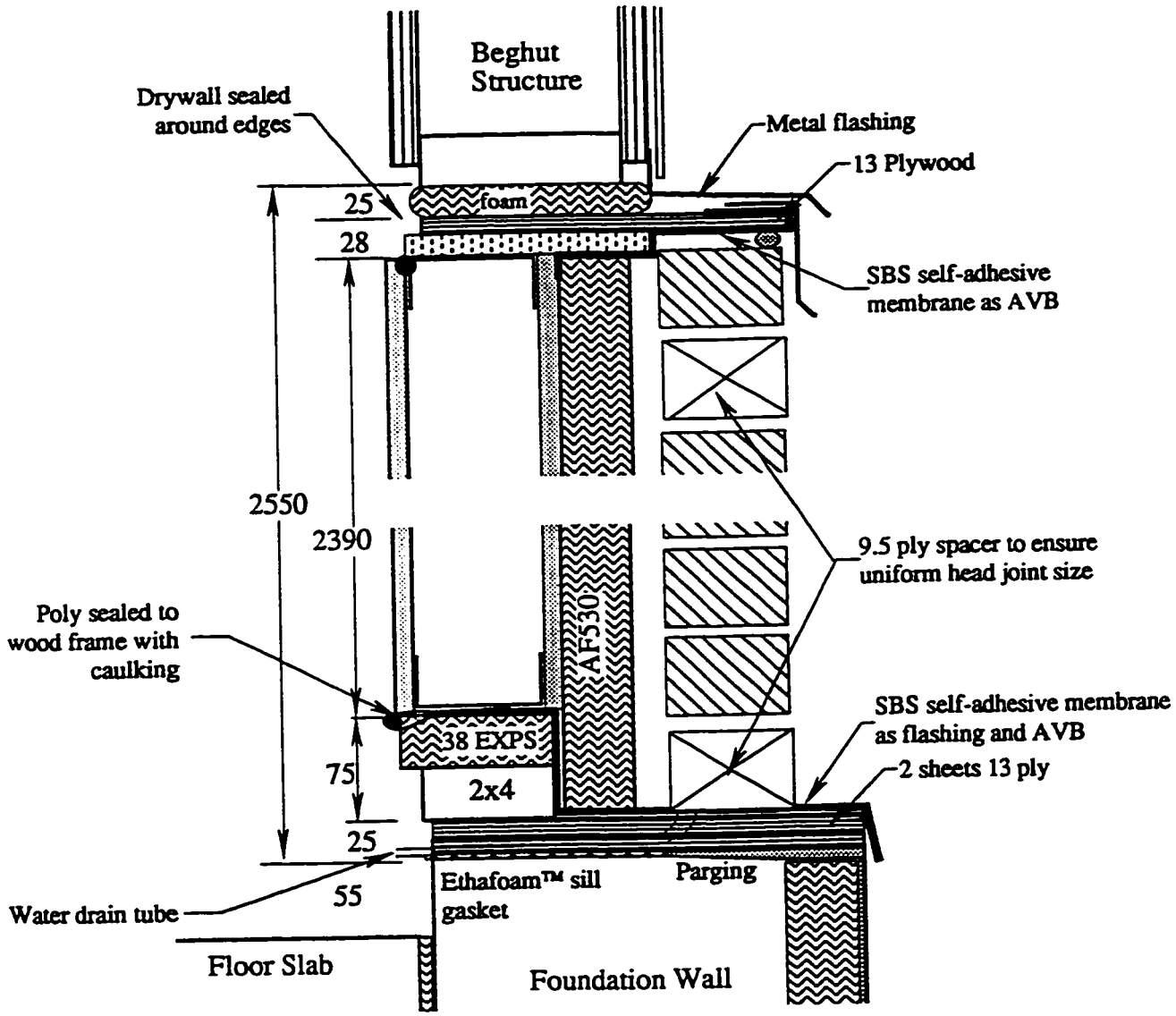

Figure A.F2 - Vertical section through F panel

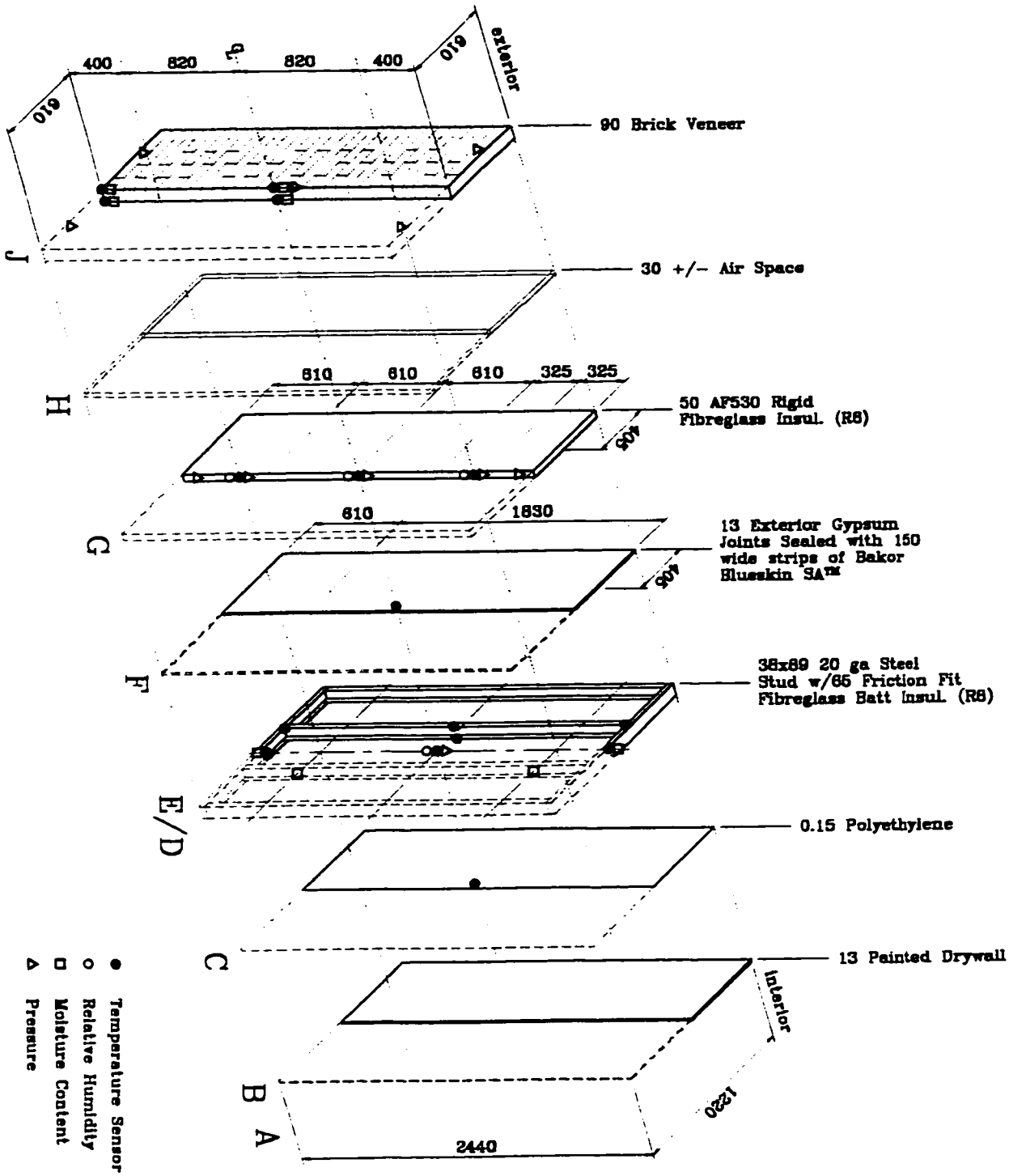

Figure A.F3 - Instrumentation isometric for F panel

A2.5 Owens-Corning W Panel

The W panel is a wood-framed, brick-veneer, filled-cavity wall intended for use in low-rise residential buildings. The composition of the W wall is typical of current commercial construction practice with the exception of the Dritherm, which is being used as an insulating and draining cavity fill. From the inside, the wall consists of:

- taped and painted 13 mm (1/2") drywall,
- 0.15 mm (0.006") polyethylene vapour barrier,
- a 38 x 89 mm (2 x 4") wood framing (see Section A3.1),
- Fibreglass Friction Fit batt (R12) in the stud space,
- a 12 mm (1/2") oriented strand board with open joints,
- a 50 mm (2") vented cavity with Dritherm insulating and draining cavity fill,
- a finger space of not more than 10 mm (3/8"), and
- an 85 mm (3-3/8") brick veneer screen with vents and weep holes (see Section A3.3).

Construction of the wood frames for the W panels was carried out in the laboratory as described in Section A3.1. Only materials which are specific to the W panels are discussed in this section. Refer to Section A3.1 for the construction of the typical wall panel frame. The W wall panels were completed in the following sequence:

1. The standard 1220 x 2440 mm (4 x 8') sheet of 12 mm (1/2") oriented strand board (OSB) sheathing was cut into four pieces to make two vertical joints and one horizontal joint (See Fig. 3.W3a). This was done in order to ensure representative jointing. Each sheet of OSB was attached using 38 mm (1 1/2") galvanized roofing nails at 200 mm (8") spacing around the perimeter and 400 mm (16") spacing in the field.

2. Three pieces of 910 mm (36") wide building paper were cut 1320 mm (52") long and were installed with a 50 mm (2") overlap between pieces and at the sides of the panel. Sheathing tape was used to temporarily fasten the building paper to the frame until

installation of the brick ties. The joints at the sides and top of the panel were sealed with sheathing tape.

3. The Dritherm insulation was delivered from the manufacturer in the United Kingdom. The 75 mm (3") thick pieces were cut to 50 mm (2") thick. The standard 455 mm (18") high pieces were cut to 405 or 810 mm (16 or 32") in length so that the vertical joints were staggered and over the studs (see Fig. 3.W3b) and to ensure representative jointing. The Dritherm was temporarily fastened to the wood framing with plastic-headed nails to prevent the insulation from falling out prior to the installation of the brick ties.

4. The wall was transported to the Beghut and installed using the procedure outlined in Section A3.2.

5. The brick veneer was installed as described in Section A3.3.

The W wall was designed in conjunction with Owens-Corning. Dritherm was used as the draining and insulating cavity fill because it has been successfully used as a partial or complete cavity fill in the UK for walls with masonry backup. Some of the physical properties of Dritherm insulation are listed in Table A.W1

	Metric	Imperial
Dimensions (as delivered)	51 x 455 x 1200 mm	2 x 18 x 48"
Thermal resistance (ASTM-C518)	RSI = 1.35 $m^2 \cdot C°/W$	R = 7.68 $ft^2 \cdot h \cdot °F/Btu$
Density (ASTM-C303)	16.8 kg/m^3	1.05 $lb./ft^3$

Table A.W1 - Some physical properties of Dritherm™

During the construction of the W panels, the Dritherm was temporarily fastened with plastic-headed nails. The brickwork was anchored to the backup with Helifix Tim ties. This raised the same issues as for the Roxul panels.

The frame, cavity insulation and brickwork of the W panel was instrumented following the typical instrumentation layout and procedure outlined in Section A3.5. Two additional moisture sensors were used to measure the moisture content of the OSB sheathing; one was located in the middle of the panel and the other 50 mm from the bottom of the OSB sheathing (125 mm from the base of the brick). The instrumentation layout specific to the W test panel is illustrated in Figure A.W2.

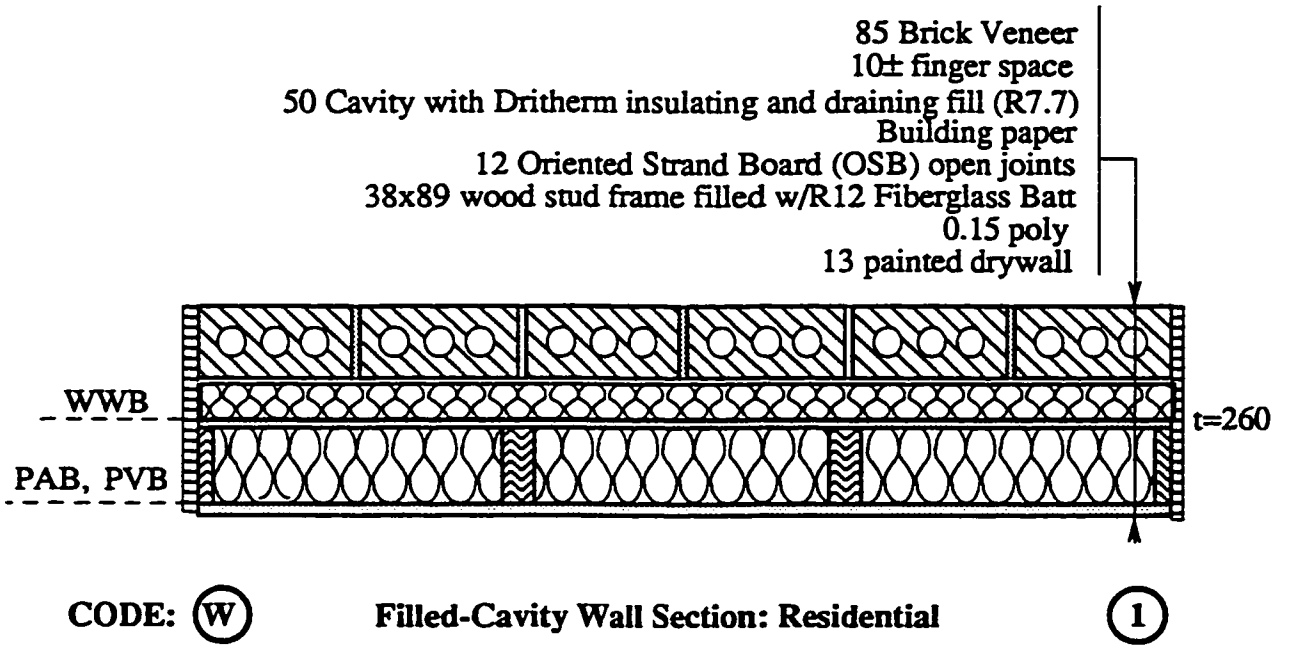

Control Layers

PAB : Primary Air Barrier
PVB: Primary Vapour Barrier
WWB: Wind and Weather Barrier

All dimensions in mm unless noted

Figure A.W1 - Horizontal section through W wall panel

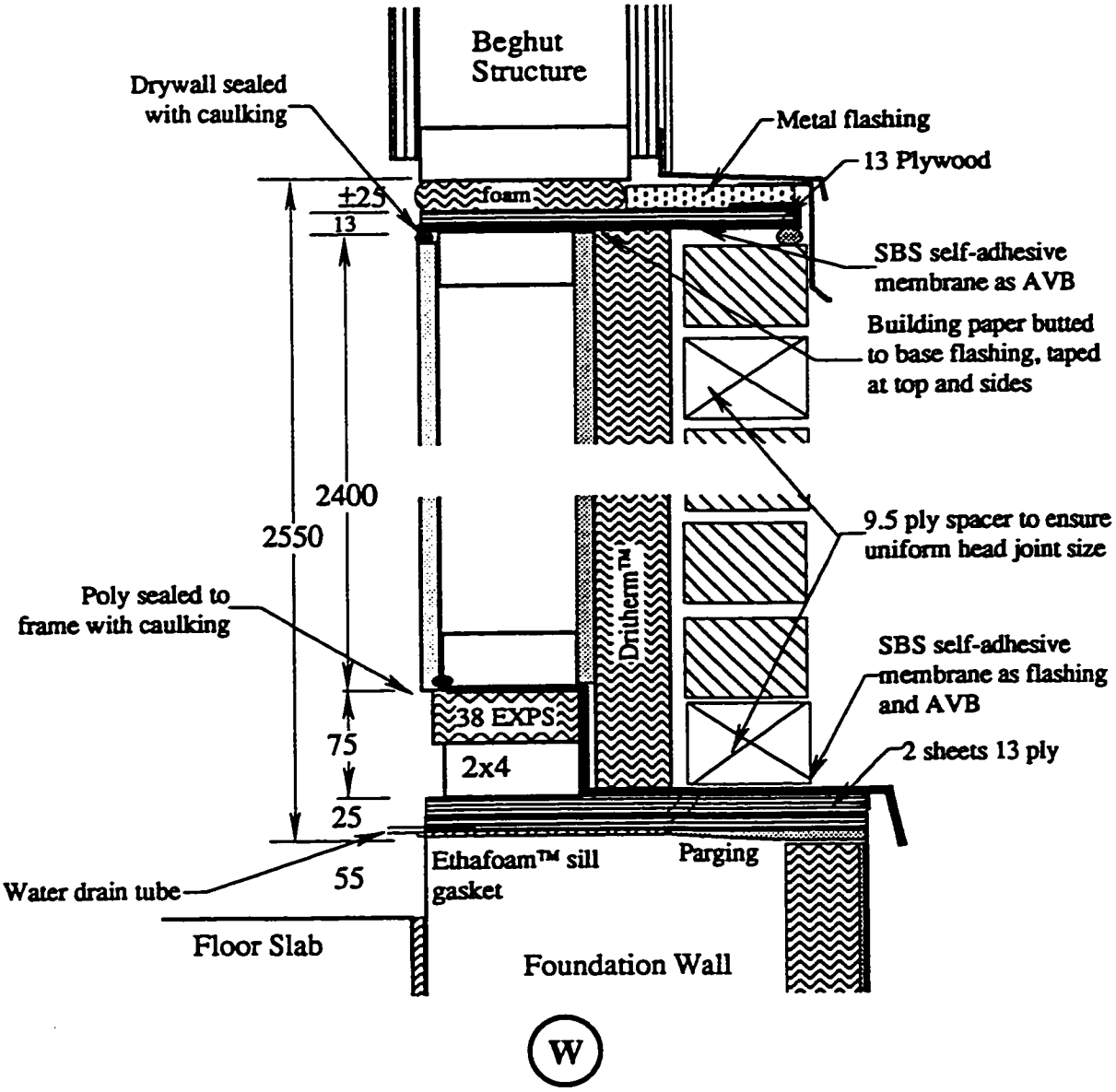

Note: All dimensions in mm unless noted

Figure A.W2 - Vertical section through W panel

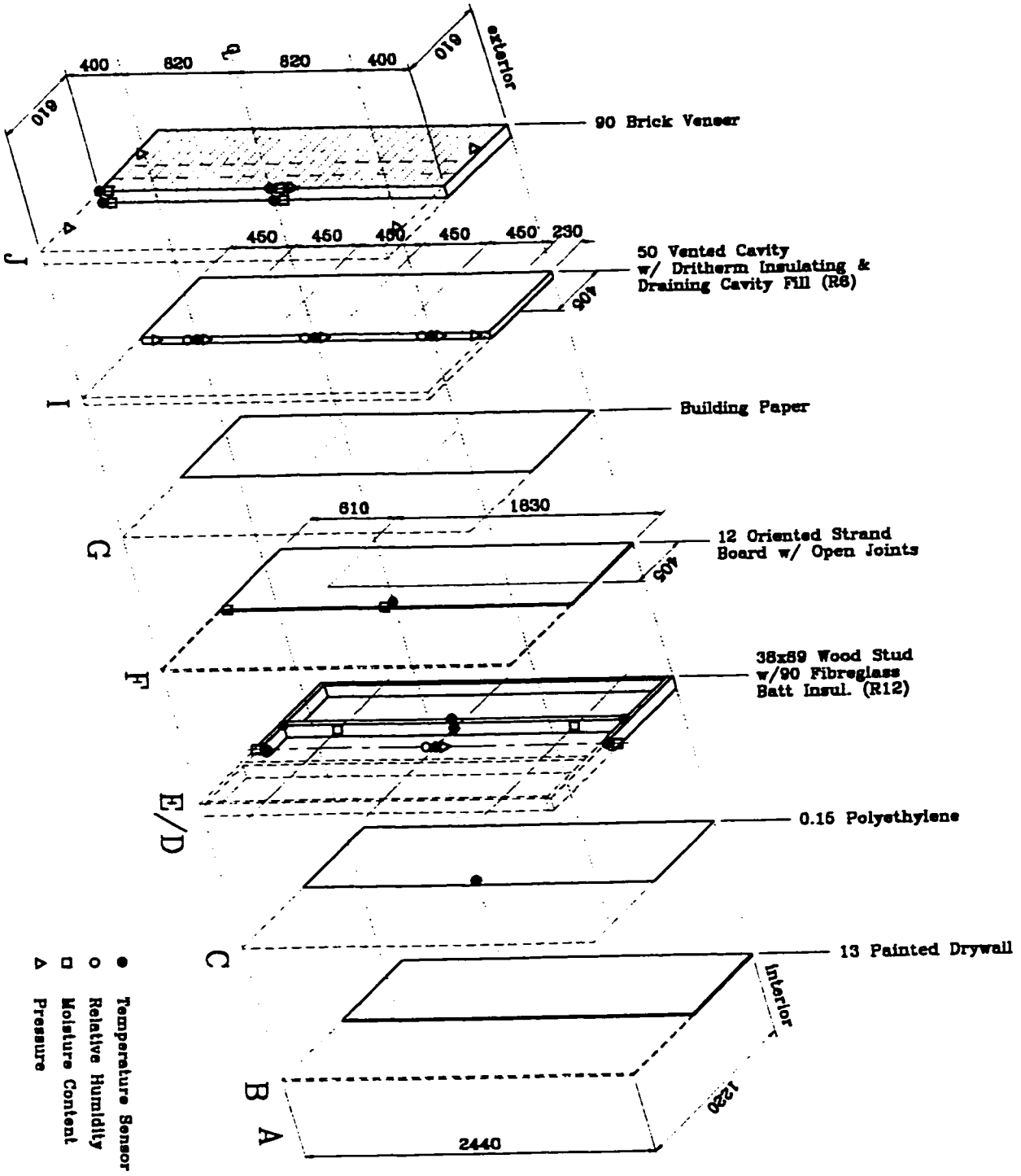

Figure A.W3 - Instrumentation isometric for W panel

A2.6 Durisol D Panels

The D panel is a wood-framed, Durisol-clad wall intended for use in low-rise residential buildings. The D wall is a prototype wall that is finished with Durisol cladding, an insulating and draining screen. From the inside, the wall consists of:

- taped and painted 13 mm (1/2") drywall,
- 0.15 mm (0.006") polyethylene vapour barrier,
- a 38 x 89 mm (2 x 4") wood stud framing (see Section A3.1),
- 90 mm (3-7/8") Fibreglass Friction Fit batt (R12) in the stud space,
- a single layer of Typar™ housewrap sealed with sheathing tape, and
- 132 mm (5-1/2") Durisol cladding (R8.75).

Construction of the wood frames for the D panels was carried out in the laboratory as described in Section A3.1. Only materials which are specific to the D panels are discussed in this section. Refer to Section A3.1 for the construction of the typical wall panel frame. The D wall panels were completed in the following sequence:

1. The Typar™ housewrap was installed on the exterior of the frame using 10 mm (3/8") staples at 200 mm (8") spacing. Sheathing tape was carefully applied to seal the housewrap to the sides of the panel to prevent leakage around the edges.

2. The wall was transported to the Beghut and installed using the procedure outlined in Section A3.2.

3. The Durisol cladding was delivered from the manufacturer in precast pieces 1195 mm (47") wide x 500 mm (20") high. Five pieces were installed one on top of the other, and the top piece was cut to approximately 450 mm (18") high to fit the remaining opening (Figure A.D3). Each piece of cladding was attached to the two central wood studs using four Helifix HRT-60 ties driven through a groove in the cladding.

The D wall was designed in conjunction with Durisol. Durisol is a wood/cement composite material which can be precast to a variety of dimensions. The material is air permeable, vapour permeable, draining, and insulating. The Durisol cladding is a prototype material and has a cementitious finish on the vertical exterior surface. The

underside of the reveals has not been finished in order to encourage air, water and vapour movement. Some of the physical properties of Durisol cladding are listed in Table A.D1.

	Metric	Imperial
Dimensions (as delivered)	132 x 500 x 1200 mm	5-1/4 x 20 x 48"
Thermal resistance (estimated)	RSI = 1.54 $m^2 \cdot C°/W$	R = 8.75 $ft^2 \cdot h \cdot °F/Btu$
Density	560 kg/m^3	35 $lb./ft^3$

Table A.D1 - Some physical properties of Durisol Cladding

The frames of the D test panels were instrumented following the typical instrumentation layout and procedure outlined in Section A3.5. Additional relative humidity and temperature sensors were installed in the Durisol cladding. Three sets of RH and temperature sensors were installed on the vertical centre line of each wall panel. One set was installed at the bottom of the wall in the middle of the Durisol cladding, one at the middle of the wall just inside of the exterior of the cladding, and one at the middle of the wall just outside the interior face of the cladding. Pressure taps in the Durisol cladding were installed in a similar locations to those in the brickwork (Section A3.3). The instrumentation layout specific to the D test panels is illustrated in Figure A.DA2.

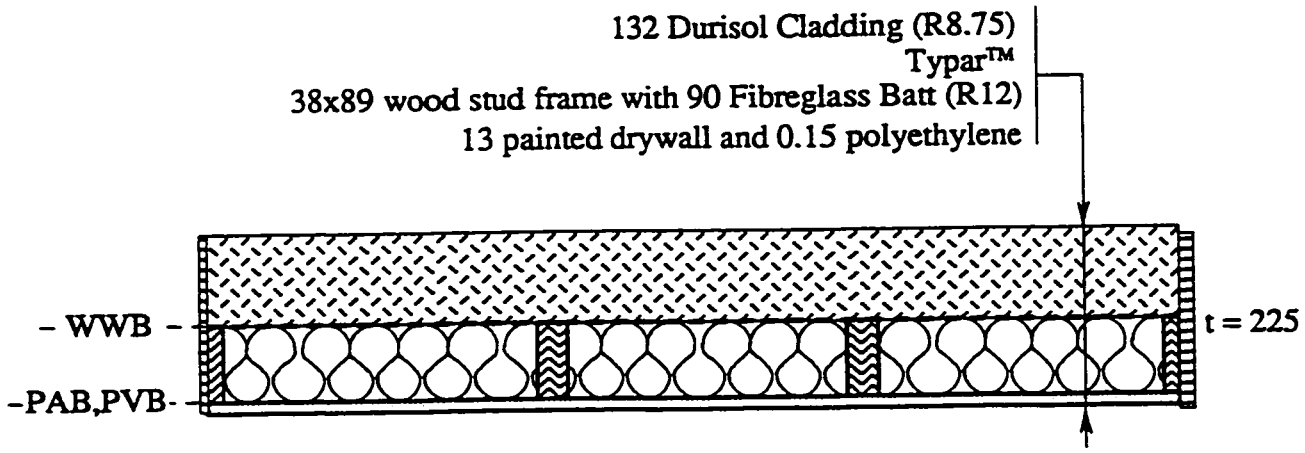

CODE: (D) **Durisol Cladding Residential Wall Section** **(4)**

All dimensions in mm unless noted otherwise

Control Layers

PAB : Primary Air Barrier
PVB: Primary Vapour Barrier
WWB: Wind and Weather Barrier

Figure A.D1 - Horizontal section through D wall panel

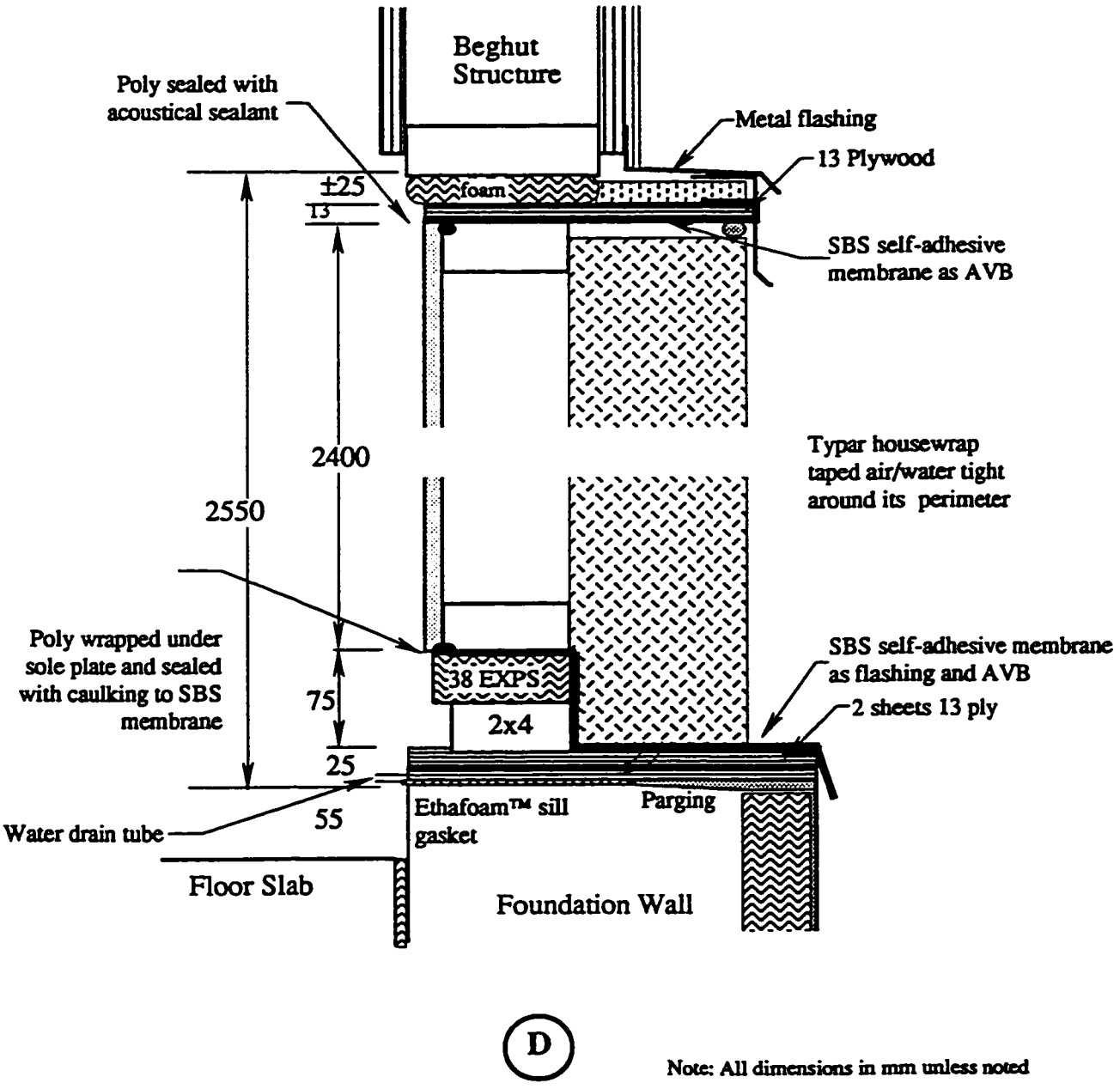

Figure A.D2 - Vertical section through D panel

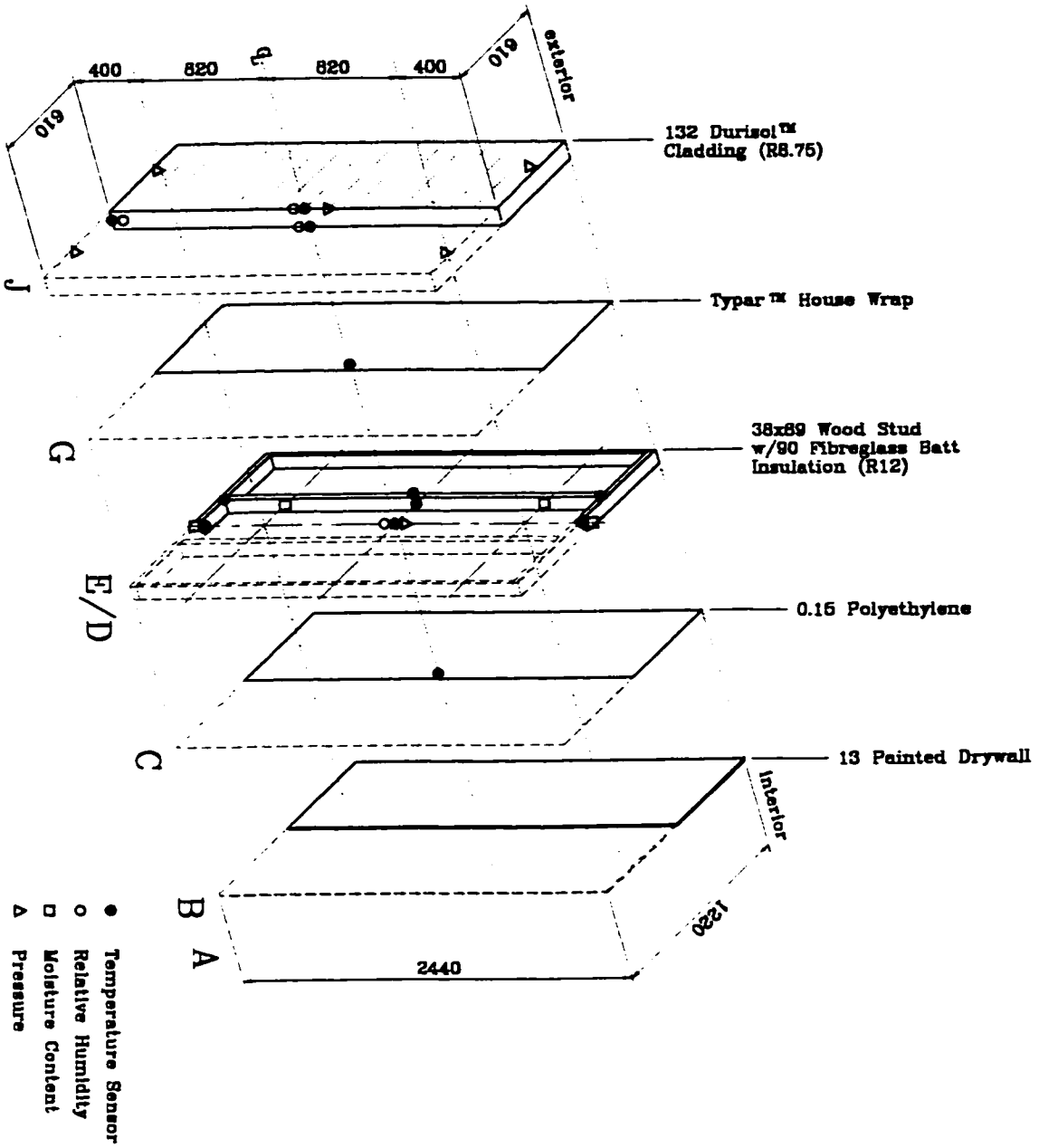

Figure A.D3 - Instrumentation isometric for D panel

A2.7 Durisol C Panel

The Durisol C panel comprises a Durisol insulated wall form with a brick veneer. It is intended for use in low-rise residential buildings. The C panel is a demonstration wall based on a Durisol block inner wythe, an insulating wall form and reinforced concrete system. From the inside, the wall consists of:

- taped and painted 13 mm (1/2") drywall,
- a 200 mm (8") reinforced concrete-filled Durisol block wall (R8),
- 50 mm (2") Styrofoam SM, Type 4 EXPS insulation (R10),
- building paper,
- a ±30 mm (1-1/8") air space, and
- an 85 mm (3-3/8") brick veneer screen with vents and weep holes (see Section A3.3).

The C wall was entirely constructed in situ at the Beghut because the materials and assembly used in wall made it impossible to do any work in the laboratory. The C wall was assembled in the following sequence:

1. The typical base detail was assembled and anchored to the top of the foundation wall using two 62 mm (2-1/2") long 6 mm (1/4") dia. Tapcon™ screws.

2. The standard Durisol block measures 890 mm (35") long x 300 mm (12") high x 200 mm (8") thick and has three cores (Figure A.C1). The ends were cut off four of these blocks to produce eight 300 mm (12") long single core blocks. One course of block is comprised of one full block (3 cores) and one part block (1 core) to make a wall panel 1150 mm (46") wide (Figure A.C1).

3. The first three courses of Durisol block were laid up dry and a 1220 mm (48") long 10M rebar was set into 50 mm (2") deep holes in the base and centred in each core.

4. The concrete was proportioned gravimetrically in the lab and transported to the site as a dry mix. The dry mix was mixed with water in a cement mixer on site and poured into the first three courses. The remaining four courses were laid up and poured two courses at a time. Three 6 x 12" standard concrete test cylinders were cast and cured

in a laboratory fog room. The strength of the sample tested at 7 days was 21.9 MPa (3180 psi) The 28 day test sample reached a strength of 28 MPa (4070 psi).

5. The building paper and extruded polystyrene insulation were installed and attached to the Durisol Block using Helifix HRT 80 brick ties and Wedge-Lok insulation clips.

6. The brick veneer was installed as described in Section A3.3.

The C panel design was developed by Durisol to demonstrate a typical application of the Durisol WallFrom, a product that has been used for years around the world. Durisol is a wood/cement composite material which can be precast in a variety of shapes. The material is air permeable, vapour permeable, draining, insulating, and has useful structural strength. The Durisol Wall Form acts as a lost formwork for a reinforced concrete wall and provides thermal insulation both during construction and in service. Some of the physical properties of the Durisol Wall Form are listed in Table A.C1.

	Metric	Imperial
Block Dimensions (as delivered)	200 x 300 x 900 mm	8 x 12 x 33"
Thermal resistance (estimated)	RSI = 1.41 $m^2 \cdot C°/W$	R = 8 $ft^2 \cdot h \cdot °F/Btu$
Surface Density (estimated)	230 kg/m^2	500 $lb./ft^2$

Table A.C1 - Some physical properties of concrete-filled Durisol Wall Form

During the construction of the C panels, the building paper and expanded polystyrene insulation were fixed to the Durisol block using Helifix HRT 80 ties. The only concern noted was the protrusion of the sharp ends of the Helifix ties after the EXPS had been attached. To prevent injury, small blocks of EXPS were impaled on the end of the tie until the mason reached this level.

The cavity insulation and brickwork of the C panel was instrumented following the typical instrumentation layout and procedure outlined in Section A3.5. Six more temperature sensors were also placed at the mid-height on the vertical centre line of the panel. Two of these sensors were located on each face of the Durisol block; one over the web and one over the core. The last two sensors are in the middle of the block: one in the web and one in the core - the sensor in the core was attached to the 10M reinforcing bar. The instrumentation layout specific to the C test panel is illustrated in Figure A.CA2.

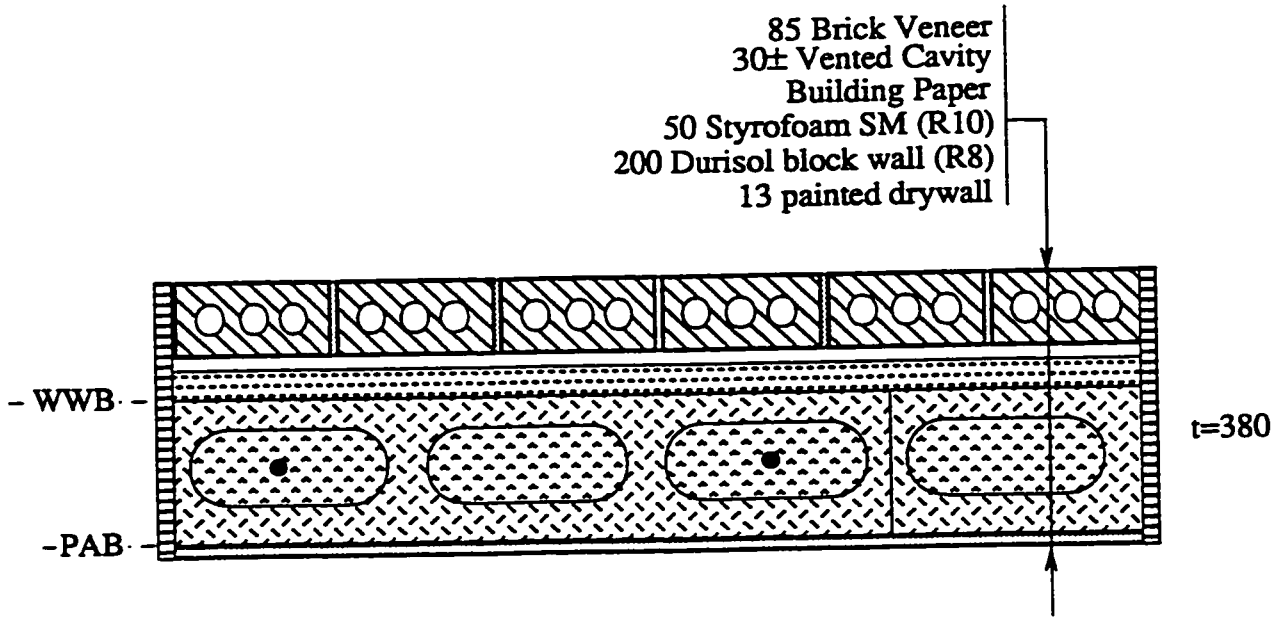

CODE: (C) Durisol Block Residential Wall Section (1)

Control Layers

PAB : Primary Air Barrier
PVB: Primary Vapour Barrier
WWB: Wind and Weather Barrier

All dimensions in mm unless noted otherwise

Figure A.C1 - Horizontal section through C wall panel

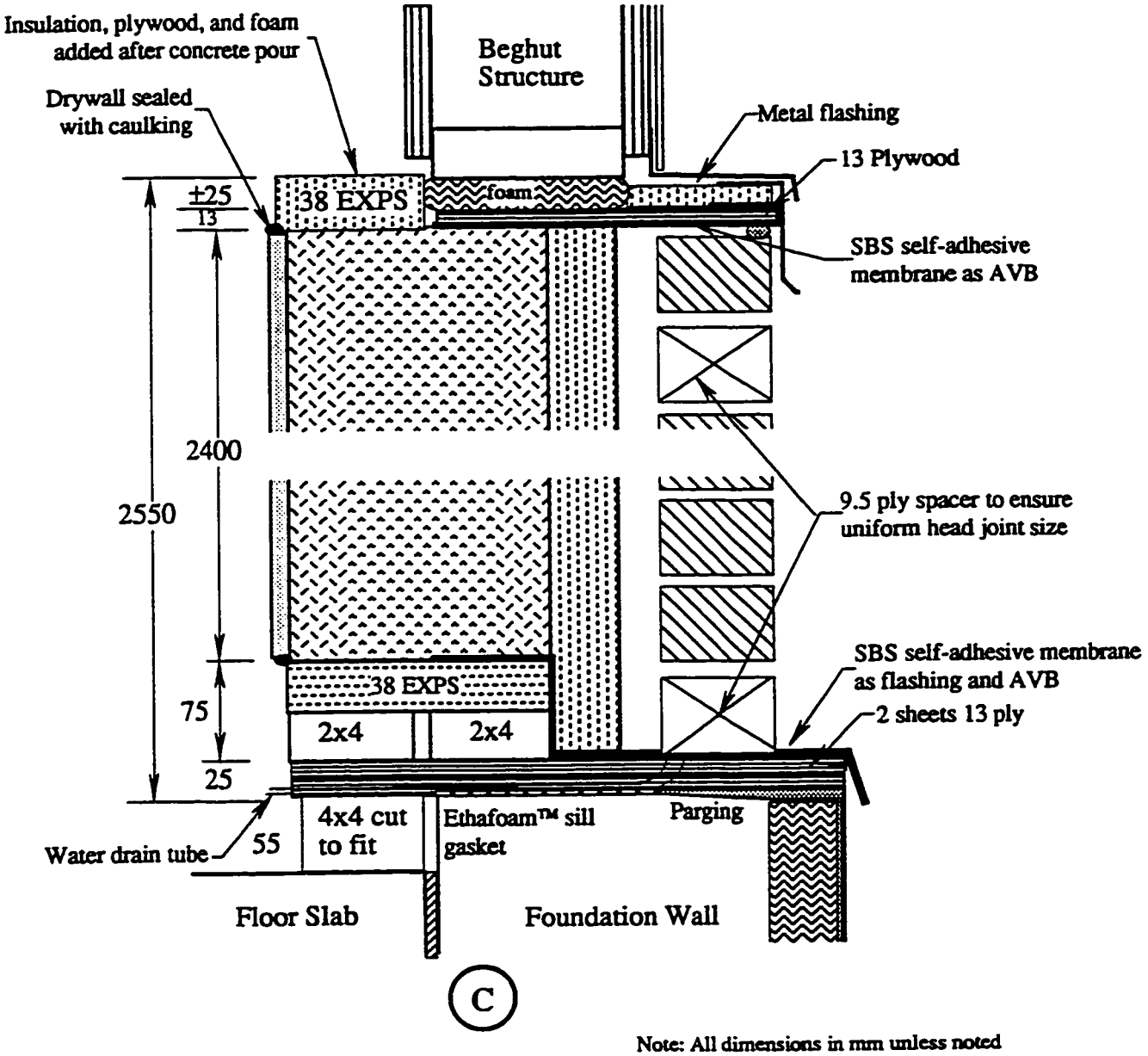

Figure A.C2 - Vertical section through C panel

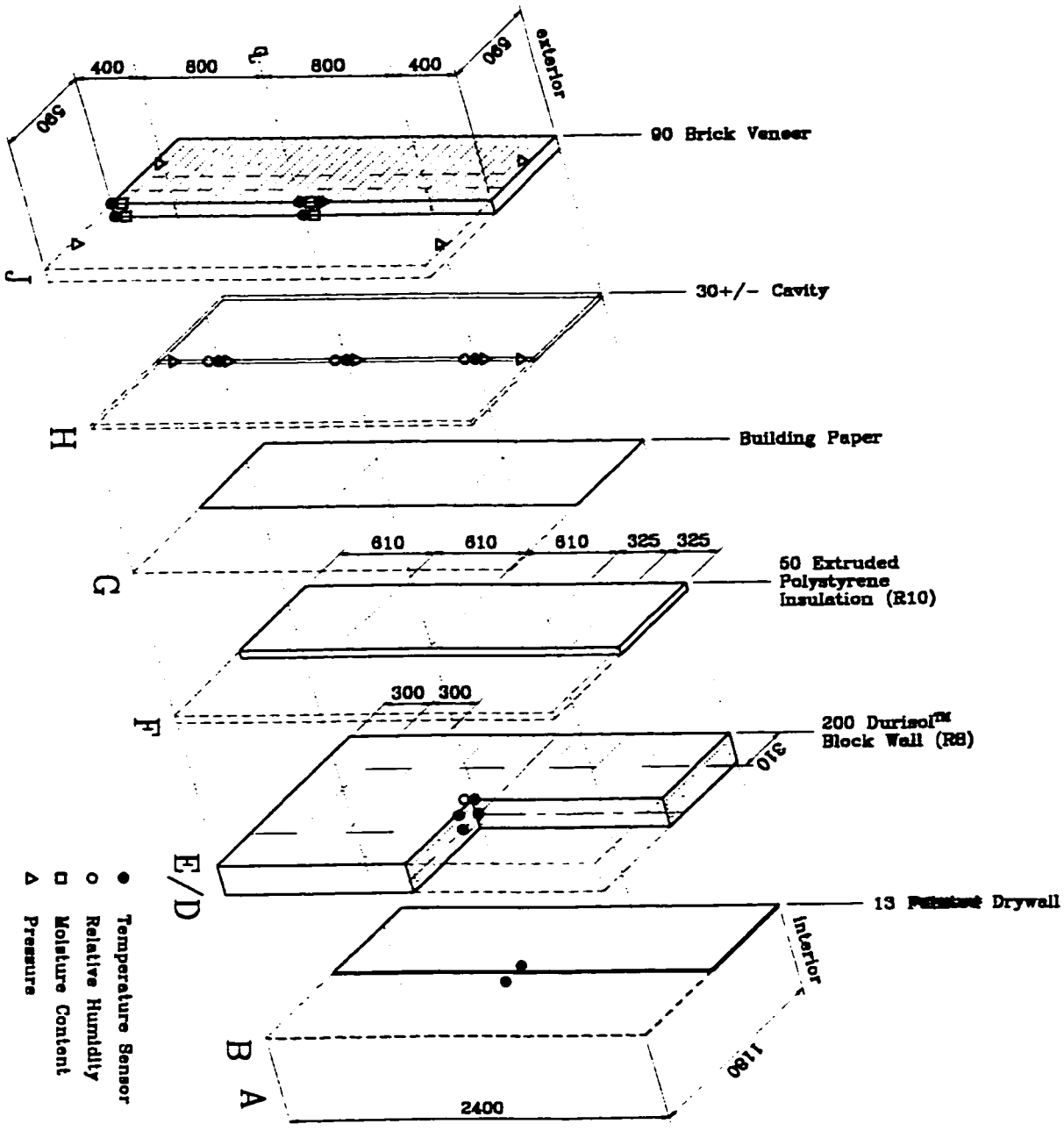

Figure A.C3- Instrumentation isometric for C panel

A2.8 Sto E Panels

The Sto E panel is a steel framed wall with an Exterior Insulated Finish System (EIFS). The composition of the E wall is typical of a high-quality, fully synthetic, non-combustible commercial EIFS wall system with the exception of the Roxul Lamella™ insulation which acts as an insulating and draining cavity fill. Each piece of the Lamella™ has grooves routed in its sides to create a vented cavity behind the Sto finish. From the inside, the wall consists of:

- taped and painted 13 mm (1/2") drywall,
- a 38 x 89 mm (2 x 4") 20 Ga. steel framing (see Section A3.1),
- Roxul Flexi-batt™ insulation in the stud space (R13),
- 13 mm (1/2") Georgia-Pacific Dense-Glas Gold™ exterior gypsum sheathing,
- Sto Flexyl ™ air/vapour/water barrier,
- 75 cavity filled with Roxul Lamella™ insulation (R11) with grooves cut for ventilation and pressure moderation, and
- Sto Silco™ finish system (Sto 'E' mesh™ embedded in Sto BTS-NC Ground Coat™, finished with Sto Silco Prime™ and Sto Silco Lit™).

Construction of the steel framing for the E panels was carried out in the laboratory as described in Section A3.1. Only materials which are specific to the E panels are discussed in the following section. Refer to Section A3.1 for the construction of the typical wall panel frame. Installation of the Sto EIF system was performed by approved Sto system installers from Walmar. The E panels were constructed in the following sequence:

1. The standard 1220 x 2440 mm (4 x 8') sheet of 13 mm (1/2") Dense-Glas Gold gypsum sheathing was cut into four pieces to make two vertical joints and one horizontal joint (See Fig. 3.E3). This was done in order to ensure representative jointing. Each piece of sheathing was attached using 32 mm (1-1/4") drywall screws at 200 mm (8") spacing around the perimeter and 400 mm (16") spacing in the field.
2. The Stoflex™ air/moisture barrier with a fibreglass reinforcing mesh was installed over the Dense-Glas Gold™ gypsum sheathing.

3. Air cores were routed in Roxul Lamella™ insulation, and the Lamella™ was instrumented and attached to the Dense-Glas Gold™ substrate using a full bed adhesive similar to Stoflex™.

4. The Roxul Lamella™ was rasped to create a flat surface and the base coat and finish coat were applied on subsequent days.

5. After the finish had cured in the laboratory for at least 2 days, the panel was transported to the Beghut and installed following the procedure described in Section A3.2.

The pressure-moderated Sto System Plus1 RS™ EIFS wall represents a new approach to EIF systems. The pressure moderation is facilitated by the addition of grooves in the joints between the 150 mm wide strips of Roxul Lamella™ cavity insulation. Roxul Lamella™, which has been used as cavity fill in EIF systems in the past, is a rock wool insulation which is cross cut so that when the Lamella™ is installed, the fibres run perpendicular to the face of the wall. Some of the physical properties of Roxul Lamella™ are listed in Table A.E1.

	Metric	**Imperial**
Dimensions (as delivered)	75 x 150 x 1220 mm	3 x 6 x 48"
Thermal resistance (ASTM-C177)	RSI = 1.90 $m^2 \cdot C^o/W$	R = 10.8 °F h ft^2 / BTU
Density (ASTM-C612)	100 kg/m^3	6.2 $lb./ft^3$

Table A.E1 - Some physical properties of Roxul Lamella™ external wall board

The E test panels are slightly modified versions of the Sto System Plus1 RS™ wall system. To more accurately simulate likely pressure fields that these walls would experience in service, the bottom of the EIFS (where the wind pressure acts on the grooves) was raised approximately 450 mm above grade. The bottom of the exterior of the test panel was finished as a face seal system. The north and south facing panels have grooves at every second Lamella™ joint, i.e., at 300 mm (12") c.c. The east and west panels have grooves at every joint, i.e., 150 mm (6" c.c.).

The frames of the E panels were instrumented following the typical instrumentation layout and procedure outlined in Section A3.5. Additional temperature sensors were installed in the north and south panels. These were located in the right-hand stud at the intersection

of the top and bottom plates. The Lamella™ (cavity insulation) was instrumented in a layout similar to that described in Section A3.5 except that six pressure taps were installed in the insulation, two each at the bottom, middle, and top of the insulation. Three of these taps were installed in the insulation midway between two vertical cores and three were installed directly in the routed core. The exterior finish was instrumented with one thermistor and five pressure taps laid out in the same configuration as for the brick veneer panels. The east panel also includes a 1" internal diameter rigid PVC pipe. The response of the pressure in the pipe (completely rigid and airtight) will be compared to the response of the panel under the same wind conditions.

The instrumentation layout specific to the E test panel is illustrated in Figure A.EA2.

Georgia-Pacific's Dense-Glas Gold™ is a premium, exterior grade siliconized-gypsum sheathing reinforced with fibreglass. The moisture absorption (5%) is approximately half that of standard exterior grade gypsum sheathing (10%) after 24 hours immersion as per the ASTM standard.

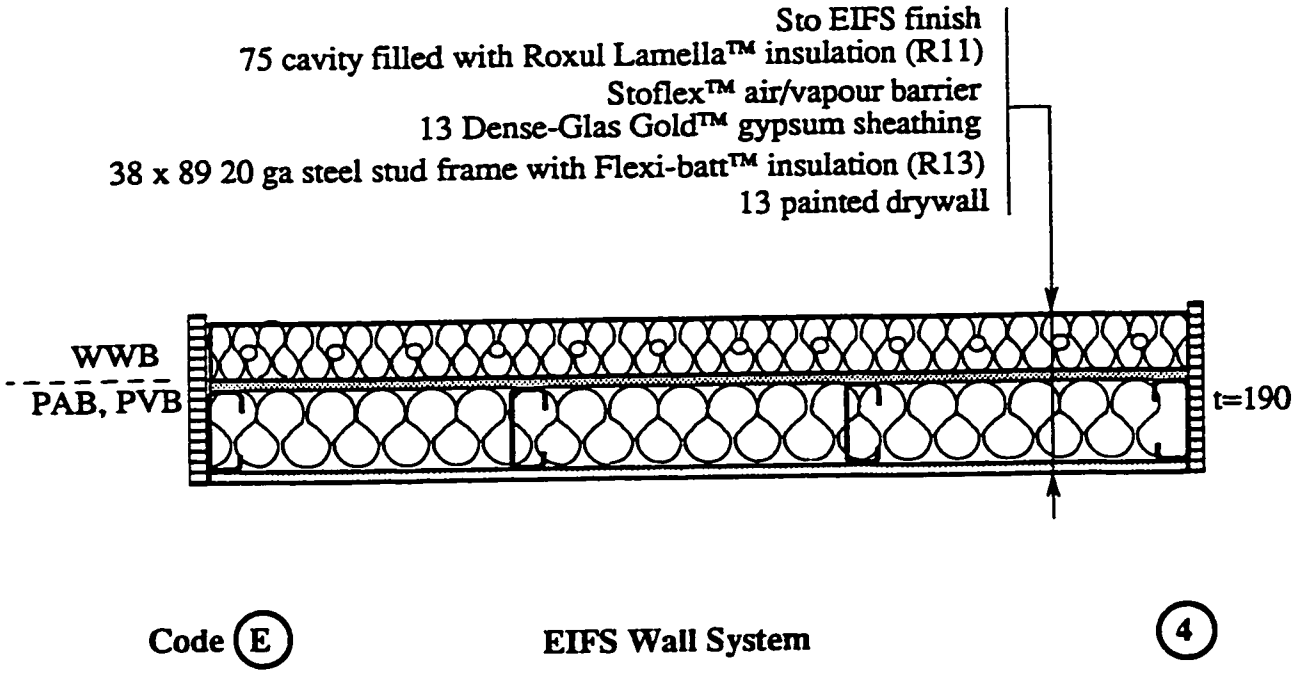

Figure A.E1 - Horizontal section through E wall panel

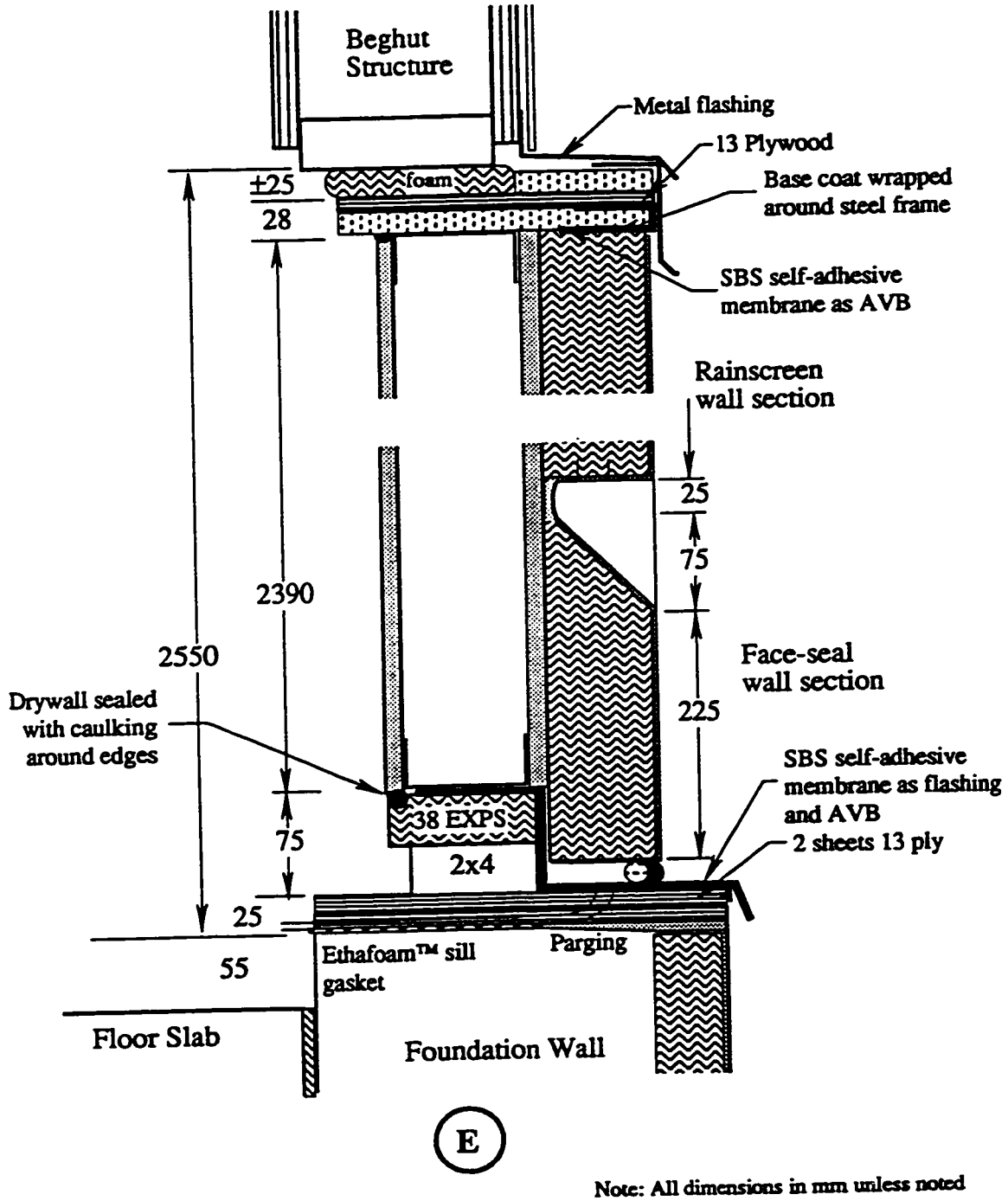

Figure A.E2 - Vertical section through E panel

Figure A.E3 - Instrumentation isometric for E panel

A2.9 Datum B Panel

The B panel is a wood-framed, brick-veneer, cavity wall intended for use in low-rise residential buildings. The composition of the B wall is typical of current residential construction practice and is intended to provide datum performance measures for low rise residential construction. From the inside, the wall consists of:

- taped and painted 13 mm (1/2") drywall,
- 0.15 mm (0.006") polyethylene vapour barrier,
- a 38 x 89 mm wood stud framing (see Section A3.1),
- fibreglass friction fit batt (R12) in the stud space,
- 32 Celfort Codebord™ extruded polystyrene insulation (R6.5),
- building paper,
- a nominal 30 mm air space, and
- an 85 mm (3-3/8") brick veneer screen (see Section A3.3).

Construction of the wood stud frames for the B panels was carried out in the laboratory as described in Section A3.1. Only materials which are specific to the B panels are discussed in this section. Refer to Section A3.1 for the construction of the typical wall panel frame. The B wall panels were completed in the following sequence:

1. The standard 1220 x 2740 mm (4 x 9') sheet of 32 mm (1-3/8"") CodeBord insulation was cut into two pieces, one 405 x 2440 mm (16 x 96") and one 810 x 2440 mm (32 x 96"), to make one vertical joint (Figure A.B3). This was done to ensure representative jointing. Each piece of CodeBord was attached using plastic headed nails at 200 mm (8") spacing around the perimeter and 400 mm (16") spacing in the field.

2. Three pieces of 910 mm (36") wide building paper were cut 1320 mm (52") long and were installed with a 50 mm (2") overlap between pieces and carried 75 mm (3") up the sides of the panel. Sheathing tape was used to temporarily fasten the building paper to the frame until installation of the brick ties. The joints at the sides and top of the panel were sealed with sheathing tape.

3. The wall was transported to the Beghut and installed following the procedure outlined in Section A3.2.

4. The brick veneer was installed as described in Section A3.3.

The B wall design was developed on the basis of an assessment of current standard low-rise residential construction practices. The Celfort Codebord™ insulation is an insulating sheathing often used in residential cavity wall applications. A wall using R 12 mineral fiber batt insulation and CodeBord™ meets the minimum level of thermal resistance mandated by the Ontario Building Code. Some of the physical properties of Celfort CodeBord™ are listed in Table A2.10.

	Metric	**Imperial**
Dimensions (as delivered)	32 x 1220 x 2740 mm	1-3/8 x 48 x 108"
Thermal resistance (ASTM-C518)	RSI > 1.14 $m^2 \cdot C°/W$	R > 6.50 °F h ft^2 / BTU
Density (ASTM-C303)	125 kg/m^3	1.6 $lb./ft^3$

Table A2.10 - Some physical properties of Celfort Codebord™

The frame, cavity insulation and brickwork of the B test panels were instrumented following the typical instrumentation layout and procedure outlined in Section A3.5. Additional temperature sensors were installed in the north and south panels. These were located in the right-hand stud at the intersection with the top and bottom plates. The instrumentation layout specific to the B test panels is illustrated in Figure A.BA2.

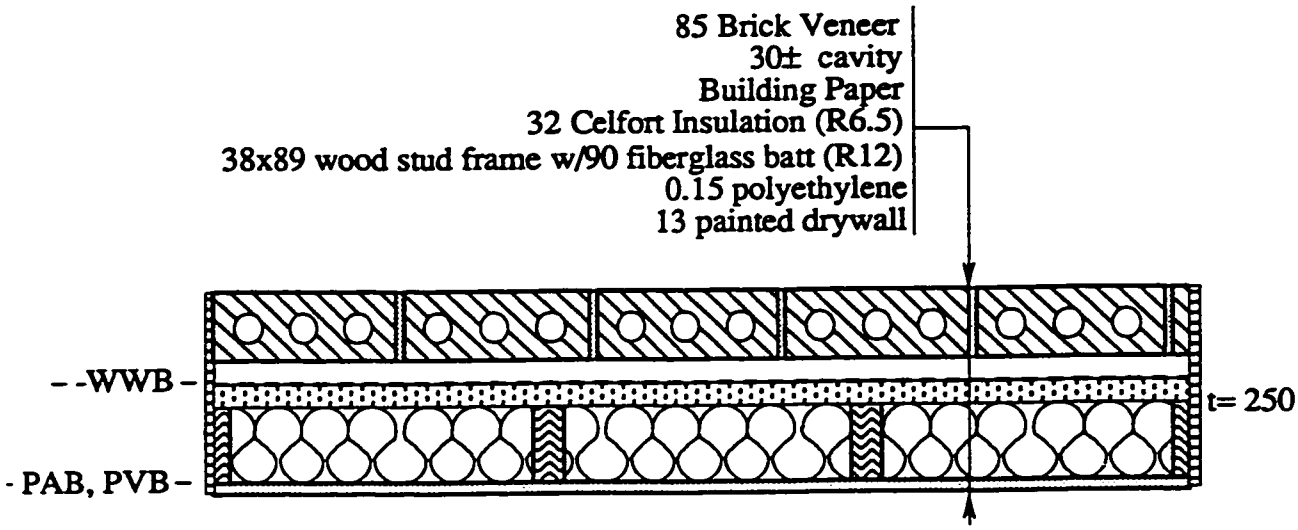

Code (B) **Datum Residential Wall Section** (4)

Control Layers
PAB : Primary Air Barrier
PVB: Primary Vapour Barrier
WWB: Weatherand Wind Barrier

All dimensions in mm unless noted otherwise

Figure A.B1 - Horizontal section through B wall panel

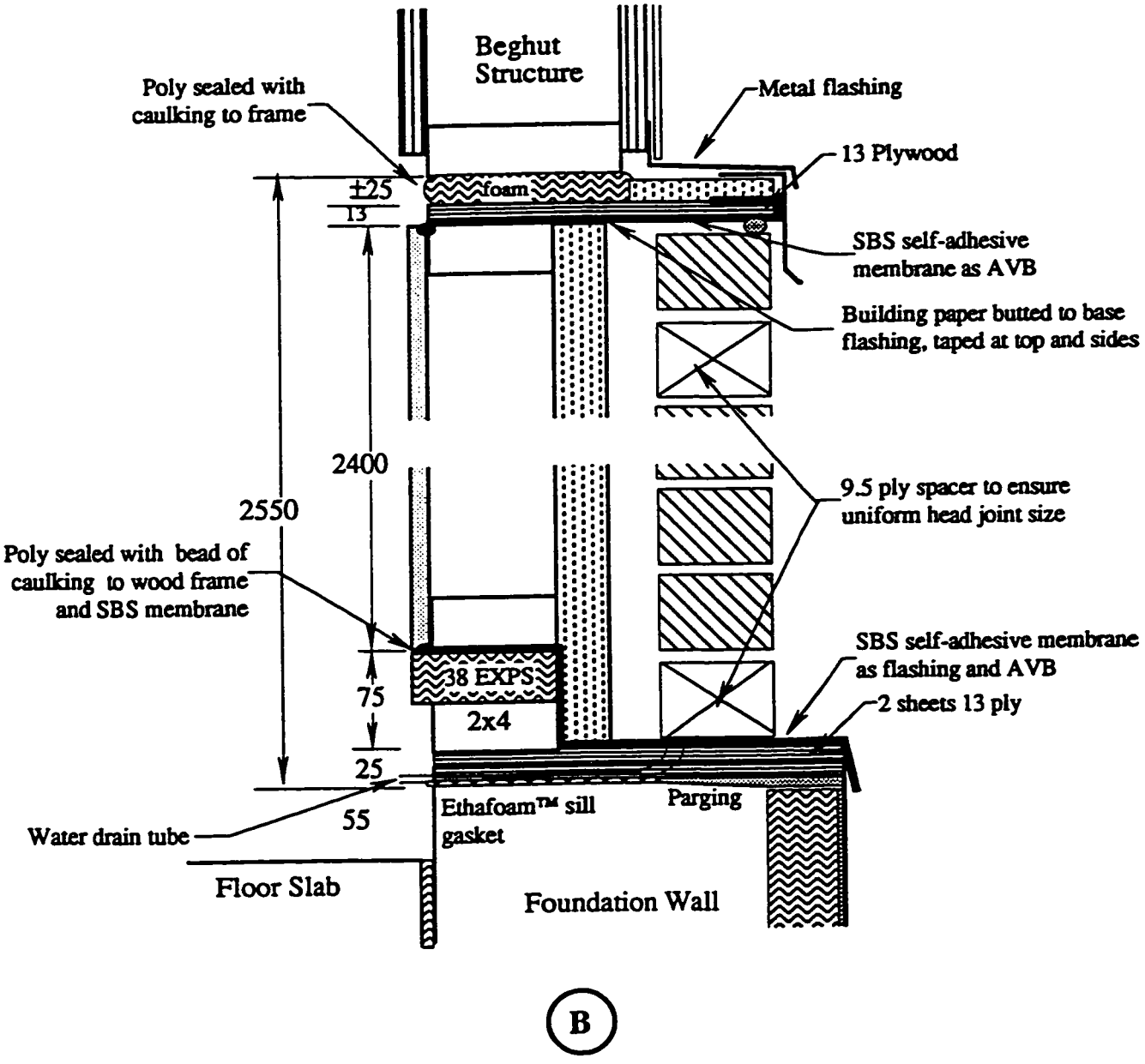

Figure A.B2 - Vertical section through B panel

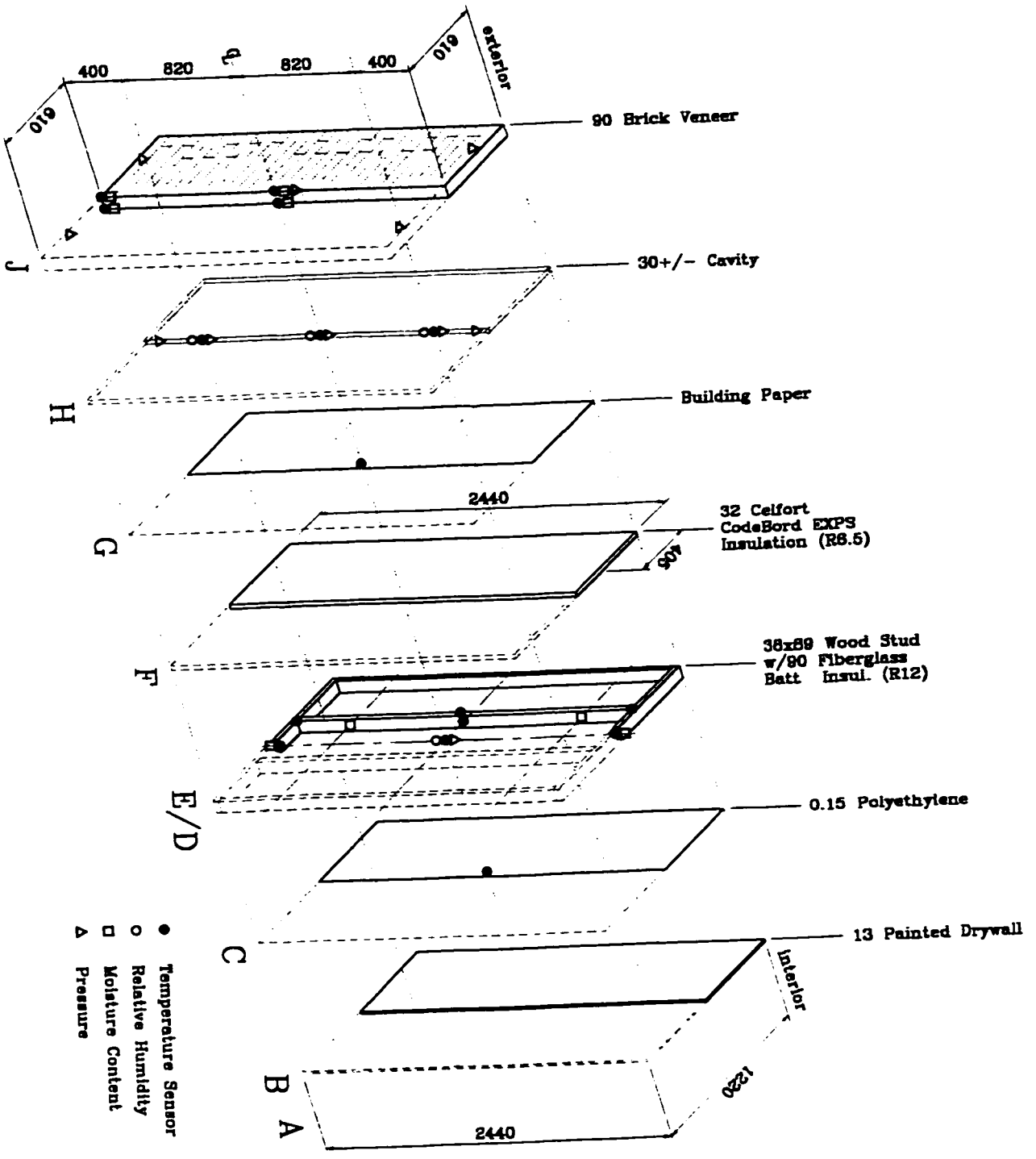

Figure A.B3 - Instrumentation isometric for B panel

A2.10 Structural S Panel

The S panel is a structural brick cavity wall intended for use in low-rise and multi-story residential buildings. The panel is a prototype wall based on a reinforced structural brick outer wythe. From the inside, the wall consists of:

- taped and painted 13 mm (1/2") drywall,
- 25 ga., 41 mm (1-5/8") deep non structural steel stud frame,
- 75 mm (3") foil faced Roxul RXL 40 insulation (R12),
- 32 mm (1-3/8") Celfort CodeBord™ EXPS insulation (R6.5),
- a 19 mm (3/4") air space, formed with strips of Celfortec foam, and
- a 110 mm (4-3/8") reinforced structural brick wythe with vents and weep holes (see Section A3.3).

The S wall was constructed entirely in situ at the Beghut because the materials and the assembly procedure used made it impossible to do any work in the laboratory. The S wall was assembled in the following sequence:

1. The typical base detail was assembled and placed on top of the foundation wall without using any fasteners. In actual practice, the reinforcing would be lapped with dowels previously cast in the concrete foundation, but in this project the wall is not being tested structurally.

2. The first course was laid and two 10 M reinforcing bars were placed in the wall, one in the second core in from the left side and one in the third core from the right side (see Figure A.S1). The brickwork was installed following a procedure similar to that described in Section A3.3. Face shell bedding (similar to blockwork) was used on the bed joints, and head joints were buttered full. The mason was asked to attempt to leave the unreinforced cores empty of mortar. As the work proceeded, cores containing the rebar were slushed full with mortar.

3. After the wall panels had set for 24 hours, they were secured to the Beghut through the top plate. Two 75 mm (3") long 6 mm (1/4") dia. Tapcon™ screws were used to attach the brickwork to the top plate; the top plate was then fixed to the Beghut structure using 100 mm (4") long # 10 wood screws.

4. The standard 1220 x 2740 mm (4 x 9') sheet of 32 mm (1-3/8") Celfortec CodeBord™ insulation was cut into two pieces, one 405 x 2440 mm (16 x 96") and one 810 x 2440 mm (32 x 96"), to make one vertical joint (Figure A.S3). This was done in order to ensure representative jointing. To create the vented cavity, the extruded polystyrene insulation was fitted with 75 mm (3") wide 19 mm (3/4") thick strips of Celfortec CodeBord™ at 16" O/C using polystyrene adhesive. Each piece of CodeBord™ was attached using Hilti IP 5/6 fasteners at 200 mm (8") spacing around the perimeter and 400 mm (16") spacing in the field. The Hilti fasteners required that a 8 mm diameter, 50 mm deep hole be drilled into the brickwork.

5. The side and top inside edges of the Celfortec CodeBord™ were sealed with acoustical sealant. The vertical joint in the field of the panel and all penetrations by the Hilti fasteners were left unsealed.

6. The Roxul RXL 40™ insulation was stacked tightly against the extruded polystyrene. No attempt was made to seal the joints in the reinforced foil facing. The 41 mm steel frame was lifted in place, plumbed independently of the RXL 40™, and fastened to the top plate with two 32 mm (1-1/2") #8 wood screws and to the bottom plate with two 75 mm (3") #8 wood screws.

7. Drywall was attached using 32 mm (1-1/4") drywall screws at 200 mm (8") centres.

The brickwork and cavity of the S test panels was instrumented following the typical instrumentation layout and procedure outlined in Section A3.5. Additional temperature, relative humidity and air pressure sensors were installed in the middle of the Roxul RXL 40™ at the middle and centre of the panel. The instrumentation layout specific to the S test panels is illustrated in Figure A.SA2. Some physical properties of the RXL 40™ and Celfortec CodeBord™ insulation are listed in Tables A.V1 and A.B1 respectively.

After air leakage testing showed that the downstream air barrier was leakier than desired, the panels were opened, and all joints between the EXPS and frame were well sealed with caulking. The drywall was reapplied and sealed. Subsequent air leakage testing showed that the drywall was tight and thet the downstream air barrier had been made much tighter.

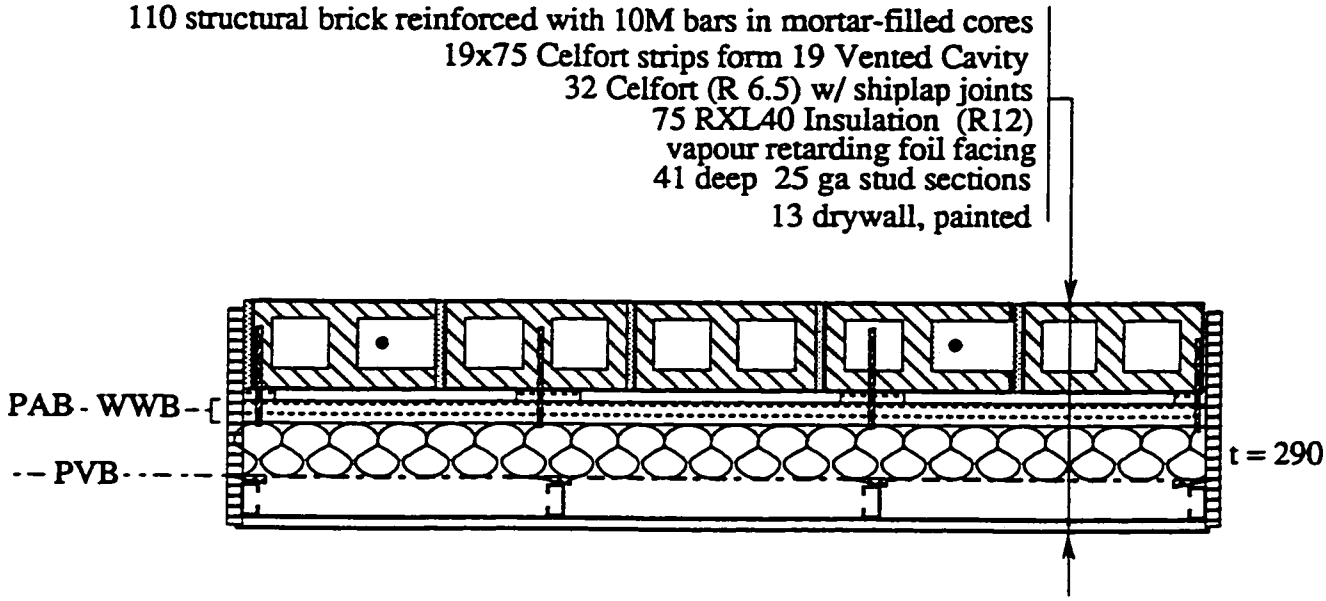

Code (S) **Structural Brick Wall** (2)

Control Layers
PAB : Primary Air Barrier
PVB: Primary Vapour Barrier
WWB: Wind/Weather Barrier

All dimensions in mm unless noted otherwise

Figure A.S1 - Horizontal section through S wall panel

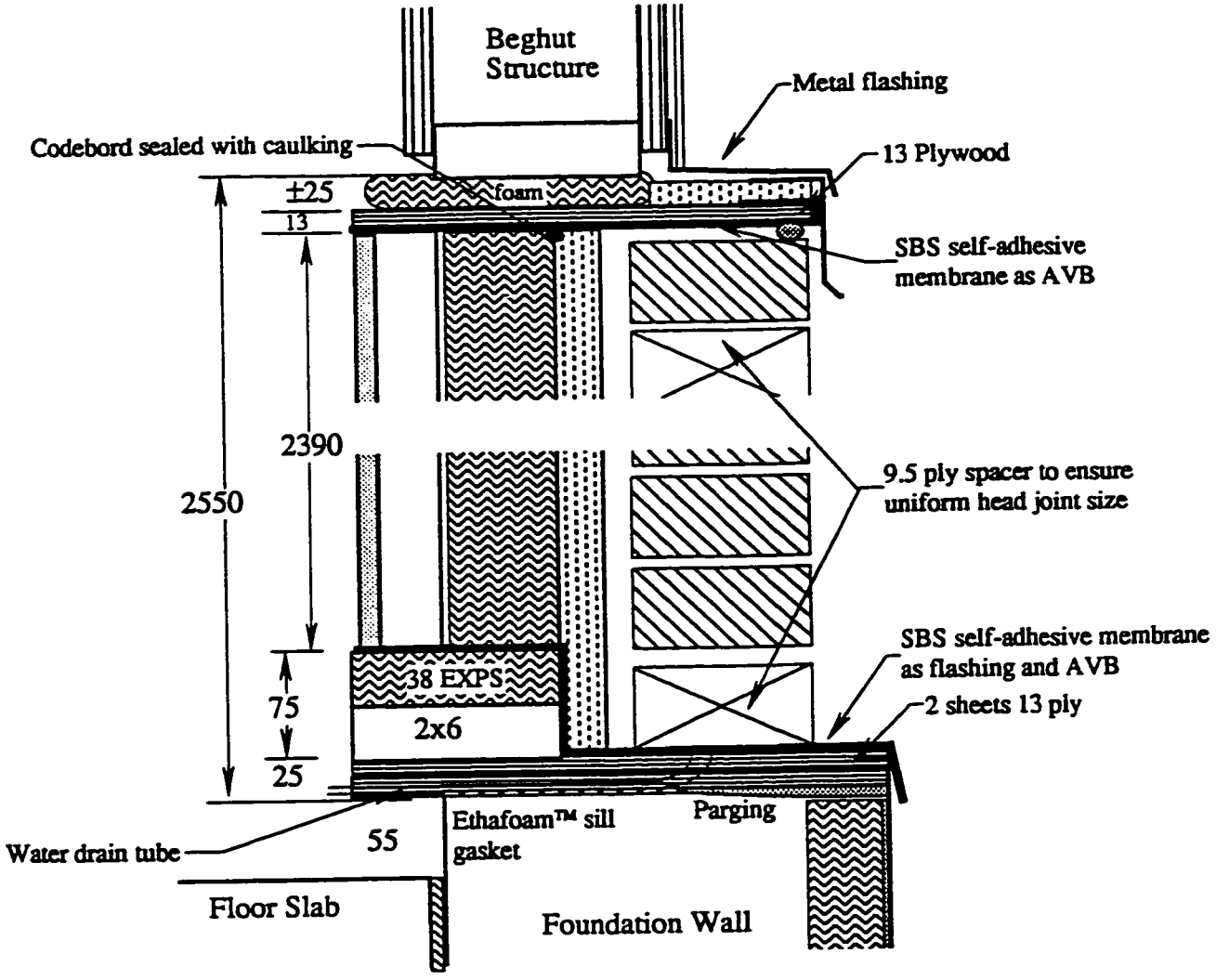

Note: All dimensions in mm unless noted

Figure A.S2 - Vertical section through S panel

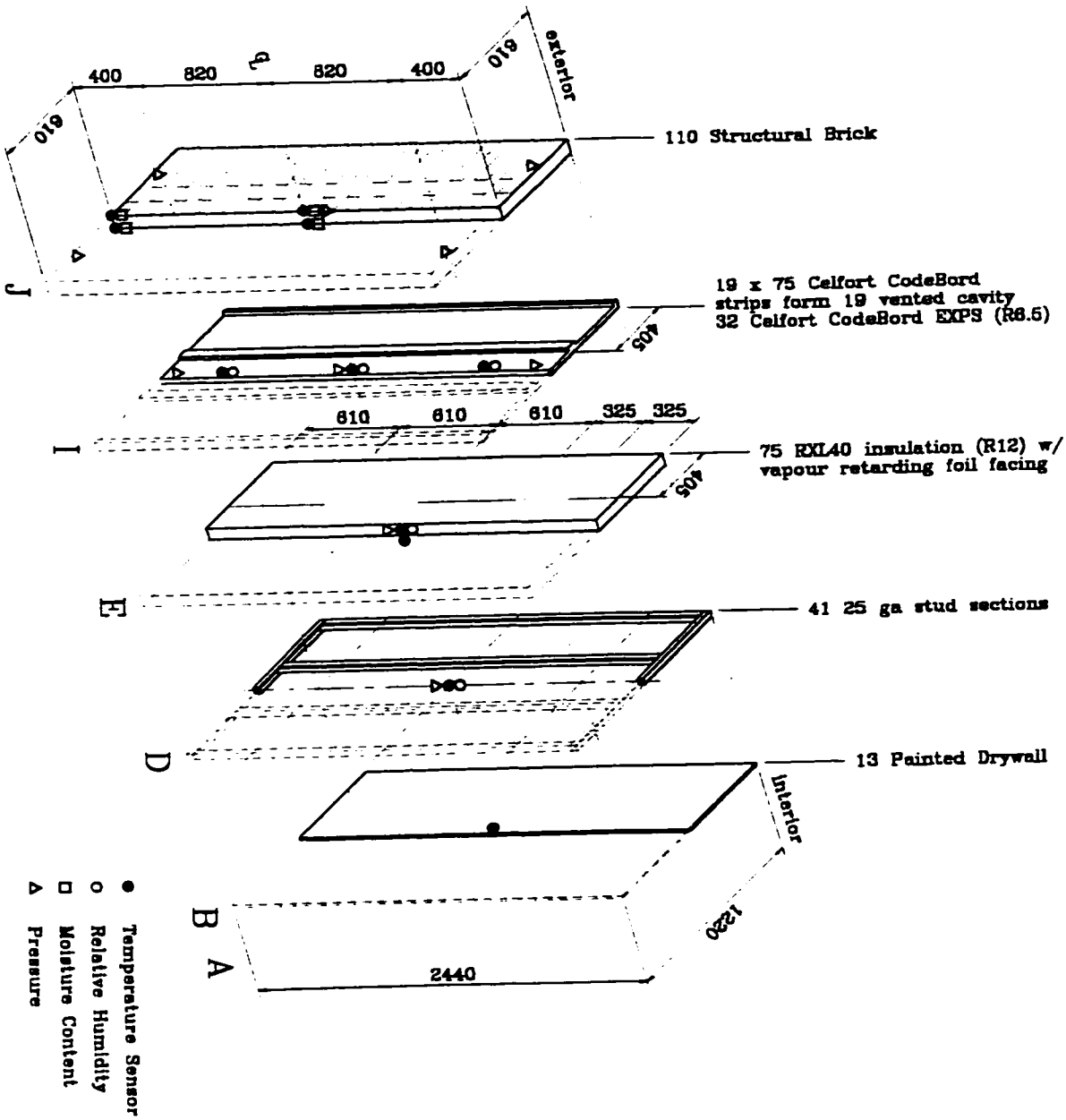

Figure A.S3 - Instrumentation isometric for S panel

A2.11 Mockup Brick Veneer Panels

Two laboratory mockups of the field brick veneer screens were built at the same time as the brickwork in the field. Figure A.M1 provides details and dimensions of these mockups. The intent of these mockups is to provide brick veneers which can be tested under controlled laboratory conditions, and to provide a realistic test bed for draining insulation tests and the study of ventilation flow and pressure moderation.

A wood frame was built with the same dimensions as the panels in the field. The wood was wrapped in an air and watertight SBS modified bitumen membrane. The frame was bolted to a heavy steel section, itself bolted to the concrete floor, and stabilized at the top by means of tensioned cable stays. The base of the brickwork was raised by 38 mm to allow water collection troughs, one on the front and one on the back of the veneer, to be installed.

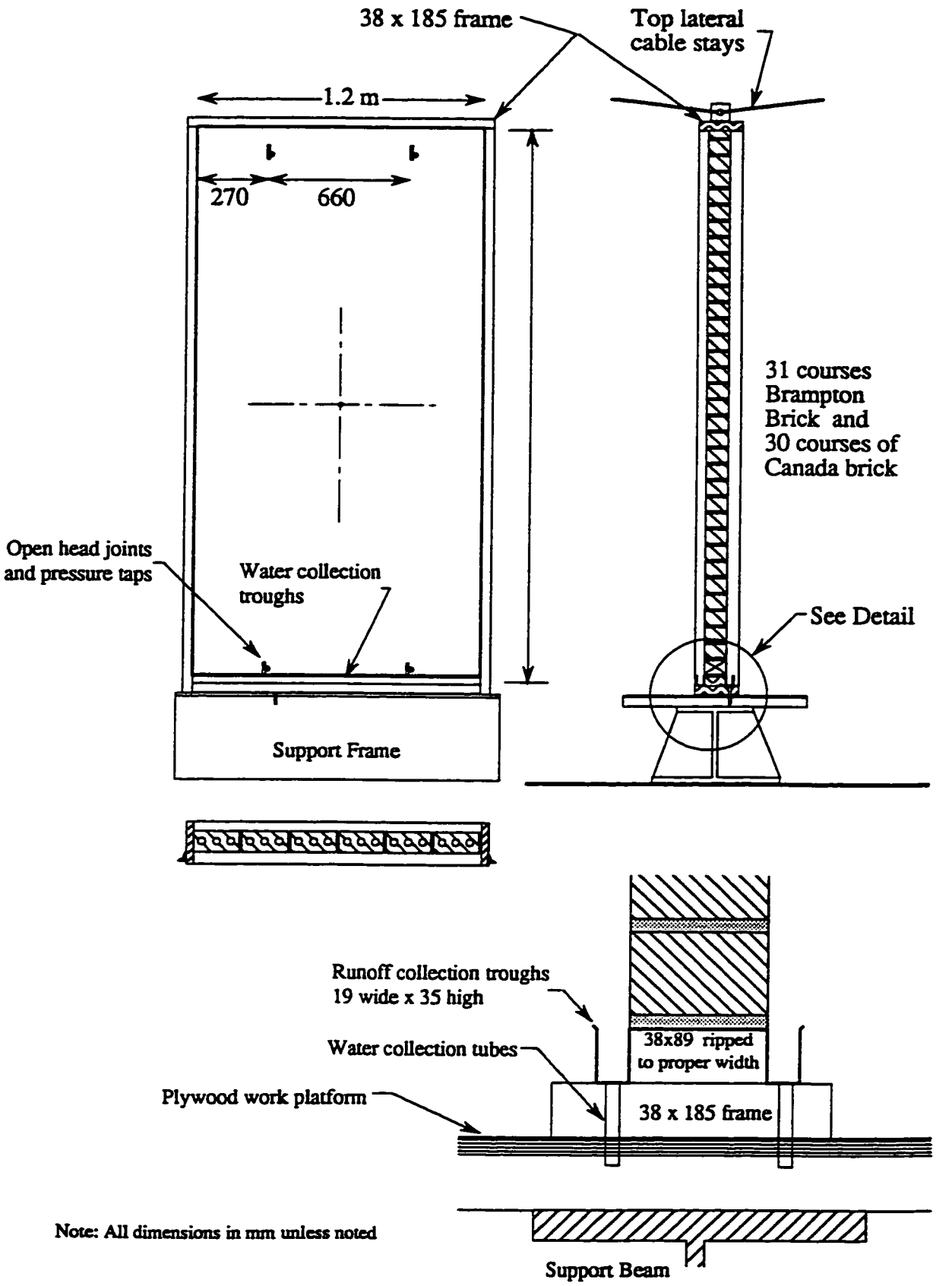

Figure A.M1 - Details of Laboratory Mockup Brick Veneer Screens

A3. TYPICAL PANEL CONSTRUCTION AND INSTALLATION PROCEDURES

The following sections discuss the typical construction details common to several types of walls, namely, framing configurations, base details, weep hole collectors, brick veneer, and special details for instrumentation. The actual materials and assembly and installation procedures vary depending on the particular make-up of each wall system.

A3.1 Construction Procedure

The E and V wall panels were assembled entirely in the laboratory. The remaining wall panels (D, R, O, F, W, B) were assembled in the laboratory except for the cladding which was installed in the field after panel installation in the Beghut. The C, S and X walls were constructed entirely in place in the Beghut because the materials and assembly procedures made it impractical to transport these walls.

The steps involved in the laboratory assembly of the framed walls are outlined below:

1. The framed wall panels were assembled flat on a raised work surface.

2. Either:
   Grade number one or better eastern white pine lumber was used for all wood framing. All pieces were selected to be straight and relatively clear of knots and other imperfections that may affect moisture content readings. Studs and plates were cut to the correct length and joined using two #10 x 89 mm (3-1/2") wood screws at each intersection. Studs were placed on 405 mm (16") centres and the frames were constructed to the dimensions shown in Figure A3.1.
   Or:
   Twenty gauge steel studs and track were used for all steel framing. These pieces were delivered precut and were assembled using two #8 x 13 mm (1/2") pan head, self-drilling, self-tapping screws at each intersection. Studs were placed on 405 mm (16") centres. The frames were constructed to the dimensions shown in Fig. A3.1. The knockouts in the steel studs along the outside edges of the panel were sealed with sheathing tape.

3. Special top and bottom assemblies were pre-built and attached to the top and bottom plates of the frames using 4 #10 x 89 mm (3-1/2") wood screws. Silicone was used to seal the penetration where wood screws passed through the steel track. The function and construction of these base assemblies is described in detail in Section A3.A2.

4. Where required, a sheet of 0.15 mm (0.006")l polyethylene was attached to the frame and sealed to the studs and plates with a bead of acoustical sealant. Drywall was then attached using 32 mm (1-1/4") drywall screws at 200 mm (8") centres.

5. Two 38 mm (1-1/2") holes were drilled through the polyethylene film and drywall, at the centre line, each 400 mm (16") above and 400 mm (16") below the panel edge, as illustrated in Figure A3.1. The hole in the upper position was fitted with a PVC threaded union and elbow for use as an instrumentation port (Figure A3.2). The lower hole was fitted with a threaded union and cleanout for air permeance testing (Figure A3.2). Both fittings were sealed with acoustical sealant and secured with a nut on the union. The panels were turned over and laid cavity side up to be instrumented and insulated.

6. Sensors were placed at the locations illustrated in Fig. A3.1. Insulation was fitted as required, and the instrumentation cables were fed through the upper instrumentation conduit and coiled beneath the panel.

7. The side of each frame was fitted with three short lengths of PVC pipe which acted as instrumentation ports for wiring in the cavity and screen. They reduced the need for penetrations through the air barrier and insulation in the walls while minimizing the amount of wiring in the cavity (Fig. A3.2). The panel was isolated from heat transfer through the sides using 16 mm (5/8") thick, foil-faced polyisocyanurate insulation. Successive layers of material were installed and instrumented as required by the design of each wall type.

Panels were temporarily covered with Typar and stored in the UW Structures Laboratory in an upright position.

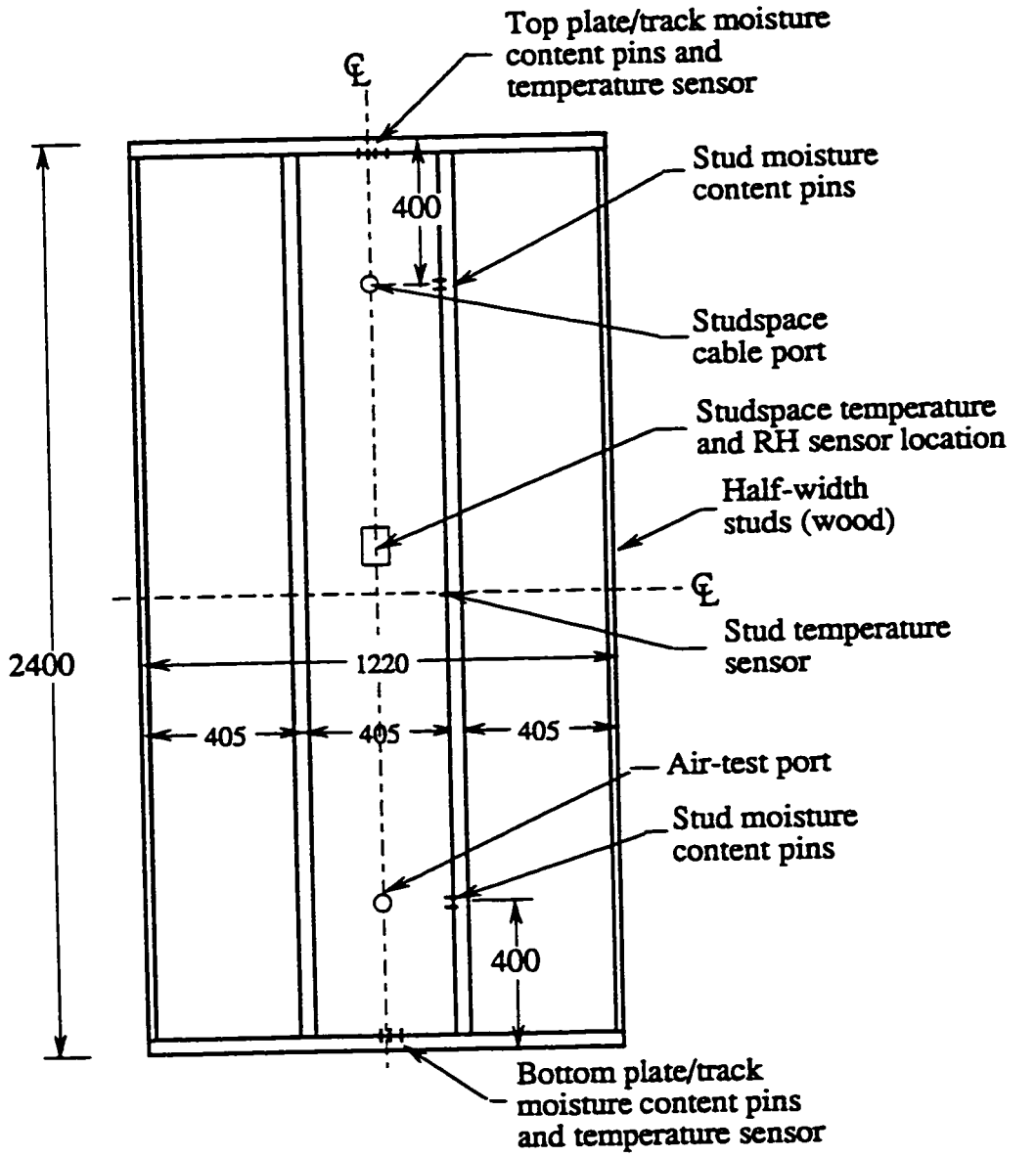

Figure A3.1 - Framing and Studspace Instrumentation

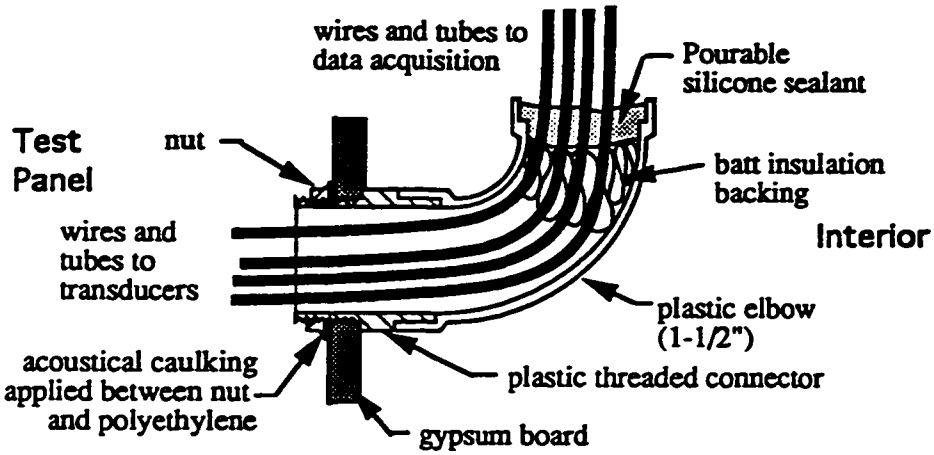

CONDUIT THROUGH DRYWALL

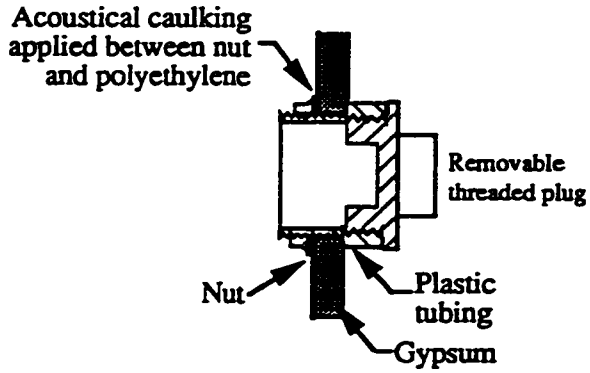

AIR-TESTING DUCT

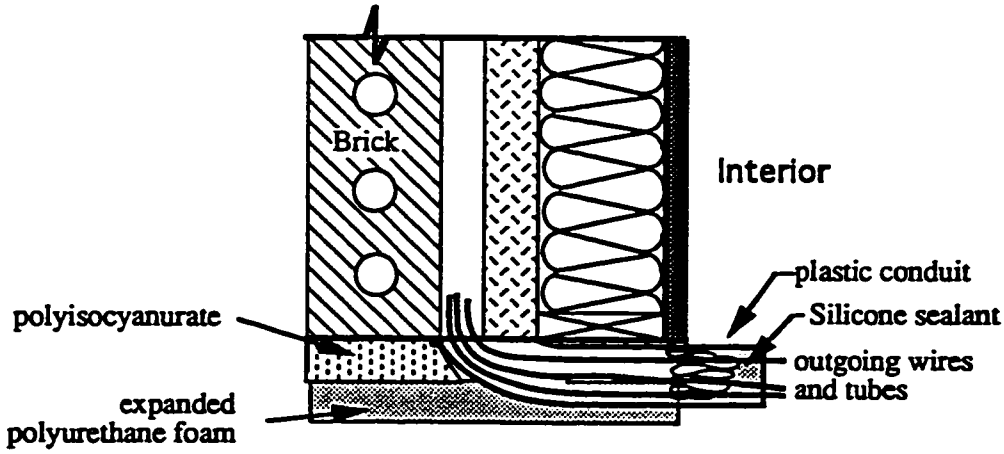

CONDUIT AT SIDE OF PANEL

Figure A3.2 - Special Details

A3.2 Installation Procedure

Panel installation was similar for all laboratory-built wall panels; details are given below:

1. Each panel was transported the 1/2 km to the Beghut in a horizontal position on the back of a 3/4 ton truck.

2. Panels were handled and tilted into place by a crew of four. Each wall was leveled, plumbed and temporarily fastened to the structure of the Beghut using two screws.

3. In addition to the temporary sheet of protective Typar installed in the lab, a polypropylene tarpaulin was used to protect the panels prior to the installation of the exterior cladding.

4. The gaps between panels were covered using Bakor Blueskin SA. This provided an air and water-tight weather barrier.

5. Over a six-week period, before and after the installation of the brickwork, the space between panels was filled with expanding polyurethane foam. This foam acted in conjunction with the polyisocyanurate rigid board insulation and Blueskin membrane to control air, water, vapour and heat flow between panels.

6. Metal flashing with a drip edge was fitted above each panel. The remaining space above the panel was foamed to isolate the panel from the Beghut and to ensure an airtight seal.

A3.3 Brickwork and Ties

All brickwork, except for the S wall panels, was installed by masons from the Ontario Masonry Training Centre (OMTC) on May 30 through June 1, 1995. The structural brickwork for the S wall panels were installed by an instructor from the OMTC on August 22, 1995. BEG personnel were present to instrument, observe, and provide quality control during all brick laying. The brick coursing, weep holes and vent holes were laid out as illustrated in Figure A3.3. Type S mortar and the same sand was used for all panels. CSR size bricks (90 x 70 x 230 mm) from either Brampton Brick or Canada Brick were used for all panels except the S panel. Table A3.1 provides details of the brickwork used on each panel, namely the manufacturers of the bricks, the type of wall tie, and the back-up used for each panel type.

Panel Type	Brick Supplier	Tie System	Back-up
R	Brampton Brick	Helifix Tim-ties	Wood framing
O	Canada Brick	Posi-lag	Steel framing
F	Canada Brick	Posi-lag	Steel framing
W	Brampton Brick	Helifix Tim-ties	Wood framing
C	Brampton Brick	Helifix HRT 60	Wood framing
B	Canada Brick	Strap ties	Wood framing
S	Canada Brick	None	Non-structural
X	Brampton Brick	None	None

Table A3.1 - Wall types, bricks and ties

During the design phase, the choice of the method of anchoring the brickwork veneer to the backup was a major issue. Experience in the UK indicated that brick ties were a source of problems in filled-cavity, brick-veneer walls. Ideally, the tie should pierce the insulation (so that water will easily flow around the tie), it should be corrosion resistant (because the level of moisture in the cavity is expected to be higher than in normal cavities), and it should allow for fast and easy installation and vertical adjustability.

The only masonry tie which met these criteria, albeit applicable for use in wood framing and Durisol block backup only, was the Helifix tie.

A special tie was developed for panels with steel framing to meet most of the criteria described above. This tie was made of a 6 mm (1/4") diameter lag bolt with a washer welded to the hexagonal head. When the mason reached one course below the prescribed location for a tie, a pilot hole was drilled at the correct height through the cavity insulation, sheathing (if any), and the outer flange of the framing. The lag bolt was then turned into the steel stud until the hole in the washer was flush with the outer face of the insulation. A trapezoidal wire tie was then inserted to connect the tie to the brickwork. This tie was dubbed the Posi-lag. In practice, the tie would be stainless steel with a self-drilling, self-tapping thread. A variation of a hook and pintle wire tie could be used to provide vertical adjustment if the ties were installed before the mason arrived. A standard plastic insulation retention washer could be snapped over the head of the tie after installation to fix the insulation in place.

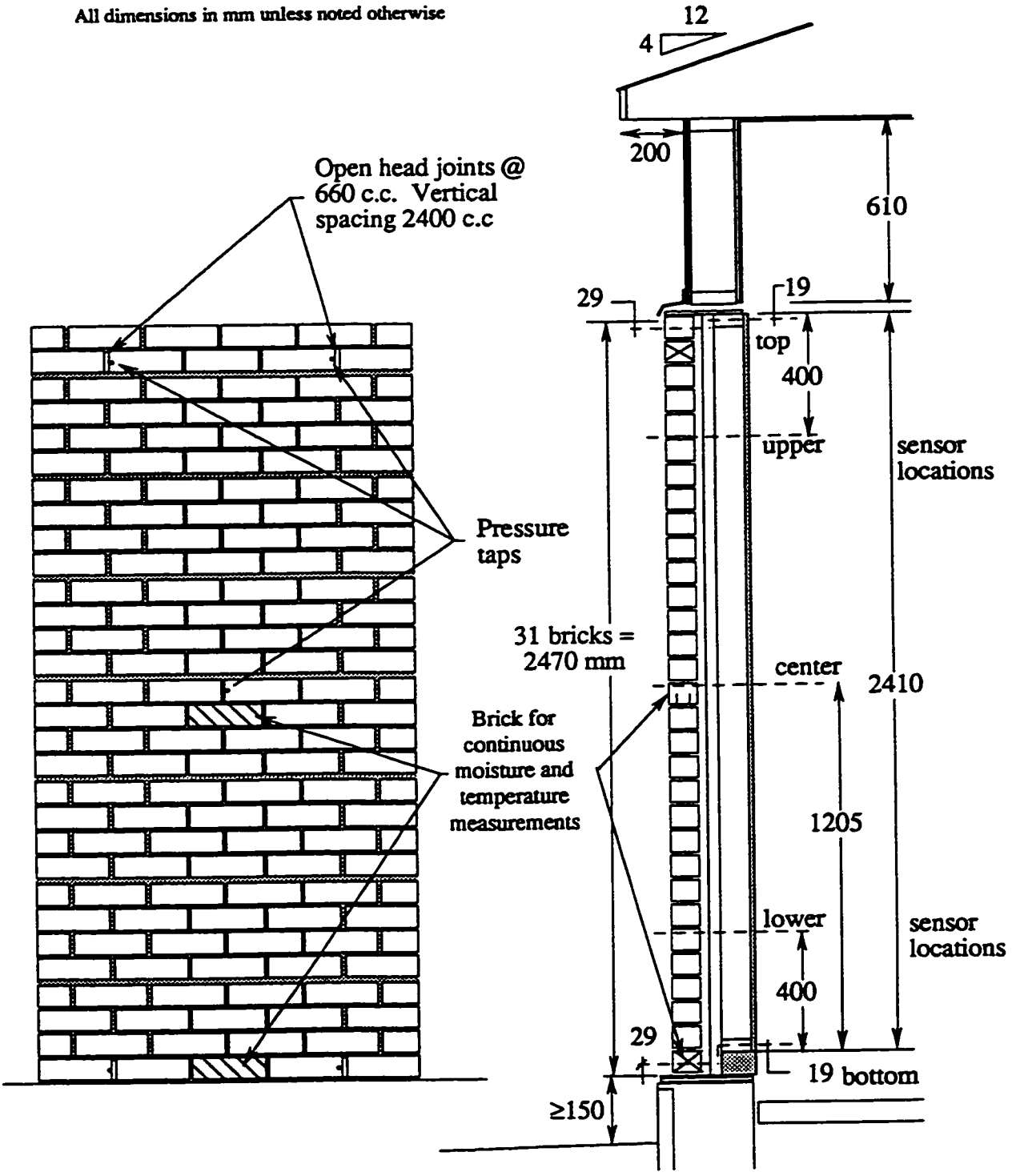

Figure A3.3 - Brickwork Details and Instrumentation

A3.4 Special Features

The following special features were incorporated into the construction of the panels to facilitate instrumentation and to enhance the performance of the experiment:

- A PVC conduit was installed as a port on the panel centre line 400 mm (16") down from the top of the frame to collect and lead wires and tubes out of the panel. This port was later sealed with a self-levelling fire stop to ensure an airtight seal (see Figure A3.2).

- Three more PVC conduits were installed as instrumentation ports on the right-hand side of each panel - one each at the middle and at 400 mm (16") from the top and bottom - to collect the wires and tubes from the cavity. These ports facilitated the instrumentation in the interior of each wall panel and avoided penetration of the sheathing (see Figure A3.2).

- An air test port was also installed on the panel centre line 400 mm up from the bottom of the frame to allow air leakage testing on each panel. This PVC fitting is similar to that used for the upper instrumentation port except that it has a screw-in plug to seal the port (see Figure A3.2).

- Half width studs were used for the end studs of each panel. These studs have a similar volume and surface area to that part of the stud which would normally be included in a 1220 mm (48") section of wall. Thus a representative 1220 mm (48") section is being modelled.

- Special top and bottom assemblies were constructed to isolate the panel from the Beghut structure and more closely simulate in-service conditions (see panel vertical section). The bottom assembly was constructed with a 75 mm (3") high step to ensure that the bottom plate/track of the frame was elevated above the base of the brickwork, as is the case with most residential and commercial wall systems. Although the 75 mm (3") step is less than a typical 250 mm (10") rim joist or 200 mm (8") reinforced concrete floor, the test panel should behave as the wall assembly would in service. Two copper weep hole tubes were fitted into grooves in each of the bottom assemblies to intercept and collect any water which may drain out of the cavity through the traditional weep holes.

A3.5 Typical Sensor Locations

The following sub-sections discuss the typical sensor locations that are common to most wall types. Actual sensor locations vary, depending on the particular construction of each panel. The variations in sensor locations are discussed in Chapter A2.

A3.5.1 Sensor Coding System

Table A3.2 outlines the seven-letter system used to identify each individual sensor in the Beghut. The first two letters, the panel identification code, identify the wall system and orientation of the test panel. The third letter, the sensor type, indicates the property measured by the sensor. The last four letters, the sensor location code, identify the location of the sensor within the wall assembly.

For example, the sensor labeled RNTENMC is a temperature sensor located in the north-facing R test panel in the middle of the batt insulation (interstitial) at the middle and centre of the panel.

A3.5.2 Sensors in Wood Framing

Each wood frame was fitted with moisture content and temperature sensors. Moisture-content and temperature sensors were located on the panel centre line at the top and bottom plates of the frame (Figure A3.1). Moisture-content sensors were also installed on the right stud (as seen from inside) at 400 mm (16") from the top and bottom of the frame. Temperature sensors were also placed at mid-height of the right stud, at the outside surface, and in the middle. A pressure tap and temperature and relative humidity sensors were installed in the middle of the batt installation at the centre and middle of each panel. In some cases, additional temperature sensors were installed at the framing intersections and/or the interior surface of the stud.

Panel Identification Code	Panel Code	R, V, O, F, W, D, C, E, B, S, and X
	Orientation	N - North E - East S - South W - West
Sensor Type	Measured Property	M - moisture content P - pressure R - relative humidity T - temperature
Sensor Location Code	Layer (if present)	A - interior air film B - drywall C - polyethylene V.B. D - stud frame E - batt insulation F - sheathing G - typar/bldg. paper H - cavity insulation I - cavity J - cladding
	Location through layer	I - inside N - interstitial O - outside
	Vertical position	T - top U - upper M - middle L - lower B - bottom
	Horizontal position (as seen from the inside)	L - left C - centre R - right

Table A3.2 - Instrumentation Coding System

A3.5.3 Sensors in Steel Framing

Each steel frame was fitted with temperature sensors and moisture content sensors. The moisture content sensors were installed in short lengths of eastern white pine to provide an indication of the level of moisture in the stud space and bottom track. Moisture content and temperature sensors were located on the panel centre line at the top and bottom plates of the frame (Figure A3.1). Moisture content sensors were also installed on the right stud (as seen from inside) at 400 mm (16") from the top and bottom of the frame. Temperature sensors were also placed at mid-height of the right stud, at the outside surface and at the inside surface. A pressure tap and temperature and relative humidity sensors were installed in the middle of the batt installation at the centre and middle of each panel. In some cases extra temperature sensors were installed at the framing intersections.

A3.5.4 Sensors in the Wall Cavity

Pressure taps and temperature and relative humidity sensors were installed on the centre line of the panel in the middle of the cavity or cavity fill at the middle and at 400 mm (16") from the top and bottom of each panel (Figure A3.3). Pressure taps were also positioned on the centre line of the panel 50 mm (2") from the top and the bottom of each panel.

A3.5.5 Sensors in the Brickwork

Two bricks in every panel were instrumented (see Fig. A3.3). The brick in the centre of the bottom course was instrumented for moisture content only. The brick in the middle course was also fitted with temperature sensors on the inside and outside surfaces. Temperature and moisture content sensors were located near the inside and outside surfaces of the bricks on the centre line of the panel in the bottom and middle courses.

Pressure taps were installed in the centre brick and in the bricks directly beside the weep holes and vent holes.

A3.6 Detailed Sensor Description

All of the test panels were instrumented to measure temperature, relative humidity, moisture content, and air pressure at various points in the panel assemblies. The typical sensor locations are described in Sections A3.5, and the specific sensor locations are given in Chapter A2. This section provides detailed descriptions of the sensors used in the instrumentation of the wall panels.

A3.6.1 Temperature Sensors

All of the panel temperature sensors are precision thermistors with a 10 000 Ohm @ 25 degrees Celsius. Two types, produced by Fenwall and YSI, have been used, both with an interchangeabililty of better than 0.2 °C. The thermistors and their soldered connection to the instrumentation wiring was coated with an electrically insulating and waterproof liquid plastic.

A3.6.2 Relative Humidity Sensors

A knowledge of the relative humidity within a wall assembly is valuable because the potential and incidence for condensation can be measured and the amount of moisture in a space in a wall will be reflected in the moisture content of the air in the panel. Two models of sensors have been used to measure relative humidity: Hycal Engineering model Survivor II and Vaisala model HMW 20 UB.

The Vaisala sensor is a wall-mounted type with the sensor and printed circuit board encased in a plastic shell, 32 mm deep, 85 mm wide and 110 mm high. The sensor is effective over a range of 0 to 100% relative humidity with an accuracy of ±2% RH. The transmitter returns a 4 to 20 milliampere current which is converted to a voltage using a simple circuit. The measured voltage is then converted to a RH percentage by the computer software. The HMW 20 UB was calibrated with a Vaisala HMK 20 single-point calibrator, itself calibrated with salt bath solutions. The calibrator registers the difference between its RH reading and that of the sensor. The difference is adjusted to read zero with the dial provided; a difference of approximately ±0.1%RH was considered satisfactory in the calibration procedure.

The Hycal sensor is a CMOS integrated circuit that has a thin film RH sensor. The sensor is housed in a metal TO-5 case (approximately 6 mm in diameter and 6 mm high) with an integral hydrophobic filter. The Survivor II outputs a voltage proportional to humidity corrected for temperature. NIST-traceable calibration data are provided for each sensor. Accuracy is better than ±2% RH from 5 to 95%RH, and long-term (5 year) drift is less than 1%RH. The very small size of the sensor results in the minimum of interference with the space being measured.

A3.6.3 Wood Moisture

Moisture-content readings were made in the steel framing as well as the wood framing. The moisture-content sensor for the wood framing consists of Delmhorst pins that were driven directly into the wood framing. The moisture-content sensor for the steel framing consists of Delmhorst pins driven into 150 x 89 x 19 mm (6 x 3-1/2 x 1-1/2") blocks of clear pine with sealed ends. The relatively small volume of the wood blocks means that the same volume of moisture will result in relatively higher moisture content reading in the steel framing.

Figure A3.5 illustrates the spacing and depth of the pin placement. The moisture content is measured by passing a 12 volt direct current between the pins. The voltage is applied for about 0.1 seconds to allow the readings to stabilize. The resistance values can be correlated with readings from a Delmhorst model RC-1D moisture meter. The software calculates the moisture content and corrects for temperature and species.

Measurement of wood moisture content is not as accurate as the measurement of temperature and relative humidity. The recorded moisture content does not necessarily represent the average moisture content of the wood. Moisture gradients are present through the wood as a result of drying/wetting of the wood and the environmental conditions that promote it, as well as wet pockets that might not represent the average moisture content. The actual accuracy of the resistance-type meters used is estimated as ±2% within the range of 6 to 25%; however, a considerable loss in accuracy can be expected outside this range. Above fiber saturation (25 to 30%), the meter will generally return lower values than actually exist, whereas below 6%, the resistance becomes so high it cannot be properly measured.

A3.6.4 Brick Moisture

Measuring brick moisture in-situ is very difficult. To provide a relative indication of moisture content trends, two bricks in each brick panel were instrumented for moisture. Resistance measurements are made just as for wood moisture content but are saved as raw resistance values. Very high resistance values are so inaccurate and variable that readings of greater than 200 Mohms are simply saved as "> 200 Mohms". The layout of the pins is shown in Figure A3.6. The moisture content pins were located along the centerline of the brick, approximately 10 mm from the inside and outside surfaces, approximately 25 mm

from the bottom of the brick. Wiring exits from the brick and into the cavity via the bed joint.

A3.6.5 Air Pressure

Air pressure can be measured at various points within the wall assemblies to assist in the evaluation of the effectiveness of the various planes of airflow resistance within a wall assembly and the response of pressure moderating chambers within the test panel. Pressure is transmitted to transducers by equal length (3.5 meter long) Tygon™ tubing (3 mm internal diameter, 6 mm external diameter). The pressure transducers are Honeywell PX-163 silicon pizeoresistive sensors with integral amplifying and temperature compensating circuitry. The transducers cover a range of -1250 to +1250 Pa, have a response time of about 1 millisecond, and can be resolved by the data acquisition system to a pressure of less than 0.1 Pa. The arrangement of tubing and transducers results in a flat frequency response of the system up to at least 30 Hz.

A second data acquisition system is used to quickly measure the pressures and meteorological information at the same time. Software controls when the acquisition begins and whether the collected data is saved or discarded.

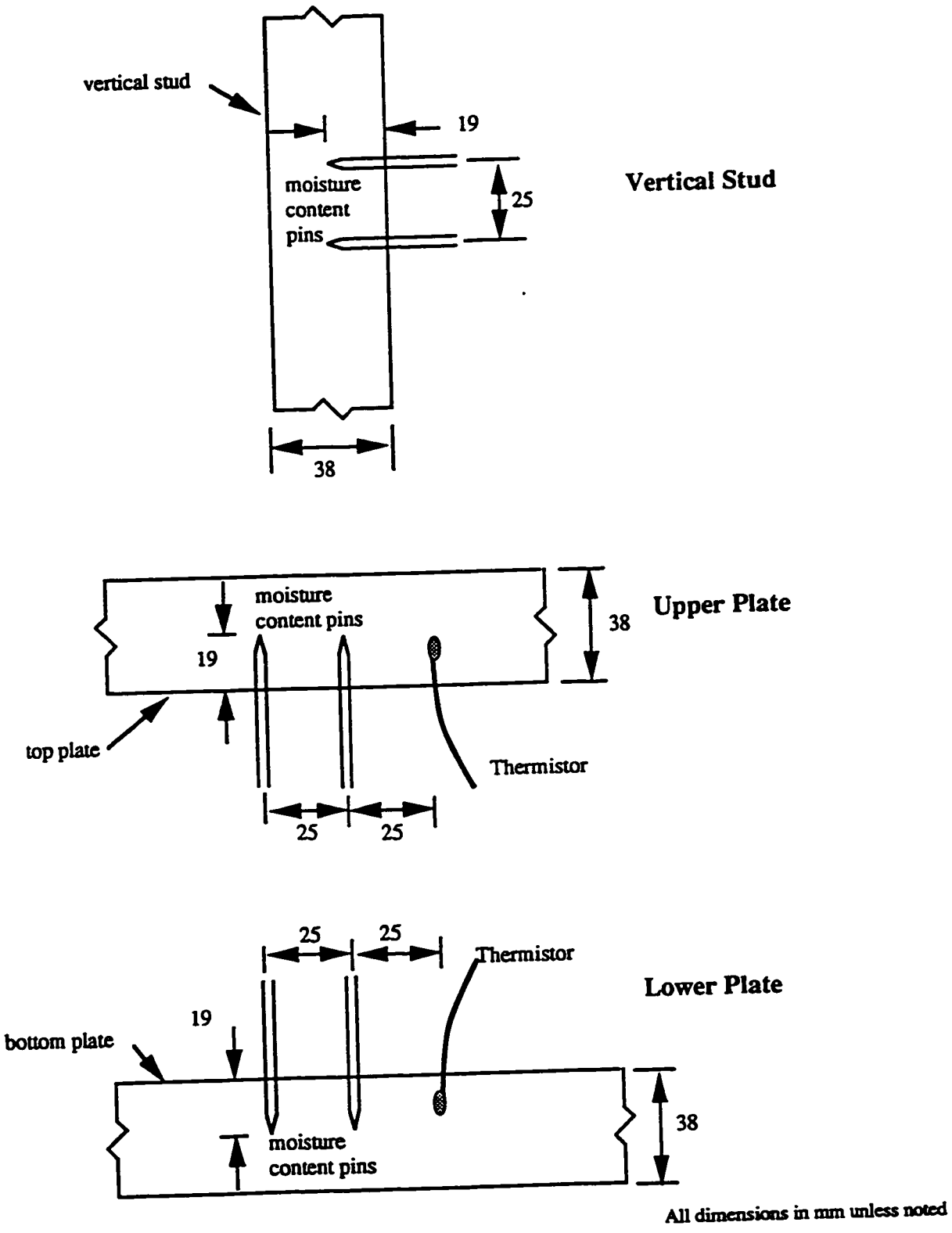

Figure A3.5 - Wood Moisture Content Instrumentation

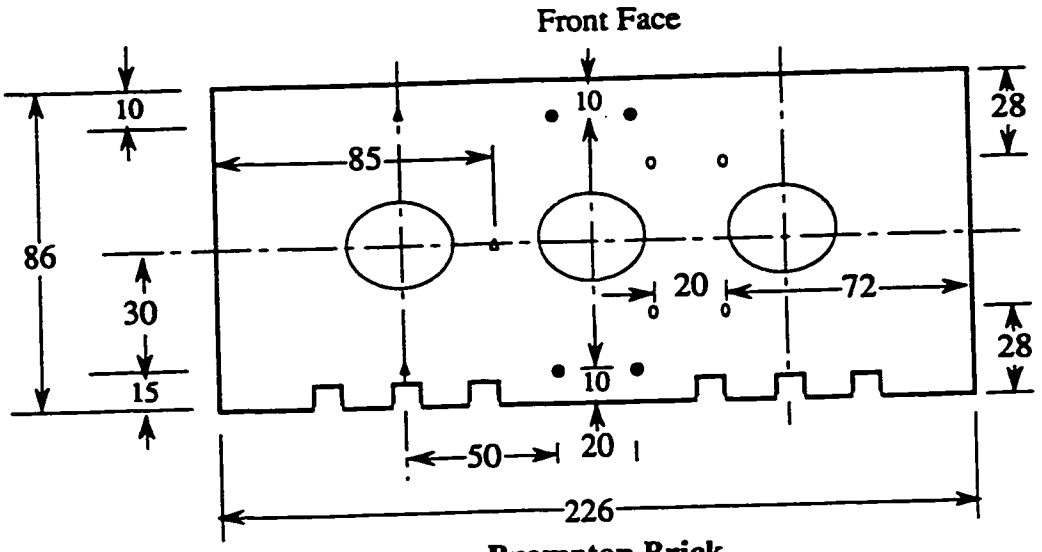

Brampton Brick

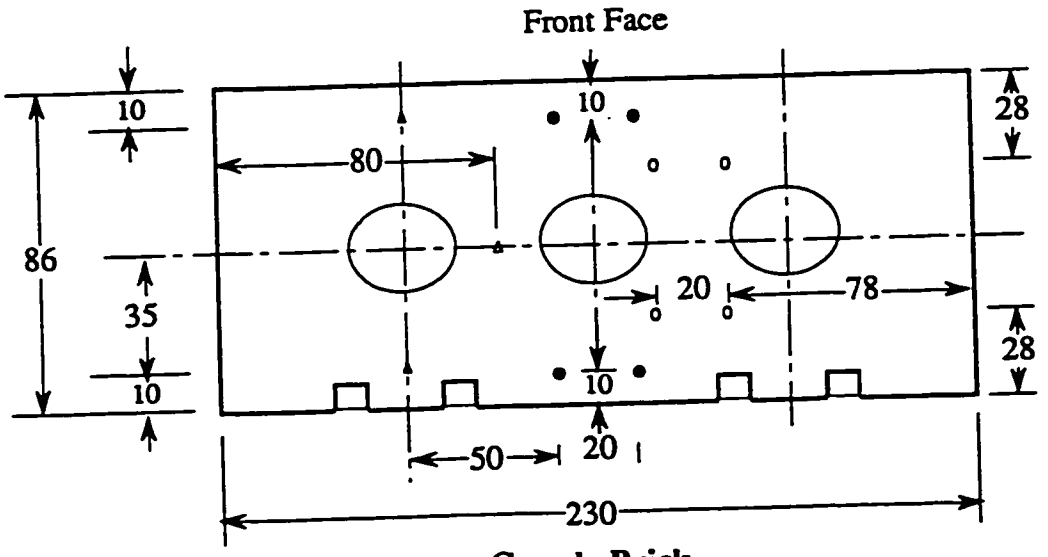

Canada Brick

Temperature measurements in middle bricks only.
Moisture measurement in bottom and middle bricks.

● ● moisture pins in all bricks

o o supplemental moisture pins in some walls

▲ temperature sensor in all middle bricks

△ supplemental temperature sensor in some middle bricks

All dimensions in mm unless noted

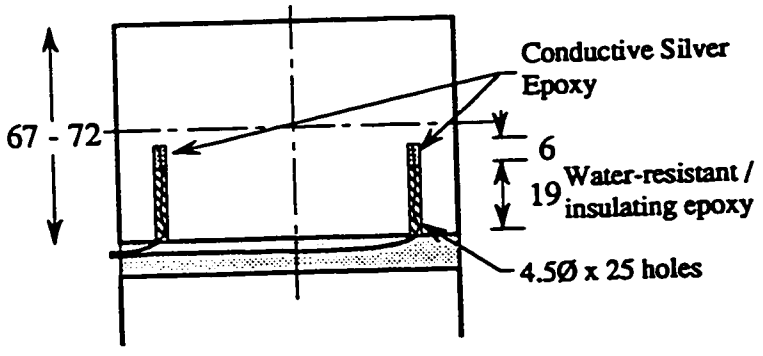

Figure A3.6 - Brick Instrumentation Details

A3.7 Miscellaneous Material Lists

Many standard building materials were used in the construction and installation of the panels. The products and specifications are listed below:

- Air sealant. Canadian Adhesives Ltd., Bulldog Grip PL Acoustic-Seal, meeting CGSB 19-GP-21-M87.
- Air and water sealant. CSL Silicones Ltd. No. 160, 30 year silicone.
- Sheathing tape. Canadian Technical Tape, Tuck Tape, CCMC #11955.
- Polyethylene sheet. Polytarp Products "super six" 0.150 mm (6 mil) thick, complies with CAN/CGSB-51.34-M86.
- Building paper. BPCO 15 lb. Plain Asphalt Felt, 914 mm wide (36") roll.
- Housewrap. Reemay Corp., Typar.
- Exterior Gypsum. Westroc Gypsum Sheathing.
- Expanding foam. Dap Canada, Dap Kwik-Foam, one component, moisture cure, polyurethane.
- Air/water sealing membrane. Bakor Blueskin SA, SBS modified bitumen self-adhering membrane.
- Masonry Cement. St Lawrence Cement Type S.
- Board Insulation. Celotex Canada Thermax 16 mm (5/8") foil-faced polyisocyanurate (RA2.5, R_v < 0.03 perms).
- Foam Adhesive. Dap Canada Foamboard Adhesive.

A4. TIMETABLE OF EVENTS

1994	July	Project conception.
	August	URIF application submitted.
1995	January	Notification of URIF funding award. Planning begins.
	April 18 - May 11	Begin construction of framed panels.
	April 29	Remove previous wall panels and instruments.
	May 16 - 26	Install R, V, O, F, W, D and B wall panels in Beghut.
	May 18	Construction of C (Durisol block) wall in Beghut.
	May 30 - June 1	Brick veneers installed on R ,O, F, W, C, B and X wall panels in Beghut.
	June 1	Construction of brick veneer test panels in lab.
	June - July	Panels sealed, inside and out.
	June 16 - 17	Installation of Durisol cladding on D walls.
	July 6 - 8	Installation of Sto finish on E walls in lab.
	July 10	Installation of E walls in Beghut.
	August 22	Construction of S wall brickwork in Beghut.
	August 24 - 29	Completion of inner wythes for S wall panels.
	July - August	Wiring of panel instrumentation to data acquisition system and panel acclimatization.
	September 2-4	Drywall sealed, primed and painted.
	September 7	Continuous monitoring of panels begins
	October 21	Continuous monitoring of driving rain begins
1996	August	Air leakage testing of panels
1997	January 1 - 31	Continuous injection of Behhut air into selected panels
	April 30	End of analysis of monitoring data
	June 1	Vent openings sealed in Wall F
	July	Water injected behind lamina of Wall EE
	Sept 24	Continuous monitoring ends

Appendix B: Selected Summary Statistics of Ventilation Pressure Measurements

Ventilation Pressure Coefficients for Each Configuration and Record

Relative Frequency Distribution of Ventilation Pressures for Each Configuration

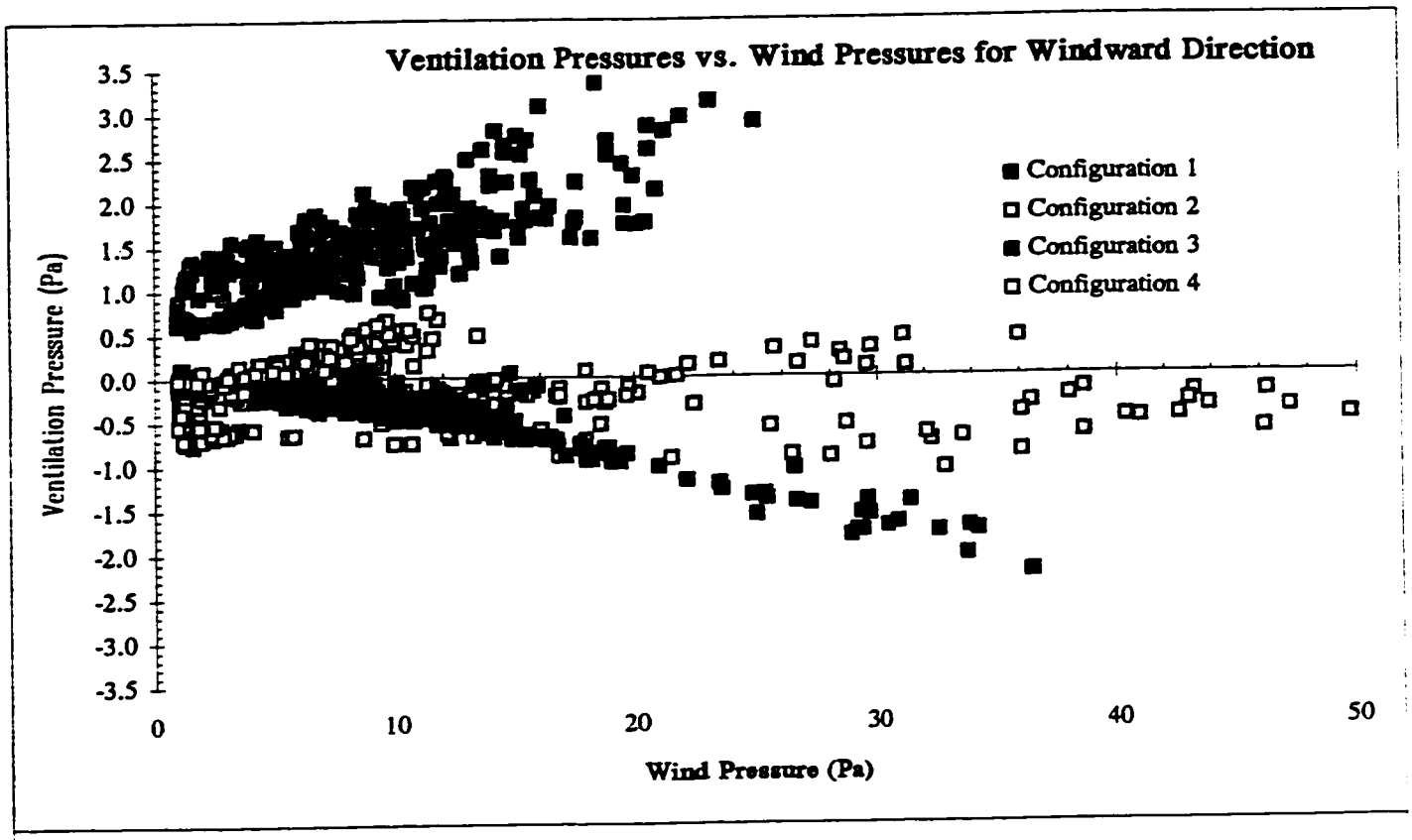
Ventilation Pressures vs. Wind Pressures for Windward Direction
Ventilation Pressure (Pa)
Wind Pressure (Pa)
Configuration 1
Configuration 2
Configuration 3
Configuration 4
3.5
3.0
2.5
2.0
1.5
1.0
0.5
0.0
-0.5
-1.0
-1.5
-2.0
-2.5
-3.0
-3.5
0
10
20
30
40
50

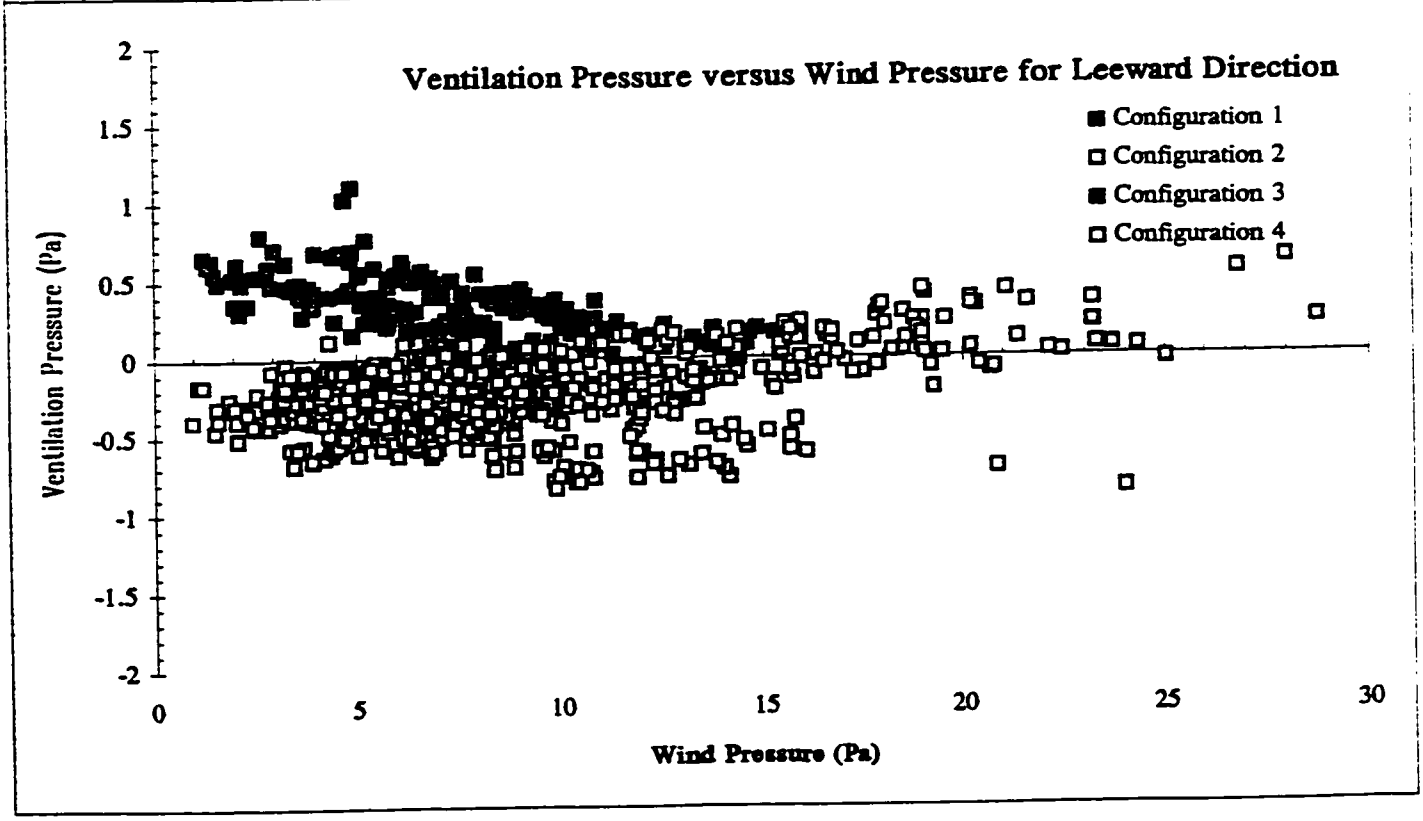
Ventilation Pressure versus Wind Pressure for Leeward Direction
Ventilation Pressure (Pa)
Wind Pressure (Pa)
Configuration 1
Configuration 2
Configuration 3
Configuration 4
2
1.5
1
0.5
0
-0.5
-1
-1.5
-2
0
5
10
15
20
25
30

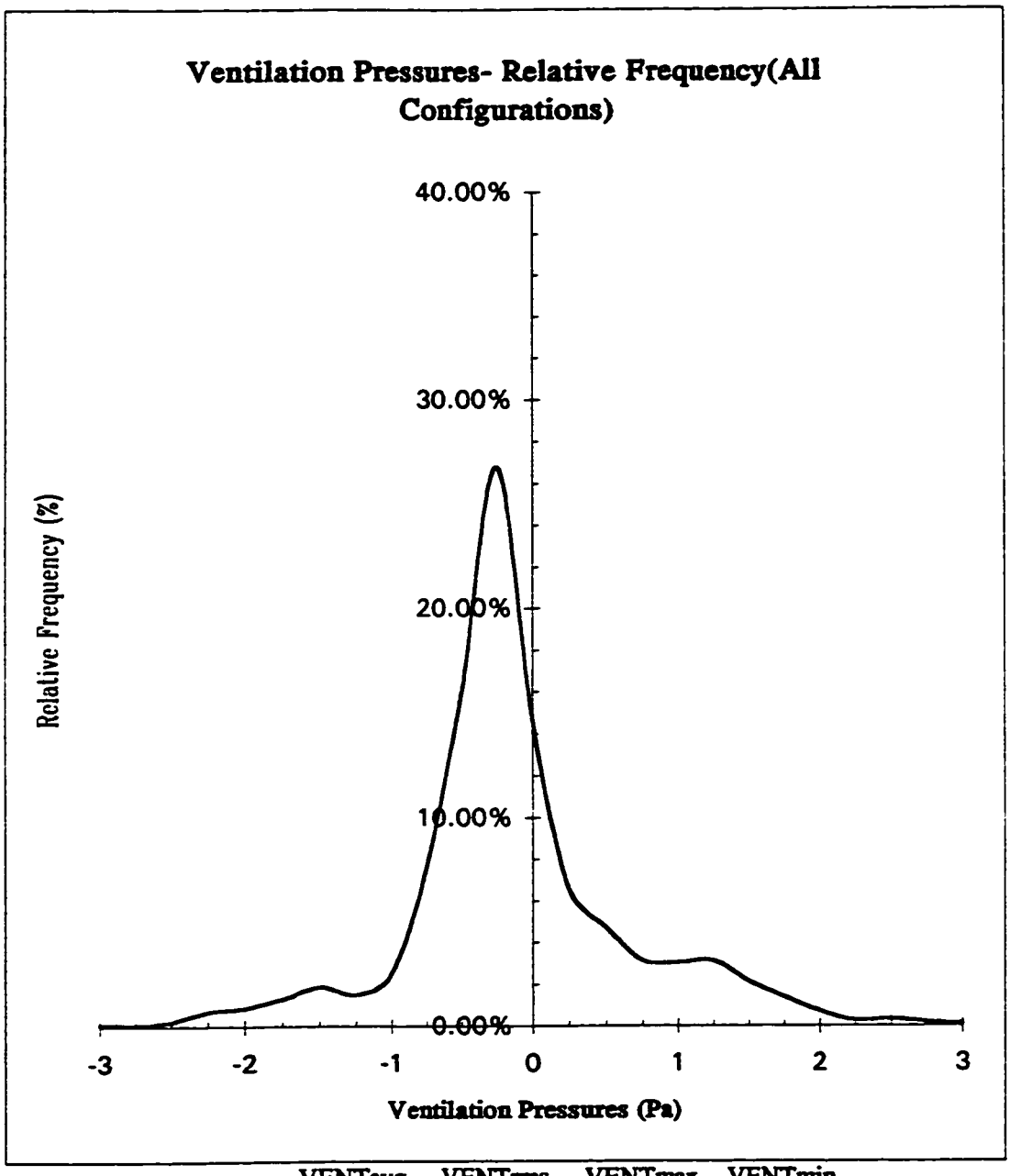

	VENTavg	VENTrms	VENTmax	VENTmin
Average	0.006	0.904	3.730	-3.915
RMS	0.775	1.139	3.811	5.086
Max	3.330	8.662	12.480	1.030
Min	-3.000	0.020	-0.620	-17.380
Range	6.330	8.642	13.100	18.410
Total Number of Records:		3287		

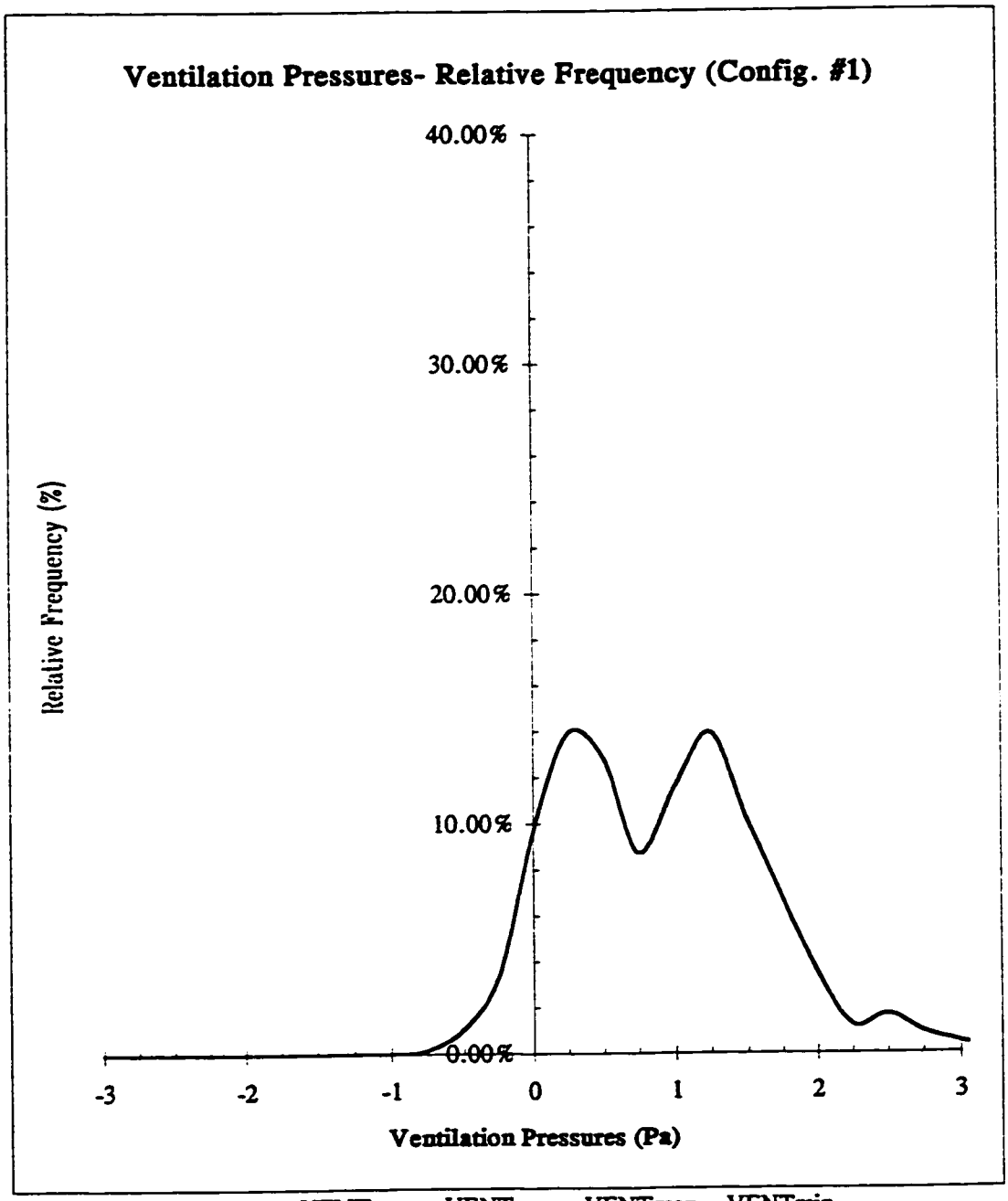

	VENTavg	VENTrms	VENTmax	VENTmin
Average	1.014	0.500	3.422	-0.461
RMS	0.701	0.379	2.691	1.438
Max	3.330	1.827	11.850	1.030
Min	-0.510	0.049	0.420	-16.770
Number:	654			

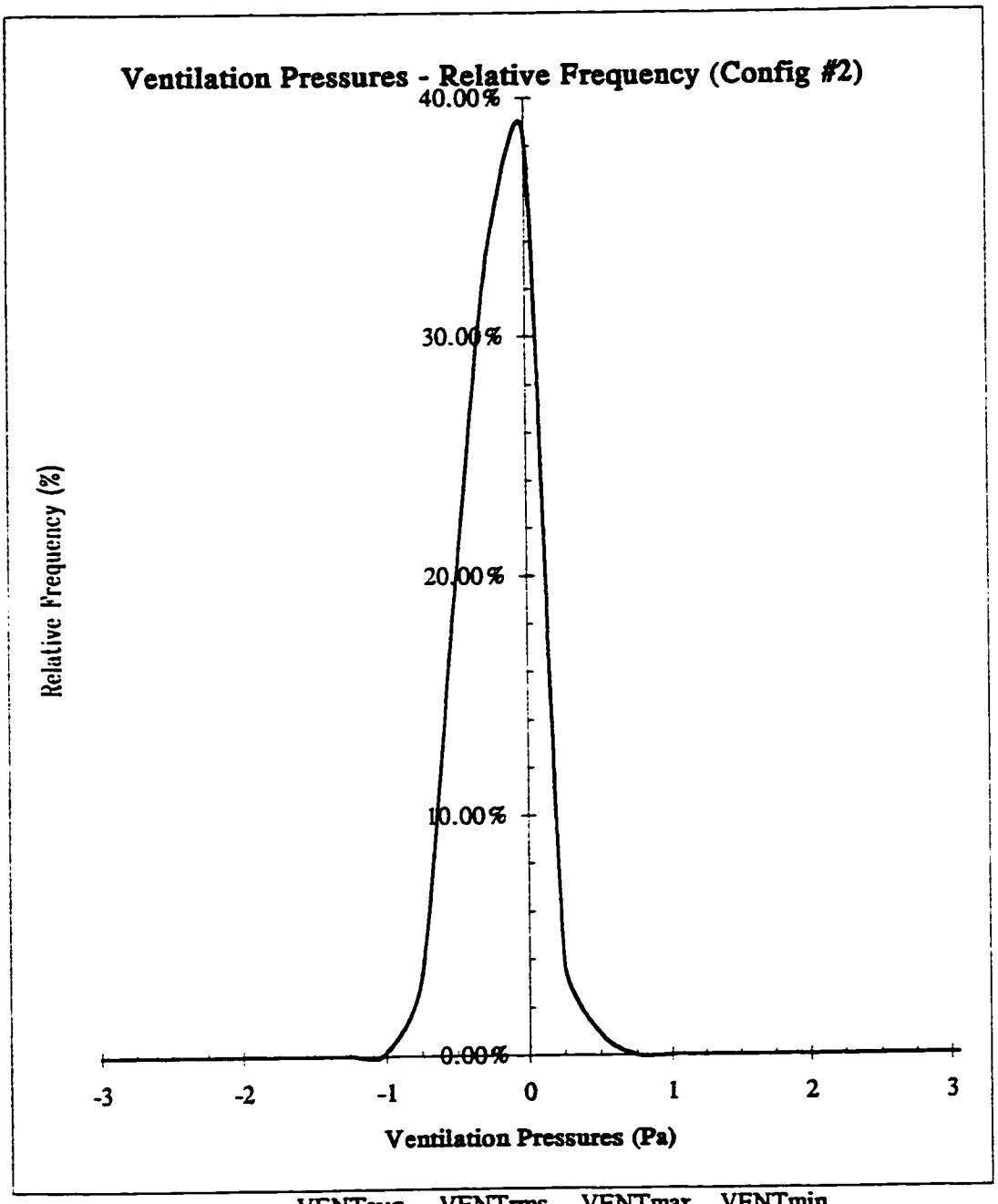

	VENTavg	VENTrms	VENTmax	VENTmin
Average	-0.308	0.402	1.493	-2.403
RMS	0.230	0.533	2.321	2.930
Max	0.440	3.537	11.900	-0.270
Min	-1.060	0.023	-0.620	-16.570
Number:	658			

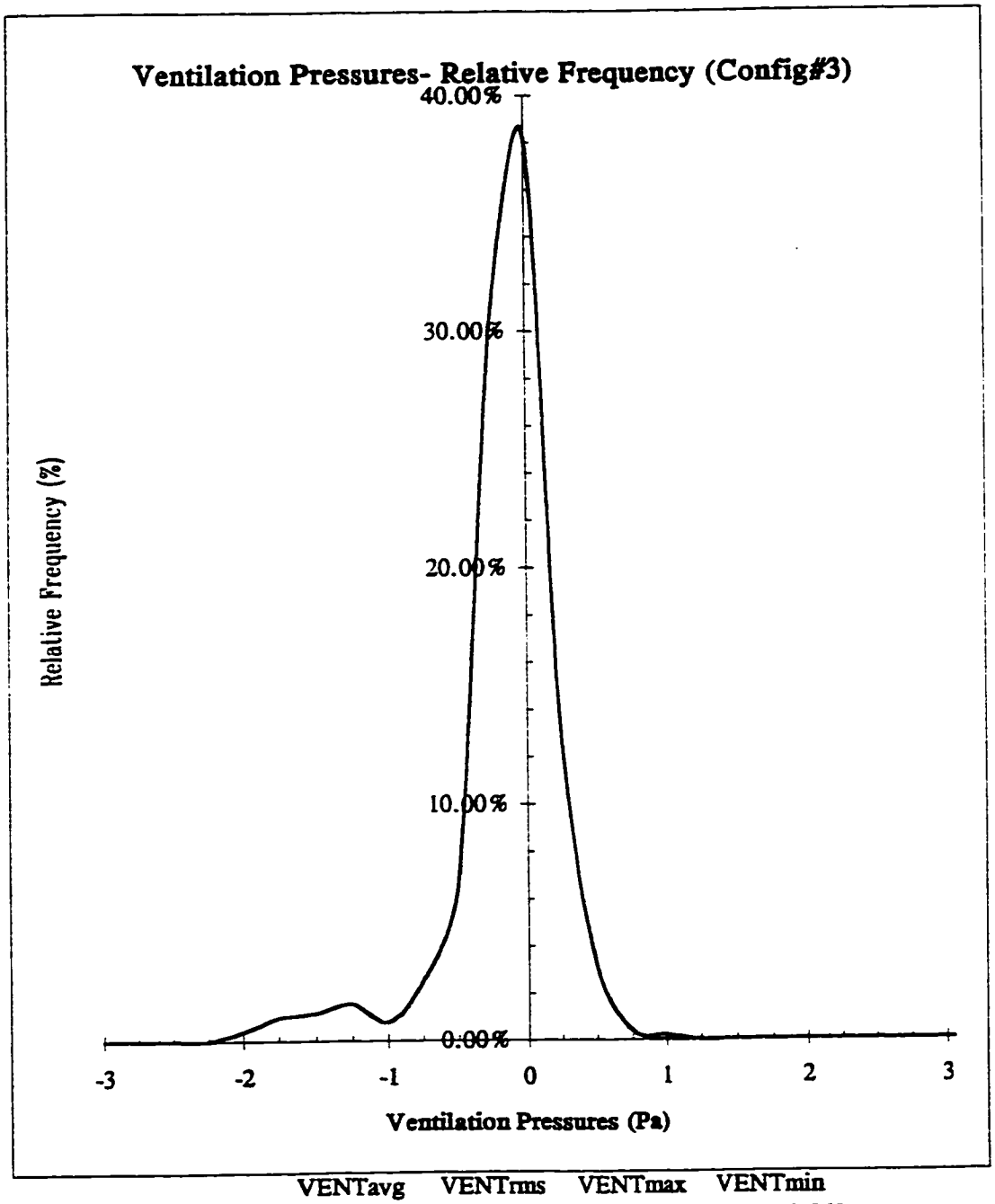

	VENTavg	VENTrms	VENTmax	VENTmin
Average	-0.262	0.483	1.792	-2.863
RMS	0.388	0.456	1.727	2.908
Max	0.770	3.026	9.880	0.010
Min	-2.230	0.020	0.000	-16.060
Number:	507			

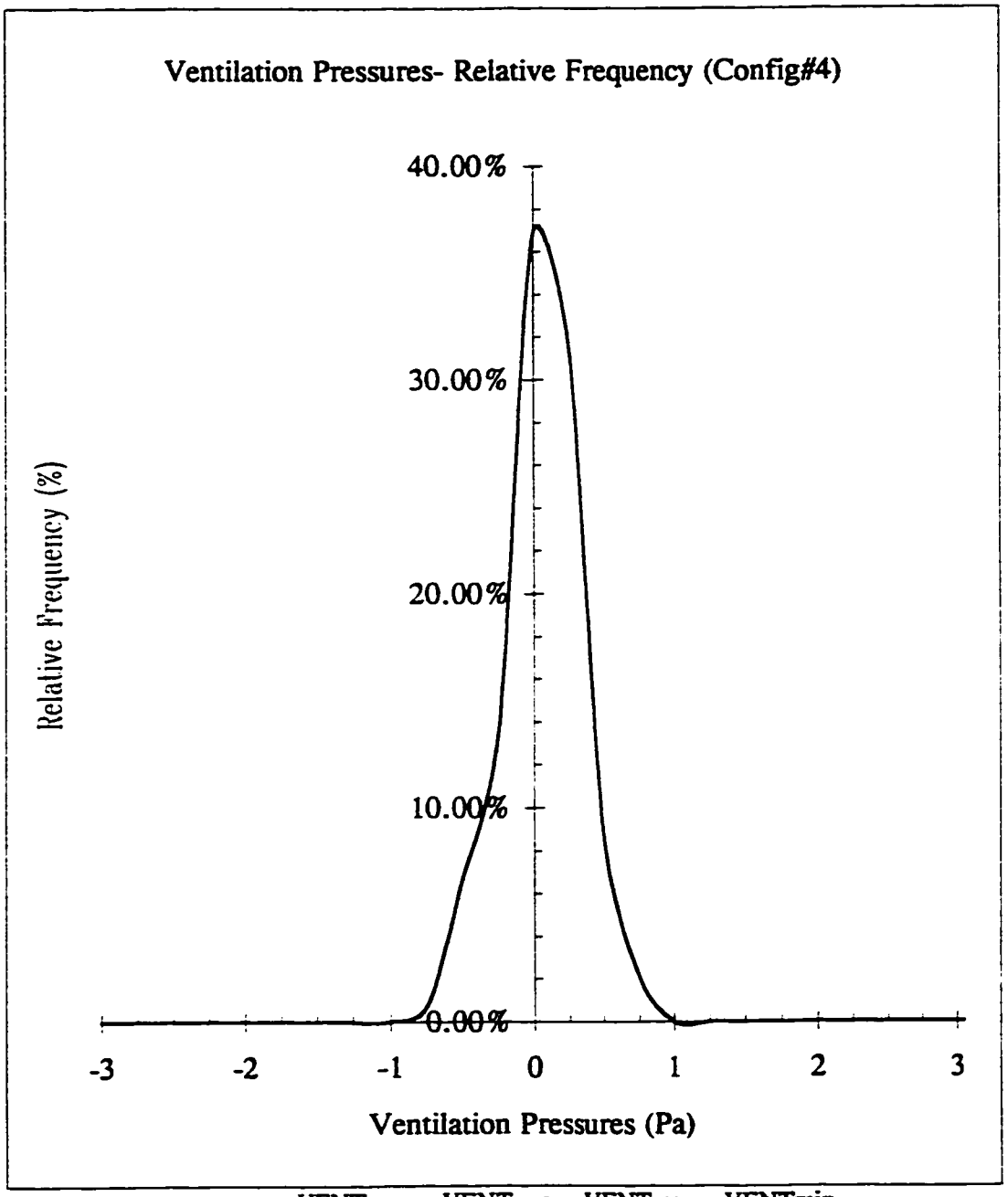

	VENTavg	VENTrms	VENTmax	VENTmin
Average	-0.053	0.542	2.715	-2.506
RMS	0.274	0.319	2.055	1.651
Max	0.750	1.723	10.270	-0.270
Min	-0.860	0.041	-0.010	-8.770
Number:	421			

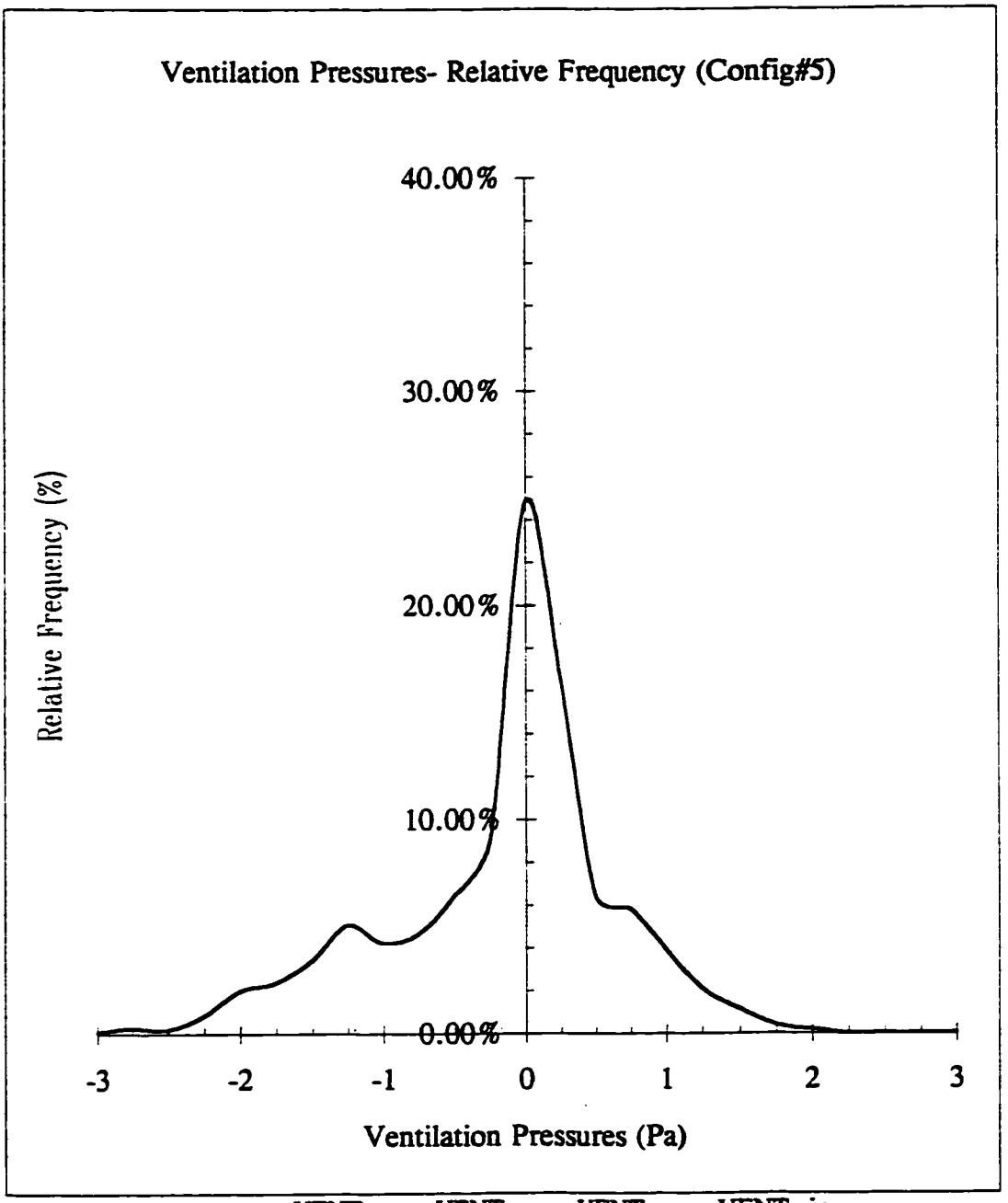

	VENTavg	VENTrms	VENTmax	VENTmin
Average	-0.272	1.820	6.676	-8.098
RMS	0.797	1.558	4.522	6.454
Max	1.850	8.662	12.480	-0.070
Min	-3.000	0.027	-0.450	-17.380
Number:	1047			

IMAGE EVALUATION
TEST TARGET (QA-3)

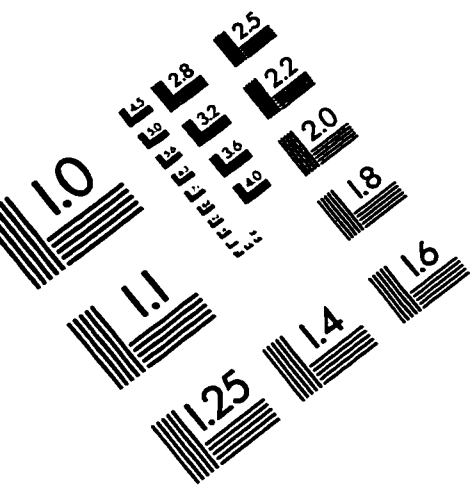

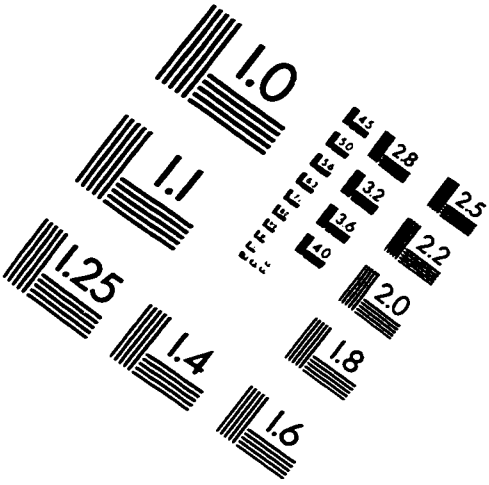

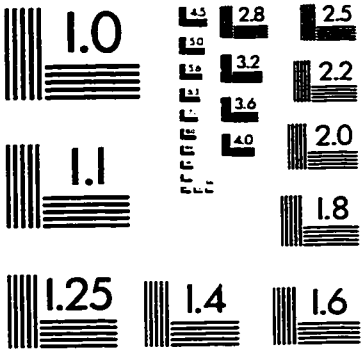

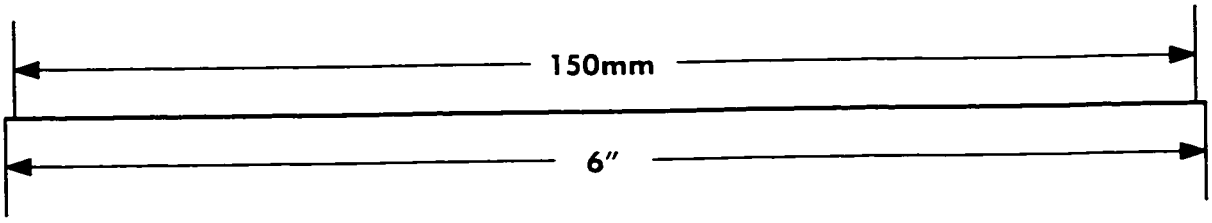

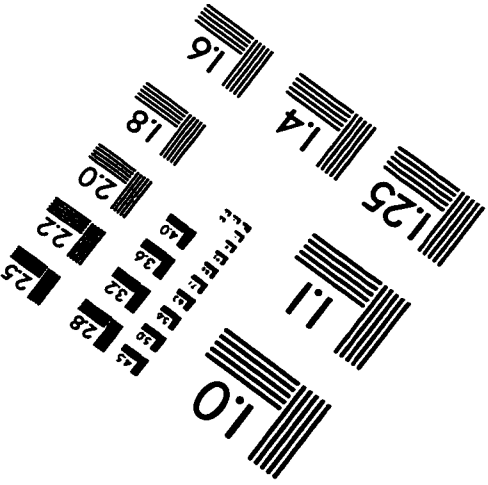

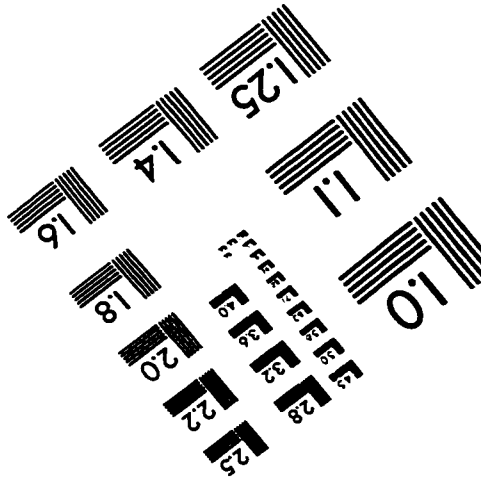

APPLIED IMAGE, Inc
1653 East Main Street
Rochester, NY 14609 USA
Phone: 716/482-0300
Fax: 716/288-5989